Functional Analysis of NET2A at the Actin-Membrane Interface of Plants

PATRICK JAMES DUCKNEY

Functional Analysis of NET2A at the Actin-Membrane Interface of Plants

Patrick James Duckney

Submitted in accordance with the requirements for the degree of Doctor of Philosophy

Department of Biosciences
Durham University

September 2016

Abstract

Recently, NET2A was characterised as a novel, plant-specific actin-binding protein that binds actin at the plasma membrane of growing pollen tubes (Deeks et al. 2012; Dixon. 2013). However, a function for NET2A has not yet been identified. Throughout the course of this investigation, several strategies were employed to elucidate the roles of NET2A in Arabidopsis, including reverse-genetic analysis, *in situ* localisation studies of NET2A in developing pollen grains and growing pollen tubes, as well as several protein-protein interaction screens.

During this study, multiple NET2 subfamily members were shown to interact with plasma membrane integral proteins, demonstrating novel mechanisms by which the actin cytoskeleton is linked to the plasma membrane in plants. Through these interactions, NET2 proteins are implicated in the regulation of pollen tube growth *in vivo* during fertilisation, and regulation of the cytoskeleton in response to extracellular signals. A role for NET2A in pollen grain development was also studied during this investigation, in which NET2A was observed to associate with the actin cytoskeleton of developing pollen grains, and undergo dynamic reorganisations in subcellular localisation timed to specific developmental events in male gametogenesis.

Reverse-genetic analysis of individual NET2 subfamily members has identified no phenotypic growth defects in pollen grain development or fertilisation. Several lines of evidence suggest functional redundancy and cooperation between individual NET2 proteins, including their involvement with common interacting partners at the plasma membrane, and interactions with one another in NET2 hetero-oligomers.

Additionally, this project describes the discovery of a novel microtubule-associated protein in Arabidopsis. This protein, named herein as MAP7A, was demonstrated to associate with microtubules directly, and localise to the pollen tube plasma membrane and generative cell nucleus.

Described in this thesis are the potential roles for NET2A and MAP7A in the regulation of the plant cytoskeleton during anisotropic cell growth.

Declaration

I confirm that this thesis and the original research described therein are my own work with the exception of figure 7.16, in which the microtubule co-sedimentation assay was performed by Dr Ian Cummins (Durham University). The creation of the *pNET2A*:NET2A-GFP and *pLAT52*:FABD2-RFP stable transgenic lines, and isolation of *net2a.1* (SALK_020898), and *net2a.2* (GABI_234H12) homozygous T-DNA mutants was undertaken by Dr Martin Dixon (Durham University). Appropriate credit has been given where reference has been made to the work of others.

No material contained in this thesis has been submitted for the award of a higher degree elsewhere.

Acknowledgements

There are many people whom I would like to thank for their support, encouragement and guidance throughout my PhD. Firstly, I would like to express my gratitude towards my supervisor, Professor Patrick Hussey, for the exceptional experience I have gained whilst working under his supervision. I would like to thank him for the opportunity to participate in his research, in which he has provided invaluable guidance and encouragement. I have thoroughly enjoyed working as part of the PMCB group.

I would like to thank Dr Michael Deeks, who mentored me during the early stages of my PhD and oversaw the investigation of NET2A prior to his departure. Dr Deeks has provided excellent theoretical insight during this project and has engaged my interest in plant cell science. I wish him all the best for the future as he develops his own research group at the University of Exeter. My predecessor, Dr Martin Dixon, also deserves special mention for his prior research on NET2A, from which the work described in this thesis has followed.

A special thanks to Dr Timothy Hawkins, who has provided exceptional technical guidance throughout my PhD, and for his advice during the writing of my thesis. I would also like to thank him for introducing me to the world of bioimaging as instructor of the undergraduate biological imaging field course, and influencing my choice in pursuing a research career in cell biology.

Additionally, I would like to express my thanks to all members of the PMCB group past and present for their advice, teamwork and cooperation during the course of my PhD. The senior members of the lab; Dr Tim Hawkins, Dr Pengwei Wang, Dr Johan Kroon, Dr Mike Deeks, Dr Andrei Smertenko, and Dr Ian Cummins have all provided a great and friendly working environment, and have offered much appreciated technical and theoretical assistance during my PhD. I give special mention to our lab manager, Dr Johan Kroon, for his rigourous organisation and smooth running of the laboratory. I would like to thank him for his excellent technical expertise and patience towards my unorthodox working procedures. I am also extremely grateful to have worked alongside fellow students, Dr Martin Dixon, Dr

David Mentlak, Jessica Fostvedt, Greg Pridgeon, Simon Bush, Jinny Zhang and Rita Catarino, who have all been supportive, helpful and great fun over the past 4 years. I especially wish Rita good luck with her future work on the pollen cytoskeleton. Finally, I am also very grateful to my great friend Simeon Johnson for all the fun over the years: I wish him all the best for his PhD!

During my time at Durham, I have had an incredible experience in learning Muay Thai under Glen Hawman with Durham University Thai Boxing Society, and with Paul Pearson at Silapa Muay Thai, Bishop Auckland. I feel privileged to have trained with these top-quality teachers and learned from their deep experiences. Learning Muay Thai has been one of my favourite aspects of my time in Durham, for which I would like to thank Glen, Paul and all members of Durham University Thai Boxing Society and Silapa Muay Thai; with special mention to my regular training partners, Adam Bending and Joe Hall.

For making it possible to study in Durham, I would like to express my gratitude to the Grevillea Trust, Durham University, for their financial support during my first year of study. Furthermore, I would like to take the opportunity to thank the Dixie Educational Foundation for their generous contribution towards my studies, for which I am most grateful.

I would also like to express my heartfelt gratitude towards my Grandmother, Ann Duckney, for her support towards my PhD. I hope that she is proud of the work I have done. Finally, many thanks to my Aunty Kath for her support and encouragement to pursue a career in science, and for the invaluable research experience she has made available to me during my undergraduate study.

Contents

Chapter 1: Introduction

Chapter 2: Materials and Methods.

Chapter 3: Reverse-Genetic Analysis of the NET2 Subfamily.

Chapter 4: *in situ* Analysis of NET2A-GFP Subcellular Localisation During Pollen Grain Development.

Chapter 5: Identifying Interacting Partners of NET2A using Protein-Protein Interaction Screens, and Investigation of NET2A Homo- and Hetero-Oligomerisation.

Chapter 6: Investigation of NET2-PRK Interactions.

Chapter 7: Characterisation of Arabidopsis MAP7s as Novel Microtubule-Binding Proteins, and Investigation of NET2A-MAP7A Interactions.

Chapter 8: Discussion.

Appendices.

List of Figures.

Chapter 1: Introduction.

Chapter 3: Reverse-Genetic Analysis of the NET2 Subfamily.

Chapter 4: *in situ* Analysis of NET2A-GFP Subcellular Localisation During Pollen Grain Development.

Chapter 5: Identifying Interacting Partners of NET2A using Protein-Protein Interaction Screens, and Investigation of NET2A Homo- and Hetero-Oligomerisation.

Chapter 6: Investigation of NET2-PRK Interactions.

Chapter 7: Characterisation of Arabidopsis MAP7s as Novel Microtubule-Binding Proteins, and Investigation of NET2A-MAP7A Interactions.

Chapter 8: Discussion.

List of Tables.

Chapter 2: Materials and Methods.

Chapter 3: Reverse-Genetic Analysis of the NET2 Subfamily.

Chapter 5: Identifying Interacting Partners of NET2A using Protein-Protein Interaction Screens, and Investigation of NET2A Homo- and Hetero-Oligomerisation.

Chapter 7: Characterisation of Arabidopsis MAP7s as Novel Microtubule-Binding Proteins, and Investigation of NET2A-MAP7A Interactions.

Chapter 1: Introduction.

1.1. Overview.

This thesis focusses on the identification of potential roles of the actin-binding protein, NETWORKED 2A (NET2A) in the regulation of the actin cytoskeleton in growing pollen tubes, and developing pollen grains.

The cytoskeleton is an essential feature of all eukaryotic cells. In plants, the cytoskeleton consists of networks of actin microfilaments and microtubules. The actin cytoskeleton is a highly dynamic filamentous network of linear actin polymers that regulates a large number of essential cellular functions including cell growth, division, organelle transport, vesicle trafficking and responses to various stimuli (Hussey et al. 2006; Deeks et al. 2007; Henty-Ridilla et al. 2014; Peremyslov et al. 2010). Precise spatiotemporal control of the dynamic actin cytoskeleton is required to coordinate these processes, and the actin cytoskeleton is regulated by a large number of actin-binding proteins that control the dynamics and organisation of actin filaments (Hussey et al. 2006; Staiger and Hussey. 2004).

The angiosperm pollen tube is an archetypal example of a ‘tip-growing’ cell, in which cell expansion occurs only at the extreme apex to form a cylindrical-shaped cell. The actin cytoskeleton is known to play a crucial role in regulating tip growth in pollen tubes and is distinctively organised for this purpose (Chen et al. 2009; Helper et al. 2001). Therefore, the growing pollen tube is a popular experimental model system on which to study the actin cytoskeleton in plant cell growth, and its regulation by various actin-binding proteins. This investigation focusses on the potential roles of the pollen-specific actin-binding protein, NET2A; recently discovered to bind actin at the plasma membrane of growing pollen tubes (Deeks et al. 2012). The recently discovered NET proteins are a novel superfamily of plant-specific actin-binding proteins that bind actin at various membrane compartments, likely serving as linkers between the actin cytoskeleton and membranes (Deeks et al. 2012; Wang et al. 2014; Wang and Hussey. 2015). The characterisation of NET2A would greatly expand our current understanding of actin-membrane interactions in plant cells, and their importance in plant cell growth and development. Furthermore, understanding the function of NET2A in the regulation of the actin cytoskeleton would also increase

our knowledge of how the actin cytoskeleton is able to regulate tip growth in anisotropically expanding plant cells.

In this chapter, the biological contexts in which NET2A is predicted to function will be discussed. Firstly, the structure and function of the actin cytoskeleton in plant cells will be described. Secondly, a comprehensive description of the events of pollen grain development will be outlined, along with the structure and function of the actin cytoskeleton throughout the developmental process. Subsequently, the mechanisms governing polarised pollen tube growth and the structure and function of actin in growing pollen tubes must also be discussed. Pollen tube growth is controlled in response to extracellular signals by pollen receptor-like kinases (PRKs; Wengier et al. 2010; Huang et al. 2014; Takeuchi and Higashiyama. 2016), which are believed to transduce external signals to the actin cytoskeleton during fertilisation. The regulation of pollen tube growth by PRKs, and the predicted involvement of NET2A with PRK signalling, will be explained in this chapter. During the course of this investigation, a role for NET2A in mediating interactions between actin and microtubules will be speculated. Therefore, actin-microtubule interactions will be introduced, along with their functions in orchestrating plant cell growth, development and division, with a special focus on their potential roles in developing pollen grains and pollen tubes. Finally, a synoptic overview of the NET protein superfamily will be presented, with the strategic intentions of this investigation to identify the functional roles of NET2A in Arabidopsis.

1.2. The Actin Cytoskeleton of Plants.

Actin is found in two forms in eukaryotic cells; as globular actin monomers (G-actin) and filamentous actin (F-actin; Steinmetz et al. 1997). The actin cytoskeleton displays a highly dynamic structure, undergoing polymerisation of F-actin filaments from soluble G-actin, and depolymerisation of F-actin to G-actin monomers (Welch et al. 1997). Nucleation of actin filaments can occur from trimers or tetramers of G-actin, acting as a ‘seed’ for actin filament formation from existing G-actin monomers (Pollard and Borisy. 2003).

The polymerisation and depolymerisation of F-actin is controlled by the nucleotide binding activity of actin subunits, which are able to bind both ATP (adenosine

triphosphate) and ADP (adenosine diphosphate) in a nucleotide binding cleft (Kabsch et al. 1990). G-actin monomers polymerising into F-actin filaments are bound to ATP, which is subsequently hydrolysed to ADP after actin monomers are incorporated into the filament. The hydrolysis of ATP to ADP by F-actin subunits is a mechanism of regulation over the dynamics of actin polymerisation and depolymerisation (de la Cruz et al. 2000): F-actin subunits bound to ADP have reduced binding affinity for surrounding subunits, making disassembly of the filament more favourable. The polymerisation, depolymerisation and seeding of actin filaments is aided by a large number of actin regulatory proteins, which will be described later (Hussey et al. 2006).

The structure of F-actin is described as a right-handed double helix, composed of two protofilaments twisted around each other to generate a double helix of 7 – 9 nm in diameter. Actin subunits are unidirectionally aligned within the protofilament, and due to the asymmetric structure of actin monomers, the resulting actin filament has polarity. The actin filament possesses a barbed end and a pointed end: assembly of actin subunits occurs as a greater rate at the barbed end, and depolymerisation occurs at a greater rate from the pointed end (Pollard and Borisy. 2003).

F-actin filaments are arranged into multiple arrays in plant cells. At interphase, F-actin exists as a dense filament system at the cell cortex, subcortical actin bundles in transvacuolar strands, and surrounding the cell nucleus (figure 1.1; Valster et al. 1997). During cell division, the distribution of actin within the dividing cell is markedly different: actin aligns with microtubules of the pre-prophase band at the initiation of prophase, and surrounds the microtubule spindle during anaphase. During telophase, actin filaments co-align with microtubules of the phragmoplast (figure 1.2).

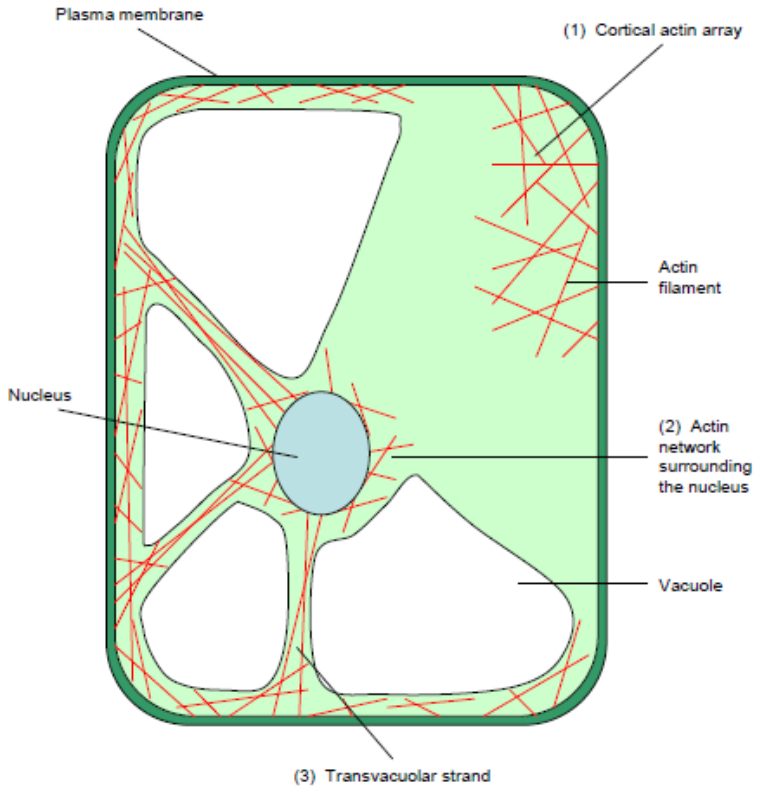

Figure 1.1: Actin Arrays in Plant Interphase Cells. (1): Dense network of cortical actin filaments. (2): Actin network surrounding the nucleus. (3): Actin bundles connecting the cell periphery and the nucleus in transvacuolar strands. Diagram from Calcutt. (2009).

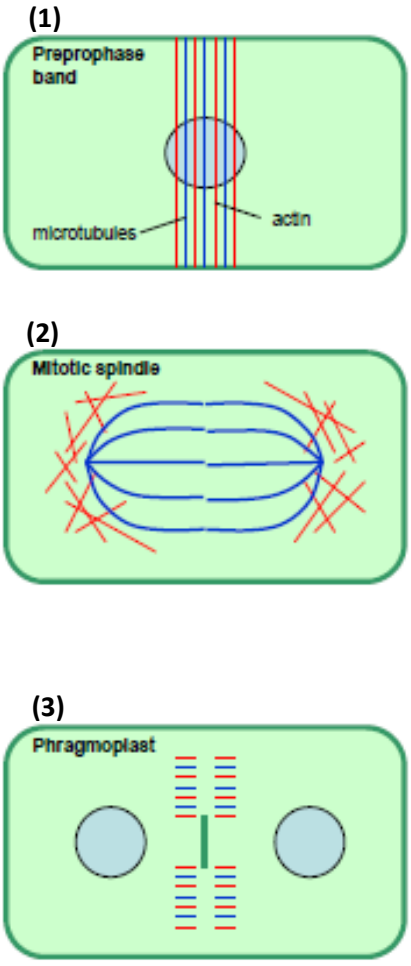

Figure 1.2: Actin Arrays in Dividing Plant Cells. (1): Actin filaments align with microtubules at the preprophase band before the start of prophase. (2): Actin forms a basket around the spindle in anaphase. (3): Actin filaments align with microtubules in the phragmoplast during cytokinesis. Diagram from Calcutt. (2009).

The actin cytoskeleton regulates a large number of subcellular processes in plant cells, including cell division, growth and morphogenesis, organelle transport, signal transduction and responses to stimuli. Actin is necessary for plant cell growth (Hussey et al. 2006): F-actin filaments are needed for anisotropic cell expansion, including the growth of interdigitating lobes of epidermal cells (Fu et al. 2002) and trichromes (Szymanski et al. 1999; Mathur et al. 1999). Actin is also required in tip growing cells, such as root hairs and pollen tubes in which cell elongation is restricted entirely to the tip. In such examples, actin filaments facilitate the transport of golgi-derived vesicles to areas of cell growth (Peremyslov et al. 2008; Rounds et al. 2014). Actin also functions in plant cell division. During pre-prophase, actin and microtubules of the pre-prophase band define the site of cell division (Kost et al. 1999; Granger and Cyr. 2000). The association of actin with the spindle during anaphase may define the position or structure of the spindle (Schmitt and Lambert. 1990), and actin guides the phragmoplast to facilitate cytokinesis during telophase (Sylvester. 2000; Wu and Bezanilla. 2014).

The trafficking of vesicles and organelles on the acto-myosin network generates a constant flow of cytosol, defined as cytoplasmic streaming. This is important for the rapid and targeted delivery of cytosolic components to specific sites of the cell which could not be achieved through Brownian diffusion (Verchot-Lubicz and Goldstein. 2010; Esseling-Ozdoba et al. 2008). Organelles including nuclei, endoplasmic reticulum, mitochondria, chloroplasts, golgi bodies and transport vesicles are known to be transported along actin filaments on myosin motors (Tamura et al. 2013; Peremyslov et al. 2010; Ueda et al. 2010; Van Gestel et al. 2002; Sattarzadeh et al. 2009; Nebenfuhr et al. 1999; Peremyslov et al. 2013). The movement of organelles by actin can also be facilitated through re-arrangements in actin filaments: chloroplasts for example are tethered to actin filaments through protein anchors, and can be re-positioned through the movement of actin filaments (Kadota et al. 2009).

There are also examples of the involvement of actin in signal transduction. Actin is important in the perception of, and responses of plant cells to biotic and abiotic stimuli, and reorganisation of the actin cytoskeleton is observed in response to many stimuli (Staiger et al. 2000). In addition to the actin-dependent re-positioning of chloroplasts described above, actin is an effector of the plant cell response to pathogens; co-ordinating trafficking of endoplasmic reticulum and golgi bodies to

the site of pathogen attack to deliver defence components (Takemoto et al. 2003; Hardham et al. 2007; Henty-Ridilla et al. 2013). The opening and closing of stomata in response to stimuli such as light and abscisic acid (ABA) is known to be dependent on actin, which undergoes reorganisation upon stimulus-induced stomatal opening and closure (Eun and Lee et al. 1997). ABA and light-induced stomatal closure are impaired in mutants defective in actin regulation (Jiang et al. 2012). Therefore, actin is important in mediating cellular responses to a wide range of stimuli. This thesis will address the potential mechanisms by which the actin cytoskeleton regulates pollen tube growth in response to external stimuli, as described in section 1.5.

1.3. Actin-Binding Proteins in Plants.

As discussed above, the actin cytoskeleton is highly dynamic in nature and undergoes constant reorganisation to regulate a large number of processes. The reorganisation of actin is regulated in a tight spatiotemporal manner by a plethora of spatially-distributed, temporally-activated actin-binding proteins (Hussey. 2004). Actin-binding proteins can be accordingly classified into three categories based on their functions: proteins that regulate actin dynamics, proteins that mediate transport activity, and proteins that organise actin filaments into higher order structures (Hussey et al. 2006). In addition, actin-binding proteins that link actin to cell membrane structures will also be discussed.

1.3.1. Actin-Binding Proteins that Regulate Actin Dynamics.

The first functional group of actin-binding proteins to be discussed are those that regulate actin dynamics. Actin-binding proteins regulate filament turnover and reorganisation of actin networks through spatiotemporal regulation of actin polymerisation and depolymerisation (Hussey et al. 2006). Profilin is a conserved actin-binding protein that serves two roles in regulating actin dynamics; when actin filaments are capped it is able to sequester G-actin monomers to prevent actin filament polymerisation (Staiger et al. 1997), but has been shown to promote polymerisation at the barbed end of uncapped filaments by acting as a nucleotide

exchange factor that converts ADP-bound G-actin to polymerisable ATP-bound monomers (Pantaloni and Carlier. 1993).

Actin-binding proteins also serve as nucleators of actin filament assembly. The conserved seven-subunit Arp2/3 complex for example, promotes barbed-end polymerisation whilst capping the pointed end of the filament. The Arp2/3 complex binds existing actin filaments and promotes the polymerisation of a new actin filament 'branch' at a 70º angle to the original filament (Hussey et al. 2006). As an additional example, formin proteins can nucleate unbranched actin filaments and also act as actin bundling proteins (Michelot et al. 2005).

Another mechanism by which actin-binding proteins can regulate actin dynamics is by capping or severing actin filaments to control polymerisation and depolymerisation. Heterodimeric capping protein regulates actin dynamics by binding to the barbed end of F-actin to prevent polymerisation (Huang et al. 2003). Actin-depolymerising factor (ADF)/Cofilin proteins sever actin filaments to promote actin turnover (Zheng et al. 2013; Henty-Ridilla et al. 2014). Villin/gelsolin proteins work to sever filaments by binding to and capping the barded end of the severed filament: as a result, rapid elongation is therefore prevented, leading to disassembly of the severed filament (Su et al. 2007).

1.3.2. Actin-Binding Proteins Regulating Transport Activity.

Transport of cargo along actin filaments is regulated by myosins: molecular motor proteins that use energy derived from ATP hydrolysis (Sellers. 2000). Myosins consist of three domains; a head domain which binds actin and ATP, a neck domain and a tail domain; specific to each myosin class and responsible for binding cargos (Hammer and Sellers. 2012). Myosin motors travel along actin filaments to facilitate transport of cargo bound to their tail domains; the hydrolysis of ATP by myosin alters the conformation of the head, exerting force on the actin filament needed for the myosin to move (Schliwa and Woehlke. 2003). In *Arabidopsis thaliana* (referred to herein as Arabidopsis), there are 17 myosins: 13 class XI myosins and 4 class VIII myosins (Reddy and Day. 2001; Peremyslov et al. 2011).

1.3.3. Actin-Binding Proteins that Regulate the Formation of Higher-Order Actin Structures.

A third functional class of actin-binding proteins are those that regulate the organisation of actin filaments into higher-order structures by interconnecting individual filaments. Formin proteins such as FORMIN1 (FH1) are able to cross-link individual actin filaments: after the nucleation of a new actin filament, FH1 detaches from the barbed end and moves to the side of the elongating actin filament to generate bundles of branched filaments (Michelot et al. 2005; Michelot et al. 2006; Cheung and Wu. 2004). Villin proteins belonging to the villin/gelsolin superfamily also bundle actin filaments; with each villin monomer binding and cross-linking actin filaments adjacently. The formation of actin bundles by villin is thought to stabilise actin bundles *in vivo* (Yokota and Shimmen. 1999; Huang et al. 2005; Su et al. 2007). Fimbrin proteins are also known to cross-link actin filaments in plant cells (McCurdy and Kim. 1998). These proteins are the only plant members of the Calponin Homology Domain Superfamily, which contains the actin cross-linking proteins α-actinin, dystrophin, filamin, and spectrin of mammals (Djinovic-Carugo et al. 2002). In Arabidopsis, five fimbrin proteins have been identified (Staiger and Hussey. 2004). LIM-domain proteins also bind and promote bundling of actin filaments in a pH and [Ca^{2+}]-sensitive manner (Papuga et al. 2010).

1.3.4. Actin-Binding Proteins that Link Actin to Membranes.

Of particular relevance to this study are actin-binding proteins that bind actin to the plasma membranes of various cell compartments. The plant formin proteins exhibit multiple functional roles; in addition to the actin-nucleating and bundling activities described above, formins such as FH1, FH4, FH5 and FH8 localise to plasma membranes where they bind actin to form physical links between actin and the plasma membrane. Plant formins can localise to the plasma membrane through transmembrane domains, binding of phospholipids and also other proteins (Cheung et al. 2010; Martiniére et al. 2011; Van Gisbergen et al. 2012; Cvrčková. 2013).

FH8 is also able to link actin to the membrane of the nuclear envelope (Xue et al. 2008). Additionally, the nuclear envelope is also linked to the actin cytoskeleton through SUN-INTERACTING NUCLEAR ENVELOPE protein-1 (SINE1; Zhou et al.

2014). SINE1 is a plant-specific member of KASH (Klarsicht/Anc/Syne-1 homology) -domain proteins which span the outer nuclear envelope to interact with SUN (SAD1/UNC84) proteins, which span the inner nuclear envelope; forming a physical connection between the inner nuclear envelope and outer nuclear envelope. The KASH-SUN protein complexes are conserved across eukaryotes (Zhou and Meier. 2013). The binding of SINE1 to actin physically tethers the nuclear envelope to the actin cytoskeleton (Zhou et al. 2014).

As described previously, the actin cytoskeleton is able to reposition chloroplasts through reorganisation of the actin cytoskeleton. This is facilitated by the tethering of chloroplast membranes to actin filaments by the actin-binding protein CHLOROPLAST UNUSUAL POSITIONING 1 (CHUP1), which is localised to the outer chloroplast envelope (Kadota et al. 2009).

As a central focus of this study, the connection of the actin cytoskeleton to various membrane compartments by the NET protein superfamily will be discussed (chapter 1.7). NET proteins have been demonstrated to bind actin at membranes through interactions with various membrane integral proteins: NET3C for example links actin to the endoplasmic reticulum through an interaction with the ER-integral protein, VAP27 (Wang et al. 2014). As elucidated in the course of this investigation, multiple members of the NET2 protein family link actin to the plasma membrane through interactions with pollen receptor-like kinase integral membrane proteins (chapter 1.5).

1.4. The Actin Cytoskeleton of Pollen.

Pollen is the male gametophyte of flowering plants. Its role is to deliver non-motile sperm through the female sporophytic tissues to the ovule, whereupon sperm is delivered to the egg cell to achieve fertilisation. Detailed descriptions of pollen grain development and pollen tube growth will be outlined below. Additionally, this section will focus on the role of actin in pollen grain development, and in the growing pollen tube.

1.4.1. Pollen Grain Development.

Pollen grains are highly specialised cells, typically tricellular or bicellular (varying between species) and possess a unique cell wall consisting of two layers: an inner layer composed of cellulose and pectin, and a tough and distinctively sculptured outer layer known as the exine, derived of sporopollenin (Borg and Twell. 2011; Blackmore et al. 2007). Pollen grain development takes place in the developing anther, following which the rupturing of the anther locules during dehiscence releases mature pollen grains, permitting their germination on the stigma (Ma. 2005; Wilson and Yang. 2004).

Developing pollen grains undergo a series of tightly regulated cell divisions over the course of pollen grain maturation (figure 1.3). The production of the male gamete is initiated by the formation of pollen mother cells (PMCs), derived from mitotic divisions of the somatic hypodermal cells of the anther primordium (Scott et al. 2004; Wilson and Yang. 2004). In developing anthers, meiotic division of diploid PMCs gives rise to a tetrad of four haploid microspores surrounded by a callosic wall. Release of microspores from the tetrad is facilitated by digestion of the tetrad cell wall by enzymes secreted from the tapetum (Scott et al. 2004): a nutritive layer of parietal cells that surrounds and supports the developing pollen grains (Scott et al. 2004; Wilson and Yang. 2004; Borg and Twell. 2011). The development of the unicellular microspore into the mature male gametophyte (or mature pollen grain) is a process known as microgametogenesis. During this process, several cell divisions occur to give rise to mature tricellular or bicellular pollen grains (depending on the species). During the first microspore division, known as pollen mitosis I (PMI), the microspore nucleus migrates to the cell periphery in which an asymmetric mitotic division generates two unequal cells: a large vegetative cell (VC), and a smaller generative cell (GC), separated by the synthesis of a callose wall. Following PMI, the callose wall separating the two cells in digested and the GC is then engulfed by the vegetative cell, forming a ‘cell-within-a-cell’, and generating a bicellular pollen grain. The engulfed GC then migrates to the centre of the pollen grain and develops an elongated morphology (Palevitz and Cresti. 1989; Cai and Cresti. 2006; Borg et al. 1989). Division of the GC in pollen mitosis II (PMII) gives rise to two sperm cells (SCs), the timing of which varies between species: in bicellular pollen, PMII occurs after pollen germination as the GC is transported in the growing pollen tube. In contrast, PMII occurs during pollen grain development, prior to anthesis, in tricellular

pollen (Twell. 2001; Borg et al. 2009; Zonia et al. 1999; Gervais et al. 1994). The vegetative cell nucleus (VCN) and two sperm cells together comprise the male-germ unit (MGU) of tricellular pollen, and are believed to be physically linked through membrane and cytoplasmic connections (McCue et al. 2011). Upon approaching maturity, developing pollen grains begin to desiccate in order to survive exposure to dry environments following dehiscence, in which the anther locules rupture in order to expel the mature pollen grains (Ma. 2005).

During the process of pollen maturation, the parietal tissues of the tapetum support the development of the maturing gametophytes, which accumulate carbohydrate and lipids secreted from the tapetum in order to support pollen tube growth (Pacini 1996), and osmoprotectants such as proline and glycine-betanine to protect cell membranes during dehydration (Schwacke et al. 1999; Borg and Twell. 2011). Additionally, the tapteum is responsible for the synthesis and deposition of components of the pollen exine, such as sporopollenin (Borg and Twell. 2011).

1.4.2. Structure of the Actin Cytoskeleton in Developing Pollen Grains.

Relative to studies on the actin cytoskeleton in growing pollen tubes, little research has been performed on the actin cytoskeleton of developing pollen grains. Previous studies on the developing pollen grains of *Nicotiana tabacum* and *Brassica napus* have shown the actin cytoskeleton to undergo dynamic rearrangements over the course of development to form distinctive arrays at specific stages of gametogenesis.

In *B. napus* pollen, the dynamic reorganisation of actin arrays during grain development has been studied from the microspore stage to anthesis (figure 1.4). In developing unicellular microspores, actin microfilaments have been observed to surround the nuclear envelope and are present throughout the cytoplasm. Interestingly, in acentric nuclei, actin filaments localise to the cytoplasmic face of the nucleus, but not the face of the nucleus adjacent to the cell cortex, indicating alterations in actin localisation accompany nuclear migration prior to PMI. During PMI, actin filaments are present at the surface of the nuclear envelope and extend into the cytoplasm at prophase, before forming a basket around the cytoplasmic face of the spindle during anaphase. Actin can be found associated with the

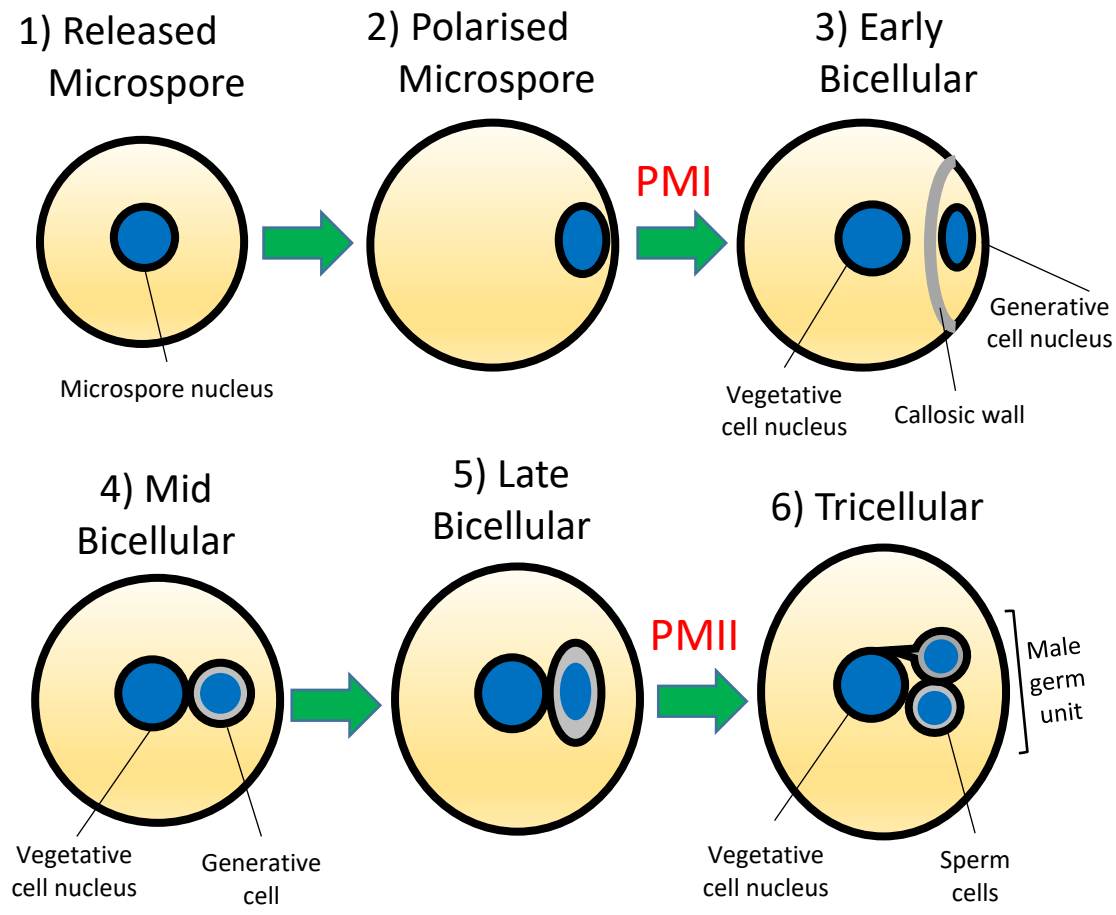

Figure 1.3: Classifications of Pollen Grain Developmental Stages. Widely accepted terminology for discreet stages of pollen grain development, describing the series of cellular events and cell divisions that occur during the development of the male gametophyte. 1). Unicellular microspore released from tetrad. 2). Microspore nucleus migrates to cell pole to form polarised microspore. 3.) Early bicellular pollen has undergone PMI to form large vegetative nucleus and smaller generative cell nucleus separated by callosic cell wall. 4.) In mid-bicellular pollen, the generative cell has been engulfed by the vegetative cell to form a 'cell-within-a-cell', both VCN and GC have migrated centrally. 5.) In late bicellular pollen, the GC elongates. In bicellular species, the VCN and GC remain in this position until germination. 6.) Tricellular species undergo PMII, in which the GC divides to form two sperm cells. A cytoplasmic projection links the SCs to the VCN to form the MGU. Original figure created based on descriptions from Borg and Twell. (2009); Borg et al. (2009).

phragmoplast during telophase in PMI. In bicellular pollen, actin filaments surround the newly formed generative nucleus and form a filamentous meshwork at the vegetative cell cortex. As the GC migrates to a central position in the developing pollen grain, highly ordered transverse actin cables align at the cortex at the equatorial regions of the pollen grains. In late bicellular pollen, the cortical transverse actin cables are no longer present, and actin microfilaments surround

the VCN, but not the GCN. After PMII, cortical actin filaments are seen in the furrows of the exine of the *B. napus* grains. Association of actin with the VCN was observed in tricellular pollen grains also (Gervais et al. 1994).

In developing pollen grains of *N. tabacum*, the actin cytoskeleton also undergoes dynamic reorganisations at specific stages of development (figure 1.5). In unicellular microspores, actin filaments were not observed during the migration of the nucleus to the cell pole. However, once having arrived at the generative cell pole, a cage of actin filaments forms around the nucleus, appearing to tether it to the cell cortex. During PMI, actin localises to the spindle and phragmoplast. In bicellular pollen, the actin microfilaments encircle both the GCN and VCN as they begin to migrate to a central position, with longer filaments radiating into the cell cytoplasm. After migration, actin is only seen to surround the VCN but not the GCN. In addition to this, a dense meshwork of actin filaments can be observed at the cell cortex (Zonia et al. 1999).

Therefore, developmentally co-ordinated reorganisations of actin arrays have been reported in multiple species, coinciding with specific stages of development. There exist striking similarities between the organisations of actin in bicellular and tricellular grains, including the association of actin with the microspore nucleus during PMI, and the VCN following PMI, and manifesting as cortical actin networks in maturing pollen grains. As described below, actin plays important roles at specific stages in pollen grain development: it is likely that the actin organisations described above have specific roles in mediating certain processes in pollen development.

1.4.3. The Function of Actin in Pollen Grain Development, and its Regulation by Actin-Binding Proteins.

Actin appears to have important roles in pollen grain development and pharmacological disruption of actin at specific stages of development has been documented to perturb specific developmental events. In studies conducted on *B. napus* and *N. tabacum*, the actin cytoskeleton has been implicated in the regulation of specific developmental events (Gervais et al. 1994; Zonia et al. 1999). Actin is believed to be crucial in regulating PMI through the positioning of the microspore nucleus to the microspore wall, and in the formation of the phragmoplast and

spindle. In early bicellular pollen the migration of the GCN and VCN to a central position appears to be actin-dependent. Additionally, actin appears to have an important role in regulating cell morphology during pollen grain development, and plays a role in the elongation of pollen grains after PMI.

Very little research has been performed on the role of actin-binding proteins in the regulation of pollen grain development, with focus lying on the roles of actin-binding proteins in growing pollen tubes. It has been reported that the actin-bundling PLIM2 protein family plays essential roles in grain development (Ye and Xu. 2013), although no explanation of their mechanism of action, or the specific processes they regulate has been presented. Members of the NET3 protein family are also necessary in pollen grain development, and the specific subcellular processes they regulate has yet to be elucidated (Wang et al. 2014). Dynamic rearrangements of the subcellular localisations of actin-associated ADF7 and ADF10 during pollen grain development indicate an important role for these proteins, potentially in regulating F-actin turnover (Bou Daher et al. 2011). In lily, a pollen-specific ADF, *Li*ADF1, stably binds and decorates actin filaments in ungerminated pollen grains and exhibits a low level of actin-depolymerising activity. Upon pollen germination, the actin-depolymerising activity of *Li*ADF1 is greatly enhanced by actin-interacting protein-1 (AIP1) to regulate dynamic reorganisations of the actin cytoskeleton as pollen grains exit dormancy and begin to germinate (Allwood et al. 2002). It is therefore apparent that pollen actin-binding proteins coordinate reorganisations of the actin cytoskeleton and modulate its dynamicity during specific events in development. However, no role for these proteins in pollen grain development has been described. It should be noted however, that mutants of certain actin-binding proteins such as FIMBRIN5 or cyclase-associated protein1 (CAP1) exhibit defects in pollen germination, which may reflect defects in pollen grain development prior to germination (Deeks et al. 2007; Wu et al. 2010).

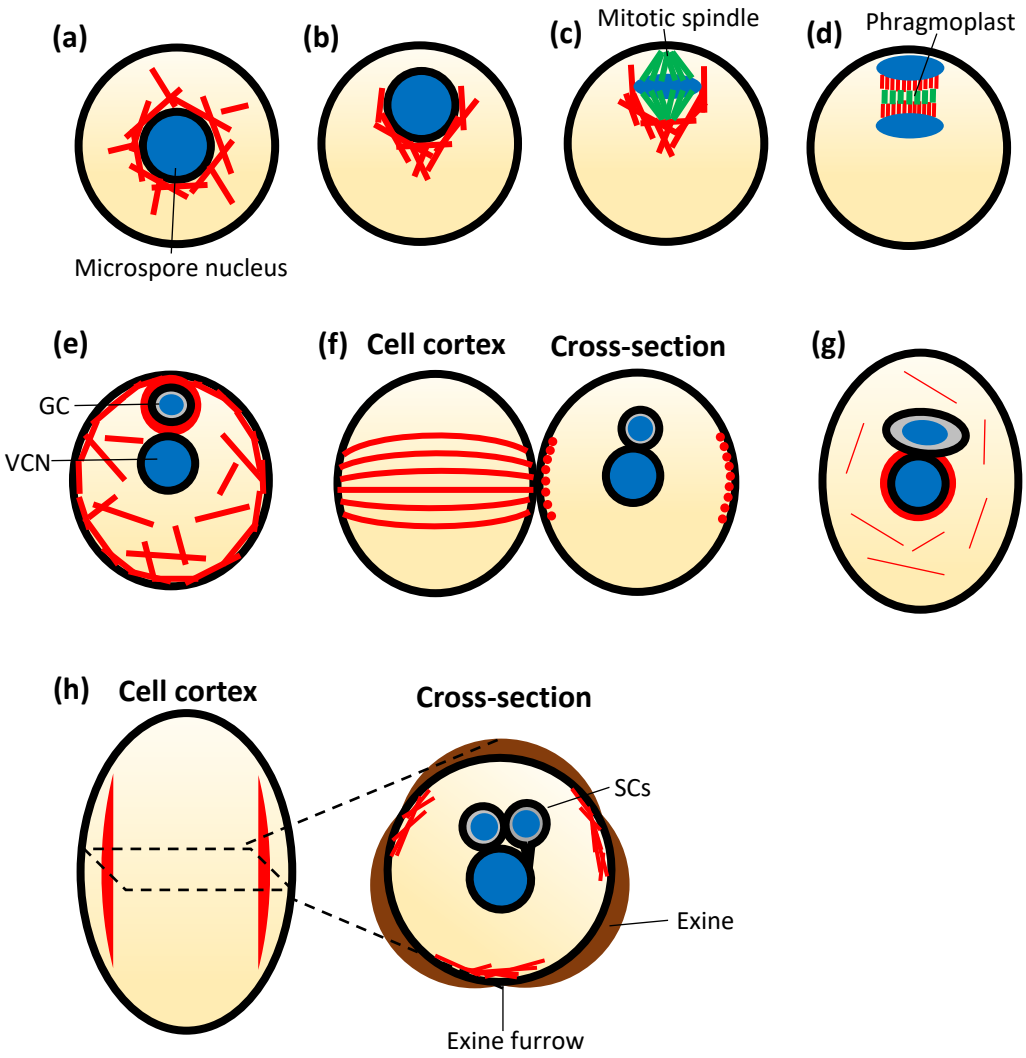

Figure 1.4. F-actin Organisation During *B. napus* Pollen Grain Development. The subcellular localisation of F-actin undergoes dynamic reorganisations at specific stages of pollen grain development. (a): at the microspore stage, F-actin surrounds the nucleus prior to nuclear migration. (b): during nuclear migration, F-actin localises asymmetrically to the cytoplasmic face of nucleus. (c): F-actin surrounds the mitotic spindle during PMI. (d): F-actin associates with the phragmoplast during telophase in PMI. (e): in early bicellular pollen, F-actin surrounds the GC. (f): following nuclear migration, F-actin forms transversely-orientated actin cables at equatorial regions of the cell cortex. (g): in late bicellular pollen, F-actin associates with the VCN, but not the GC, and fine F-actin filaments are present in the cytoplasm. (h): in tricellular pollen, F-actin localises to the cell cortex specifically associated with the furrows of the exine. Original figure created based upon descriptions from Gervais et al. (1994). F-actin filaments are depicted in red, cell nuclei in blue, and microtubules in green.

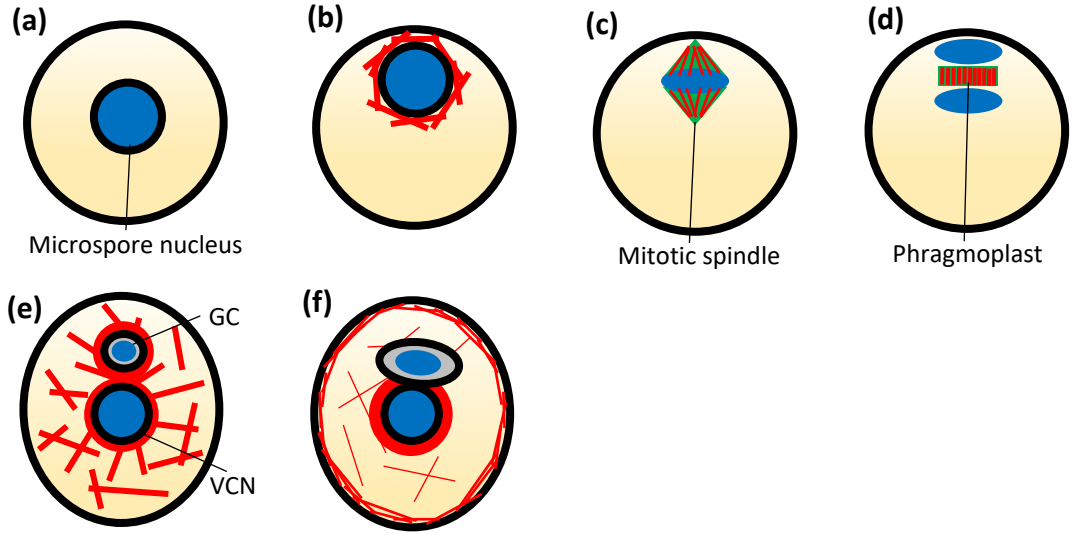

Figure 1.5. F-actin Organisation During *N. tabacum* Pollen Grain Development. The subcellular localisation of F-actin undergoes dynamic reorganisations at specific stages of pollen grain development. (a): F-actin was not observed prior to polarised migration of the microspore nucleus. (b): during nuclear migration, F-actin localises to the microspore nuclear envelope, connecting it to the cell cortex. (c): F-actin associates with the mitotic spindle during PMI. (d): F-actin associates with the phragmoplast during telophase in PMI. (e): following PMI, F-actin surrounds the GC and VCN, and actin filaments extend throughout the cytoplasm. (f): in mature bicellular pollen, F-actin surrounds the VCN, and a fine meshwork of actin filaments are present at the cell cortex. Fine actin filaments also extend throughout the cytoplasm. Original figure created based upon descriptions from Zonia et al. (1999). F-actin filaments are depicted in red, cell nuclei in blue, and microtubules in green.

1.4.4. The Growing Pollen Tube.

The delivery of non-motile sperm cells to the female gamete during fertilisation is dependent on pollen tube growth. Upon adhesion to the surface of the stigma, pollen grains germinate to form a pollen tube which extents rapidly, penetrating the style tissue and transmitting tract whilst navigating a path to the ovules. Upon arrival at the ovule, the pollen tube then ruptures in order to discharge the sperm cells to achieve fertilisation of the egg (figure 1.6; Cheung et al. 2010; Vidali and Helper. 2001).

Pollen tube extension is classical example of ‘tip growth’ in which cell expansion is limited entirely to the cell tip (Chen et al. 2009), resulting in the formation of a cylindrical shaped structure of uniform width (Helper et al. 2001). The pollen tube

can be divided into three distinct zones: the apical region, the subapex (or shoulder), and the shank region (figure 1.7), each with a distinct cytoplasmic organisation (Chen et al. 2009). The tip-focussed expansion of pollen tubes requires strict maintenance of cell polarity; the regulation of which has been extensively documented. Oscillatory fluctuations in tip-focussed $[Ca^{2+}]_{cyt}$, pH, reactive oxygen species (ROS) and phosphatidylinositol gradients are known to regulate the polarised growth of pollen tubes by establishing tip polarity (Helper et al. 2006; Steinhorst and Kudla. 2013; Potocký et al. 2007; Ischebeck et al. 2008). Tip-focussed gradients of $[Ca^{2+}]_{cyt}$, the phosphatidylinositol, phosphatidylinositol-4,5-bisphosphate [$PtdIns(4,5)P_2$], and perhaps pH, are believed to regulate the actin cytoskeleton (Ischebeck et al. 2011; Lovy-Wheeler et al. 2006; Steinhorst and Kudla. 2013), which has a highly organised and distinctive organisation in growing pollen tubes. A detailed description of the actin cytoskeleton of pollen tubes will be described below.

The polar organisation of the actin cytoskeleton of growing pollen tubes acts a framework for the targeting of golgi-derived secretory vesicles to the pollen tube tip through acto-myosin transport. Exocytosis of synthetic vesicles at the tip permits unidirectional cell expansion, whilst simultaneous endocytosis at the tip recycles excess plasma membrane and secreted components (Moscatelli and Idilli. 2009). The polarised exocytosis of synthetic growth components at the pollen tube tip is involved in the establishment of the pollen tube cell wall, which in turn supports the tip-focused growth of pollen tubes (Geitmann et al. 2010). The cell wall provides mechanical stabilisation of the pollen tube cylinder under high internal turgor pressures (Parre and Geitmann. 2005a), which drive growth through local expansion of the cell wall (Aouar et al. 2010).

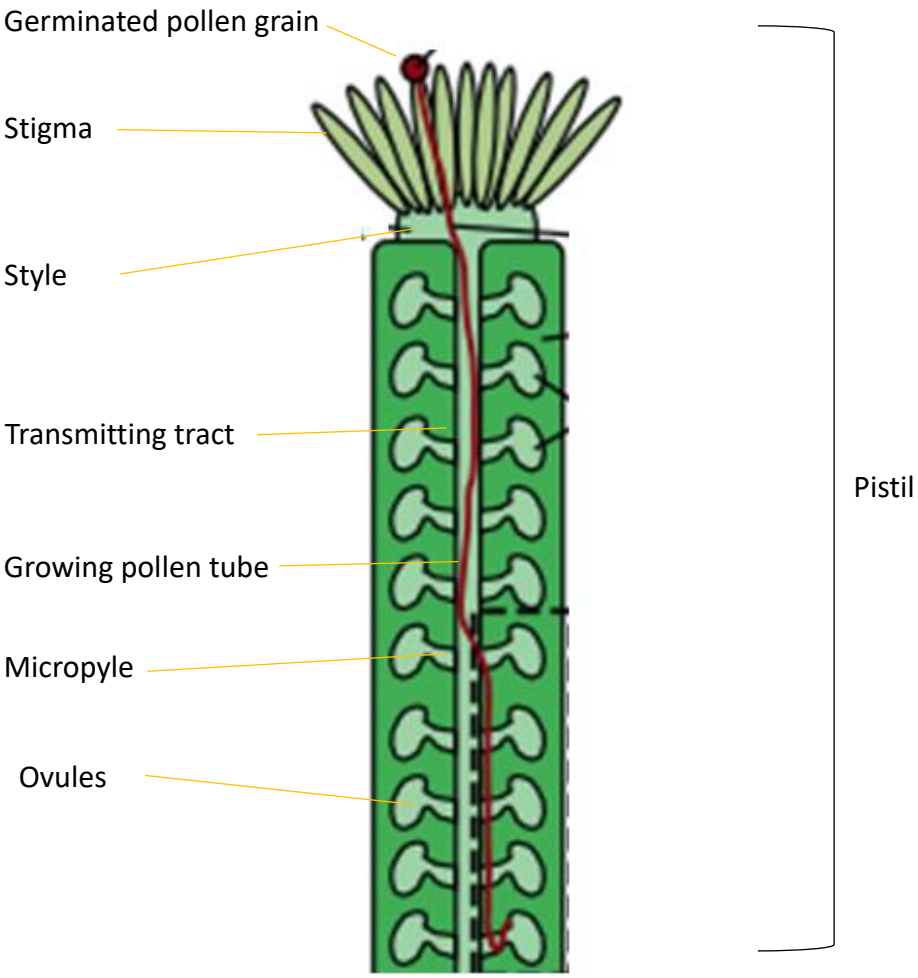

Figure 1.6: Pollen Tube Growth Through the Pistil During Fertilisation in Angiosperms. Pollen grains germinate on the stigma. The extending pollen tube penetrates and grows through the stigma and style sporophytic tissues and travels down the transmitting tract. Following guidance signals from the pistil, the pollen tubes enter the micropyle and grow to the ovules to deliver sperm to the egg cell. Adapted from Stewman et al. (2010).

Turgor-driven cell expansion is permitted at areas of high cell extensibility and low rigidity, but is restricted from regions of low cell wall extensibility, and high rigidity. The spatial regulation of pollen tube cell wall composition through targeted vesicle trafficking is used to modulate its local mechanophysical properties. By maintaining low cell wall rigidity at the poll tube tip, and high rigidity at the shank, cell expansion is permitted at the tip, whilst radial expansion is restricting at the shank, therefore maintaining the constant cylindrical shape of the pollen tube. The pollen tube cell wall consists primarily of pectin, cellulose and callose, the precursors of which are deposited at the tip apoplast via exocytosis. Pectin and callose play major roles in controlling anisotropic cell growth in pollen tubes (Geitmann. 2010). Pectin exists in

two forms: methyl-esterified pectin, which forms a non-rigid cell wall matrix, and de-esterified pectin, which binds calcium to form cross-links, resulting in a dense, rigid cell wall (Peaucelle et al. 2012). Pectin is secreted at the cell tip in its esterified form by golgi-derived secretory vesicles (Wolf et al. 2009). The enzyme, pectin methyl esterase, which converts methyl-esterified pectin to de-esterified pectin, is secreted to the shoulder regions of the pollen tube tip, which causes the pectin cell wall to rigidify as the cell wall matures and becomes shank (Bosch et al. 2005; Parre and Geitmann. 2005a). Additionally, pectin methyl esterase inhibitors (PMEIs) are secreted at the pollen tube apex, to prevent the rigidification of the pectin cell wall by esterases. PMEIs are selectively removed from the subapical regions of the pollen tube by endocytosis, permitting the rigidification of pectin by PME in the shank (Wolf et al. 2009; Palin and Geitmann. 2012). Therefore, through spatial regulation of pectin composition by targeted vesicle trafficking, pectin cell wall rigidity is maintained at the shank, and relaxed at the tip, restricting cell expansion to the apex. Similarly, callose deposition, restricted from the pollen tube apex, is believed to stabilise the mechanical rigidity of the shank cell wall through interactions with cellulose microfibrils (Ferguson et al. 1998; Geitmann and Parre. 2005b; Chebli et al. 2012).

Therefore, many factors are known to be important in the regulation of pollen tube growth. The pollen tube is highly responsive to its extracellular environment, and responds to a large number of extracellular signals in order to navigate through the pistil tissues to the ovule (Takeuchi and Higashiyama. 2016; Palanivelu and Preuss. 2006; Qu et al. 2015a). Therefore, the processes regulating pollen tube growth and guidance must be modulated in response to extracellular signals. Further descriptions of the regulation of pollen tube growth in response to extracellular cues are provided in sections 1.4.7.2 and 1.5.

1.4.5. The Structure of Actin in Growing Pollen Tubes.

The actin cytoskeleton is organised differently in the apex, subapex and shank of growing pollen tubes (Chen et al. 2009). In the shank, actin is organised into thick longitudinal cables which facilitate actomyosin-based trafficking of organelles to and from the apical region of the pollen tube. Cortical actin cables at the pollen tube shank mediate anterograde transport of organelles and golgi-derived secretory

vesicles to the tip, whilst medial actin cables facilitate retrograde transport for the recycling of vesicles and organelles. This actin arrangement mediates what is known as ‘reverse-fountain’ cytoplasmic streaming, and prevents large organelles (but not secretory vesicles) entering the apical region, creating a ‘clear zone’ devoid of organelles (Qu et al. 2015b). The existence and arrangements of actin filaments at the proximal regions of the tube are subject to debate, mainly due to different observations of actin in cells prepared using different methods (Qu et al. 2015b). However, the general consensus is as follows: at the subapex, short, fine actin filaments are arranged into an ‘actin fringe’ which deliver secretory vesicles to the apical plasma membrane to permit cell expansion (Lovy-Wheeler et al. 2005; Chen et al 2009; Qu et al. 2015b). At the extreme apex, filaments are less abundant and are highly dynamic (Qu et al. 2015b).

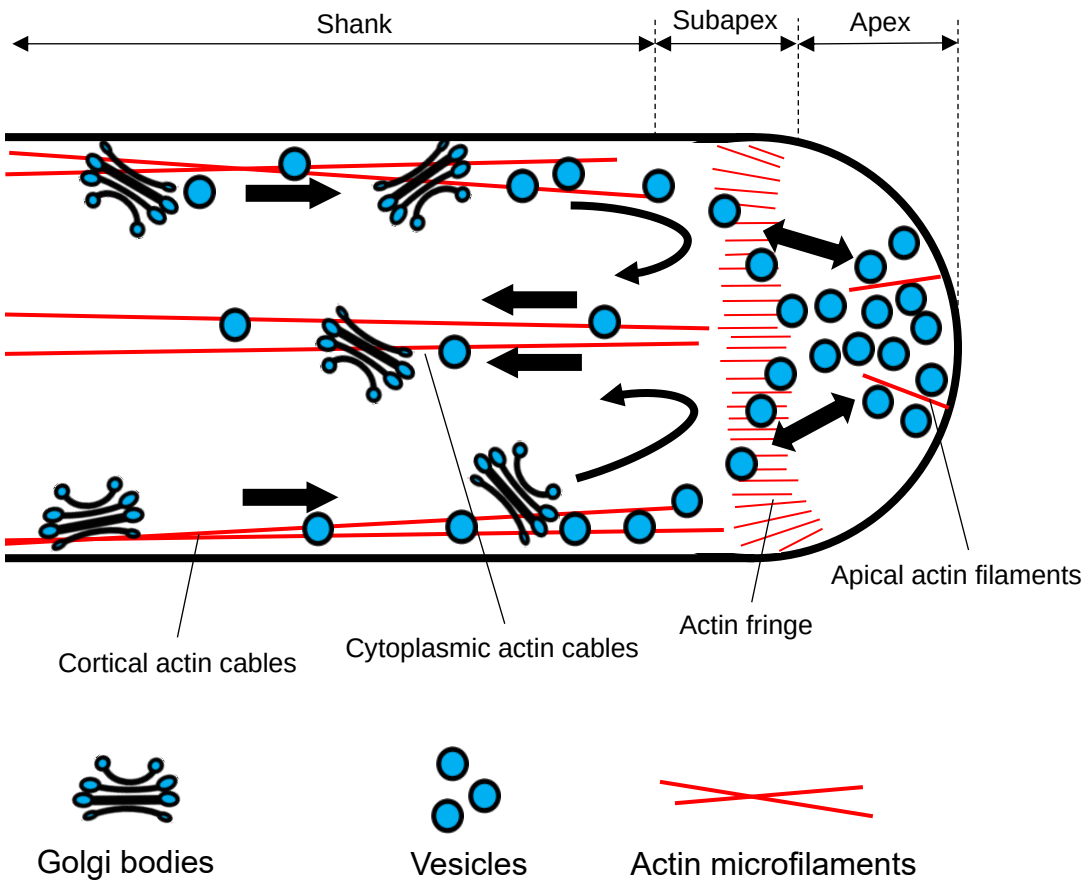

Figure 1.7: The Structure of the Actin Cytoskeleton in Growing Pollen Tubes. Only a few dynamic filaments exist in the tip. Short longitudinal actin filaments make up an actin fringe in the shoulder. In the shank, longitudinal actin cables at the cortex mediate rapid, long-range anterograde trafficking of organelles and secretory vesicles. Cytoplasmic cables mediate retrograde trafficking. Original figure.

1.4.6. The Function of Actin in Pollen Tubes.

Actin is known to be vital for pollen tube growth; needed for germination, elongation, and cytoplasmic streaming, as determined by pharmacological studies (Vidali et al. 2001; Gibbon et al. 1999). Disruption of actin in pollen tubes induces defects in cytoplasmic streaming, cytoplasmic organisation, transport of organelles (Vidali et al. 2001; Gibbon et al. 1999), and it is believed that actin is vital in transport and fusion of secretory vesicles at the tip (Qu et al. 2015b; Lee et al. 2008). Indeed, disruption of the actin cytoskeleton induces mislocalisation of the secreted pectin cell wall, showing the importance of actin in polarised, targeted secretion (Rounds et al. 2014). The actin cytoskeleton has been demonstrated to be involved in the regulation of exocytosis and endocytosis in the pollen tube shank region (Moscatelli et al. 2012). It should be noted that in addition to actin-dependent exocytosis and endocytosis, actin-independent exocytosis and endocytosis have also been observed at the pollen tube tip, which may be regulated instead by microtubules (Idilli et al. 2013; Moscatelli et al. 2012).

The actin cytoskeleton of pollen tubes is thought to be involved in the regulation of cellular processes other than polarised cell growth. The actin cytoskeleton is a target of the self-incompatibility (SI) response of outcrossing plant species, in which self-incompatible pollen is inhibited from reaching the ovules in order to prevent self-fertilisation. The disruption of actin during the SI response is thought to be causative of programmed cell death, through unknown mechanisms (Staiger and Franklin-Tong. 2003; Bosch et al. 2008; Eaves et al. 2014). As described in section 1.5, regulation of actin in response to extracellular signals may be important in regulating the navigation of the pollen tube through the female pistil tissue to the ovules.

The importance of the actin cytoskeleton in pollen is underscored by defects in pollen tube growth arising from loss of function mutations of actin-binding proteins, which are described below (Qu et al. 2015b; Staiger et al. 2010).

1.4.7. Actin-Binding Proteins in Pollen Tubes.

A number of actin-binding proteins are known to exist in pollen tubes, many of which are known to play important roles in pollen germination and the regulation of tip growth (Qu et al. 2015b; Staiger et al. 2010). As described previously, actin-binding proteins function to regulate actomyosin transport, actin dynamics and the formation of higher-order actin structures. It has been established that members of the myosin XI family are necessary for regulating trafficking of vesicles on actin networks in pollen (Madison et al. 2015). However, this section will focus on the role of actin-binding proteins in the organisation of the actin cytoskeleton in growing pollen tubes, through regulation of actin dynamics and formation of higher-order structures.

1.4.7.1. Regulation of Actin by Actin-Binding Proteins in the Pollen Tube Tip.

Specific examples of actin-binding proteins that regulate the organisation of actin at the pollen tube tip have been documented, which function to nucleate and sever actin filaments to maintain a distinctive actin array that is dynamically reorganised during rapid cell growth (Qu et al. 2015b). Nucleation of actin at the pollen tube tip is performed by FORMIN1 (FH1) and FORMIN5 (FH5) in Arabidopsis (Cheung and Wu. 2004; Cheung et al. 2010). Interestingly, it appears that the Arp2/3 complex is predicted not to play a major role in the nucleation of actin filaments in pollen, suggesting this role may be played primarily by formins and perhaps profilins (Qu et al. 2015b; Staiger et al. 2010). FH5 acts to anchor actin filaments of the apex to the apical pollen tube membrane, and serves a crucial role in facilitating apical vesicle transport and normal pollen tube growth (Cheung et al. 2010; Qu et al. 2015b). Severing of actin filaments at the pollen tube apex by actin-binding proteins is important in the regulation of pollen tube growth. VILLIN2 (VLN2) and VILLIN5 (VLN5) sever actin filaments in the pollen tube apex to promote actin turnover, and are required for the organisation of the subapical actin fringe (Qu et al. 2013; Qu et al. 2015b). Interestingly, various microtubule-binding proteins have also been reported to bind and sever actin filaments in the subapical regions of growing pollen tubes to facilitate actin turnover. MICROTUBULE-ASSOCIATED PROTEIN-18 (MAP18), and MICROTUBULE-DESTABILISING PROTEIN 25 (MDP25), have both been demonstrated to bind microtubules in vegetative tissues, but bind and sever actin filaments in the pollen tube subapical regions to drive filament turnover. Both

MAP18 and MDP25 are important in regulating the organisation of the subapical actin fringe and facilitating normal pollen tube growth (Zhu et al. 2013; Qin et al. 2014; Qu et al. 2015b).

Therefore, regulation of the organisation of the actin cytoskeleton at the pollen tube tip by actin-binding proteins that nucleate and sever actin filaments is highly important in facilitating normal pollen tube growth. However, this investigation will focus on the role of actin-binding proteins localised to the shank of growing pollen tubes, which are likely to regulate the organisation of actin in the pollen tube shank. Examples of actin-binding proteins known to organise longitudinal actin cables in the pollen tube shank are outlined in section 1.4.7.3.

1.4.7.2. Regulation of Apical Actin Dynamics by Rop GTPase Signalling.

Apical actin filaments facilitate the exocytosis of secretory vesicles at the pollen tube apex during tip growth (Lee et al. 2008). The regulation of apical actin filaments during polar cell growth is controlled by small GTPases of the Rho family, designated Rops (Rho of plants; Mucha et al. 2011; Lin et al. 1996).

Rop GTPases are ‘molecular switches’ that bind the guanine nucleotides, GTP or GDP. GTP-bound Rops are active, and can localise to plasma membrane and interact with downstream effector proteins, whilst GDP-bound Rops are inactive, and are sequestered in the cytosol. Rop GTPases are able to hydrolyse GTP to GDP at a slow rate, and control of Rop activity is largely regulated by RopGEFs (Rop guanine nucleotide exchange factors), and RopGAPs (Rop GTPase-activating proteins). RopGAPs promote the hydrolysis of Rop-bound GTP to GDP, inactivating Rop. RopGEFs serve to activate Rop proteins, by exchanging the bound GDP for GTP, permitting interaction of Rops with downstream effectors. The action of RopGEFs can be prevented by Rop guanine nucleotide dissociation inhibitors (GDIs), preventing the exchange of GDP for GTP (Mucha et al. 2011).

Rops are considered to be key regulators of pollen tube growth, and are found localised to the apical membrane corresponding to the zone of cell expansion (Lin et al. 1996). In Arabidopsis, inhibition of the pollen-specific Rop1 has been reported to result in the depletion of apical F-actin and cessation of pollen tube growth, whilst

overactivation of Rop1 signalling induces depolarisation of the pollen tube tip through the stabilisation of apical filaments (Fu et al. 2001; Gu et al. 2005). Rop1 activates two downstream pathways to regulate apical actin dynamics and delivery of exocytotic vesicles to the pollen tube tip. Two Rop1 effectors; Rop-Interactive CRIB-containing proteins (RICs); RIC3 and RIC4, are activated by Rop1. RIC4 promotes the assembly of F-actin at the apex. Conversely, RIC3 promotes the accumulation of $[Ca^{2+}]_{cyt}$ at the apex which promotes disassembly of F-actin filaments. Careful balance of these two counteracting pathways co-ordinates actin dynamics at the pollen tube tip. RIC4-dependent actin assembly accumulates secretory vesicles at the apex of the pollen tube, and RIC3-dependent disassembly of F-actin permits their fusion with the apical membrane, explaining a possible mechanism of how actin dynamics are regulated to facilitate exocytosis at the pollen tube apex, and cell expansion (Lee et al. 2008; Gu et al. 2005). Other Rops, such as Rop2 and Rop5 also appear to have roles in pollen tube growth by regulation of the actin cytoskeleton through unknown mechanisms; perhaps not specifically restricted to the pollen tube apex (Feng et al. 2016).

As discussed in chapter 1.5.3.2, the maintenance of tip growth by Rops is believed to be responsive to external signals perceived by membrane receptors. There are proven examples of cell signalling cascades involving the regulation of actin by Rops downstream of signal perception. For example, the co-ordination of leaf epidermal cell expansion is believed to be regulated by Rop signalling to the actin cytoskeleton downstream of auxin and ABA perception by membrane receptors (Miyawaki and Yang. 2014). The control of tip polarity by Rop GTPases is regulated by RopGEFs, RopGAPs and RopGDIs, which function to maintain Rop localisation and activity specifically at the apical pollen tube membrane (Klahre and Kost. 2006; Klahre et al. 2006; Gu et al. 2006). Rop regulatory proteins such as RopGEFs are believed to be signalling components downstream of membrane receptor proteins, which work to maintain polarised cell growth in response to the perception of external stimuli (Zhang and McCormick. 2007; Chang et al. 2013; Takeuchi and Higashiyama. 2016). As discussed in chapter 1.5.3.2, Rop GTPases may be involved in signal transduction to the actin cytoskeleton to regulate polarised cell growth in pollen.

1.4.7.3. Actin-Binding Proteins that Organise Actin in the Pollen Tube Shank.

Examples of actin-binding proteins functioning to nucleate, bundle/stabilise and sever actin filaments in the pollen tube shank have also been described, and are known to have important roles in the formation and organisation of longitudinal actin cables, needed for normal pollen tube growth (Qu et al. 2015b). Nucleation of actin filaments in the pollen tube shank is known to be performed by FH3, and pollen of *fh3* mutants display depolarised cell growth (Ye et al. 2009; Qu et al. 2015b). Various actin-binding proteins are implicated in the organisation of actin filaments into longitudinal actin bundles in the pollen tube shank. In contrast to their role as actin-severing proteins in the pollen tube tip, VLN2 and VLN5 function to stabilise and bundle actin filaments in the shank region; regulating the formation of longitudinal actin cables (Zhang et al. 2010; Bao et al. 2012; Qu et al. 2013; Qu et al. 2015b). A similar role has been suggested for the actin-bundling LIM proteins, such as CROLIN1 (Jia et al. 2013; Qu et al. 2015b). FIMBRIN5 (FIM5) bundles actin filaments into organised longitudinal cables, subsequently maintaining organised cytoplasmic streaming and anisotropic growth (Wu et al. 2010; Su et al. 2012; Qu et al. 2015b). Turnover of actin filaments is facilitated by ADFs in the pollen tube shank, and ADF7-mediated severing of longitudinal actin cables is vital for normal pollen tube growth (Zheng et al. 2013). In Lily, *Li*ADF1-mediated severing of actin filaments is promoted by AIP1, and spatially controlled by pH and phosphoinositides (Allwood et al. 2002). This indicates a high level of complexity in the mechanisms regulating the dynamic organisation of actin during pollen tube growth.

Therefore, the highly organised structure of the actin cytoskeleton in the pollen tube shank is regulated by a host of actin-binding proteins that regulate actin dynamics and the formation of higher-order actin structures to achieve normal pollen tube growth. This underscores the importance of the actin cytoskeleton in the regulation of plant cell growth, and of the actin-binding proteins that regulate its organisation. Dixon et al. (2013) observed NET2A to bind actin at the shank plasma membrane of growing pollen tubes. During the course of this study, NET2A will be demonstrated to link the actin cytoskeleton to the plasma membrane, which is likely to have significant implications on the organisation of longitudinal cortical actin cables in the shank region of the growing pollen tube.

1.5. Pollen Receptor-Like Kinases (PRKs).

A wide variety of pollen receptor proteins interpret a large number of extracellular signals from both male and female reproductive tissues, to regulate many aspects of pollen tube growth during fertilisation (Qu et al. 2015a). Examples include the S-LOCUS RECEPTOR KINASE (SRK) and the receptor protein, Papaver SELF-INCOMPATIBILITY POLLEN S-DETERMINANT (PrpS), which regulate pollen incompatibility responses downstream of external signal perception. Downstream of ligand binding, STERILITY-REGULATING KINASE-1 and -2, (SKM1 and SKM2), maintain pollen tube growth under stress. Meanwhile MITOGEN-ACTIVATED PROTEIN KINASE-3 and -6, (MPK3 and MPK6), and the kinase proteins LOST IN POLLEN TUBE GUIDANCE-1 and 2 (LIP1 and LIP2) mediate pollen tube guidance to the ovule tissue in response to female guidance cues. Furthermore, ANXUR1 and ANXUR2 receptor kinases regulate the delivery of sperm to the female gametophyte (Qu et al. 2015a). This study will focus on another type of signalling receptor; the Pollen Receptor-Like Kinases (PRKs), which transduce external growth signals to the actin cytoskeleton during the regulation of pollen tube growth and fertilisation; a process in which NET2 proteins are shown to be implicated during this investigation.

1.5.1. Pollen Receptor-Like Kinases (PRKs) as Regulators of Pollen Tube Growth.

Pollen receptor like-kinases are a subgroup of the leucine-rich repeat (LRR) group of Receptor-Like Kinase (RLKs), that are expressed specifically, or preferentially in pollen. The LRR subfamily of RLKs all possess an extracellular domain with a characteristic LRR motif, a transmembrane domain, and an intracellular serine/threonine kinase domain (Kim et al. 2002; Shiu and Bleeker. 2001). In plants, RLKs have been widely implicated in the perception of extracellular signals and the regulation of plant development and stress responses (Dievart and Clark. 2004; Osakabe et al. 2013). The first PRK to be identified was *Petunia inflata* PRK1 (*Pi*PRK1; Mu et al. 1994): a pollen-specific LRR-RLK with serine/threonine and tyrosine kinase activity. Since, more PRK proteins have been characterised in other species including *Lycopersicon esculentum, Zea mays* and Arabidopsis. Described below are the characterised PRKs of *P. inflata*, *L. esculentum* and Arabidopsis, their

roles in the regulation of pollen tube growth and the signalling pathways with which they are involved.

1.5.1.1. PRKs in *Petunia inflata*.

*Pi*PRK1, the first pollen receptor-like kinase to be characterised, is a pollen-specific PRK protein with demonstrated Ser/Thr and Tyr kinase activity, known to be essential for pollen development (Mu et al. 1994; Lee et al. 1996). Of central focus in this study is the previously reported interaction between *Pi*PRK1, and *Petunia inflata* Kinase-Interacting Protein-1 (*Pi*KIP1); a Petunia orthologue of Arabidopsis NET2C and NET2D (Skirpan et al. 2001; Deeks et al. 2012), which has been demonstrated to possess a functional actin-binding NAB domain (Calcutt. 2009). This interaction implicates a role for NET2 proteins in the regulation of pollen tube growth by PRKs, and is also suggestive of a role for *Pi*PRK1 in the regulation of the actin cytoskeleton in pollen.

1.5.1.2. PRKs in *L. esculentum*.

Three PRKs: the closely related *Le*PRK1, *Le*PRK2, and the more distantly related *Le*PRK3, have thus far been characterised in *L. esculentum* (figure 1.8; Kim et al. 2002; Muschietti et al. 1998). The three *Le*PRKs are demonstrated to localise to the pollen tube plasma membrane with overlapping but distinct distributions at different regions of the growing pollen tube. *Le*PRK1 and *Le*PRK2 are known to possess functional kinase domains, and are differentially phosphorylated in response to binding of pistil-specific signals, indicating specific roles for each kinase in pollen tubes (Muschietti et al. 1998). As described below, *Le*PRK1 and *Le*PRK2 have been shown to perceive and transduce a host of pistil-specific signalling ligands, and are known to regulate the actin cytoskeleton during pollen tube growth. It is believed that *Le*PRKs are able to form homodimers (Löcke et al. 2010) and heterodimers (Wengier et al. 2003) in pollen, and that their phosphorylation-dependent dimerisations and dissociations may be involved in the transduction of extracellular signals (see below; Wengier et al. 2003). *Le*PRK1 and *Le*PRK2 are closely related to *At*PRK1 and *At*PRK2 of Arabidopsis, whereas *Le*PRK3 is more closely related to

*At*PRK3 and *At*PRK6, which form an evolutionary subclade in Arabidopsis (figure 1.8; Chang et al. 2013), indicating these protein subclades may be evolutionarily and functionally parallel between species.

1.5.1.3. PRKs in Arabidopsis.

To date, 8 PRKs have been characterised in Arabidopsis (figure 1.8; Chang et al. 2013; Takeuchi and Higashiyama. 2016). Three distinct subclades of evolutionarily related *At*PRKs were initially identified, consisting of *At*PRK1 & *At*PRK2, *At*PRK3 & *At*PRK6, and *At*PRK4 & *At*PRK5 (Chang et al. 2013). More recently *At*PRK7 has been characterised as a more distant relative of the *At*PRK1 & *At*PRK2 subclade, and *At*PRK8 is known to be a more distant relative of *At*PRK3 & *At*PRK6. As described above, *At*PRK1 & *At*PRK2 appear to be Arabidopsis orthologues of *Le*PRK1 and *Le*PRK2, whereas *At*PRK3 & *At*PRK6 are orthologues of *Le*PRK3 (Chang et al. 2013).

Certain Arabidopsis PRKs have been shown to possess active kinase domains: *At*PRK1, *At*PRK2 and *At*PRK3 have all been demonstrated to be able to phosphorylate other proteins (Chang et al. 2013), and *At*PRK2 is postulated to have an active kinase domain (Zhao et al. 2013). *At*PRK4 and *At*PRK5 however, are thought to possess catalytically inactive kinase domains, with evolutionarily conserved consensus protein sequences characteristic of inactive kinases (Wrzaczek et al. 2015). However, the conserved consensus sequence of inactive kinases is also present in the kinase domain of *Pi*PRK1, which has been demonstrated to phosphorylate *Pi*KIP1 *in vitro* (Mu et al. 1994; Skirpan et al. 2001). Whether *At*PRK4 and *At*PRK5 are able to phosphorylate downstream signalling intermediates with or without a functional kinase domain remains to be determined.

Each *At*PRK has been demonstrated to play a role in the regulation of pollen tube polar cell growth in response to perception of pistil-secreted guidance cues, with functional redundancy to one another. This indicates the importance of Arabidopsis PRKs as transducers of external signals (Chang et al. 2013; Takeuchi and Higashiyama. 2016).

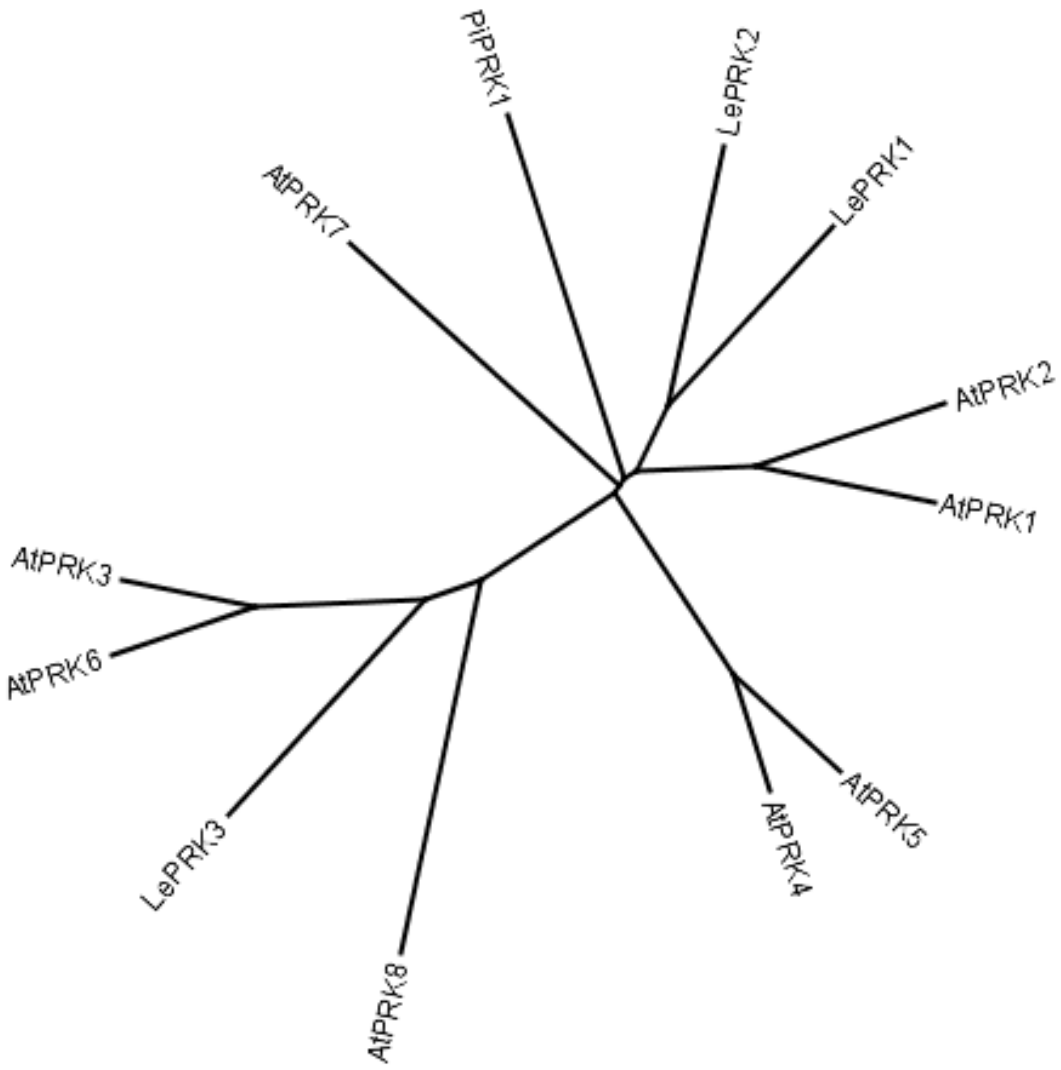

Figure 1.8. Phylogenetic Relationship of Selected Pollen Receptor-Like Kinases from *Arabidopsis thaliana*, *Lycopersion esculentum* and *Petunia inflata*. Phylogenetic tree of relative protein sequence conservation of characterised PRKs from *A. thaliana* (*At*PRK1 – 8), *L. esculentum* (*Le*PRK1 - 3) and *P. inflata* (*Pi*PRK1). The phylogenetic tree was created using Geneious® 10.1.3 software (Biomatters Ltd). Original figure.

1.5.2. External Signal Perception by Pollen Receptor-Like Kinases.

Pollen Receptor-Like Kinases are known to bind a variety of extracellular signalling ligands, many of which have been demonstrated to regulate pollen tube growth through PRK signal transduction. For years, examples of the extracellular ligands known to bind PRKs were only characterised in *L. esculentum*. More recently however, the signalling ligands of *At*PRKs are beginning to be elucidated.

1.5.2.1. Signalling Ligands Detected by *Le*PRKs.

In *L. esculentum*, four extracellular binding partners are known to bind *Le*PRKs, the first of which to be characterised is LAT52; a pollen-secreted extracellular binding partner of *Le*PRK2, required for pollen germination and fertilisation (Tang et al. 2002; Muschietti et al. 1994). LAT52 is only able to bind *Le*PRK2 prior to pollen germination, indicating a role for LAT52 signalling and *Le*PRK2 in pollen grain germination (Tang et al. 2002). LAT52 is known to abolish an interaction between *Le*PRK1 and *Le*PRK2 with another extracellular signalling ligand in *L. esculentum*, *Le*SHY: a pollen-specific peptide so-called to reflect the 'shy' phenotype of *leshy* mutant pollen (Tang et al. 2004; Guyon et al. 2004). Mutants of the *Le*SHY orthologue in Petunia, (*Pi*SHY), have been shown to be defective in fertilisation due to failure of pollen tubes to reach the ovules (Guyon et al. 2004). A third extracellular signalling ligand in *L. esculentum*, *Lycopersicon esculentum* STIGMA-SPECIFIC PROTEIN-1 (*Le*STIG1), is a pistil-secreted peptide bound by *Le*PRK1 and *Le*PRK2, that can outcompete LAT52 for binding to the extracellular domain of *Le*PRK2. Exogenous application of *Le*STIG1 to pollen germinated *in vitro* has been shown to promote pollen tube growth, and greatly increase the length of the germinated tubes (Tang et al. 2004). It is believed that the promotion of pollen tube growth by *Le*STIG1 is in some way dependent on extracellular phosphatidylinositol-3-phosphate, with which it is known to bind (Huang et al. 2014). Interestingly, application of *Le*SHY did not have an effect on pollen tube elongation (Tang et al. 2004), indicating that specific ligands of each *Le*PRK may constitute different signals to be transduced differentially during pollen tube growth and guidance. In mutants of *Le*PRK2, the responsiveness of pollen to *Le*STIG1 was found to be diminished, effectively proving that *Le*PRK2 is responsible for transduction of the *Le*STIG1 extracellular signal (Huang et al. 2014). Meanwhile, mutants of *Le*STIG1 have been demonstrated to exhibit reduced pollen tube growth rate and fertilisation efficiency *in vivo*, understating the importance of the perception of extracellular signalling ligands by PRKs during fertilisation (Huang et al. 2014). Likewise, another *Le*PRK2 ligand, STYLE INTERACTOR FOR *Le*PRKS (STIL) has also been shown to promote pollen tube elongation *in vitro* (Wengier et al. 2010).

The mechanisms by which *Le*PRKs transduce extracellular signals has also been a matter of intensive focus. *Le*PRK1 and *Le*PRK2 are known to respond to and transduce protein factors in tomato style extract (Wengier et al. 2003): in this study,

it was reported that application of extract results in the dissociation of the *Le*PRK1-*Le*PRK2 protein complex, downstream of *Le*PRK2 de-phosphorylation. Binding of STIL to *Le*PRK2 has been reported to induce *Le*PRK2 de-phosphorylation, providing an example as to how the *Le*PRK complex may be dissociated during the promotion of pollen tube germination and growth by extracellular signals. Controlled regulation of phosphorylation of *Le*PRKs is likely to play an important role in signal transduction during pollen tube growth: *Le*PRK2 is highly phosphorylated in the pollen plasma membrane, and exists in multiple phosphorylated forms (Salem et al. 2011). Phosphorylation of residues at two independent sites of *Le*PRK2 have antagonistic effects on pollen tube elongation: whilst phosphorylation of residues at one site was observed to result in increased pollen tube length, phosphorylation of specific residues at the other site decreased tube length. Simultaneous phosphorylation or de-phosphorylation of residues at both sites appears to have no additive effect on pollen tube length, indicating that multiple antagonistic phosphorylation of *Le*PRK2 may be a mechanism of fine-tuning pollen tube length (Salem et al. 2011). To date, it is thus far unknown as to what direct effects *Le*PRK dimerisation and phosphorylation status may have on the downstream signalling intermediates involved in the transduction of external signals, and how exactly these factors may regulate pollen tube growth. However, it is known that *Le*PRKs bind and regulate the activity of RopGEF proteins through phosphorylation: it is possible that *Le*PRKs regulate Rop-controlled polarised cell growth in response to external stimuli (Zhang et al. 2008; Koathien et al. 2005). Further descriptions on the control of Rop signalling by PRKs will be discussed below.

1.5.2.2. Signalling Ligands of *At*PRKs.

*At*PRKs are also known to bind extracellular ligands and are believed to be responsible for signal transduction during the targeting of pollen tubes to the egg during fertilisation.

*At*PRK6 has recently been demonstrated to be vital in the sensing of the pollen tube chemoattractant, *At*LURE1; one of various signalling peptides secreted from the synergid cells of the ovule in order to guide pollen tube growth into the micropyle

(Takeuchi and Higashiyama. 2016; Takeuchi and Higashiyama. 2012). Upon perception of *At*LURE1, *At*PRK6 localises asymmetrically at the pollen tube tip, facing the diffusing gradient of the *At*LURE1 attractant, perhaps to direct pollen tube growth towards the source of the attractant. The function of *At*PRK6 in perceiving and responding to *At*LURE1 is functionally redundant to *At*PRK3 and *At*PRK1, and the responsibility of pollen tube targeting to the ovules *in vivo* is shared between *At*PRK1, *At*PRK3, *At*PRK6 and *At*PRK8. It appears that different *At*PRKs share overlapping roles in signal perception *in vivo* (Takeuchi and Higashiyama. 2016).

Similarly to the *Le*PRKs of *L. esculentum*, dimerisation of *At*PRKs is observed in Arabidopsis: homodimerisation of *At*PRK6, as well as heterodimerisation of *At*PRK3 and *At*PRK6 has been reported, paralleling the interactions between *Le*PRK1 and *Le*PRK2 discussed above. However, it has yet to be seen whether perception of *At*LURE1 can induce dissociation of these complexes downstream of signal perception, as reported in *L. esculentum.* Interestingly, *At*PRK6 has been shown to interact with LIP1 and LIP2, which also perceive and mediate pollen tube attraction to *At*LURE, and are responsible for targeting of pollen tubes into the micropyle *in vivo (*Takeuchi and Higashiyama. 2016; Liu et al. 2013). It is possible that different, overlapping signalling pathways are involved in the responses of pollen tubes to a single female signalling ligand.

*At*PRK4 and *At*PRK5 have been shown to bind the extracellular signalling ligand, GRIM REAPER (GRI), in the regulation of ROS-induced cell death in Arabidopsis leaf tissue (Wrzaczek et al. 2015). Although it is unknown as to whether this interaction may occur in pollen, it can be expected that GRI may serve as an extracellular signalling ligand to be perceived by *At*PRK4 and *At*PRK5 during fertilisation. GRI is a STIG domain-containing protein, conserved with tobacco STIG1: mutants of which are defective in fertilisation (Wrzaczek et al. 2009). In *L. esculentum*, *Le*STIG1 binds *Le*PRK2 to promote pollen tube growth (Tang et al. 2004), and it is highly likely that GRI may be perceived by *At*PRK4 and *At*PRK5 for a similar purpose.

The mechanisms of signal transduction upon binding of extracellular ligands by *At*PRKs is unknown, and no downstream phosphorylation or protein-protein interaction events have been described to occur as a direct result of signal

perception. However, it is known that *At*PRKs can interact with, and phosphorylate certain signalling effectors, as will be discussed below.

1.5.3. Potential Downstream Effectors of PRKs.

1.5.3.1. *Pi*ORP1: A Downstream Interacting Partner of *Pi*PRK1.

Petunia inflata oxysterol-binding protein-related protein1 (*Pi*ORP1) was identified as an interactor of *Pi*PRK1 (Skirpan et al. 2006). *Pi*ORP1, like *Pi*PRK1 is preferentially expressed in pollen, and is phosphorylated by *Pi*PRK1 *in vitro*, indicating a signalling role for this protein downstream of *Pi*PRK1, specifically in pollen. The function of *Pi*ORP1 in pollen has yet to be identified, however it can be predicted to bind sterols, sphingolipids and phosphoinositides through its oxysterol-binding domain, as has been reported in oxysterol-binding proteins in yeast (Beh et al. 2012). In yeast, disruption of oxysterol-binding protein function has been reported to cause defects in polarised exocytosis and mislocalisation of Rho GTPases (Kozminski et al. 2006). It is possible that ORP proteins have roles in controlling tip-driven growth downstream of PRK signalling through co-ordination of Rop GTPases and polarised exocytosis.

1.5.3.2. RopGEFs as Downstream Interactors of PRKs.

RopGEFs are known to be interacting partners of PRK receptors from studies on *L. esculentum* and Arabidopsis. This indicates a signalling link between PRKs and Rops, in which perception of extracellular ligands may promote pollen tube growth through regulation of the actin cytoskeleton.

The *L. esculentum* RopGEF, Kinase Partner Protein (KPP), has been demonstrated to interact with *Le*PRK1 and *Le*PRK2. KPP is phosphorylated by *Le*PRK1 and *Le*PRK2, and is involved in the regulation of pollen tube growth downstream of these kinase proteins: the specific mechanism by which this occurs, however, has not yet been elucidated (Kaothien et al. 2005). However, it is known that RopGEFs regulate Rop signalling in pollen, which is vital in maintaining normal pollen tube growth

(Mucha et al. 2011). Overexpression of KPP results in depolarised cell growth and defective F-actin organisation in the pollen tube tip, consistent with defects in Rop signalling (Kaothien et al. 2005).

In Arabidopsis, *At*PRKs are also known to interact with RopGEFs, to activate Rop1-regulated cell growth. RopGEF1 was identified as an interactor of both *At*PRK2, and Rop1; through which *At*PRK2 is able to promote Rop1 activity (Chang et al. 2013). *At*PRK1, *At*PRK3, and *At*PRK4 also interact with RopGEF1, and *At*PRK1, *At*PRK2 and *At*PRK3 are known to phosphorylate Rop1 directly (Chang et al. 2013), perhaps indicating a direct signalling mechanism for regulation of the Rop1 pathway downstream of external ligand binding. RopGEF12 also regulates pollen tube growth downstream of recruitment to the membrane by *At*PRK2. The activity of both RopGEF1 and RopGEF12 appear to be controlled by phosphorylation, however it appears that *At*PRK2 kinase activity is not required for an interaction between RopGEF12 and *At*PRK2 to occur (Zhang and McCormick. 2007; Zhao et al. 2013). The means by which PRKs regulate RopGEFs has yet to be determined. The mechanism by which Rop signalling is controlled by *At*PRKs is likely to be very complex: PRK6 for example has been shown to interact with RopGEF8, RopGEF9, RopGEF12 and RopGEF13, which may each regulate different downstream signalling pathways. RopGEF8 for example does not interact with Rop1, and it is therefore likely to regulate an alternative signalling pathway (Gu et al. 2006).

1.5.3.3. NET2 Proteins as Downstream Interactors of PRKs.

Petunia inflata Kinase-Interacting Protein1 (*Pi*KIP1) is also an interactor of *Pi*PRK1. (Skirpan et al. 2001). *Pi*KIP1 is a self-interacting, pollen-specific protein that is phosphorylated by *Pi*PRK1, indicating that it may function downstream of *Pi*PRK1. Interestingly, functional kinase activity of *Pi*PRK1 appears to be important for the two proteins to interact *in vitro*. It is therefore likely that an interaction between *Pi*PRK1 and *Pi*KIP1 may be promoted by phosphorylation of *Pi*KIP1 by *Pi*PRK1, downstream of signal perception by *Pi*PRK1. Of particular significance to this study, *Pi*KIP1 is a Petunia orthologue of the Arabidopsis NET2 family, and is evolutionarily related to NET2C and NET2D (Skirpan et al. 2001; Deeks et al. 2012). It has been demonstrated that *Pi*KIP1 has a functional NET actin-binding (NAB) domain, characteristic of all NET proteins, that mediates the association of NETs with actin

(Deeks et al. 2012; Calcutt. 2009). Therefore, the interaction of *Pi*KIP1 with *Pi*PRK1 may represent a link between the actin cytoskeleton and plasma membrane, with potential functions in signal transduction during pollen tube growth.

1.5.4. Summary: Potential Regulation of the Actin Cytoskeleton by PRKs.

PRKs have an important role in regulating pollen tube growth and navigation during fertilisation. They are implicated in the maintenance of normal pollen tube growth, and in the perception of extracellular signals secreted from male and female reproductive tissues.

The mechanisms by which PRK proteins regulate pollen tube growth appears to involve their regulation of the actin cytoskeleton. To date, most research has focussed on the activation of Rop signalling at the pollen tube tip through interactions with RopGEFs: most likely driving tip growth through targeted exocytosis at the apex through RIC3/RIC4-controlled actin dynamics (figure 1.9a). ORPs may also be speculated to be involved in regulating polar exocytosis in cooperation with Rop GTPases downstream of PRK signalling (figure 1.9b).

An alternative mechanism linking PRKs to the regulation of the actin cytoskeleton will be investigated in this report: As described previously, the Petunia NET2 orthologue, *Pi*KIP1, is a potential actin-binding protein, and may regulate the actin cytoskeleton downstream of external signal perception by *Pi*PRK1 (figure 1.9a).

The way in which PRKs are able to regulate pollen tube growth is yet unknown, and is likely to be very complex. It is believed that PRK phosphorylation of downstream effectors and dissociation of PRK complexes may initiate signal transduction. It is apparent that PRKs appear to have overlapping roles in the signals they perceive, and the downstream pathways that they regulate (figure 1.9a).

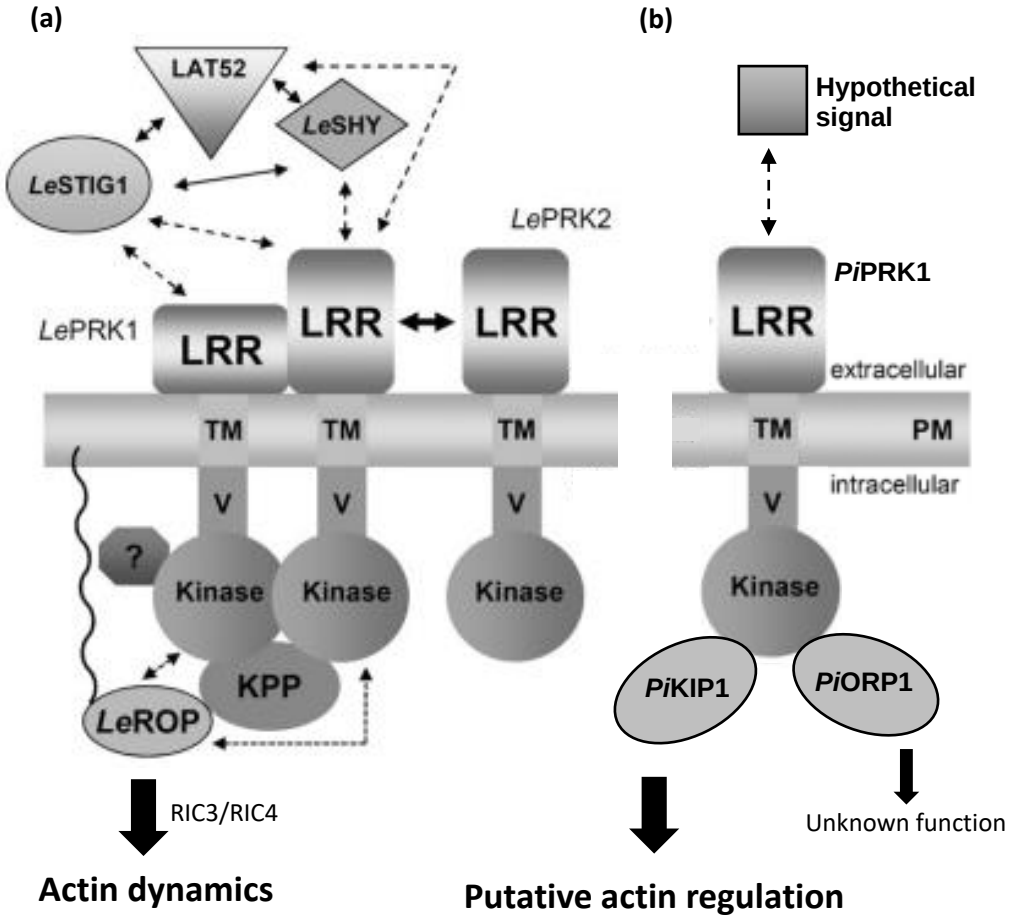

Figure 1.9: Putative Mechanisms of PRK Signal Transduction. Figure depicts postulated signalling mechanisms of PRKs drawn from studies on *L. esculentum* (*Le*PRK1 and *Le*PRK2) and *P. inflata* (*Pi*PRK1), in which PRK signalling mechanisms are best characterised. (a): extracellular signal transduction through *Le*PRK1 and *Le*PRK2. *Le*PRK2 binds the extracellular ligands, LAT52, *Le*SHY, STIL and *Le*STIG1 (which is also recognised by *Le*PRK1). Extracellular ligand perception by *Le*PRK2 induces dissociation of *Le*PRK dimers, and de-phosphorylation of *Le*PRK2. *Le*PRK1 and *Le*PRK2 control pollen tube growth through the Rop signalling pathway. *Le*PRK1 and *Le*PRK2 bind and phosphorylate the RopGEF, KPP, which regulates actin dynamics through activation of *Le*ROP. (b): *Pi*PRK1 may recognise a yet uncharacterised extracellular ligand. *Pi*PRK1 binds and phosphorylates *Pi*ORP1 (with unknown function), and the putative NET2 orthologue, *Pi*KIP1, which is likely to function in the regulation of the actin cytoskeleton. Modified from Löcke et al. (2010).

1.6. Actin-Microtubule Interactions in Plants.

In this investigation, a novel microtubule-associated protein, named MAP7A, was identified as a potential interactor of NET2A. The existence of an interaction between actin-binding and microtubule-associated proteins may serve as a physical link between the two cytoskeletal arrays, potentially facilitating actin-microtubule associations in plants. This section will describe a brief overview of the structure and

function of microtubule arrays in plant cells, with a focus on pollen grain development and pollen tube growth. Our current understanding of actin-microtubule interplay in plants will be discussed, as will their functions, and mechanisms by which the two cytoskeletal components are known to interact. It is likely that actin and microtubules may share functional roles in pollen, and a physical interaction may be facilitated by an interaction between MAP7A and NET2A.

1.6.1. Structure and Function of Plant Microtubule Arrays.

Microtubules form highly distinctive localisation patterns over the course of the cell cycle in order to perform specialised functions associated with cell growth, regulation of cell morphology and division.

At interphase, microtubule filaments form characteristic cortical arrays, localising to the cell cortex, transversely to the cell axis of elongation. The interphase cortical microtubule array defines cell morphology by directing the plane of growth. In growing cells, the interphase cortical microtubule array serves to guide the movement of membrane-embedded cellulose synthase complexes, therefore defining orientation of cellulose microfibrils deposited into the cell wall (Baskin. 2001; Gutierrez et al. 2009; Hashimoto. 2015). Microtubules therefore determine the orientation of cellulose microfibrils added to the cell wall; deploying them perpendicular to the axis of elongation to resist internal turgor pressure and radial cell expansion, therefore promoting anisotropic growth. Pharmacological disruption of microtubules in interphase cells impairs their ability to grow anisotropically, and induces radial expansion (Lloyd. 2009).

Prior to prophase, microtubules localise to an array known as the pre-prophase band: in which densely packed cortical microtubules align transversely, specifically at the equatorial region of the cell, encircling the cell nucleus (Hashimoto. 2015). The location of the microtubule preprophase band defines the future site of cell division, and pharmacological disruption of the preprophase band causes plant cells to divide along abnormal division planes (Vanstralenen et al. 2006). During prophase, microtubules form the mitotic spindle; two mirrored sets of polarised microtubules extending from each pole of the two daughter cells. By metaphase, the spindle microtubules extend to the condensed chromosomes to facilitate their

separation in anaphase (Dhonkushe et al. 2006). In telophase, cytokinesis is performed by the phragmoplast: an array of two mirrored sets of short polarised microtubules orientated towards the plane of cell division. The phragmoplast is responsible for the formation of the new cell plate; directing the transport of golgi-derived vesicles containing synthetic cell wall-building materials to the division site. Radial extension of the cell plate is accomplished by centrifugal expansion of the phragmoplast in order to separate the newly formed daughter cells (Hashimoto. 2015).

1.6.2. The Microtubule Cytoskeleton of Pollen Grains.

As described previously, the angiosperm male gametophyte is an elaborately specialised cell type, that undergoes a complex series of cell divisions and has a unique morphology. The microtubule cytoskeleton is highly important in regulating pollen development and is also implicated in aiding tip growth in pollen tubes. Described below are the structures and functions of microtubule arrays that mediate the development and growth of the highly specialised male gametophyte (figure 1.10).

In the developing pollen grains of dicotyledonous angiosperms, the microtubule cytoskeleton undergoes dynamic rearrangements to mediate specific developmental processes associated with nuclear migrations and cell division. In the unicellular microspores of tobacco, the microtubule cytoskeleton facilitates nuclear migration and cell division in PMI. Prior to nuclear migration, long bundles of microtubules form from punctae at the surface of the nucleus to form a dense basket surrounding the nucleus. The microtubule basket is asymmetrical: one side is flat, whereas the other projects a ‘microtubule tail’, connecting the nuclear basket to the microspore wall to which the nucleus migrates (Zonia et al. 1999; Oh et al. 2010). Migration of the nucleus to the microspore wall before PMI is mediated by the microtubule basket, and pharmacological disruption of the microtubule basket prevents nuclear migration and entry in PMI (Zonia et al. 1999). Following migration of the nucleus to the microspore wall, the microtubules surrounding the cell nucleus form the spindle, which is required for the separation of chromosomes during PMI (Zonia et al. 1999). PMI is an asymmetric cell division, perhaps resulting from the asymmetric structure of the microtubule spindle during PMI, which is broader at the

generative pole (Oh et al. 2010). Microtubules assemble into the phragmoplast at telophase of PMI to form a hemispherical callosic cell plate between the GCN and VCN to complete asymmetric cell division (Oh et al. 2010). The phragmoplast is also asymmetrically structured and the generative face of the phragmoplast is shorter than that of the vegetative face. Genetic disruption of the phragmoplast in Arabidopsis induces defects in cell plate formation and asymmetric cell division, showing the importance of the microtubule phragmoplast in mediating asymmetric division (Oh et al. 2010; Twell et al. 2002; Pastuglia et al. 2006).

Following PMI, cytoplasmic microtubules in the generative cell form a basket-like structure at the GC cortex, with a cytoplasmic microtubule tail that connects the GC membrane to the VCN (Oh et al. 2010; McCue et al. 2011). In tricellular pollen grains of Maize, the generative cell microtubules are likely to regulate PMII during pollen development, and have been observed to form a spindle structure involved in the separation of chromosomes into the daughter sperm cells (Kliwer and Dresselhaus. 2010). In species such as tobacco, in which mature pollen is bicellular, PMII takes place in the growing pollen tube, in which generative cell microtubules form a spindle and phragmoplast to facilitate the division of the generative cell into two sperm cells. PMII in pollen tubes can be disrupted by treatment with microtubule disrupting drugs, indicating the importance of the GC cytoplasmic microtubules in the regulation PMII (Palevitz. 1993; Joos et al. 1994). It can be inferred from these studies that PMII will be similarly regulated by microtubules in tricellular pollen also. In both bicellular and tricellular species of pollen, the sperm cell nuclei arising from PMII are surrounded by microtubules which extend cytoplasmic tails; physically linking the two nuclei together and to the vegetative cell nucleus (McCue et al. 2011; Kliwer and Dresselhaus. 2010; Palevitz. 1993). Following PMI, a dense network of cortical microtubule filaments could be observed in tobacco pollen grains, persisting throughout pollen grain maturation (Zonia et al. 1999).

1.6.3. The Microtubule Cytoskeleton of Pollen Tubes.

In growing pollen tubes, two distinct subpopulations of microtubules have been observed. Short, dynamic, randomly aligned microtubules filaments are present in the tip, and immobile, longitudinally-orientated cortical microtubule bundles exist in the shank (Idilli et al. 2013; Cheung. 2008). Additionally, sperm cell microtubules (or

generative cell microtubules in bicellular pollen) are seen connecting the nuclei of the MGU.

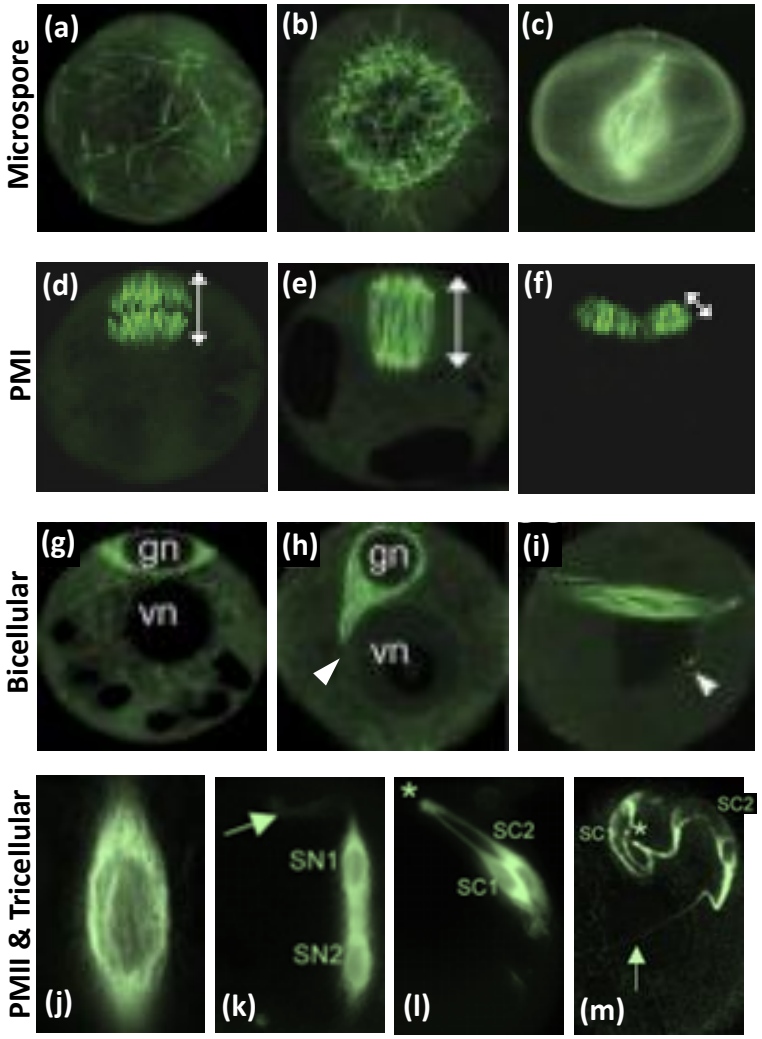

Figure 1.10: Microtubule Organisation During Pollen Grain Development. The microtubule arrays of developing pollen have been studied from the microspore to bicellular stages in *N. tabacum*, in which mature pollen grains are bicellular (Zonia et al. 1999; Oh et al. 2010). The organisation of microtubules during and after PMII has been studied in *Zea mays*, in which pollen is tricellular (Kliwer and Dresselhaus. 2010). (a)–(i): microtubule organisation in the developing bicellular pollen grains of *N. tabacum*. (j)–(m): microtubule organisation during and after PMII in tricellular *Z. mays* pollen. (a)–(c): microtubule arrays in developing microspores. (a): cytoplasmic microtubules are present in microspores prior to nuclear migration. (b): microtubules form a cage around the migrating nucleus in polarising microspores. (c): prior to PMI, the microtubule cage surrounds the migrating nucleus and connects it to the cell cortex. (d)–(f): microtubule organisation during PMI. Microtubules assemble into the metaphase spindle (d), anaphase spindle (e), and phragmoplast during telophase (f). (g)–(i): microtubule organisation in bicellular pollen following PMI. MTs surround the GCN following PMI (g), and during the subsequent nuclear migration (h). A microtubule tail connects the GC to the VCN (white arrow). (i): a cortical network of MTs is present within the GC in mature bicellular pollen, and a microtubule tail connects the GC to the VCN (white arrow). (j)–(m): microtubule organisation during and after PMII in tricellular pollen. (j): microtubules assemble into the mitotic spindle in the GC during PMII. (k): a continuous network of microtubules surrounds the newly formed SCs following PMII, connected to the VC by a microtubule tail (arrow). (l): in maturing pollen, SC microtubules surround and interconnect the SCN (asterisk). In mature pollen, a continuous network of SC microtubules surrounds and connect both SCN and connect them to the VCN through the cytoplasmic projection (arrow). GN = generative nucleus. VC = vegetative nucleus. SC1 = sperm cell 1, SC2 = sperm cell 2. SN1 = sperm nucleus 1. SN2 = sperm nucleus 2. (a), (b), (d), (e), (f), (g), (h) and (i): taken from Oh et al. (2010). (c): taken from Zonia et al. (1999). (j)-(m): taken from Kliwer and Dresselhaus. (2010).

The potential roles of microtubules in growing pollen tubes are poorly understood relative to those of actin (Onelli et al. 2015; Idilli et al. 2013; Romagnoli et al. 2007). It is known that the microtubule cytoskeleton does play a role in regulating pollen tube growth, and pharmacological disruption of microtubules has been observed to have slight effects on the ability of pollen tubes to maintain growth direction and pollen tube diameter (Gossot and Geitmann. 2007; Idilli et al. 2013). As described previously, actomyosin-mediated cytoplasmic streaming is well-known to drive pollen tube growth. Although microtubule motor proteins are known to exist in pollen, it has not yet been established whether long-range microtubule-based organelle trafficking may contribute to pollen tip extension (Onelli et al. 2015; Romagnoli et al. 2007; Cai et al. 2000). It is known however, that apical microtubules are important in driving slow, actin-independent exocytosis at the extreme apex (Idilli et al. 2013). Golgi-derived vesicles and mitochondria isolated from pollen are able to move along microtubules, indicating that they could be transported along microtubules *in vivo*. However, their rate of transport along microtubules is much slower than their movement along actin filaments, suggesting that microtubules may be responsible for 'fine positioning' of organelles in pollen tubes, as opposed to rapid, long-range transport (Romagnoli et al. 2007). Furthermore, whereas recycling of plasma membrane by actin-dependent endocytosis occurs in the shank region, microtubules mediate actin-independent endocytosis of apical membrane to the early endosome (Idilli et al. 2013).

The roles of the microtubule cytoskeleton in the synthesis of the pollen tube cell wall are also relatively poorly understood. The cortical microtubule arrays of anisotropically-extending somatic cells are well known to direct the orientation of cellulose microfibrils of the cell wall (Baskin. 2001; Gutierrez et al. 2009). In growing pollen tubes, the orientation of the longitudinally-orientated microtubule bundles is mirrored by longitudinally-arranged cellulose microfibrils and cellulose synthase complexes (Chebli et al. 2012). Interestingly however, there is little evidence to suggest a direct role for microtubules in the guidance of cellulose synthase complexes in pollen tubes, which are seemingly unaffected by the pharmacological disruption of the microtubule cytoskeleton. Instead, the guidance of cellulose synthase in growing pollen tubes seems to be a role for actin (Cai et al. 2011). The deposition of callose in the distal regions of the pollen tube is however dependent on a direct association of callose synthase with microtubules (Cai et al. 2011).

Microtubules have been speculated to play a role in the organisation of the MGU in pollen tubes. As described above, microtubules physically interconnect the nuclei of the MGU and facilitate PMII in the pollen tubes of plant species bearing bicellular pollen grains (McCue et al. 2011; Kliwer and Dresselhaus. 2010; Palevitz. 1993). It has been hypothesised that these microtubules may serve to maintain the integrity and organisation of the MGU (Palevitz et al. 1993; McCue et al. 2011). The MGU maintains proximity to the growing tip, and the transport of the MGU during pollen tube growth is likely to be dependent on microtubules: disruption of microtubules in tobacco pollen tubes causes the MGU to remain in the distal regions of the tube, or to remain in the pollen grain as the pollen tube extends (Heslop-Harrison et al. 1988; Joos et al. 1994; Astrom et al. 1995).

1.6.4. Actin-Microtubule Interactions in Plants.

Thus far, the structure and functions of actin and microtubules in plant cells been described, specifically focussing on the cytoskeletal arrays of pollen. In mammalian cells, interactions between the actin and microtubule arrays of the cytoskeleton are important in the regulation of cell division, motility, adhesion and organelle trafficking in many cell types (Coles and Bradke. 2015). Likewise, interactions between actin and microtubule arrays have been observed in plants and are also likely to have important functions in the regulation of plant cell growth and development. Discussed below are examples of actin-microtubule interactions observed in plants and their potential functions.

Associations of actin and microtubules have been visualised in many of the cytoskeletal arrays that form over the course of the plant cell cycle. Co-localisation of transversely-aligned actin and microtubule filaments has been documented in the elongating interphase cells of Arabidopsis hypocotyls, and undergo dynamic re-arrangements in tandem with one another (Sampathkumar et al. 2011). The interactions of actin and microtubules appear to be necessary for the integrity of each cytoskeletal component: re-polymerisation of actin following pharmacological disruption occurs along microtubule tracks, and is dependent on the microtubule cytoskeleton. Conversely, recovery of microtubules following disruption is dependent on actin. Stimulus-induced rearrangements of the actin cytoskeleton require an intact microtubule cytoskeleton, showing the co-dependence of both

cytoskeletal arrays in regulating cytoskeletal dynamics. These observations suggest that the organisation of one cytoskeletal array can affect the organisation of the other (Sampathkumar et al. 2011). Interplay between actin and microtubules during interphase is important in the regulation of anisotropic cell growth. In studies performed on elongating Arabidopsis root cells, mild pharmacological or genetic disruption of actin or microtubules alone induced no morphological defects, whereas mild disruption of both actin and microtubules together prohibited anisotropic growth and induced radial swelling of developing cells (Collings et al. 2006). This indicates functional synergy between actin and microtubules in the regulation of anisotropic cell growth.

Cooperation of actin and microtubules has also been observed at multiple stages of plant mitosis. Association of the two cytoskeletal networks occurs during the formation of the preprophase band (Kost et al. 1999; Granger and Cyr. 2000), which requires both actin and microtubules to assemble correctly (Eleftheriou and Palevitz 1992; Mineyuki and Palevitz. 1990). Actin has also been reported to be important in the formation of the mitotic spindle (Traas et al. 1989), and associates with microtubules of the phragmoplast, in which the establishment of a normal division plane cannot occur in the absence of actin (Sylverster. 2000; Wu and Benzilla. 2014; Gunning and Wick. 1985). Therefore, the actin cytoskeleton functions alongside the microtubule cytoskeleton in each mitotic microtubule array to coordinate cell division.

There are few examples of proteins that cross-link actin and microtubules in plants. Members of the plant formin family appear to have roles in mediating the associations of actin and microtubules in plant cells. Arabidopsis FH14 associates with actin and microtubules *in vivo*, and genetic disruption of FH14 induces defects in both actin and microtubule arrays. Similarly, Arabidopsis FH4 contains both actin and microtubule-binding domains, and appears to serve as an interface between actin and microtubules *in vivo* (Deeks et al. 2010). CH domain-containing kinesins (KCHs), a subset of kinesin-14 microtubule motor proteins can bind microtubules through their internal kinesin motor domain. Dimerisation of KCH is likely to permit them to bind actin, through the bringing together of CH domains to generate high affinity to actin filaments. KCHs are important in cell elongation and division and can bind and bundle both actin and microtubules. Therefore, KCHs may serve as mediators of actin-microtubule interactions in plants (Schneider and Persson. 2015).

MICROTUBULE-ASSOCIATED PROTEIN 190 (MAP190) can bind and induce bundling of actin and microtubules *in vitro* (Igarashi et al. 2000), however it is unknown as to whether MAP190 may mediate actin-microtubule interactions *in vivo*. Similarly, SB401, isolated from *Solanum berthaultii* also binds and bundles actin and microtubules *in vitro*, perhaps through dimerisation (Huang et al. 2007). Interactions between actin-binding proteins and microtubule-associated proteins can also mediate links between the two cytoskeletal components: an interaction between the actin-binding NET3C and microtubule-binding VAP27 has been shown to serve as a linker complex between the two proteins at specific endoplasmic reticulum-plasma membrane (ER-PM) contact sites (Wang et al. 2014).

1.6.5. Actin-Microtubule Interactions in Pollen.

Although the roles of actin and microtubules in pollen have been studied for many years, little attention has been given to the potential role of interactions or interplay between the two cytoskeletal networks in pollen development or pollen tube growth. It has been observed that actin and microtubules physically associate and appear to align in pollen tubes (Piersson et al. 1989). Both cytoskeletal elements form longitudinally-aligned cables in the pollen tube shank, as described previously. It is likely that similar associations between the two cytoskeletal networks may occur in pollen as described in somatic cells above. There appears to be synergy in the interplay of actin and microtubules in the regulation of pollen tube growth: light disruption of either actin or microtubules in pollen tubes has only mild effects on pollen tube growth and morphology. However, disruption of both cytoskeletal networks leads to inhibition of pollen tube growth. It has been hypothesised that microtubules may stabilise actin filaments or guide their polymerisation during pollen tube growth, and vice versa (Gossot and Geitmann. 2007). It is also possible that actin and microtubules may share overlapping, or functionally redundant roles in pollen tubes: it has been described above that actin and microtubules are able to facilitate vesicle trafficking, organelle transport and cell wall deposition in pollen tubes, and it is possible that the disruption of one cytoskeletal array may be compensated for by the functions of the other.

Although little work has been performed on the interactions of actin and microtubules in developing pollen grains, it can be hypothesised that the two arrays

should interact. As described above, interactions between actin and microtubules occurs multiple times during mitosis in somatic cells; in the preprophase band, spindle and phragmoplast. Multiple cell divisions occur during pollen grain development, making it highly likely that these developmental events could be sites of actin-microtubule cooperation. Furthermore, actin and microtubules are known to surround the microspore nucleus before PMI and the generative nucleus following PMI, and regulate the associated nuclear migrations. It is also possible that actin and microtubules may cooperate in the migration of nuclei during pollen grain development therefore.

Reports of proteins known to mediate interactions between actin and microtubules in pollen is sparse. However, it is known that certain microtubule-binding proteins are able to regulate actin in growing pollen tubes. MAP18 for example is demonstrated to bind and regulate microtubules in somatic cells, but binds and severs actin filaments in growing pollen tubes to regulate pollen tube growth (Wang et al. 2007; Zhou et al. 2013). Similarly, MDP25 is a microtubule-associated protein that binds and destabilises microtubules in expanding hypocotyl cells, but severs actin filaments in growing pollen tubes (Li et al. 2011; Qin et al. 2014). It is possible that proteins such as MAP18 and MDP25 may serve different functions in somatic cells and pollen; binding microtubules in the latter and actin in the former. They may however serve to bind and regulate both cytoskeletal components simultaneously, and coordinate their activities in pollen.

1.7. The NET Protein Superfamily.

1.7.1. The Discovery of the NET Proteins.

Deeks et al. (2012) originally characterised the NETWORKED (NET) proteins as a superfamily of plant-specific actin-binding proteins that bind actin at various membrane structures. The NETs were first identified using a high-throughput screen to analyse the subcellular localisations of various proteins (Escobar et al. 2003). In this screen, an Arabidopsis cDNA library was cloned into a tobacco mosaic virus expression vector to express the cDNA fragments as GFP fusion proteins in *Nicotiana benthamiana* leaf epidermal cells. Analysis of the subcellular localisation

of the expressed constructs revealed one particular fragment to bind the actin cytoskeleton: this fragment was identified as amino acids 1 – 288 of a previously uncharacterised protein encoded by the gene locus At3g22790, later named NET1A (Deeks et al. 2012).

It was identified that the actin-binding activity of NET1A was facilitated through amino acids 1 – 94; through which it could associate with actin *in vivo.* This N-terminal region was designated the NET actin-binding (NAB) domain, representing a novel, plant-specific actin-binding motif (Deeks et al. 2012). In Arabidopsis, thirteen proteins are known to contain an N-terminal NAB domain and comprise the NET protein superfamily (Deeks et al. 2012). These proteins can be subdivided into four separate subfamilies defined by comparisons of shared sequence homology within the NAB domains of each protein, structural organisation of the protein C-termini and protein size (figure 1.11; Deeks et al. 2012; Hawkins et al. 2014). Therefore, each protein subfamily shares a highly conserved N-terminal NAB domain, as well as regions of predicted coiled-coil domains at the protein C-termini. Proteins of each NET family have been demonstrated to associate with actin directly through their NAB domain. NET proteins appear to associate with actin in a characteristic 'beads-on-a-string' pattern, in which they form discreet punctae that align along actin filaments (Deeks et al. 2012).

Extensive characterisation of NET proteins from each subfamily has since been performed (Calcutt. 2009; Ingle. 2011; Dixon. 2013; Bush. 2015; Wang et al. 2014; Mentlak. 2015). It has been effectively demonstrated that members of each NET subfamily associate with a different membrane system in plant cells. The NET1 subfamily consists of NET1A, NET1B, NET1C and NET1D (Deeks et al. 2012). NET1A has been shown to localise to transverse walls of cells of the stellar files and root tip and was enriched a plasmodesmata (Deeks et al. 2012; Calcutt. 2009). It has been observed that NET1C and NET1D also associated with the plasma membrane of root cells (Ingle. 2011). Members of the NET1 family are reported to have important roles in the regulation of root growth, in a functionally redundant manner (Calcutt. 2009; Ingle. 2011).

NET2A, NET2B, NET2C and NET2D comprise the NET2 protein family (Deeks et al. 2012). Characterisation of the NET2 protein family has demonstrated these proteins to be preferentially or specifically expressed in pollen. NET2A forms

discreet foci at the plasma membrane of growing pollen tubes, and associates with actin filaments in developing pollen grains (Dixon et al. 2013). *Pi*KIP1 is known to be an orthologue of NET2C and NET2D in *Petunia inflata* and has been shown to have a functional actin-binding NAB domain (Skirpan et al. 2001; Calcutt. 2009; Deeks et al. 2012). This implicates members of the NET2 protein family as potential interactors of PRK proteins in Arabidopsis pollen tubes.

As described by Deeks et al. (2012), NET3A, NET3B and NET3C make up the NET3 protein family. Members of the NET3 subclade are also known to bind actin at specific membrane compartments. NET3A appears to bind actin at the nuclear membrane as demonstrated by studies on BY2 cell lines, and NET3C binds actin at ER-PM contact sites of the endoplasmic reticulum (Deeks et al. 2012; Wang et al. 2014). At ER-PM contact sites, NET3C interacts with VAP27; an ER-integral protein that also binds microtubules, and it appears that NET3C may serve to link actin and microtubules at membrane compartments. NET3B and NET3C are reported to be essential to the development of the male and female gamete, with functional redundancy to one another (Wang et al. 2014). Additionally, NET3 is known to self-interact.

Recently, characterisation of the NET4 protein subfamily (consisting of NET4A and NET4B) has been performed (Hawkins (unpublished data); Mentlak. 2015; Deeks et al. 2012). NET4A and NET4B bind actin at the tonoplast of root cells. NET4B is known to both homo-dimerise through self-interaction, and can form heterodimers through interaction with NET4A (Mentlak et al. 2015). It is predicted that the actin-binding activity of NET4B is controlled by phosphorylation *in vivo*, and phosphorylation of a Tyr residue at the protein C-terminus is predicted to activate NET4B actin-binding activity (Bush. 2015). This may provide interesting insights as to how the subcellular localisations of other NETs may be influenced by phosphorylation.

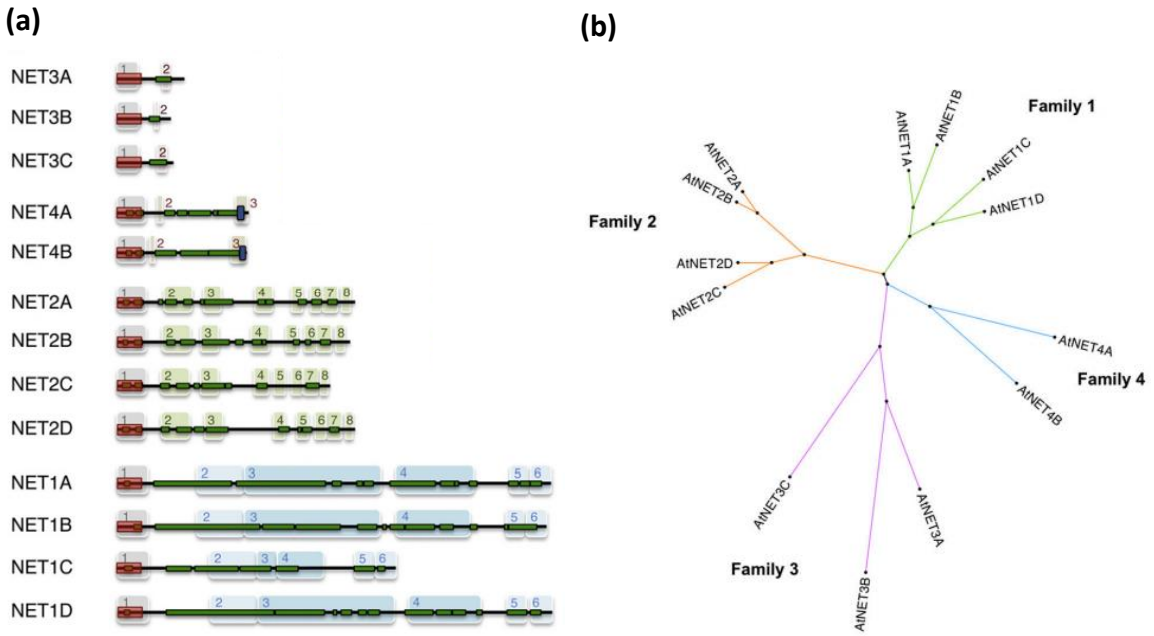

Figure 1.11. Conservation of the NETWORKED Protein Superfamily. (a): schematic diagram of NET protein structure and conservation. Diagram includes relative positions of the NAB domains (red) and predicted coiled-coil regions (dark green). Regions of homology conserved within each NET subfamily are denoted by the numbered coloured tiles. Taken from Deeks et al. (2012). (b): cladogram of relative NET protein sequence conservation. Individual members of the NET protein superfamily are grouped into 4 separate subfamilies based on protein structure and sequence conservation. Taken from Hawkins et al. (2014).

1.7.2. Previous Characterisation of the NET2 Subfamily.

The NET2 protein family has been extensively characterised, with particular focus on NET2A (Dixon. 2013; Deeks et al. 2012). Using bioinformatic analysis, members of the NET2 protein family were predicted to be largely pollen-specific: NET2A, NET2B and NET2C are expressed exclusively within the male gametophyte in which NET2D is also preferentially expressed. Expression of NET2D is also active in root hair cells. Interestingly, the divergence of the *NET2* gene subfamily corresponds to the evolutionary emergence of angiosperms, and the use pollen tubes to deliver non-motile, non-flagellated sperm during fertilisation (Hawkins et al. 2014). This may indicate a specific role for the NET2 proteins in regulating the delivery of sperm during fertilisation in angiosperms. NET2A and NET2D are most strongly expressed during pollen grain development. Expression of NET2A, NET2C and NET2D is upregulated following penetration of the style by the pollen tube, and NET2B is expressed specifically after this event (Dixon. 2013; Leydon et al. 2013). It is therefore likely that NET2A and NET2D may function during pollen grain

development, and that NET2A, NET2B, NET2C and NET2D may serve important functions during pollen tube growth. Consistent with this hypothesis, NET2B expression is reported be controlled by a group of three pollen-expressed MYB transcription factors necessary for the delivery of sperm during fertilisation (Leydon et al. 2013).

Each NET2 family member has a functional actin-binding NAB domain, which can associate with actin *in vivo* (Dixon et al. 2013). Additionally, *Pi*KIP1 also possesses a functional NAB domain (Calcutt. 2009), showing that it too may serve as a functional actin-binding protein in Petunia. The association of NET2A with actin has been demonstrated in growing pollen tubes, in which NET2A forms discreet foci at the plasma membrane which align on actin filaments, in the 'beads-on-a-string' pattern characteristic of NET proteins (Deeks et al. 2012). Importantly, these membrane foci were restricted to the shank region of the pollen tube and were absent from the pollen tube tip (Deeks et al. 2012).

Reverse-genetic analysis was employed to identify a potential role for NET2A in Arabidopsis. One potential loss-of-function *net2a* mutant was selected for investigation, and it was reported that no severe defects in pollen development or pollen tube growth could be attributed to the loss of NET2A. However, mild defects were observed in the *net2a* mutant, including slight morphological defects in the vegetative nucleus of mature pollen grains, and altered distribution and dynamics of mitochondria in growing pollen tubes (Dixon. 2013). It was later determined throughout the course of the current investigation described in this thesis, that the *net2a* mutant described above was transcriptionally active, accounting for the lack of a severe phenotypic defect.

As described previously, an observed interaction between *Pi*KIP1 and *Pi*PRK1 (Skirpan et al. 2001) implicates NET2 proteins in the regulation of pollen tube growth, perhaps in response to external signals. *Pi*KIP1, as a potentially functional actin-binding protein, may form a physical connection between the actin cytoskeleton and the plasma membrane through an interaction with *Pi*PRK1, and may regulate the actin cytoskeleton in response to external signals perceived by *Pi*PRK1. Whether or not this interaction occurs *in vivo* is unknown, as is the nature and the function of the interaction. However, it is known that *Pi*KIP1 is phosphorylated by *Pi*PRK1 (Skirpan et al. 2001), indicating a potential signalling link

between the two proteins. It is also known that *Pi*KIP1 is able to self-interact, as has been reported for members of the NET3 and NET4 protein families. It is therefore likely that Arabidopsis NET2 proteins may also self-interact.

Therefore, NET2A has been characterised as a pollen-specific actin-binding protein that binds actin in developing pollen grains and at the plasma membrane of growing pollen tubes. NET2A is likely to play an important role in pollen grain development, pollen tube growth and fertilisation through previously unreported mechanisms of action. However, these potential functions of NET2A remain to be elucidated. Throughout the course of this investigation, functional analysis of NET2A will be performed, to characterise the roles of NET2A in pollen and elucidate novel mechanisms of cytoskeletal regulation in plant cell growth and development.

1.8. Characterisation of NET2A Function: Strategic Approach.

Multiple approaches were adopted to characterise the function of NET2A in Arabidopsis. Chiefly, identification and characterisation of potential interacting partners of NET2A was performed, in order to better understand the cellular processes that NET2A may be involved in, through interactions with other proteins. Additionally, reverse genetic analysis of NET2 proteins, and *in situ* analysis of NET2A subcellular localisation was also undertaken, to shed light on the potential functions and importance of NET2A in Arabidopsis.

Firstly, reverse genetic analysis was employed to identify potential roles for the NET2 family, which is discussed in Chapter 3. As described before, phenotypic analysis was previously performed on a *net2a* mutant which I later determined to be transcriptionally active. During this investigation, identification of *net2a* transcriptional null mutants was performed, on which to investigate the role of NET2A. *net2b* and *net2d* mutants were also identified and analysed, to determine if NET2B and NET2D have roles in pollen development and fertilisation, and ascertain if they may be involved in similar processes to NET2A.

Chapter 4 describes the characterisation of NET2A subcellular localisation in developing pollen grains. It was previously reported that NET2A-GFP decorates filamentous networks in developing pollen grains (Dixon. 2013); perhaps those of

actin. The actin cytoskeleton undergoes several dynamic rearrangements during pollen grain development in order to regulate specific developmental processes, in which NET2A may play an important role. To better understand the potential role of NET2A in gametogenesis, NET2A-GFP subcellular localisation was analysed over the course of pollen grain development and its associations with actin at each developmental stage was investigated. By analysing the subcellular structures at which NET2A associates with actin during specific stages of development, it might be possible to predict its potential roles in pollen maturation. In order to study this, stable transgenic Arabidopsis plants expressing NET2A-GFP under its native promoter were analysed. Lines stably co-expressing NET2A-GFP and actin marker constructs were developed to visualise the associations of NET2A-GFP and actin throughout pollen grain development.

As described in chapter 5, multiple interaction screens were performed to identify potential interacting partners of NET2A, so that it might be possible to determine which subcellular processes NET2A may be involved in. Homomeric interactions between NET2A and itself, as well as heteromeric interactions between NET2A and NET2B were identified in these protein-protein interaction screens. Explained in this chapter are the principles of tandem-affinity purification coupled to mass spectroscopy (TAP-MS), and the split-ubiquitin yeast-2-hybrid (SU-Y2H) system: protein-protein interaction screens that were used to identify potential interacting partners of NET2A. Additionally, Förster resonance energy transfer - fluorescence lifetime imaging microscopy (FRET-FLIM) was also performed to characterise an interaction between NET2A and NET2B identified in the TAP-MS screen.

In chapter 6, investigations of the interactions between NET2 proteins and PRKs will be described. Firstly, *in vivo* analysis of the previously characterised interaction between *Pi*KIP1 and *Pi*PRK1 (Skirpan et al. 2001) was performed using FRET-FLIM, in order to ascertain whether the two proteins may interact *in vivo*, and elucidate the nature and potential functions of the interaction. Subsequently, identification of potential interactions between NET2A and *At*PRKs was performed using the Clontech Matchmaker GAL4 Y2H system, and FRET-FLIM. Identification of an interaction between NET2A and *At*PRKs would allow investigation of the interaction in the model organism, Arabidopsis, in which NET2A has already been well characterised. Finally, investigation of the associations of NET2A and putative *At*PRK interacting partners was performed in growing pollen tubes. Stable

transgenic Arabidopsis lines expressing *At*PRK-fluorophore fusions under the control of a pollen-specific promoter were generated, to analyse the subcellular localisation of *At*PRKs *in vivo*. These lines were crossed with stable transgenic plants natively expressing NET2A-GFP, so that the associations of NET2A and *At*PRKs could be visualised in Arabidopsis pollen tubes.

Finally, chapter 7 describes the characterisation of At3g24100; a potential interactor of NET2A isolated in the SU-Y2H screen. Preliminary investigations of this protein, herein referred to as MAP7A, performed during this project indicated it to be a microtubule-associated protein, therefore warranting its full characterisation. Firstly, brief bioinformatic analysis revealed the gene and protein structures of MAP7A, and identified potential functional protein domains. Related proteins, sharing sequence homology with MAP7A were identified, including another Arabidopsis protein named in this study as MAP7B. Following this, MAP7A microtubule-binding activity was assessed *in vivo*: MAP7A-GFP fluorophore fusions were expressed in *N. benthamiana* leaf epidermal cells alongside cytoskeletal marker constructs to visualise co-localisation of MAP7A-GFP and microtubules. Pharmacological disruption of microtubules was performed to ascertain whether MAP7A-GFP may associate with microtubules *in vivo*. *In vitro* microtubule-binding assays were also performed to determine whether MAP7A may associate with microtubules directly. Subsequently, the interactions between MAP7A and NET2A were investigated using the Y2H system and FRET-FLIM in order to corroborate the interaction observed in the SU-Y2H system. Analysis of MAP7A and MAP7B *in situ* was carried out by investigating the transcriptional expression patterns of MAP7A and MAP7B using the GUS reporter system. Anti-MAP7A antibodies were generated and used to analyse the subcellular localisation of MAP7A in pollen tubes using immunofluorescence microscopy. Finally, reverse genetic analysis of MAP7A and MAP7B was performed to identify the potential roles of MAP7 proteins in Arabidopsis.

Chapter 2: Materials and Methods.

2.1. Materials.

2.1.1. Plant Material.

Nicotiana benthamiana plants were used for the transient expression of fluorophore fusion proteins in leaf epidermal cells for analysis of subcellular localisation, drug studies and FRET-FLIM. *Arabidopsis thaliana* Columbia (Col-0) ecotype was used as the background line for the creation of *pMAP7A*:MAP7A-GUS, *pMAP7B*:MAP7B-GUS, *CaMV35s*:MAP7A-GFP, *pLAT52*:*At*PRK4-GFP, *pLAT52*:*At*PRK5-GFP, *pLAT52*:*At*PRK4-RFP and *pLAT52*:*At*PRK5-RFP stable transgenic lines. The Col-0 seeds were obtained from Lehle Seeds. *Petunia inflata* used for cloning experiments was obtained from B&T World Seeds. Narcissus tissue used for immunofluorescence with anti-MAP7A antibodies was obtained from Durham University Botanical Gardens.

The *pNET2A*:NET2A-GFP and *pLAT52*:FABD2-RFP Arabidopsis stable transgenic lines were created by Dr. Martin Dixon using the *Agrobacterium tumefaciens* floral dipping method.

The SALK and GABI_KAT T-DNA insertion lines were obtained from NASC and were used for the creation of the *net2a, net2b, net2d, map7a and map7b* homozygous lines, and the generation of the *map7a*/*map7b* double mutant line.

2.1.2. Bacterial Strains.

The Agrobacterium strain, GV3101 was used for transient transformation of *N. benthamiana* leaf epidermal cells and for stable transformation of Arabidopsis. The following *Escherichia coli* strains were used: DH5α for cloning, DB3.1 for amplifying empty Gateway vectors and Rosetta 2 for protein induction and expression.

2.1.3. Yeast Strains.

Two strains of *Saccharomyces cerevisiae* were used for yeast-2-hybrid (Y2H) assays: Y187 was used for transformation of bait constructs. AH109 was used for transformation of prey constructs and autoactivation tests.

2.1.4. Vectors and Constructs.

All vectors used were commercially available, with the following exceptions; (1): the pBI101G vector was developed by Dr. Martin Kieffer (University of Leeds) in order to create a Gateway compatible version of the pBI101 vector (Clontech). (2): pH7RGW52 was created by Dr Michael Deeks (University of Exeter), to drive strong, pollen-specific expression of C-terminal RFP fusions in pollen, under the *pLAT52* promoter. (3): pB7FGW52 was created during this project to drive strong, pollen-specific expression of C-terminal GFP fusion proteins under the *pLAT52* promoter. (4): pMDC83-mCherry was created during this project to drive constitutive expression of C-terminal mCherry fusion proteins under the *CaMV 35s*: promoter. Table 2.1 summarises the vectors used in this project.

Vector Name	Vector Function	Vector Size (bp)	Resistance	Supplier
pDONR207	Gateway entry vector	5585	Gentamycin (bacteria)	Invitrogen
pBI101G	Gateway β-glucuronidase expression vector under endogenous promoter	12200	Kanamycin (bacteria and plants)	University of Leeds
pET28a	Expression vector with N-terminal 6xHIS-tag	5369	Kanamycin (bacteria)	Novagen
pMDC43	Gateway expression vector for N-terminal GFP fusion under 2x35S promoter	12460	Kanamycin (bacteria). Hygromycin (plants)	University of Zurich via ABRC
pMDC83	Gateway expression vector for C-terminal GFP fusion under 2x35S promoter	12513	Kanamycin (bacteria). Hygromycin (plants)	University of Zurich via ABRC

pMDC83-mCherry	Gateway expression vector for C-terminal mCherry fusion under 2x35S promoter	12581	Kanamycin (bacteria). Hygromycin (plants)	Durham University
pB7FGW2	Gateway expression vector for C-terminal GFP fusion under 35S promoter	11628	Spectinomycin (bacteria). BASTA (plants)	Ghent University via ABRC
pH7RGW2	Gateway expression vector for C-terminal RFP fusion under 35S promoter	12253	Spectinomycin (bacteria). Hygromycin (plants)	Ghent University via ABRC
pB7FGW52	Gateway expression vector for C-terminal GFP fusion under *pLAT52* promoter	11140	Spectinomycin (bacteria). BASTA (plants)	Durham University
pH7RGW52	Gateway expression vector for C-terminal RFP fusion under *pLAT52* promoter	11765	Spectinomycin (bacteria). Hygromycin (plants)	Durham University
pMDC107	Gateway expression vector for C-terminal GFP fusion under endogenous promoter	11738	Kanamycin (bacteria) Hygromycin (plants)	University of Zurich via ABRC
pGADT7	Gateway prey vector for Y2H studies. N-terminal GAL4 activation domain fusion	10399	Ampicillin (bacteria) Leucine (yeast)	Durham University
pGBKT7	Gateway bait vector for Y2H studies. N-terminal GAL4 DNA binding domain fusion	9715	Kanamycin (bacteria) Tryptophan (yeast)	Durham University

Table 2.1: Cloning and Expression Vectors used in this Project.

2.2. Molecular Biology Methods.

2.2.1. Transformation of *E. coli* Using Electroporation.

DH5α or DB3.101 strain *E. coli* were streaked onto solid LB-media (20 g/L LB (Melford) and 10 g/l agar (Melford)) from glycerol stocks and left to grow for 16 hours at 37 °C. A single colony was used to inoculate an overnight culture of 5 ml liquid LB media (20 g/L LB), which was grown overnight for 16 hours at 37 °C. ≈ 250 µl overnight culture was used to inoculate 10 ml liquid LB media, which was grown for 2 - 3 hours at 37 °C. The culture was centrifuged at 11,000 RPM for 30 seconds at 4 °C, and the resultant pellet was suspended in 1 ml sterile distilled water chilled to 4 °C. The cells were centrifuged and resuspended twice more. The cells were then

centrifuged and resuspended in 200 µl ice-cold sterile distilled water, and placed in a chilled electroporation cuvette (2 mm gap electroporation cuvettes; VWR). 1 µl plasmid DNA (50-100 ng/µl) was added to the cells which were electroporated at 2.5 kV using the BioRad MicroPulser. 400 µl liquid LB media was added to the cells, which were incubated at 37 °C with shaking for 1 hour in order to recover. The cells were then spread on solid LB agar plates supplemented with the appropriate plasmid selection marker (table 2.1).

2.2.2. Preparation of Chemically-Competent Agrobacterium GV3101 Strains.

GV3101 cells were streaked from glycerol stocks onto solid LB media supplemented with 10 µg/ml gentamicin (Melford) and 40 µg/ml rifampicin (Melford). The bacteria were grown at 30 ºC for 2 days. Single colonies were used to inoculate an overnight culture of 10 ml LB media supplemented with 10 µg/ml gentamicin and 40 µg/ml rifampicin and grown for 16 hours at 30 °C. 1 ml of the overnight culture was used to inoculate 100 ml LB supplemented with 10 µg/ml gentamicin and 40 µg/ml rifampicin, which was grown for approximately for ≈ 6 hours until the culture grew to an optical density (OD_{600}) of 0.6. The cells were then centrifuged at 3000 x g for 5 minutes at 4 °C. The resultant pellet was resuspended using 50 ml ice-cold 0.15 M NaCl (BDH). Cells were incubated at 4 °C for 15 mins. A second centrifugation at 3,000 x g was performed for 5 minutes at 4 °C. The pellet was resuspended in 5 ml 20 mM $CaCl_2$ (BDH) at 4 °C, and aliquots of 100 µl were frozen in liquid nitrogen and stored at -80 °C.

2.2.3. Transformation of Chemically-Competent Agrobacterium Strains using the Heat Shock Method.

≈ 500 ng plasmid DNA was added to each aliquot of frozen chemically competent cells at -80 °C on dry ice. Cells were subsequently incubated at 37 °C for 5 mins using a water bath. 400 µl liquid LB medium was added to the cells, which were then incubated with shaking at 30 °C for 2 – 5 hours to allow their recovery. Cells were centrifuged at 3,000 x g for 3 minutes and resuspended in 100 µl liquid LB medium. The cells were spread on solid LB media supplemented with 10 µg/ml gentamicin,

40 µg/ml rifampicin plus plasmid selection. The plated bacteria were left to grow for 3 days at 30 °C.

2.2.4. Plasmid DNA Purification.

The Promega Wizard Plus SV Miniprep DNA Purification System was used for plasmid purification. Cells of overnight cultures were pelleted by centrifugation, and lysed with lysis solution. Alkaline phosphatase was subsequently added to inactivate released bacterial proteins that may affect DNA purity. After 5 minutes, a neutralisation solution was used to terminate the lysis. The lysate was cleared through centrifugation and transferred to a binding column containing a DNA binding matrix. The binding column was washed with buffer and the DNA was eluted in 50-100 µl nuclease-free water.

2.2.5. Analytical Restriction Digests.

Restriction digests were used to confirm the identities of purified plasmids. The reactions were performed using a mix consisting of 1 µl of the appropriate 10x reaction buffer, 0.5 µl restriction enzyme, 3 µl purified plasmid DNA (as described in 2.2.4), and 5.5 µl sterile distilled water. Digest reactions were incubated at 37 °C for 1 hour and resolved using agarose gel electrophoresis (2.2.6).

2.2.6. Agarose Gel Electrophoresis.

Agarose gels were prepared by dissolving 1% - 3% (w/v) Agarose Low EEO (Melford) in 1x TAE buffer (40 mM Tris acetate (Fisher), 1 mM EDTA (Ethylenediaminetetraacetic acid, Sigma)) with heating. 3 µl /100 ml ethidium bromide (BDH) was added and the gel mixture was poured into casting trays to set. DNA Loading Buffer Blue (Bioline; 5x stock) was added to DNA samples prior to loading into the wells. Hyperladder I, Hyperladder 25 bp (Bioline) or 2-Log DNA Ladder (NEB) were used as standards of DNA molecular weight. Gel

electrophoresis was performed using an electrophoresis tank containing 1x TAE. Gels were run at 100 - 200 volts and imaged using the Bio-Rad Gel-Doc 1000.

2.2.7. RNA Purification.

Total mRNA was extracted from whole Arabidopsis inflorescences using the Spectrum Plant Total RNA Kit (Sigma). 30 - 80 mg of tissue was flash-frozen in sterile Eppendorf tubes and ground at – 80 ºC using a liquid-nitrogen cooled micropestle. The ground tissue was lysed using 500 µl lysis buffer supplemented with 10 µl/ml ß-mercaptopethanol (Sigma). Samples were vortexed thoroughly for 1 minute and were incubated at 56 ºC for 5 minutes. The lysate was transferred to a filtration column and centrifuged at 16,000 x g for 1 minute to remove debris. 500 µl binding solution was added to the filtered lysate and the resulting solution was transferred to an RNA-binding column containing an RNA-binding matrix. The lysate was centrifuged at 16,000 x g for 1 minute to bind the RNA to the matrix.

An on-column DNase digestion was performed to remove genomic DNA contamination using the RNase-Free DNase Set (Qiagen). The binding column was washed with wash buffer and DNase I was applied to the RNA-binding matrix. The DNase I digestion was performed for 15 minutes at room temperature before the digestion was terminated by washing the column with wash buffer. RNA was eluted using 30 µl RNase-free water.

2.2.8. cDNA Synthesis.

cDNA was synthesised from Arabidopsis total RNA, using the GoScript Reverse Transcription System (Promega) with oligo(dT)15 primers and GoScript reverse transcriptase enzyme. Heating steps were performed using the G-Storm (GRI) PCR machine.

Firstly, the following reaction components were mixed in a PCR tube: 1 µl oligo$(dT)_{15}$ primer (0.5 µg/reaction), 3 µg RNA, and nuclease-free water was added to a final volume of 10.2 µl. Samples were heated at 70 ºC for 5 minutes and were then cooled

to 4 ºC. A reverse transcription mix consisting of 4 µl GoScript 5x Reaction buffer, 1.8 µl $MgCl_2$ (final concentration 2.25 mM), 1 µl PCR nucleotide mix (final concentration of 0.5 mM for each dNTP), 1 µl recombinant RNasin ribonuclease inhibitor and 1 µl GoScript reverse transcriptase, was added to the PCR tube. The mixture was heated at 25 ºC for 5 minutes to permit primer annealing, before an extension step at 42 ºC for one hour was performed for first-strand cDNA synthesis. The reaction was terminated using an inactivation step at 70 ºC for 15 minutes.

2.2.9. Genomic DNA Extractions using the Edwards Preparation Method.

Preparations of genomic DNA extracts were made from Arabidopsis leaf tissue. (Edwards et al. 1991). Leaf tissue was ground in 400 µl Edwards buffer (250 mM NaCl, 200 mM TrisHCl (Fisher) pH 7.5, 25 mM EDTA (Ethylenediaminetetraacetic acid (Sigma)), 0.5% (w/v) sodium dodecyl sulphate (SDS, (BDH)). The samples were centrifuged at 16,000 x g for 5 minutes, and 200 µl was collected and mixed with an equal volume of isopropanol (BDH) to precipitate genomic DNA. Samples were incubated at 4 ºC for 10 minutes, before being centrifuged at 16, 000 x g for 5 minutes. The supernatant was removed and the DNA pellet was dried at 37 ºC for 15 minutes to remove any residual isopropanol. The genomic DNA pellet was resuspended in 100 µl 1 x TE buffer (10mM Tris.HCl pH 8.0, 1mM EDTA).

2.2.10. Amplification of DNA Fragments using the Polymerase Chain Reaction.

Amplification of DNA fragments of interest from genomic DNA, cDNA or purified plasmid DNA was performed using the polymerase chain reaction (PCR). PCR using Q5 DNA polymerase (NEB) was performed for functions requiring high-fidelity replication, otherwise MyTaq DNA polymerase (Bioline) was used.

2.2.10.1. PCR using Q5 DNA Polymerase.

For PCR using Q5 DNA polymerase, the following components were assembled per 50 µl reaction: 10 µl 5x Q5 reaction buffer, 1 µl 10mM dNTPs (made from 100 mM stocks of dATP, dGTP, dCTP and dTTP), 2.5 µl forward primer, 2.5 µl reverse primer (both 10 µM stocks, Eurofins/IDT), 1 µl DNA template, 0.5 µl Q5 High-Fidelity DNA Polymerase, 32.5 µl nuclease-free water. The PCR programme was run using the following stages:

Stage	Temperature (ºC)	Time	Cycles
Initial Denaturing	98	30 seconds	1
Denaturing	98	10 seconds	35 - 45
Annealing	55 – 72	20 seconds	
Extension	72	30 seconds/kb	
Final extension	72	2 minutes	1

Table 2.2: Standard Thermocycling Programme for PCR with Q5 DNA Polymerase

Annealing temperature was adjusted depending on the melting temperature of the primers used, and extension time was modified to suit the size of the amplicon of interest. Annealing temperature was typically set at 5 °C below the predicted melting temperature of the primers, and an extension time of 30 seconds/Kb of amplicon was used.

2.2.10.2. PCR using MyTaq DNA Polymerase.

MyTaq DNA polymerase was used when high-fidelity of replication was not essential, such as for genotyping and RT-PCR. A typical 20 µl reaction mixture consisted of 10 µl 5x MyTaq Reaction Buffer, 1 µl forward primer, 1 µl reverse primer (10 µM stocks, Eurofins/IDT), 0.5 µl template, 0.5 µl MyTaq DNA Polymerase, 7 µl nuclease-free water. The PCR programme was run using the following stages:

Stage	Temperature (ºC)	Time	Cycles
Initial Denaturing	95	30 seconds	1
Denaturing	95	15 seconds	25 - 35
Annealing	55 – 65	15 seconds	
Extension	72	10 seconds/kb	
Final extension	72	1 minute	1

Table 2.3: Standard Thermocycling Programme for PCR with MyTaq DNA Polymerase

An extension time of 10 s/Kb was allowed, and the annealing temperature was set at 5 °C below the predicted melting temperature of the primers.

2.2.11. Cloning Using the Invitrogen Gateway Cloning System

2.2.11.1. BP Reaction.

The BP reaction was used to insert PCR-amplified DNA fragments of interest into the entry vector, pDONR207. Each BP reaction consisted of 75 ng PCR fragment insert, 75 ng pDONR207, made up to a total volume of 4 µl with 1x TE buffer. 1 µl BP Clonase II enzyme mix added and the reaction was incubated at 25 °C for 1 – 24 hours. The reaction was subsequently terminated by Proteinase K digestion: 0.5 µl Proteinase K was added to the BP reaction, which was then incubation at 37 °C for 15 minutes.

DH5α cells were transformed with the recombinant entry vector (as described in 2.2.1). The transformed cells were selected on LB agar plates supplemented with 10 µg/ml gentamicin.

2.2.11.2. LR Reaction.

To transfer DNA fragments of interest from an entry vector to a destination vector, the LR reaction was used. A list of the destination vectors used in this project is

provided in 2.1.4. Each LR reaction consisted of 75 ng recombinant entry vector and 75 ng destination vector made to a total volume of 4 µl with 1x TE buffer. 1 µl LR Clonase II was added and the reaction mixture as incubated at 25 °C for 1 - 24 hours. To terminate the reaction, 0.5 µl Proteinase K was added, and the reaction was incubated at 37 °C for 15 minutes.

DH5α cells were transformed with the recombinant destination vector as described in 2.2.1. The transformed cells were selected on LB agar plates supplemented with the appropriate antibiotic as indicated in 2.1.4.

2.2.12. Recombinant Cloning using Restriction Digestion.

The expression construct, MAP7A-pET28a, and the destination vectors pMDC83-mCherry and pB7FGW52, were created using restriction cloning. To create these constructs, regions of DNA from the target vectors were excised using double restriction digest, and replaced with a DNA fragment of interest (insert DNA) by ligation with T7 DNA ligase. Insert DNA was PCR amplified (2.2.10.1) with added restriction sites at each end of the fragment. The added restriction sites matched the restriction sites of the target vector, to which the insert fragment ends would be ligated.

2.2.12.1. Purification of PCR Products.

Before restriction cloning could be performed, purification of the insert PCR product was performed using the Promega Wizard SV Gel and PCR Clean-Up System.

Firstly, crude PCR product was mixed in 1:1 volumes with a membrane-binding solution, and the mixture was added to a DNA-binding spin column, which contains a DNA-binding matrix. The column was centrifuged for 1 minute at 16,000 x g to bind the PCR product to the column. The DNA was washed by the addition of 750 µl wash buffer followed by centrifugation at 16,000 x g for 1 minute. A second wash step was performed using 250 µl wash buffer and centrifugation at 16,000 x g for 5 minutes. The purified DNA was eluted in 30 µl nuclease-free water.

2.2.12.2. Generation of Compatible Ends using Restriction Digests.

Large-scale double restriction digestion of purified target vectors and insert DNA (purified PCR product) was performed to create 'sticky-ended' DNA fragments suitable for ligation. For digestion of PCR products, the following components were assembled: 20 µl purified PCR product (100 – 200 ng/µl), 5 µl first restriction enzyme, 5 µl second restriction enzyme, 10 µl appropriate 10x reaction buffer, made to 100 µl with nuclease-free water. For restriction digest of the target vector, the following components were assembled: 30 µl target vector (50 – 100 ng), 5 µl first restriction enzyme, 5 µl second restriction enzyme, 30 µl appropriate 10x reaction buffer, made to 300 µl with nuclease free water. The insert and target vector digestion reactions were vortexed thoroughly and centrifuged for 1 minute at 16,000x g to ensure complete mixing and total digestion of DNA. The reactions were incubated overnight at 37 ºC.

2.2.12.3. Ligation of DNA Fragments into Target Vectors.

Restriction digestion of purified PCR products and target vectors was performed as described above. 5 µl calf intestinal alkaline phosphatase (Fermentas) was added to the digested target vectors and incubated at 37 ºC for 30 minutes to inactivate the restriction enzymes. The insert digestions were not treated with phosphatase. Chloroform (BDH) was added at a 1:1 volume ratio to the digested vector solution, which was subsequently centrifuged at 16,000 x g for 5 minutes to inactivate the phosphatase and separate the DNA into the aqueous supernatant. The supernatant, containing the digested target vector DNA was transferred into a microcentrifuge tube. The digested target vector and the digested PCR product were purified separately using the Promega Wizard SV Gel and PCR Clean-Up System as described above.

The purified digested PCR products were ligated into the digested target vectors using T7 DNA Ligase (NEB). Each ligation was performed using a 1:1, 3:1 and 10:1 molar ratio of insert:vector. A 10 µl ligation reaction was composed of: 1 µl 10x T7 DNA Ligase Buffer, 1 – 9 µl (200 ng) linearised target vector, 1 – 9 µl insert DNA, 1 µl T7 DNA Ligase, and made up to a total volume of 10 µl. Background control reactions were set up containing no PCR product (to test for re-ligation of excised

vector fragments) or no ligase (to test for undigested vector). The ligation reactions were incubated at room temperature for 1 hour, and were then transformed into DH5α cells as described in 2.2.1.

2.2.13. DNA Sequencing.

All DNA sequencing reactions were performed by Durham University Biological Sciences Genomics, using an Applied Biosystems 3730 DNA Analyser.

2.2.14. Agrobacterium-Mediated Transformation of *N. benthamiana* Leaf Epidermal Cells.

Adapted from the protocol used by Sparkes et al. (2006). Agrobacterium GV3101 cells transformed with the construct of interest (as described in 2.2.1.2) were used to inoculate an overnight culture of 5 ml LB media supplemented with 10 μg/ml gentamicin, 40 μg/ml rifampicin plus the appropriate plasmid selection marker. Also, an overnight culture of GV3101 cells containing the p19 protein was prepared in 5 ml LB (supplemented with 10 μg/ml gentamicin, 40 μg/ml rifampicin, 100 μg/ml kanamycin), in order to suppress gene silencing in *N. benthamiana.* Each culture was grown for 16 hours at 30 °C, before being centrifuged at 3,000 x g for 10 minutes. The cell pellet was resuspended in 1 ml infiltration buffer (50 mM MES (2-(N-morpholino) ethanesulfonic acid (Sigma)), 28 mM D-glucose (Melford), 2 mM $Na_3PO_4.12H_2O$ (trisodium orthophosphate), 100 μM acetosyringone (3',5'-Dimethoxy-4'-hydroxyacetophone (Fluka), from 200 mM stocks in DMSO). Using centrifugation and resuspension in infiltration buffer, the cells were washed twice more and were finally resuspended in 1 ml infiltration buffer. A 1:10 dilution of the cell suspension was made, with which the OD_{600} of the solution was measured. The cells were then diluted in 1ml infiltration buffer to a final OD_{600} of 0.01 – 0.1. The p19 construct was added at a 1:1 ratio with other constructs.

Infiltration of *N. benthamiana* leaves was performed by injection of bacterial suspension into the underside of the leaf using a needleless syringe.

2.2.15. Stable Transformation of Arabidopsis through Floral Dipping.

Based on the protocol used by Clough and Bent (1998). Floral dipping was performed on Arabidopsis plants at 6-8 weeks old. In preparation for floral dipping, the stems could be cut back to the rosette up to two times, to promote the growth of more stems bearing an increased number of inflorescences. Immediately before floral dipping, siliques and open flowers were removed to increase the frequency of transformants amongst the progeny.

Agrobacterium GV3101 cells transformed with the construct of interest were used to start an overnight culture by inoculating 5 ml liquid LB media (supplemented with 10 µg/ml gentamicin, 40 µg/ml rifampicin, plus the appropriate plasmid selection marker) which was grown overnight at 30 °C for 16 hours. This culture was used to inoculate 500 ml LB media (supplemented with the same antibiotics), which was grown overnight with shaking at 30 °C for 16 hours. The culture was pelleted by centrifugation at 3,500 x g for 30 minutes and resuspended in 1 L dipping buffer (5 % (w/v) sucrose (Melford) and 0.02 % (v/v) Silwett L-77 (Lehle Seeds)).

The pre-prepared Arabidopsis plants were dipped, upside down, into the cell solution with gentle agitation for 1 minute. Dipped plants were placed in a sealed plastic bag and placed in a shaded environment at room temperature for 24 hours to maintain humidity and prolong the viability of the agrobacterium during transformation. The dipped plants were returned to normal growth conditions. The dipping procedure, (without pruning) could be repeated 5 – 10 days later. The plants were contained, allowed to mature, and seeds were collected when the plants had matured.

2.3. GAL4 Yeast-2-Hybrid System.

2.3.1. Yeast Transformations.

Y187 and AH109 yeast strains were streaked onto solid YPDA plates (20 g/L peptone (Melford), 10 g/L yeast extract (Merck), 30 mg/L adenine hemisulphate (Sigma), 2% D-glucose, 1g/L agar, pH 6.5) and grown for 2 – 3 days at 30 ºC.

Single yeast colonies were used to inoculate an overnight culture of 10 ml liquid YPDA. The OD_{600} of the culture was measured and subsequently diluted to an OD_{600} of 0.2 in a final volume of 100 ml YPDA. The culture was grown in an Erlenmeyer flask with shaking at 30 ºC for 4 hours, before the culture was pelleted by centrifugation at 1800 x g for 5 minutes. The cell pellet was resuspended in 50 ml sterile distilled water. The cells were centrifuged again as before, and the pellet was resuspended in 1.5 ml Li/TE buffer (10 mM Tris.HCl (Fisher) pH 7.5, 1mM EDTA, 100 mM lithium acetate (Sigma)). Cells were centrifuged at 16,000 x g for 15 seconds in a microcentrifuge tube, and resuspended in 1.2 ml Li/TE buffer.

Deoxyribonucleic acid sodium salt (ssDNA; Sigma) was used as a DNA carrier for the yeast transformation. The ssDNA was resuspended in sterile distilled water and shredded by forcing the solution through a 19 – gauge syringe needle. The ssDNA was denatured immediately before use by heating at 95 ºC for 5 minutes followed by rapid cooling on ice.

Per transformation, the following components were assembled in a pre-chilled microcentrifuge tube: 600 µl PEG/Li/TE buffer (40 % (w/v) PEG-4000 (polyethylene glycol 4000; BDH), 100 mM lithium acetate, 10 mM Tris.HCl, 1 mM EDTA pH 7.5) 100 µl yeast cells, 160 µl denatured ssDNA (2 mg/ml), 1 µg plasmid DNA. The cells were mixed gently by pipetting and incubated at 30 ºC for 30 minutes. 10 µl DMSO was added to the mixture, which was incubated at 42 ºC for 15 minutes. The cells were centrifuged at 16,000 x g for 15 seconds and the pellet was resuspended in 1ml sterile distilled water. The centrifugation step was repeated and the cells were resuspended in 0.9% (w/v) NaCl solution. Dilutions of 1/10 and 1/100 were prepared in 0.9 % NaCl. Each dilution was spread on solid SD minimal growth media (SD media; 6.9 g/L yeast nitrogen base without amino acids (Formedium), 10 g/L agar, 2 % (w/v) D-glucose, pH 5.8, plus 100 ml/l of the appropriate 10x dropout solution), supplemented with 50 µg/ml kanamycin. The plates were incubated for 2 – 5 days at 30 ºC.

The 10x dropout solution was prepared in advance. 2.2 g dropout mix was firstly dissolved in 400 ml sterile distilled water to make 10x -WLHA dropout solution. The dropout mix consisted of 3 g L-isoleucine, 15 g L-valine, 2 g L-arginine HCl, 3 g L-lysine, 2 g L-methionine, 5 g L-phenylalanine, 20 g L-threonine, 3 g L-tyrosine, 2 g L-uracil. To make a required 10x dropout media, the following amino acids could

then be added: A (80 mg L-adenine hemisulphate), H (80 mg L-histidine HCl monohydrate), L (400 mg L-leucine) and W (80 mg L-tryptophan). All amino acids were obtained from Sigma.

2.3.2. Autoactivation Tests.

To test autoactivation of reporter genes, each construct was transformed into the AH109 yeast reporter strain as described above. Three individual colonies from each transformation were each resuspended in 1 ml sterile distilled water and dropped on SD plates with the appropriate nutritional selection, supplemented with 50 µg/ml Kanamycin and specific amounts of 3AT (3-Amino-1,2,4-triazole, Sigma) as described below.

Yeast transformed with pGBKT7 expression constructs were dropped onto SD plates with the following nutritional selection: -W, -WH, -WH + 2.5 mM 3AT, -WH + 5 mM 3AT, and -WA.

Yeast transformed with pGADT7 expression constructs were dropped onto SD plates with the following nutritional selection: -L, -LH, -LH + 2.5 mM 3AT, -LH + 5 mM 3AT, and -LA.

Dropped colonies were allowed to dry and the plates were incubated for 5 – 7 days at 30 ºC. The plates were then imaged using a desktop image scanner.

2.3.3. Yeast One-on-One Mating Tests.

Bait constructs in pGBKT7 were transformed into the Y187 yeast strain, and prey constructs in pGADT7 were transformed into the AH109 yeast strain. Yeast matings were performed as follows: firstly, single Y187 bait colonies were resuspended in 100 µl sterile distilled water. 10 µl was dropped onto solid YPDA plates and the colony was allowed to dry. Subsequently, single AH109 prey colonies were similarly resuspended in 100 µl sterile distilled water and 10 µl was dropped directly on top

of the dried drop containing the bait cells. The drops were allowed to dry and the plates were incubated at 30 ºC for 24 hours.

Once the yeast colonies had grown, nutritional selection was performed to isolate diploid arising from the matings. With exceptions (as described below) selection of diploids was performed as follows: a small quantity of mated cells from each colony was resuspended in 100 µl sterile distilled water, and 10 µl was dropped onto solid -WL SD plates supplemented with 50 µg/ml kanamycin. The plates were grown for 2 – 5 days at 30 ºC.

An exception to this was in the selection of diploid yeast arising from the mating of AH109 yeast containing NET2A-pGADT7 with Y187 yeast containing *At*PRK1, *At*PRK2, *At*PRK3, *At*PRK4, *At*PRK5, or *At*PRK6 in pGBKT7. Following mating, these cells were selected as follows: entire colonies were resuspended in 100 µl sterile distilled water and all 100 µl of the suspension was spread on onto solid -WL SD plates supplemented with 50 µg/ml kanamycin. The plates were grown for 2 – 5 days at 30 ºC.

Selected diploids were resuspended in 100 µl sterile distilled water and 10 µl of the suspension was dropped onto -WL, -WLH, -WLH + 2.5 mM 3AT and -WLH + 5 mM 3AT and -WLA SD plates supplemented with 50 µg/ml kanamycin. The drops were allowed to dry and the plates were grown at 30 ºC for 3 – 5 days. The plates were the imaged using a desktop image scanner.

2.4. *In vitro* Protein Methods.

2.4.1. Expression and Purification of 6xHIS-Tagged Proteins.

Rosetta 2 strain *E. coli* cells were transformed with MAP7A-pET28a (as described in 2.2.1) and spread onto LB plates supplemented with 50 µg/ml kanamycin and 30 µg/ml chloramphenicol (Duchefa), and grown at 37 °C.

One colony was used to inoculate an overnight culture of 10 ml liquid LB media supplemented with 50 µg/ml kanamycin and 30 µg/ml chloramphenicol. 100 µl of the overnight culture was used to inoculate 10 ml of LB media (containing the same

antibiotics), which was grown for 6 hours at 37 ºC with shaking. Protein expression was induced using autoinduction: after 6 hours, 300 µl cells were used to inoculate 600 ml autoinduction media (AIM; 34.85 g/L, (Formedium)) in an Erlenmeyer flask. The culture was grown overnight at 37 °C with shaking. The cells were pelleted by centrifugation at 6,000 x g for 10 minutes at 4 ºC using a Beckman Coulter Avanti J-20 XP centrifuge with a JLA 10.500 rotor. The cell pellet could be frozen until needed.

The pellet was resuspended in sonication buffer, consisting of 50 mM phosphate buffer pH 8 (46.6 mM Na_2HPO_4 (di-sodium hydrogen orthophosphate dehydrate: BDH) and 3.4 mM NaH_2PO_4 (sodium dihydrogen phosphate; Sigma)), 0.5 M NaCl, 10 mM imidazole (Sigma). The cells were lysed using sonication and centrifuged at 16,000 x g at 4 ºC for 10 minutes to pellet cell debris.

The cell lysate was added to a column containing nickel nitrilotriacetic acid (Ni-NTA) agarose beads (Qiagen), which has been equilibrated prior to use with sonication buffer. The cell lysate was passed through the column 4 times using a syringe attached to the base, in order to bind the 6xHIS-tagged protein to the Ni-NTA beads. The beads were subsequently washed with using column wash buffer (50 mM phosphate buffer pH 8, 0.5 mM NaCl and 20 mM imidazole) by drawing the wash buffer through the column using a syringe. The wash step was repeated a further 3 times. The 6xHIS-tagged protein was then eluted from the column using elution buffer (50 mM phosphate buffer pH 8, 0.5 mM NaCl and 300 mM imidazole). SDS-PAGE gel electrophoresis was performed to confirm expression of the protein (2.4.2) and the purified protein was then dialysed as follows.

For use in microtubule co-sedimentation assays, the purified protein was dialysed into 2x buffer C, consisting of 100 mM PIPES (Piperazine-N,N'-bis-(2-ethanesulfonic acid), Melford), 2 mM EGTA (Ethyleneglycol-bis(2-aminoethyl)-N,N,N',N'-tetra-acetic acid, (Fluka,)) 0.4 mM $MgCl_2$ (BDH), 20% (v/v) glycerol (Fisher) pH 6.8. The purified protein was pipetted into dialysis tubing and sealed, before being placed into 1L pre-chilled 2x buffer C, and was incubated at 4 ºC overnight.

For use in antibody preparation, the purified protein was dialysed into 1x PBS solution (137 mM NaCl, 2.7 mM KCl (Melford), 10 mM Na_2HPO_4, 1.8 mM KH_2PO_4 (potassium phosphate monobasic (Sigma), pH 7.4). The purified protein was

pipetted into dialysis tubing and sealed, before being placed into 1 L chilled 1x PBS and was incubated at 4 ºC overnight.

A Bradford assay (Bio-Rad Protein Assay) was performed to determine the concentration of the protein using a spectrophotometer set at a wavelength of 595 nm. The dialysed protein was flash frozen in liquid nitrogen and stored at -80 ºC.

2.4.2. SDS-Polyacrylamide Gel Electrophoresis (SDS-PAGE).

SDS-PAGE was performed using the Bio-Rad Mini Protean II system. Firstly, the resolving gel was cast, containing 15% (v/v) acrylamide (Protogel, 30% (w/v acrylamide, 0.8% (w/v) bisacrylamide), 0.1% (w/v) SDS, 375 mM Tris pH 8.8, 0.1% (w/v) ammonium persulphate (APS; Melford), 0.04% TEMED (NNN'N'-Tetramethylethylenediamine (Fluka)). The resolving gel was covered in a layer of isopropanol and left to set. Once the resolving gel had set, the isopropanol was removed and stacking gel was added. The stacking gel contains 5% acrylamide, 125 mM Tris pH 6.8, 0.1% (w/v) SDS, 0.1% (w/v) APS, 0.002% (v/v) TEMED).

Prior to loading, purified recombinant protein was diluted 2.5x in 5x Laemmli buffer (300 mM Tris-HCl, pH 6.8, 10% (w/v) SDS (BDH), 50% (v/v) glycerol, 25% (v/v) ß-mercaptoethanol (Sigma), 0.05% (w/v) bromophenol blue (Sigma)) and heated at 95 ºC for 5 minutes with intermittent vortexing. Total protein extracts prepared in 2x Laemmli buffer (2.4.5) could be loaded directly. Samples were equilibrated to room temperature and centrifuged for 2 minutes at 16,000 x g. Electrophoresis was performed in an SDS-PAGE tank filled with 1x running buffer (25 mM Tris, 192 mM glycine (Sigma), 0.1% SDS). Initially, electrophoresis was run at 100 V, until the protein reached the resolving gel. Subsequently, the voltage was increased to 150 – 200 V. To visualise proteins in SDS-PAGE gels, the gels were stained using InstantBlue Ultrafast Protein Stain (Expedeon).

2.4.3. MALDI-TOF Analysis of SDS-PAGE Protein Gel Bands.

The sequence of the purified proteins was confirmed using MALDI-TOF-MS analysis. SDS-PAGE was used to separate protein samples. The resulting acrylamide gels were subsequently sent to the Durham School of Biological and Biomedical Sciences (SBBS) Proteomics service. Protein band digestion was performed for analysis using a 4800 Plus MALDI TOF/TOF Analyzer (Sciex). Data-files were processed using GPS Explorer (3.6) software (Sciex) for protein identification from the SwissProt database (September 2013 release).

2.4.4. Production of Polyclonal Antibodies.

Polyclonal antibodies to MAP7A were raised in mice against recombinant 6xHIS-MAP7A, purified from *E. coli* and dialysed into 1x PBS buffer (2.4.1). Approximately 50 µg of the purified MAP7A antigen was used per injection. The antigen was mixed 1:1 with Freund's complete adjuvant (FCA) for the first inoculation and Freund's incomplete adjuvant (FIA) for all subsequent injections. Five mice were inoculated a total of 4 times at days 0, 14, 28 and 42. At day 49, the terminal bleed was collected and the serum was separated. The terminal bleeds were used for Western blot analysis and immunofluorescence labelling. Antibody production (including animal care, injections, test-bleeds and serum collection) was performed in-house by the Durham University Life Science Support Unit (LSSU).

2.4.5. Extraction of Total Protein for Antibody Tests.

Total protein from Arabidopsis Col-0 whole inflorescences was used to test the mouse polyclonal anti-MAP7A antibodies. The inflorescences were ground to a fine powder in liquid nitrogen using a pestle and mortar. Using a spatula pre-cooled in liquid nitrogen, the ground tissue was immediately added to 2 x Laemmli buffer preheated to 95 ºC. Samples were heated at 95 ºC for 5-10 minutes with intermittent vortexing. Samples were centrifuged at 16,000 x g and stored at -20 ºC until needed.

2.4.6. Western Blotting.

To analyse proteins using Western blotting, prepared protein samples were separated using SDS-PAGE as described above. The acrylamide gel was not stained using Instant Blue. Transfer of proteins onto nitrocellulose membranes (Whatman) was performed in a tank filled with transfer buffer (48 mM Tris, 39 mM glycine, 0.375% (w/v) SDS, 20% (v/v) methanol) at 20 V overnight. Following transfer, the membrane was washed in distilled water, and the proteins were visualised by staining the membrane with a 1/100 dilution of Ponceau stain (0.1% Ponceau S (w/v: Sigma) in 5% acetic acid (v/v: Fisher)). The membrane was subsequently washed for 5 minutes in distilled water to de-stain the membrane.

The nitrocellulose membranes were first incubated for 5 minutes in 2x TBST (20 mM Tris pH 7.4, 300 mM NaCl, 0.1% (v/v) Tween 20 (Sigma)). Subsequently, the nitrocellulose membranes were incubated for 30 – 60 minutes in blocking buffer, consisting of 2x TBST + 5% (w/v) dried skimmed milk powder (Tesco). The nitrocellulose membranes were incubated with anti-MAP7A primary antibody diluted in blocking buffer, either for 1 hour at room temperature, or overnight at 4 ºC. The membranes were then washed three times in 2x TBST; (the first wash for 15 minutes, the second for 10 minutes and the final for 5 minutes). The membranes were then incubated with anti-mouse IgG secondary antibodies conjugated to horseradish peroxidase (HRP; Amersham) diluted 1:1000 in blocking buffer. The membranes were then washed again three times in 2x TBST; (15 minutes, 10 minutes and 5 minutes). Antibody binding was detected with the application of ECL Western Blotting Detection Reagent (Amersham Biosciences). The strips were incubated in ECL for 5 minutes and luminescence was captured using X-ray film (SLS), which was developed using the Compact X4 automatic X-ray film processor (Xograph Imaging Systems).

2.4.7. Microtubule Co-Sedimentation Assay.

Aliquots of high molarity PIPES tubulin (purified by Dr Ian Cummins, Durham University), and purified recombinant 6xHIS-MAP7A in 2x buffer C (2.4.1) were defrosted on ice. To remove denatured insoluble protein, the tubulin and 6xHIS-MAP7A samples were separately ultracentrifuged at 90,000 rpm at 4 ºC for 10

minutes using a Beckman Optima TLX ultracentrifuge fitted with a TLA 120.1 rotor. The supernatant containing soluble protein was removed and placed on ice. A Bradford assay was performed to measure the protein concentration of the tubulin and 6xHIS-MAP7A in the supernatants using a spectrophotometer set at a wavelength of 595 nm.

Co-sedimentation reactions were assembled in pre-chilled ultracentrifuge tubes kept on ice. Each reaction consisted of 10 µM tubulin, 10 µM 6xHIS-MAP7A, 1 mM GTP, made up to a total volume of 100 µl with 2x buffer C. As controls, a co-sedimentation reaction with no tubulin was set up, and a reaction with no 6xHIS-MAP7A was also assembled.

The ultracentrifuge tubes containing the co-sedimentation reactions were transferred to a TLA 120.1 rotor pre-heated to 37 ºC, which was incubated at 37 ºC for 20 minutes to promote polymerisation of tubulin. The reactions were then ultracentrifuged at 70,000 rpm at 37 ºC for 10 minutes. The supernatant was removed and diluted 4:1 in 5x Laemmli buffer. The pellet was resuspended in 125 µl 1x Laemmli buffer. Samples were heated for 5 minutes at 95 ºC and analysed using SDS-PAGE (2.4.2).

2.5. Cell Biology.

2.5.1. Preparation of Poly-L-Lysine Slides.

Poly-L-lysine slides were used to adhere cells to coverslips for staining and imaging. To make poly-L-lysine slides, fresh coverslips were incubated overnight in 0.1 M HCl (Fisher). The coverslips were washed 10 times in sterile distilled water and placed in 70% ethanol. The acid-washed coverslips were placed on filter paper and allowed to air dry. 100 µg/ml poly-L-lysine solution (Sigma: from 1 mg/ml stock in 1x PBS) was applied and spread evenly on the top of the coverslip with a pipette tip. The slides were left for 20 minutes, and were then washed in sterile distilled water. The slides were left face-up to dry, after which they were ready for use.

2.5.2. Pollen Germination.

2.5.2.1. *In vitro* Germination of Arabidopsis Pollen.

Arabidopsis pollen grains could be germinated using solid or liquid germination medium.

Solid pollen germination medium consisted of 18% (w/v) sucrose, 0.01% (w/v) H_3BO_4 (BDH), 1 mM $Ca(NO_3)_2$ (Fisher), 1 mM $MgSO_4$, (BDH) and 1 mM $CaCl_2$, 0.5% (w/v) Agarose Type VII-A (Sigma), pH 7 with KOH (Sigma). Mature pollen grains of open Arabidopsis flowers were gently blotted onto 1 ml solid pollen germination media, which was incubated at 22 ºC in a dark humid environment for > 3 hours (Li et al. 1999).

Liquid germination media consisted of 1 mM $Ca(NO_3)_2$, 1 mM $CaCl_2$, 1 mM $MgCl_2$, 0.01% (w/v) H_3BO_4, 18% (w/v) sucrose, 0.5% (w/v) agarose, pH 6.0 with KOH. Mature pollen grains of open Arabidopsis flowers were gently botted onto poly-L-lysine slides, and 30 µl liquid germination media was added directly on top. The slides were incubated at 22 ºC in a dark humid environment for > 3 hours (Deeks et al. 2007).

2.5.2.2. Semi *in vivo* Germination of Arabidopsis Pollen.

Semi *in vivo* germination of Arabidopsis pollen was performed as described by Qin et al. (2009). Mature pollen from open Arabidopsis flowers was manually dusted onto the excised stigmas of opening flowers, cut below the style. The excised pollinated pistils were placed vertically on solid pollen germination media (2.5.2.1) and were incubated at 22 ºC in a dark humid environment to permit the pollen to germinate into the stigma. After 1 hour of incubation, the pistils were re-positioned horizontally, to allow the germinated pollen tubes to grow across the solid pollen germination media after having grown through the pistil tissue. The samples were incubated again at 22 ºC in a dark humid environment for a further 3 hours, after which the growth of the pollen tubes through the pistil was clearly visible.

2.5.2.3. *In vitro* Germination of Narcissus Pollen.

Narcissus pollen was germinated in daffodil pollen germination medium consisting of 7.5% (w/v) glucose, 1 mM $Ca(NO_3)_2$ and 1 mM H_3BO_4, pH 6.7 with KOH. Anthers of daffodil flowers were placed in a Falcon tube with 10 ml daffodil pollen germination medium and vortexed to release the pollen. The resulting pollen suspension was poured into a petri dish and was incubated at room temperature for 2 - 3 hours with gentle agitation to permit aeration (Heslop-Harrison and Heslop-Harrison. 1992).

2.5.3. Confocal Laser Scanning Microscopy (CLSM).

2.5.3.1. Live Cell Imaging.

CLSM was used to visualise fluorophore fusion proteins expressed in *N. benthamiana* leaf epidermal cells using Agrobacterium-mediated infiltration (2.2.14). Imaging of fusion proteins was performed 2 – 5 days post-infiltration. Leaf sections were prepared and mounted on glass slides in sterile distilled water with the abaxial surface in contact with the coverslip. Likewise, CLSM was used to visualise fluorophore fusion proteins in growing pollen tubes. Pollen tubes were germinated as described in section 2.5.2.1, and mounted onto microscope slides for imaging. To image developing pollen grains of *pNET2A*:NET2A-GFP/*pLAT52*:FABD2-RFP stable transgenic lines, small incisions were made in the anther wall of transgenic plants to expose the developing grains. Whole anthers were mounted onto microscope slides and imaged.

Imaging was performed using a Leica SP5 confocal laser scanning microscope, with x40 or x63 oil immersion lenses. Specific fluorophores were visualised using different imaging settings. For GFP, excitation was performed using the 488 nm 20 mW argon laser, visualised with detection of 505 -530 nm emission. For RFP, excitation was performed using the 543 nm 12 mW HeNe laser, visualised by detection of 600 - 650 nm emission. mCherry was excited using the HeNe 595 nm laser, visualised using 600 – 650 nm emission detection. Depending on signal strength, the laser power used typically ranged between 30 - 50 %, and a smart gain of 800 – 1000 mV was used for PMT detectors. When using the HyD detector, a smart gain of 70 – 100% was typically used. Sequential scans were used for co-

localisation experiments, and the separate channels were overlaid using the ImageJ 64 software.

2.5.3.2. Immunofluorescence Imaging.

Likewise, immunofluorescence imaging was performed using the Leica SP5 confocal laser scanning microscope, with x40 or x63 oil immersion lenses. The nucleic acid stain, DAPI (4',6-diamidino-2-phenylindole) was excited using the 405 nm UV laser and visualised through detection of 415 – 450 nm emission. FITC (fluorescein isothiocyanate) was excited using the 488 nm 20 mW argon laser, visualised using detection of 490 – 525 emission. TRITC (tetramethylrhodamine-5-isothiocyanate) and Rhodamine were excited using the 543 nm 12 mW HeNe laser, visualised by detection of 600-700 nm emission. Sequential scans were used for co-localisation experiments, and the separate channels were overlaid using ImageJ 64 software.

2.5.4. FRET-FLIM.

FRET-FLIM was performed to assess putative protein-protein interactions between GFP-fusion proteins (donors) and RFP-fusion proteins (acceptors). Here, measurements were taken of the fluorescence lifetime of a donor GFP fusion protein, which had been expressed alone in *N. benthamiana* leaf epidermal cells using Agrobacterium-mediated infiltration (2.2.14). Fluorescence lifetime measurements of the GFP donor fusion were made again in the presence of an expressed FRET acceptor (an RFP/mCherry fusion protein), to compare the donor fluorescence lifetime when expressed alone, and when co-expressed with an acceptor. The experiment was performed using a Leica SP5 confocal laser scanning microscope with a PicoQuant FLIM LSM upgrade kit, using a x63 1.2NA water immersion lens, and running the Leica SMD FLIM Wizard. Data acquisition and analysis was performed using the PicoQuant SymPhoTime 32 software. GFP was excited with a pulsed 470 nm laser and photons counted using an internal spectral FLIM PMT detector, with a detection bandwidth of 505 – 530 nm fluorescence emission. Image acquisition was performed with the above settings until 1000

photons had been detected in the brightest pixel. Average fluorescence lifetimes were subsequently calculated using tail fitting. Data analysis and calculation of fluorescence lifetime was performed using the PicoQuant SymPhoTime 32 software.

2.5.5. Cytoskeleton-Disrupting Drug Treatments on *N. benthamiana* Leaves.

Disruption of the microtubule cytoskeleton was achieved by incubating leaf sections in 200 µM Amiprophosmethyl (Fluka, prepared from 20 mM stock in DMSO) for 1 hour. As a control, leaf sections were incubated in 0.2% DMSO, representing the highest concentration of DMSO used in the APM treatments.

Disruption of the actin cytoskeleton was performed by incubating leaf sections for 30 minutes in 50 µM Latrunculin B (Sigma, prepared from 10 mM stock in DMSO) or 40 µM Cytochalasin D (Calbiochem, prepared from 10 mM stock in DMSO). As a negative control, leaf sections were incubated in 0.5% DMSO, representing the highest concentration of DMSO used in these treatments.

2.5.6. Immunofluorescent Labelling of Narcissus Pollen Tubes.

Immunofluorescent labelling of MAP7A was performed in Narcissus pollen tubes, germinated as described in 2.5.2.3. Where transfer of pollen tubes was necessary, suspensions of pollen tubes were pipetted using a Gilson Pipetman p1000 with pipette tips cut back ≈ 1 cm from the end, as not to shear the pollen tubes during pipetting. Fixation of the pollen tubes and subsequent wash steps were performed in a 40 – 60 µm mesh strainer inserted into the wells of a 6-well plate.

Growing pollen tubes suspended in daffodil germination media were gently pipetted into the strainer inserted in a 6-well plate. To fix and permeablise the pollen tubes, the strainer was placed in a fresh well containing 4 ml fixative solution, for 30 minutes. The fixative solution consisted of 0.25 M PIPES, 0.1 M EGTA, 0.2 M $MgSO_4$, 3.7% (w/v) paraformaldehyde (Sigma), 0.02% (v/v) glutaraldehyde (Agar Scientific), 100 µM MBS ester (m-maleimidobenzoyl-N-hydroxysuccinimide ester;

Sigma), 0.02% (w/v) saponin (Sigma). The cells were washed by transferring the strainer to a new well containing 4 ml PEM buffer (0.25 M PIPES, 0.1 M EGTA, 0.2 M $MgSO_4$) for five minutes. Two more identical washes were performed by transferring the strainer to 4 ml fresh PEM buffer. Specimens were treated with cell wall-digesting enzymes for 30 minutes at room temperature, by transferring the insert to a new well containing 4 ml cell wall digestion mix (1% cellulase (Duchefa), 1% macerosyme (Duchefa), 1% pectolyase (Duchefa), 1% dricelase (Duchefa), 0.4 M mannitol (Sigma), 5 mM EGTA, 15 mM MES, pH 5). The cells were then washed 3 times in 1x PBS for 5 minutes each by transferring the strainer from well to well.

The cells were then attached to poly-L-lysine coverslips. 200µl of pollen tubes suspended in 1x PBS were pipetted onto the poly-L-lysine slides and left to adhere for 15 minutes in a humid chamber. Each coverslip was then placed face-up in a well of a 6-well plate, and 3 ml 1x PBS was carefully added. After 10 minutes, the PBS was decanted to wash the cells. Two more identical washes in PBS were performed.

Non-specific binding of antibodies was blocked by incubating the cells in blocking buffer, consisting of 2 % (w/v) bovine serum albumin (BSA: Melford) in 1x PBS. The coverslips were carefully placed face-up in a humid chamber and 200 µl blocking buffer was added to the surface of the coverslip. The samples were incubated in blocking buffer for 30 minutes at room temperature.

The specimens were then probed with primary antibody. Anti-MAP7A antibodies were diluted 1:200 - 1:300 in blocking buffer. If labelling of microtubules was also required, the rat anti-alpha tubulin antibody, YL1/2, (Serotec) was included at a dilution of 1:200. 200 µl primary antibody solution was added to the surface of each coverslip in a humid chamber. The samples were incubated in primary antibody solution overnight at 4 ºC. Samples were washed three times in 1x PBS in a 6-well plate as before. The specimens were then probed with secondary antibody, applied to the surface of coverslip in a humid chamber. FITC-conjugated donkey anti-mouse IgG secondary antibody (Jackson Immuno Research) was used to detect anti-MAP7A antibodies and was diluted 1:50 in blocking buffer. If labelling of microtubules was performed, TRITC-conjugated goat anti-rat IgG secondary antibodies (Jackson Immuno Research) were included at the dilution of 1:50. If labelling of the actin cytoskeleton was required, rhodamine-phalloidin (Molecular

Probes Inc) was added to the antibody solution at a final concentration of 0.825 nM. The samples were left for 1 hour at room temperature in a dark environment.

The coverslips were washed 3 times in 1x PBS as before. If DAPI-staining of the cell nuclei was required, DAPI (Sigma) was added to the penultimate wash at a final concentration of 4 µg/ml (diluted from a stock solution of 10 mg/ml in DMSO).

The samples were mounted in Vectashield (Vector Laboratories) and imaged using CLSM (2.5.3.2).

2.5.7. DAPI Staining of Pollen Grains.

DAPI-staining was used to determine the developmental stage of developing pollen grains of *pNET2A*:NET2A-GFP stable transgenic Arabidopsis plants, and analyse potential defects in the nuclear morphologies of dehiscent pollen grains of T-DNA mutant lines.

DAPI-staining of pollen grains was performed as described by Park et al. (1998). Whole anthers were mounted on a microscope slide in 10 µl DAPI staining solution (0.1 M phosphate buffer, pH 7 (57.8 mM Na_2HPO_4, 42.2 mM NaH_2PO_4), 1 mM EDTA, 0.1% Triton X-100 (Sigma), 0.4 µg/ml DAPI). The anthers were gently squashed under a coverslip to release the pollen grains into the DAPI staining solution. The samples were left for 10 – 30 minutes, and imaged with CLSM using a 405 nm UV excitation laser and detection of 415 – 450 nm emission.

2.5.8. DAPI Staining of Pollen Tubes.

DAPI staining was used to visualise and compare the nuclei of pollen tubes from Col-0, *map7a.1, map7b.1* and *map7a.1/map7b.1* plants. Pollen tubes were germinated on poly-L-lysine coverslips in liquid pollen germination medium as described in 2.5.2.1. The pollen germination media was removed and replaced with 100 µl fixative solution (0.25 M PIPES, 0.1 M EGTA, 0.2 M $MgSO_4$, 100 µM MBS ester and 0.02% (w/v) saponin). The samples were incubated for 30 minutes in a

humid chamber. The coverslips were placed in wells of a 6-well plate and gently washed with 3 ml 1x PBS for 10 minutes, before the PBS was decanted. The coverslips were immersed in 4 µg/ml DAPI in 1x PBS for 10 minutes. The DAPI solution was decanted and the samples were again washed in 1x PBS for 10 minutes. The samples were mounted in Vectashield and imaged using CLSM (2.5.3.2).

2.5.9. GUS Histochemical Staining.

Tissue from *pMAP7A:GUS* and *pMAP7B:GUS* stable transgenic plants was incubated in GUS staining solution (0.1 M phosphate buffer (61 mM Na_2HPO_4 and 39 mM NaH_2PO_4), 10 mM EDTA, 0.1% (v/v) Triton X-100, 0.5 mM potassium ferricyanide (Sigma), 0.5 mM potassium ferrocyanide (Sigma), pH 7, 1 mM X-Gluc (20 mM stock in DMSO (Sigma)).

To stain 7-10 day old seedlings, samples were vacuum infiltrated in 300 µl GUS buffer for 5 minutes using an Eppendorf Concentrator 5301. *pMAP7B*:GUS seedlings were incubated for 1 - 3 hours at 37 ºC depending on signal strength. *pMAP7A*:GUS seedlings were incubated for 48 hours at 37 ºC to verify lack of expression. The seedlings were cleared of pigment through serial incubations in increasing strengths of ethanol (10%, 30%, 50%, 70% and 100%).

For staining of floral tissue, whole inflorescences of 5 - 6 week-old plants were vacuum infiltrated in GUS buffer for 5 minutes. Samples were incubated at 37 ºC for 1 - 3 hours depending on signal strength. Stained tissue was repeatedly washed in 70% ethanol to clear the samples of pigment.

Samples were imaged using a Leica M165FC fluorescent stereo microscope fitted with a Panasonic 3CCD HD Camera and running Streamcatcher 1.8.0.0 software.

2.5.10. Phenotypic Analysis of Seed Set.

To assess the fertility of Arabidopsis T-DNA mutant lines, the number of seeds produced per silique was counted in each line. Siliques of plants at 6 – 8 weeks old were taken and cleared of chlorophyll using multiple washes in 70% ethanol. Following removal of chlorophyll, developing seeds were clearly visible and were counted under an Olympus SZH10 Research Stereo Microscope. Image acquisition was performed using the QImaging QICAM digital camera and Improvision Openlab 5.5.0 software.

2.6. Plant Growth Conditions.

2.6.1. *Nicotiana benthamiana* Growth Conditions.

N. benthamiana seeds were sown directly onto compost (seed and modular compost plus sand; F2 + S (Levington)) to establish a seedling nursery. The nursery was covered with a plastic propagator lid to maintain humidity and was transferred to a growth chamber under a 16/8 hour day/night photoperiod (daytime light intensity of 150 µmol/m^2sec), with temperatures of 24 °C and 21 °C during the day and night respectively. After approximately 3 weeks, the seedlings were transplanted into individual 10 cm pots and returned to the growth chamber until 5 – 6 weeks old.

2.6.2. Arabidopsis Growth Conditions.

Seeds were surface sterilised by first washing in 70% ethanol for 15 minutes, and then in 6% sodium hypochlorite (BDH) + 0.1% triton X-100 for 15 minutes. The seeds were then washed 3 times in sterile distilled water. Sterilised seeds were sown in Petri dishes onto half-strength Murashige and Skoog (½MS) basal salt mixture (Duchefa; pH 5.7 with KOH) containing 0.8% (w/v) plant agar (Duchefa). Plates were sealed with micropore tape (3M) and placed in darkness for 3 days at 4 °C to stratify the seeds. Subsequently, the plates were transferred to a temperature-controlled Sanyo growth cabinet with a 16/8 hour photoperiod (daytime light intensity of 150 µmol/m^2sec), and temperatures of 22 °C and 16 °C during the

day and night respectively. After 12 – 15 days growth, seedlings were transferred into plastic trays containing compost (seed and modular compost plus sand; F2 + S (Levington)) that had been autoclaved to remove pests. Plants were grown in the Sanyo growth cabinet or a walk-in growth chamber using the growth settings described above. Trays were covered with a propagator lid to retain humidity until the plants were fully established.

2.6.3. Cross-Pollination of Arabidopsis Plants.

Cross-pollination of Arabidopsis plants was used to generate the *pNET2A*:NET2A-GFP/*pLAT52*:FABD2-RFP and *pNET2A*:NET2A-GFP/*pLAT52*:*At*PRK4-RFP stable transgenic lines, and the *map7a.1/map7b.1* double T-DNA mutant line. Cross-pollination was performed under a dissection microscope using forceps. Unopened flowers from one transgenic line were dissected and the anthers removed to prevent self-pollination. Anthers taken from the second transgenic line were brushed against the papillae of the stigma to cover it in pollen. After 3 – 4 days, successful pollination was indicated by purple colouring of the silique. Mature siliques were carefully removed and placed in a microcentrifuge tube to dry.

2.6.4. Arabidopsis Seed Collection.

The ARACON container system (Betatech) was used to collect seeds from individual Arabidopsis plants. ARACON bases were placed centrally over rosettes, and Aracon tubes enclosed the stem following floral bolting. Plants were grown to maturity and senescence in Sanyo growth cambers or a growth room, and seeds were collected and left to dry for a minimum of 2 weeks.

2.6.5. Selection of Transgenic Arabidopsis Plants.

Arabidopsis plants were stably transformed through the floral dipping method and seeds of the dipped plants were collected and dried (2.2.15). Seeds were sown on

½ MS media plates (2.6.2) containing the appropriate antibiotic or herbicide to select for plants transformed with the construct of interest, and also supplemented with 200 µg/ml timentin (Ticarcillin: Melford) to prevent growth of residual Agrobacterium. Seeds were sown on 3 – 4 20 mm Petri dishes (Fisher), which would typically yield 10 – 30 transformants. After 12 – 15 days, plants growing on selective media were transferred to soil and grown as described in section 2.6.2.

Chapter 3: Reverse-Genetic Analysis of the NET2 Subfamily.

3.1. Further Reverse-Genetic Analysis of *NET2A.*

3.1.1. Introduction.

In this study, reverse genetics was employed to elucidate the functional role of NET2A in Arabidopsis. Identification of a phenotype arising from the mutation of a specific gene can help to shed light on the normal function of the endogenous protein that it encodes, and the cellular processes that it may be involved in.

A previous study using reverse genetic analysis of *NET2A*, potentially identified a *net2a* loss-of-function mutant. In that study, the T-DNA mutant line, SALK_020898, was selected for investigation as a transcriptional null mutant, and a *net2a* knockout line (Dixon. 2013). The SALK_020898 T-DNA mutants, hereafter referred to as *net2a.1*, was shown to have no major phenotype in growing pollen tubes, but exhibited a minor defect in the morphology of the vegetative nucleus in a small proportion of developing pollen grains (Dixon. 2013). Further analysis during the course of this study suggests that in contrast to the observations of Dixon. (2013), *net2a.1* was in fact not a transcriptional null mutant, and produced an abundance of *NET2A* transcript. It is possible that the subtle differences observed between the *net2a.1* mutant and Col-0 control may have been due to experimental variation arising from the invasive specimen preparation techniques used in this experiment. Analysis of the *net2a.1* mutant was subsequently abandoned, and alternative *net2a* mutants were identified for further investigation. In addition to this, *net2b* and *net2d* mutants were also identified and investigated to widen our understanding of the roles of the NET2 protein family in Arabidopsis.

3.1.2. Re-analysis of the SALK_020898 (*net2a.1*) T-DNA Line as a Transcriptional Null Mutant.

3.1.2.1. Analysing the Transcriptional Activity of *NET2A* in the SALK_020898 (*net2a.1*) T-DNA Mutant Line.

RT-PCR was employed to determine whether the transcription of *NET2A* was abolished in the *net2a.1* mutant. RNA was extracted from *net2a.1* mutant plants and used as a template from which to synthesise cDNA. The cDNA generated from each sample therefore represents the total mRNA transcribed in the collected tissue, and can be used as template for RT-PCR, in order to analyse the transcriptional activity of a specific gene. RT-PCR involves PCR amplification of gene coding sequences with gene-specific primers using cDNA as template. If an mRNA transcript is present amongst the total mRNA in a collected sample, the sequence will be present in the generated cDNA and can be amplified by PCR. If the mRNA is absent, no PCR amplification will be observed. Therefore, if the *net2a.1* mutant was indeed a transcriptional null, no *NET2A* transcript would be detectable by RT-PCR.

RNA was extracted from whole inflorescences of *Col-0* and *net2a.1* plants as described in chapter 2.2.7. The total quantity of RNA used for cDNA synthesis was normalised to 1 µg, and cDNA was generated using the GoScript Reverse Transcriptase System with oligo(dT)15 primers, as described in chapter 2.2.8. The resulting cDNA was used as template for RT-PCR reactions.

Figure 3.1 shows a schematic diagram of the SALK_020898 T-DNA allele of *NET2A*, with the locations of the primers used for RT-PCR. The primers 2A_DS-F and 2A_DS-R were designed to PCR amplify a 229 bp fragment of *NET2A*, which could only be observed if *NET2A* was transcriptionally active in the sample from which the cDNA was generated. Using these primers, RT-PCR was performed on floral cDNA from Col-0, *net2a.1*, and on deionised water; included as a negative control to ensure that PCR product could only be amplified from cDNA. Amplification of a 187 bp fragment of the housekeeping gene *ELONGATION FACTOR*-1α (EF-1α) was also performed as a positive control, to ensure similar quantities of Col-0 and *net2a.1* template cDNA were used for RT-PCR (Czechowski et al. 2005).

Figure 3.1: Schematic Diagram of the *net2a.1* (SALK_020898) T-DNA Mutant Allele, Including the Positions of Primers used for RT-PCR Analysis. Promoter regions are shown in green, exons in blue, introns in grey and the 3' UTR in yellow. The T-DNA insertions are represented by the red triangle. Primers used for genotyping (2A_DS-F and 2A_DS-R) are represented by white arrows, labelled with the identity of each specific primer. Numbers below the gene diagram correspond to base pairs after the start codon.

The results of the RT-PCR on the *net2a.1* mutant are displayed in figure 3.2. The 2A_DS-F and 2A-DS-R primers were able to amplify a 229 bp fragment from Col-0 floral cDNA, indicating that the primers were able to detect the *NET2A* transcript using RT-PCR. The 229 bp band was also detected in cDNA generated from *net2a.1* floral cDNA, demonstrating that the *NET2A* transcript was also detectable in the *net2a.1* mutant. No band was detected in the H_2O control, showing that no amplification of PCR product had resulted from contamination of the PCR reaction mixture with DNA template. Using the *EF-1a* gene-specific primers, equal amounts of PCR product were generated from both Col-0 and *net2a.1* cDNA, demonstrating that similar quantities of cDNA template were used for RT-PCR on both lines.

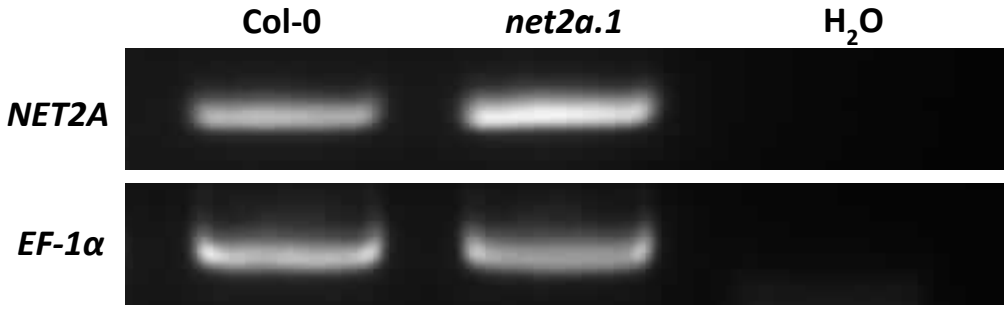

Figure 3.2: RT-PCR Analysis of *NET2A* Transcriptional Activity in the *net2a.1* Mutant. Top row: 223 bp band amplified using the *NET2A* gene-specific primers 2A_DS-F and 2A_DS-R. Bottom row: 187 bp band amplified from the housekeeping gene, *EF-1α*, as a positive control. RT-PCR was performed on cDNA extracted from Col-0 (left column), *net2a.1* (centre column), and H_2O (right column).

The detection of *NET2A* transcript in the *net2a.1* mutant shows that the mutant allele is transcriptionally active, in contrast to previous reports (Dixon. 2013). It was determined that the 229 bp PCR band generated from *net2a.1* cDNA could not have been amplified from contaminating gDNA, which can persist in cDNA from the RNA extraction process. Using primers to amplify a 256 bp fragment of the *Actin-2* (*ACT2*) transcript sequence, it is possible to detect and discern amplicons generated from cDNA, and those generated from gDNA. The *ACT2* primer annealing sites lie either side of an intron in the *ACT2* gene, which is spliced and removed from the *ACT2* transcript. The 256 bp fragment amplified by the *ACT2* primers corresponds to the *ACT2* transcript lacking the intron sequence, whereas the *ACT2* amplicons generated from gDNA include the intron sequence and have size of 342 bp. Therefore, detection of amplicons at 342 bp with *ACT2* primers is indicative of gDNA contamination of template cDNA. Using the *ACT2* primers, RT-PCR was performed on *net2a.1* cDNA to ensure it contained no gDNA template. As shown in figure 3.3, no PCR band of 342 bp was observable in cDNA generated from *net2a.1* mutant, indicating it contained no contaminating gDNA. Therefore, the 229 bp amplicon generated from *net2a.1* cDNA using 2A_DS-F and 2A_DS-R must have been from *NET2A* transcript template, proving that *NET2A* must still be transcriptionally active in the *net2a.1* mutant.

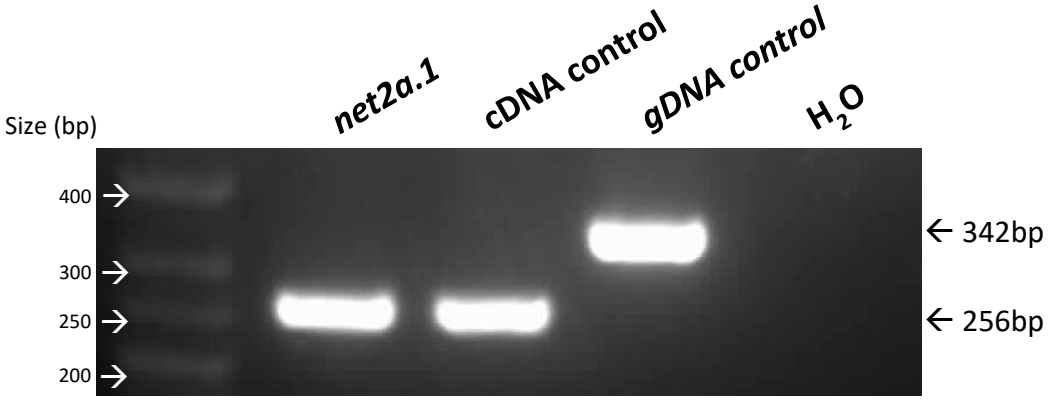

Figure 3.3: RT-PCR Analysis of gDNA Contamination in *net2a.1* cDNA Samples. PCR amplification was performed with *ACT2*-specific primers. *net2a.1* = amplicon generated using *net2a.1* cDNA. cDNA control = cDNA known to be free of gDNA contamination was used as template. gDNA control = gDNA used as template. H_2O = PCR reaction performed on deionised water. Bioline Hyperladder 25bp was used as a molecular weight marker.

It was therefore concluded that the *net2a.1* T-DNA line was in fact not a transcriptional null mutant of *NET2A*, and further analysis of this mutant line was subsequently abandoned. Although it is possible that the SALK_020898 T-DNA insertion may have reduced the transcription of *NET2A* in the *net2a.1* mutant, (as is frequently reported of mutant lines with T-DNA insertions lying in gene promoter regions (section 3.1.3.2; Wang. 2008)), further attempts to quantify potential reductions in *NET2A* transcription were not undertaken. The quantity of PCR product amplified from the *NET2A* transcript in the *net2a.1* mutant cDNA appeared roughly similar to that of Col-0. This indicates that little difference, if any, existed between the levels of *NET2A* transcript in the Col-0 and *net2a.1* mutant cDNA: and thorough quantification of this difference would not be worthwhile. Furthermore, Western-blot analysis of NET2A protein levels in *net2a.1* mutant flowers was not performed: it was concluded that any small variations in *NET2A* transcript levels in the *net2a.1* mutant would not result in a difference in NET2A protein levels that could be accurately quantified using western blotting. Instead, alternative *net2* mutants were identified and investigated, in order to elucidate the functional role of NET2A and other NET2 family members in Arabidopsis.

3.2. Analysis of Alternative *net2* T-DNA Mutant Lines.

3.2.1. An Introduction to T-DNA Mutants.

As described above, the previously described T-DNA insertion mutant, *net2a.1* (SALK_020898), was shown not to be a transcriptional null mutant and was not studied further. Therefore, in order to elucidate the functional role of NET2A using reverse genetics, alternative *net2a* mutants were analysed.

In addition to this, wider analysis of the other NET2 family members was also performed: there may exist potential redundancy between the closely related NET2 family members, as has been reported in the NET1 and NET3 subfamilies (Wang et al. 2014; Calcutt. 2009; Ingle. 2011). NET2A and NET2B are demonstrated to interact with each other (chapter 5), and both share common interacting partners in *At*PRK4 & *At*PRK5 (chapter 6), indicating that NET2A may share functional roles with other NET2s. Therefore, investigating other members of the NET2 protein

family may provide insight into the functional role of NET2A itself. Furthermore, the potential for functional redundancy between NET2s may result in no phenotype being observable from mutation of a single family member, as the absence of one gene may be compensated for by the function of another. In this case, generation of transgenic lines in which multiple gene family members have been knocked out would be required to elicit an observable phenotype. Therefore, identification and characterisation of mutant lines for each NET2 family member will be required before this can be achieved.

Readily available T-DNA insertion lines are a commonly used resource for the generation and acquisition of Arabidopsis mutants. T-DNA insertion mutants are generated through *Agrobacterium tumefaciens*-mediated T-DNA insertion at random sites in plant genomic DNA: commonly ranging in size from 5 - 25 kb, the insertion of the T-DNA into the promoter or coding region of a host gene is capable of disrupting gene function (Krysan et al. 1999). Curated by the Nottingham Arabidopsis Stock Centre (NASC), mass-generated T-DNA insertion lines by groups such as the SALK Institute Genomic Analysis Laboratory (SIGnAL) and GABI-Kat, are made publicly available, providing a rich resource from which to obtain potential T-DNA mutants. For example, SIGnAL have demonstrated the generation and cataloguing of 88,000 insertions, resulting in mutagenesis of 21,700 genes at the time of publication (Alonso et al. 2003).

This section describes the identification of *net2a, net2b and net2d* mutants from promising candidate T-DNA insertion lines obtained from NASC, validation of transcriptional inactivation of the corresponding *NET2* gene, and subsequent phenotypic analysis of the confirmed mutants.

3.2.2. Analysis of *net2a*, *net2b*, *net2c* and *net2d* T-DNA Insertion Lines.

The SIGnAL T-DNA Express Arabidopsis Gene Mapping Tool provides a summary of identified T-DNA insertion events and their insertion positions in Arabidopsis chromosomes, as mapped by PCR and sequencing analysis. Using this tool, desirable T-DNA insertion lines were identified, in which the expression of the conveying *NET2* gene may be disrupted.

The position of a T-DNA insertion within a gene is very important in determining its effect and potency in disrupting gene expression. It is known that T-DNA insertions lying in the exons are highly effective in abolishing gene transcription. However, the effects of those lying in introns can be negated by removal of the T-DNA sequence from the transcript during splicing, and T-DNA inserted in promoter regions are likely to reduce gene expression as opposed to abolishing it (Wang. 2008). Therefore, only desirable T-DNA insertions, likely to result in the knockout of *NET2* transcription, were selected to investigate. Schematic maps of selected T-DNA alleles with the positions of their T-DNA insertions (as identified by sequencing of insert genotyping PCRs (3.1.3.3, figure 3.5)), are shown in figure 3.4, and summarised in table 3.1.

Available *net2a* T-DNA lines were previously analysed by Dixon. (2013). In addition to SALK_020898, the T-DNA lines SALK_065094 and GABI_234H12 were also investigated: qRT-PCR analysis indicated ≈100% levels of *NET2A* transcript downstream of the T-DNA insertion sites in both of these lines, indicating that *NET2A* transcription had not been abolished. Investigation of SALK_065094 and GABI_234H12 was subsequently discontinued. SALK_065094 lies in the *NET2A* promoter, seemingly having no effect on *NET2A* transcription. Meanwhile, GABI_234H12 lies in the second exon of the *NET2A* coding sequence (figure 3.4, table 3.1). Exon-located T-DNA insertions have been reported to be very effective in disrupting transcription (Wang. 2008). It is therefore very likely that the GABI_234H12 T-DNA insertion should have an effect on *NET2A* transcription, despite the presence of transcript detected by Dixon. (2013). It could be that transcription of the *NET2A* coding region downstream of the GABI_234H12 T-DNA insertion may be driven by an element within the T-DNA itself, whilst endogenous *NET2A* transcript could potentially be absent (Wang et al. 2008). Further transcriptional analysis of *NET2A* in the GABI_234H12 T-DNA line was therefore commenced to investigate this. The GABI_234H12 mutant will be referred to as *net2a.2* in this study.

Two promising *net2b* T-DNA mutant lines were selected for investigation: GABI_486H12 and GABI_132E08, both located early within the second exon of the *NET2B* coding sequence. GABI_486H12 will be referred to as *net2b.1*, and GABI_132E08 as *net2b.2*.

For NET2D, two T-DNA insertion mutants were selected for analysis: SALK_042729 and SALK_035401 are located in the second exon of the *NET2D* coding sequence

and are highly likely to disrupt *NET2D* transcription. The selected T-DNA lines were available as homozygous seed stocks and were therefore preferable to the other available T-DNA insertion mutant lines, SALK_003561 and SALK_003553; which were available as segregating lines from which a homozygote for the T-DNA allele must be screened and isolated. SALK_042729 will henceforth be referred to as *net2d.1*, and SALK_035401 as *net2d.2*.

NET2A

GABI_234H12
(*net2a.2*)

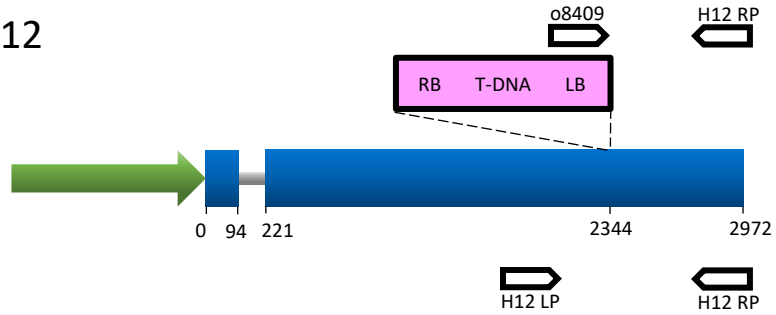

NET2B

GABI_486H12
(*net2b.1*)

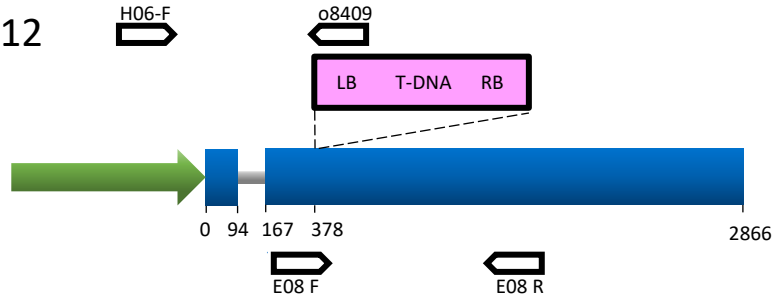

GABI_132E08
(*net2b.2*)

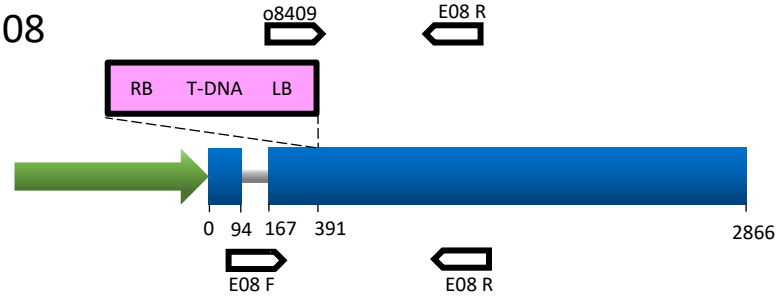

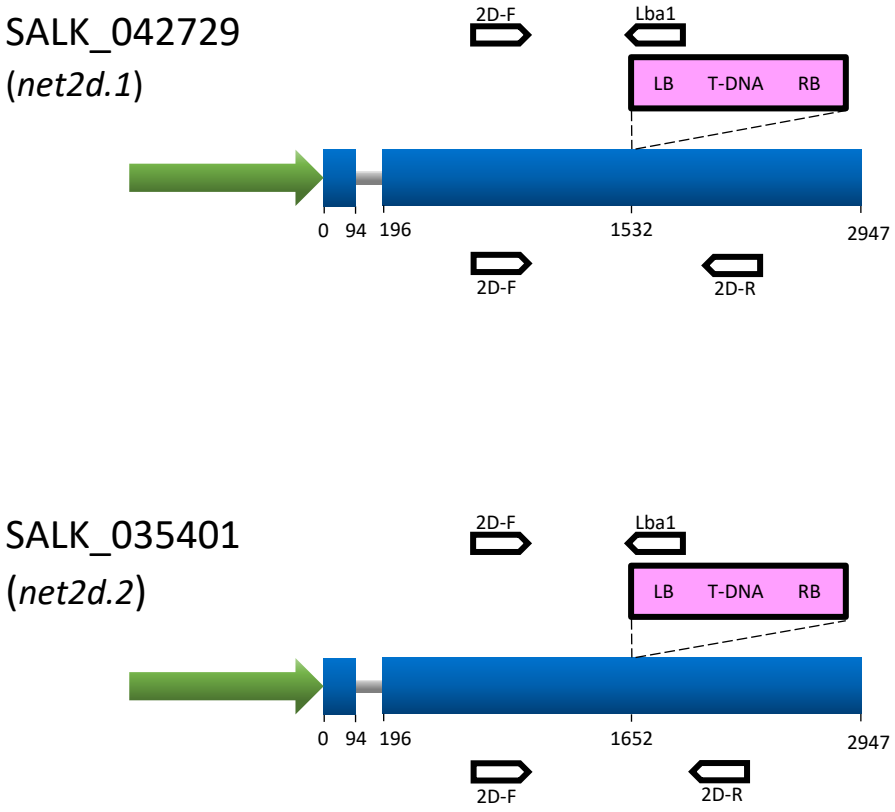

Figure 3.4: Schematic Diagram of T-DNA Mutant Alleles Selected for Analysis, Including Positions of the T-DNA Insertion Sites and Primers used for Genotyping. Promoter regions are shown in green, exons in blue and introns in grey. The T-DNA insertions are represented by the pink box, labelled with the left border (LB) and right border (RB). Primers used for genotyping are represented by white arrows, with insert-specific primers above, and gene-specific primers below the gene. Numbers below the gene diagram correspond to base pairs after the start codon.

A relatively poor selection of T-DNA insertion mutant lines was available for NET2C. Only one desirable T-DNA line, GABI_322B10, was found to exist and was located in the *NET2C* promoter region (-90 bp), making it less likely to have a pronounced effect on *NET2C* transcription than an exon-located T-DNA insertion. With a poor selection of *net2c* T-DNA mutant candidates available, reverse-genetic analysis of NET2C using T-DNA mutant lines was not pursued further.

3.2.3. Identification of Homozygous *net2a*, *net2b* and *net2d* T-DNA Mutants.

In order to knock-out a gene of interest, T-DNA mutant lines must be homozygous for the T-DNA mutant allele to eliminate transcription of the WT allele. Therefore, PCR genotyping was performed to screen for and confirm homozygosity of the T-DNA mutant alleles in each mutant line.

PCR genotyping involves two types of PCR reactions, both performed on genomic DNA extracted from T-DNA mutant plants. The first, called the 'insert PCR', is used to determine the presence of the T-DNA insertion in a gene of interest, by amplifying a PCR product using a gene-specific primer and a primer specific to the T-DNA left border. Using agarose gel electrophoresis, the presence of the T-DNA insertion can be confirmed only if a band of the predicted size, known as the 'insert band', is observed.

Having confirmed the presence of the T-DNA insert, the second PCR genotyping reaction performed is the 'WT PCR', in which a pair of gene specific-primers, flanking the T-DNA insertion site are used to amplify a PCR product, (typically of ≈1kb). This 'WT band' is only visible on an agarose gel if a plant carries the WT allele of a gene of interest: a T-DNA insertion, ranging in size from 5 - 25 kb, is too large for taq polymerase to extend in the time permitted to extend the 1 kb band specified using the gene specific primers. Therefore, if a plant is homozygous for the T-DNA mutant allele of a gene of interest, no 'WT PCR' band will be observable.

Genomic DNA was extracted from T-DNA insertion mutants and Col-0, (chapter 2.2.9) and PCR genotyping was performed. Table 3.1 displays the primers used for the insert PCR and WT PCR reactions, and the predicted sizes of PCR bands observable using agarose gel electrophoresis. Homozygotes of the *net2a.2* T-DNA mutant, GABI_234H12, had been previously identified by Dr Martin Dixon (2013).

Mutant Line	T-DNA Allele	Insert Position	Insertion Type	Primers for Insert PCR	Insert PCR Size (bp)	Primers for WT PCR	WT PCR Size (bp)
NET2A							
net2a.1	GABI_234H12	2330	exon	o8409 + H12 RP	543	H12 LP + H12 RP	1080
NET2B							
net2b.1	GABI_486H06	378	exon	o8409 + H06-F	1133	E08-F + E08-R	996
net2b.2	GABI_132E08	391	exon	o8409 + E08-R	925	E08-F + E08-R	996
NET2D							
net2d.1	SALK_042729	1380	exon	2D-F + Lba1	1049	2D-F + 2D-R	1048
net2d.2	SALK_035401	1403	exon	2D-F + Lba1	1069	2D-F + 2D-R	1048

Table 3.1: Details of *net2a*, *net2b* and *net2d* T-DNA Insertion Mutants Selected for Analysis. Included are the locations of the T-DNA insertions for each mutant, the primers used for PCR genotyping and the expected sizes of insert and WT PCR bands.

Figures 3.5 and 3.6 show examples of insert PCR and WT PCR reactions performed on homozygotes of each T-DNA mutant line analysed. The insert PCRs clearly indicate that the T-DNA inserts were present in the mutant lines of interest, as shown by the presence of the predicted PCR band for each allele (table 3.1). Corresponding bands were not amplified from Col-0 genomic DNA, demonstrating that PCR amplification of each insert band was reserved specifically to the T-DNA allele of interest.

The WT PCRs demonstrate the absence of the WT allele of the conveying gene of interest in each T-DNA mutant described above. Using the primers described in table 3.1, predicted WT bands were clearly observable following WT PCR on Col-0 genomic DNA, but were conspicuously absent when performed on genomic DNA of the mutant of interest. This indicates insertion of the T-DNA allele into both chromosomal copies of the gene of interest, and demonstrates the plant to be homozygous for the T-DNA allele in question.

Having identified plants homozygous for each of the described *net2* T-DNA alleles, RT-PCR was performed to confirm that transcription of the conveying *NET2* genes had been disrupted.

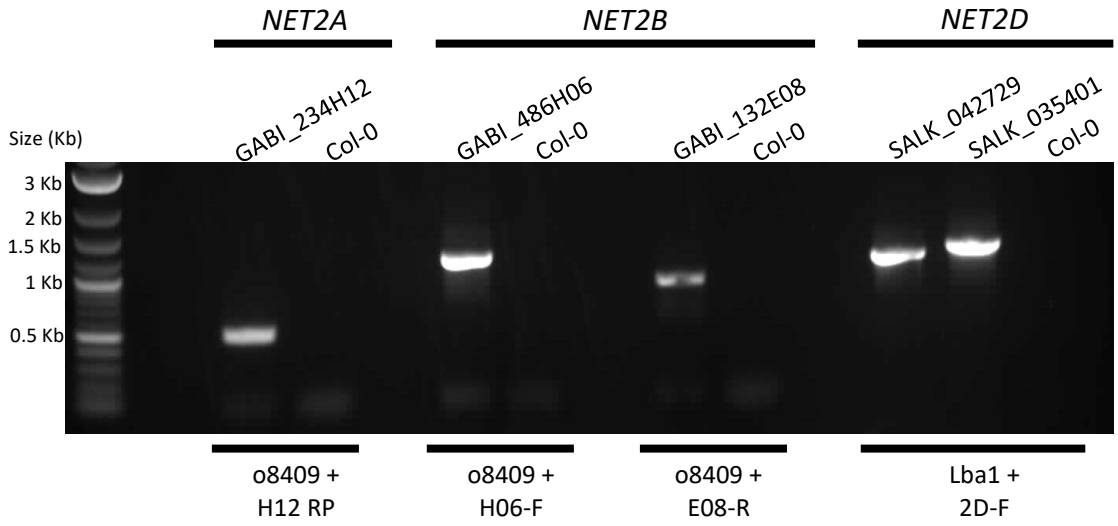

Figure 3.5: Example Insert PCR Reactions Performed to Genotype *net2a*, *net2b* and *net2d* T-DNA Mutants. PCR reactions performed on genomic DNA extracted from homozygous T-DNA mutant lines and Col-0 control plants. The insert-specific primers used to amplify the insert band are stated below the gel. 2-Log DNA ladder was used as a molecular weight marker.

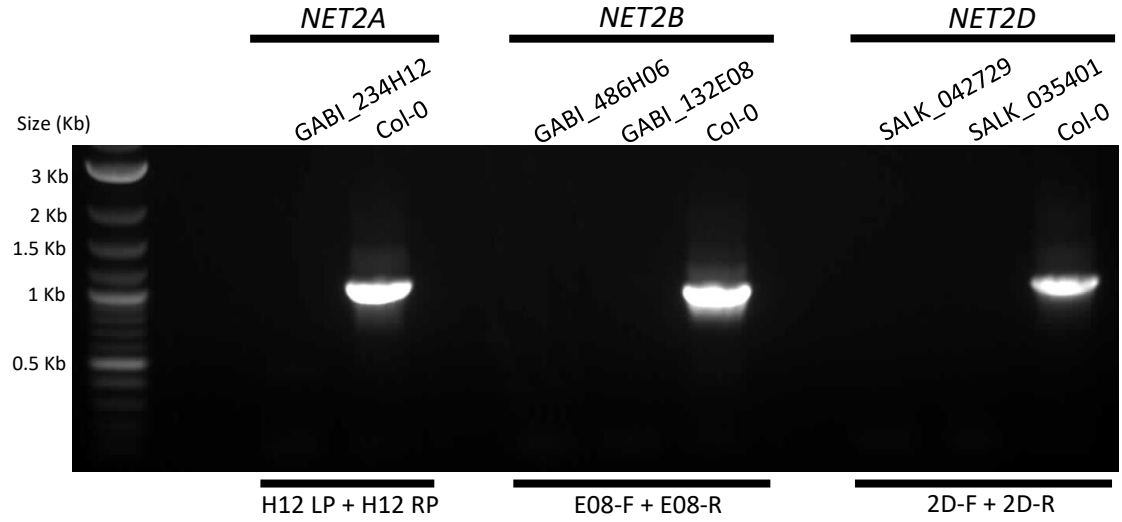

Figure 3.6: Example WT PCR Reactions Performed to Genotype *net2a*, *net2b* and *net2d* T-DNA Mutants. PCR reactions performed on genomic DNA extracted from homozygous T-DNA mutant lines and Col-0 control plants. The gene-specific primers used to amplify the WT band are stated below the gel. 2-Log DNA ladder was used as a molecular weight marker.

3.2.4 Confirmation of *NET2A*, *NET2B* and *NET2D* Transcript Absence in *net2a*, *net2b* and *net2d* T-DNA Mutants using RT-PCR.

In the previous section, it was confirmed that each of the T-DNA mutant lines described were homozygous for their respective T-DNA mutant alleles. RT-PCR was therefore performed to ensure that the transcriptional activity of each mutant allele was abolished in the corresponding T-DNA mutant lines.

RNA extraction and cDNA synthesis was performed as described in chapter 2.8 and 2.9, to generate cDNA for use as template for RT-PCR. Using the specific primer combinations listed in table 3.2 and figure 3.7, PCR amplification of target sequences upstream and downstream of the T-DNA insertion sites of each mutant allele was performed, as well as sequences spanning the T-DNA insertion site itself. Using these primer combinations, RT-PCR was performed to detect transcript in Col-0 positive control cDNA, T-DNA mutant cDNA, and on deionised water; included as a negative control. As a positive control, RT-PCR amplification of the housekeeping gene*, EF-1α*, was also performed to ensure similar cDNA template quantity was used for each reaction (Czechowski et al. 2005).

Figure 3.8 shows the results of the RT-PCR reactions performed to investigate the transcriptional activity of the *net2a.2*, *net2b.1*, *net2b.2*, *net2d.1* and *net2d.2* T-DNA mutant alleles.

Analysis of *NET2A* transcriptional activity in the *net2a.2* mutant line was performed. Using RT-PCR on Col-0 cDNA template, it was determined that the primer pairs listed in table 3.2 were able to detect and amplify the correct target cDNA sequences. The upstream and flanking primer pairs were unable to amplify the corresponding PCR fragments from *net2a.2* cDNA, however transcript could be detected downstream of T-DNA insertion site using the downstream primers. Detection of a downstream band in the *net2a.2* mutant was also reported previously (Dixon. 2013), and it should be noted that no gDNA contamination could be detected in the *net2a.2* cDNA using RT-PCR with *ACT2* primers (figure 3.9). It is possible that the region downstream of the GABI_234H12 T-DNA insertion is still endogenously transcribed in the *net2a.2* mutant line, or it could be that an element within the T-DNA itself is able to promote transcription of the downstream *NET2A* genomic sequence. Regardless, no endogenous *NET2A* transcript could be detected upstream of the T-DNA insertion site, or using primers flanking the T-DNA insertion site, indicating that the GABI_234H12 T-DNA insertion had disrupted transcription at these sites in the *net2a.2* mutant.

NET2A

net2a.2

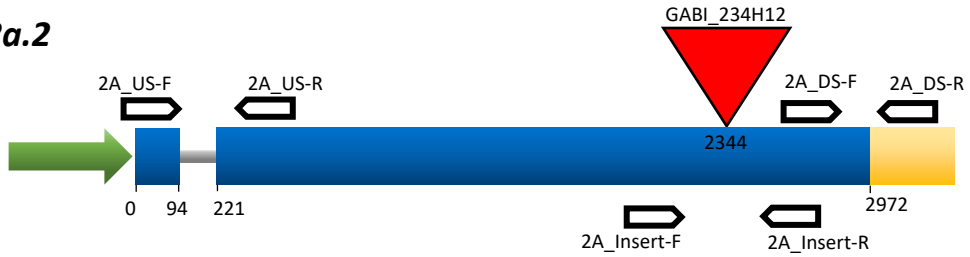

NET2B

net2b.1

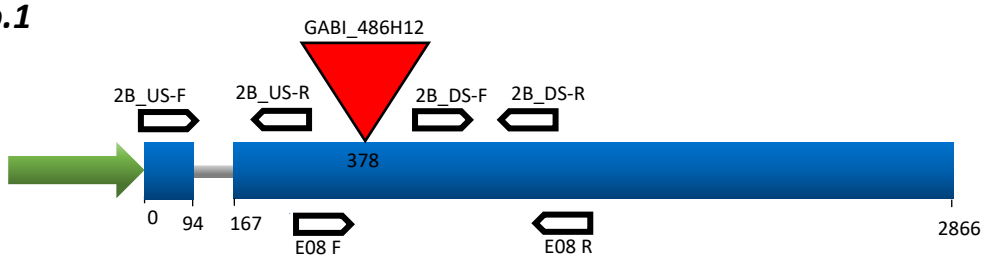

net2b.2

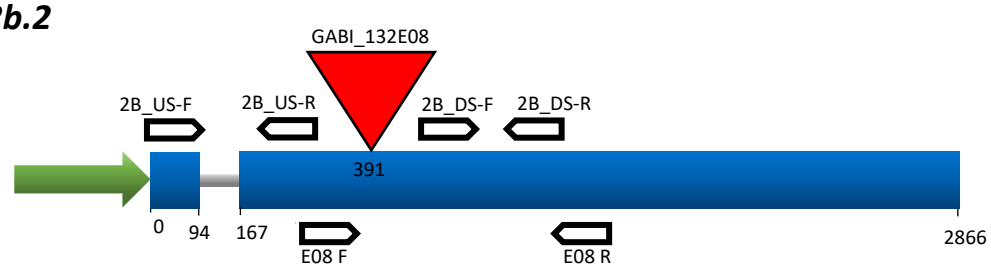

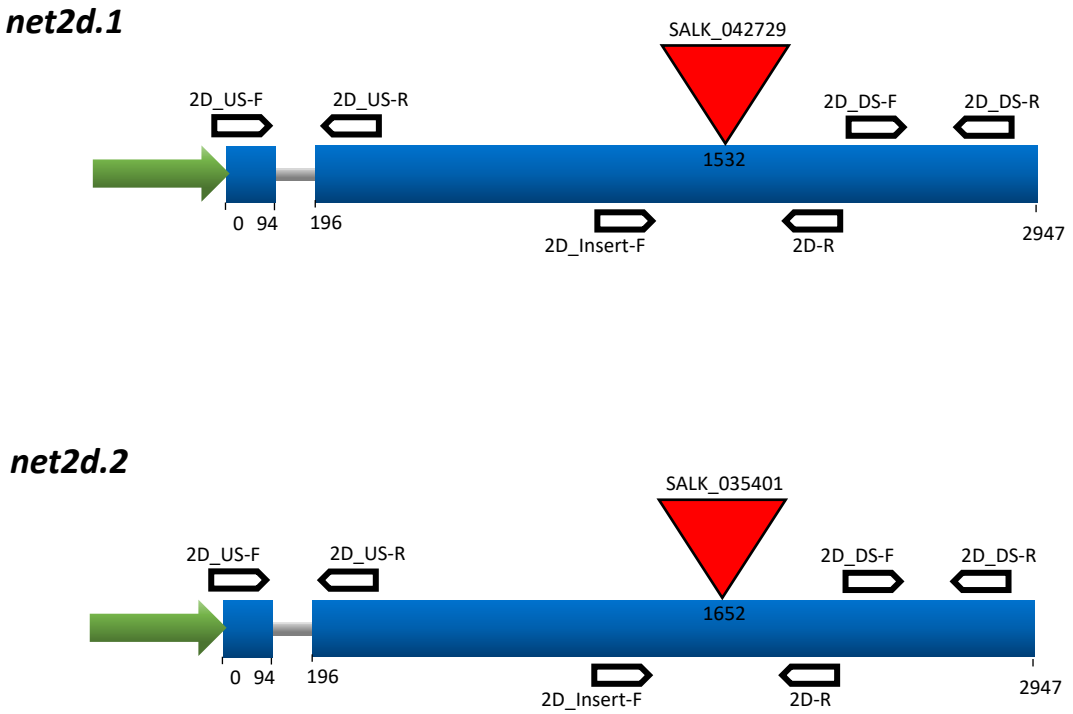

Figure 3.7: Schematic Diagram of *net2* T-DNA Mutant Alleles, Including Positions of Primers used for RT-PCR Analysis of Transcriptional Activity. Promoter regions are shown in green, exons in blue, introns in grey and the 3' UTR in yellow. The T-DNA insertions are represented by the red triangle. Primers used for RT-PCR are represented by white arrows, labelled with the identity of each specific primer. Numbers below the gene diagram correspond to base pairs after the start codon.

Gene	Mutant Line	Upstream Primers	Upstream Band Size	Flanking Primers	Flanking Band Size	Downstream Primers	Downstream Band Size
NET2A	*net2a.2*	2A_US-F + 2A_US-R (1)	362 bp	2A_Insert-F + 2A_Insert-R (2)	222 bp	2A_DS-F + 2A_DS-R (3)	229 bp
NET2B	*net2b.1*	2B_US-F + 2B_US-R (4)	174 bp	E08-F + E08-R (5)	996 bp	2B_DS-F + 2B_DS-R (6)	168 bp
	net2b.2						
NET2D	*net2d.1*	2D_US-F + 2D_US-R (7)	174 bp	2D_Insert-F + 2D-R (8)	550 bp	2D_DS-F + 2D_DS-R (9)	280 bp
	net2d.2						

Table 3.2: List of Primers used for RT-PCR Analysis of *net2a.2*, *net2b.1*, *net2b.2*, *net2d.1* and *net2d.2* Mutant Transcriptional Activity. Upstream primers are used to amplify PCR product from template sequences upstream of the T-DNA insert. Flanking primers amplify gene-specific sequences spanning the T-DNA insertion site of the corresponding mutant. Downstream primers amplify sequences downstream of the T-DNA insertion site. Included are the predicted sizes of amplicons generated using each primer set. Numbers associated with each primer pair correspond to the amplified PCR products shown in figure 3.8. Diagrammatic details of the locations of each primer are displayed in figure 3.7, and the sequences of each primer are shown in appendix 1.

RT-PCR was then employed to confirm that the transcriptional activity of *NET2B* was disrupted in the *net2b.1* and *net2b.2* mutants. Due to the close proximity of the GABI_486H06 and GABI_132E08 T-DNA insertion sites, the same primer sets could be used to analyse both *net2b.1* and *net2b.2* mutant lines. RT-PCR on Col-0 cDNA, using primer sets targeting the regions upstream of, downstream of, and spanning the T-DNA insertion sites generated amplicons of predicted size. In the *net2b.1* mutant, no upstream or downstream band was amplified, nor was a band using primers flanking the GABI_486H06 T-DNA insertion site. This indicates the *net2b.1* line is a full transcriptional null mutant. In contrast, upstream and downstream bands could be amplified from *net2b.2* cDNA. Notably however, no band could be amplified using primers flanking the GABI_132E08 T-DNA insertion site, indicating that the *net2b.2* cDNA had not been contaminated with DNA from another line: amplification of a PCR fragment of predicted size using the primers E08-F and E08-R could only occur if WT DNA template were present. Furthermore, no contaminating gDNA could be detected in the *net2b.2* cDNA using *ACT2* primers (figure 3.9). It is possible that endogenous transcription of *NET2B* continues through the T-DNA insert in the *net2b.2* mutant, in which case the sequence of the T-DNA would be included in, and interrupt, the open reading frame of the *NET2B* mRNA transcript; rendering it non-functional (Wang. 2008).

The *net2d.1* and *net2d.2* mutant lines were also analysed for *NET2D* transcriptional activity using RT-PCR. In a similar fashion to the *net2b* mutant lines described above, the *net2d.1* and *net2d.2* mutants could be analysed using the same primer sets, due to the close proximity of the SALK_042729 and SALK_035401 T-DNA insertion sites. Using primers designed to amplify PCR product upstream of, downstream of, and across the SALK_042729 and SALK_035401 T-DNA insertion sites, it was that amplicons of the correct size could be generated from Col-0 cDNA by RT-PCR. However, the corresponding PCR products could not be amplified from the cDNA of *net2d.1* and *net2d.2* mutants, indicating that both lines constitute complete transcriptional null mutants.

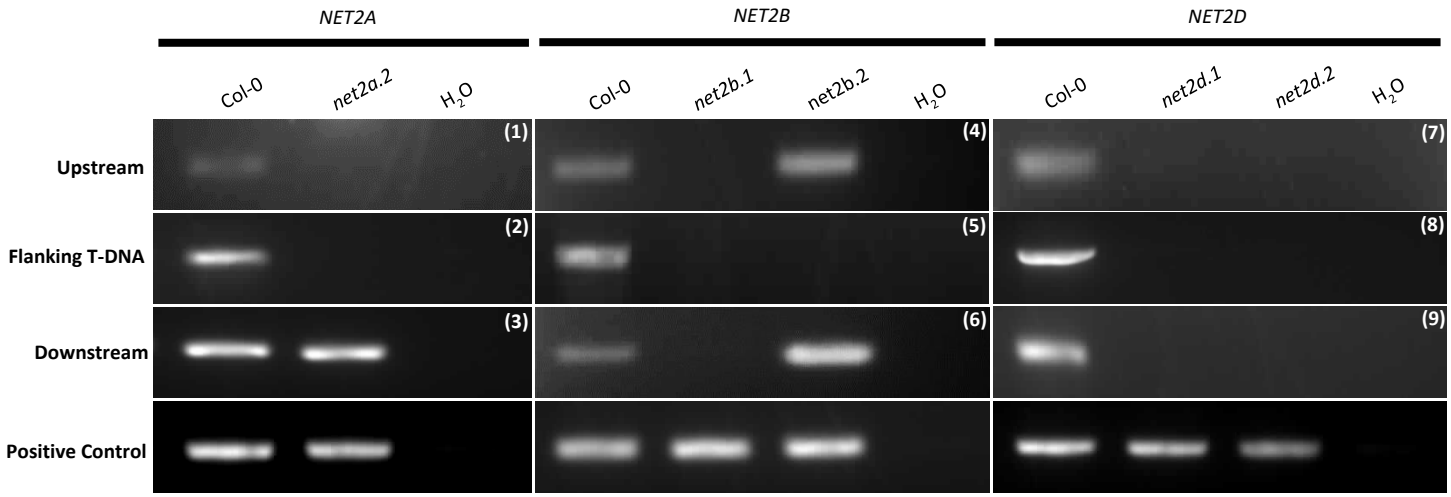

Figure 3.8: Analysis of the Transcriptional Activity of *net2a.2*, *net2b.1*, *net2b.2*, *net2d.1* and *net2d.2* Mutants using RT-PCR. Using gene-specific primers**,** bands were generated by PCR amplification of sequences upstream (top row), across (second row) and downstream (third row) of the T-DNA insertion site of each mutant. To ensure each cDNA sample contained similar quantities of cDNA template, amplification of a 187 bp sequence from the housekeeping gene, EF-1α, was performed (bottom row). RT-PCR using each gene-specific primer set was performed on Col-0 cDNA, the corresponding *net2* mutant cDNA, and deionised water as a negative control. The numbers in the top right-hand corner of each panel correspond to the specific primer pairs used to amplify the PCR product, as shown in table 3.2. The predicted sizes of the PCR products amplified are also shown in table 3.2.

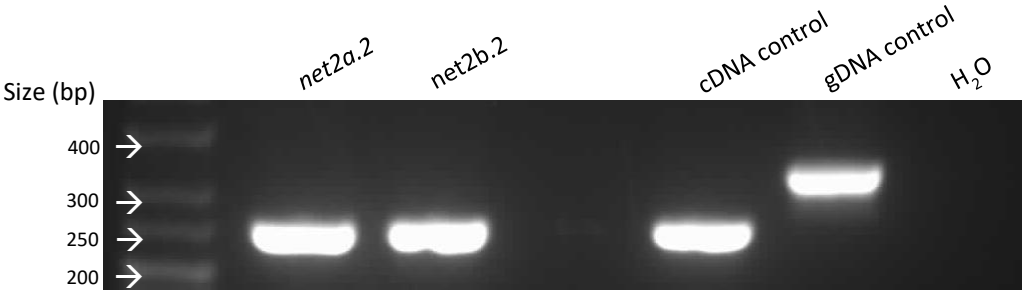

Figure 3.9: RT-PCR Analysis of gDNA Contamination in *net2a.2 and net2b.2* cDNA Samples. PCR amplification was performed with *ACT2*-specific primers. *net2a.2* = amplicon generated using *net2a.2* cDNA. *net2b.2* = amplicon generated using *net2b.2* cDNA. cDNA control = cDNA known to be free of gDNA contamination was used as template. gDNA control = gDNA used as template. H_2O = PCR reaction performed on deionised water. Bioline Hyperladder 25 bp was used as a molecular weight marker.

In summary, the transcriptional activity of the described T-DNA alleles was shown to be disrupted. The *net2b.1*, *net2d.1* and *net2d.2* mutant lines were shown to display abolished transcription of their respective mutant alleles. The *net2a.2* mutant appeared to partially transcribe NET2A, whilst the *net2b.2* mutant seemed to exhibit full transcription of *NET2B*. However, the transcription of each mutant allele is nonetheless disrupted in both lines by the presence of the T-DNA inserts. Therefore, it was confirmed that the *net2a.2*, *net2b.1*, *net2b.2, net2d.1* and *net2d.2* T-DNA lines were genuine mutants of their respective *NET2* genes. Subsequently, phenotypic analysis of each mutant line was performed to investigate the potential roles of NET2A, NET2B and NET2D *in vivo*.

3.3. Phenotypic Analysis of *net2a*, *net2b* and *net2d* Single Mutants.

Having identified *net2a*, *net2b* and *net2d* transcriptional knockout mutants, phenotypic analysis was performed to identify potential functions of the mutant genes. To successfully identify a phenotype associated with a specific protein, phenotypic analysis must be performed on the tissues at the specific developmental stages in which the protein is biologically active.

Phenotypic analysis of *net2a*, *net2b* and *net2d* mutants was performed on semi-*in vivo* (SIV)-germinated pollen tubes, in which pollen is germinated on excised pistils and permitted to grow through the stigma and style (Qin et al. 2009). SIV-germinated pollen tubes were used for phenotypic analysis for two reasons: firstly, previous analysis by Dixon. (2013), has shown that expression of *NET2A*, *NET2B* and *NET2D* is increased in pollen tubes following penetration of the stigma. NET2B in particular, is only expressed at high levels following penetration of the female tissue by growing pollen tubes (Dixon. 2013), under control of transcription factors required for sperm release during fertilisation (Leydon et al. 2013). This suggests that the NET2s may be important in regulating pollen tube growth following penetration of the stigma. Furthermore, the NET2 proteins interact with PRKs (chapter 6), which regulate pollen tube growth and navigation through the pistil by regulating the actin cytoskeleton in response to external signals from the pistil (chapter 1.5). This suggests the NET2 proteins may be involved in regulating pollen tube guidance through involvement with PRK signalling. Phenotypes for specific PRKs are only observable in SIV-germinated pollen, in which only after penetration of the stigma do pollen tubes gain competence to recognise pistil-secreted guidance cues (Palanivelu and Preuss. 2006; Takeuchi and Higashiyama. 2016). Taken together, it can be expected that *NET2A*, *NET2B* and *NET2D* are likely to play a role in pollen tube growth following penetration of the stigma and during fertilisation. Therefore, phenotypic analysis of *net2a*, *net2b* and *net2d* mutants was performed on SIV-germinated pollen. In addition to this, the potential roles of NET2 proteins in fertilisation was performed by analysing the seed set of each mutant.

Furthermore, phenotypic analysis of *NET2A* and *NET2D* was performed on mutant pollen grains. *NET2A* and *NET2D* are most strongly expressed in developing tricellular pollen grains (Dixon. 2013), indicating they may play a role in gametogenesis or germination. In addition to this, NET2A-GFP associates with actin filaments in the maturing gametophyte (chapter 4), suggesting that NET2A may regulate actin during development. As discussed in chapter 1.4.1, the actin cytoskeleton is known to play important roles in pollen gametogenesis: to determine whether *NET2A* and NET2D may play a role in pollen grain development through regulation of actin, phenotypic analysis of pollen grains was performed using two approaches. Firstly, staining of mature pollen grains with the nucleic acid stain, 4',6-Diamidino-2-Phenylindole, Dihydrochloride (DAPI) was performed to visualise the cell nuclei. During pollen maturation, pollen grains undergo a series of developmentally regulated cell divisions (chapter 1.4.1), making it possible to

identify the specific developmental stage of pollen grains by analysis of the cell nuclei. DAPI staining of pollen grain nuclei is a commonly used method to determine whether grains have successfully completed development, and identify defects in cell division (Parks et al. 1998), as well as in nuclear morphology and organisation (Lalanne and Twell. 2002). The actin cytoskeleton is known to be important in regulating the division and positioning of nuclei during pollen grain development (Gervais et al. 1994; Zonia et al. 1999), and analysis of pollen grain nuclear morphology using DAPI staining may highlight potential nuclear morphology defects in *net2a* and *net2d* mutants. Secondly, the germination rates of pollen from *net2a* and *net2d* mutants was analysed to determine if NET2A and NET2D may be necessary in pollen germination, which is also known to be dependent on actin (Gibbon et al. 1999). NET2B is not predicted to be expressed in pollen grains (Dixon. 2013; Leydon et al. 2013) and therefore phenotypic analysis of pollen grains of *net2b* mutants was not performed.

3.3.1. Phenotypic Analysis of *net2a* and *net2d* Pollen Grains using DAPI Staining.

Pollen grains of *net2a.2*, *net2d.1* and *net2d.2* plants did not display any obvious morphological defects and appeared indistinguishable from Col-0 pollen grains. DAPI staining of dehisced pollen was performed to determine if the grains of mutant plants had successfully matured, and to investigate potential nuclear defects arising in the *net2a* or *net2d* mutants. A minimum of 75 pollen grains was analysed in each of the Col-0, *net2a.2*, *net2d.1* and *net2d.2* lines. As shown in figure 3.10, the DAPI stained nuclei of *net2a* and *net2d* mutant pollen grains appeared to be indistinguishable from those of Col-0 plants: the mutant pollen grains had reached maturity, as indicated by the centrally organised vegetative nucleus closely associated by two sperm nuclei (Chapter 1.4.1; Lalanne and Twell. 2002). The pollen grain nuclei of *net2a* and *net2d* mutants did not display an observable morphological defects. These observations were consistent in all pollen grains analysed.

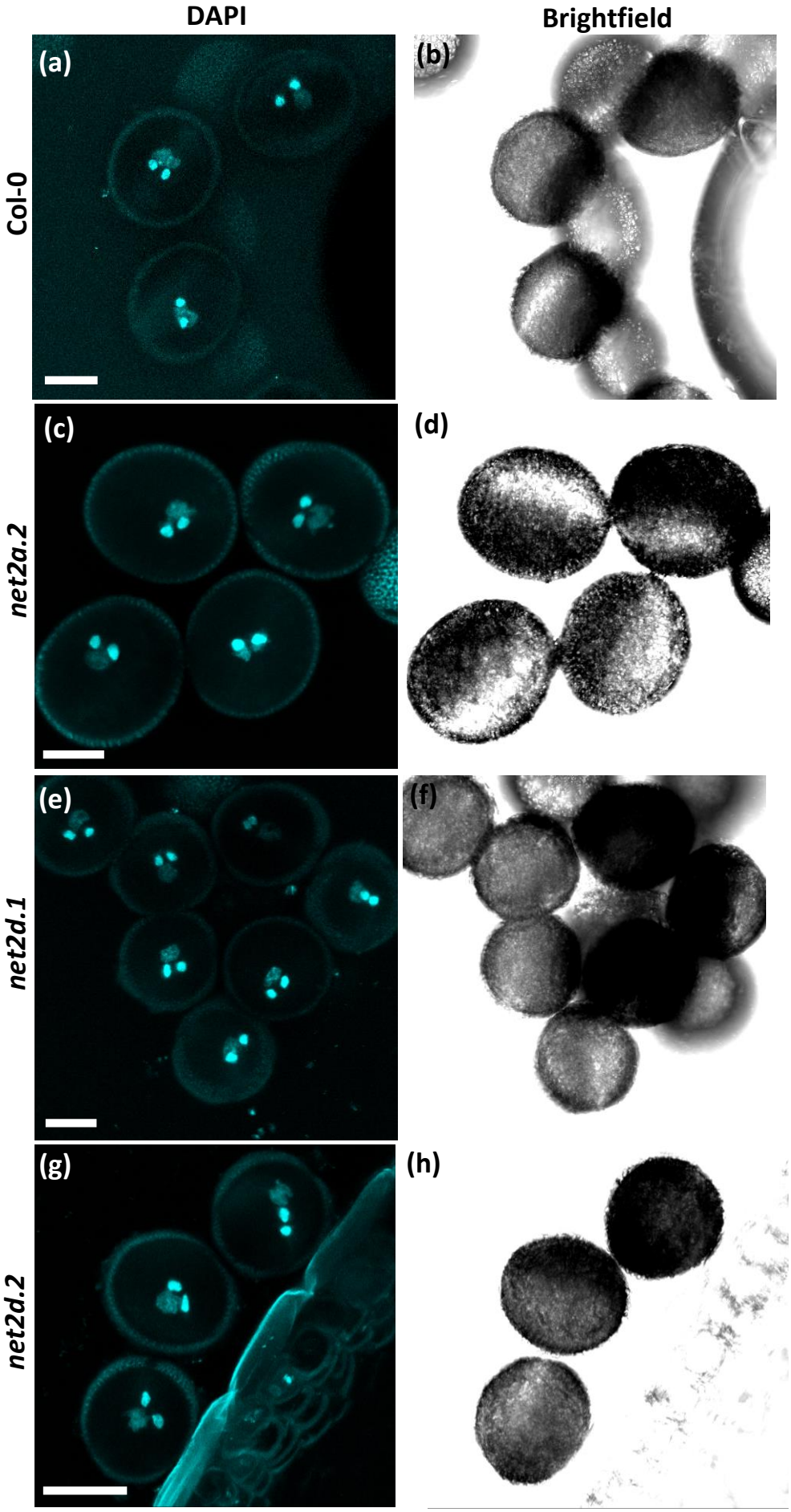
DAPI
Brightfield
Col-0
net2a.2
net2d.1
net2d.2
(a)
(b)
(c)
(d)
(e)
(f)
(g)
(h)

Figure 3.10 (above): Analysis of *net2a* and *net2d* Mutant Pollen Grain Development and Nuclear Morphology using DAPI Staining. (a) and (b): Col-0 pollen grains. (c) and (d): *net2a.2* pollen grains. (e) and (f): *net2d.1* pollen grains. (g) and (h): *net2d.2* pollen grains. (a), (c), (e) and (g): DAPI stained nuclei visualised by CLSM using 405 nm excitation and 415 – 500 nm emission detection. (b), (d), (f) and (h): brightfield images of the same cells. Scale bar: 10 µm.

3.3.2. Analysis of Pollen Germination Efficiency in *net2a, net2b* and *net2d* Mutants.

It was then investigated as to whether NET2A or NET2D may be important in regulating pollen grain germination. To study this, the germination frequencies of pollen grains was analysed after 24 hours incubation on solid pollen germination media (chapter 2.5.2.1). Failure of mutant pollen to germinate, or reduced frequencies of germination in mutant pollen would indicate a role for NET2A or NET2D in the initiation of pollen germination. Pollen from Col-0, *net2a.2*, *net2d.1* and *net2d.2* plants were germinated for 24 hours as described in chapter 2.5.2.1**,** and confocal laser scanning microscopy (CLSM) was used to acquire brightfield images of germinated pollen grains, in order to quantify the percentage of pollen that had germinated in each line. For each line analysed, roughly equal numbers of pollen grains were analysed from 3 individual plants, to account for natural variations in pollen germination efficiency occurring from plant to plant.

Figure 3.11 shows example images of pollen from each mutant line after 24 hours of incubation in germination medium, and the germination rates of pollen grains from each mutant line. As shown, pollen from *net2a.2*, *net2d.1* and *net2d.2* mutant plants was able to germinate extensively, producing a large number of pollen tubes after 24 hours of incubation. The exact percentage of pollen that successfully germinated after 24 hours was found to be markedly similar in Col-0, and the *net2a* and *net2d* mutants. In one experiment, depicted by the green bars in figure 3.11, the average pollen germination rate of *net2a.2* and *net2d.1* plants was observed to be 67.1 ± 8.4 % and 70.6 ± 8.6 % respectively, which was remarkably similar to that of Col-0 plants analysed on the same day (65.9 ± 6.5 %). In a different experiment (depicted by the blue bars), the average pollen germination rate from *net2d.2* plants was found to be 53.2 ± 9.1 % compared to 48.3 ± 5.2 % in Col-0. Statistical analysis indicated no significant difference in pollen germination rate between *net2a.2*, *net2d.1* or *net2d.2* mutant lines and the respective Col-0 controls (appendix 2.1).

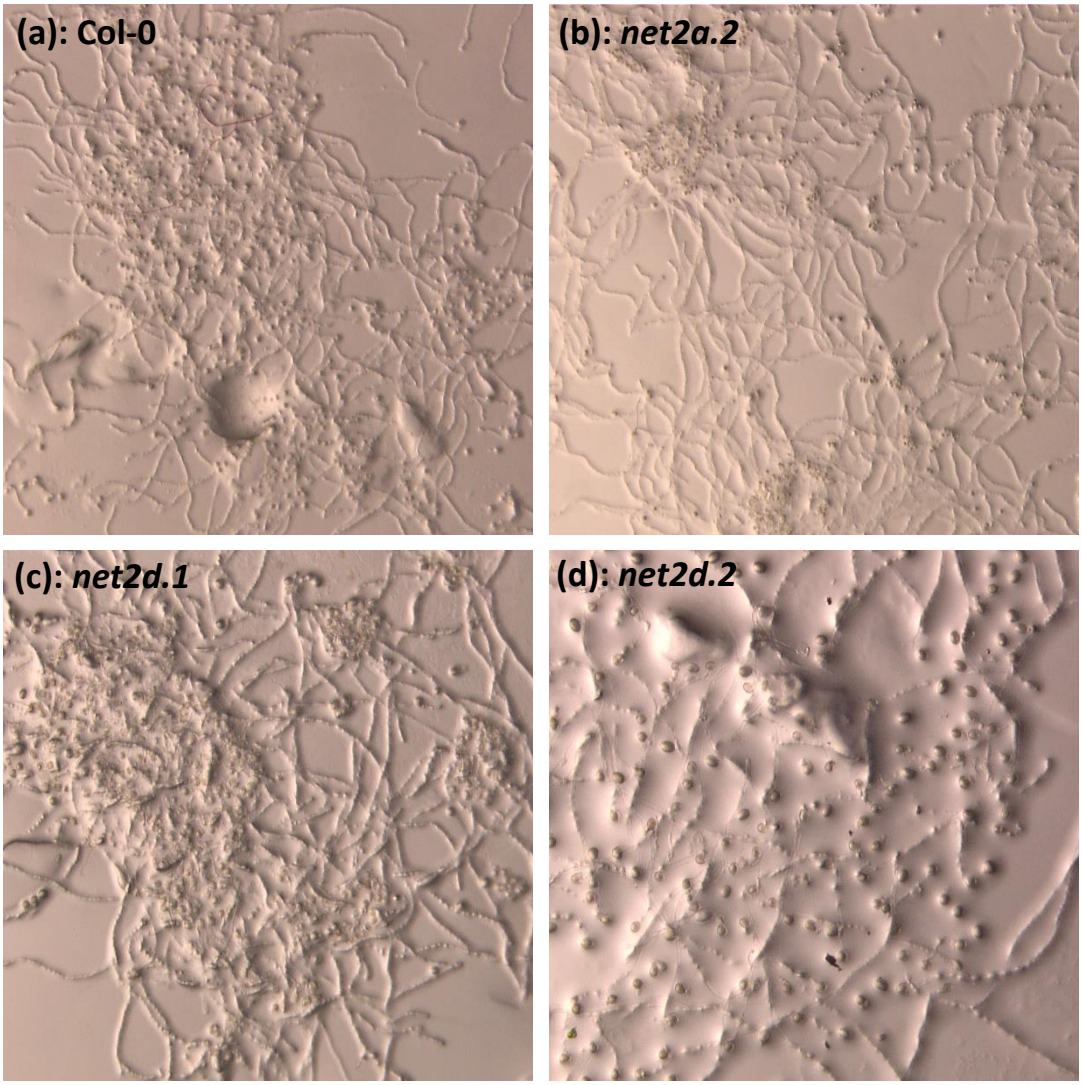

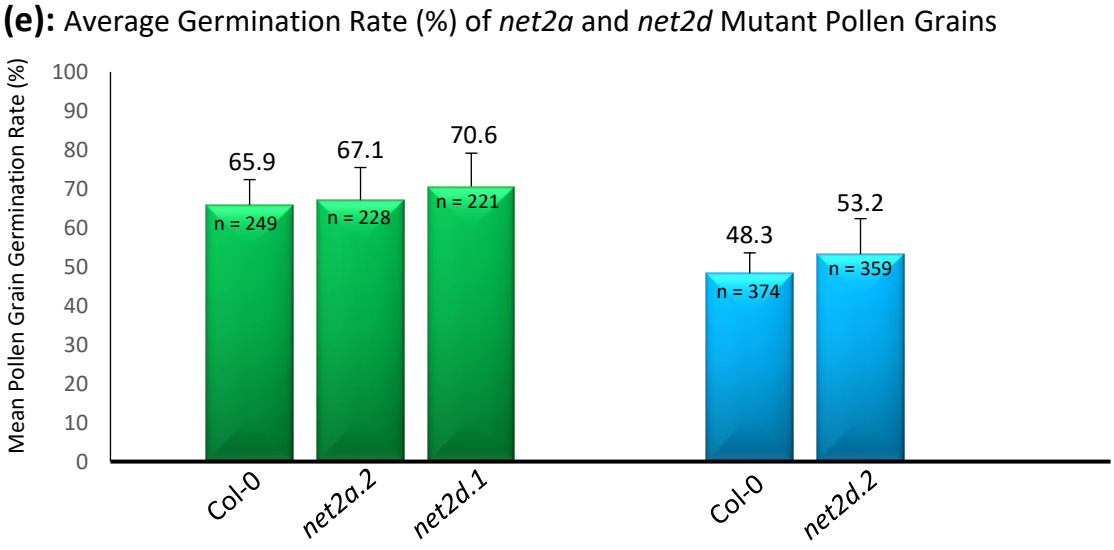

Figure 3.11: Germination of *net2a* and *net2d* Mutant Pollen Grains *in vitro*. Pollen grains of Col-0 plants and *net2a.2*, *net2d.1* and *net2d.2* mutants were germinated *in vitro* for 24 hours to assess their ability to germinate. Widefield images of germinated pollen from (a): Col-0, (b): *net2a.2*, (c): *net2d.1* and (d): *net2d.2* plants left to germinate for 24 hours. (e): chart represents the average germination rate (%) of pollen grains from Col-0, *net2a.2*, *net2d.1* and *net2d.2* plants after 24 hours. Green and blue bars represent results of independently performed experiments. n = number of pollen tubes analysed.

The results show that pollen of the *net2a* and *net2d* mutants were not impaired in their ability to germinate, and that NET2A and NET2D, alone, had no essential role in regulating pollen germination.

3.3.3. Analysis of SIV-Germinated Pollen Tubes in *net2a*, *net2b* and *net2d* Mutants.

The roles of NET2A, NET2B and NET2D in pollen tube growth were investigated through analysis of SIV-germinated pollen. Pollen from of Col-0, *net2a.2, net2b.1, net2b.2, net2d.1* and *net2d.2* mutant plants was germinated under semi *in vivo* conditions, as described in chapter 2.5.2.2, and pollen tubes extending from the excised pistils were analysed using CLSM. In addition to analysis of pollen tube morphology, average pollen tube growth rate and pollen tube width was quantified, all of which are known to be regulated by actin (Gu et al. 2003; Deeks et al. 2007; Takeuchi and Higashiyama. 2016).

As shown in figures 3.12 and 3.13, pollen of *net2a.2*, *net2b.1*, *net2b.2*, *net2d.1* and *net2d.2* mutants was successfully germinated under semi-*in vivo* conditions. The mutant pollen tubes were able to grow through the pistil tissue, extending throughout the germination media in a similar manner to Col-0 pollen tubes with no noticeable morphological defects. Under analysis using time-lapse confocal microscopy, the mutants did not appear to have greatly reduced growth rates, compared to Col-0 pollen tubes analysed during the same experiment. As shown in figure 3.14, it was found that on average, *net2a.2* mutant pollen tubes extended at a rate of 2.11± 0.43 µm/min, compared to Col-0 pollen tubes analysed in the same experiment, which extended at a rate of 2.64 ± 0.34 µm/min. Statistical analysis indicated a significant difference between the growth rates of *net2a.2* and Col-0 pollen tubes, however, the actual average rates of elongation did not differ considerably between *net2a.2* and Col-0 pollen tubes, and it could not be concluded that *net2a.2* mutant pollen tubes exhibited highly reduced rates of elongation. The average growth rates of *net2b.1* and *net2b.2* pollen tubes was determined to be 2.52 ± 0.46 µm/min, and 2.37 ± 0.37 µm/min, compared to Col-0 pollen analysed in the same experiment, which elongated at an average rate of 2.41 ± 0.67 µm/min. Statistical analysis revealed no significant difference between the growth rates of *net2b.1* or *net2b.2* mutant pollen tubes compared to the Col-0 controls, and it is clear that the *net2b* mutant pollen tubes did not show a significantly reduced rate of elongation. Likewise, pollen tubes of *net2d* mutants did not display highly reduced rates of elongation. *net2d.1* pollen

tubes grew at an average rate of 2.44 ± 0.37 µm/min, whereas Col-0 pollen analysed in the same experiment grew at an average rate of 2.64 ± 0.34 µm/min. Although this difference was found to be statistically significant (appendix 2.2), the growth rates of Col-0 and *net2d.1* mutant pollen tubes were, clearly, highly similar. The difference between Col-0 and *net2d.2* pollen tube growth rates were not statistically significant: *net2d.2* pollen tubes displayed an average growth rate of 1.84 ± 0.46 µm/min and Col-0 pollen analysed during that experiment grew at a rate of 2.10 ± 0.42 µm/min. It could therefore not be concluded that pollen tube growth rate was greatly reduced in the *net2d.1* and *net2d.2* mutants. It is clear from this data that loss of NET2A, NET2B or NET2D function did not greatly impair the growth rate of SIV-germinated pollen tubes, indicating that they, individually, play no crucial role in maintaining pollen tube growth rate.

The average diameter of *net2a*, *net2b* and *net2d* pollen tubes did not appear to differ from that of Col-0 pollen tubes. The diameter of pollen tubes can vary along the length of the cell; to ensure consistency in analysis between samples, the diameter of growing pollen tubes was measured 5 µm behind the growth tip of each tube. As demonstrated in figure 3.15, the average diameter of Col-0 pollen was 5.99 ± 1.1 µm, and was remarkably similar to the average diameters of *net2a*, *net2b* and *net2d* mutant pollen tubes, which differed from that of Col-0 by no more than 0.29 µm (<5% of the average width of Col-0 pollen tubes). No significant difference in pollen tube diameter was observed between any of the *net2* mutants analysed and the Col-0 controls (appendix 2.3).

It can be concluded that no defects were observable in SIV-germinated pollen of *net2a*, *net2b* and *net2d* mutants, in which the pollen tube morphologies, growth rates and diameters did not differ significantly from that of Col-0. It can therefore be concluded that NET2A, NET2B and NET2D alone play no essential role in regulating pollen tube growth.

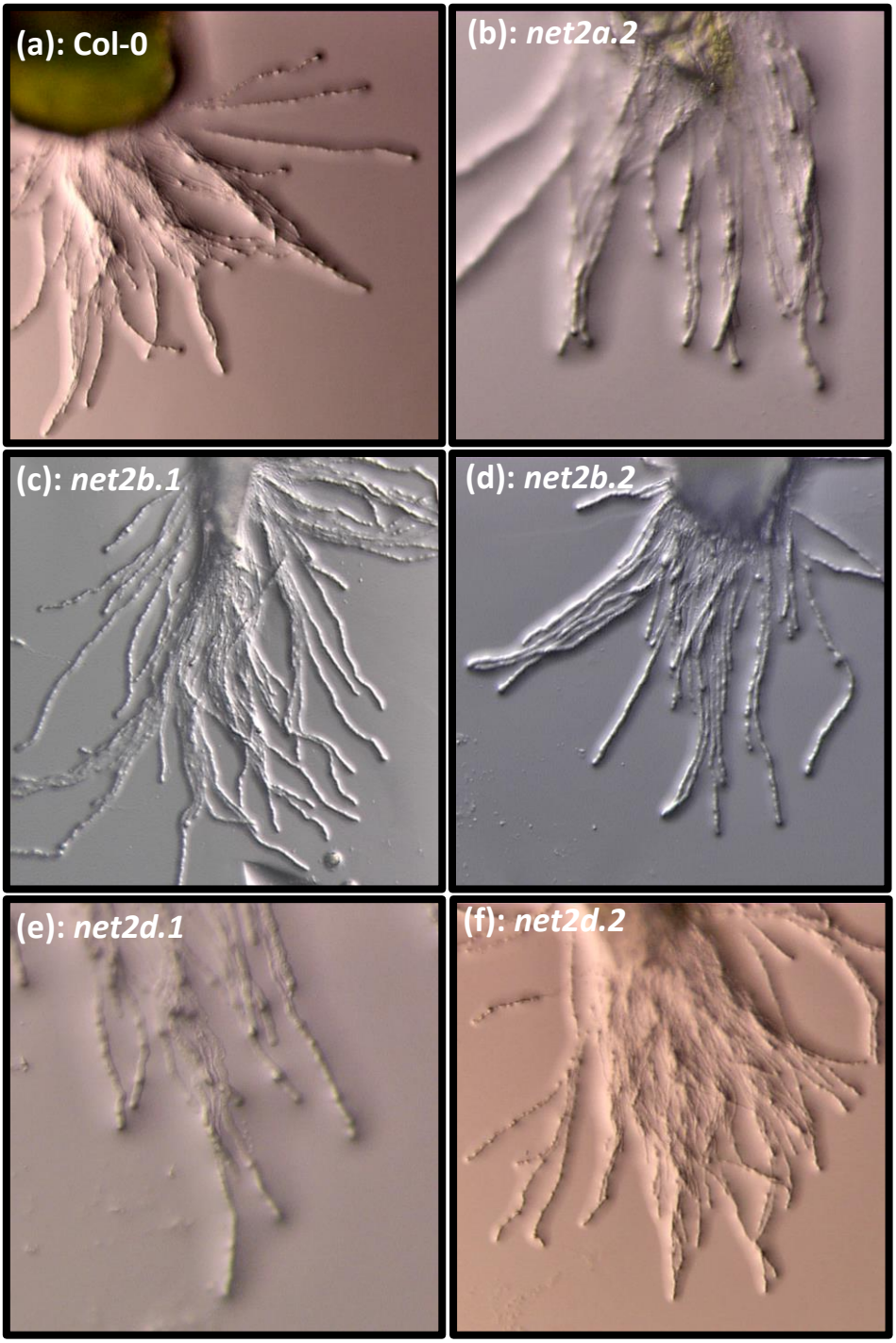

Figure 3.12*: Semi-in vivo Germ*ination of *net2a net2b* and *net2d* Mutant Pollen. Pollen grains of Col-0 plants and *net2a.2*, *net2b.1, net2b.2*, *net2d.1* and *net2d.2* mutants were germinated under semi-*in vivo* conditions. Widefield images of SIV-germinated pollen tubes from (a): Col-0, (b): *net2a.2*, (c): *net2b.1,* (d): *net2b.2,* (e): *net2d.1* and (f): *net2d.2* plants, growing from excised pistils.

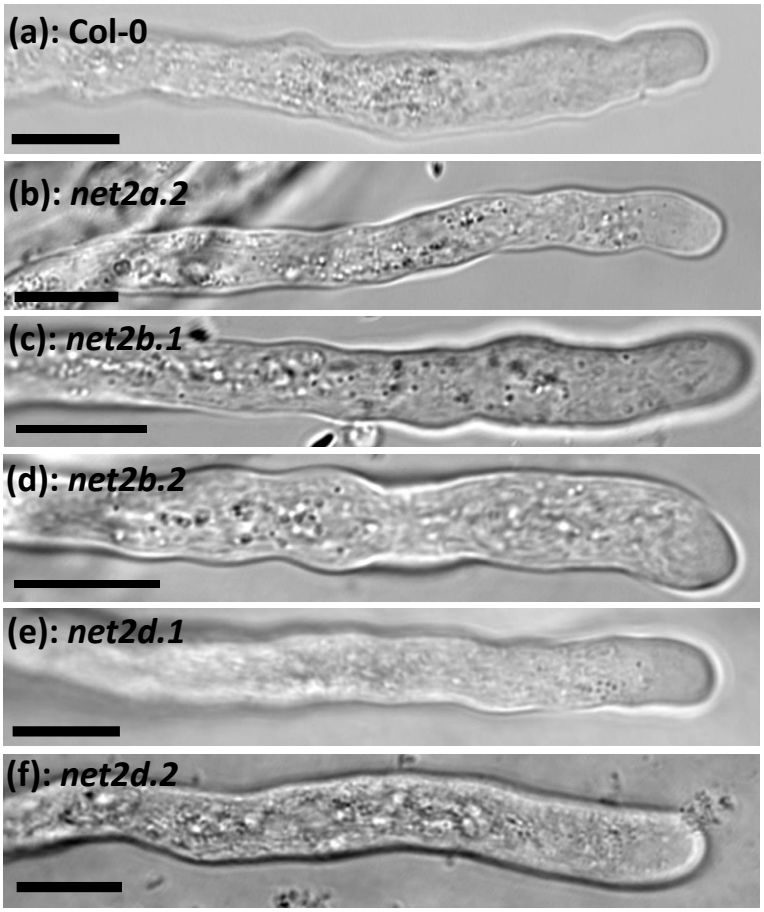

Figure 3.13*:* Example SIV-Germinated *net2a*, *net2b* and *net2d* Pollen Tubes. Brightfield images of SIV-germinated pollen tubes from Col-0 plants and *net2a.2, net2b.1, net2b.2, net2d.1* and *net2d.2* mutants acquired using CLSM. Scale bar: 10 µm

3.3.4. Analysis of *net2a, net2b* and *net2d* Mutant Seed Set.

It is possible that NET2A, NET2B or NET2D may regulate processes involved in fertilisation that are not observable during *in vitro* germination assays. During fertilisation, delivery of sperm by the pollen tube to the egg cells results in the formation of an embryo which develops into a seed. If fertilisation cannot occur then no seed will be formed, instead leaving an unfertilised ovule in its place. Therefore, pollen-specific defects in fertilisation can manifest in reduced seed production within a silique. To determine if the mutant pollen tubes were impaired in their ability to perform fertilisation, analysis of the seed set of *net2a.2, net2b.1, net2b.2, net2d.1* and *net2d.2* plants was analysed. Maturing siliques were collected from both Col-0 and mutant plants and cleared in 70% ethanol to remove pigment from the siliques, permitting visualisation of developing seeds. For each mutant line, 5 siliques were analysed from 3 individual plants in order to account for potential variation between individual plants.

(a). Comparison of Pollen Tube Growth Rate Between Col-0 and *net2a.2.*

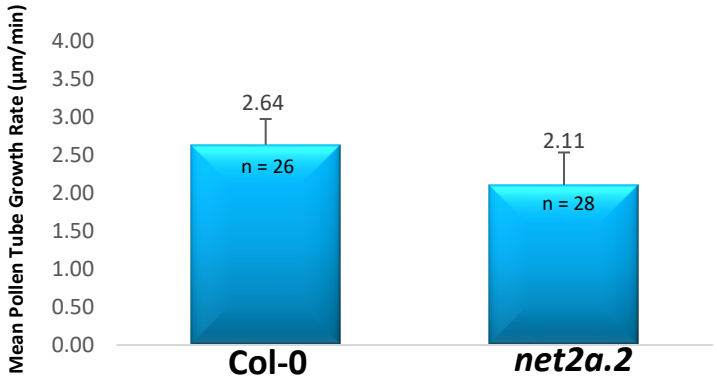

(b). Comparison of Pollen Tube Growth Rate Between Col-0, *net2b.1* and *net2b.2.*

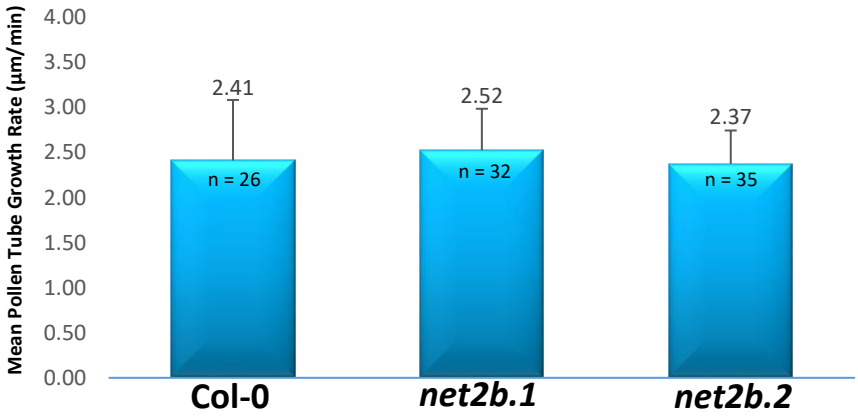

(c). Comparison of Pollen Tube Growth Rate Between Col-0 and *net2d.1.*

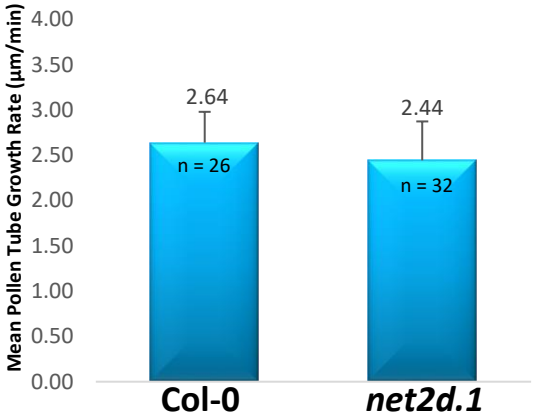

(d). Comparison of Pollen Tube Growth Rate Between Col-0 and *net2d.2.*

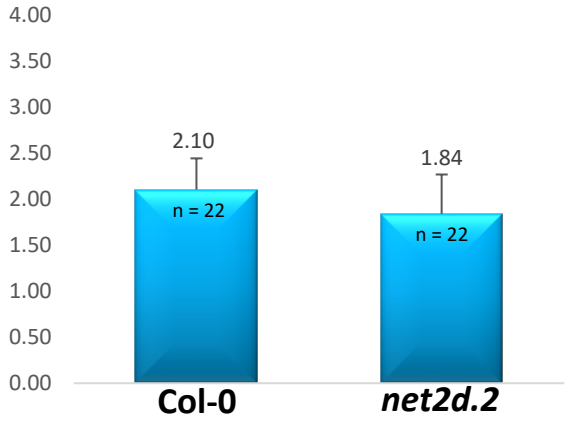

Figure 3.14*: Quantitative Analysis of Pollen Tube Growth Rate of *net2a, net2b* and *net2d* Mutant Pollen Tubes. Pollen grains of Col-0 plants and *net2a.2*, *net2b.1, net2b.2*, *net2d.1* and *net2d.2* mutants were germinated under semi-*in vivo* conditions. Time-lapse imaging using CLSM was used to acquire brightfield images of growing pollen tubes at regular intervals, in order to visualise the growth of pollen tubes over time (µm/min). (a) growth rate of *net2a.2* pollen tubes compared to Col-0 pollen tubes analysed in the same experiment. (b): growth rate of *net2b.1* and *net2b.2* pollen tubes, compared to Col-0 pollen tubes analysed in the same experiment. (c): growth rate of *net2d.1* pollen tubes and corresponding Col-0 controls. (d): growth rate of *net2d.2* pollen tubes and corresponding Col-0 controls. n = number of pollen tubes analysed.

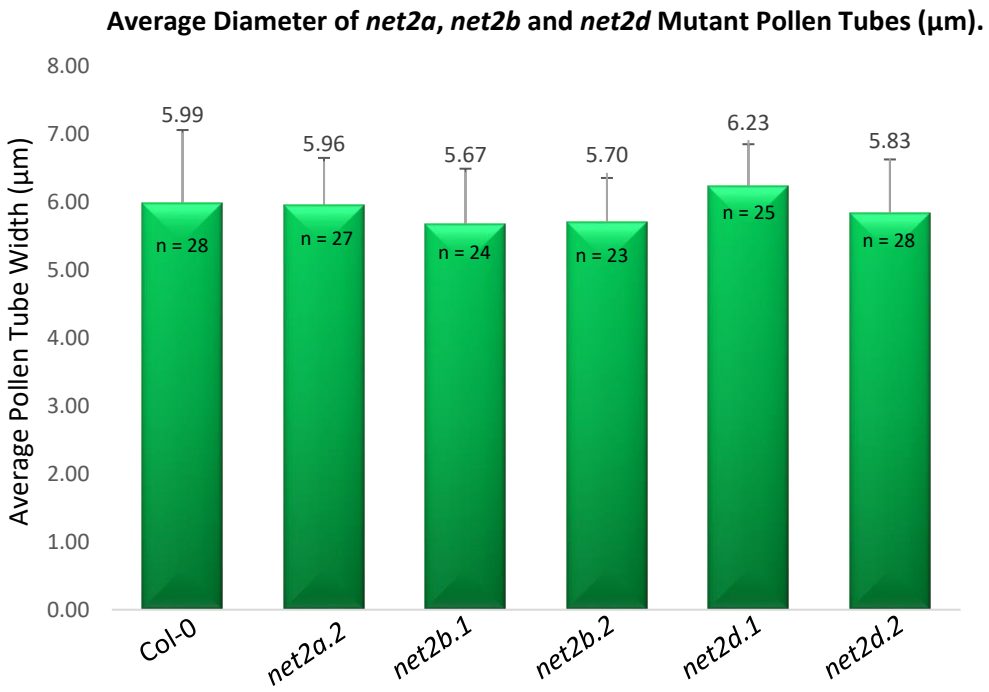

Figure 3.15*: Quantitative Analysis of net2a, net2b* and *net2d* Mutant Pollen Tube Diameter. Pollen grains of Col-0 plants and *net2a.2, net2b.1, net2b.2, net2d.1* and *net2d.2* mutants were germinated under semi-*in vivo* conditions. CLSM was used to acquire brightfield images of growing pollen tubes. ImageJ image analysis software was used to measure the diameters of each pollen tube 5 µm behind the tip. n = number of pollen tubes analysed.

Figure 3.16. shows the seed set of the Col-0, *net2a.2, net2b.1, net2b.2, net2d.1* and *net2d.2* mutant plants observed in this study. As expected, the average fertilisation efficiency of Col-0 plants was very high, with 96.8 ± 3.3 % of available ovules successfully fertilised to form developing seeds. No apparent reduction in fertilisation efficiency was observed in *net2a.2, net2b.1, net2b.2, net2d.1* and *net2d.2* mutant plants, with no mutant line exhibiting an average fertilisation efficiency lower than 96.3 ± 3.8 %. It is possible that minor defects in fertilisation could exist in the *net2a, net2b* or *net2d* mutants that could not be detected using this experimental approach: the amount of pollen tubes germinating and penetrating the stigma greatly outnumber the available ovules, meaning that small reductions in pollen fertility may not be detected. However, it can be confidently assumed that no severe reduction in pollen tube fertility could be detected in this study.

3.4. Summary.

In this section, further functional analysis of NET2A was performed, expanding on previous studies performed on the *net2a* mutant, *net2a.1.* During the course of this study, it was suggested that the *net2a.1* mutant allele appeared to be transcriptionally active and further work on this mutant line was discontinued.

Subsequently, an alternative *net2a* mutant was identified on which to perform reverse genetic analysis. In addition to this, *net2b* and *net2d* T-DNA mutants were also identified, in the likelihood that individual NET2 family members shared functionally redundancy. During this study, identification, isolation and validation of *net2a*, *net2b* and *net2d* mutants was achieved to characterise five transcriptionally-disrupted *net2* T-DNA mutant lines.

Phenotypic analysis of *net2a*, *net2b* and *net2d* mutant pollen was performed at all developmental stages at which *NET2A*, *NET2B* and *NET2D* are expressed, ranging from pollen grain development to fertilisation, to identify potential phenotypes that could arise from their loss of function. No phenotypic defects were observable in pollen grain development and germination, pollen tube growth and morphology, and fertilisation *in vivo*. The actin cytoskeleton is known to play vital roles in each of these processes, and it is highly likely that the NET2 protein family will play a role in regulating one or more of these processes. As described above, functional redundancy between related proteins means that a loss-of-function of one protein can be compensated for by the function of another. Therefore, multiple members of a protein family may need to be knocked out to elicit a phenotype. The NET2 subfamily consists of four members, making it highly likely that the loss of function of one NET2 protein can be compensated for by the function of another. Therefore, no essential function can be prescribed solely to NET2A, NET2B or NET2D. Generation and analysis of Arabidopsis mutants lacking expression of multiple NET2 family members must be performed in order to assign a functional role to the NET2 protein family.

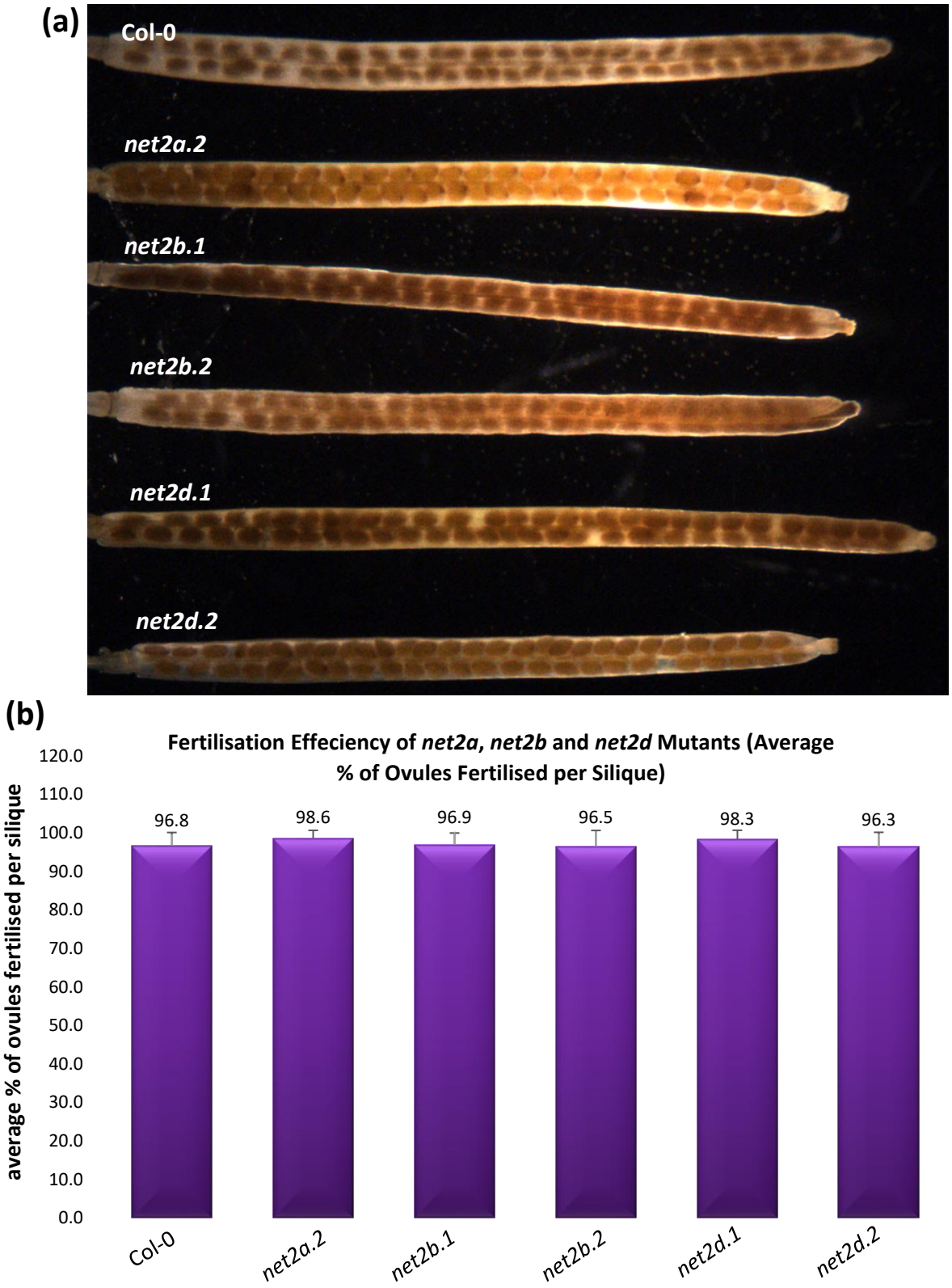

Figure 3.16*:* Quantitative Analysis of *net2a, net2b* and *net2d* Mutant Seed Set. Developing siliques of Col-0, *net2a.2*, *net2b.1*, *net2b.2*, *net2d.1* and *net2d.2* plants were collected and their seed content quantified. (a): Example siliques collected from Col-0, *net2a.2*, *net2b.1*, *net2b.2*, *net2d.1* and *net2d.2* plants, with developing seeds clearly visible. (b): Quantification of average fertilisation efficiency (% ovules fertilised to produce seeds) of Col-0, *net2a.2*, *net2b.1*, *net2b.2*, *net2d.1* and *net2d.2* plants. For each line, 5 siliques were analysed from 3 individual plants.

Chapter 4: *in situ* Analysis of NET2A-GFP Subcellular Localisation During Pollen Grain Development.

4.1. Introduction.

Previous studies have revealed NET2A-GFP to localise to punctae at the plasma membrane of the pollen tube shank (Deeks et al. 2012; Dixon. 2013). Initial studies have also indicated that NET2A-GFP decorates a filamentous network in developing pollen grains (Dixon. 2013). Therefore, thorough analysis was performed to fully characterise NET2A-GFP subcellular localisation during pollen grain development, and its associations with the actin cytoskeleton. Detailed sequential analysis of NET2A-GFP subcellular localisation in pollen grains was performed, at incremental stages of pollen development. NET2A-GFP exhibited distinctive localisation patterns, which underwent dynamic reorganisations associated with specific stages of the pollen developmental programme. The patterns formed by NET2A-GFP during pollen grain development, here termed 'NET2A-GFP arrays', are briefly summarised in figure 4.1, and can be observed to form 4 discreet and successive arrangements: the punctate array, the transverse array, the filamentous array and the cortical array. It was demonstrated in this study that NET2A-GFP associated with actin filaments in most of the NET2A-GFP arrays.

The structure of the actin cytoskeleton in developing pollen has been characterised in *Brassica napus* (Gervais et al. 1994) and *Nicotiana tabacum* (Zonia et al. 1999); undergoing distinctive reorganisations at specific stages of pollen development. As shown in this study, the organisation of the actin cytoskeleton in developing Arabidopsis pollen follows similar patterns to *B. napus* and *N. tabacum*; undergoing a series of dynamic rearrangements timed to specific cellular events in pollen development. Although the actin cytoskeleton has been previously investigated throughout pollen development, high-resolution imaging of actin subcellular localisation using CLSM has not been performed, and the dynamic rearrangements of the actin network has yet to be characterised in the model organism, Arabidopsis.

This section outlines the characterisation of actin organisation throughout Arabidopsis pollen grain development using high-resolution imaging. The focus of this study lies on the association of NET2A with the actin cytoskeleton during pollen

grain development; analysing the subcellular localisations of NET2A-GFP at each developmental stage, and the co-localisation of NET2A-GFP with actin. The association of NET2A with actin during the course of pollen grain development may indicate an interesting role for NET2A in gametogenesis.

Subsequently, the subcellular localisation of NET2A-GFP was analysed in pollen grains undergoing germination, therefore completing a synopsis of NET2A localisation in developing pollen grains, from the onset of NET2A expression to pollen tube germination.

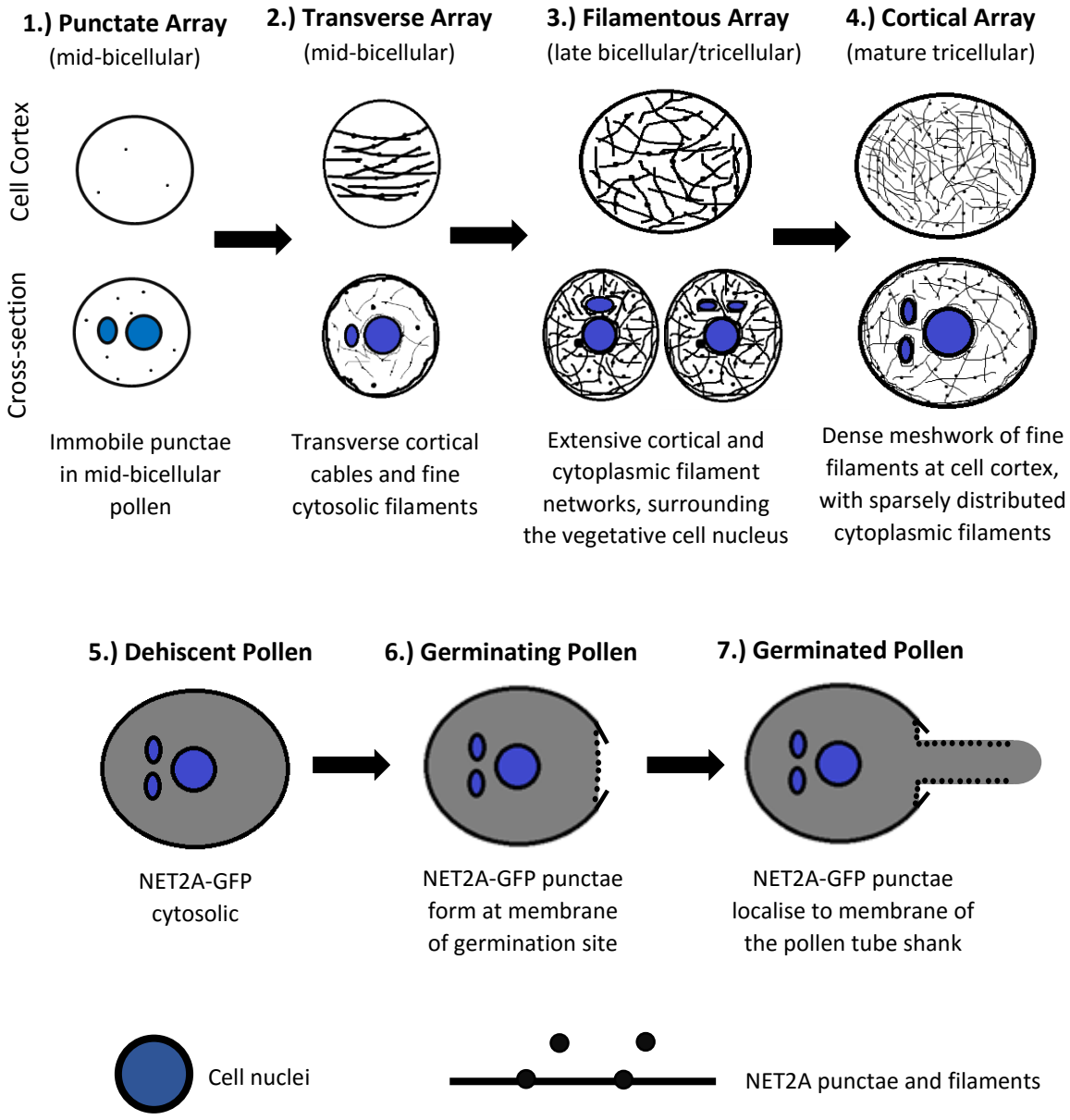

Figure 4.1: Diagrammatic Representation of NET2A-GFP Subcellular Localisation During Pollen Grain Development. Included are the descriptive titles assigned to the characterised NET2A-GFP arrays, and the developmental stages of pollen grain development at which they are observed.

4.2. Analysis of NET2A-GFP Subcellular Localisation Throughout the Course of Pollen Grain Development.

4.2.1. Strategy for Characterisation of NET2A-GFP Subcellular Localisation Throughout Pollen Grain Development.

Three methods were used to characterise the dynamic reorganisation of NET2A in developing pollen grains. Firstly, the subcellular localisation of NET2A-GFP was analysed in the developing pollen grains of Arabidopsis plants transformed with *pNET2A*:NET2A-GFP, which stably express NET2A-GFP under control of the *pNET2A* promoter (Dixon. 2013). Visualisation of NET2A-GFP subcellular localisation was performed using CLSM, and serial analysis of pollen from each bud in a single inflorescence was performed in order to observe NET2A-GFP at progressive stages of gametogenesis. Thus, it was possible to determine sequential changes in NET2A-GFP subcellular localisation throughout pollen maturation. Secondly, staining of pollen grains with the nucleic acid stain, DAPI (4',6-diamidino-2-phenylindole); a commonly used method of determining the developmental stage of developing pollen grains (Park and Twell. 1998), was employed to identify the specific developmental stage of pollen grains in which NET2A-GFP was being analysed. It was observed that the DAPI staining protocol disrupted NET2A-GFP subcellular localisation in developing pollen grains. Therefore, separate analysis of NET2A-GFP and DAPI staining was performed on pollen grains partitioned from a single bud. Finally, co-visualisation of NET2A-GFP with actin was accomplished using the actin marker, FABD2-RFP (FIMBRIN ACTIN-BINDING DOMAIN 2-RFP). *pLAT52*:FABD2-RFP Arabidopsis transgenic lines stably expressing FABD2-RFP under the strong pollen-specific promoter, *pLAT52,* were previously developed by Dr Martin Dixon (Durham University). Cross-pollination of *pLAT52*:FABD2-RFP and *pNET2A*:NET2A-GFP plants was performed to generate offspring expressing both constructs. Therefore, co-visualisation of NET2A-GFP and FABD2-RFP-labelled actin was made possible within single pollen grains, allowing analysis of NET2A association with the actin cytoskeleton throughout pollen development.

Using these experimental methods, sequential reorganisations of NET2A-GFP subcellular localisation and dynamic associations with the actin cytoskeleton could be attributed to a specific stage of pollen grain development. Described below is a summary of each NET2A-GFP array observed sequentially throughout specific

stages in pollen grain development, and the association of NET2A-GFP with the actin cytoskeleton.

4.2.2. Array 1: NET2A-GFP Punctate Array.

At the earliest developmental stage at which its expression could be visualised, NET2A-GFP was seen to localise to intense, discreet punctae in the developing pollen grain (figure 4.2). The punctae did not seem to be associated with the pollen grain cortex, and could be seen distributed throughout the interior of the cell. Brief time-lapse analysis of the pollen grains revealed that the punctae were non-motile. The precise developmental stage of the pollen grains was determined using DAPI staining of grains from the same buds as those analysed for NET2A-GFP localisation (chapter 2.5.7). It was revealed that the NET2A-GFP punctate array was exhibited by developing pollen grains at the mid-bicellular stage: the diffusely-stained vegetative nucleus, and an intensely stained generative nucleus detached from the wall of the developing grain, could be observed (figure 4.3). This NET2A-GFP array was seen in >100 pollen grains, could be observed consistently in different individual plants, and was analysed in 4 independently transformed *pNET2A*:NET2A-GFP transgenic lines. At this developmental stage, co-visualisation between NET2A-GFP and actin could not be performed, due to poor expression of the FABD2-RFP actin marker construct.

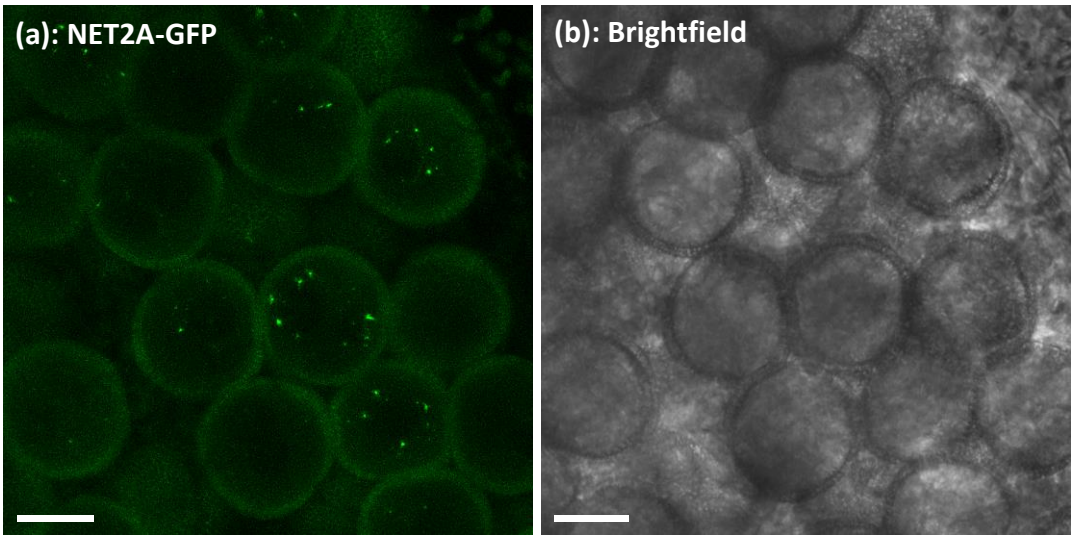

Figure 4.2: Array 1 - NET2A-GFP Punctate Array: Punctate subcellular localisation of NET2A-GFP, (termed NET2A-GFP array 1), in mid-bicellular pollen grains from *pNET2A*:NET2A-GFP stable transgenic plants. (a): NET2A-GFP subcellular localisation. (b): Brightfield image of the same cells. Scale bar = 10 µm.

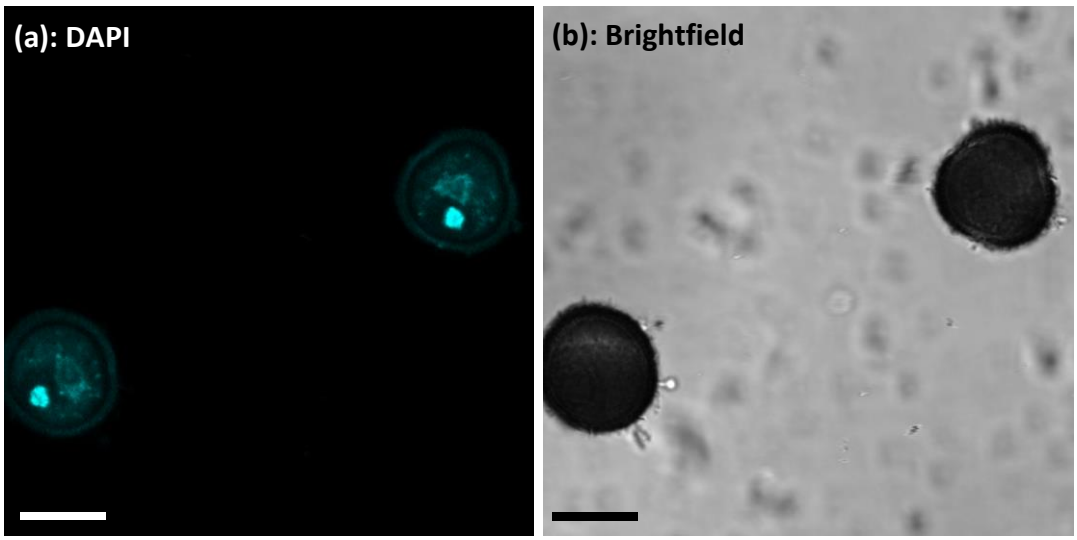

Figure 4.3: DAPI Staining of NET2A-GFP Punctate Array Pollen Grains: pollen grains taken from the same buds as grains exhibiting NET2A-GFP array 1 were stained with DAPI. (a): visualisation of DAPI-stained pollen grain nuclei. (b): brightfield image of the same cells. Scale bar: 10 µm.

4.2.3. Array 2: NET2A-GFP Transverse Array.

Upon analysis of developing pollen grains from older floral buds, NET2A-GFP could be seen to display a markedly different subcellular localisation pattern. In addition to the punctae observed in array 1, NET2A-GFP appeared to decorate prominent cables at the cell cortex, in the 'beads-on-a-string' pattern characteristic of NET proteins (figure 4.4). These cables were highly organised in a transverse orientation; aligned perpendicular to the cell longitudinal axis and the grooves of the exine (figure 4.5). Finer NET2A-GFP-decorated filaments were observed extending throughout the cytoplasm, with a beads-on-a-string pattern. The NET2A-GFP transverse array was studied in >100 pollen grains and was observable in 4 independently transformed transgenic lines. Developmental staging of the pollen grains using DAPI staining indicated that the NET2A-GFP transverse array also occurred in mid-bicellular pollen. Co-visualisation of NET2A-GFP and the actin marker, FABD2-RFP, was performed in plants expressing both constructs to ascertain whether the filaments decorated by NET2A-GFP were those of the actin cytoskeleton. As shown in figure 4.6, striking co-localisation of NET2A-GFP and FABD2-RFP-decorated filaments was clearly apparent, indicating that NET2A-GFP associated with actin at this stage of pollen development. The presence of transversely organised actin cables at the cell cortex has been reported to exist in

B. napus pollen, specifically at the mid-bicellular stage of development (Gervais et al. 1994). However, in contrast to such previous observations, actin was not observed to associate with the generative cell nucleus in Arabidopsis. The data presented in this section shows the organisation of actin in Arabidopsis and *B. napus* to be similar in mid-bicellular pollen, and that NET2A is associated with the actin cytoskeleton during this stage of development.

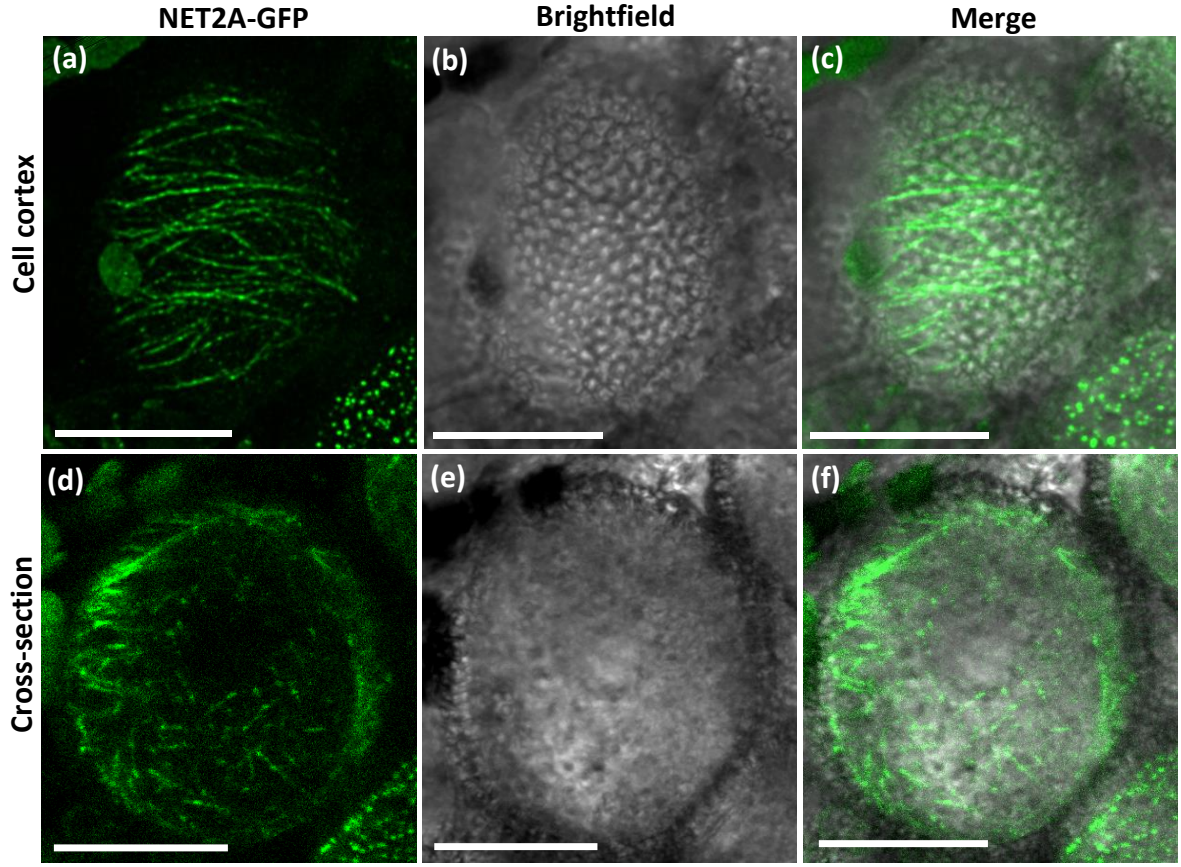

Figure 4.4: Array 2 - NET2A-GFP Transverse Array. Subcellular localisation of NET2A-GFP to transverse cortical actin cables, and fine actin cytoplasmic filaments and punctae, (termed NET2A-GFP array 2), in mid-bicellular pollen grains of *pNET2A*:NET2A-GFP stable transgenic plants. (a) and (d): NET2A-GFP subcellular localisation. (b) and (e): Brightfield image of the same cells (c): merge of (a) and (b). (f): merge of (d) and (e), respectively. (a)-(c): cell cortex. (d)-(f): cross section of the cell. Scale bar: 10 µm.

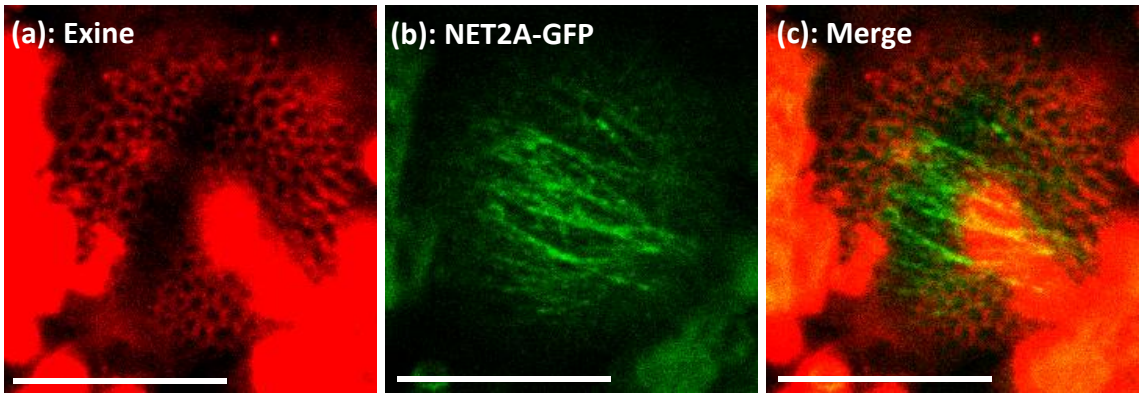

Figure 4.5: Co-visualisation of Cortical Transverse NET2A-GFP Cables with the Pollen Exine. Cortical actin cables align perpendicular to the pollen grain exine groove and the cell longitudinal axis. (a): exine (pollen grain coat) autofluorescence, imaged to visualise the exine groove and reference the cell longitudinal axis, using a 405 nm excitation laser and 600 - 700 nm wavelength emission detection. (b): NET2A-GFP visualised using a 488 nm excitation laser and 505 - 530 nm wavelength emission detection. (c): merge of (a) and (b). Scale bar: 10 µm.

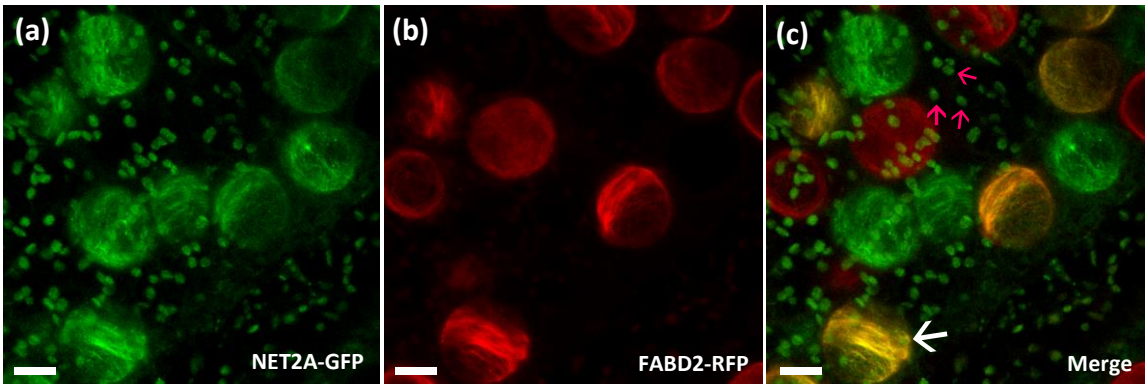

Figure 4.6: Co-localisation of the NET2A-GFP Transverse Array with Actin in Developing Pollen Grains. (a): NET2A-GFP subcellular localisation visualised using a 488 nm excitation laser and 505-530 nm emission detection. (b): FABD2-RFP subcellular localisation visualised using a 543 nm excitation laser and 600 - 650 nm detection. (c): merge of (a) and (b). White arrows indicate pollen grains. Pink arrows indicate autofluorescence from chloroplasts in the anther wall. Scale bar: 10 µm.

4.2.4. Array 3: NET2A-GFP Filamentous Array.

Later in development, following the pre-described NET2A-GFP transverse array, NET2A-GFP was observed to decorate a highly filamentous network distributed throughout the developing pollen grain. This localisation pattern was termed the NET2A-GFP filamentous array. As shown in figure 4.7, NET2A-GFP filament networks were prominent at the pollen grain cortex and extended throughout the cell cytoplasm, decorating the filaments with a beads-on-a-string pattern. In contrast to the filaments of the NET2A-GFP transverse array, the cortical filaments of the NET2A-GFP filamentous array did not appear to have any specific orientation to the cell axis. Both cortical and cytoplasmic filaments were observed to be highly static using time-lapse imaging. NET2A-GFP also formed a ring-like structure in the centre of the cell, which was connected with the cytoplasmic filament network. The NET2A-GFP ring was demonstrated to encircle the vegetative nucleus using DAPI staining. Although the DAPI staining procedure appeared to result in disruption of NET2A-GFP subcellular localisation in immature pollen grains, the NET2A-GFP ring of the filamentous array remained intact, and could be seen to surround the vegetative nucleus (figure 4.9). The NET2A-GFP filamentous array was consistently observable in >100 pollen grains analysed, and was studied in 5 independently transformed *pNET2A:*NET2A-GFP stable transgenic lines. Developmental staging of pollen grains using DAPI staining revealed the NET2A-GFP filamentous array to exist in late bicellular and early tricellular pollen grains (figure 4.8).

In plants co-expressing NET2A-GFP and FABD2-RFP, clear co-localisation between NET2A-GFP and actin was evident at cortical and cytoplasmic filaments, and at the nuclear periphery. It can therefore be assumed that NET2A interacts with actin filaments during this stage of pollen grain development. Previous studies on actin organisation in developing pollen grains of *B. napus* and *N. tabacum* also report the association of actin with the vegetative nucleus, but not the generative cell nucleus in late bicellular grains (Gervais et al. 1994; Zonia et al. 1999). This substantiates the hypothesis that NET2A may associate with actin surrounding the vegetative cell nucleus. Observations of cortical and cytoplasmic filament networks were also reported in *N. tabacum* pollen grains at this stage in development (Zonia et al. 1999).

The data presented in this section shows the actin cytoskeleton to surround the vegetative cell nucleus of Arabidopsis late bicellular and early tricellular pollen,

where NET2A can be found associated. Also described is an extensive cortical and cytoplasmic actin filament system decorated by NET2A-GFP.

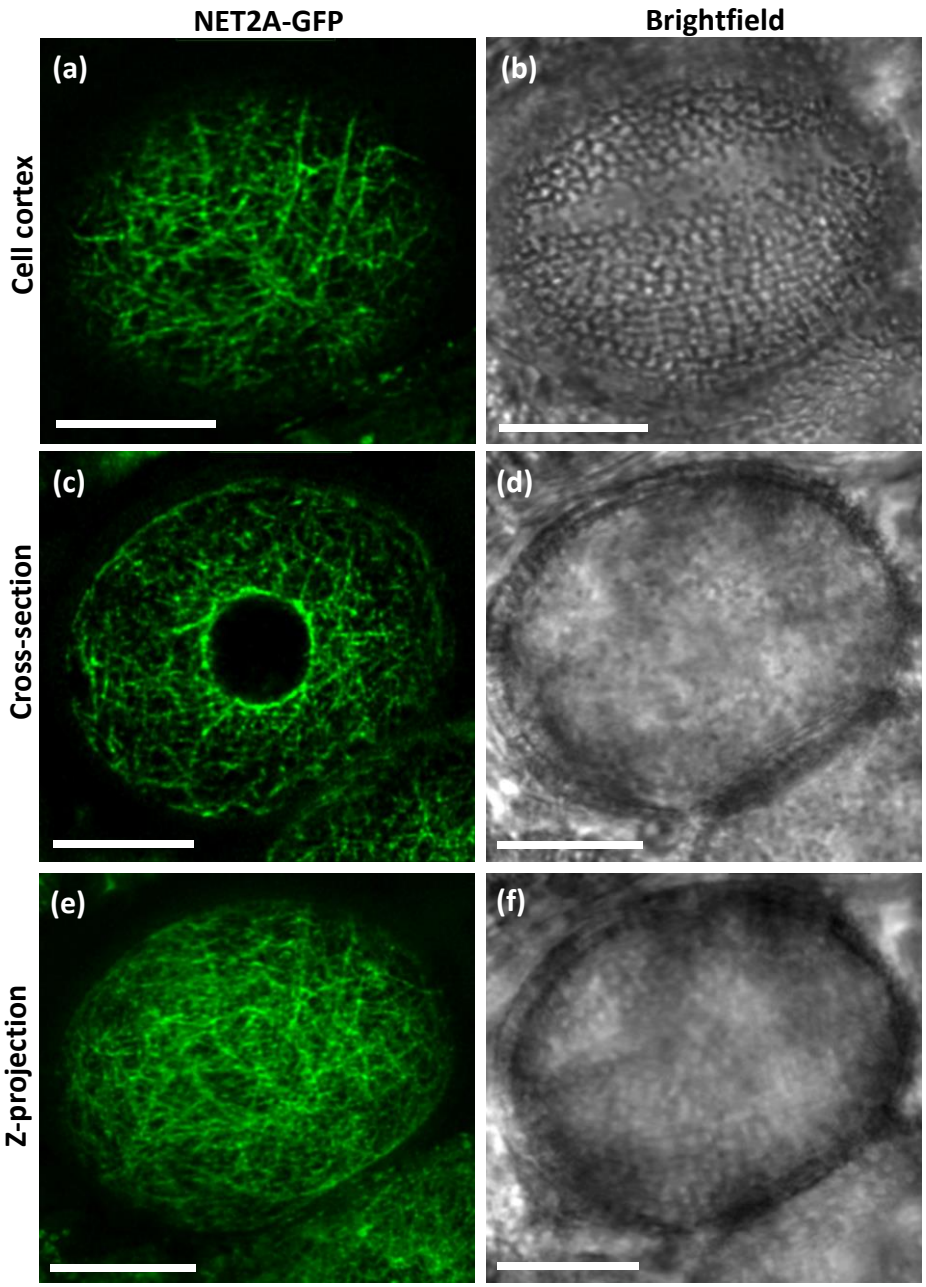

Figure 4.7: Array 3 - NET2A-GFP Filamentous Array. Subcellular localisation of NET2A-GFP to cortical and cytoplasmic filament networks, and enclosing the vegetative nucleus in late-bicellular/early tricellular pollen grains of *pNET2A*:NET2A-GFP stable transgenic plants. (a), (c) and (e): NET2A-GFP subcellular localisation. (b), (d) and (f): Brightfield image of the same cells. (a) and (b): cell cortex. (c) and (d): cell cross-section. (e) and (f): Z-projection. Scale bar: 10 µm.

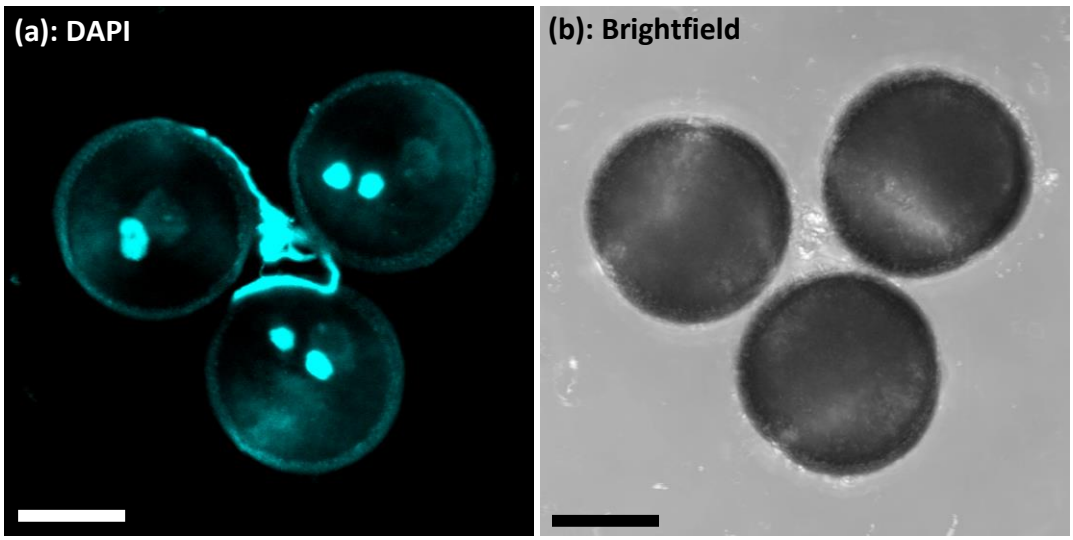

Figure 4.8: DAPI Staining of NET2A-GFP Filamentous Array Pollen Grains: pollen grains taken from the same buds as grains exhibiting the NET2A-GFP filamentous array were stained with DAPI. (a): visualisation of DAPI-stained pollen grain nuclei. (b): brightfield image of the same cells. Scale bar: 10 µm.

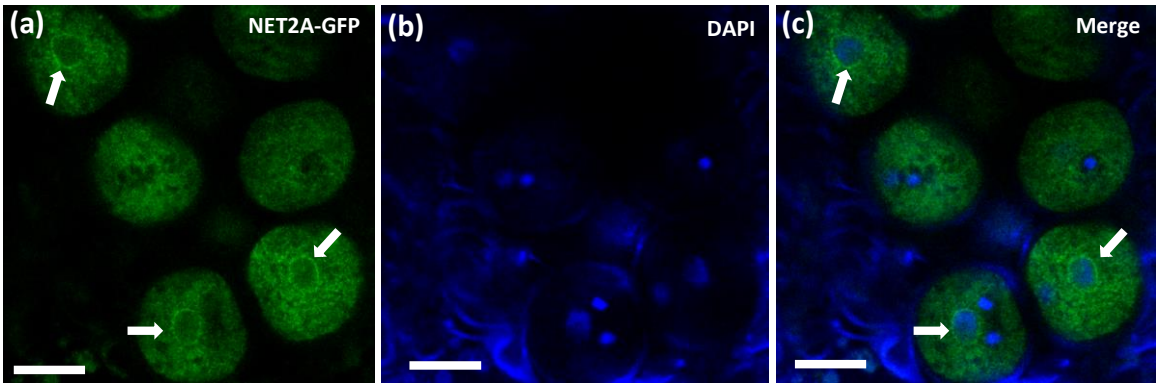

Figure 4.9: Localisation of the NET2A-GFP Filamentous Array to Vegetative Cell Nucleus of Developing Pollen Grains. Pollen grains exhibiting the NET2A-GFP filamentous array were stained with DAPI. (a): NET2A-GFP visualised with a 488 nm excitation laser and 505 – 530 nm emission detection. (b) DAPI staining of pollen nuclei visualised using a 405 nm excitation laser and 415 – 470 nm emission detection. (c): merge of (a) and (b). The DAPI staining procedure resulted in disruption of the NET2A-GFP filamentous network, but the central NET2A-GFP ring persists (white arrows), and localises to the periphery of the vegetative cell nucleus (c). Scale bar: 10 µm.

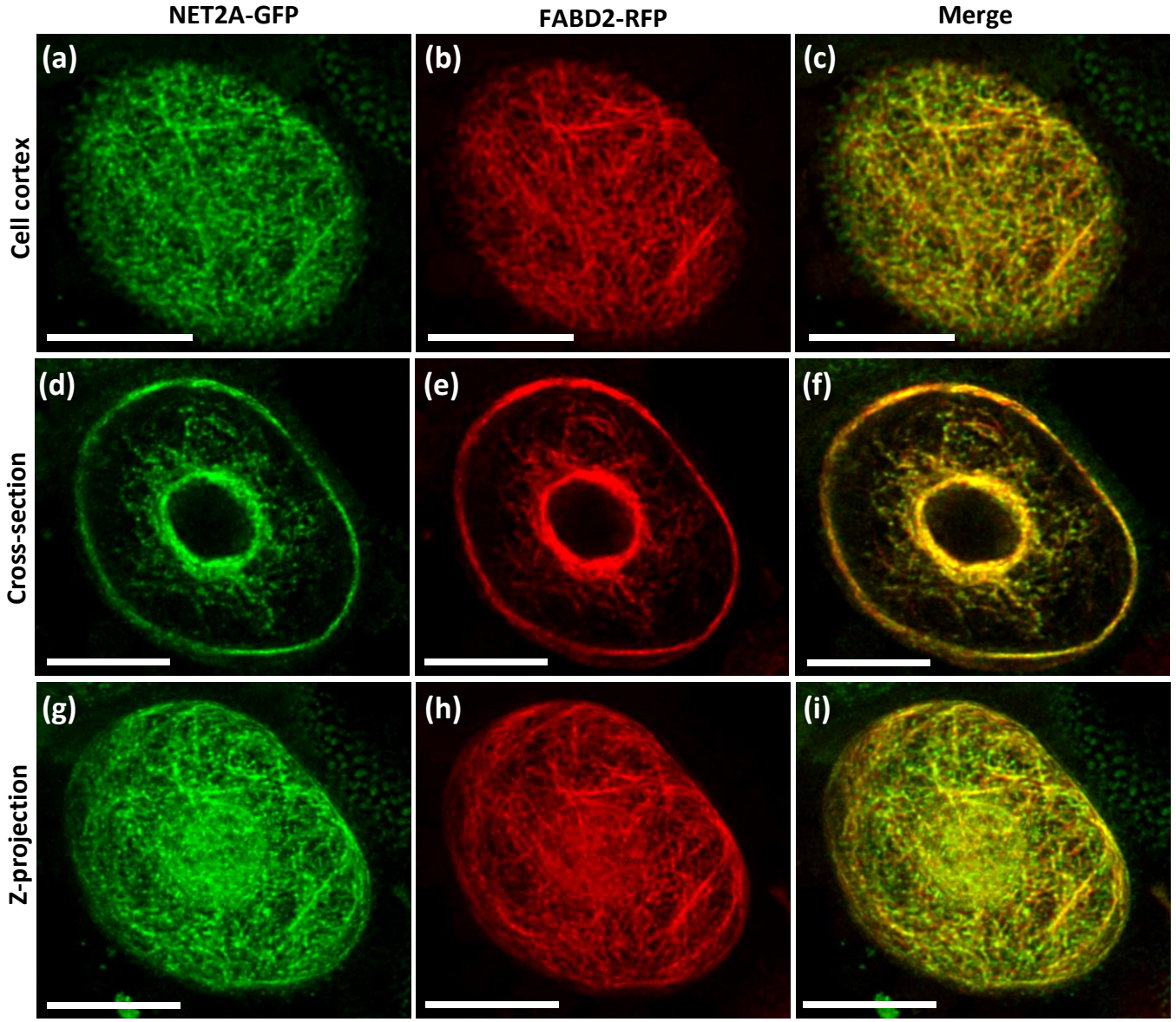

Figure 4.10: Co-localisation of the NET2A-GFP Filamentous Array with Actin in Developing Pollen Grains. (a), (d) (g): NET2A-GFP subcellular localisation visualised using a 488 nm excitation laser and 505 - 530 nm emission detection. (b), (e) and (h): FABD2-RFP subcellular localisation visualised using a 543 nm excitation laser and 600 - 650 nm detection. (c): merge of (a) and (b). (f): merge of (d) and (e). (i): merge of (g) and (h). Scale bar: 10 µm.

4.2.5. Array 4: NET2A-GFP Cortical Array.

At later stages of development, one further NET2A-GFP array was observable in maturing pollen grains before dehiscence. The NET2A-GFP cortical array consists of a dense meshwork of fine NET2A-GFP filaments at the pollen grain cortex, with a sparser network of fine filaments extending throughout the cytoplasm (figure 4.11, 4.12). These filaments displayed the characteristic NET family beads-on-a-string pattern. At this stage of pollen grain development, NET2A-GFP no longer formed an intense ring around the vegetative cell nucleus as observed in the prior NET2A-GFP filamentous array. The NET2A-GFP cortical array was counted in > 100 pollen grains and was studied in five independently transformed *pNET2A*:NET2A-GFP stable transgenic lines. DAPI staining of grains revealed the NET2A-GFP cortical array to be specific to maturing tricellular pollen grains; apparent by the tightly centralised organisation of the male germ unit (figure 4.13). Co-visualisation of NET2A-GFP and FABD2-RFP revealed the NET2A-GFP cortical array to co-localise with the actin cytoskeleton at both cortical and cytoplasmic filaments (figure 4.14). Similar actin arrangements have been reported in maturing pollen grains of *N. tabacum* (Zonia et al. 1999), and cortical actin localisation at the pollen grain furrow has been reported in mature *B. napus* pollen at anthesis. Following the NET2A-GFP cortical array, NET2A-GFP is reported to adopt a cytosolic subcellular localisation in dehiscent pollen grains (Dixon. 2013).

4.2.6. NET2A-GFP Subcellular Localisation in Dehiscent Pollen Grains During Pollen Tube Germination.

Previous research by Dixon. (2013), shows the localisation of NET2A-GFP to be cytosolic in dehiscent pollen grains, before localising to punctae at the plasma membrane of growing pollen tubes following germination (Dixon. 2013; Deeks et al. 2012). However, changes in the distribution of NET2A-GFP localisation during the early stages of pollen grain germination have not yet been studied. Pollen of *pNET2A*:NET2A-GFP stable transgenic lines was germinated by incubation in germination media for 3 hours, so that the subcellular localisation of NET2A-GFP could be studied in grains undergoing germination. As previously described,

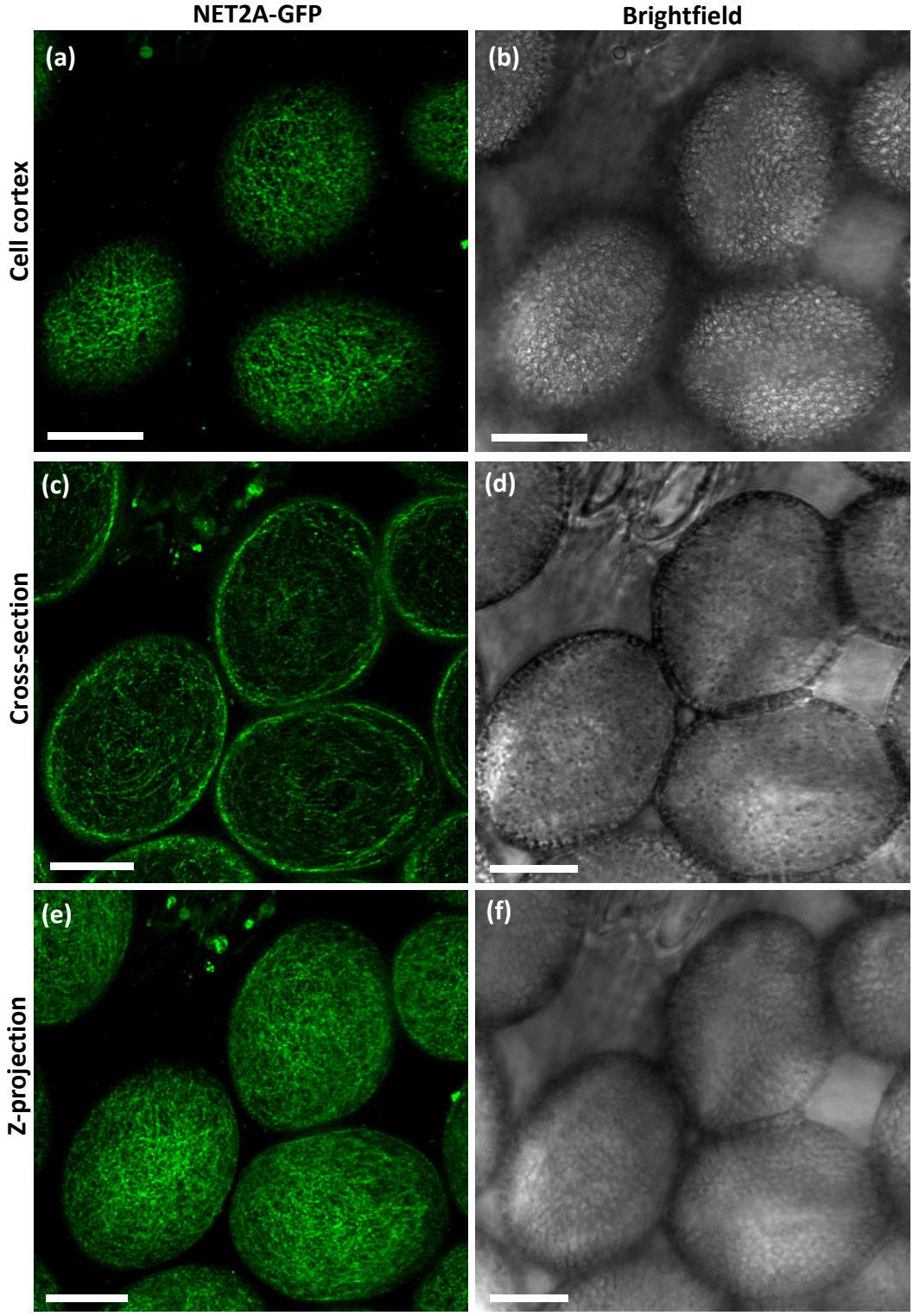

Figure 4.11: Array 4 - NET2A-GFP Cortical Array. Subcellular localisation of NET2A-GFP to fine cortical and cytoplasmic filament networks in maturing tricellular pollen grains of *pNET2A*:NET2A-GFP stable transgenic plants. (a), (c) and (e): NET2A-GFP subcellular localisation. (b), (d) and (f): Brightfield image of the same cells. (a) and (b): cell cortex. (c) and (d): cell cross section. (e) and (f): Z-projection. Scale bar: 10 µm.

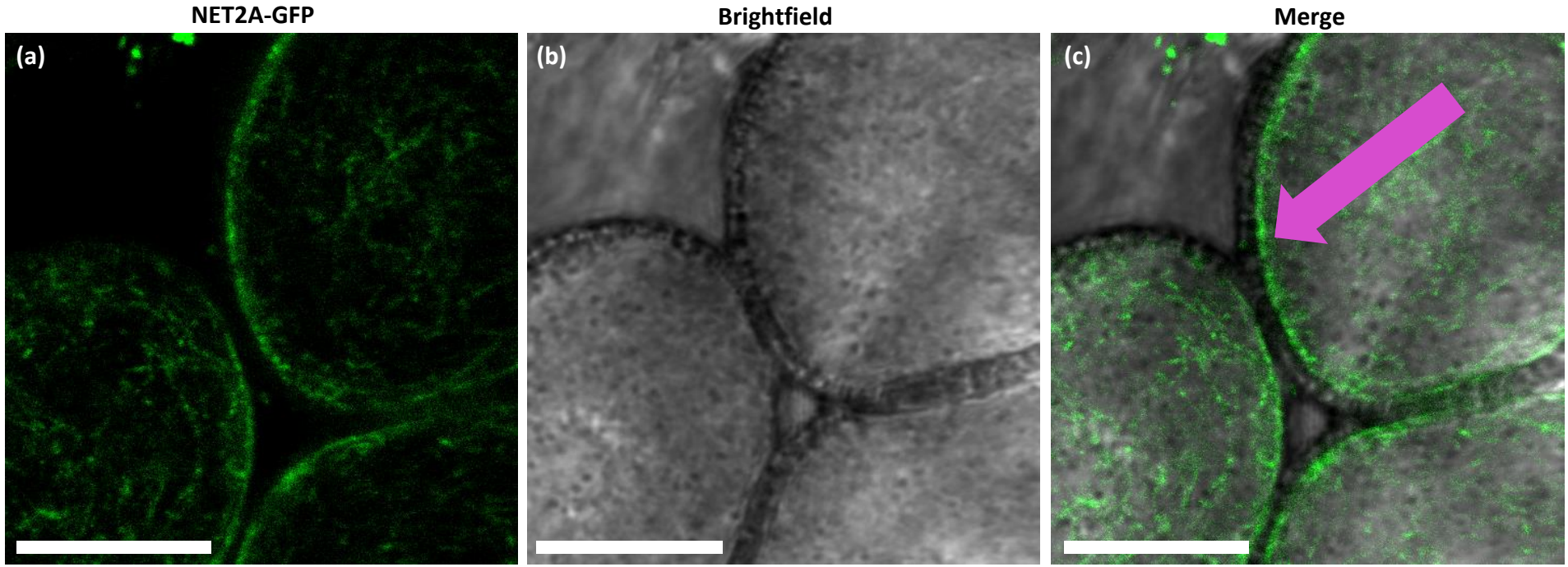

Figure 4.12: NET2A-GFP Cortical Array Localisation at the Pollen Grain Cortex. Close-up of pollen grain displayed in figure 4.11, showing NET2A-GFP localisation to pollen tube cortex (pink arrow). (a): NET2A-GFP subcellular localisation. (b): Brightfield image of the same cells. (c): merge of (a) and (b). Scale bar: 10 µm.

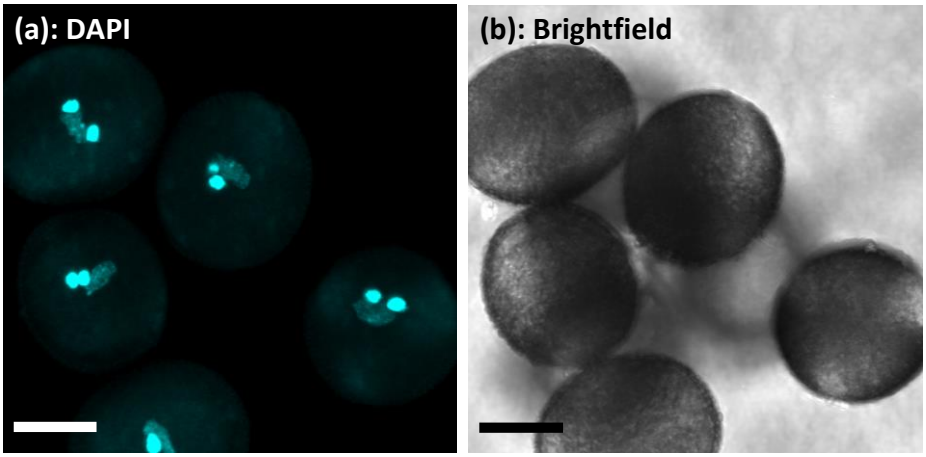

Figure 4.13: DAPI Staining of NET2A-GFP Cortical Array Pollen Grains. Pollen grains taken from the same buds as grains exhibiting the NET2A-GFP cortical array were stained with DAPI. (a): visualisation of DAPI-stained pollen grain nuclei. (b): brightfield image of the same cells. Scale bar: 10 µm.

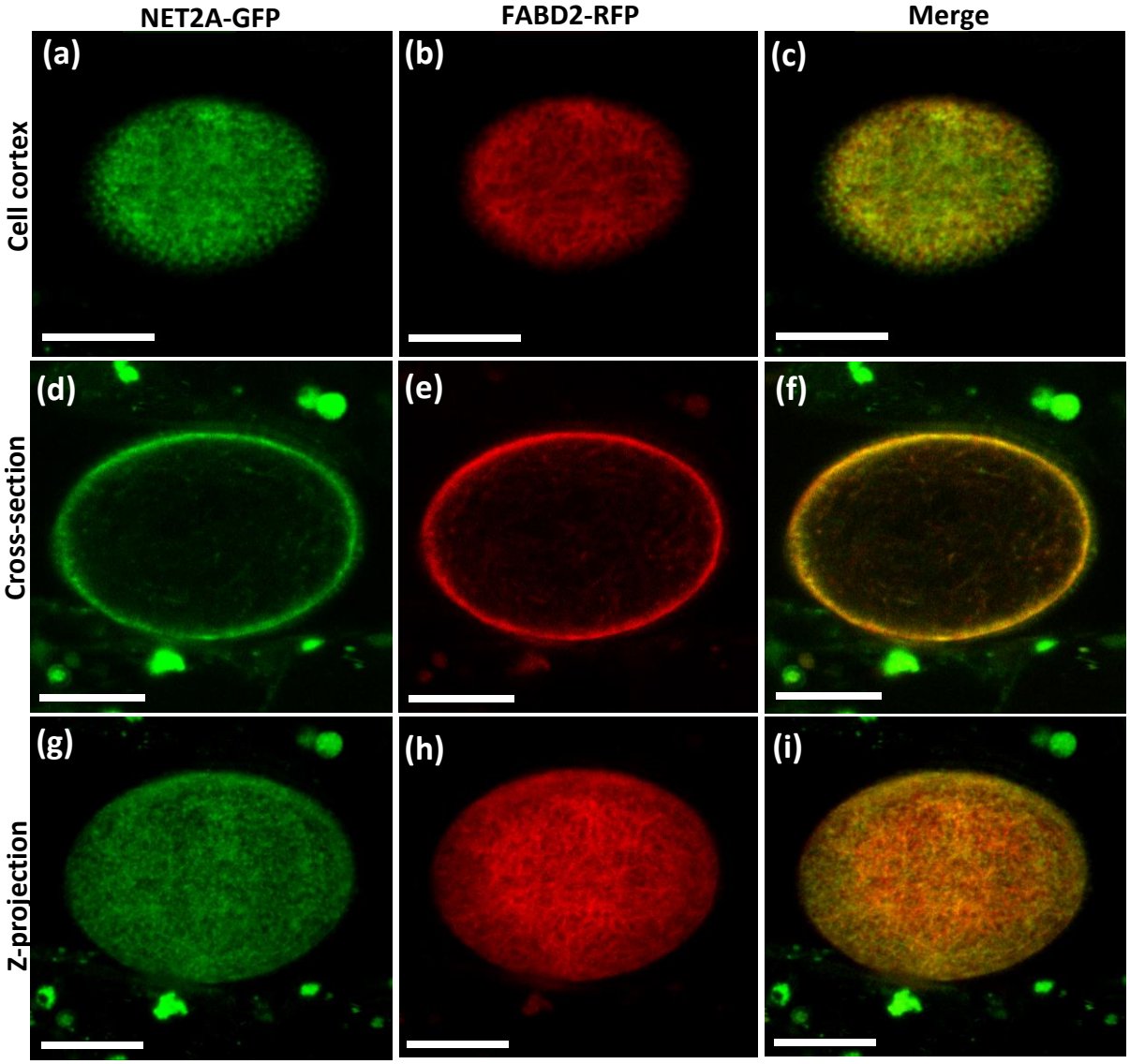

Figure 4.14: Co-localisation of the NET2A-GFP Cortical Array with Actin in Developing Pollen Grains. (a), (d) (g): NET2A-GFP subcellular localisation visualised using a 488 nm excitation laser and 505-530 nm emission detection. (b), (e) and (h): FABD2-RFP subcellular localisation visualised using a 543 nm excitation laser and 600-650 nm detection. (c): merge of (a) and (b). (f): merge of (d) and (e). (i): merge of (g) and (h). Scale bar: 10 µm.

NET2A-GFP could be seen to reside in the pollen grain cytosol in ungerminated pollen (figure 4.15). This was observed in pollen grains that had been analysed before germination could occur, and in pollen grains that had not germinated after 3 - 6 hours of incubation. It is therefore likely that the cytosolic distribution of NET2A-GFP in ungerminated pollen is not a result of pollen inviability or damage to the cell, and naturally precedes the formation of punctae at the pollen tube plasma membrane.

The subcellular localisation of NET2A-GFP in pollen grains undergoing germination was then analysed. As shown in figure 4.16, the depicted pollen grain has begun to germinate (towards the bottom-right corner), with the incipient pollen tube protruding from the exine. NET2A-GFP appeared to form discreet foci specifically at the plasma membrane facing the pollen tube germination site, which were not present at other regions of the plasma membrane. Shortly after the formation of a discernible pollen tube, NET2A-GFP localised to the plasma membrane of the pollen tube shank as described by Deeks et al. (2012), and regions of the grain plasma membrane surrounding the pollen tube germination site (figure 4.17).

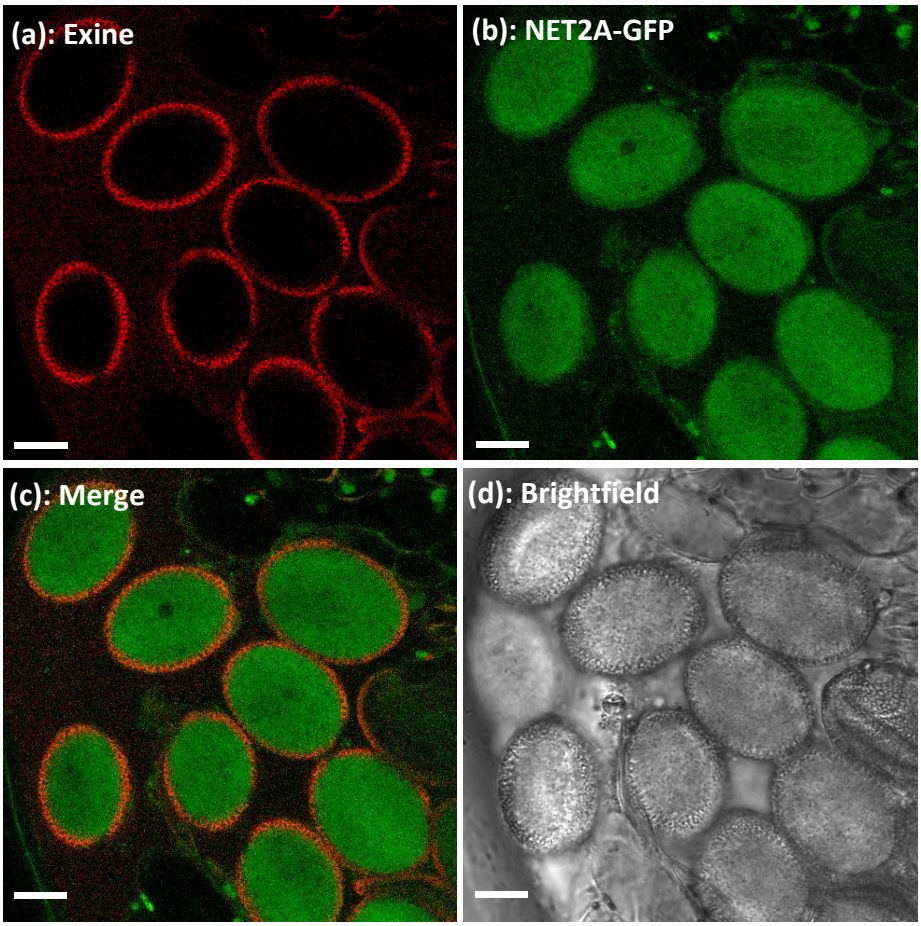

Figure 4.15: NET2A-GFP Localisation in Dehiscent Pollen Grains. (a): exine autofluorescence visualised using a 488 nm excitation laser and 600 – 700 nm emission. (b): NET2A-GFP visualised using a 488 nm excitation laser and 505 – 530 nm emission detection. (c): merge of (a) and (b). (d): brightfield image of the same cells. Scale bar: 10 µm.

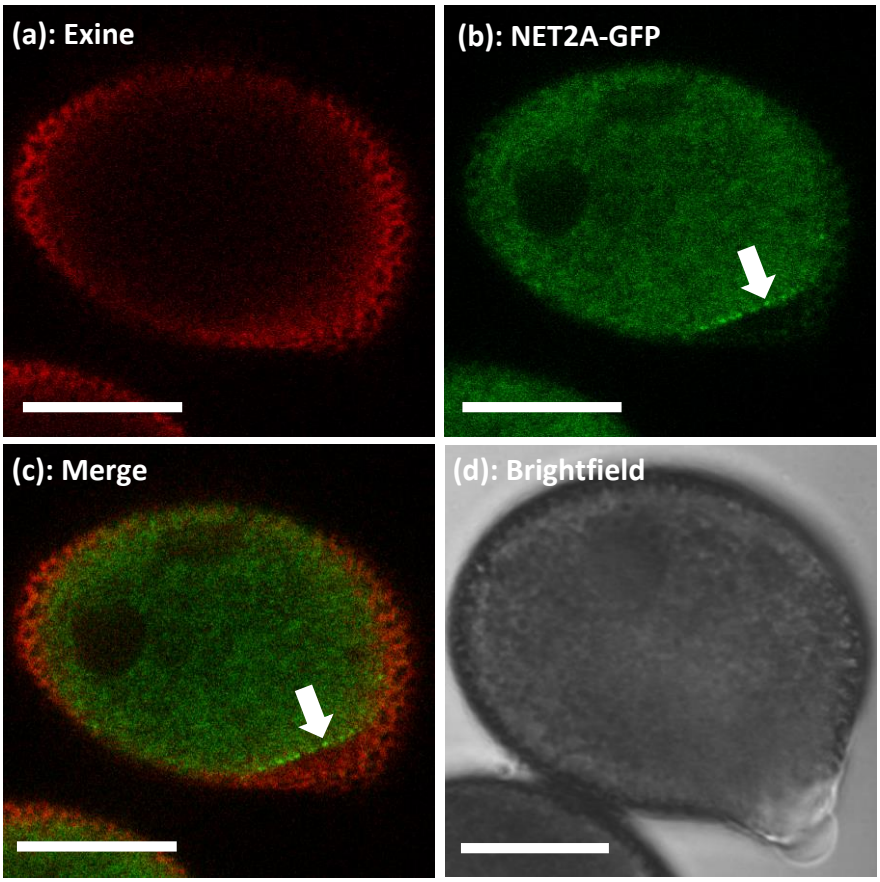

Figure 4.16: NET2A-GFP Localisation in Germinating Pollen Grains. (a): exine autofluorescence visualised using a 488 nm excitation laser and 600 – 700 nm emission detection. (b): NET2A-GFP visualised using a 488 nm excitation laser and 505 – 530 nm emission detection. (c): merge of (a) and (b). (d): brightfield image of the same cell. Scale bar: 10 µm.

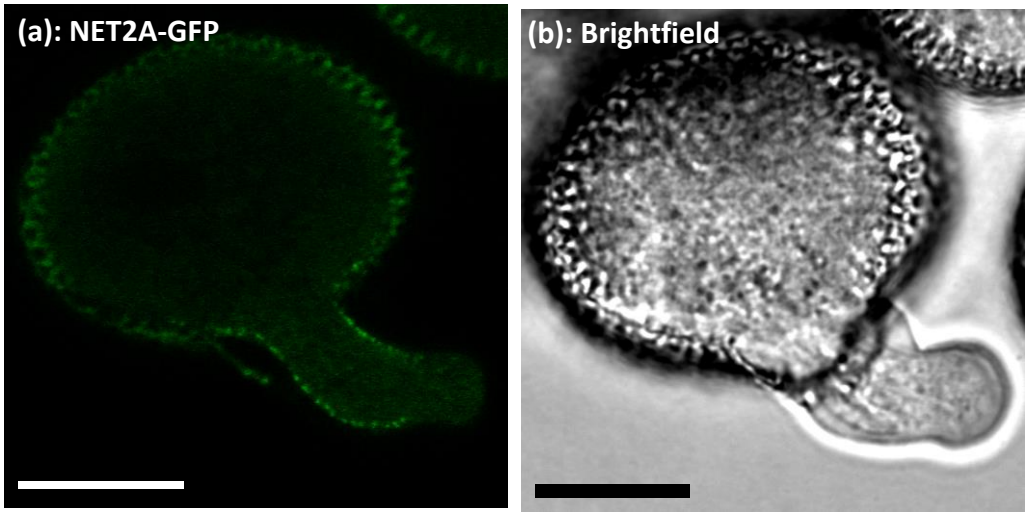

Figure 4.17: NET2A-GFP Localisation in Newly Germinated Pollen. (a): NET2A-GFP subcellular localisation. (b): brightfield image of the same cell. Scale bar: 10 µm.

4.3. Conclusion.

In this section, *in situ* analysis of NET2A-GFP subcellular localisation was performed on developing pollen grains. The observations of the dynamic reorganisations of the actin cytoskeleton in Arabidopsis pollen draw significant similarities to those previously reported in *Brassica napus* (Gervais et al. 1994) and *Nicotiana tabacum* (Zonia et al. 1999). Throughout the course of pollen grain development, NET2A-GFP could be seen to associate with the actin cytoskeleton, perhaps indicating a functional role for NET2A in the regulation of actin during gametogenesis.

NET2A-GFP exhibited distinctive subcellular localisations throughout pollen grain development; undergoing a series of dynamic reorganisations co-ordinated with the pollen developmental programme. NET2A-GFP expression was first observed during mid-bicellular pollen as immobile NET2A-punctae distributed throughout the cell; a pattern which was termed the NET2A-GFP punctate array. Co-localisation of these NET2A-GFP punctae could not be co-visualised with actin during this stage of pollen development due to poor expression of the actin marker, FABD2-RFP. In studies on *B. napus* and *N. tabacum*, actin filaments have been observed at the vegetative and generative cell nuclei prior to the formation of transverse cortical actin cables in bicellular pollen (Gervais et al. 1994; Zonia et al. 1999), and it is possible that the NET2A punctae may associate with actin filaments at the pollen grain nuclei in Arabidopsis. Proceeding the NET2A-GFP punctate array, NET2A-GFP localised to transverse cortical cables and fine cytoplasmic filaments, in a pattern termed the NET2A-GFP transverse array, which also occurred in mid-bicellular pollen. NET2A-GFP decorated actin filaments at this stage in pollen development. In accordance with this study, the actin cytoskeleton of *B. napus* has also been shown to organise to transverse actin cables during mid-bicellular pollen. Subsequently in late bicellular and early tricellular pollen, NET2A-GFP decorated actin filament networks at the cell cortex, throughout the cytoplasm and surrounding the vegetative cell nucleus. This localisation pattern was termed the NET2A-GFP filamentous array. Observations of the actin cytoskeleton surrounding the vegetative cell nucleus have been recorded in late bicellular pollen grains in *B. napus* and *N. tabacum,* with similar cortical and cytoplasmic filaments described in *N. tabacum* (Gervais et al. 1994; Zonia et al. 1999). The association of NET2A-GFP with the vegetative cell nuclear periphery in pollen grains may prove to be another

example of actin-membrane interactions mediated by the NET protein family (Deeks et al. 2012; Wang et al. 2014). In maturing tricellular pollen, the NET2A-GFP cortical array was observed, in which NET2A-GFP co-localised with a dense meshwork of fine actin filaments at the cell cortex and sparsely distributed filaments throughout the cytoplasm. Such dense cortical actin networks have been described in *N. tabacum* pollen grains nearing maturation (Zonia et al. 1999). In line with previous observations of actin subcellular localisation in developing pollen grains, the data described in this section indicates that the actin cytoskeleton of Arabidopsis is co-ordinated in a similar manner to that of *B. napus* and *N. tabacum* throughout pollen grain development. The association of NET2A with actin throughout development may indicate a role for NET2A in regulating the actin cytoskeleton during pollen grain maturation.

NET2A-GFP was cytosolic in dehiscent pollen grains, in accordance with previous observations (Dixon. 2013; Deeks et al. 2012). Upon initiation of pollen germination, NET2A-GFP foci were seen to form at the cortical membrane in direct vicinity of the incipient pollen tube germination site. In recently germinated pollen tubes, NET2A-GFP punctae were present in the pollen tube shank membrane as described by Deeks et al. (2012). During pollen tube germination, actin filaments have been reported to organise longitudinally within the grain towards the germination site, partially extending into the nascent tube (Volger et al. 2015). It is plausible that NET2A may play a role in pollen tube initiation by binding actin at the plasma membrane at the site of pollen tube germination.

Chapter 5: Identifying Interacting Partners of NET2A using Protein-Protein Interaction Screens, and Investigation of NET2A Homo- and Hetero-Oligomerisation.

5.1. Introduction.

As outlined in previous sections, reverse-genetic analysis and *in situ* localisation studies were performed to investigate the role of NET2A in Arabidopsis. In addition to these experimental approaches, identification of interaction partners of a protein of interest can elucidate the cellular functions with which that protein may be associated with. As described below, multiple protein-protein interaction screens were performed throughout the course of this study in order to identify proteins that may potentially interact with NET2A. Identification of interacting partners would contextualise the role of NET2A against characterised cellular processes; elucidating the potential roles of NET2A in Arabidopsis.

Three approaches were used to identify NET2A-interacting candidates, which will be described in this subchapter. Two protein-protein interaction screens; tandem-affinity purification coupled to mass spectrometry (TAP-MS), and split-ubiquitin yeast-2-hybrid (SU-Y2H) screens, were performed, to identify potential interacting partners of NET2A. In addition, Förster resonance energy transfer - fluorescence lifetime imaging microscopy (FRET-FLIM) was employed to corroborate the interactions of screened interacting candidates *in vivo*.

The data presented indicates that NET2A is able to interact with itself, as shown by TAP-MS and SU-Y2H interaction screens, and also with NET2B, as indicated in TAP-MS studies and FRET-FLIM. Additionally, other potential interacting partners of NET2A are listed, further investigation of which was beyond the scope of this project.

5.2. Identification of NET2A-Interacting Partners Using the TAP-MS System.

5.2.1. An Introduction to the TAP-MS System.

TAP-MS was performed by the Ghent University Plant Systems Biology (PSB) AP-MS Platform. Tandem affinity purification coupled to mass spectroscopy (TAP-MS) was performed to identify potential interacting proteins of NET2A. In TAP-MS, a protein of interest (known as the bait protein) is isolated, in order to co-purify the components of protein complexes with which it associates *in vivo*. Mass spectrometry is then performed to elucidate the identity of proteins in the purified complexes, which may interact with the bait protein directly, or indirectly.

The tandem-affinity purification was performed on *Arabidopsis thaliana* cell cultures expressing the bait construct, NET2A-GS^{Rhino} (Figure 5.1). The NET2A-GS^{Rhino} bait construct is a fusion protein of NET2A joined to a GS^{Rhino} double affinity tag, which itself, consists of a proteinG tag fused to a streptavidin binding peptide (SBP), separated by a human rhinovirus 3C protease cleavage site (Van Leen et al. 2014). ProteinG tags facilitate protein purification using an IgG resin, whilst SBP fusions allow purification with streptavidin-conjugated beads. Using GS^{Rhino}-tagged proteins as bait allows a two-step purification process: firstly, protein complexes containing the bait construct are isolated from total protein on an IgG resin. After washing of the isolated complex, its elution from the IgG resin is achieved through incubation with human rhinovirus 3C protease, and cleavage of the bait-SBP construct from the proteinG tag. Following this, a second purification step with streptavidin-conjugated beads is performed, and contaminating proteins are washed away in order to isolate and identify protein complexes with high stringency. Proteins of purified complexes are subsequently separated by size using SDS-PAGE gel electrophoresis and identified using high sensitivity mass spectrometry.

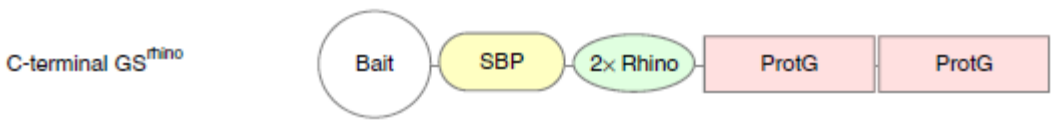

Figure 5.1: Schematic of the TAP-MS GS^{Rhino} Tag. The bait protein is fused to a GS^{Rhino} tag, consisting of ProteinG tags fused to streptavidin binding peptide (SBP), separated by a human rhinovirus 3C protease cleavage site. This facilitates the two-step protein purification process described above. Taken from Van Leen et al. (2014).

5.2.2. Cloning and Expression of NET2A-GS^{Rhino} in Arabidopsis Cell Culture.

The full-length NET2A coding sequence was PCR amplified from Arabidopsis floral cDNA, and inserted into pDONR207 using gateway cloning. Subsequent generation and expression of the NET2A-GS^{Rhino} expression construct in Arabidopsis cell culture was performed by the Ghent University PSB AP-MS platform. A western blot of transformant total protein, probed with anti-GS^{Rhino} antibodies, was provided by Ghent PSB, as proof of NET2A-GS^{Rhino} expression in cell culture (figure 5.2). An intense band of ≈150 KDa was observed, corresponding to NET2A-GS^{Rhino}, which has a predicted MW of 141 KDa. Fainter bands of lower MW can be attributed to degradation products of NET2A-GS^{Rhino}.

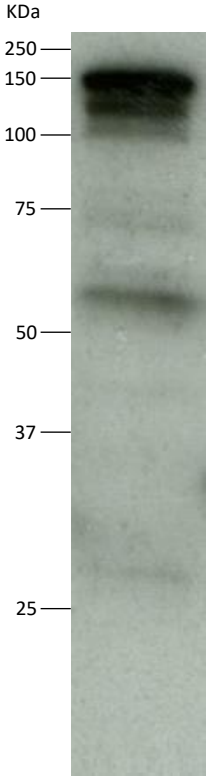

Figure 5.2: Western Blot Analysis of NET2A-GS^{Rhino} Expression in *Arabidopsis thaliana* Cell Culture. Western blot provided by the Ghent University PSB AP-MS Platform, as proof of NET2A-GS^{Rhino} expression in Arabidopsis cell culture. Total protein from Arabidopsis cell culture expressing NET2A-GS^{Rhino} was analysed with anti-GS^{Rhino} antibodies.

5.2.3. Candidate Interactors of NET2A Identified in the TAP-MS Screen.

Having confirmed that the NET2A-GS^{Rhino} bait construct was stably expressed in *Arabidopsis* cell culture, TAP-MS was performed by the Ghent University PSB AP-MS Platform.

Candidate interactors of NET2A were screened using two different protein extraction methods used to isolate protein complexes containing the NET2A-GS^{Rhino} bait. The

first employed the detergent Triton X-100 as a method of protein extraction from plant tissue sample, the second used the detergent, Digitonin. Various detergents are known to have differential effects on protein-protein interactions, so multiple detergent extraction methods were employed in order to screen interactions between proteins that might be disrupted with one detergent extraction method. Using two detergent extractions can also increase the stringency of the screen: candidate interactors isolated in multiple detergent extraction methods may be more likely to be genuine protein complex components.

Table 5.1 shows a list of candidate interacting proteins of NET2A, identified in the TAP-MS screen.

Gene Locus	Protein Description	Detergent Extraction Method
At1g58210	NET2A (NETWORKED 2A)	Digitonin and triton-X100
At1g09720	NET2B (NETWORKED 2B)	Digitonin and triton-X100
At1g62390	CMLP1 (CLUMPED CHLOROPLASTS 1)	Digitonin only
At1g04080	PRP39/TETRATRICOPEPTIDE (TRP)-LIKE SUPERFAMILY PROTEIN	Digitonin only
At4g35800	NRPB1 (RNA POLYMERASE II LARGE SUBUNIT)	Digitonin only

Table 5.1: Candidate Interactors of NET2A Identified in the TAP-MS Screen. Detailed are the gene loci and descriptive names of proteins identified as interactors of NET2A, with the detergent extraction methods with which they were isolated.

Of the potential interactors listed in Table 5.1, NET2A and NET2B were selected for further investigation as true interactors of NET2A. NET2A and NET2B were isolated in both digitonin and triton-X100 TAP-MS extraction methods, indicating a high likelihood that these proteins may genuinely exist in complex with NET2A. Also, previous work has shown other members of the NET superfamily to form homo-oligomers and hetero-oligomers with other members within the same NET family. NET3C for example, has been shown to self-interact (Wang et al. 2014), whilst NET4A and NET4B are able to form homodimers, and heterodimerise with each other (Mentlak. 2015). It is therefore likely that members of the NET2 family may also bind each other. Thus, NET2A and NET2B were selected for further confirmation as potential interactors of NET2A.

CLMP1 is known to be involved in chloroplast partitioning during mitosis (Yang et al. 2011). It has also been observed to localise to microtubules of the cell plate during division and interact with the microtubule-binding protein, TANGLED (Su. 2012). In addition to this, expression of CLMP1 in *Saccharomyces pombe* resulted in alterations in actin organisation and defects in cell morphology (Xia et al. 1996). Despite the interesting implications of a possible interaction between NET2A and CLMP1, there remained insufficient time to demonstrate and characterise CLMP1 as an interactor of NET2A, and no further investigation of this protein was performed.

PRP39 and NRPB1 were not studied further. PRP39 is putatively involved in mRNA splicing, and is a homologue of the yeast pre-mRNA processing protein, Prp39p (Wang et al. 2007). NRPB1 is a component of RNA POLYMERASE II. It is highly unlikely that NET2A is involved in the same subcellular processes as these proteins, and therefore PRP39 and NRPB1 were not investigated further.

To validate the data yielded from the TAP-MS screen, FRET-FLIM was performed to corroborate the observed interactions between NET2A and NET2B. A homomeric interaction between NET2A and itself was identified in a split-ubiquitin yeast-2-hybrid screen as described in section 5.4, confirming the interaction observed by TAP-MS.

5.3. Analysis of NET2A-NET2B Interactions *in vivo* Using FRET-FLIM.

5.3.1. An Introduction to FRET-FLIM.

The results of the TAP-MS screen described in the previous section had identified candidate proteins that may complex with NET2A. A second method of investigating protein-protein interactions was employed to validate whether the proteins co-purified with NET2A in the TAP-MS screen were genuine NET2A-interacting proteins. Employed to this end was FRET-FLIM; a non-invasive imaging method of analysing direct interactions of fluorophore-tagged proteins *in vivo*. FRET-FLIM combines two major principles: FRET, (Förster resonance energy transfer), combined with FLIM (fluorescence lifetime imaging microscopy).

FRET is a process of energy transfer from an excited fluorophore (donor) to another molecule (acceptor). This process is known to quench donor fluorophore excitation, and reduce the fluorescence lifetime of the donor. In this system, the acceptor is usually another fluorophore which can absorb emitted energy from the donor fluorophore.

FLIM is a method of measuring the fluorescence lifetime of a specific fluorophore. Fluorescence lifetime is an intrinsic property of all fluorophores, defined by the average time it spends in an excited state before returning to ground state during photon emission. This fluorescence lifetime is sensitive to the local microenvironment of the fluorophore: this phenomenon can be exploited to investigate protein-protein interactions, as interacting proteins lying in direct proximity of the fluorophore may induce detectable changes in its fluorescence lifetime if FRET occurs between them. FRET between two proteins is only possible if they lie within 10 nm of each other (a distance known as the Förster distance), and therefore resulting reductions in donor fluorophore lifetime can be attributed to a close physical relationship with an acceptor (figure 5.3; Sun et al. 2011).

In FRET-FLIM, putative interacting partners are co-expressed as fluorophore-tagged fusion proteins *in vivo*. If the two fusion proteins physically interact, FRET will occur between the donor and acceptor fluorophores, reducing the fluorescence lifetime of the donor fluorophore. Before FRET-FLIM could be performed, appropriate donor and acceptor fluorophore-fusion proteins were developed and expressed *in vivo*, as described in the next section.

5.3.2. Generation of FRET-FLIM Donor and Acceptor Constructs; NET2A-GFP and NET2B-RFP.

In order for FRET to occur between them, donor and acceptor fluorophore pairs must possess overlapping spectral profiles: the emission spectrum of the donor fluorophore must be shared with the absorption spectrum of the acceptor for energy transfer to occur (figure 5.4). Variations of CFP/YFP, and GFP/RFP donor/acceptor fluorophore pairs are popular combinations for use in FRET-FLIM, as these commonly used fluorophore tags possess the desired overlapping spectral properties required for FRET. In this study, GFP-fusion proteins were used as donor

constructs, and RFP-fusion proteins as acceptors. A summary of generated donor and acceptor constructs for use in FRET-FLIM is shown in table 5.2 and figure 5.5.

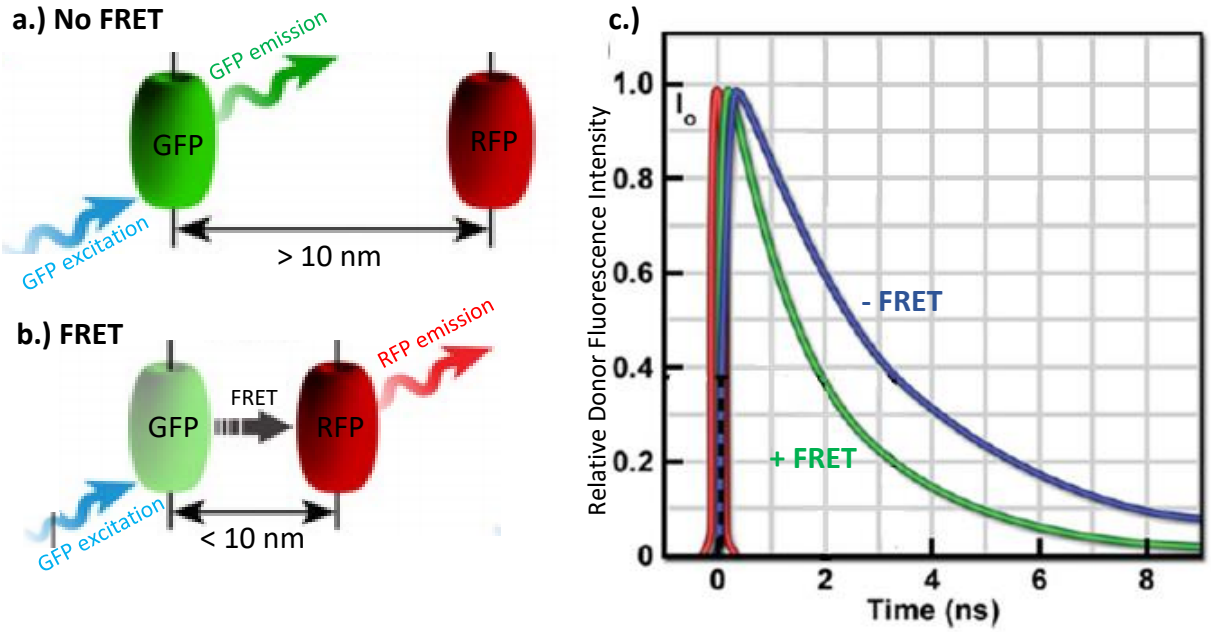

Figure 5.3: The Principles of FRET and Fluorescence Lifetime. (a) and (b): FRET occurs between donor (GFP) and acceptor (RFP) molecules only when within 10 nm proximity. When >10 nm apart, GFP is excited and emits energy as fluorescence. When within 10 nm of an acceptor, excited GFP transfers energy to RFP via FRET. (c) shows a profile of donor fluorescence lifetime: immediately following excitation, a sharp peak in fluorescence emission is observed, which decays over time. When the donor undergoes FRET, the fluorescence is quenched and fluorescence lifetime is greatly reduced. (a) and (b) are adapted from Ishikawa et al. (2012). (c) adapted from Day and Davidson. (2012).

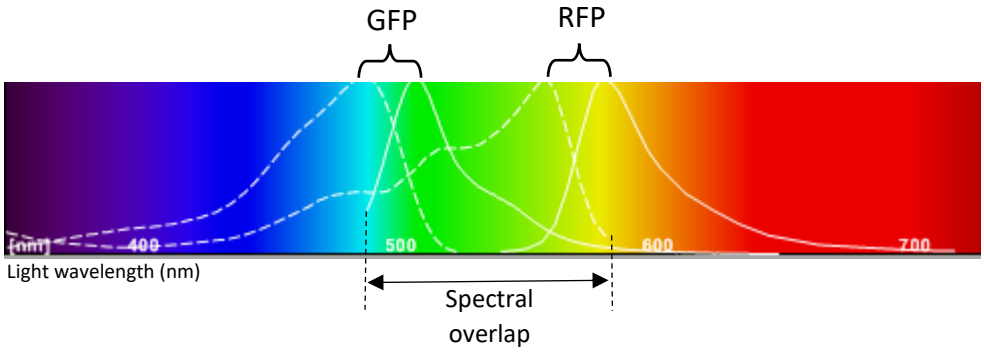

Figure 5.4: FRET Requires Spectral Overlap Between Two Fluorophores. Excitation (dashed lines) and emission (solid lines) spectra of GFP and RFP. The wavelengths of light emitted by GFP overlap with the wavelengths of light absorbed by RFP during excitation. The ability of RFP to absorb wavelengths of light emitted by GFP permits FRET between the two fluorophores.

Interaction Studied	Donor Construct	Acceptor Construct
NET2A and NET2B	NET2A-GFP	NET2B-RFP
Positive Control	GFP-RFP	

Table 5.2: The Protein-Protein Interactions to be Investigated using FRET-FLIM, and the Donor and Acceptor Construct Pairs Used.

To generate the NET2A-GFP expression construct, the full length NET2A coding sequence was cloned into pB7FGW2 from NET2A-pDONR207 using gateway cloning. pB7FGW2 facilitates the expression of proteins as C-terminal GFP fusions under the expression of a *CaMV 35s* promoter.

The full length NET2B coding sequence was PCR amplified from *Arabidopsis thaliana* gDNA and cloned into pDONR207 using gateway cloning. NET2B was then cloned into pH7RGW2 to drive expression of full length NET2B-RFP under control of a *CaMV 35s* promoter.

As a positive control, a GFP-RFP fusion protein construct was generated to physically link the GFP donor and RFP acceptor in direct proximity, and guarantee FRET. Such constructs have been used previously to demonstrate decreases in GFP fluorescence lifetime, resulting from FRET between physically associated GFP and RFP fusions (Wang et al. 2014). To generate this construct, the coding sequence of the RFP fluorophore, DsRED, was PCR amplified from pH7RGW2 and cloned into pDONR207 using gateway cloning. The DsRED coding sequence was then cloned into pMDC43 to express DsRED with an N-terminal GFP tag under the control of a *CaMV 35s* promoter.

Having generated the donor and acceptor expression constructs for use in FRET-FLIM, the resulting fusion proteins were expressed in *Nicotiana benthamiana* leaf epidermal cells using agrobacterium-mediated transformation, and their subcellular localisation analysed *in vivo*.

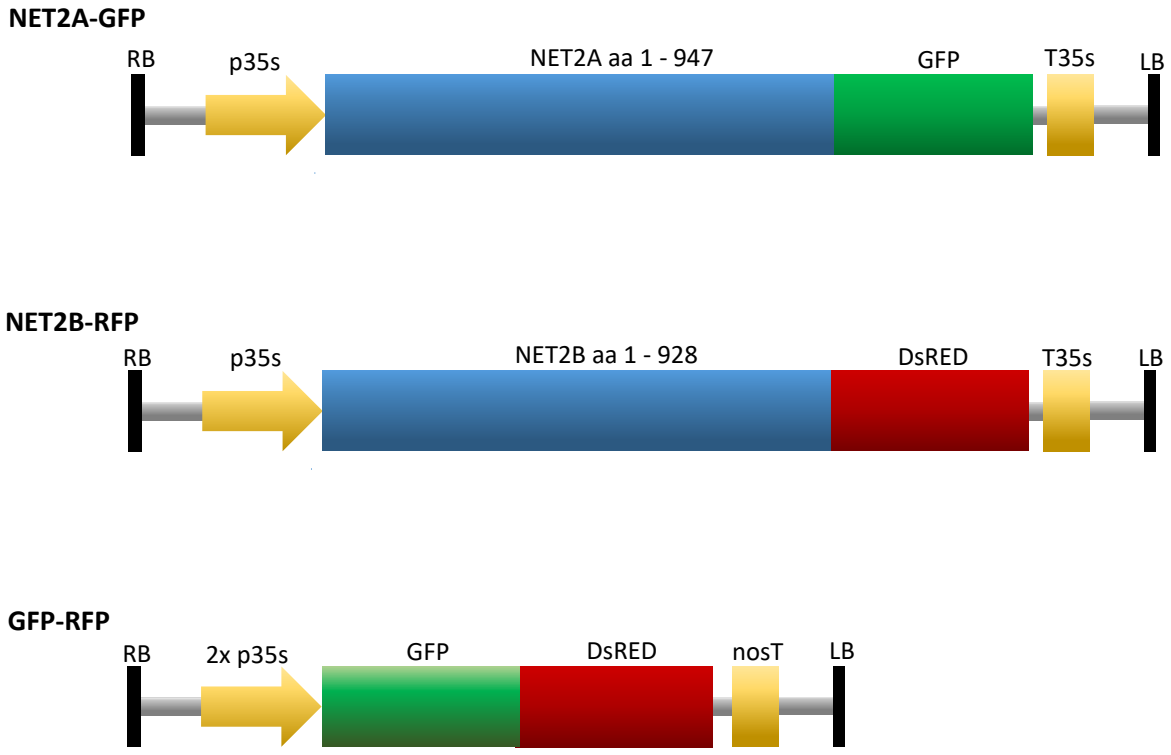

Figure 5.5: Schematics of Expression Constructs Listed in Table 5.2, used to Express Donor and Acceptor Fluorophore Fusions *in vivo* for use in FRET-FLIM: NET2A-GFP was generated using the vector pB7FGW2, NET2B-RFP was generated using pH7RGW2, and GFP-RFP was generated using pMDC43. RB = T-DNA right border. p35s = CaMV 35s promoter sequence. T35s = CaMV 35s terminator sequence. nosT = nopaline synthase terminator sequence. LB = T-DNA left border.

5.3.3. Analysis of NET2A-GFP and NET2B-RFP Subcellular Localisation *in vivo.*

Having generated the necessary donor and acceptor FRET-FLIM expression constructs outlined above, agrobacterium-mediated transformation was used to facilitate their expression in *Nicotiana benthamiana* leaf epidermal cells, so that their subcellular localisation could be observed.

Agrobacterium tumefaciens is a natural plant pathogen, which integrates transfer-DNA (T-DNA) into the host genome to promote tumour formation during infection (Zupan and Zambryski. 1995). The ability of Agrobacterium to transfer DNA into plant genomes has been manipulated as a method of plant transformation, in order to introduce and express recombinant DNA constructs of interest in host plants. The

genes necessary for inducing tumour formation have been removed from the T-DNA, and genetic expression constructs of interest can be inserted, facilitating their mobilisation and integration into host DNA.

Nicotiana benthamiana leaf epidermal cells are a commonly used system for the expression of transgenes using Agrobacterium-mediated transformation (Kapila et al. 1997), and can be used to study the subcellular localisation of fluorophore-tagged fusion proteins. During this procedure, the apoplastic space of *N. benthamiana* leaf tissue is infiltrated with a solution of agrobacterium, permitting the transfer of T-DNA to cells in the local vicinity, and the expression of transgenic constructs in *N. benthamiana* leaf tissue.

Using agrobacterium-mediated transformation, NET2A-GFP and NET2B-RFP were expressed in *N. benthamiana* leaf epidermal cells, and their subcellular localisations observed using CLSM. Using this method, co-expression of NET2A-GFP and NET2B-RFP was performed, to analyse their potential co-localisation and see if they could possibly interact i*n vivo*. Following this, FRET-FLIM was performed on leaf epidermal cells co-expressing the donor and acceptor FLIM constructs, to analyse whether they may interact physically.

The subcellular localisations of NET2A-GFP and NET2B-RFP and can be shown in figure 5.6. Expectedly, full length NET2A-GFP and NET2B-RFP were observed to decorate a filamentous network in *N. benthamiana* leaf epidermal cells, forming punctae on filaments in accordance with the described subcellular localisations of NET2A, and other NET proteins observed by Deeks et al. (2012). In addition to this, the NET2-fusion proteins were observed to form protein aggregates, which were especially prominent at the nuclear envelope. These aggregates are likely to be artefacts of protein overexpression, resulting from constitutive expression under the *CaMV 35s* promoter. The formation of aggregates was reduced by infiltrating the leaf tissue with lower concentrations of agrobacterium, thus reducing expression of the fusion proteins. Due to variability in expression levels of the fusion constructs from cell to cell, protein aggregates could still be observed in highly-expressing cells.

Having analysed the subcellular localisation of the NET2A and NET2B fluorophore fusions designed for FRET-FLIM, potential co-localisation of the subcellular localisations of donor and acceptor FRET-FLIM constructs was investigated.

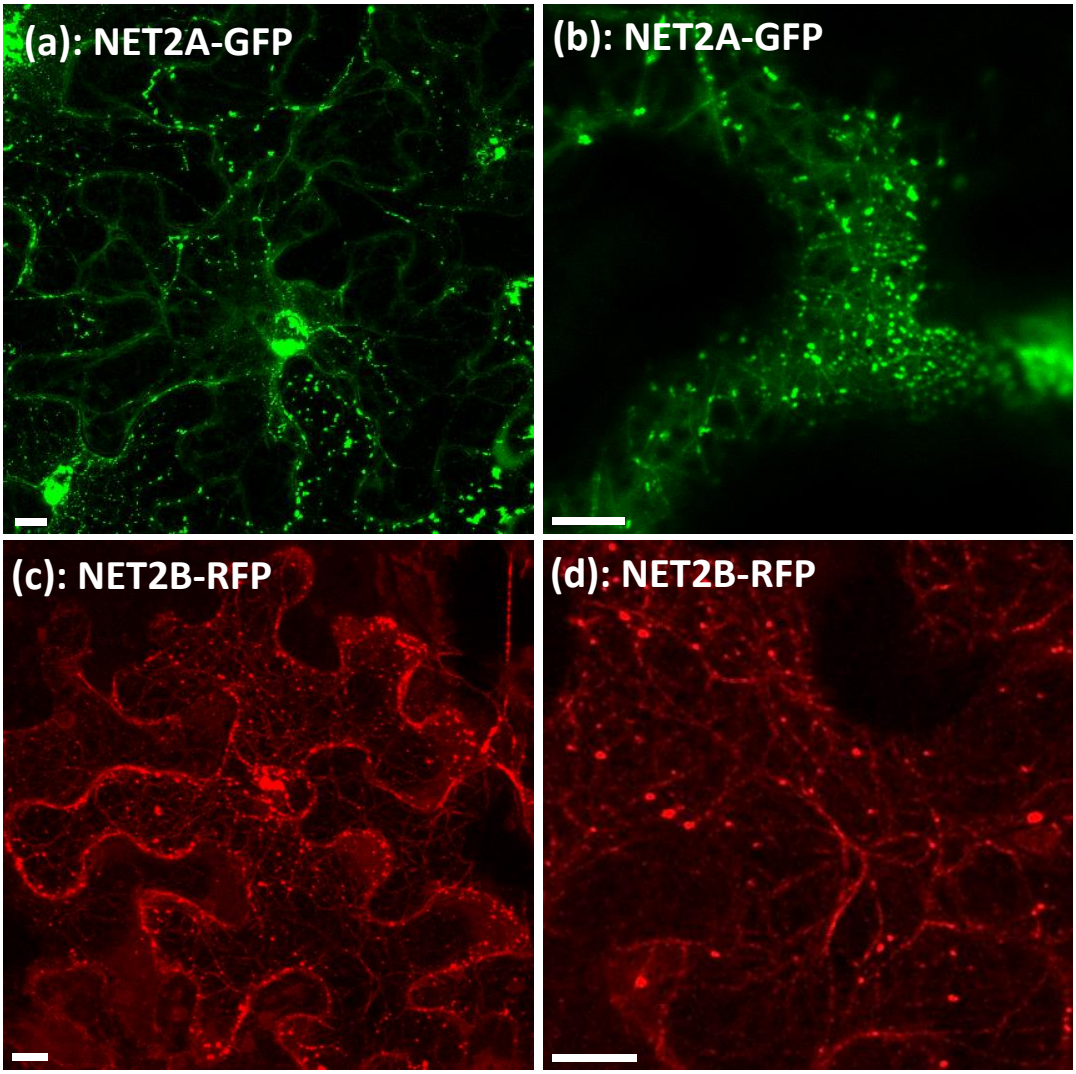

Figure 5.6: The Subcellular Localisation of NET2A-GFP and NET2B-RFP in *N. benthamiana* Leaf Epidermal Cells. (a) and (b): NET2A-GFP localisation. (c) and (d): NET2B-RFP localisation. Scale bar: 10 µm.

5.3.4. Co-Localisation of NET2A-GFP with NET2B-RFP *in vivo*.

For two proteins to physically interact, it is necessary for them to reside at the same subcellular localisation at a point in time. Therefore, the potential co-localisation between the NET2A-GFP FRET-FLIM donor and NET2B-RFP acceptor constructs was analysed. The distinct spectral properties of GFP with those of RFP permits the discreet visualisation of GFP and RFP fusion proteins. After sequential imaging of GFP and RFP, an overlay of each image is created to visualise the co-localisation between the GFP and RFP-fusion proteins.

Using agrobacterium-mediated transformation, the donor and acceptor fusion proteins were co-expressed in *N. benthamiana* leaf epidermal cells. Potential co-

localisation between the GFP donor and RFP acceptor fusion protein constructs was analysed using CLSM. GFP was visualised using a using a 488 nm excitation laser and detection of fluorescence emission of 505 – 530 nm. RFP was visualised using a 543 nm excitation laser and detection of fluorescence emission of 600 - 650 nm.

Figure 5.7 shows the co-localisation between NET2A-GFP with NET2B-RFP. Unsurprisingly, NET2A-GFP was clearly observed to co-localise with NET2B-RFP, appearing to co-localise on actin filaments and also at the punctae that lie on them. It should be noted that no bleedthrough between channels was observed when one of the fluorophore constructs was expressed alone under identical imaging conditions.

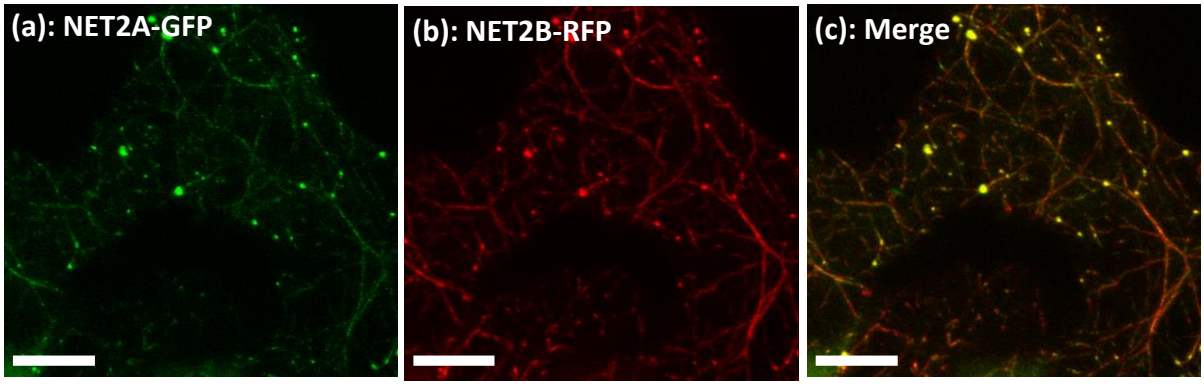

Figure 5.7: Co-localisation of NET2A-GFP with NET2B-RFP *in vivo*. *N benthamiana* leaf epidermal cells co-expressing NET2A-GFP and NET2B-RFP. (a) and (d): NET2A-GFP visualised using a 488 nm excitation laser and detection of 505 – 530 nm emission. (b): NET2B-RFP, visualised using a 543 nm excitation laser, and detection of 600 – 650 nm emission. (c): and overlay of images (a) and (b), with yellow indicating regions of co-localisation between NET2A-GFP and NET2B-RFP. Scale bar: 10 µm.

3.3.5. FRET-FLIM Analysis of NET2A-NET2B Interactions.

Having confirmed the co-localisation of the NET2A-GFP and NET2B-RFP fusion proteins *in vivo*, FRET-FLIM was performed to ascertain whether they may interact directly.

FRET-FLIM was performed on *N. benthamiana* leaf epidermal cells expressing donor and acceptor FRET-FLIM constructs, using the Leica SP5 CLSM running the Leica SMD FLIM Wizard program. The 470 nm pulse laser was used to excite the GFP-fusion protein donor constructs. Fluorescence lifetime calculation was performed using the PicoQuant SymPhoTime 32 curve fitting software. During fluorescence lifetime calculation, a χ^2 value close to 1, which is indicative of good curve fitting, was ensured for all measurements (Wang et al. 2014).

To investigate a potential interaction between NET2A and NET2B, FRET-FLIM was performed on leaf sections expressing either the NET2A-GFP donor construct alone, or co-expressing NET2A-GFP alongside the NET2B-RFP acceptor construct. Comparison of the fluorescence lifetime of NET2A-GFP, with that of NET2A-GFP + NET2B-RFP was made, to ascertain whether the NET2B-RFP acceptor could reduce the fluorescence lifetime of the NET2A-GFP donor. A reduction in NET2A-GFP fluorescence lifetime by NET2B-RFP would indicate the occurrence of FRET between the two fluorophores, implicating a close physical interaction of the two fusion proteins. As a positive control, FRET-FLIM was performed on *N. benthamiana* leaf epidermal cells expressing the GFP-RFP fusion protein.

Figures 5.8 and 5.9 show the average fluorescence lifetimes of the NET2A-GFP donor when expressed alone, and when co-expressed with the NET2B-RFP acceptor. The data clearly indicates a significant drop in the fluorescence lifetime of NET2A-GFP when co-expressed alongside NET2B-RFP, compared to NET2A-GFP expressed alone. This reduction in average fluorescence lifetime of 0.28 ns is highly similar to that observed in FRET-FLIM experiments used analyse the published interaction between NET3C and VAP27 (Wang et al. 2014). It is accepted that FRET occurrence, and therefore a protein-protein interaction, can be confidently confirmed if the normal fluorescence lifetime of a GFP donor construct is reduced by ≈ 0.2 ns or more, when in the presence of an acceptor construct (Danquah et al. 2011; Jeshtadi et al. 2010; Osterrieder et al. 2009; Sparkes et al. 2010; Stubbs et al. 2005). The observed reduction in fluorescence lifetime is highly indicative of FRET occurring between NET2A-GFP and NET2B-RFP, and therefore a close physical interaction between the two proteins. In comparison, the average fluorescence lifetime of the GFP-RFP fusion protein was 2.06 ± 0.04 ns. Using two separate experimental approaches to investigate protein-protein interactions (TAP-MS and FRET-FLIM), NET2B has been demonstrated to interact directly with NET2A.

Constructs Expressed	Mean GFP Fluorescence Lifetime	Standard Deviation	n
NET2A-GFP	2.47 ns	0.03	10
NET2A-GFP + NET2B-RFP	2.19 ns	0.09	9
GFP-RFP positive control	2.06 ns	0.04	5

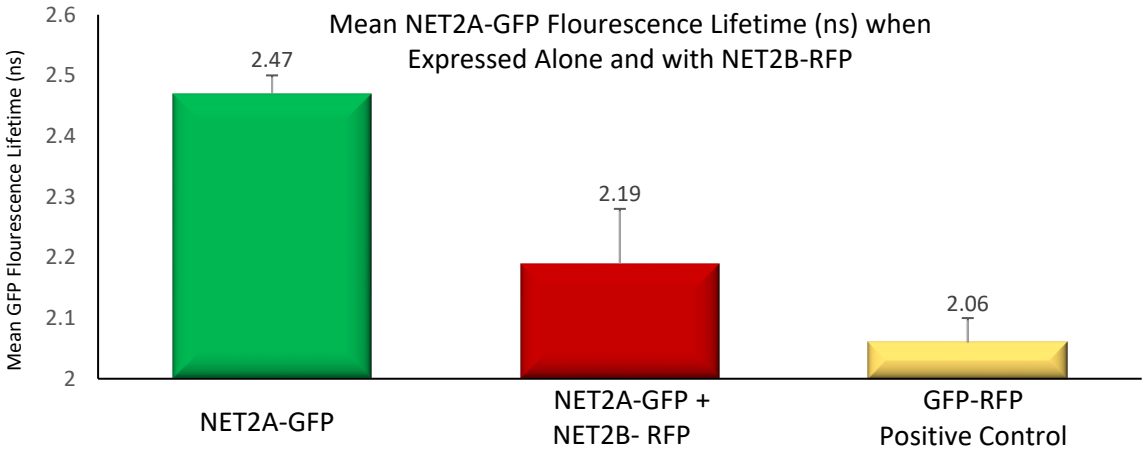

Figure 5.8: NET2B-RFP Induces a Decrease in NET2A-GFP Fluorescence Lifetime when Co-expressed in *N. benthamiana* Leaf Epidermal Cells. n = number of cells analysed

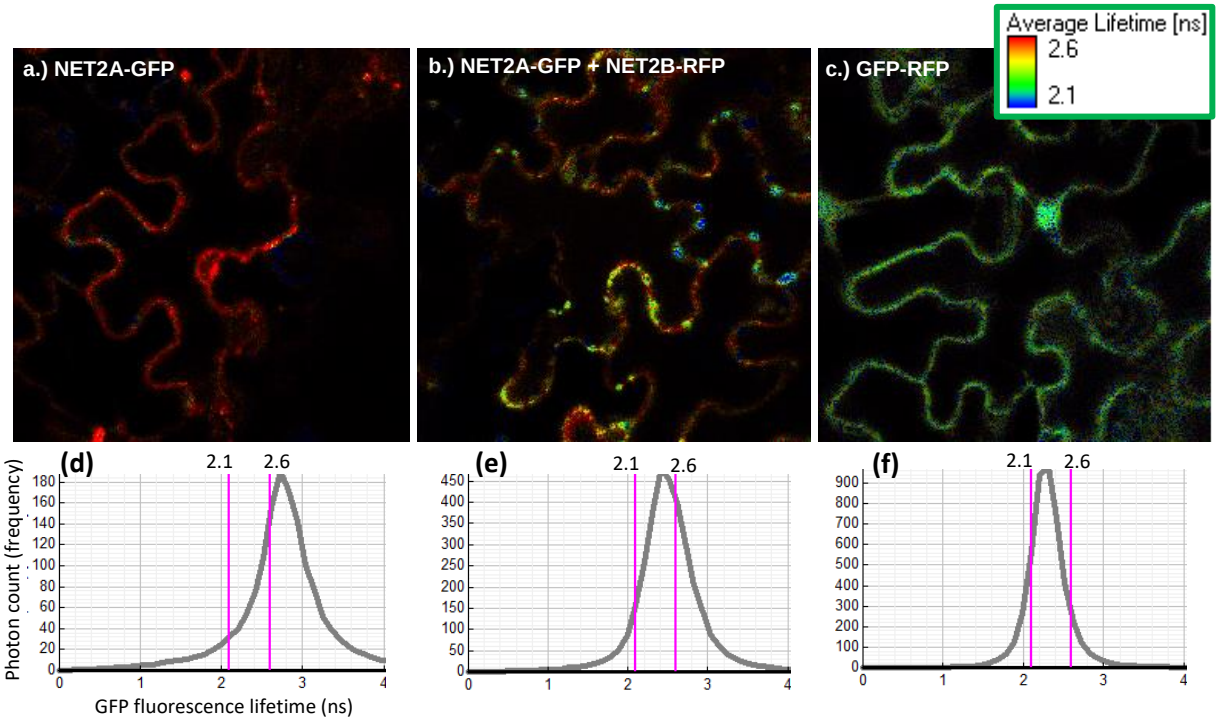

Figure 5.9: Visualisation of NET2A-GFP Fluorescence Lifetime *in vivo* when Expressed Alone, and with NET2B-RFP. (a)–(c): Example images of GFP fluorescence detected in *N. benthamiana* leaf epidermal cells, pseudocoloured according to GFP fluorescence lifetime. (d)-(f): charts associated with images (a)-(c) respectively, show the frequency distributions of the fluorescence lifetimes (ns) of detected photons in each image. A leftward shift in peak GFP fluorescence lifetime is indicative of reduced average lifetime. (a) and (d): NET2A-GFP expressed alone. (b) and (e): NET2A co-expressed with NET2B-RFP. (c) and (f): GFP-RFP positive control.

5.4. Screening for Interacting Partners of NET2A using the Split Ubiquitin Yeast-2-Hyrid System.

NET2A was observed to interact with itself in the TAP-MS interaction screen. Validating this interaction, NET2A was identified as an interactor of itself in a split ubiquitin yeast-2-hybrid (SU-Y2H) screen. Therefore, NET2A-NET2A interactions were corroborated using two experimental approaches, confirming that NET2A is able to bind itself to form homo-dimers, or homo-oligomers.

This section describes the principles of the SU-Y2H screen, that was performed by the DUALhunter Screening service, DualsystemsBiotech, and outlines the proteins identified as interactors of NET2A in this screen. In addition to identifying a NET2A-NET2A interaction, another protein of interest, At3g24100, was identified as NET2A-interacting protein. The characterisation of At3g24100, named MAP7A in this study, will be described in chapter 7.

5.4.1. An Introduction to the Split Ubiquitin Yeast-2-Hybrid System.

The yeast-2-hybrid (Y2H) system is a method of investigating direct protein-protein interactions in *Saccharomyces cerevisiae* yeast cells, in which an interaction results in the ability of the yeast to survive and grow on selective media. The occurrence of an interaction results in the activation of a transcription factor, endowing the yeast with an ability to transcribe genes necessary for survival on selective media.

In the SU-Y2H system, protein-protein interactions will result in liberation of an artificial transcription factor, through the recombining of two halves of ubiquitin; Cub (the ubiquitin C-terminal moiety), and Nub (the ubiquitin N-terminal moiety), to form a functional, split-ubiquitin complex. This formation of a functional split-ubiquitin molecule (which is fused to the transcription factor), acts as a proteolytic cleavage signal by ubiquitin-specific proteases, to release the transcription factor from sequestration. In this assay, the artificial transcription factor PLV (ProteinA-LexA-VP16) is fused to Cub, which is in turn bound to a bait protein of interest, which is tethered to the membrane by fusion to the yeast integral membrane protein, Ost4p. To screen for potential interactors of the bait protein, the bait-Cub construct is co-expressed alongside prey-Nub fusion proteins. If the bait and prey proteins interact,

it will permit the recombining of Cub and Nub to form split ubiquitin, and release PLV, so that it may transcribe genes necessary for survival (figure 5.12).

The SU-Y2H interaction screen was conducted in the yeast reporter strain, NMY32. The NMY32 reporter strain (*MATa trp1 leu2 his3 ade2 LYS::2LexA-HIS3 ade2::LexA-ADE2 URA3::LexA-lacZ*) has loss of function mutations in the genes *TRP1* (necessary for tryptophan synthesis), *LEU2* (leucine synthesis), *HIS3* (histidine synthesis), *ADE2* (adenine synthesis; Möckli et al. 2007), meaning that culture media must be supplemented with these nutrients for NMY32 to survive and grow. On selective media lacking one or more of these nutrients, growth cannot occur. The strain contains the reporter genes *LYS::2LexA-HIS3* and *ade2::LexA-ADE2,* that permit the expression of *HIS3* and *ADE2* under the control of PLV, as well as *URA3::LexA-lacZ* for the expression of *LacZ*. The release of PLV from sequestration during an interaction between bait and prey permits transcription of *HIS3* and *ADE2*, permitting growth on selective media lacking histidine (-H) and adenine (-A), and the expression of *LacZ* for colorimetric assays.

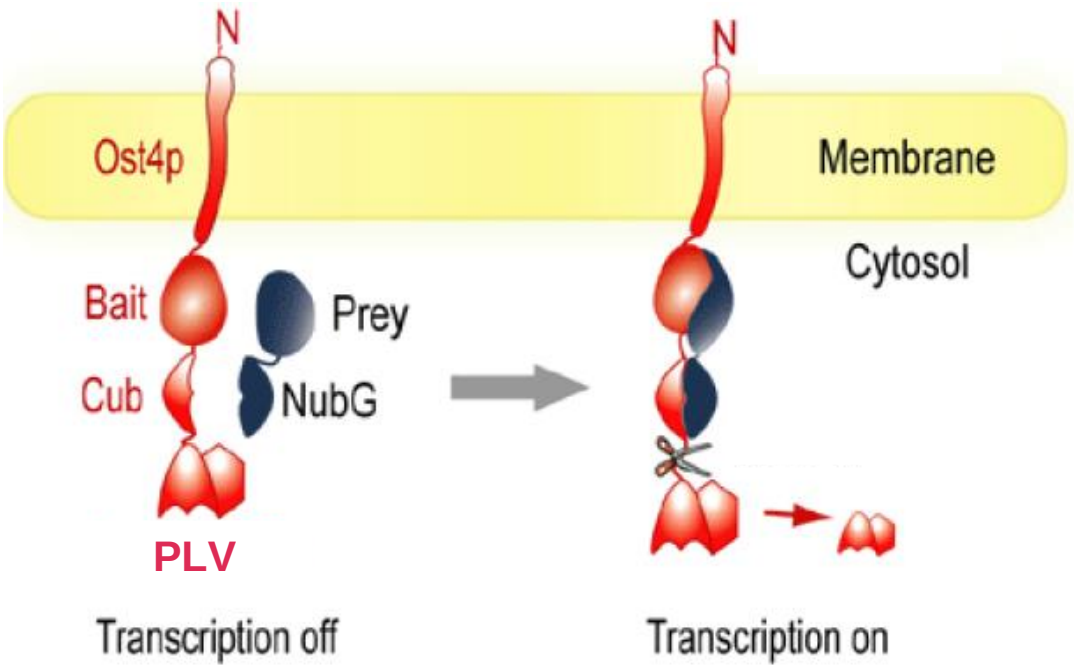

Figure 5.10: Split Ubiquitin Yeast-2-Hybrid Mechanism of Action. The interaction of the prey and bait constructs re-constitutes a functional split ubiquitin molecule through the bringing together of Cub and Nub. Split ubiquitin is recognised by ubiquitin-specific proteases that release the PLV transcription factor, permitting transcription of reporter genes. Figure taken from the Dualhunter screening report.

5.4.2. Screening for Interactors of NET2A using the Dualhunter Split Ubiquitin Yeast-2-Hybrid System.

The generation of the bait construct and its transformation into yeast was performed by DualsystemsBiotech. pDONR207-NET2A was sent to DualsystemsBiotech as template for PCR amplification. The full-length NET2A coding sequence was inserted into the *SfiI* restriction sites of pDHB1 using restriction cloning, to permit the expression of Ost4p-NET2A-Cub-PLV in yeast. pDHB1 carries the selection marker, *LEU2* (necessary for leucine synthesis), permitting growth and selection of transformants on selective plates lacking leucine (-L). The construct was transformed into NMY32 using DualsystemsBiotech proprietary protocols.

It is known that the expression of a bait construct in yeast reporter strains can autonomously activate reporter transcription, giving rise to false positive results. The *HIS3* reporter gene is known to have 'leaky expression' and can activate in absence of an interaction (Van Criekinge and Beyaert. 1999). Varying levels of 3-amino-triazole (3AT) can competitively inhibit *HIS3* reporter activation to reduce the basal level of *HIS3* activity. It was determined by DualsystemsBiotech that 2.5 mM 3AT was sufficient to prevent NMY32 bearing pDHB1-NET2A growing on -H media.

Prey cDNAs from a normalised *Arabidopsis thaliana* cDNA library were cloned into the prey vector, pPR3-N, using DualsystemsBiotech proprietary protocols. pPR3-N contains the reporter gene, *TRP1* (necessary for tryptophan synthesis), permitting growth and selection of transformants on media lacking tryptophan (-W). The cDNA library in pPR3-N was transformed into NMY32 bearing pDHB1-NET2A using DualsystemsBiotech proprietary protocols. Transformants were grown on -L, (to select for the bait construct), -W (to select for the prey construct), -A and -H (to select for activation of reporter genes resulting from protein-protein interaction), and 2.5 mM 3AT media. Plasmid rescue of colonies growing on selective media was then performed, and sequencing of the prey cDNA inserts using pPR3-N specific primers elucidated the identities of the prey proteins interacting with the NET2A bait.

5.4.3. Potential Interactors of NET2A Identified in the Dualhunter Split Ubiquitin Yeast-2-Hybrid Screen.

Table 5.3 indicates the list of prey proteins isolated in the split ubiquitin Y2H using NET2A as bait.

Of particular significance, NET2A was pulled back as an interactor of itself, confirming the same interaction observed in the TAP-MS screen. Specifically, the prey cDNA clone isolated was NET2A (aa 36 - 136), indicating that NET2A homomeric interactions may be facilitated through this protein domain. $NET2A^{36\text{-}136}$ lies mostly within the NET2A NAB domain, encoded by aa 1 – 95 (Dixon. 2013), perhaps indicating that the NET2A NAB domain may function in facilitating interactions with other NET2s: $NET2A^{36\text{-}136}$ is highly conserved with $NET2B^{36\text{-}136}$, and it may be tentatively postulated that NET2A-NET2B interactions could also occur through this domain. Having confirmed a homomeric NET2A-NET2A interaction using two independent experimental methods, it can be assumed with confidence that NET2A is a genuine interactor of itself.

Locus	Protein Description	Hits
At1g58210	NET2A (NETWORKED 2A)	1
At3g24100	Putative Uncharacterised Protein	1
At2g29980	FAD3 (FATTY ACID DESATURASE 3)	1
At2g41160	RBL18 (RHOMBOID-LIKE PROTEIN 18)	1
At2g06520	PSBX (PHOTOSYSTEM II SUBUNIT X)	1
At2g21170	TIM (TRIOSEPHOSPHATE ISOMERASE)	1

Table 5.3: List of Prey Proteins Pulled Back from the Split Ubiquitin Yeast-2-Hybrid Screen using Full-Length NET2A as Bait. Detailed are the gene loci and descriptive names of proteins identified as interactors of NET2A, and the number of times they were isolated (hits).

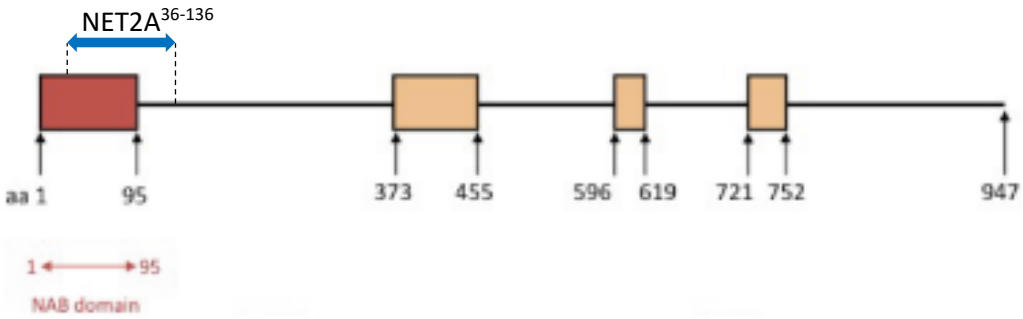

Figure 5.11: Predicted NET2A Protein Structure, Featuring the Fragment Shown to Interact with the NET2A-Bait Construct in the SU-Y2H Screen. Red box: NAB domain. Orange box: predicted coiled-coil domains. Blue arrow: NET2A prey cDNA (aa 36-136) pulled back in the SU-Y2H screen using full-length NET2A as bait. Figure modified from Dixon. (2013).

A second protein of interest, At3g24100; a previously uncharacterised protein, was also pulled back as an interactor of NET2A. Specifically, a prey cDNA clone encoding a fragment of At3g24100 (aa 5 – 38) was rescued from yeast colonies growing on selective media, indicating that this protein fragment is able to bind NET2A. At3g24100, named MICROTUBULE-ASSOCIATED PROTEIN 7A (MAP7A) in this study, was characterised during this investigation as belonging to a highly conserved family of SERF (small ERD-rich family) proteins, and was observed to bind microtubules *in vivo*, during initial studies. Full characterisation of this protein will be described in chapter 7.

The remaining proteins listed as interactors of NET2A were not selected for further investigation. FAD3 is a metabolic enzyme localised to the ER, which is involved in the synthesis of 18:3 fatty acids (Lou et al. 2014; Ohlrogge. 1991). PSBX, a component of photosystem II (García-Cerdán et al. 2009), and the metabolic enzyme TIM (Chen and Thelen. 2010), are both located at chloroplasts and are unlikely to have involvement with NET2A in pollen. RBL18 is a rhomboid-like protein, thought to be an integral membrane protein with intramembrane serine protease activity (Tripathi and Sowdhamini. 2006). These proteins were deemed less likely to be involved with NET2A *in vivo*, and insufficient time could be dedicated to corroborating them as genuine interactors of NET2A. Therefore, no further research was performed on these proteins.

5.5. Conclusion.

This chapter describes the confirmation of NET2A-NET2A and NET2A-NET2B interactions, using a variety of experimental approaches.

Firstly, this section reports a homomeric interaction between NET2A and itself. NET2A was indicated as a self-interacting protein in two independent protein-protein interaction screens, effectively eliminating the possibility that the identified interaction was a false positive observation arising in one of the interaction studies. It can be confidently assumed that NET2A interacts with itself in a homomeric interaction. NET2B was also shown to be an interactor of NET2A in two different protein-protein interaction screens. Firstly, NET2B was isolated in complex with NET2A in the TAP-MS screen. FRET-FLIM confirmed that NET2B interacts with NET2A *in vivo,* through a direct physical association. Using two experimental methods to prove this interaction allows confident conclusion that NET2B is a true interactor of NET2A. This interaction suggests that NET2A and NET2B may co-operate in cellular function *in vivo*.

Other proteins of interest were also identified as potential interactors of NET2A. At3g24100, named in this study as MAP7A, is a novel microtubule-binding protein, and will be characterised in chapter 7. As well as this, CLMP1; isolated in the TAP-MS screen, has also been reported to have potential involvement with the cell cytoskeleton, and is an important regulator of cell architecture. An interaction between NET2A and CLMP1 might be of great significance in plant cytoskeletal research, however characterisation of this interaction was not possible as there was insufficient time remaining in which to investigate CLMP1 further.

The discovery of homo- and hetero-oligomerisations of NET2 proteins has significant implications with regards to our understanding of how the NET2s function *in vivo*. Discussed in chapter 3 is the potential functional redundancy between individual NET2 proteins; postulated from the observations that single *net2* mutants display no phenotype. Here, it is demonstrated that NET2A and NET2B are likely to be involved in the same cellular processes, as concluded from their interactions with each other, perhaps further suggesting that NET2A and NET2B are functionally redundant in the processes they regulate. As discussed in chapter 6, both NET2A and NET2B are demonstrated to interact with the same *At*PRK receptor kinases, further indicating functional redundancy between NET2 proteins.

The oligomerisation of NET2 proteins is likely to determine their activity, and may modulate their function. Different NET2s may have different affinities for binding actin filaments, and may regulate the actin cytoskeleton differentially. NET2A and NET2B have overlapping but distinct temporal and developmental expression patterns in pollen; with NET2A expressed from pollen grain development to fertilisation, whereas NET2B is expressed only after the growing pollen tube penetrates the stigma during fertilisation (Dixon. 2013; Leydon et al. 2013). It is possible that during germination and early pollen tube growth, NET2 punctae consist of only NET2A homo-oligomers that perform one specific function, however as NET2B is expressed during the navigation of the pollen tube through the pistil tissue, hetero-oligomers consisting of NET2A and NET2B may become more prevalent. This shift in composition of NET2 proteins at punctae at the plasma membrane may alter the activity and function of NET2A at these plaques to regulate actin differently, and coordinate processes specific to the later stages of fertilisation.

Chapter 6: Investigation of NET2-PRK Interactions.

6.1. Introduction.

In chapter 5, potential interactors of NET2A were identified using multiple protein-protein interaction screens. In addition to this, a NET2 protein has been highlighted as a potential interactor of a Pollen Receptor-Like Kinase (PRK) in a past study. According to Skirpan et al. (2001), the Petunia NET2 orthologue, *Petunia inflata* KINASE-INTERACTING PROTEIN-1 (*Pi*KIP1) was identified as an interactor of *Petunia inflata* POLLEN RECEPTOR-LIKE KINASE-1 (*Pi*PRK1). PRKs are acknowledged to regulate pollen tube growth downstream of external signal perception, through signalling to the actin cytoskeleton (chapter 1.5). It has been demonstrated that *Pi*KIP1 possesses a functional actin-binding NAB domain, suggesting that the *Pi*PRK1-*Pi*KIP1 interaction may constitute a physical link between the plasma membrane and actin cytoskeleton, with potential functions in the transduction of external signals in growing pollen tubes. The interaction between *Pi*PRK1 and *Pi*KIP1, initially characterised using Y2H and *in vitro* assays (Skirpan et al. 2001), has not been studied further, and no analysis of the *Pi*PRK1-*Pi*KIP1 complex has been performed *in vivo.* In addition to this, no orthologous interaction between NET2A and a PRK protein has been identified in Arabidopsis. Identification of an *At*PRK interaction partner of NET2A would be of great importance in determining the role of NET2A in Arabidopsis, and would implicate NET2A in the transduction of external growth signals essential for pollen tube growth and fertilisation.

Therefore, investigation of the interactions between NET2s and PRKs was performed to determine if NET2A may play a role in the regulation of pollen tube growth, guidance and fertilisation under control of PRK signalling. Firstly, analysis of *Pi*PRK1-*Pi*KIP1 interactions was performed *in vivo*, to corroborate earlier *in vitro* studies (Skirpan et al. 2001). Subsequently, screening of an *At*PRK interactor of NET2A was performed using the GAL4 Y2H system and FRET-FLIM assays. Additionally, investigation of interactions between *At*PRKs and NET2B was also undertaken, to determine whether multiple NET2 family members may share

functional redundancy to each other in their involvement with *At*PRKs in Arabidopsis. Finally, analysis of NET2-PRK interactions was performed in Arabidopsis pollen tubes, to further explore the nature and potential function of the interactions between the actin-binding NET2 proteins, and the PRK membrane-bound signalling receptors

6.2. *In vivo* Analysis *Pi*KIP1-*Pi*PRK1 Interactions Using FRET-FLIM.

6.2.1. Introduction.

An interaction between the Petunia NET2 orthologue, *Pi*KIP1, and *Pi*PRK1 has been demonstrated using Y2H and *in vitro* assays (Skirpan et al. 2001). However, no further studies on the interactions of *Pi*PRK1 and *Pi*KIP1 have since been reported, and the interaction has not yet been investigated *in vivo*. *Pi*KIP1, which is known to have a functional, actin-binding NAB domain (Calcutt. 2009), may link the actin cytoskeleton to the plasma membrane through direct association with *Pi*PRK1 *in vivo*. Here described are the experiments performed to confirm and characterise the interaction of *Pi*KIP1 and *Pi*PRK1 *in vivo.*

6.2.2. Analysis of *Pi*KIP1-GFP and *Pi*PRK1-RFP Subcellular Localisation *in vivo.*

Agrobacterium-mediated transformation was used to express *Pi*KIP1-GFP and *Pi*PRK1-RFP in leaf sections of *N. benthamiana.* To generate the *Pi*KIP1-GFP expression construct, the coding sequence of full-length *Pi*KIP1 (aa 1 – 974) was PCR amplified from cDNA extracted from Petunia anthers and cloned into pDONR207. *Pi*KIP1 was cloned into pH7FGW2 to express *Pi*KIP1 with a C-terminal GFP tag under the *CaMV:* 35s promoter. The coding sequence of full-length *Pi*PRK (aa 1 – 763) was PCR amplified from Petunia anther cDNA and cloned into pDONR207 using gateway cloning. *Pi*PRK1 was then cloned into pH7RGW2 to facilitate expression of *Pi*PRK1 as a C-terminal RFP fusion protein under control of the *CaMV 35s*: promoter. *Pi*KIP1-GFP and *Pi*PRK1-RFP were expressed in *N.*

benthamiana leaf tissue using agrobacterium-mediated transformation and visualised using CLSM.

Figures 6.2 and 6.3 show the localisation of *Pi*KIP1-GFP and *Pi*PRK1-RFP in *N. benthamiana* leaf epidermal cells. In contrast to the previous observations of the subcellular localisation of *Pi*KIP1$^{1-93}$-GFP in *N. benthamiana* (Calcutt. 2009), full-length *Pi*KIP1-GFP did not bind to actin filaments, but localised to the cytosol. As expected, *Pi*PRK1-RFP localised to the periphery of *N. benthamiana* epidermal cells, presumably at the plasma membrane. *Pi*PRK1-RFP appeared to be absent from the cytosol and internal membrane systems. Having established the subcellular localisations of *Pi*KIP1-GFP and *Pi*PRK1-RFP *in vivo*, potential co-localisation of *Pi*KIP1-GFP and *Pi*PRK1-RFP was investigated.

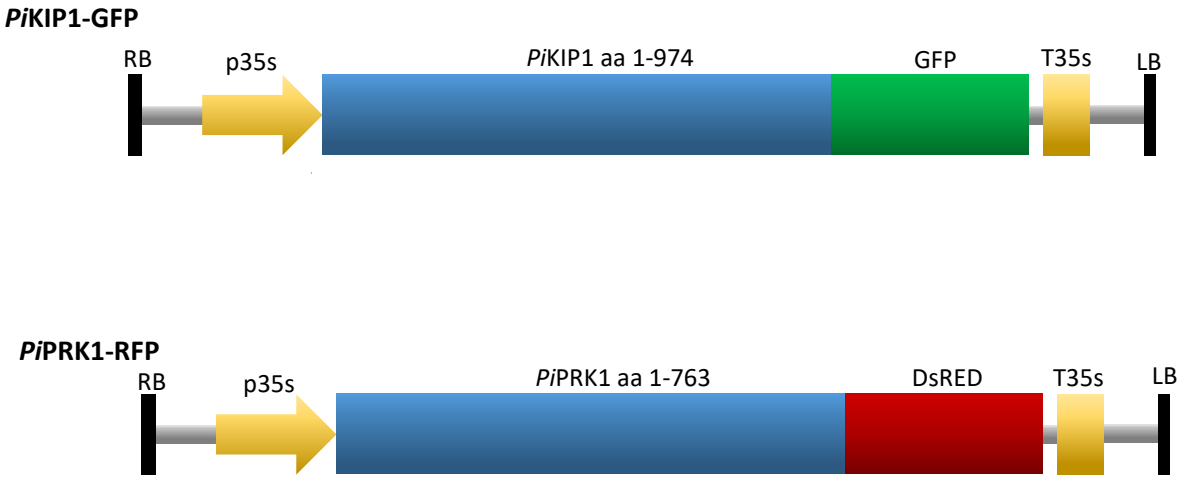

Figure 6.1: Schematics of Expression Constructs used to Express Donor and Acceptor Constructs *in vivo* for use in FRET-FLIM: *Pi*KIP1-GFP was generated using the vector pH7FGW2, and *Pi*PRK1-RFP was generated using pH7RGW2. RB = T-DNA right border. p35s = CaMV 35s promoter sequence. T35s = CaMV 35s terminator sequence. sequence. LB = T-DNA left border.

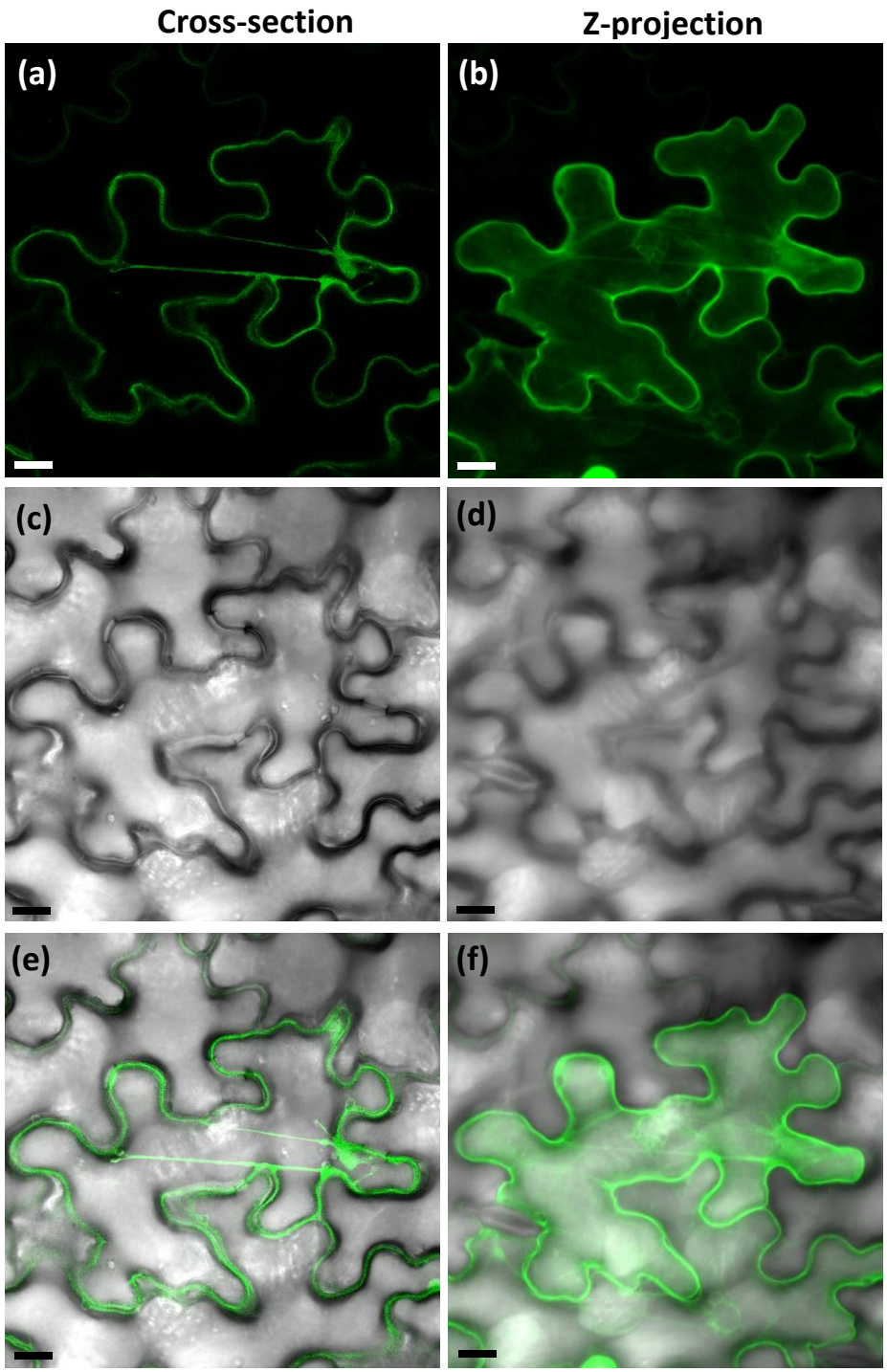

Figure 6.2: *Pi*KIP1-GFP Expressed in *N. benthamiana* Leaf Epidermal Cells Using Agrobacterium-Mediated Transformation. (a) and (b): *Pi*KIP1-GFP visualised using a 488 nm laser and 505 – 530 nm emission detection. (c) and (d): brightfield images of the same cell. (e): overlay of (a) and (c). (f): overlay of (b) and (d). (a), (c) and (e): single z-plane representing a cross section of a cell. (b), (d) and (f): Z-projection of the same cell. Scale bar: 200 µm.

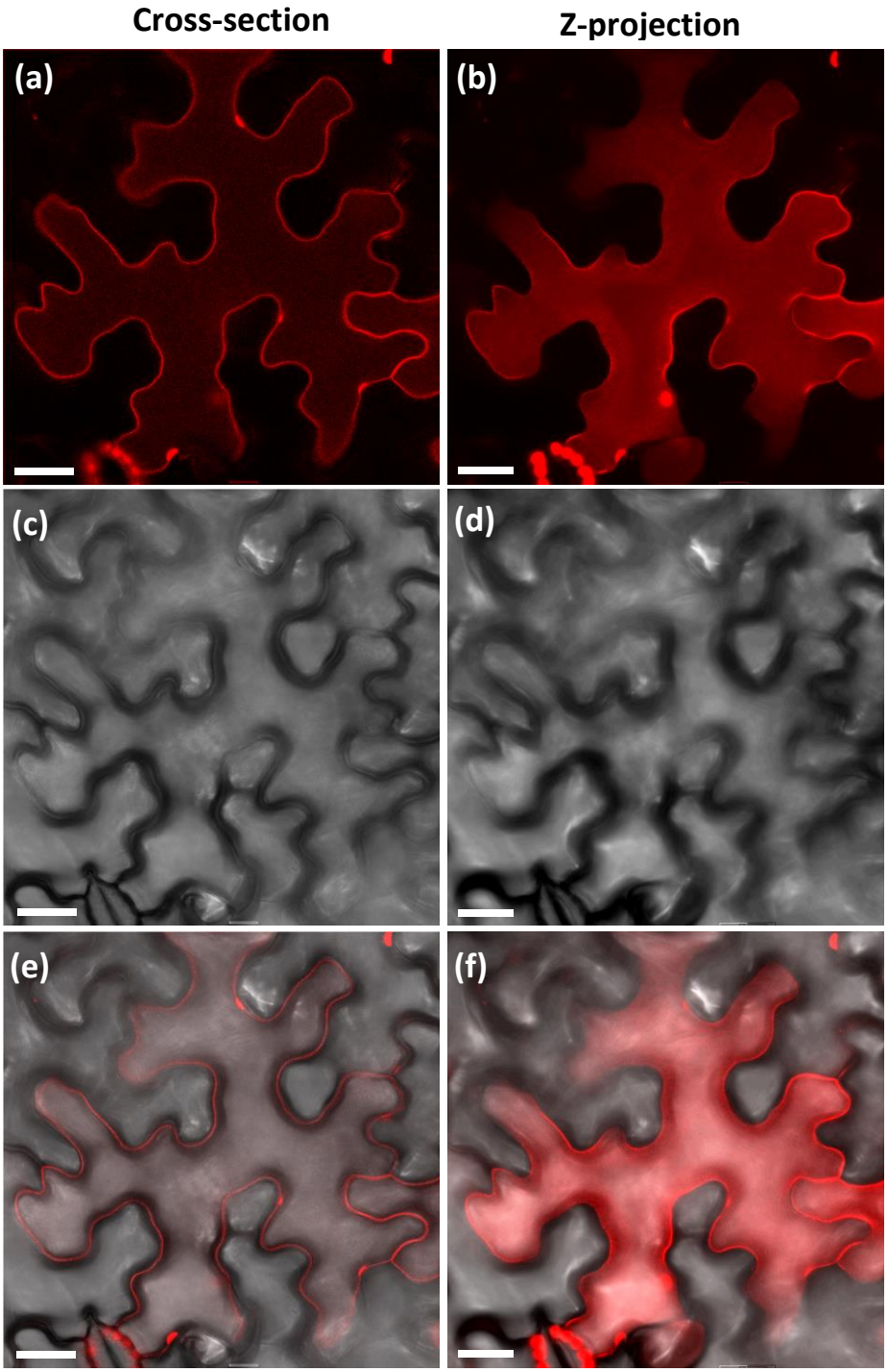

Figure 6.3: *Pi*PRK1-RFP Expressed in *N. benthamiana* Leaf Epidermal Cells Using Agrobacterium-Mediated Transformation. (a) and (b): *Pi*PRK1-RFP visualised using a 543 nm excitation laser and 600 – 650 nm emission detection. (c) and (d): brightfield images of the same cell. (e): overlay of (a) and (c). (f): overlay of (b) and (d). (a), (c) and (e): single z-plane representing a cross section of a cell. (b), (d) and (f): Z-projection of the same cell. Scale bar: 200 µm.

6.2.3. Analysis of *Pi*KIP1-GFP and *Pi*PRK1-RFP Co-localisation *in vivo*, and Recruitment of *Pi*KIP1-GFP to the Plasma Membrane by *Pi*PRK1-RFP.

Co-localisation of *Pi*KIP1-GFP and *Pi*PRK1-RFP was assessed *in vivo*. Agrobacterium-mediated transformation was used to co-express *Pi*KIP1-GFP and *Pi*PRK1-RFP in *N. benthamiana* leaf tissue to permit their visualisation in the same cells.

Figure 6.4 shows the co-localisation of *Pi*KIP1-GFP and *Pi*PRK1-RFP in *N. benthamiana* leaf epidermal cells. As previously described, *Pi*PRK1-RFP localised to the plasma membrane, where it was observed to co-localise with *Pi*KIP1-GFP. In contrast to the cytosolic localisation of *Pi*KIP1-GFP when expressed alone, *Pi*KIP1-GFP appeared to be absent from the cytosol and localised entirely to the plasma membrane when co-expressed with *Pi*PRK1-RFP (figure 6.5). It can be concluded that *Pi*PRK1-RFP elicits a change in *Pi*KIP1-GFP subcellular localisation, and recruits it from the cytoplasm to the plasma membrane in *N. benthamiana* leaf epidermal cells. FRET-FLIM was performed to investigate whether *Pi*KIP1-GFP and *Pi*PRK1-RFP interact directly *in vivo*.

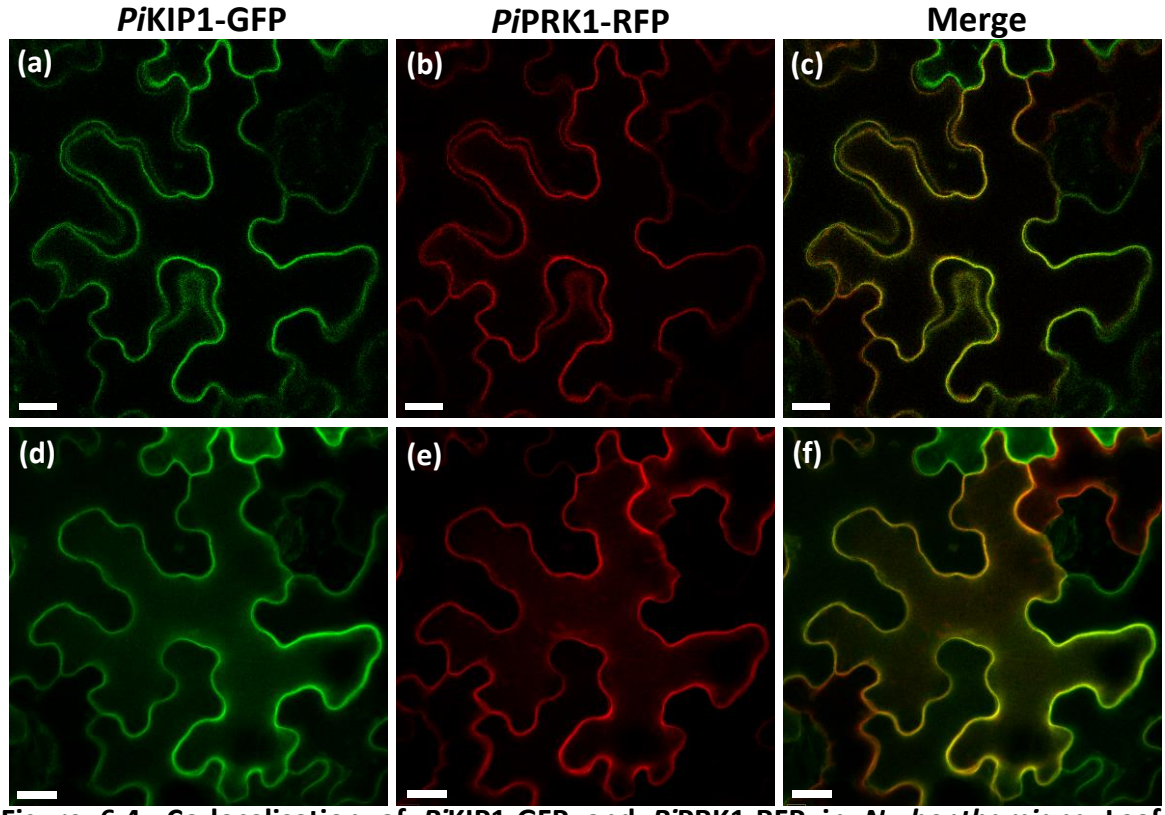

Figure 6.4: Co-localisation of *Pi*KIP1-GFP and *Pi*PRK1-RFP in *N. benthamiana* Leaf Epidermal Cells. (a) and (d): *Pi*KIP1-GFP visualised using a 488 nm excitation laser and 505 – 530 nm emission detection. (b) and (e): *Pi*PRK1-RFP visualised in the same cell using a 543 nm excitation laser and 600 – 650 nm emission detection. (c): overlay of (a) and (b). (f): overlay of (d) and (e). Images (a) – (c) are single z-plane images representing a cross-section the cell. (d) - (f): z-projection of the same cell. Scale bar: 200 µm.

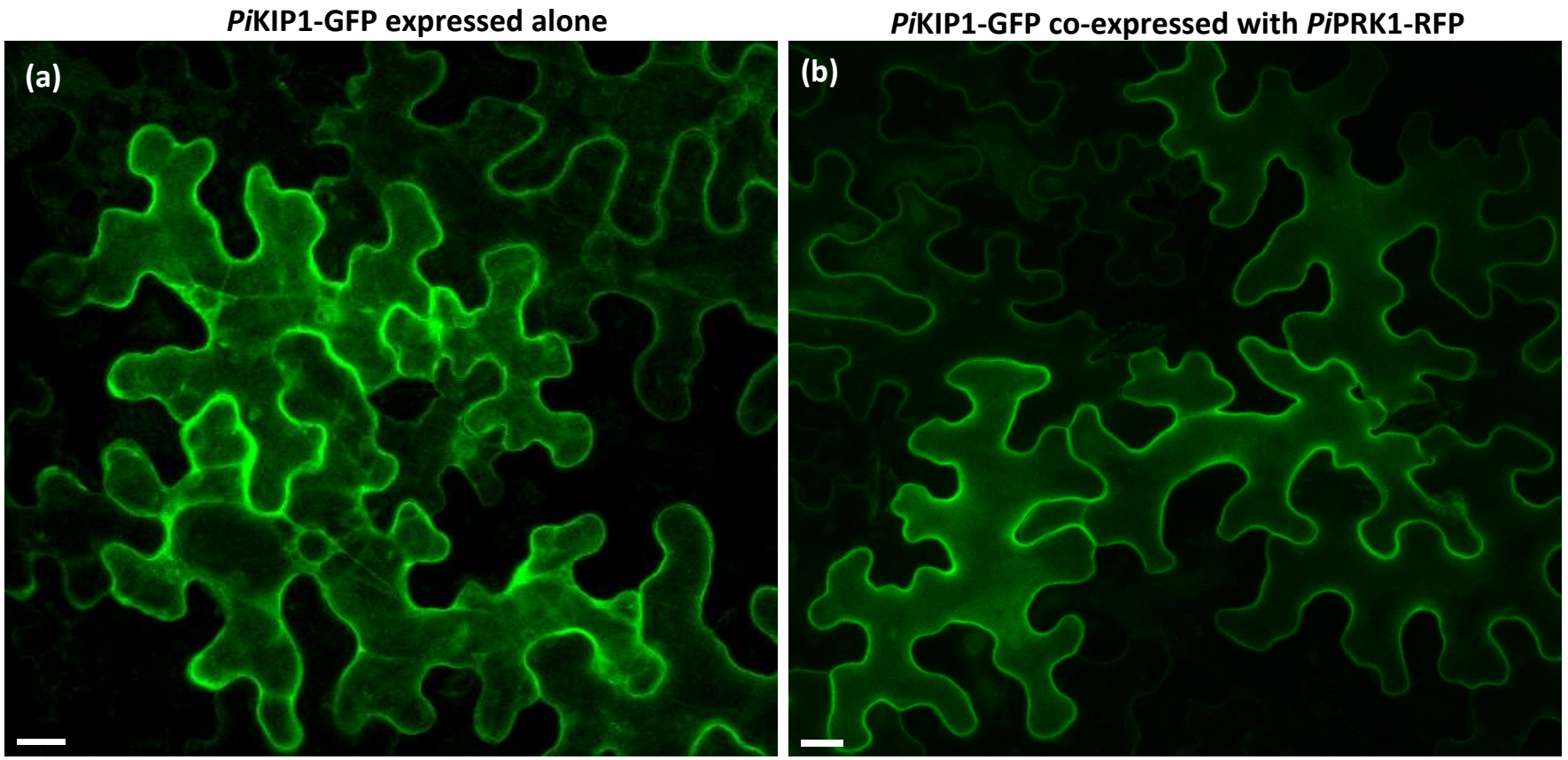

Figure 6.5: Subcellular Localisation of *Pi*KIP1-GFP When Expressed Alone, and When Co-expressed with *Pi*PRK1-RFP. *Pi*KIP1-GFP visualised in *N. benthamiana* leaf epidermal cells using a 488nm excitation laser and detection of 505 – 530 nm emission. (a): *Pi*KIP1-GFP expressed alone. (b) *Pi*PRK1-RFP co-expressed with *Pi*PRK1-RFP. Scale bar: 200 µm.

6.2.4. FRET-FLIM Analysis of *Pi*KIP1-GFP and *Pi*PRK1-RFP Interactions.

To investigate whether *Pi*KIP1-GFP and *Pi*PRK1-RFP may interact directly, FRET-FLIM was performed as described in chapter 2.5.4, and 5.3. *Pi*KIP1-GFP was used as a FRET-FLIM donor construct and *Pi*PRK1-RFP as an acceptor. Agrobacterium-mediated transformation was used to express *Pi*KIP1-GFP alone, or co-express *Pi*KIP1-GFP alongside *Pi*PRK1-RFP in *N. benthamiana* leaf epidermal cells. Leaf epidermal cells transiently expressing the fusion protein, GFP-RFP, were analysed as a positive control.

The results of the FRET-FLIM interaction assay between *Pi*KIP1-GFP and *Pi*PRK1-RFP are displayed in figure 6.6 and 6.7. The average fluorescence lifetime of *Pi*KIP1-GFP when expressed alone was observed to be 2.56 ± 0.03 ns. In contrast, the average fluorescence lifetime of *Pi*KIP1-GFP when co-expressed with *Pi*PRK1-RFP was 2.15 ± 0.07 ns, constituting a large average fluorescence lifetime reduction of 0.41 ns. The fluorescence lifetime of *Pi*KIP1-GFP when co-expressed with *Pi*PRK1-RFP was similar to that of the GFP-RFP positive control, which was observed to be 2.11 ± 0.03 ns. Therefore, the FRET-FLIM experiment indicates that *Pi*KIP1-GFP physically interacts with *Pi*PRK1-RFP *in vivo*, confirming previous reports of an interaction between *Pi*KIP1 and *Pi*PRK1 observed in Y2H assays (Skirpan et al. 2001).

6.2.5. Summary.

In this section, *in vivo* analysis of an interaction between *Pi*KIP1 and *Pi*PRK1 was performed. Using FRET-FLIM, it was demonstrated that *Pi*KIP1-GFP and *Pi*PRK1-RFP physically interact *in vivo*, confirming previous reports of an interaction between *Pi*KIP1 and *Pi*PRK1 demonstrated by Y2H (Skirpan et al. 2001). Furthermore, it was observed that *Pi*KIP1-GFP, which exhibited cytoplasmic localisation when expressed alone, was recruited to the plasma membrane by *Pi*PRK1-RFP in *N. benthamiana* leaf epidermal cells, where the two fusion proteins could be seen to co-localise markedly. It is possible therefore, that PRK proteins may function to recruit NET2 proteins to the pollen tube plasma membrane, thus serving as a link between the membrane and actin cytoskeleton. Having established that an interaction between PRK and NET2 proteins exists in Petunia, investigation of potential interactions between NET2A and *At*PRKs was commenced in the model organism, *Arabidopsis*.

Constructs Expressed	Mean GFP Fluorescence Lifetime	Standard Deviation	n
*Pi*KIP1-GFP	2.56 ns	0.03	10
*Pi*KIP1-GFP + *Pi*PRK1-RFP	2.15 ns	0.07	10
GFP-RFP positive control	2.11 ns	0.03	10

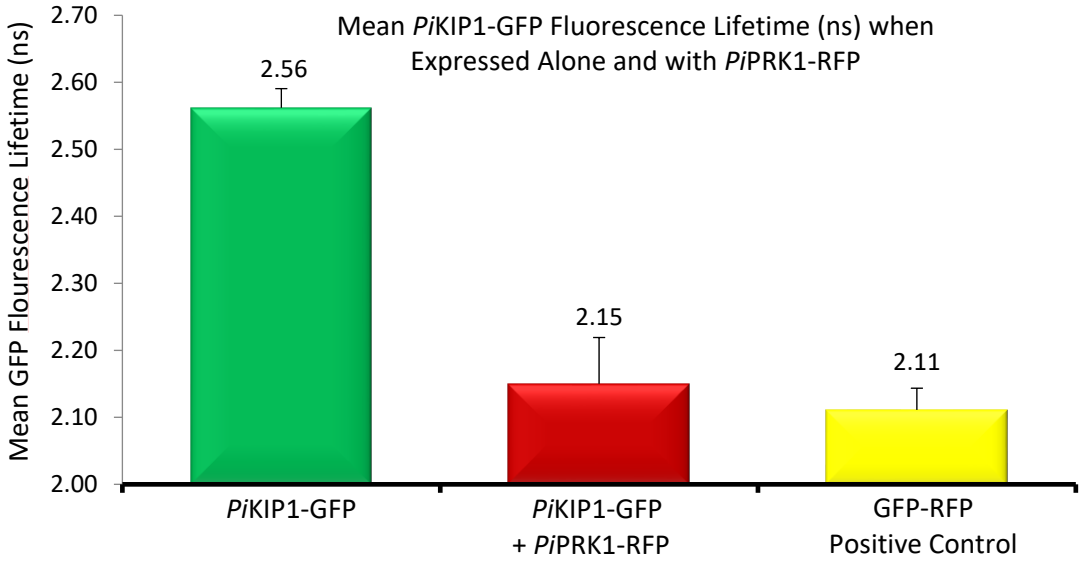

Figure 6.6: *Pi*PRK1-RFP Induces a Decrease in *Pi*KIP1-GFP Fluorescence Lifetime when Co-expressed in *N. benthamiana* Epidermal Cells. n = number of cells analysed.

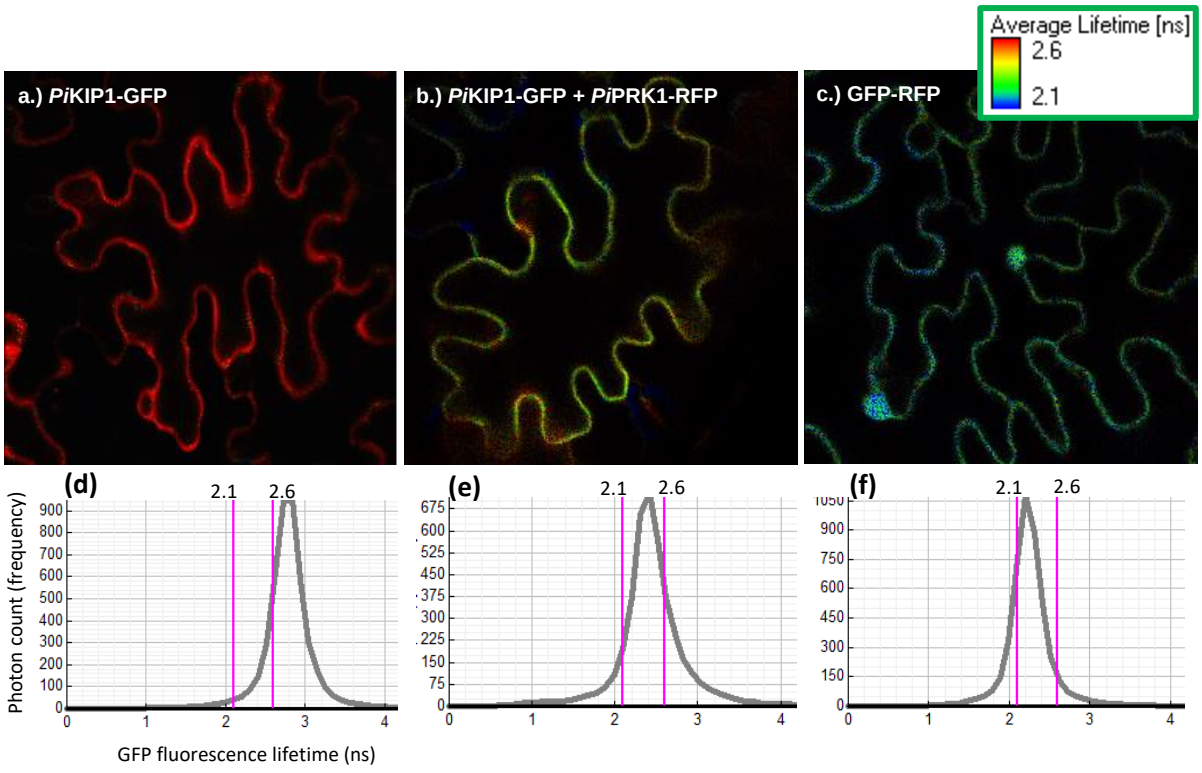

Figure 6.7: Visualisation of *Pi*KIP1-GFP Fluorescence Lifetime *in vivo* when Expressed Alone, and with *Pi*PRK1-RFP. (a)–(c): Example images of GFP fluorescence detected in *N. benthamiana* epidermal cells, pseudocoloured according to GFP fluorescence lifetime. (d)-(f): charts associated with images (a)-(c) respectively, show the frequency distributions of the fluorescence lifetimes (ns) of detected photons in each image. A leftward shift in peak GFP fluorescence lifetime is indicative of reduced average lifetime (a) and (d): *Pi*KIP1-GFP expressed alone. (b) and (e): *Pi*KIP1-GFP co-expressed with *Pi*PRK1-RFP. (c) and (f): GFP-RFP positive control.

6.3. Identification of *At*PRK Interaction Partners of NET2A.

6.3.1. Introduction.

The above section describes the validation of a previously observed interaction between the *Petunia inflata* proteins *Pi*KIP1, and *Pi*PRK1, identified in a Y2H screen (Skirpan et al. 2001). *Pi*KIP1 is a petunia orthologue of NET2A, with a functional actin-binding NAB domain (Calcutt. 2009), whose interaction with *Pi*PRK1 may represent a physical link between the plasma membrane and actin cytoskeleton, with a potential role in transduction of external signals to the actin cytoskeleton during pollen tube growth and guidance (chapter 1.5). In this section, an orthologous interaction between NET2A and *Arabidopsis thaliana* Pollen Receptor-Like Kinases (*At*PRKs) was investigated. Identification of NET2-PRK interactions in Arabidopsis would permit practical and convenient functional analysis of the interaction in the model organism Arabidopsis, in which regulation of cell signalling, the cytoskeleton and cell growth is better characterised. An interaction between NET2A and the *At*PRK4/*At*PRK5 subclade was identified using the matchmaker Y2H system, and validated using FRET-FLIM, with which both NET2A and NET2B were observed to interact with *At*PRK4 and *At*PRK5.

6.3.2. Investigating NET2A-*At*PRK Interactions Using the Clontech Matchmaker Y2H System.

Previously, an interaction between *Pi*KIP1 and *Pi*PRK1 was identified in a Y2H screen using the GAL4 Y2H system (Skirpan et al. 2001). Therefore, the Clontech Matchmaker GAL4 Y2H system was used to replicate the Y2H conditions performed by Skirpan et al. (2001) to identify an orthologous interaction between NET2A and an *Arabidopsis* PRK. The Matchmaker Y2H uses a similar principle to that of the SU-Y2H (described in chapter 5.4), in that an interaction between bait and prey proteins within yeast cells permits transcription of selective marker genes required for growth on selective media. In contrast to the SU-Y2H, in which bait-prey interactions result in the release of a transcription factor downstream of the formation of split-ubiquitin, the matchmaker system relies on the formation of functional GAL4 transcription factor through bait-prey interaction. In this system, the bait protein is fused to the GAL4 DNA binding domain (BD), and the prey protein to

the GAL4 activator domain (AD). An interaction between bait and prey proteins will bring the GAL4 BD and AD into close proximity, creating functional GAL4 that drives transcription of the reporter genes *HIS3*, *ADE3* and *LacZ*, (described in chapter 5.4), and growth on selective media.

6.3.2.1. Generation, Transformation and Validation of Bait and Prey Fusion Protein Constructs in Yeast.

In this study, an interaction screen between NET2A and each known *At*PRK was performed. *At*PRK1, *At*PRK2, *At*PRK3, *At*PRK4, *At*PRK5 and *At*PRK6 were characterised at the time of this experiment and were selected for investigation (Chang et al. 2013). The more recently characterised *At*PRK7 and *At*PRK8 (Takeuchi and Higashiyama. 2016) were not tested as interactors NET2A.

According to Skirpan et al. (2001), an AD-KIP1 (AD-KIP1$^{333-724}$) prey clone was pulled back as an interactor of BD-*Pi*PRK1$^{408-720}$ in the Y2H screen, using the cytoplasmic domain of *Pi*PRK1 (aa 408 – 720) as bait. To identify an orthologous interaction between Arabidopsis NET2A and an *At*PRK protein, the conditions of the *Pi*KIP1-*Pi*PRK1 Y2H were replicated. Therefore, AD-NET2A was used as prey to screen against BD-fusions of the cytoplasmic domains of *At*PRKs 1 – 6 (*At*PRK1$^{280-662}$, *At*PRK2$^{268-647}$, *At*PRK3$^{270-633}$, *At*PRK4$^{303-679}$, *At*PRK5$^{305-686}$ and *At*PRK6$^{287-659}$), which are hereafter referred to as ‘BD-PRKs’ throughout the course of this report.

The vectors pGBKT7 and pGADT7 were used to express proteins as BD-bait and AD-prey fusion proteins in yeast. pGBKT7 carries the selection marker *TRP1*, enabling growth on -W plates, and pGADT7 carries *LEU2*, for growth on -L plates. Full-length NET2A was cloned into pGADT7, to generate the prey construct AD-NET2A. The cytoplasmic domains of *At*PRKs 1 – 6 were cloned into pGBKT7 to express the bait constructs BD-*At*PRK1, BD-*At*PRK2, BD-*At*PRK3, BD-*At*PRK4, BD-*At*PRK5, BD-*At*PRK6. To generate these constructs, the coding sequences of the *At*PRK intracellular domains were PCR amplified using full-length *At*PRK1-pB7FGW2, *At*PRK2-pB7FGW2, *At*PRK3-pB7FGW2, *At*PRK4-pMDC83, *At*PRK5-pB7FGW2, and *At*PRK6-pB7FGW2 as template (see section 6.3.3.2). The *At*PRK intracellular domains were cloned into pDONR207 using gateway cloning, and were then cloned into pGBKT7.

As described in chapter 5.4, autoactivation of selection markers by BD- and AD-constructs can give rise to false positive results. Therefore, it was assessed whether the generated constructs were able to autoactivate transcription of selection markers in the yeast reporter strain, AH109, which carries the reporter genes *HIS3* and *ADE2*. pGADT7-NET2A, pGBKT7-*At*PRK1, pGBKT7-*At*PRK2, pGBKT7-*At*PRK3, pGBKT7-*At*PRK4, pGBKT7-*At*PRK5 and pGBKT7-*At*PRK6 were transformed into AH109 (as described in chapter 2.3.1), and grown on selective media. AH109 yeast containing AD-NET2A was grown on -L medium (to select for the prey construct), -LH (to select for autoactivation of *HIS3*), -LH + 2.5 mM 3AT (to repress potential autoactivation of *HIS3*) and -LA (to select for autoactivation of *ADE2*). AH109 yeast containing BD-*At*PRK1, BD-*At*PRK2, BD-*At*PRK3, BD-*At*PRK4, BD-*At*PRK5, BD-*At*PRK6, were grown on -W (to select for the bait construct), -WH (to select for autoactivation of *HIS3*), -WH + 2.5 mM 3AT and -WH + 5 mM 3AT (to repress potential autoactivation of *HIS3*), and -WA (to select for autoactivation of *ADE2*). Figure 6.8(a) shows the growth of AH109 yeast containing the AD-NET2A prey construct on selective media. After 3 days, growth was clearly observed on -L agar, however no growth was observed on -LH or -LH + 2.5 mM 3AT indicating that the *HIS3* reporter was not autoactivated by the AD-NET2A prey construct. Likewise, no growth was observed on -LA, indicating no transcription of *ADE2* occurred in the absence of a bait-prey interaction. Figure 6.8(b) shows the growth of AH109 yeast containing the bait constructs on selective agar. On -W agar, yeast containing each bait construct was able to grow on -W medium. On -WH, AH109 yeast containing BD-*At*PRK1, BD-*At*PRK2, BD-*At*PRK3, BD-*At*PRK4 or BD-*At*PRK6, were unable to grow, indicating that autoactivation of the *HIS3* reporter was not induced by these bait constructs. However, BD-*At*PRK5 appeared to autoactivate expression of *HIS3*, and growth of AH109 containing the BD-*At*PRK5 bait construct was clearly observable after 3 days of growth on -WH media. This growth was suppressed by addition of 2.5 mM 3AT to the selective media. Therefore, interaction studies on -H media were supplemented with 2.5 mM 3AT to prevent autoactivation of the *HIS3* reporter gene. None of the bait constructs were able to induce autoactivation of the *ADE2* reporter gene, and no growth of was seen on -WA media after 3 days.

(a): Prey Construct Autoactivation

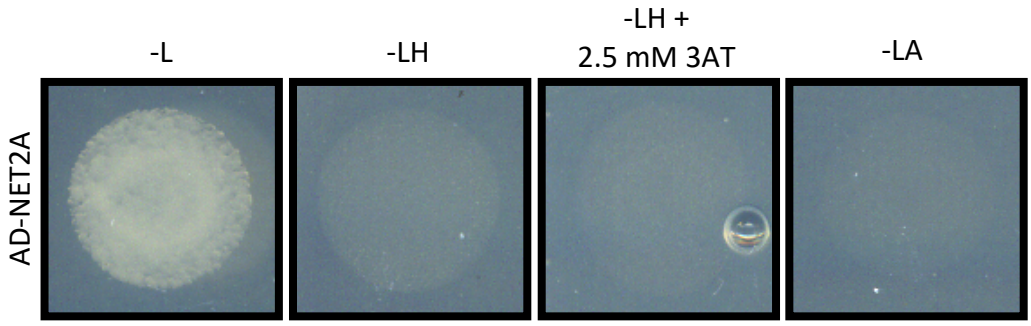

(b): Bait Construct Autoactivation

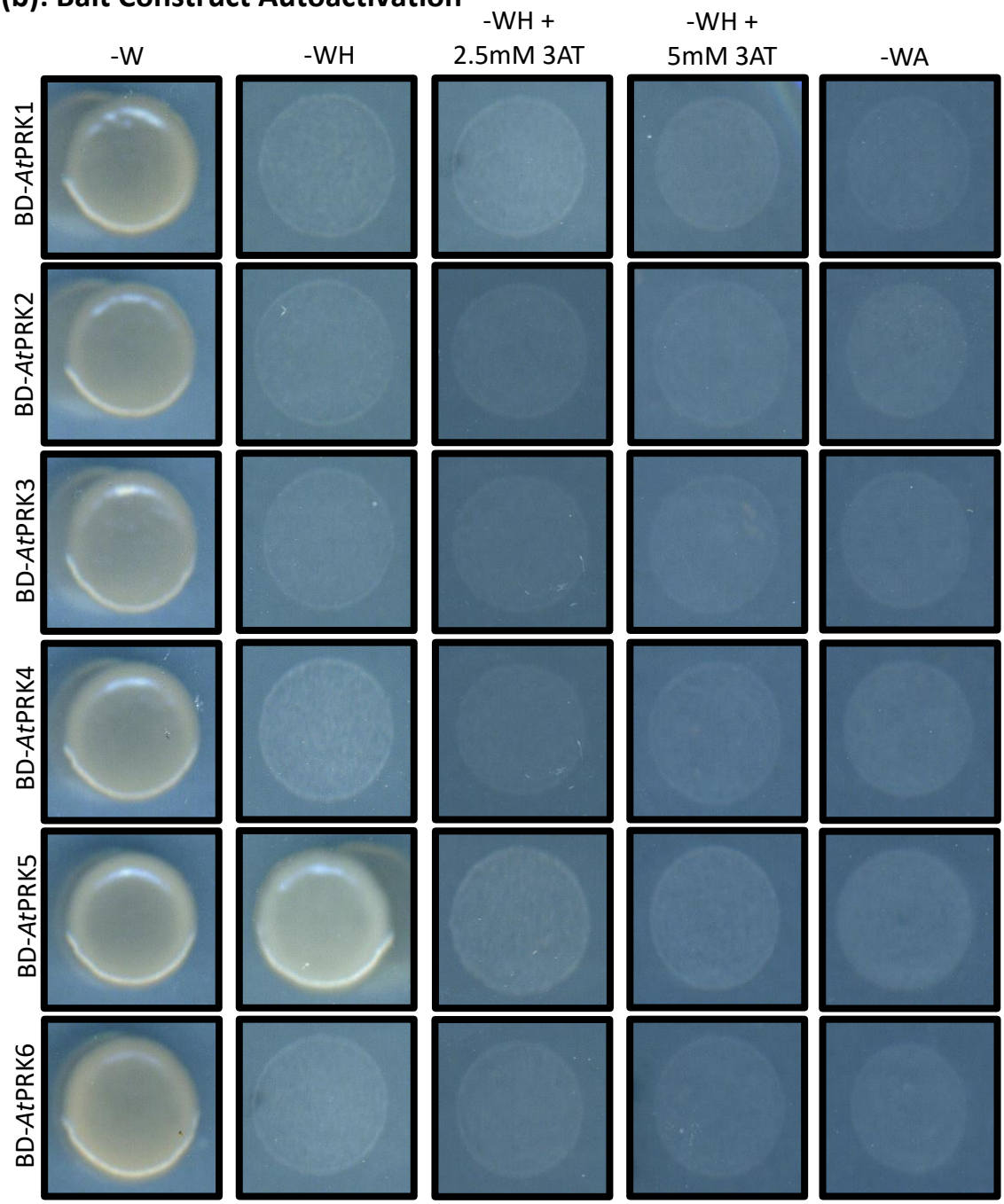

Figure 6.8: Autoactivation Assays of AD-NET2A in pGADT7, and BD-*At*PRK Cytoplasmic Domains in pGBKT7. Constructs were transformed into the AH109 yeast reporter strain. Yeast containing the AD-NET2A prey construct in pGADT7 were selected on -L media. Yeast containing the BD-*At*PRK bait constructs in pGBKT7 were selected on -W media. The yeast were then selected on media also lacking -H, -H + 3AT and -A to determine whether the constructs could autoactivate expression of *HIS3* and *ADE2*.

6.3.2.2. Identification of *At*PRK4 and *At*PRK5 as Interactors of NET2A using the Clontech Matchmaker Y2H System.

After determining the conditions necessary to prevent autoactivation of *HIS3* and *ADE2* by the aforementioned bait and prey constructs, interactions between NET2A and *At*PRKs 1 – 6 were investigated. Bait constructs in pGBKT7 were transformed into the yeast strain Y187, and were mated with AH109 yeast containing the prey construct AD-NET2A in pGADT7. Mating of Y187 and AH109 strain yeast generates diploid yeast cells containing both prey and bait constructs, allowing potential interactions between the bait and prey proteins. As negative controls, the prey plasmid constructs were mated with empty pGBKT7, and bait plasmids with empty pGADT7, to ensure that autoactivation of reporter genes did not occur in the absence of a genuine interaction. Diploid yeast resulting from the one-on-one matings were grown on selective -WL agar to select for cells carrying both bait and prey constructs. The resulting diploid cells were then selected on -WLH media to select for activation of the *HIS3* reporter gene as a result of an interaction between bait and prey constructs. The -WLH media was supplemented with 2.5 mM 3AT to suppress autoactivation of reporter genes as described above. These selection conditions were used to replicate those used by Skirpan et al. (2001) to identify the interaction between *Pi*PRK1 and *Pi*KIP1, therefore maximising the chances of identifying an orthologous interaction between Arabidopsis NET2A and *At*PRKs.

As shown in figure 6.9, an interaction between NET2A and *At*PRK4 & *At*PRK5 was observed, whilst no interaction between NET2A the other *At*PRKs (*At*PRK1, *At*PRK2, *At*PRK3 and *At*PRK6) could be detected. Diploid yeast containing AD-NET2A and each BD-*At*PRK were able to grow on -WL selective media, however on -WLH + 2.5 mM 3AT media, only yeast containing AD-NET2A with BD-*At*PRK4, and AD-NET2A with BD-*At*PRK5 were able to survive and grow, indicating activation of the *HIS3* reporter in these diploids as a result of protein-protein interaction. The

failure to grow of diploids containing BD-*At*PRK1, BD-*At*PRK2, BD-*At*PRK3 and BD-*At*PRK6, indicates that these proteins do not interact with NET2A in the Y2H system. Control diploid cells containing AD-NET2A and empty pGBKT7 were unable to grow on selective media, as were diploids containing empty pGADT7 and each BD-*At*PRK. This demonstrates that diploid yeast containing these prey and bait constructs were unable to grow on selective media in the absence of a protein-protein interaction. It should be noted that no growth of diploids containing AD-NET2A and BD-*At*PRK4, or AD-NET2A and BD-*At*PRK5, was observed on -WLA selective media (data not shown). Likewise, no *ADE2* nutritional selection of yeast was reported during the investigation of the interaction between *Pi*KIP1 and *Pi*PRK1 (Skirpan et al. 2001). *HIS3* nutritional selection is a relatively weak form of selection compared to *ADE2* selection (James et al. 1996), indicating that the interaction of NET2A with *At*PRK4 & *At*PRK5 may be weak or transient. The observed interaction described above parallels that of the pre-described *Pi*KIP1-*Pi*PRK1 interaction, and is sufficient to prove that NET2A interacts with *At*PRK4 & *At*PRK5 in the GAL4 Y2H system.

Therefore, by replicating the Y2H experiments performed by Skirpan et al. (2001), an interaction between NET2A and *At*PRK4 & *At*PRK5 was identified. Subsequently, the observed interactions were corroborated by FRET-FLIM, as described below.

,

Figure 6.9 (Below): One-on-One Y2H Assays Between AD-NET2A and BD-*At*PRK 1 – 6. (a): The prey construct AD-NET2A was mated against empty pGBKT7, BD-*At*PRK1, BD-*At*PRK2, BD-*At*PRK3, BD-*At*PRK4, BD-*At*PRK5 and BD-*At*PRK6. (b): As a negative control, empty pGADT7 was mated against BD-*At*PRK1, BD-*At*PRK2, BD-*At*PRK3, BD-*At*PRK4, BD-*At*PRK5 and BD-*At*PRK6. Diploids were grown on the selective medias -WL to select for diploids, and -WLH +2.5 mM 3AT to select for positive interactions through activation of *HIS3*.

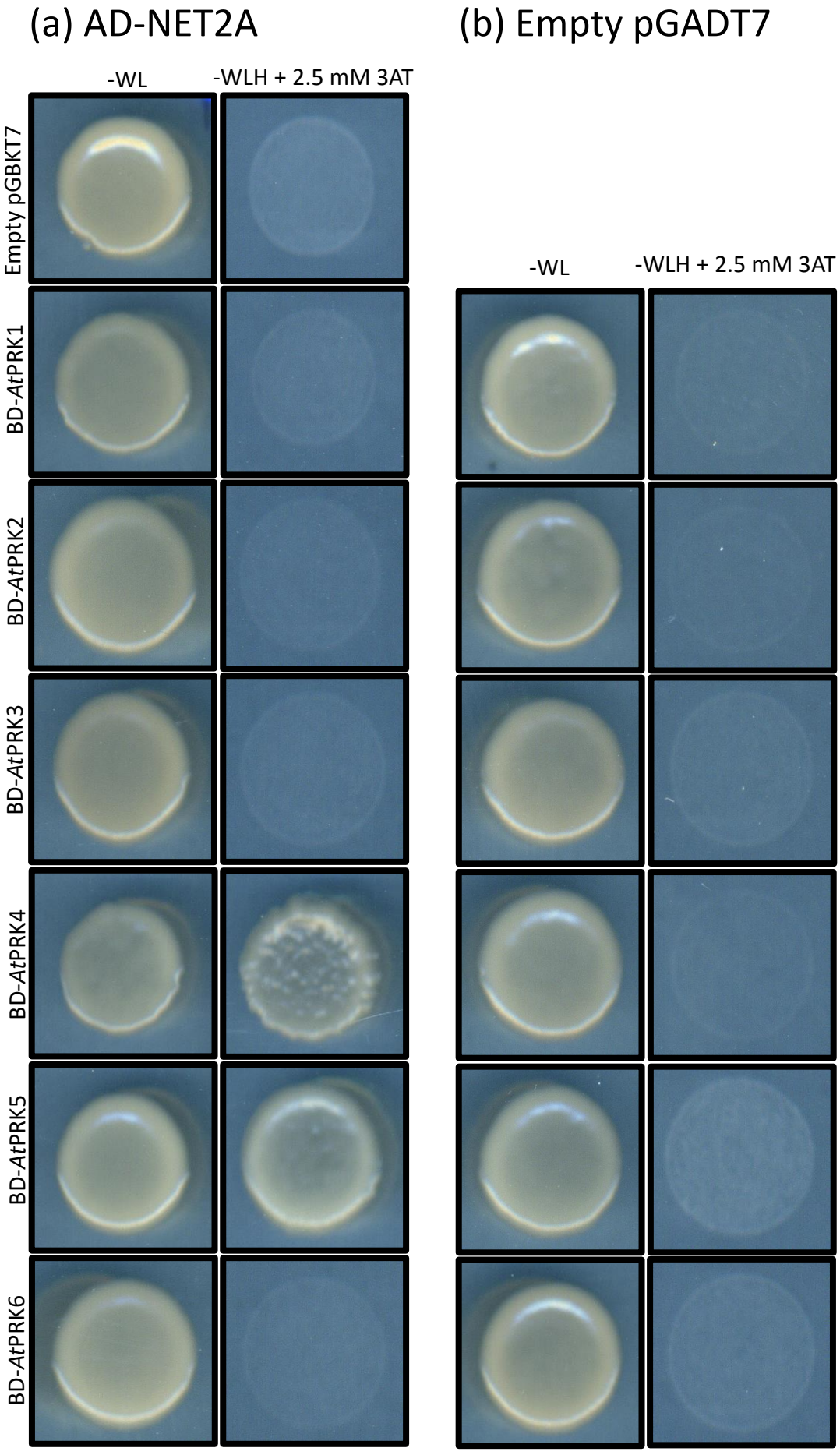
(a) AD-NET2A
(b) Empty pGADT7
-WL
-WLH + 2.5 mM 3AT
Empty pGBKT7
BD-AtPRK1
BD-AtPRK2
BD-AtPRK3
BD-AtPRK4
BD-AtPRK5
BD-AtPRK6
-WL
-WLH + 2.5 mM 3AT

6.3.3. Analysis of NET2-*At*PRK Interactions *in vivo* using FRET-FLIM.

6.3.3.1. Introduction.

Having identified interactions between NET2A & *At*PRK4, and NET2A & *At*PRK5, FRET-FLIM was performed to corroborate the Y2H results, and investigate the interactions *in vivo*. In addition to this, an interaction of NET2B with *At*PRK4 & *At*PRK5 was also studied to determine whether other NET2s may interact with *At*PRK proteins. NET2B has already been demonstrated to interact with NET2A, and it is possible that NET2B is functionally redundant to NET2A in its interactions with *At*PRK proteins. In section 6.2, cytosolic *Pi*KIP1-GFP was seen to be recruited to the plasma membrane by *Pi*PRK1-RFP in the *N. benthamiana* system. Investigation of a similar phenomenon involving recruitment of NET2A and NET2B to the membrane by *At*PRK4 and *At*PRK5 was carried out to expand our understanding of the function of NET2-*At*PRK interactions in Arabidopsis.

6.3.3.2. Generation and Expression of NET2A and *At*PRK Donor and Acceptor Constructs for FRET-FLIM.

FRET-FLIM was performed using donor and acceptor FRET-FLIM constructs expressed in *N. benthamiana* leaf epidermal cells as described previously. To investigate interactions between NET2A and *At*PRKs, FRET-FLIM was performed using C-terminal GFP fusions of each *At*PRK as donor constructs, in combination with a NET2A-mCherry acceptor construct. To generate the *At*PRK-GFP fusions, the full-length coding sequences of full-length *At*PRK1, *At*PRK2, *At*PRK3, *At*PRK4, *At*PRK5 and *At*PRK6, were PCR amplified from Arabidopsis Col-0 floral cDNA, and cloned into pDONR207 using gateway cloning. *At*PRK1, *At*PRK2, *At*PRK3, *At*PRK5, and *At*PRK6 were cloned into the expression vector pB7FGW2, and *At*PRK4 was cloned into pMDC83 (figure 6.11), both of which facilitate the expression of each *At*PRK as a C-terminal GFP fusion protein under the *CaMV 35s*: promoter.

To generate the NET2A-mCherry construct, the expression vector, pMDC83-mCherry was created. pMDC83-mCherry is a modified version of pMDC83 (Curtis and Grossniklaus. 2003) in which the GFP coding sequence has been excised and replaced with the mCherry coding sequence, to facilitate expression of proteins as

C-terminal mCherry fusions under control of the *CaMV 35s*: promoter. To create pMDC83-mCherry, the mCherry coding sequence was PCR amplified with *5'AscI* and *3'BstB*I restriction sites. *AscI/BstBI* double restriction digest was performed on pMDC83 to cut the vector either side of, and excise the GFP coding sequence. *AscI/BstBI* double restriction digest was also used on the *5'AscI-mCherry-3'BstBI* PCR product to generate sticky ends compatible for ligation into the *AscI/BstBI* sites of pMDC83. Ligation of the mCherry coding sequence into the pMDC83 *AscI/BstBI* sites was performed using T7 DNA ligase to generate pMDC83-mCherry (figure 6.10; see appendix 3.1 for sequence). The coding sequence of full-length NET2A was cloned into pMDC83-mCherry from NET2A-pDONR207 using gateway cloning, to express NET2A-mCherry under control of the *CaMV 35s*: promoter (figure 6.11).

To investigate the interaction between NET2B and each *At*PRK, NET2B-GFP was used as a FRET-FLIM donor construct, and *At*PRK-RFP fusion proteins were used as acceptors. Using the *At*PRK-pDONR207 entry clones described above, *At*PRK1, *At*PRK3, *At*PRK4, *At*PRK5 and *At*PRK6 were cloned into pH7RGW2 to facilitate their expression as C-terminal RFP fusion proteins under control of the *CaMV 35s:* promoter. *At*PRK2 was cloned into pMDC83-mCherry to facilitate its expression as a C-terminal mCherry fusion protein under control of the *CaMV 35s*: promoter.

pMDC83-mCherry

Figure 6.10: **Schematic Diagram of the pMDC83-mCherry Expression Vector used for Expression of C-terminal mCherry Fusion Proteins Under the *CaMV* 35s: Promoter.** The vector is a modified version of pMDC83, (Curtis and Grossniklaus. 2003) in which the pMDC83 GFP6 coding sequence has been excised and replaced with that of mCherry. RB: right border. yellow arrow: *CaMV 35s:* promoter sequence. Green boxes: AttR1 and AttR2 gateway recombination sites. Blue box: ccdB gateway cassette. Purple: coding sequence for C-terminal mCherry tag. Yellow box: Tnos terminator. LB: left border.

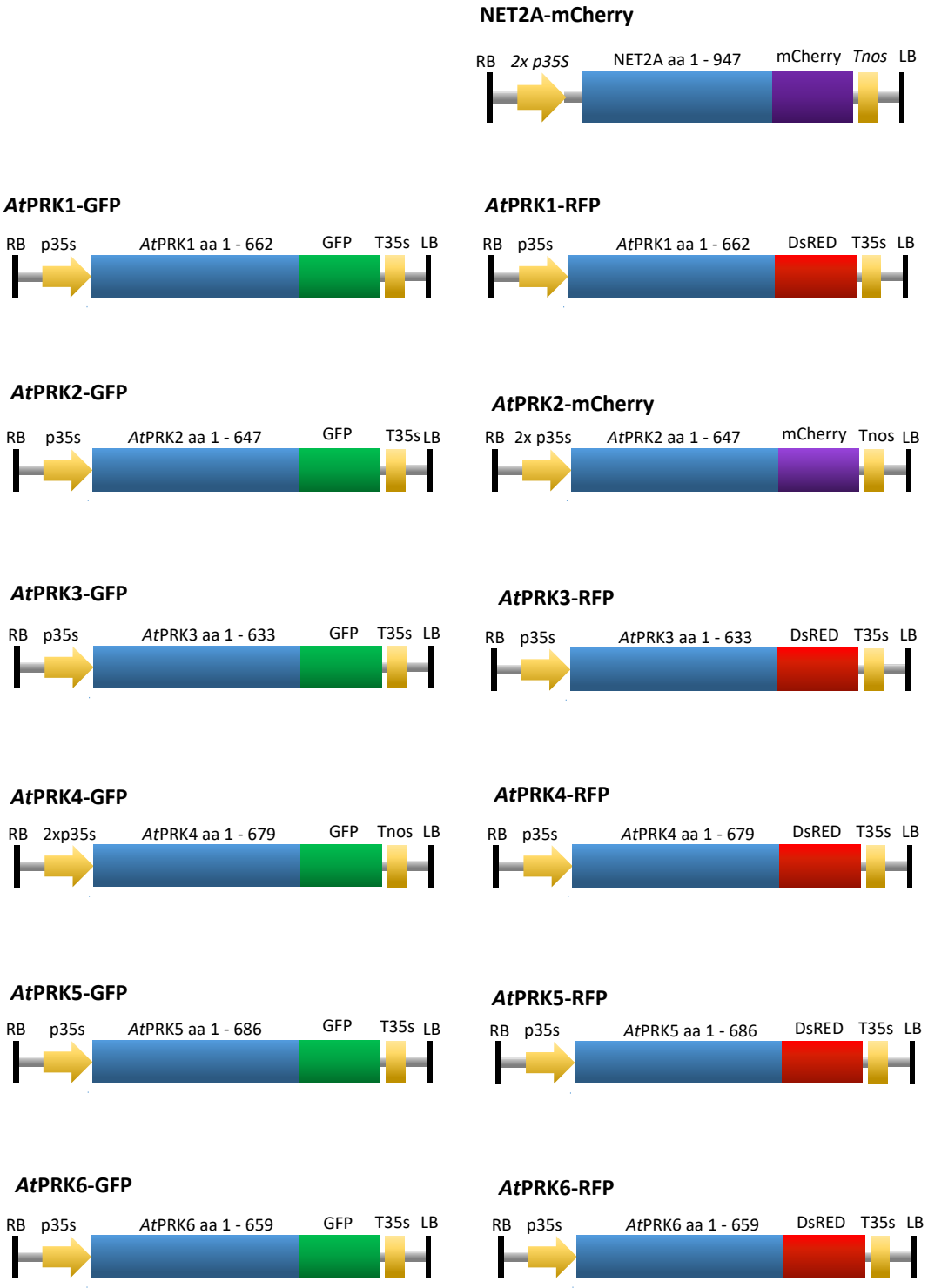

Figure 6.11: Schematic Diagrams of Expression Constructs Used to Express *At*PRK and NET2A Donor and Acceptor Constructs *in vivo* for use in FRET-FLIM: *At*PRK1-GFP, *At*PRK2-GFP, *At*PRK3-GFP, *At*PRK5-GFP and *At*PRK6-GFP were generated using the pB7FGW2 expression vector. *At*PRK4-GFP was created using the pMDC83 expression vector. NET2A-mCherry and *At*PRK2-mCherry was generated using the vector pMDC83-mCherry, *At*PRK1-RFP, *At*PRK3-RFP, *At*PRK4-RFP, *At*PRK5-RFP, and *At*PRK6-RFP was generated using pH7RGW2. RB = T-DNA right border. p35s = CaMV 35s promoter sequence. T35s = CaMV 35s terminator sequence. nosT = nopaline synthase terminator sequence. LB = T-DNA left border.

The generated constructs were expressed in *N. benthamiana* leaf epidermal cells using agrobacterium-mediated transformation, and their subcellular localisations analysed using CLSM. As shown in figure 6.12, NET2A-mCherry appeared to decorate a filament system when expressed in *N. benthamiana*; presumably binding to the actin cytoskeleton in a similar manner to NET2A-GFP as described in section 5.3.2. NET2A-mCherry appeared to localise to punctae at the cell cortex that aligned on filaments in the 'beads-on-a-string pattern' typical of NET proteins (Deeks et al. 2012). In cells exhibiting higher levels of expression, NET2A-mCherry also formed protein aggregates, perhaps due to overexpression of the construct under the *CaMV 35s:* promoter.

Analysis of the subcellular localisation of *At*PRK fluorophore fusion proteins was then performed in *N. benthamiana* leaf epidermal cells. As expected, GFP and RFP fluorophore fusions of *At*PRK2, *At*PRK4, *At*PRK5 and *At*PRK6 were found to localise almost entirely to the cell cortex, presumably at the plasma membrane. Faint labelling of cytoplasmic strands could be observed in some cells, perhaps due to the localisation of the *At*PRK fusion proteins to the membranes of transvacuolar strands resulting from saturation of the plasma membrane. Consistent with these observations, a plasma membrane localisation of *At*PRK fluorophore fusions has been reported for *At*PRK4, *At*PRK5 and *At*PRK6 in *N. benthamiana* leaf epidermal cells previously (Takeuchi and Higashiyama. 2016; Wrzaczek et al. 2015), and *At*PRK2 fluorophore fusions are known to localise to the plasma membrane of growing pollen tubes (Zhang and McCormick. 2007). *At*PRK1 and *At*PRK3 fluorophore fusion proteins also appeared to label the cytosol and endoplasmic reticulum of *N. benthamiana* leaf epidermal cells, especially in the case of *At*PRK1-GFP, which exhibited a prominent ER localisation.

Having analysed the subcellular localisations of the NET2A and *At*PRK donor and acceptor fluorophore-fusion constructs described above, FRET-FLIM was performed to corroborate the Y2H results described above.

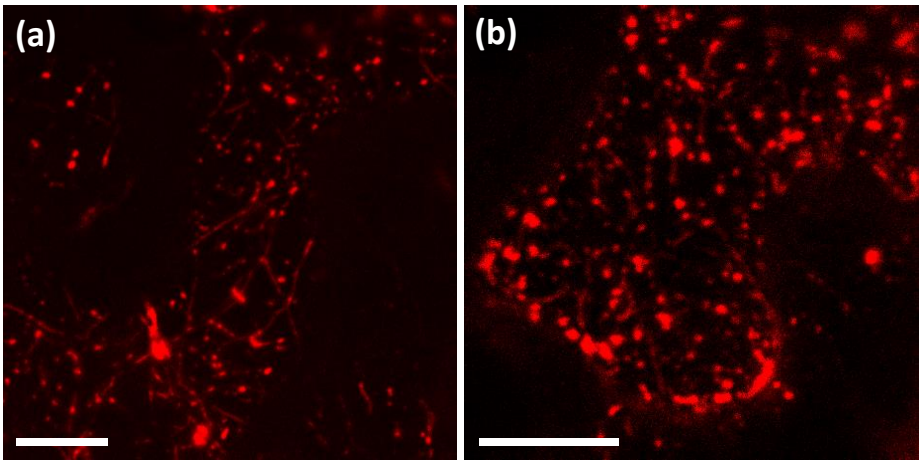

Figure 6.12: The Subcellular Localisation of NET2A-mCherry in *N. benthamiana* Leaf Epidermal Cells. (a) and (b): *N. benthamiana* leaf epidermal cells expressing NET2A-mCherry. Scale bar: 10 µm

6.3.3.3. FRET-FLIM Analysis of NET2A-*At*PRK Interactions *in vivo.*

FRET-FLIM was then performed to determine whether NET2A-mCherry may physically associate with *At*PRK1-GFP, *At*PRK2-GFP, *At*PRK3-GFP, *At*PRK4-GFP, *At*PRK5-GFP and *At*PRK6-GFP *in vivo*. Each *At*PRK-GFP fusion was expressed both alone, and with NET2A-mCherry in *N. benthamiana* leaf epidermal cells using agrobacterium-mediated transformation, and FRET-FLIM was performed to investigate a potential interaction between the constructs as previously described. The fluorescence lifetimes of each *At*PRK-GFP construct were measured when expressed alone and compared to when co-expressed with NET2A-mCherry, to observe potential reductions in fluorescence lifetime arising from FRET.

As displayed in figures 6.14 and 6.15, it was observed that NET2A-mCherry was unable to significantly reduce the GFP fluorescence lifetimes of *At*PRK1-GFP, *At*PRK2-GFP, *At*PRK3-GFP and *At*PRK6-GFP, which exhibited similar lifetime values whether expressed alone, or with NET2A-mCherry. As no reduction in the fluorescence lifetimes of *At*PRK1-GFP, *At*PRK2-GFP, *At*PRK3-GFP and *At*PRK6-GFP was induced by NET2A-mCherry, it could be determined that FRET did not

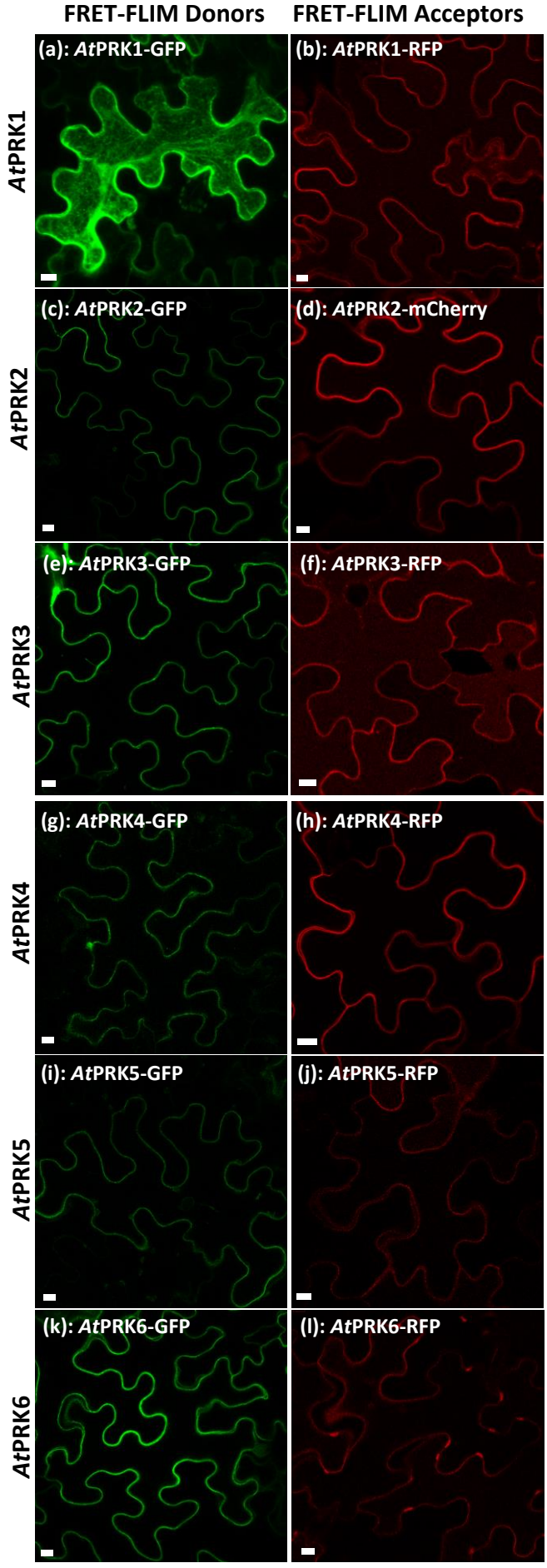

Figure 6.13: Subcellular Localisation of *At*PRK-Fluorophore Fusion Proteins in *N. benthamiana* Leaf Epidermal Cells. (a), (c), (e), (g), (i) and (k): C-terminal GFP fusion proteins for use as FRET-FLIM donors. (b), (d, (f), (h), (j) and (l): C-terminal RFP fusion proteins for use as FRET-FLIM acceptors. Scale bar: 10 µm.

occur between these *At*PRK-GFP fusions and NET2A-mCherry. Therefore, NET2A-mCherry was not observed to interact with *At*PRK1-GFP, *At*PRK2-GFP, *At*PRK3-GFP and *At*PRK6-GFP in this experimental system. This observation was in accordance with the Y2H experiment described above, in which NET2A was not observed to interact with these *At*PRKs.

In contrast, the fluorescence lifetimes of *At*PRK4-GFP and *At*PRK5-GFP were reduced considerably when co-expressed with NET2A-mCherry. The fluorescence lifetime of *At*PRK4-GFP when expressed alone was observed to be 2.45 ± 0.02 ns, which was reduced to 2.22 ± 0.06 ns when co-expressed with NET2A-mCherry, constituting a reduction in fluorescence lifetime of 0.23 ns. This value is comparable to the reduction in GFP fluorescence lifetimes reported between interacting proteins previously (chapters 5.3 and 6.2; Wang et al. 2014). This observation is indicative of FRET between *At*PRK4-GFP and NET2A-mCherry, and a physical interaction between the two proteins. This result corroborates the interaction between *At*PRK4 and NET2A observed using the Y2H system. Similarly, the fluorescence lifetime of *At*PRK5-GFP was reduced from 2.51 ± 0.02 ns when expressed alone to 2.15 ± 0.07 ns when co-expressed with NET2A-mCherry. This large decrease of 0.36 ns in *At*PRK5-GFP fluorescence lifetime induced by NET2A-mCherry, indicates FRET between the two proteins and a physical association of NET2A-mCherry and *At*PRK5-GFP *in vivo*. This result corroborates the observed interaction between NET2A and *At*PRK5 in the Y2H experiment described previously.

Therefore, interactions of NET2A with *At*PRK4 and NET2A with *At*PRK5 were demonstrated using both Y2H and FRET-FLIM assays. It can be concluded with confidence that NET2A is able to specifically bind members of the *At*PRK4/*At*PRK5 subclade, but not *At*PRK1, *At*PRK2, *At*PRK3, or *At*PRK6. As described in chapter 5, NET2B was demonstrated to heterodimerise with NET2A. In the next section, an interaction between NET2B and *At*PRK4 & *At*PRK5 was also demonstrated using FRET-FLIM.

6.3.3.4. Investigating NET2B – *At*PRK Interactions Using FRET-FLIM.

Having confirmed that NET2A is able to interact with both *At*PRK4 and *At*PRK5, it was investigated as to whether other members of the NET2 family may also interact with PRK proteins in *Arabidopsis*. As the closest protein family member and an interactor of NET2A, it is possible that NET2B may interact with *At*PRK proteins too. NET2A and NET2B may share functional redundancy by interacting with a common *At*PRK subgroup (*At*PRK4 and *At*PRK5), or perhaps NET2B may interact with a different set of *At*PRKs from an alternative subgroup (such as *At*PRK1 & *At*PRK2, or *At*PRK3 & *At*PRK6); thus indirectly linking the role of NET2A to the function of these *At*PRKs through an interaction with NET2B. To investigate this possibility, FRET-FLIM was performed to study potential interactions between NET2B and each *At*PRK.

FRET-FLIM was performed as previously described. NET2B-GFP was used as a FRET-FLIM donor construct, and *At*PRK1-RFP, *At*PRK2-mCherry, *At*PRK3-RFP, *At*PRK4-RFP, *At*PRK5-RFP and *At*PRK6-RFP were used as FRET-FLIM acceptor constructs. NET2B-GFP was expressed in *N. benthamiana* leaf epidermal cells using agrobacterium-mediated transformation, alone, and with each *At*PRK-RFP FRET-FLIM acceptor construct. Therefore, it was possible to investigate whether each of the *At*PRK acceptor constructs was able to induce a decrease in the fluorescence lifetime of NET2B-GFP and identify a potential interaction.

The results of the FRET-FLIM experiment between NET2B and the *At*PRK proteins are shown in figures 6.16 and 6.17. The results indicate that NET2B-GFP interacts specifically with *At*PRK4-RFP and *At*PRK5-RFP. NET2B-GFP was not observed to interact with *At*PRK1-RFP, *At*PRK2-mCherry, *At*PRK3-RFP or *At*PRK6-RFP; none of which were able to induce a decrease in the average fluorescence lifetime of NET2B-GFP by more than 0.04 ns. In contrast, *At*PRK4-RFP was able to reduce the average fluorescence lifetime of NET2B-GFP from 2.50 ± 0.04 ns to 2.22 ± 0.14 ns, constituting a reduction of 0.28 ns. *At*PRK5-RFP reduced the fluorescence lifetime of NET2B-GFP by 0.36 ns, to an average value of 2.14 ± 0.09 ns. These relatively large decreases in NET2B-GFP fluorescence lifetime are indicative of FRET occurring between NET2B-GFP and *At*PRK4-RFP & *At*PRK5-RFP. It be assumed that NET2B-GFP interacts with *At*PRK4-RFP and *At*PRK5-RFP when co-expressed in *N. benthamiana*.

The specific interaction of NET2B with *At*PRK4 and *At*PRK5, closely resembles the specificity of NET2A in its interaction with the same *At*PRK subclade. It can therefore be concluded that NET2A and NET2B share functional redundancy in their involvement with *At*PRK4 and *At*PRK5.

	Mean Donor GFP Fluorescence Lifetime			
Donor Construct	**Expressed without NET2A-mCherry**	**n**	**Co-expressed with NET2A-mCherry**	**n**
*At*PRK1-GFP	2.50 ± 0.03 ns	6	2.49 ± 0.02 ns	6
*At*PRK2-GFP	2.57 ± 0.02 ns	10	2.54 ± 0.03 ns	10
*At*PRK3-GFP	2.47 ± 0.02 ns	10	2.52 ± 0.02 ns	10
*At*PRK4-GFP	2.45 ± 0.02 ns	6	2.22 ± 0.06 ns	6
*At*PRK5-GFP	2.51 ± 0.02 ns	6	2.15 ± 0.07 ns	6
*At*PRK6-GFP	2.43 ± 0.04 ns	10	2.43 ± 0.07 ns	10
GFP-mCherry	2.07 ± 0.03 ns			12

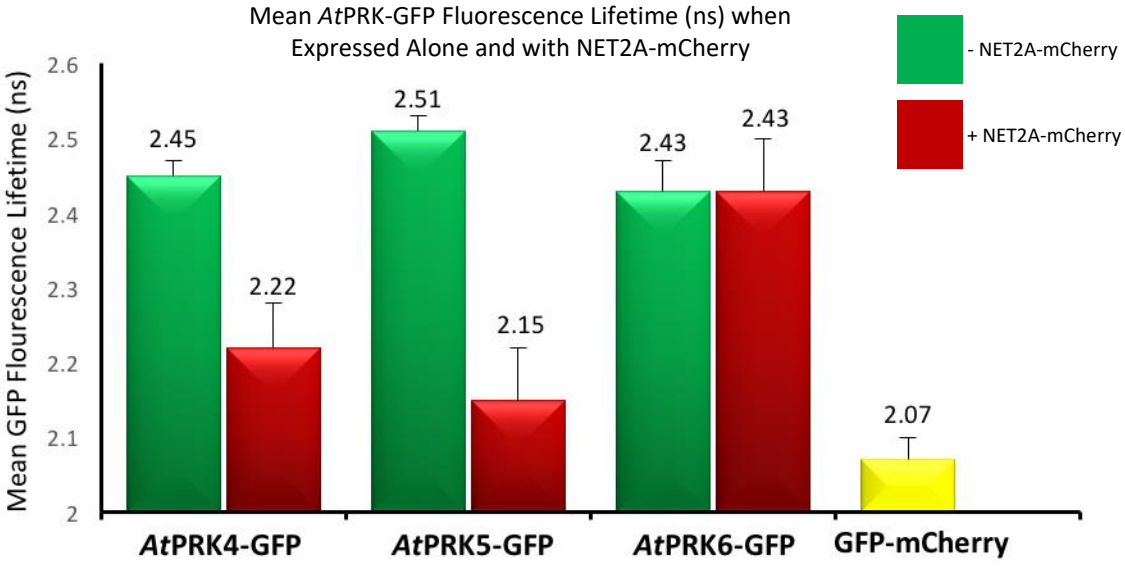

Figure 6.14: NET2A-mCherry Induces Decreases in the GFP Fluorescence Lifetime of *At*PRK4-GFP and *At*PRK5-GFP when Co-expressed in *N. benthamiana* Leaf Epidermal Cells. The GFP fluorescence lifetimes of *At*PRK1-GFP, *At*PRK2-GFP, *At*PRK3-GFP and *At*PRK6-GFP, remained relatively unaffected by NET2A-mCherry. n = number of cells analysed.

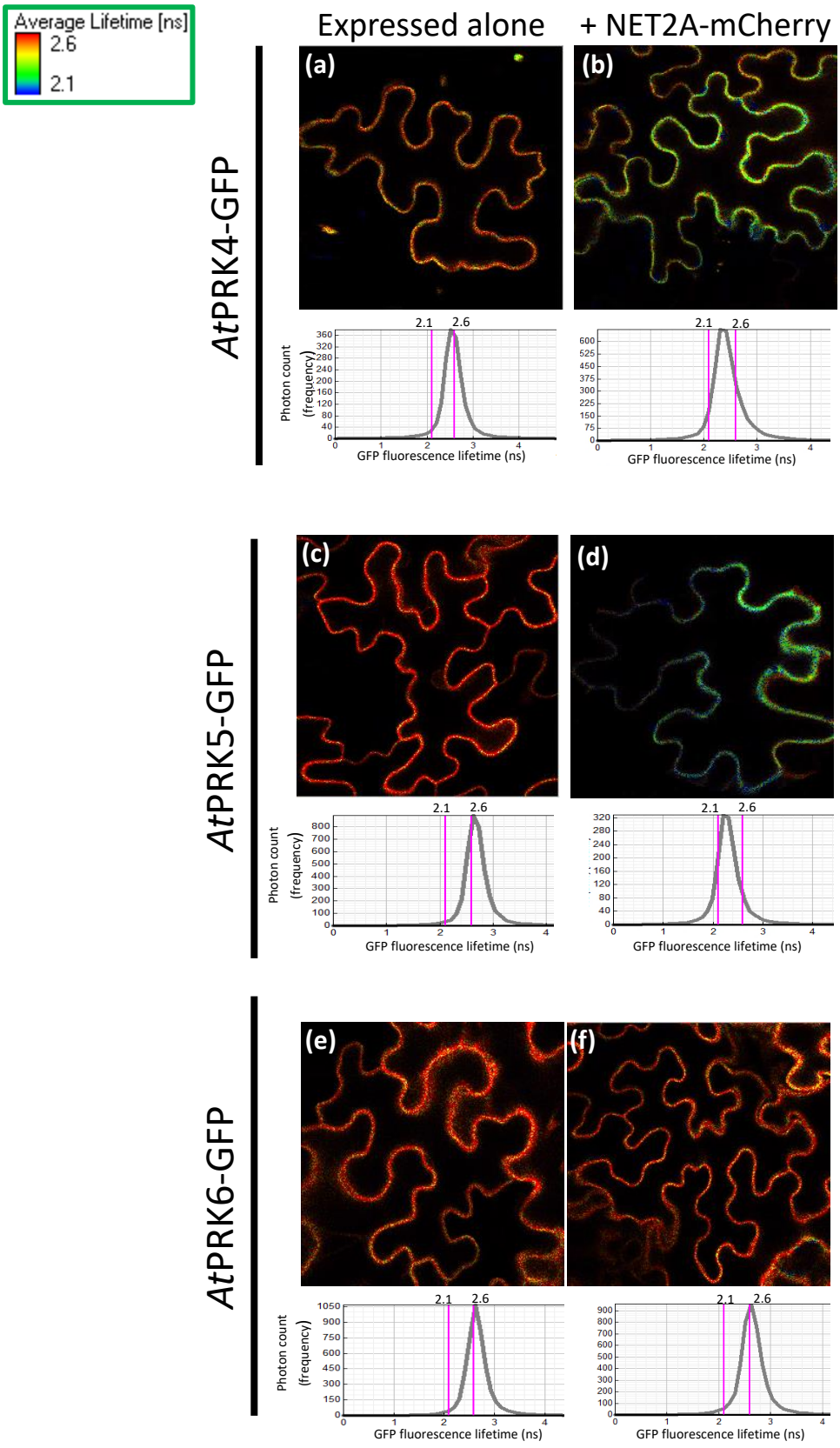
Average Lifetime [ns]
2.6
2.1
Expressed alone
+ NET2A-mCherry
AtPRK4-GFP
AtPRK5-GFP
AtPRK6-GFP
(a)
(b)
(c)
(d)
(e)
(f)
2.1
2.6
Photon count (frequency)
GFP fluorescence lifetime (ns)

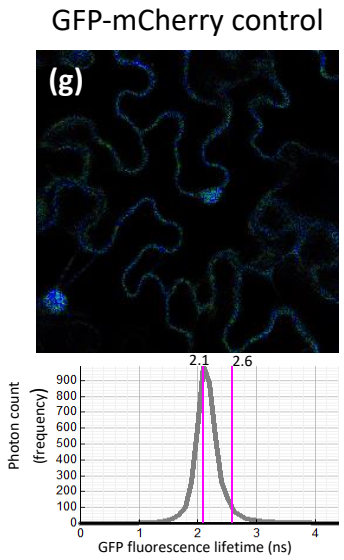

Figure 6.15: Visualisation of *At*PRK4-GFP, *At*PRK5-GFP and *At*PRK6-GFP Fluorescence Lifetimes *in vivo* when Expressed Alone, and with NET2A-mCherry. Example images of GFP fluorescence detected in *N. benthamiana* leaf epidermal cells, pseudocoloured according to GFP fluorescence lifetime, with associated graphs showing the frequency distributions of the fluorescence lifetimes (ns) of detected photons in each image. A leftward shift in peak GFP fluorescence lifetime is indicative of reduced average lifetime. (a) *At*PRK4-GFP expressed alone. (b): *At*PRK4-GFP co-expressed with NET2A-mCherry. (c): *At*PRK5-GFP expressed alone. (d): *At*PRK5-GFP co-expressed with NET2A-mCherry. (e): *At*PRK6-GFP expressed alone. (f): *At*PRK6-GFP co-expressed with NET2A-mCherry. (g): GFP-mCherry positive control.

Constructs Expressed	Mean GFP Fluorescence Lifetime	Standard Deviation	n
NET2B-GFP	2.50	0.04	10
NET2B-GFP + *At*PRK1-RFP	2.46	0.03	10
NET2B-GFP + *At*PRK2-mCherry	2.50	0.04	10
NET2B-GFP + *At*PRK3-RFP	2.48	0.02	10
NET2B-GFP + *At*PRK4-RFP	2.22	0.14	10
NET2B-GFP + *At*PRK5-RFP	2.14	0.09	10
NET2B-GFP + *At*PRK6-RFP	2.47	0.06	10
GFP-RFP	1.99	0.04	5
GFP-mCherry	2.03	0.05	5

Mean NET2B-GFP Fluorescence Lifetime (ns) When Expressed Alone and with *At*PRK-RFP Fusion Proteins.

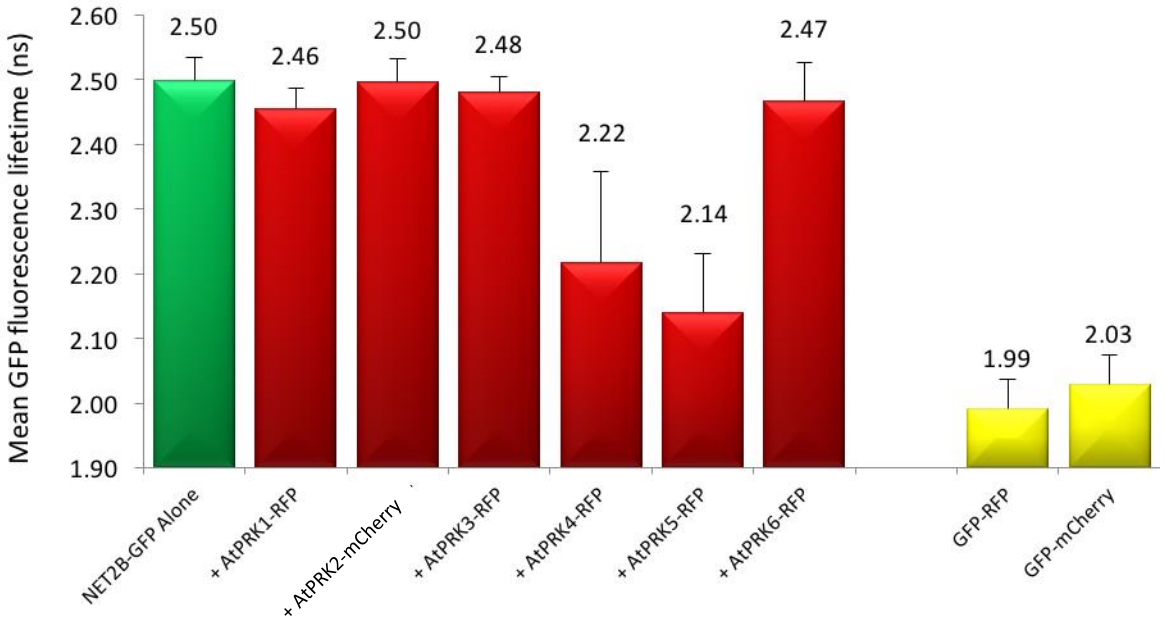

Figure 6.16: *At*PRK4-RFP and *At*PRK5-RFP Induce Significant Reductions in the Fluorescence Lifetime of NET2B-GFP when Co-expressed in *N. benthamiana* Leaf Epidermal Cells. The GFP fluorescence lifetime of NET2B-GFP, remained relatively unaffected by *At*PRK1-RFP, *At*PRK2-mCherry, *At*PRK3-RFP and *At*PRK6-RFP. n = number of cells analysed.

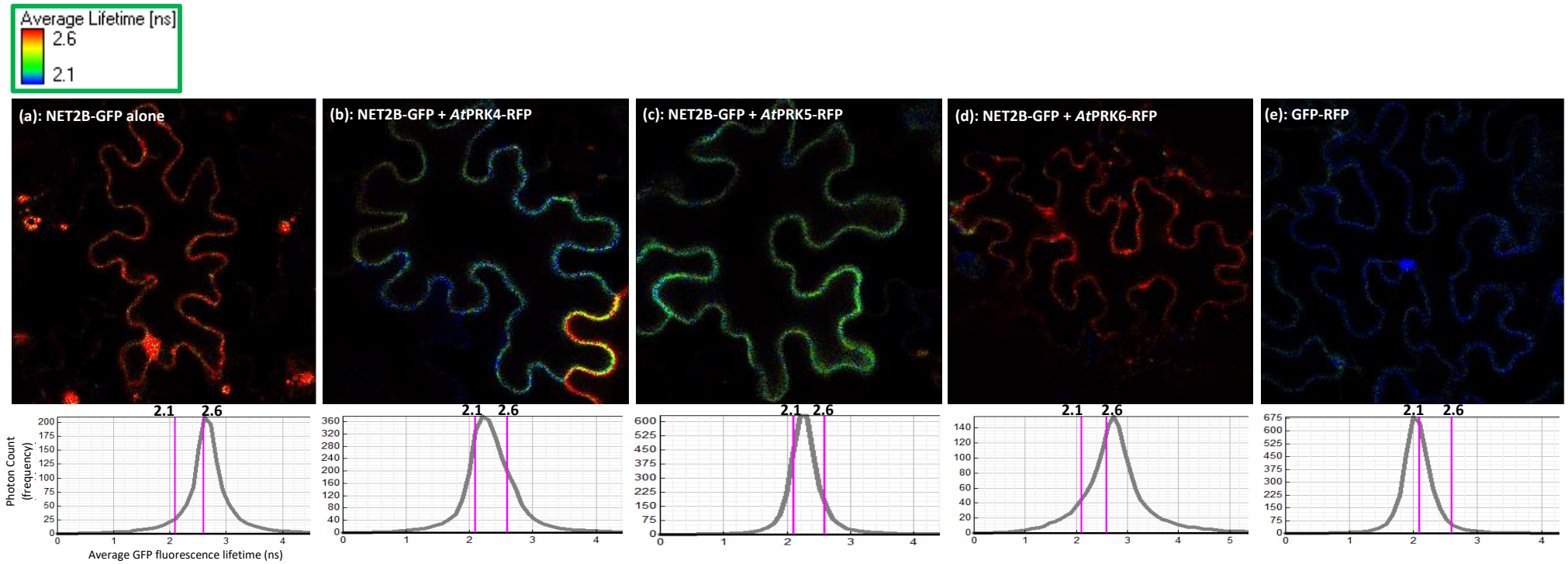

Figure 6.17: Visualisation of NET2B-GFP Fluorescence Lifetime *in vivo* when Expressed Alone, and with *At*PRK4-RFP, *At*PRK5-RFP and *At*PRK6-RFP. Example images of GFP fluorescence detected in *N. benthamiana* epidermal cells, pseudocoloured according to GFP fluorescence lifetime, with associated graphs showing the frequency distributions of the fluorescence lifetimes (ns) of detected photons in each image. A leftward shift in peak GFP fluorescence lifetime is indicative of reduced average lifetime. (a) NET2B-GFP expressed alone. (b): NET2B-GFP co-expressed with *At*PRK4-RFP (c): NET2B-GFP co-expressed with *At*PRK5-RFP. (d): NET2B-GFP co-expressed with *At*PRK6-RFP. (e): GFP-RFP positive control.

6.3.3.5. *At*PRK4-RFP and *At*PRK5-RFP Recruit NET2A-GFP and NET2B-GFP to the Plasma Membrane of *N. benthamiana* Leaf Epidermal Cells.

As described above, both NET2A and NET2B were found to interact with *At*PRK4 and *At*PRK5, but not *At*PRK1, *At*PRK2, *At*PRK3 and *At*PRK6. This interaction between Arabidopsis NET2 proteins and *At*PRK4 & *At*PRK5, is mirrored by a previously discovered interaction of between *Pi*KIP1, and *Pi*PRK1 (Skirpan et al. 2001). *Pi*PRK1-RFP was observed to recruit *Pi*KIP1-GFP to the plasma membrane when co-expressed in *N. benthamiana* leaf epidermal cells (section 6.2.3), and it is also possible that the subcellular localisation of NET2A and NET2B may similarly be re-organised by *At*PRK4 and *At*PRK5. As described below, the effects of *At*PRK4 & *At*PRK5 on the subcellular localisations of NET2A & NET2B were investigated, to determine whether they too may recruit NET2 proteins to the plasma membrane.

Using agrobacterium-mediated transformation, NET2A-GFP and NET2B-GFP were expressed in *N. benthamiana* leaf epidermal cells either alone, or alongside *At*PRK4-RFP or *At*PRK5-RFP to see if the *At*PRK proteins could induce alterations in the subcellular localisation of the NET2s. As a negative control, NET2A-GFP and NET2B-GFP were co-expressed with *At*PRK6-RFP, which was shown not to interact with the NET2 proteins in Y2H and FRET-FLIM assays.

As shown in figures 6.18 - 6.21, *At*PRK4-RFP and *At*PRK5-RFP induced drastic alterations in the subcellular localisations of NET2A-GFP and NET2B-GFP. NET2A-GFP and NET2B-GFP localised to filaments and punctae when expressed alone (6.18 and 6.20). When co-expressed with *At*PRK5-RFP, both NET2A-GFP and NET2B-GFP were found to co-localise with *At*PRK5-RFP at the plasma membrane (figures 6.19 and 6.21), and were absent from actin filaments (figures 6.18 and 6.20). When co-expressed with *At*PRK4-RFP, NET2A-GFP and NET2B-GFP were also not observed to localise to filaments or punctae (figures 6.18 and 6.20), instead co-localising with *At*PRK4-RFP at the plasma membrane, and also appeared to reside in the peripheral cytoplasm (figures 6.19 and 6.21). It is possible that the localisation of NET2A-GFP and NET2B-GFP to the cytosol may be due to a weak or transient interaction between the NET2s and *At*PRK4, meaning that the NET2s are not permanently associated with the membrane. However, it was clearly observable that *At*PRK4-RFP was able to drastically alter the subcellular localisation of NET2A-GFP and NET2B-GFP *in vivo*. In contrast, NET2A-GFP and NET2B-GFP

were still observed to localise to actin filaments and punctae when co-expressed with *At*PRK6-RFP (figures 6.18 and 6.20).

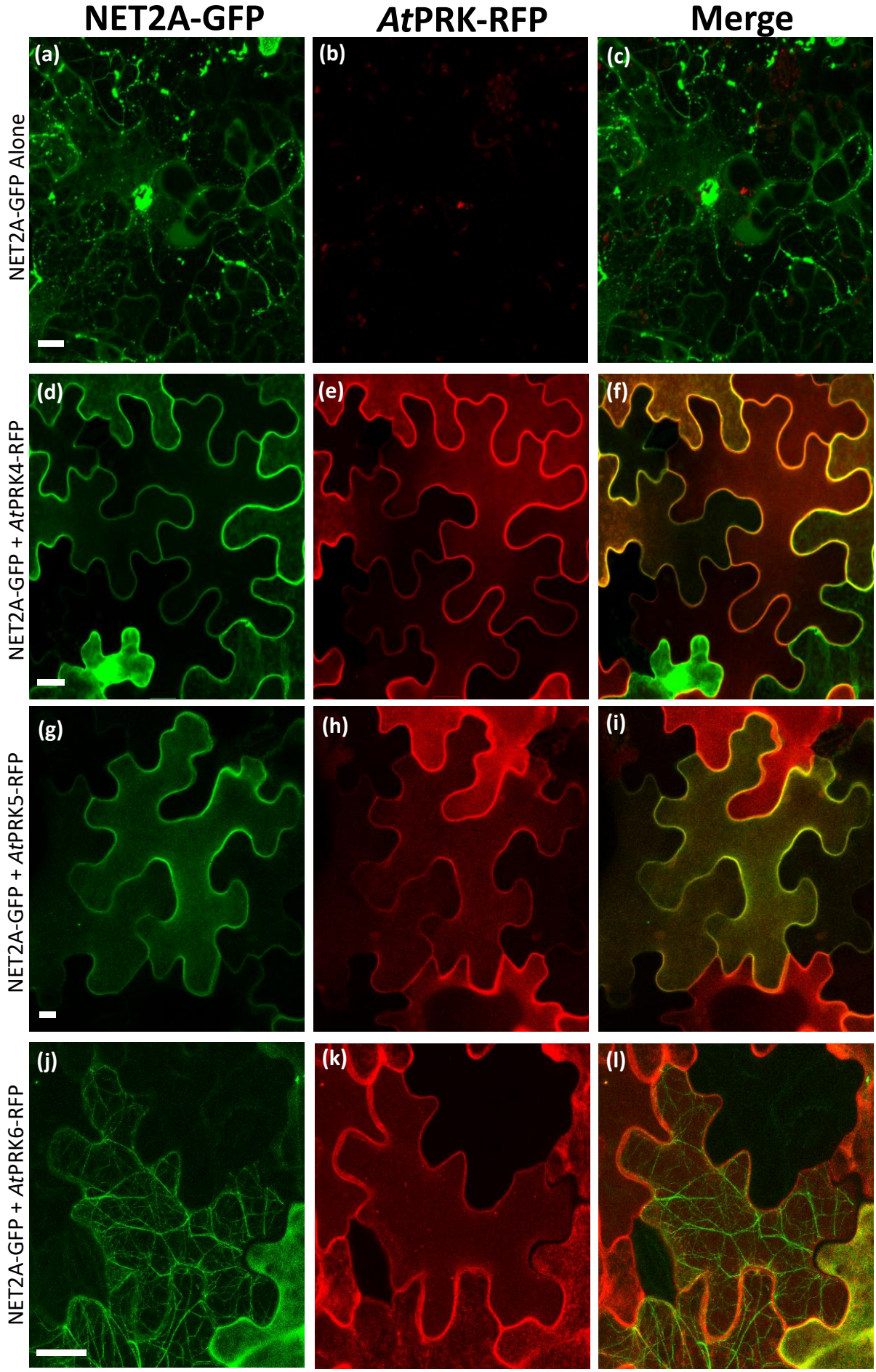

Figure 6.18: *At*PRK4-RFP and *At*PRK5-RFP Induce Changes in NET2A-GFP Subcellular Localisation in *N. benthamiana* Leaf Epidermal Cells. *N. benthamiana* leaf epidermal cells expressing NET2A-GFP either alone, or in combination with *At*PRK4-RFP, *At*PRK5-RFP, or *At*PRK6-RFP; included as a negative control. (a), (b) and (c): subcellular localisation of NET2A-GFP when expressed alone. (d), (e) and (f): NET2A-GFP subcellular localisation when co-expressed with *At*PRK4-RFP. (g), (h) and (i): NET2A-GFP subcellular localisation when co-expressed with *At*PRK5-RFP. (j), (k) and (l): NET2A-GFP subcellular localisation when co-expressed with *At*PRK6-RFP. (a), (d), (g) and (j): NET2A-GFP visualised using a 488 nm excitation laser and 505 - 530 nm emission detection. (b), (e), (h) and (k): *At*PRK-RFP fluorophore fusion proteins visualised using a 543 nm excitation laser and 600 – 650 nm emission detection. (c): overlay of (a) and (b). (f): overlay of (d) and (e). (i): overlay of (g) and (h). (l): overlay of (j) and (k). Scale bar: 10 µm.

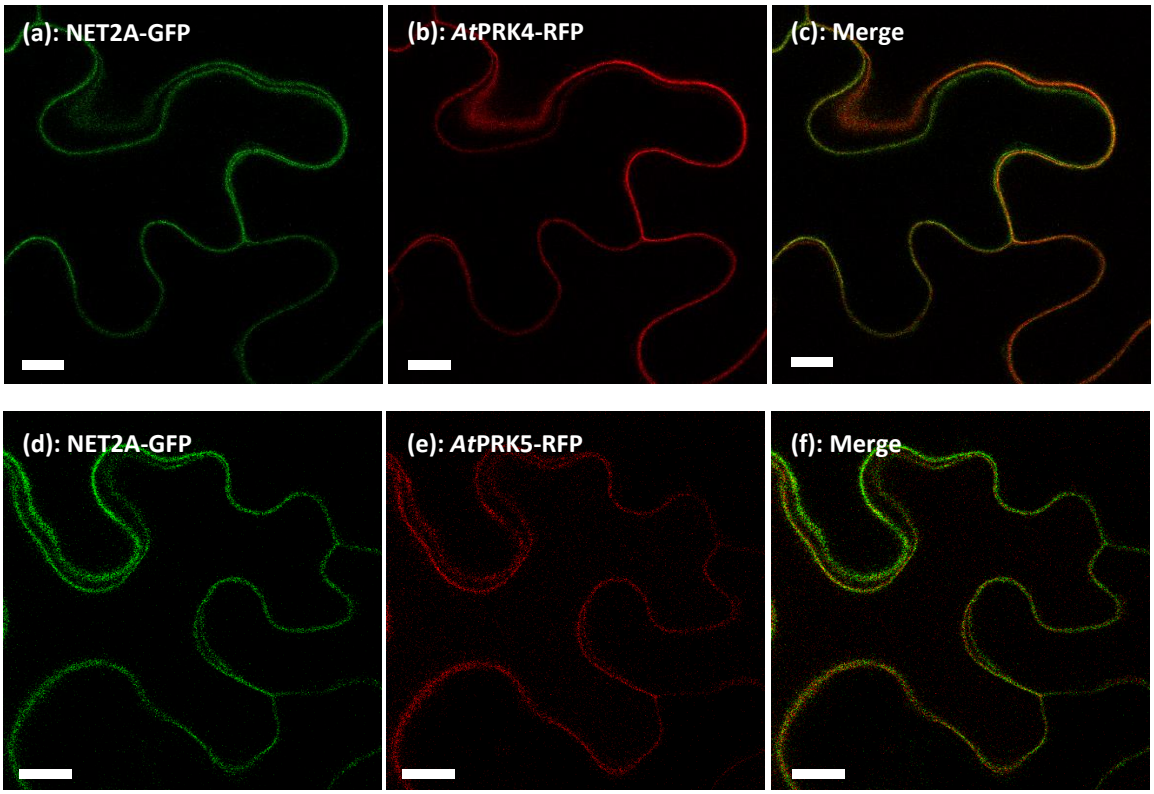

Figure 6.19: Co-localisation of NET2A-GFP with *At*PRK4-RFP and *At*PRK5-RFP in *N. benthamiana* Leaf Epidermal Cells. *N. benthamiana* leaf epidermal cells co-expressing NET2A-GFP in combination with *At*PRK4-RFP or *At*PRK5-RFP. (a), (b) and (c): subcellular localisation of NET2A-GFP when co-expressed alone with *At*PRK4-RFP. (d), (e) and (f): NET2A-GFP subcellular localisation when co-expressed with *At*PRK5-RFP. (a) and (d), NET2A-GFP visualised using a 488 nm excitation laser and 505-530 nm emission detection. (b) and (e), *At*PRK-RFP fluorophore fusion proteins visualised using a 543 nm excitation laser and 600 – 650 nm emission detection. (c): overlay of (a) and (b). (f): overlay of (d) and (e). Scale bar: 10 µm.

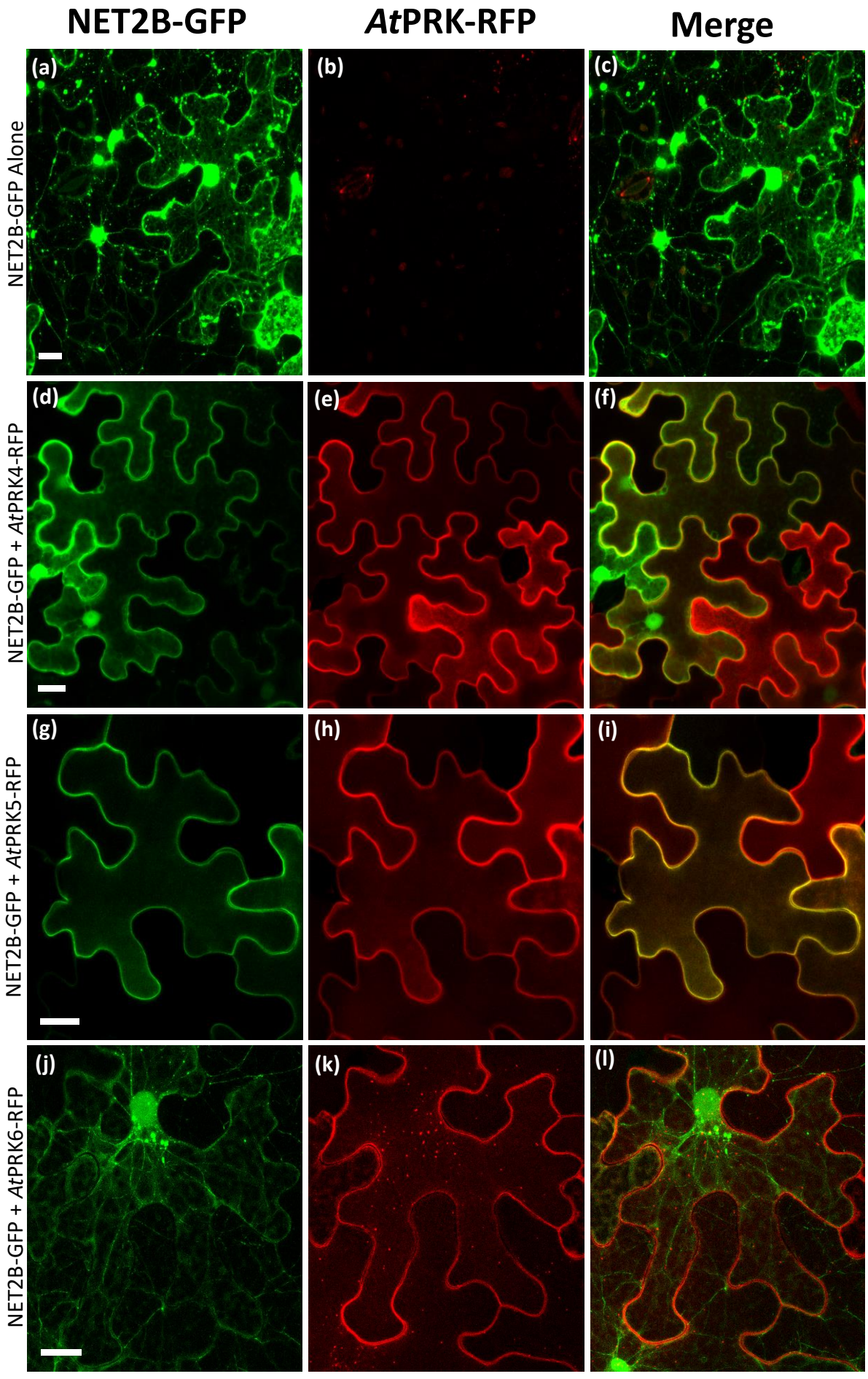
NET2B-GFP
AtPRK-RFP
Merge
NET2B-GFP Alone
NET2B-GFP + AtPRK4-RFP
NET2B-GFP + AtPRK5-RFP
NET2B-GFP + AtPRK6-RFP
(a)
(b)
(c)
(d)
(e)
(f)
(g)
(h)
(i)
(j)
(k)
(l)

Figure 6.20: *At*PRK4-RFP and *At*PRK5-RFP Induce Changes in NET2B-GFP Subcellular Localisation in *N. benthamiana* Leaf Epidermal Cells. *N. benthamiana* leaf epidermal cells expressing NET2B-GFP either alone, or in combination with *At*PRK4-RFP, *At*PRK5-RFP, or *At*PRK6-RFP; included as a negative control. (a), (b) and (c): subcellular localisation of NET2B-GFP when expressed alone. (d), (e) and (f): NET2B-GFP subcellular localisation when co-expressed with *At*PRK4-RFP. (g), (h) and (i): NET2B-GFP subcellular localisation when co-expressed with *At*PRK5-RFP. (j), (k) and (l): NET2A-GFP subcellular localisation when co-expressed with *At*PRK6-RFP. (a), (d), (g) and (j): NET2B-GFP visualised using a 488 nm excitation laser and 505 - 530 nm emission detection. (b), (e), (h) and (k): *At*PRK-RFP fluorophore fusion proteins visualised using a 543 nm excitation laser and 600 – 650 nm emission detection. (c): overlay of (a) and (b). (f): overlay of (d) and (e). (i): overlay of (g) and (h). (l): overlay of (j) and (k). Scale bar: 10 µm.

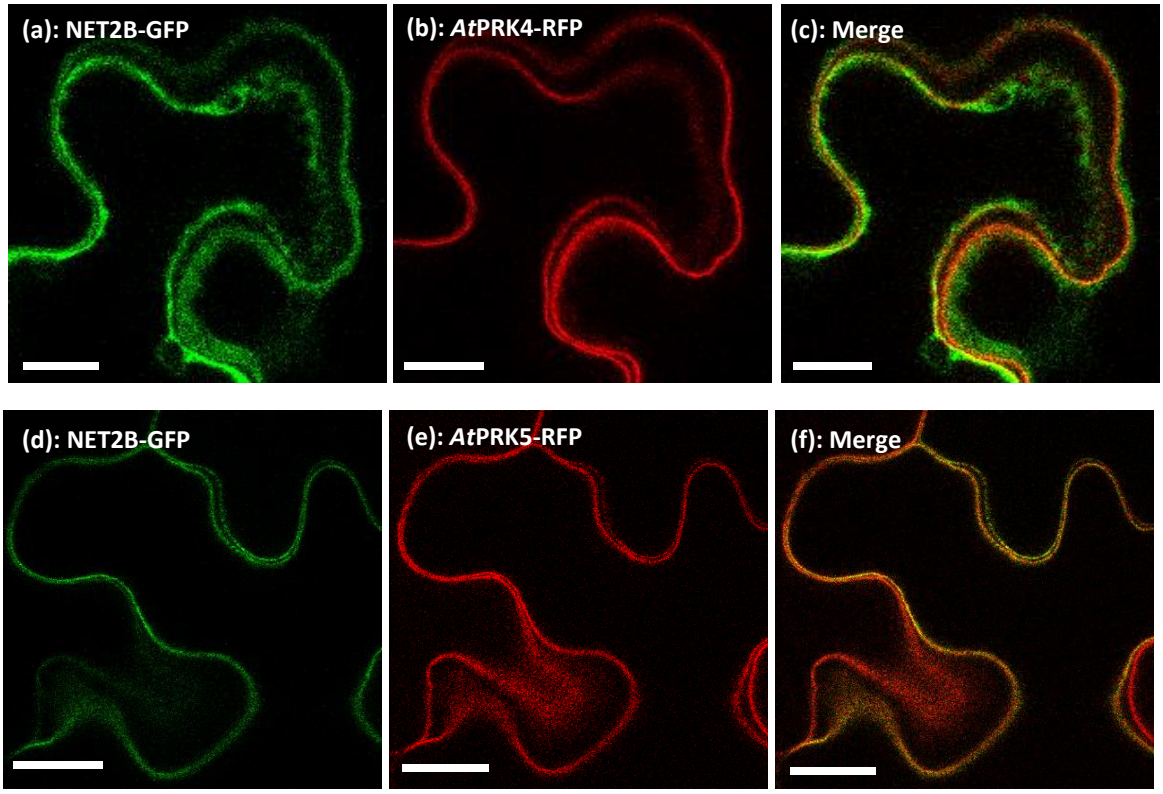

Figure 6.21: Co-localisation of NET2B-GFP with *At*PRK4-RFP and *At*PRK5-RFP in *N. benthamiana Leaf Epidermal Cells*. *N. benthamiana* leaf epidermal cells co-expressing NET2B-GFP in combination with *At*PRK4-RFP or *At*PRK5-RFP. (a), (b) and (c): subcellular localisation of NET2B-GFP when co-expressed with *At*PRK4-RFP. (d), (e) and (f): NET2B-GFP subcellular localisation when co-expressed with *At*PRK5-RFP. (a) and (d), NET2B-GFP visualised using a 488 nm excitation laser and 505 – 530 nm emission detection. (b) and (e), *At*PRK-RFP fluorophore fusion proteins visualised using a 543 nm excitation laser and 600 – 650 nm emission detection. (c): overlay of (a) and (b). (f): overlay of (d) and (e). Scale bar: 10 µm.

A change in NET2A-GFP & NET2B-GFP subcellular localisation induced by *At*PRK4-RFP & *At*PRK5-RFP may indicate a functional role for the interaction between NET2s and *At*PRKs. It is possible that *At*PRK4 & *At*PRK5 may be able to influence the subcellular localisation of NET2A & NET2B downstream of external signal perception. As described above, *At*PRK4-RFP and *At*PRK5-RFP abolished the binding of NET2-GFP to actin filaments, perhaps indicating that *At*PRK4 and *At*PRK5 may regulate NET2 actin-binding *in situ*. The co-localisation of NET2A-GFP & NET2B-GFP with *At*PRK4-RFP & *At*PRK5-RFP at the plasma membrane of *N. benthamiana* leaf epidermal cells may indicate a role for these *At*PRKs in the recruitment of NET2 proteins to the plasma membrane in growing pollen tubes.

6.3.5.6. Summary.

Discussed above is the use of FRET-FLIM to confirm the interactions between NET2A and *At*PRK4 & *At*PRK5 identified using the GAL4 Y2H system. The interactions between NET2A and the *At*PRK4/*At*PRK5 subclade of *At*PRKs is orthologous to the interaction of *Pi*PRK1 and *Pi*KIP1 in Petunia.

Using FRET-FLIM, it was then determined that NET2B also interacts exclusively with *At*PRK4 and *At*PRK5, further corroborating the specificity of the NET2 proteins in their interactions with the *At*PRK4 & *At*PRK5 subclade. This data also indicates that NET2A shares functional redundancy with NET2B through its interactions with *At*PRK4 and *At*PRK5.

Finally, it was determined that *At*PRK4 & *At*PRK5 were able to induce significant changes in the subcellular localisation of NET2A & NET2B; seemingly abolishing their binding of actin and recruiting them to the plasma membrane. This result may be indicative of a functional role for NET2A & NET2B downstream of *At*PRK4 & *At*PRK5 signalling.

Having characterised an interaction between NET2 proteins and *At*PRK4 & *At*PRK5 using Y2H and FRET-FLIM assays, analysis of the identified NET2-*At*PRK associations was subsequently conducted in pollen tubes, in which both NET2s and *At*PRKs are endogenously expressed.

6.4. Analysis of NET2-*At*PRK Interactions in Arabidopsis Pollen Tubes.

6.4.1. Introduction.

The *At*PRK4/*At*PRK5 subclade of Arabidopsis pollen receptor-like kinases were demonstrated to be interacting partners of the NET2 subfamily. Therefore, potential co-localisation between NET2A and *At*PRK4 & *At*PRK5 was visualised in germinating pollen tubes, so that the interaction could be investigated *in vivo*. Described in this section is the generation of stable transgenic Arabidopsis lines expressing *At*PRK4 and *At*PRK5 as fluorophore fusion proteins, for analysis of their subcellular localisation i*n vivo*, and co-localisation with NET2A.

6.4.2. Generation of *pLAT52*:*At*PRK4-GFP, *pLAT52*:*At*PRK5-GFP, *pLAT52*:*At*PRK4-RFP and *pLAT52*:*At*PRK5-RFP Stable Transgenic Arabidopsis Lines.

*At*PRK4 and *At*PRK5 were expressed in Arabidopsis pollen tubes with either C-terminal GFP or RFP fluorophore tags, under the strong pollen-specific promoter, *pLAT52.* To facilitate the expression of *pLAT52*-driven C-terminal RFP fusion proteins, the expression vector, pH7RGW52 was used. This vector, created by Dr Michael Deeks (University of Exeter), is a modified version of the gateway vector pH7RGW2, in which the *CaMV 35s* promoter has been replaced by *pLAT52*. To facilitate expression of *pLAT52*-driven C-terminal GFP fusion constructs, the expression vector pB7FGW52 was generated through modification of pB7FGW2 (Karimi et al. 2002), by replacement of the *CaMV 35s* with *pLAT52.*

Restriction subcloning was performed in order to generate pB7FGW52. The 567 bp *pLAT52* insert fragment was PCR amplified from template provided by Professor David Twell, University of Leicester, with added 5' *SacI* and 3' *SpeI* restriction sites using the primers listed in Appendix 1. *SacI*/*SpeI* double restriction digestion was performed on pB7FGW2 to cut the vector either side of, and excise the *CaMV 35s* promoter. The *SacI*/*SpeI* double digest was also performed on the 5'SacI-*pLAT52*-

3'SpeI PCR fragment to generate sticky ends compatible for ligation into the *SacI/SpeI* restriction site of pB7FGW2. Using T7 DNA ligase, *pLAT52* was ligated into the pB7FGW2 *SacI/SpeI* restriction site to generate pB7FGW52 (figure 6.22, see Appendix 3 for sequence).

To generate the *pLAT52*:*At*PRK4-GFP and *pLAT52*:*At*PRK5-GFP expression constructs, the full-length coding sequences of *At*PRK4 and *At*PRK5 were cloned into pB7FGW52 from *At*PRK4-pDONR207 and *At*PRK5-pDONR207 using gateway cloning. *pLAT52*:*At*PRK4-RFP and *pLAT52*:*At*PRK5-RFP were generated through gateway cloning of the full-length *At*PRK4 and *At*PRK5 coding sequences into pH7RGW52 from *At*PRK4-pDONR207 and *At*PRK5-pDONR207.

Arabidopsis Col-0 plants were stably transformed with *At*PRK4-pB7FGW52, *At*PRK5-pB7FGW52, *At*PRK4-pH7RGW52 and *At*PRK5-pH7RGW52 using floral dipping as described in chapter 2.15. Seed from the T_0 parent plants was collected and sown on ½ MS agar supplemented with 10 µg/ml BASTA to select for *At*PRK4-pB7FGW52, *At*PRK5-pB7FGW52 transformants, or 40 µg/ml hygromycin B to select for *At*PRK4-pH7RGW52 and *At*PRK5-pH7RGW52 transformants. Manual screening of GFP or RFP fluorescence was performed on flowers of selected plants to confirm expression of the fusion proteins in pollen.

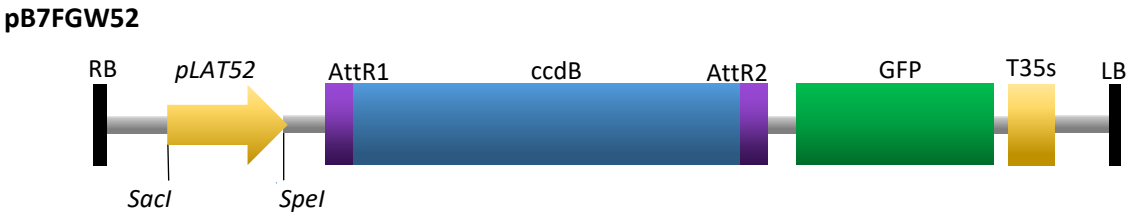

Figure 6.22: **Schematic Diagram of the pB7FGW52 Expression Vector used for Expression of C-terminal GFP Fusion Proteins Under the *pLAT52* Promoter.** The vector is a modified version of pB7FGW2, (Plant Systems Biology, Ghent University) in which the pB7FGW2 *CaMV 35s*: promoter has been excised and replaced with *pLAT52*. RB: right border. yellow arrow: *pLAT52* promoter sequence. Purple boxes: AttR1 and AttR2 gateway recombination sites. Blue box: ccdB gateway cassette. Green box: coding sequence for C-terminal GFP tag. Yellow box: T35s terminator. LB: left border. The sequence of pB7FGW52 is detailed in Appendix 3.

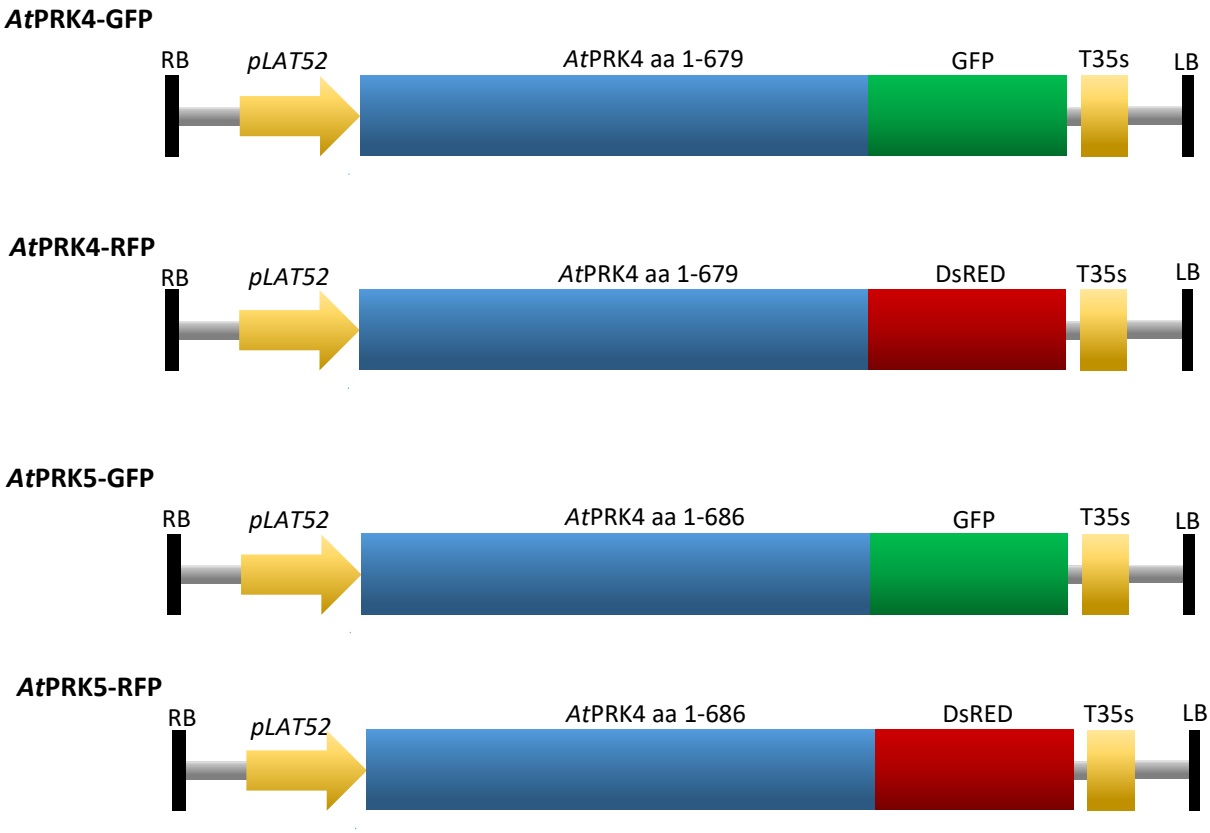

Figure 6.23: **Schematic Diagram of the Expression Constructs used Drive Stable Expression of *At*PRK4 and *At*PRK5 Fluorophore Fusion Proteins in Arabidopsis Pollen.** *At*PRK4-GFP and *At*PRK5-GFP expression constructs were generated using the pB7FGW52 expression vector. *At*PRK4-RFP and *At*PRK5-RFP were generated using the pH7RGW52 expression vector. RB = T-DNA right border. p35s = CaMV 35s promoter sequence. T35s = CaMV 35s terminator sequence. LB = T-DNA left border.

6.4.3. Subcellular Localisation of *At*PRK4 and *At*PRK5 Fluorophore Fusion Proteins in Arabidopsis Pollen Tubes.

The subcellular localisation of *pLAT52*-driven *At*PRK4-GFP, *At*PRK4-RFP, *At*PRK5-GFP and *At*PRK5-RFP was analysed in growing pollen tubes. Pollen from stable transgenic plants was germinated *in vitro* as described in chapter 2.5.2.1 and the subcellular localisations of the *At*PRK-fluorophore fusion proteins was analysed using CLSM.

Firstly, the subcellular localisations of C-terminal GFP fusions of *At*PRK4 and *At*PRK5 were analysed in Arabidopsis pollen tubes. The subcellular localisation of *pLAT52*-driven *At*PRK4-GFP is displayed in figure 6.24, and *At*PRK5-GFP in figure 6.25. It was observed that *pLAT52*-expressed *At*PRK4-GFP and *At*PRK5-GFP fusion proteins localised predominantly to the plasma membrane of growing pollen tubes, with fluorescence also detected in the cell cytoplasm. At the pollen tube

plasma membrane, *At*PRK4-GFP and *At*PRK5-GFP were observed to localise to discreet foci which were highly prominent at the membrane of the pollen tube shank region, but were absent from the membranes of the pollen tube apex.

A plasma membrane localisation was also observed for *At*PRK4-RFP and *At*PRK5-RFP in growing pollen tubes (figure 6.26 and 6.27), and to a lesser extent, the cell cytosol. Similar to *At*PRK4-GFP and *A*tPRK5-GFP fluorophore fusions, *At*PRK4-RFP and *At*PRK5-RFP could be visualised at punctae at the pollen tube plasma membrane, which were highly prominent in the shank region but were absent at the growing tip.

It can be expected that endogenous *At*PRK4 and *At*PRK5 can localise to punctae at the pollen tube shank *in situ*, perhaps in a manner specific to the *At*PRK4/*At*PRK5 subclade. The formation of shank-specific punctae by both GFP and RFP fusions of *At*PRK4 and *At*PRK5 indicates that the observed punctae are not a result of protein mislocalisation induced by the fluorophore tags. Furthermore, the subcellular localisation of *At*PRK4 and *At*PRK5 described above does not appear to be an artefact of overexpression by the strong *pLAT52* promoter: no such localisations have been observed for *pLAT52*-expressed *At*PRK1 and *At*PRK2 in tobacco pollen tubes (Lee et al. 2008; Zhao et al. 2013). Indeed, the observed subcellular localisation of *At*PRK4 and *At*PRK5 described above appears to be specific to this *At*PRK subclade: *At*PRK1 appears to localise strongly at the tip of tobacco pollen tubes and does not form punctae at the shank membrane, nor does *At*PRK2 (Lee et al. 2008; Zhao et al. 2013). Also, it has also been reported that natively expressed *At*PRK3 and *At*PRK6 appear to localise prevalently to the pollen tube tip, and are present only minimally at shank membrane where they are distributed with an even and non-punctate pattern (Takeuchi and Higashiyama. 2016). It is likely that the distribution of *At*PRK4 and *At*PRK5 detailed above is specific to the *At*PRK4/*At*PRK5 subgroup, indicating a specific role for these *At*PRKs. Of particular significance, the subcellular localisation of *At*PRK4 and *At*PRK5-fluorophore fusion proteins displays a strikingly similar pattern to that reported for NET2A-GFP, which has been characterised as an interactor of *At*PRK4 and *At*PRK5 above. Subsequently therefore, investigation of potential co-localisation between NET2A and *At*PRK4 & *At*PRK5 was performed, as described below.

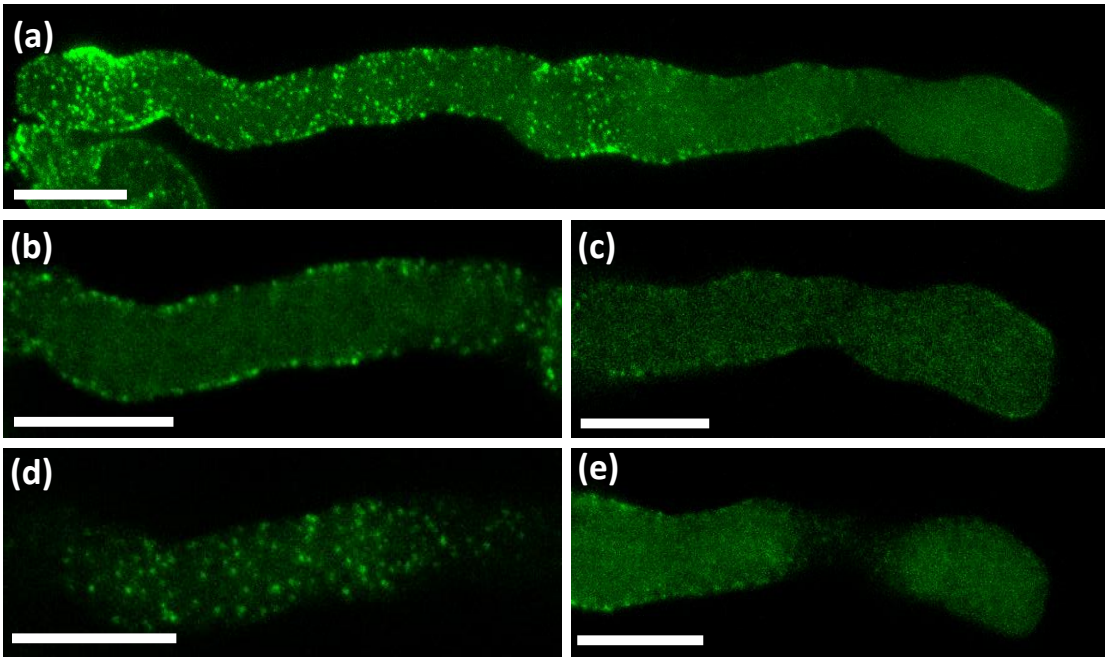

Figure 6.24: Subcellular Localisation of *pLAT52*-Driven *At*PRK4-GFP in Arabidopsis Pollen Tubes. (a): Z-projection of whole pollen tube. (b): Medial cross-section of pollen tube shank. (c): Medial cross-section of pollen tube tip. (d): Cortex of pollen tube shank. (e): Cortex of pollen tube tip. Scale bar: 10 µm.

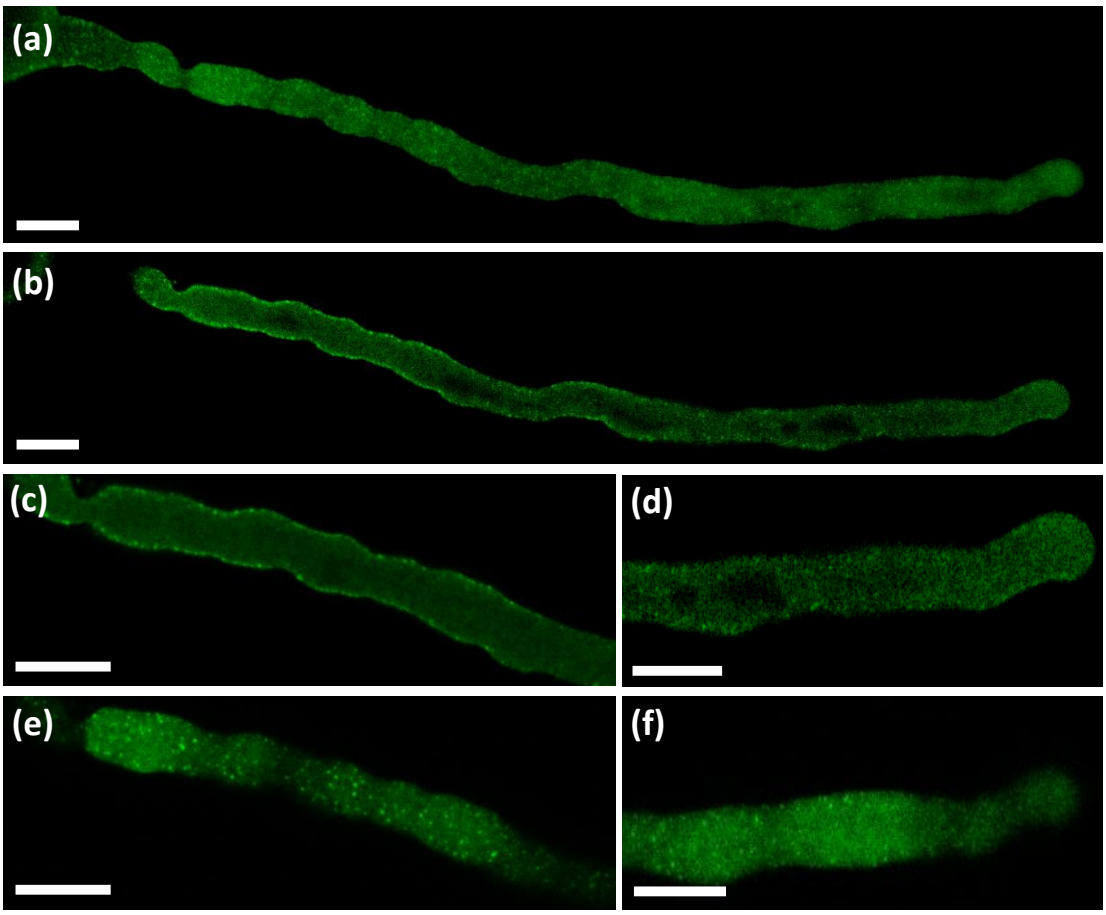

Figure 6.25: Subcellular Localisation of *pLAT52*-Driven *At*PRK5-GFP in Arabidopsis Pollen Tubes. (a): Z-projection of whole pollen tube. (b): Medial cross-section of whole pollen tube shank. (c): Medial cross-section of pollen tube shank. (d): Medial cross-section of pollen tube tip. (e): Cortex of pollen tube shank. (f): Cortex of pollen tube tip. Scale bar: 10 µm.

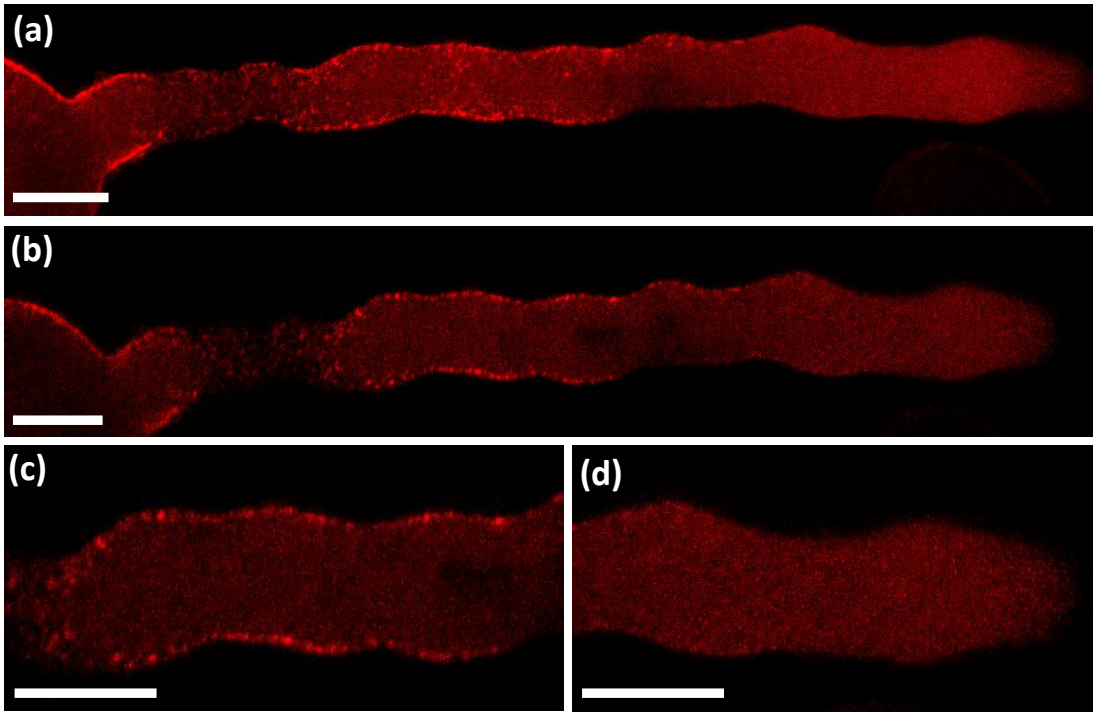

Figure 6.26: Subcellular Localisation of *pLAT52*-Driven *At*PRK4-RFP in Arabidopsis Pollen Tubes. (a): Z-projection of whole pollen tube. (b): Medial cross-section of whole pollen tube. (c): Medial cross-section of pollen tube shank. (d): Medial cross-section of pollen tube tip. Scale bar: 10 µm.

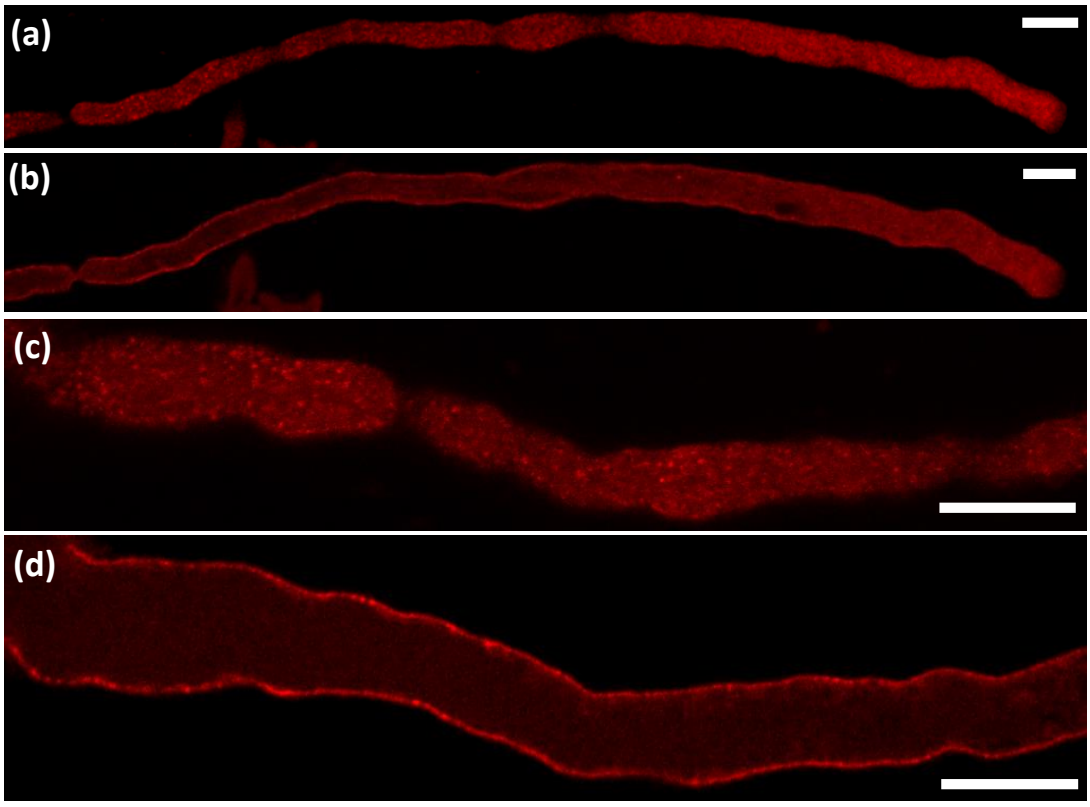

Figure 6.27: Subcellular Localisation of *pLAT52*-Driven *At*PRK5-RFP in Arabidopsis Pollen Tubes. (a): Z-projection of whole pollen tube. (b): Medial cross-section of whole pollen tube. (c): Cortex of pollen tube shank. (d): Medial cross-section of pollen tube shank. Scale bar: 10 µm.

6.4.4. Analysis of NET2A-GFP and *At*PRK4-RFP Co-localisation in Growing Pollen Tubes.

Having analysed the subcellular localisation of *At*PRK4 and *At*PRK5 fluorophore fusion proteins in growing pollen tubes, co-localisation between NET2A and *At*PRK4 & *At*PRK5 was investigated. *pNET2A*:NET2A-GFP stable transgenic Arabidopsis lines natively expressing NET2A-GFP have been used to visualise the subcellular localisation of NET2A in pollen tubes previously (Deeks et al. 2012; Dixon. 2013), and so were used in this experiment. Therefore, *At*PRK4-RFP and *At*PRK5-RFP were required for co-visualisation with NET2A-GFP. This study focusses on the co-localisation between NET2A-GFP and *At*PRK4-RFP in growing pollen tubes, as insufficient time was available to generate and analyse plants co-expressing *pNET2A*:NET2A-GFP and *pLAT52*:*At*PRK5-RFP during the course of the project. *pNET2A*:NET2A-GFP stable transgenic Arabidopsis plants were cross-pollinated with *pLAT52*:*At*PRK4-RFP lines to generate F1 progeny expressing both constructs, which were used for subsequent analysis.

Figure 6.28 shows the subcellular localisations of NET2A-GFP and *At*PRK4-RFP co-expressed in growing pollen tubes. NET2A-GFP and *At*PRK4-RFP could be seen to co-localise at punctae at the pollen tube plasma membrane. Interestingly, although many NET2A-GFP and *At*PRK4-RFP punctae clearly co-localised, some NET2A-GFP punctae could be observed unassociated with *At*PRK4-RFP foci. Likewise, some *At*PRK4-RFP punctae were not found to co-localise with punctae of NET2A-GFP (figure 6.29). It is possible that there exist subpopulations of *At*PRK4 that are not co-localised with NET2A at a single point in time: as NET2A punctae are aligned on actin filaments (Dixon. 2013), perhaps only *At*PRK4 punctae in direct vicinity of the actin filaments may bind NET2A. Alternatively, these *At*PRK4 punctae may also co-localise with other NET2 family members that do not co-localise with NET2A in pollen tubes. It is also possible that some NET2A punctae bind distinct and spatially separated interacting partners to *At*PRK4 at the plasma membrane, accounting for NET2A punctae that do not associate with *At*PRK4: it is possible that *At*PRK5 may be such an interacting protein and may not co-localise with *At*PRK4 *in vivo*. However, clear co-localisation between NET2A-GFP and *At*PRK4-RFP punctae was revealed at the plasma membrane of growing pollen tubes. It can therefore be concluded that NET2A and *At*PRK4 co-localise, and physically associate *in vivo*.

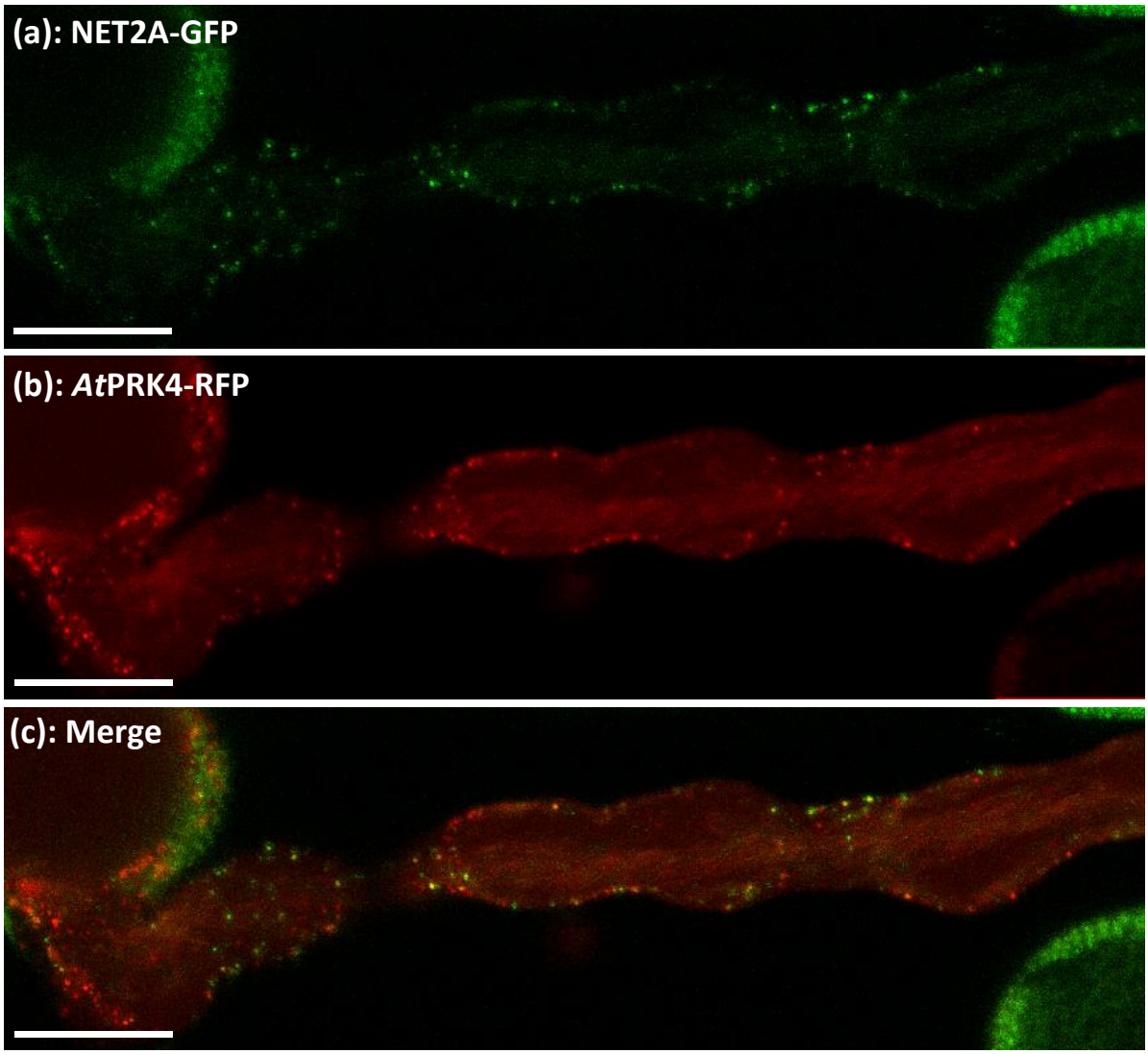

Figure 6.28: Co-localisation of NET2A-GFP and *At*PRK4-RFP in Arabidopsis Pollen Tubes. Pollen tubes of plants co-expressing *pNET2A*:NET2A-GFP and *pLAT52:At*PRK4-RFP were germinated *in vitro* and analysed using CLSM. (a): Subcellular localisation of NET2A-GFP visualised using a 488 nm excitation laser and detection of 505 - 530 nm emission. (b): *At*PRK4-RFP visualised using a 543 nm excitation laser and detection of 600 – 650 nm emission. (c): overlay of (a) and (b). Scale bar: 10 µm.

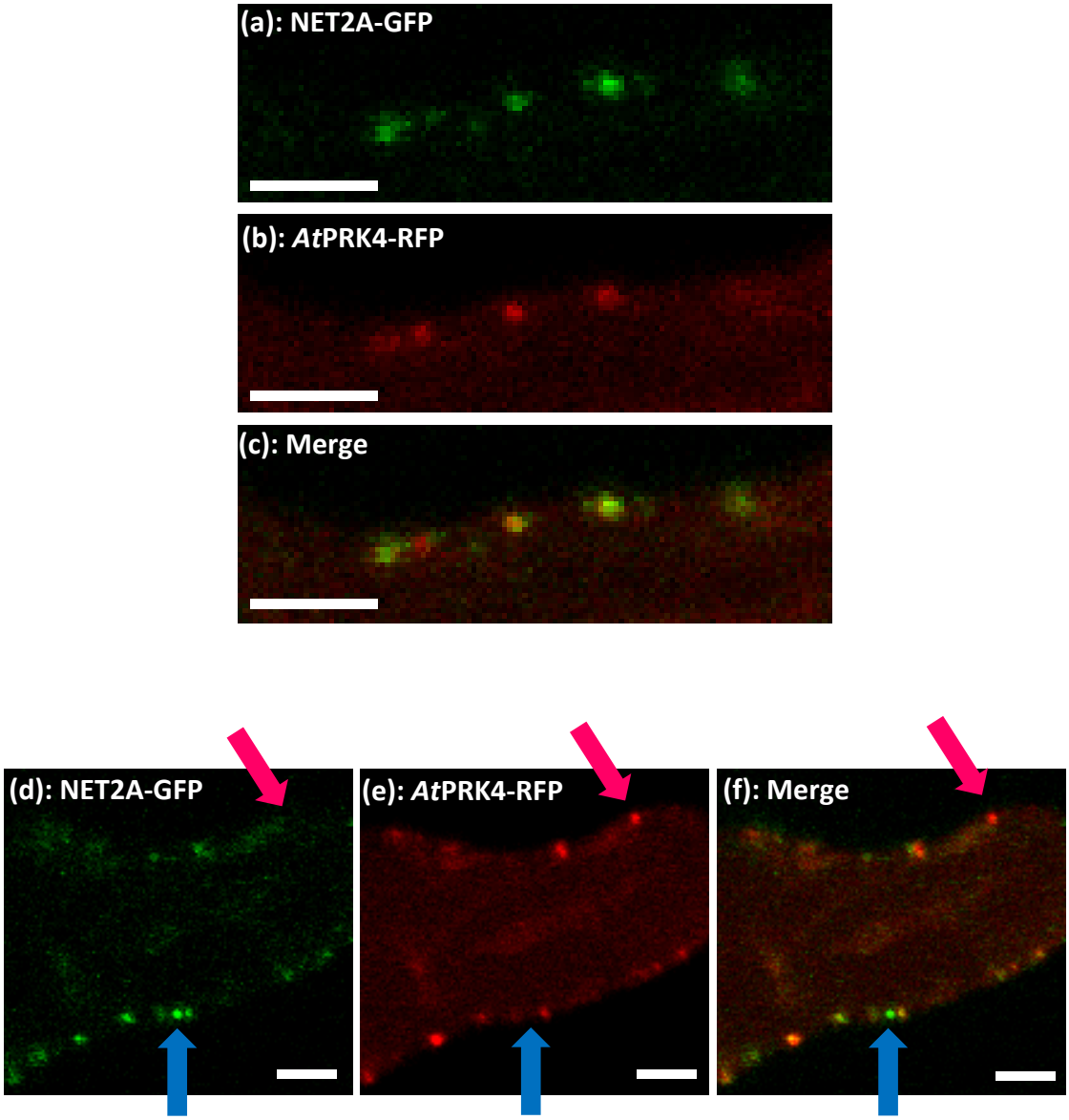

Figure 6.29: High-Magnification Analysis of NET2A-GFP and *At*PRK4-RFP Co-localisation in Arabidopsis Pollen Tubes. Pollen tubes of plants co-expressing *pNET2A*:NET2A-GFP and *pLAT52:At*PRK4-RFP were germinated *in vitro* and analysed using CLSM. (a) – (c) depict NET2A-GFP and *At*PRK4-RFP co-localising at the pollen tube membrane. (d) – (f) show examples of unassociated NET2A-GFP and *At*PRK4-RFP punctae. (a) and (d): Subcellular localisation of NET2A-GFP visualised using a 488 nm excitation laser and detection of 505 - 530 nm emission. (b) and (e): *At*PRK4-RFP visualised using a 543 nm excitation laser and detection of 600 – 650 nm emission. (c) and (f): overlay of (a) & (b), and (d) & (e) respectively. Blue arrow: NET2A-GFP punctae unassociated with *At*PRK4-RFP punctae. Pink arrow: *At*PRK4-RFP punctae unassociated with NET2A-GFP punctae. Scale bar = 2 µm.

6.4.5. Summary.

In chapter 6.3, *At*PRK4 and *At*PRK5 were proven to be interacting partners of NET2A. Subsequently, co-localisation between NET2A and *At*PRK4 & *At*PRK5 was investigated in growing pollen tubes. *At*PRK4 and *At*PRK5 were expressed in pollen as C-terminal GFP and RFP fusion proteins under the *pLAT52* promoter in order to visualise their subcellular localisations in growing pollen tubes. It was determined that *At*PRK4 and *At*PRK5 localise to punctae at the shank plasma membrane of growing pollen tubes, in a pattern that appears to be specific to the *At*PRK4/*At*PRK5 subclade and distinct from the reported subcellular distributions of *pLAT52*-expressed *At*PRK1 and *At*PRK2, and natively expressed *At*PRK3 and *At*PRK6 (Lee et al. 2008; Zhao et al. 2013; Takeuchi and Higashiyama. 2016.) This may be suggestive of a functional niche specific for *At*PRK4 and *At*PRK5 in Arabidopsis pollen tubes. Co-localisation between NET2A-GFP and *At*PRK4-RFP punctae was clearly observable at the pollen tube plasma membrane, indicating a physical association of NET2s and *At*PRKs in growing pollen tubes. It can be speculated that *At*PRK4 and *At*PRK5 may have a specific role in binding actin to the plasma membrane of growing pollen tubes through their associations with NET2 proteins.

6.5. Conclusion.

This section describes the characterisation of interactions between NET2 and PRK proteins. Firstly, *in vivo* analysis of the interactions of the Petunia NET2 protein, *Pi*KIP1, and *Pi*PRK1 corroborated previous reports of the two proteins interacting *in vitro* (Skirpan et al. 2001). *Pi*KIP1 is known to possess a functional actin-binding NAB domain (Calcutt. 2009), indicating that it may play a similar role in Petunia to Arabidopsis NET2A, in binding actin at the plasma membrane of growing pollen tubes. The observed interaction between *Pi*KIP1 and *Pi*PRK1 *in vivo* may suggest that *Pi*KIP1 binds *Pi*PRK1 at the plasma membrane of Petunia pollen tubes. This hypothesis was supported by the recruitment of *Pi*KIP1 to the plasma membrane by *Pi*PRK1 in transient expression studies in *N. benthamiana.* It is likely that *Pi*KIP1 may be a signalling component downstream of external signal perception by *Pi*PRK1. *Pi*PRK1 is known to phosphorylate *Pi*KIP1, which is important for the interaction to occur (Skirpan et al. 2001). Control of *Pi*KIP1 phosphorylation by

*Pi*PRK1 downstream of external signal perception may determine the subcellular localisation of *Pi*KIP1, and its regulation of the actin cytoskeleton.

Investigation of NET2 -PRK interactions was subsequently initiated in Arabidopsis, in which the NET2 protein family is better characterised. Therefore, observed NET2-PRK interactions could be contextualised against the many known signalling mechanisms demonstrated to regulate pollen tube growth in this model organism. By replicating previous experiments used to identify *Pi*KIP1 as an interactor or *Pi*PRK1, NET2A was demonstrated to interact with *At*PRK4 and *At*PRK5, which belong to a specific evolutionary subclade of *At*PRK proteins. NET2A did not interact with *At*PRK1, *At*PRK2, *At*PRK3 or *At*PRK6. These results were confirmed using FRET-FLIM, showing that the interactions occurred *in vivo*. Therefore, it was determined that Arabidopsis NET2A is able to bind *At*PRKs in a parallel manner to that observed between *Pi*KIP1 and *Pi*PRK1.

Using FRET-FLIM, NET2B was also shown to interact with *At*PRK4 and *At*PRK5 specifically, but not with *At*PRK1, *At*PRK2, *At*PRK3 or *At*PRK6. This underscores the specificity of the interaction of Arabidopsis NET2 proteins with the *At*PRK4/*At*PRK5 subgroup of *At*PRKs, perhaps indicating a niche functional role for this *At*PRK subgroup in growing pollen tubes. Furthermore, the data indicates that NET2A and NET2B may be functionally redundant to each other in their interactions with *At*PRK4 and *At*PRK5; perhaps involved in the same mechanisms of actin regulation.

In a parallel manner to that observed for *Pi*KIP1 and *Pi*PRK1, drastic changes in the subcellular localisations of NET2A and NET2B were induced by *At*PRK4 and *At*PRK5. The two *At*PRKs were both observed to abolish the actin-bound localisation of NET2A and NET2B, and appeared to recruit them to plasma membrane, reminiscent of *Pi*KIP1 recruitment by *Pi*PRK1. This is likely to be indicative of a signalling mechanism by which NET2 proteins can be regulated by *At*PRK4 and *At*PRK5. It has already been discussed above that *Pi*KIP1 is phosphorylated by *Pi*PRK1 to promote an interaction between the two proteins (Skirpan et al. 2001), and therefore recruitment of *Pi*KIP1 to the plasma membrane. It is therefore very likely that a similar signalling mechanism exists in Arabidopsis pollen tubes, in which NET2s are recruited by *At*PRK4 and *At*PRK5 dependent on phosphorylation.

Finally, the interactions between NET2A and *At*PRK4 & *At*PRK5 were analysed in Arabidopsis pollen tubes. It was observed that *At*PRK4 and *At*PRK5 localised to punctae at the shank membrane of growing pollen tubes, in a pattern distinct from that reported for *At*PRK1, *At*PRK2, *At*PRK3 or *At*PRK6 (Lee et al. 2008; Zhao et al. 2013; Takeuchi and Higashiyama. 2016), perhaps indicating a functional niche for the *At*PRK4/*At*PRK5 subgroup. These shank-specific punctae are highly reminiscent of those formed by NET2A in growing pollen tubes. Indeed, co-localisation of NET2A and *At*PRK4 was observed at these punctae, indicating that these foci are the sites of interaction between the membrane and cytoskeleton. This result confirmed that interactions between NET2s and *At*PRK proteins occur *in vivo*, at the plasma membrane of Arabidopsis pollen tubes.

In summary, multiple Arabidopsis NET2 proteins were demonstrated to interact specifically with *At*PRK4 and *At*PRK5, which comprise a single, evolutionarily conserved subclade of *At*PRKs. Interactions between NET2s and PRKs appear to occur at discreet foci at the shank region of the pollen tube plasma membrane. It is likely that *At*PRK4 and *At*PRK5 regulate NET2 proteins by modulating their subcellular localisation and actin-binding activity through phosphorylation. This complex may therefore constitute a signalling module by which *At*PRK4 and *At*PRK5 may be able to regulate the actin cytoskeleton, perhaps downstream of external signal perception.

Chapter 7: Characterisation of Arabidopsis MAP7s as Novel Microtubule-Binding Proteins, and Investigation of NET2A-MAP7A Interactions.

7.1. Introduction.

In chapter 5.4.3, potential interactors of NET2A were examined in a SU-Y2H screen. One prey cDNA fragment identified as a potential interactor of NET2A was aa 5 – 38 of a previously uncharacterised protein encoded by the gene locus At3g24100. This protein, referred to as MICROTUBULE-ASSOCIATED PROTEIN-7A (MAP7A) in this study (due to its predicted MW of ≈7 kDa), was selected for further characterisation and investigation as an interactor of NET2A. Initial studies on MAP7A, involving its transient expression in *N. benthamiana* leaf epidermal cells, indicated it to be a potential cytoskeletal associated protein, therefore warranting further detailed analysis its functions and its potential interaction with NET2A in Arabidopsis.

As detailed throughout the course of this chapter, a number of different approaches were used to characterise the novel MAP7A protein. Firstly, bioinformatic analysis was employed to analyse the gene and protein structures of MAP7A, and identify conserved protein domains that might be shared with other functionally and evolutionarily related proteins in both Arabidopsis and other species. As a result of this study, a related protein named MAP7B was identified as a family member of MAP7A and was also selected for further investigation. Analysis of MAP7A cytoskeletal-binding activity was then assessed. Using a series of *in vivo* and *in vitro* functional studies, MAP7A and MAP7B were characterised as microtubule-binding proteins. Thus, having concluded that MAP7A may play an important role in regulating the cell cytoskeleton, further investigation of a potential interaction between NET2A was MAP7A was performed. In addition to this, detailed investigation into the potential functions of MAP7 proteins in Arabidopsis was undertaken, using *in situ* analysis of MAP7A and MAP7B expression patterns and subcellular localisation, and reverse-genetic analysis using loss-of-function *map7a*

and *map7b* mutants. Thus, MAP7A and MAP7B were characterised as novel Arabidopsis microtubule-associated proteins expressed preferentially in pollen.

Characterisation of novel Arabidopsis microtubule-binding proteins would be highly valuable in advancing current understanding of how the cytoskeleton may regulate plant growth, development and signalling. To date, the role of microtubules in pollen tube growth is only recently beginning to be elucidated (Onelli et al. 2015), and understanding the regulation of microtubules by MAP7s may contribute to revealing the emerging importance of the microtubule cytoskeleton in pollen tubes. Identification of an interaction between NET2A and the MAP7A would implicate NET2A in mediating interactions between actin and microtubules, which is believed to be important in the regulation of pollen tube growth and fertilisation (Gossot and Geitmann. 2007). This in turn could elucidate an important role for NET2A in the regulation of microtubule-dependent processes in pollen tubes.

7.2. Bioinformatic Analysis of MAP7 Proteins.

7.2.1. Introduction.

Bioinformatic analysis is the application of computational tools to access biological information. Large quantities of generated data stored in online databases can be accessed using various software programmes to describe or predict specific characteristics of a protein or gene, including sequence and structural analysis, transcriptomics, metabolomics, and bio-ontologies (Rhee et al. 2006). In this section, bioinformatics was used to analyse the protein sequence of MAP7A, and identify related proteins with similar sequences.

Analysis of the MAP7A protein secondary structure revealed it to contain a highly conserved Small ERD Rich Factor (SERF) domain, present in proteins found in kingdoms Animalia and Fungi. Thus, MAP7A was found to be a member of a family of Arabidopsis SERF proteins, compromising MAP7A, MAP7B and MAP7C. The MAP7 protein structure was determined to be comprised of two domains; a conserved N-terminal SERF domain, conserved in *Planta*, *Animalia* and *Fungi*, and a relatively unconserved C-terminal domain. This section describes the

bioinformatics tools used to characterise the Arabidopsis MAP7s as members of a conserved family of SERF proteins.

7.2.2. Investigation of MAP7A Nucleotide and Protein Sequences.

Information regarding MAP7A was obtained from The Arabidopsis Information Resource, (TAIR), a centralised database of information pertaining to Arabidopsis genetics, molecular biology and protein sequences. MAP7A, encoded by the gene At3g24100, had an open reading frame of 673 bp, consisting of 3 exons (1 – 7 bp, 392 – 485 bp, and 573 – 673 bp), which encoded a protein of 69 aa with a predicted MW of 7.3 kDa. Therefore, At3g24100 was designated MAP7A. The database classified MAP7A as an 'uncharacterised SERF protein family member', defined as such by a Pfam (protein family) 4F5 domain, or 'SERF' protein domain. SERF proteins are described as short proteins of unknown function, rich in aspartate, glutamate, lysine and arginine (Scharf et al. 1998).

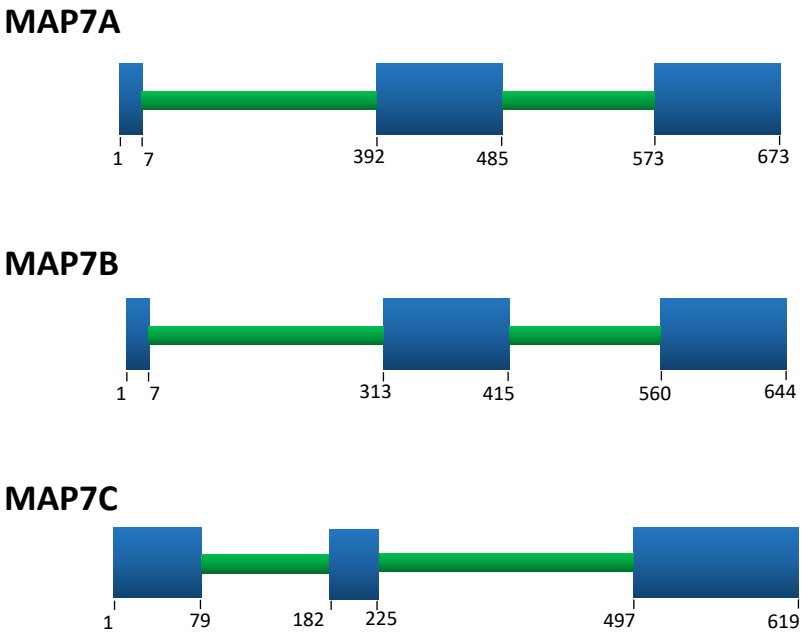

Figure 7.1: Schematic Diagrams of *MAP7A, MAP7B* and *MAP7C* Gene Structures. Exons are represented by blue boxes and introns by green boxes. Numbers below the diagrams indicate the start and end positions (bp) of exons.

7.2.3. Identification of the Arabidopsis SERF Proteins, MAP7B and MAP7C as Relatives of MAP7A.

The National Centre of Biotechnology Information (NCBI) database also provides access to centralised information related to genomics and molecular biology of all organisms studied. The NCBI Basic Local Alignment Search Tool protein-protein search programme (BLASTp), is a computational tool that compares protein sequences to find regions of local similarity between proteins. The BLASTp tool was used to identify Arabidopsis proteins with similar protein sequences with MAP7A, to identify evolutionarily related proteins that may serve similar molecular functions.

The BLASTp tool identified one Arabidopsis protein with high sequence homology to MAP7A, encoded by the gene locus At4g13615. In this alignment, the BLASTp tool identified residues 1 - 44 of At4g13615 as being conserved with residues 1 – 44 of MAP7A; sharing 91% amino acid identity. As described by the TAIR database, At4g13615 consists of an ORF of 644 bp, with 3 exons situated at 1 – 7 bp, 313 – 415 bp and 560 – 644 bp, encoding a 7.2 kDa protein of 71 residues (figure 7.1). The protein encoded by At4g13615 was named MAP7B in this study. According to the TAIR database, MAP7B is also an uncharacterised SERF protein with a Pfam 4F5 domain, through which MAP7B may be related to MAP7A.

Using the TAIR database, one further Arabidopsis protein bearing a Pfam 4F5 SERF domain was listed: At2g23090 consists of an ORF of 618 bp with exons situated at 1 – 79 bp, 182 – 224 bp and 497 – 618 bp, and encodes an 8.4 kDa protein of 81 aa (figure 7.1). This protein was termed MAP7C in this study.

7.2.4. Predicted Protein Structures of MAP7A, MAP7B and MAP7C.

Having characterised the gene and protein structure of MAP7A, and its putative SERF protein family members, the predicted secondary structures of the MAP7 proteins was analysed. To investigate, the Simple Modular Architecture Research Tool (SMART) programme was used. The SMART programme is used to identify protein domains within a protein sequence through local alignments against a database of sequences of conserved protein family (Pfam) domains (Finn et al. 2014).

Using the SMART programme, conserved protein domains were identified from the primary protein sequences of MAP7A, MAP7B and MAP7C (figure 7.2; table 7.1). A Pfam 4F5 SERF domain was identified in MAP7A (aa 1 – 36), MAP7B (aa 1 – 36) and in MAP7C (aa 3 – 37). This conserved domain was present at the N-terminus of each protein and can be considered to define the Arabidopsis MAP7 protein family. A region of low complexity was detected at the C-termini of MAP7A (39 – 69) and MAP7B (39 – 71), which are defined as simple sequence regions with significant biases in amino acid composition (Wootton and Federhen. 1996). A region of low complexity was shown to be present within the Pfam 4F5 SERF domain of MAP7C, at aa 14 – 32, but not at the protein C–terminus.

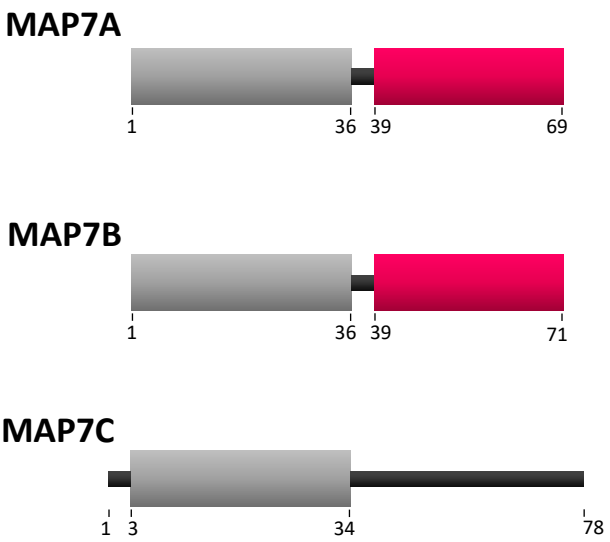

Figure 7.2: Predicted Secondary Protein Structures of MAP7A, MAP7B, MAP7C. The protein secondary structures were predicted using the SMART programme. Grey boxes represent Pfam 4F5 SERF domains. Pink boxes represent regions of low complexity. Numbers underneath the diagrams represent the start and end point (amino acids) of the labelled protein domain. Not included in this diagram is a region of low complexity in the protein sequence of MAP7C, occurring between aa 14 – 32.

Protein	Predicted Protein Domains	Position (aa)
MAP7A	4F5 SERF domain	1 - 36
	Region of low complexity	39 – 69
MAP7B	4F5 SERF domain	1 - 36
	Region of low complexity	39 - 71
MAP7C	4F5 SERF domain	3 - 37
	Region of low complexity	14 - 32

Table 7.1: List of Secondary Protein Structures Possessed by MAP7A, MAP7B and MAP7C Predicted Using the SMART Programme.

7.2.5. Predicted Protein Sequence Similarity of MAP7A with MAP7B and MAP7C.

Having established the protein domains present in MAP7A, MAP7B and MAP7C, regions of conserved sequence homology shared between the MAP7 proteins were investigated to identify conserved functional domains. Global sequence alignments between MAP7 proteins was performed using the European Molecular Biology Open Software Suite (EMBOSS) Needle programme, which uses the Needleman-Wunsch algorithm to calculate an optimal alignment along the entire length of two protein sequences. The EMBOSS Needle tool was used to separately analyse the protein sequence similarity of MAP7A with MAP7B and MAP7C, along the full length of the protein, within their N-terminal Pfam 4F5 SERF domains, and C-terminal domains. This permitted analysis of protein sequence conservation between full length proteins and within specific subdomains. The alignments were generated using the EBLOSUM62 protein weighting matrix, 10 gap opening penalty, 0.5 gap extension penalty.

As shown in table 7.2, full-length MAP7A exhibited a high level of similarity in amino acid composition with MAP7B, sharing 78.9% amino acid identity, and 80.3% amino acid similarity. It was observed that MAP7A and MAP7B displayed a higher degree of amino acid conservation within the Pfam 4F5 SERF domain, sharing 91.7% amino identity within amino acids 1 – 36 of both proteins. A lower degree of conservation was observed between the C-termini of MAP7A and MAP7B, with

61.8% amino acid identity and 64.7% amino acid similarity detected between MAP7A aa 39 – 69 and MAP7B aa 39 – 71. Although the conservation of amino acids in the C-terminal domains of these proteins is lower compared to the N-terminal SERF domains, a high degree of conservation was still observed. It is clear that the protein sequence of MAP7A and MAP7B is highly conserved along the full length of the protein, with particularly high conservation within the N-terminal Pfam 4F5 SERF domain. A diagram of the protein sequence alignments between MAP7A and MAP7B was created using the ClustalX software (Larkin et al. 2007) visualised using Jalview (figure 7.3; Waterhouse et al. 2009; Thompson et al. 1997).

Protein domain aligned	MAP7A domain location (aa)	MAP7B domain location (aa)	Length of alignment (aa)	% aa Identity	% aa similarity	% gaps	Score
Full-length protein	1 - 69	1 – 71	71	78.9	80.3	2.8	276.0
Pfam 4F5 SERF domain	1 - 36	1 – 36	36	91.7	91.7	0	169.0
C-terminus	39 - 69	39 – 71	34	61.8	64.7	8.8	96.0

Table 7.2: Protein Sequence Alignments of MAP7A and MAP7B Performed Using the EMBOSS Needle Programme. Alignments were performed between the sequences of full length proteins, Pfam 4F5 domains and C-terminal domain**.**

The protein sequence conservation between MAP7A and MAP7C was then analysed. As shown in table 7.3, there was relatively little similarity in the protein sequences of full-length MAP7A and MAP7C, sharing 18.7% amino acid identity and 27.5% amino acid similarity. Within the N-terminal Pfam 4F5 SERF domains of MAP7A and MAP7C, 23.3% amino acid identity and 32.6% similarity was observed. The C-terminal regions of MAP7A and MAP7C held only 11.6% amino acid identity and 20.9% similarity. A low degree of conservation between MAP7A and MAP7C was observed in this study. A relatively high degree of sequence similarity was observed between the N-terminal Pfam SERF domains of the two proteins compared to the protein's C-termini, however this conservation was comparatively low compared to the Pfam 4F5 SERF domains of MAP7A and MAP7B. Due to its

relatively low degree of conservation with MAP7A, MAP7C was deemed less likely to share functional conservation with MAP7A, and was not studied further.

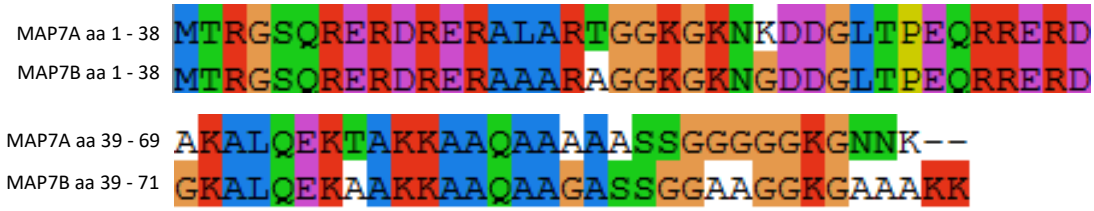

Colour	Residue at Position	(Threshold, Residue Group)
Blue	A, I, L, M, F, W, V	(+60%, WLVIMAFCHP)
	C	(+60%, WLVIMAFCHP)
Red	R, K	(+60%,KR) (80%, K,R,Q)
Green	N	(+50%, N), (+85%, N,Y)
	Q	(+60 %, KR), (+50%, QE), (+85%, Q,E,K,R)
	S, T	(+60% WLVIMAFCHP) (+50%, TS) (+85%,S,T)
Pink	C	(100%, C)
Magenta	E	(+60%,K,R), (+50%,QE), (+85%,E,Q,D)
	D	(+60%,K,R), (+85%,K,R,Q), (+50%,ED)
Orange	G	(+0%, G)
Cyan	H,Y	(+60%, WLVIMAFCHP), (+85%,W,Y,A,C,P,Q,F,H,I,L,M,V)
Yellow	P	(+ 0%, P)

Figure 7.3: Visual Projection of Protein Sequence Alignments of MAP7A and MAP7B Performed Using the ClustalX Programme. (a) Global alignment of full-length MAP7A and MAP7B amino acid sequences generated using ClustalX, coloured using the default colour scheme, in which residues are coloured based on their properties and conservation. (b) Key of the ClustalX colour scheme in which colour is assigned if the threshold value is met or exceeded. The amino acids needed to exceed the minimum threshold are indicated, with the minimum percentage needed to exceed the threshold value. Where listed residues are separated by commas (such as 'K,R,Q'), the colour is assigned when one individual amino acid meets or exceeds the threshold. Where amino acids are grouped without commas (such as 'ED'), the colour is assigned when any combination of residues exceeds the threshold value.

Protein domain aligned	MAP7A domain location (aa)	MAP7C domain location (aa)	Length of alignment (aa)	% aa Identity	% aa similarity	% gaps	Score
Full-length protein	1 - 69	1 – 78	91	18.7	27.5	35.2	32.0
Pfam 4F5 SERF domain	1 – 36	3 – 37	43	23.3	32.6	37.2	27.5
C-terminus	39 - 69	39 – 78	43	11.6	20.9	27.9	7.0

Table 7.3: Protein Sequence Alignments of MAP7A and MAP7C Performed Using the EMBOSS Needle Programme. Alignments were performed between the sequences of full length proteins, Pfam 4F5 domains and C-terminal domains**.**

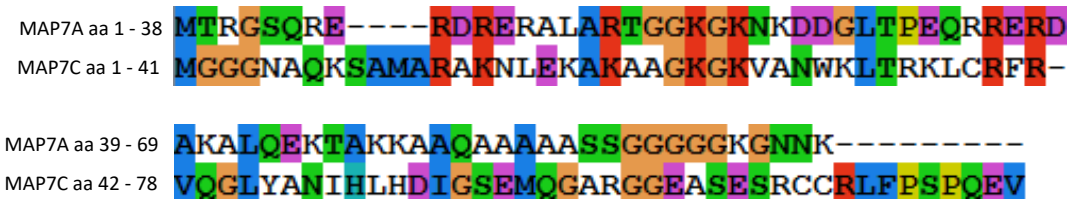

Figure 7.4: Visual Projection of Protein Sequence Alignments of MAP7A and MAP7C Performed Using the ClustalX Programme. Global alignment of full-length MAP7A and MAP7C amino acid sequences generated using ClustalX, coloured using the default colour scheme (figure 7.3), in which residues are coloured based on their properties and conservation.

7.2.6. Investigating Orthologues of MAP7A in other Kingdoms of Life.

Thus far, Arabidopsis MAP7A and its related family member, MAP7B, have been shown to possess an N-terminal Pfam 4F5 SERF domain which defines the MAP7 protein family, and is very highly conserved between MAP7A and MAP7B. In this section, conservation of the MAP7A protein sequence with proteins in other kingdoms of life was investigated, demonstrating MAP7A to be related to orthologous SERF proteins in Animalia and Fungi.

Using the NCBI BLASTp tool, the MAP7A protein sequence was compared with known protein sequences in Kingdoms Animalia and Fungi. MAP7A was observed to have a high degree of similarity to proteins in Animalia and Fungi: in this section, the conservation of MAP7A with SERF proteins of the model organisms, *Homo*

sapiens (SERF2C), *Caenorhabditis elegans* (MOAG-4) and *Saccharomyces cerevisiae* (YDL085C-A) was described, as representative examples of MAP7A sequence conservation in Kingdoms Animalia and Fungi.

The MAP7A protein sequence was observed to display a high degree of similarity with the *H. sapiens* protein, SERF2C; a 59 aa protein containing an N-terminal Pfam 4F5 SERF domain (aa 1 – 38). The NCBI BLASTp programme detected a significant degree of similarity between MAP7A aa 1 – 48 and SERF2C aa 1 – 50. Using the EMBOSS-Needle tool, it was observed that full length MAP7A and SERF2C share 32.4% amino acid identity and 52.1% amino acid similarity. A relatively high degree of similarity was observed between the MAP7A and SERF2C N-terminal domains using EMBOSS Needle, with the two sequences sharing 42% amino acid identity, and 68% amino acid similarity. Conversely, the C-termini of MAP7A (aa 49 – 69) and SERF2C (aa 51 – 59) were not well conserved, sharing 7.7% amino acid similarity. Therefore, MAP7A is related to SERF2C through its N-terminal region (aa 1 – 48), containing the Pfam 4F5 SERF domain. In humans, SERF2C is a protein of unknown function that has been implicated in the pathogenesis of spinal muscular atrophy (Sharf et al. 1998), and in the pathogenesis of age-related neurological diseases such as Huntington's, Parkinson's and Alzheimer's diseases, through the promotion of protein aggregate formation (van Ham et al. 2010). It is also possible that MAP7A may be involved in the regulation of protein aggregation in Arabidopsis.

Protein domain aligned	MAP7A domain location (aa)	SERF2C domain location (aa)	Length of alignment (aa)	% aa Identity	% aa similarity	% gaps	Score
Full-length protein	1 - 69	1 – 59	71	32.4	52.1	19.7	101.5
Conserved N-terminal region	1 - 48	1 – 50	50	42.0	68.0	4.0	106.5
C-terminus	49 - 69	51 – 59	26	7.7	7.7	84.6	11.0

Table 7.4: Protein Sequence Alignments of MAP7A and SERF2C Performed Using the EMBOSS Needle Programme. Alignments were performed between the sequences of full length proteins, Pfam 4F5 domains and C-terminal domains**.**

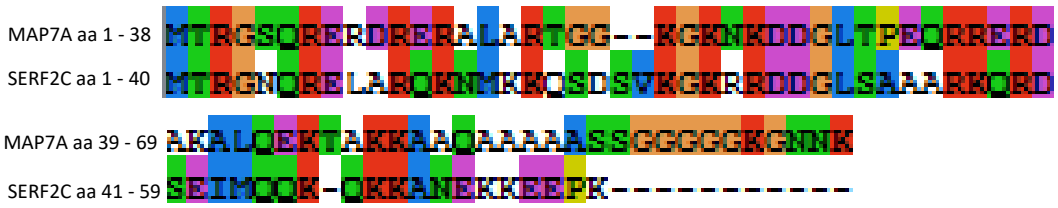

Figure 7.5: Visual Projection of Protein Sequence Alignments of MAP7A and *H. sapiens* SERF2C Performed Using the ClustalX Programme. Global alignment of MAP7A and SERF2C amino acid sequences generated using ClustalX, coloured using the default colour scheme (figure 7.3), in which residues are coloured based on their properties and conservation.

The NCBI BLASTp tool showed the MAP7A protein sequence was also found to be similar to *C. elegans* MOAG-4 (MODIFIER OF AGGREAGTION – 4): a protein of 82 residues with an N-terminal Pfam 4F5 SERF domain. Specifically, BLASTp indicated that the MAP7A N-terminus (aa 1 – 45) was found to be significantly similar with the N-terminus of MOAG-4 (aa 1 – 52). The EMBOSS-Needle programme indicated the full-length MAP7A protein sequence to contain 36.7% amino acid composition to full-length MOAG-4, and an amino acid similarity of 48.9%. High conservation was detected in the N-terminal regions of the two proteins (38.5% amino acid identity, and 57.7% amino acid similarity). The C-terminal domains of MAP7A (aa 46 – 69) and MOAG-4 (aa 70 – 82) were less conserved, sharing 16.7% amino acid identity, and 20.8% amino acid similarity. Therefore, it can be assumed that MAP7A is related to MOAG-4 through the protein's N-terminal domains (MAP7A aa 1 – 45), which carries the Pfam 4F5 SERF domain. Similarly, to SERF2C of *H. sapiens*, MOAG-4 has also been shown to play a role in the formation of protein aggregates involved in the pathogenesis of neurological diseases in *C. elegans* (van Ham et al. 2010), indicating its function is conserved across the Animal Kingdom.

Protein domain aligned	MAP7A domain location (aa)	MOAG-4 domain location (aa)	Length of alignment (aa)	% aa Identity	% aa similarity	% gaps	Score
Full-length protein	1 – 69	1 – 82	90	36.7	48.9	32.2	101.0
Conserved N-terminal region	1 - 45	1 – 52	52	38.5	57.7	13.5	74.5
C-terminus	46 - 69	70 – 82	24	16.7	20.8	45.8	13.0

Table 7.5: Sequence Alignments of MAP7A and MOAG-4 Performed Using the EMBOSS Needle Programme. Alignments were performed between the sequences of full length proteins, Pfam 4F5 domains and C-terminal domains**.**

Figure 7.6: Visual Projection of Sequence Alignments of MAP7A and *C.elegans* MOAG-4 Performed Using the ClustalX Programme. Global alignment of MAP7A and MOAG-4 amino acid sequences generated using ClustalX, coloured using the default colour scheme (figure 7.3), in which residues are coloured based on their properties and conservation.

Finally, the NCBI BLASTp tool showed the MAP7A protein sequence to be similar to that of the *S. cerevisiae* protein, YDL085C-A; a 68 aa protein bearing an N-terminal Pfam 4F5 SERF domain (aa 1 – 36). The BLASTp tool identified MAP7A aa 1 – 45, specifically, as having significant homology to YDL085C-A (aa 1 – 45). It was observed using the EMBOSS-Needle programme that the protein sequences of full-length MAP7A and YDL085C-A were less conserved than between MAP7A and SERF2C or MOAG-4, sharing 27.5% amino acid identity and 42.5% amino acid similarity. The N-terminal domain of YDL085C (aa 1 – 45) showed a degree of similarity to MAP7A (aa 1 – 45) comparable to that observed between MAP7A and SERF2C or MOAG-4; sharing 35.6% amino acid identity and 60% amino acid similarity. Conversely, the C-terminal domains of MAP7A (aa 46 – 69) and YDL085C-A (aa 46 – 68) were poorly conserved with only 9.8% similarity. It can be

assumed that MAP7A is related to YDL085C-A through the N-terminal SERF domain. A role for SERF proteins in Fungi has not yet been investigated, and can provide no predictions as to the role of MAP7A in Arabidopsis.

Protein domain aligned	MAP7A domain location (aa)	YDL085C-A domain location (aa)	Length of alignment (aa)	% aa Identity	% aa similarity	% gaps	Score
Full-length protein	1 – 69	1 – 68	80	27.5	42.5	28.8	72.0
Conserved N-terminal region	1 - 45	1 – 45	45	35.6	60.0	0	76.0
C-terminus	46 - 69	45 – 68	41	4.9	9.8	82.9	9.0

Table 7.6: Sequence Alignments of MAP7A and YDL085C-A Performed Using the EMBOSS Needle Programme. Alignments were performed between the sequences of full length proteins, Pfam 4F5 domains and C-terminal domains**.**

Figure 7.7: Visual Projection of Sequence Alignments of MAP7A and *S. cerevisiae* YDL085C-A Performed Using the ClustalX Programme. Global alignment of MAP7A and YDL085C-A amino acid sequences generated using ClustalX, coloured using the default colour scheme (figure 7.3), in which residues are coloured based on their properties and conservation.

The protein sequence of MAP7A was shown to be significantly similar with those of the SERF proteins SERF2C, MOAG-4 and YDL085C-A, demonstrating conservation of the MAP7A protein sequence in SERF proteins across Planta, Animalia and Fungi. It was observed that the N-terminal regions of these proteins, which contain the Pfam 4F5 SERF domain, were especially well conserved, whereas relatively little conservation was observed in the C-termini of these proteins. It can therefore be concluded that MAP7A is part of a family of conserved SERF proteins, related through its N-terminal SERF domain.

7.2.6. Summary.

Throughout the course of this section, bioinformatic analysis was used to elucidate the gene structure and protein sequence of MAP7A, as well as MAP7B and MAP7C; putative relatives of MAP7A identified above. Analysis of MAP7A, MAP7B and MAP7C protein secondary structures revealed that each protein contained an N-terminal Pfam 4F5 SERF domain, defining them as members of the SERF protein family.

The protein sequence of MAP7A was shown to be highly conserved with MAP7B, particularly between the protein's N-termini. A lower degree of conservation was observed between MAP7A and MAP7C, indicating that the two proteins are less likely to share a functional relationship: therefore, no further research was performed on MAP7C.

It was determined that Arabidopsis MAP7A was related to SERF proteins present in Kingdoms Animalia and Fungi through its N-terminal region, which was shown to be conserved with SERF2C of *H. sapiens,* MOAG-4 of *C. elegans* and YDL085C-A of *S. cerevisiae*. The C-termini of these proteins were much less conserved.

From the bioinformatic analysis of MAP7A performed in this section, arbitrary designation of protein subdomains could be applied to MAP7A. MAP7A aa 1 – 46 was shown to contain sequences of high similarity to the N-termini of the SERF proteins MAP7B, SERF2C, MOAG-4 and YDL085C-A described above, all of which contain a Pfam 4F5 SERF domain. Therefore, MAP7A aa 1 – 46 was designated as the conserved N-terminal SERF domain. The MAP7A C-terminus (aa 47 – 69),

although conserved with MAP7B, was poorly conserved in SERF proteins in Animalia and Fungi. This region was designated the unconserved C-terminal domain. As described in section 7.3, the conserved MAP7A N-terminal SERF domain was determined in this investigation to contain a novel microtubule-binding domain, which is likely to be conserved between SERF proteins across Kingdoms.

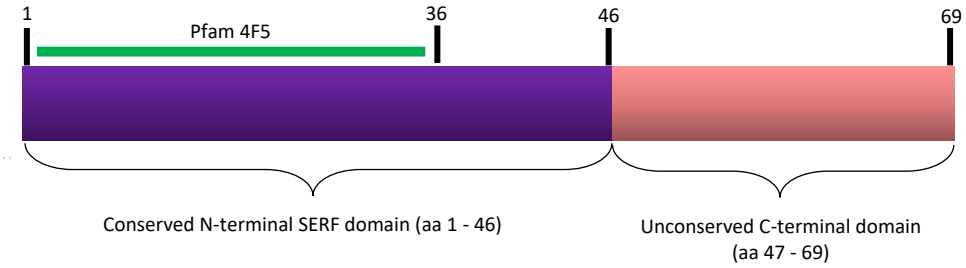

Figure 7.8: A Schematic Diagram of MAP7A Subdomains Based on Bioinformatic Analysis of Protein Secondary Structure and Sequence Conservation. Amino acids 1 – 46, represented by the purple box were shown to be highly conserved with other SERF proteins in Planta, Animalia and Fungi, and contains the Pfam 4F5 domain. This domain was arbitrarily designated as the conserved N-terminal SERF domain. Amino acids 47 – 69 (pink box) are relatively unconserved between SERF proteins, and was arbitrarily designated as the unconserved C-terminal domain. The Pfam 4F5 domain is represented by the green line.

7.3. *In vivo* and *in vitro* Analysis of MAP7A Association with Microtubules.

7.3.1. Introduction.

As explained previously, MAP7A was identified as a potential interacting partner of NET2A in a SU-Y2H screen (chapter 5.4.3). Subsequently, preliminary studies were performed in which the subcellular localisation of MAP7A was visualised in transient expression studies in *N. benthamiana*. The initial analysis indicated that MAP7A may associate with the microtubule cytoskeleton *in vivo*. This section outlines the experiments performed to characterise MAP7A and MAP7B as a novel family of microtubule-associated proteins. Analysis of MAP7-GFP subcellular localisation *in vivo* indicated that MAP7 proteins bind microtubules *in planta,* whilst *in vitro* microtubule binding assays were employed to demonstrate that the MAP7s are able to associate with microtubules directly.

7.3.2. *In vivo* Analysis of MAP7A.

7.3.2.1. Subcellular Localisation of MAP7A-GFP in *N. benthamiana* Leaf Epidermal Cells.

To investigate the subcellular localisation of the MAP7s *in vivo*, agrobacterium-mediated transient expression assays were performed to express MAP7-GFP fusion proteins in *N. benthamiana* leaf epidermal cells.

The coding sequences of full-length MAP7A (aa 1 - 69) and MAP7B (aa 1 - 71) were PCR amplified from Arabidopsis floral cDNA and cloned into pDONR207 using gateway cloning. MAP7A and MAP7B were subsequently cloned into the expression vector pB7FGW2, facilitating their expression as C-terminal GFP fusion proteins under control of the *CaMV 35s* promoter (7.9a and 7.9b).

Figure 7.9 shows the subcellular localisation of MAP7A-GFP (c and e) and MAP7B-GFP (d and f) in *N. benthamiana* leaf epidermal cells. Both proteins were observed

to have decorated a mesh-like network of filaments within the cell, similar to those formed by the microtubule marker, Kinesin Motor Domain (KMD)-GFP (h). Alongside filaments, MAP7A-GFP and MAP7B-GFP could additionally be seen to localise to the cell cytoplasm and nucleoplasm, similar to cells expressing the GFP_{cyt} control (g). However, the filamentous networks formed by the MAP7-GFP fusion proteins were markedly absent from cells expressing GFP_{cyt}, demonstrating that the GFP tag was not responsible for influencing their localisation to a filamentous network. The MAP7A-GFP and MAP7B-GFP filaments appeared to be relatively consistent in width, compared to the filament systems labelled by the microtubule marker, KMD-GFP (g), and their filaments did not seem to form bundles. The filament systems formed by MAP7A-GFP appeared to be remarkably static when analysed using time-lapse imaging: the filaments did not appear to move dynamically, and could be seen to undergo elongation or shrinkage only very rarely.

Both MAP7A-GFP and MAP7B-GFP formed punctae that aligned along filaments and varied in size. It appears that MAP7A and MAP7B localise to punctae *in vivo*, however it is also possible that the observed phenomenon are artefacts; specifically, protein aggregates resulting from ectopic and constitutive overexpression of the fusion proteins under the *CaMV 35s* promoter.

Actin and microtubules form the two main filament systems plant cells. Given the observed filamentous subcellular localisation of MAP7A-GFP and MAP7B-GFP, it is possible that the MAP7s associate with one of these cytoskeletal elements *in vivo*. Therefore, it was investigated as to whether the MAP7-GFP filament networks may associate with actin or microtubules *in vivo.*

7.3.2.2. Co-localisation of MAP7A-GFP with Microtubules.

To further investigate whether the MAP7-GFP filament systems described above may co-align with actin or microtubule networks *in vivo*, MAP7A-GFP was transiently co-expressed with the microtubule marker, mCherry-TUA5 and the actin marker, RFP-Lifeact in *N. benthamiana*. CLSM was used to visualise the two constructs in the same cell in order to study their spatial co-localisation.

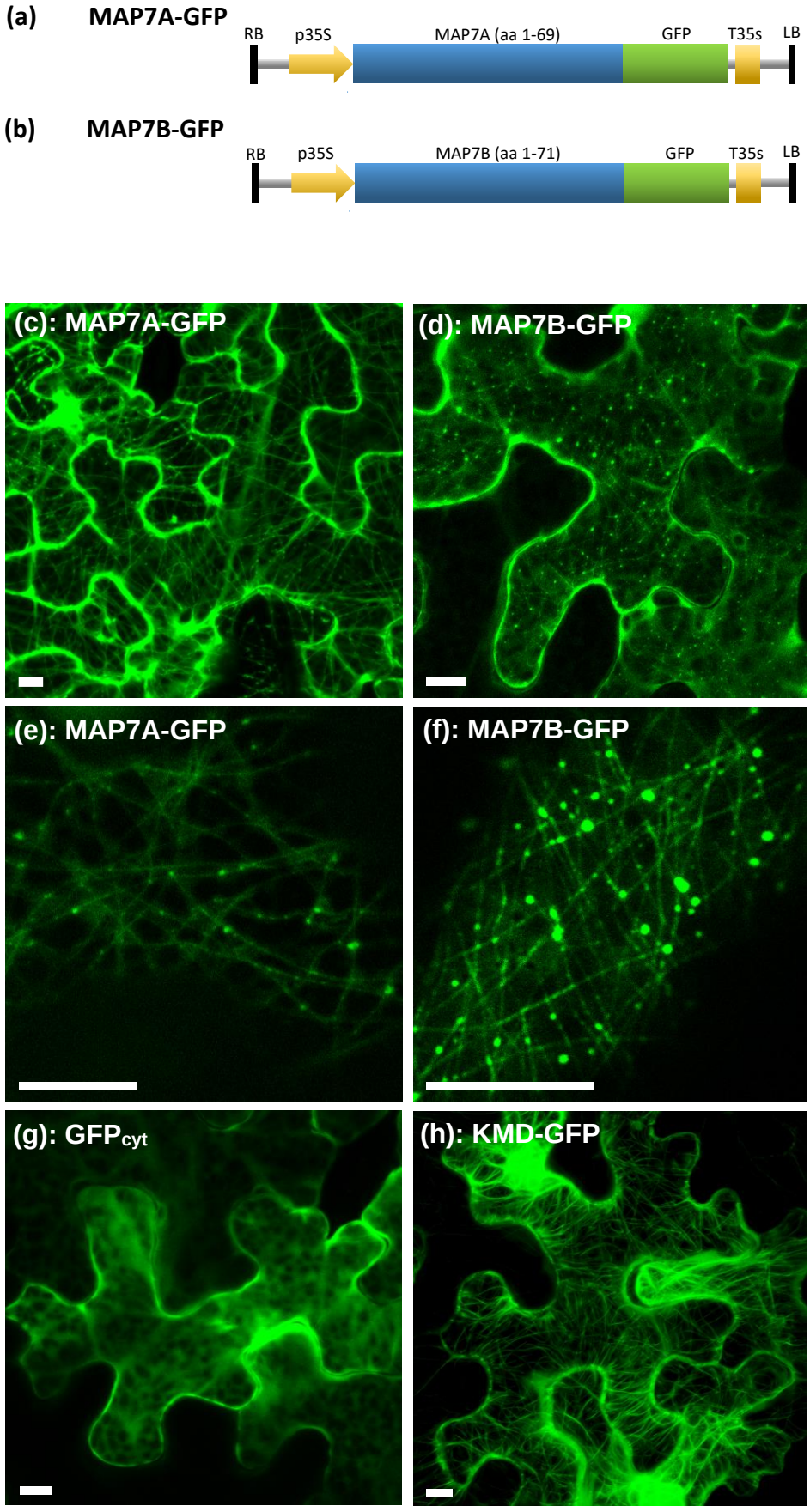

Figure 7.9: Subcellular Localisation of MAP7A-GFP and MAP7B-GFP in *N. benthamiana* Leaf Epidermal Cells. (a) and (b): Schematic diagram of MAP7A-GFP and MAP7B-GFP constructs generated using pB7FGW2. RB = T-DNA right border. p35s = CaMV 35s promoter sequence. T35s = CaMV 35s terminator sequence. LB = T-DNA left border. (c) and (e): MAP7A-GFP localisation. (d) and (f): MAP7B-GFP localisation. (g): GFP_{cyt} expressed by the pMDC43 vector. (h): KMD-GFP localisation. Scale bar: 10 µm.

As shown in figure 7.10, MAP7A-GFP filaments clearly co-aligned with the microtubule network labelled by mCherry-TUA5. In addition to this, the MAP7A-GFP punctae described above were also localised to the microtubule cytoskeleton, with 91 ± 0.05 % (n=1250) punctae associated with microtubule filaments.

Conversely, MAP7A-GFP filaments did not co-localise with the actin cytoskeleton, but maintained a close spatial relationship with actin filaments, perhaps due to the reported dynamic interactions between microtubule and actin networks in plant cells (Collings. 2008; Sampathkumar et al. 2011). It should be noted that no bleedthrough was observed in tissue expressing GFP or RFP fusion constructs alone.

The results indicate that the MAP7A-GFP filament network co-localises with the microtubule cytoskeleton *in vivo*. To further investigate whether MAP7s bear a physical association with the microtubule cytoskeleton, pharmacological analysis was employed as described in the next section.

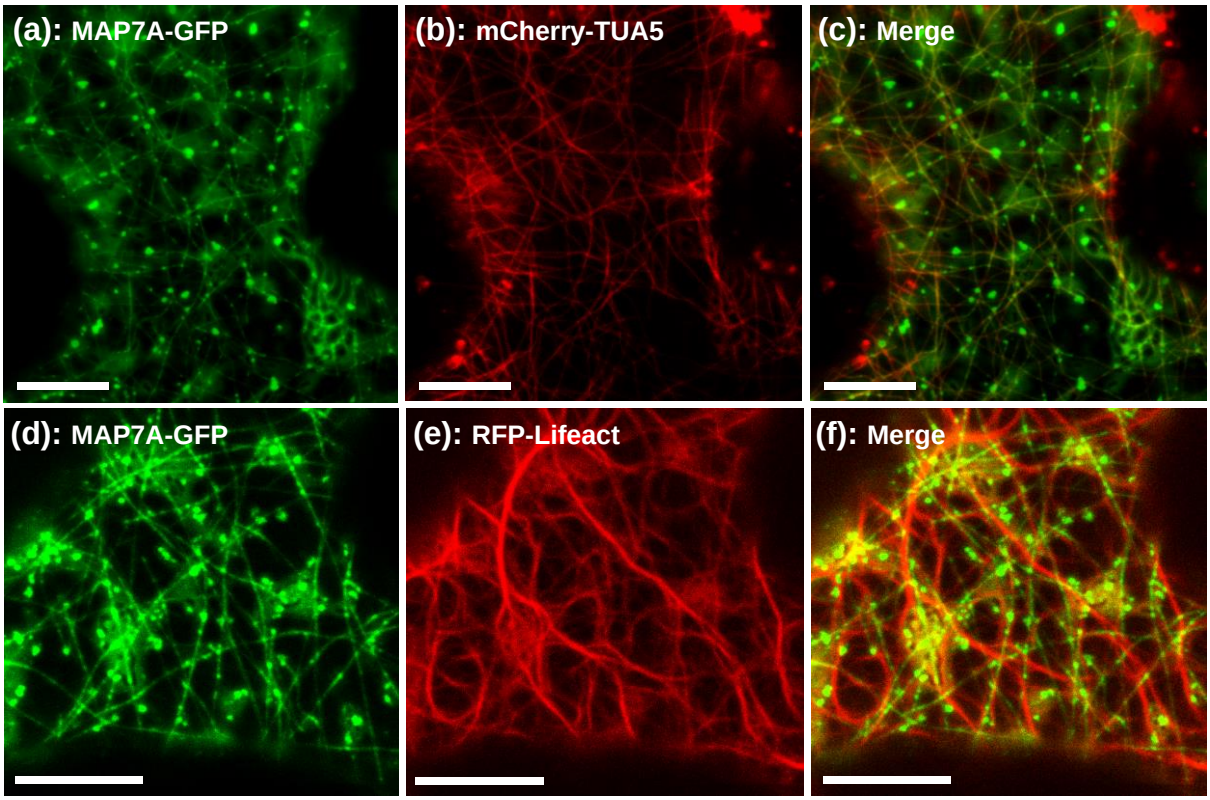

Figure 7.10: Co-localisation of MAP7A-GFP with Microtubules and Actin. (a)-(c): *N. benthamiana* leaf epidermal cells co-expressing MAP7A-GFP and the microtubule marker, mCherry-TUA5. (a) MAP7A-GFP visualised using 488 nm excitation. (b) mCherry-TUA5 in the same cell visualised using 594 nm excitation. (c): Co-localisation of MAP7A-GFP and mCherry-TUA5 in overlaid images. (d)-(f): Cells expressing MAP7A-GFP and the actin marker, RFP-Lifeact. (d): MAP7A-GFP visualised using 488 nm excitation. (e) RFP-Lifeact in the same cell visualised using 543 nm excitation. (f): Co-localisation of MAP7A-GFP and RFP-Lifeact in overlaid images. Scale bar: 10 µm.

7.3.2.3. Effects of Pharmacological Disruption of the Microtubule and Actin Cytoskeleton on MAP7A-GFP Localisation *in vivo*.

MAP7A and MAP7B may physically associate with the microtubule or actin cytoskeleton *in vivo.* Therefore, pharmacological disruption of the microtubule and actin cytoskeleton was performed on sections of *N. benthamiana* leaf tissue expressing MAP7A-GFP, to determine whether their filamentous localisation was dependent on microtubule or actin networks.

For microtubule disruption, the microtubule-depolymerising drug, amiprophos-methyl (APM), was used. APM is a herbicide that specifically disrupts plant microtubules (Morejohn and Fosket. 1984) by preventing addition of new subunits (Murthy et al. 1994).

Incubation of leaf sections in 200 µM APM for 2 hours was sufficient to induce depolymerisation of the microtubule network, as indicated by the short fragments of depolymerised microtubules observed in figure 7.11e, compared to the untreated, intact microtubule cytoskeleton shown in figure 7.11a. APM is dissolved in dimethyl sulphoxide (DMSO), and so leaf sections were treated with 1% DMSO; the final concentration present in APM treatment solution, to show that DMSO alone was unable to induce microtubule depolymerisation (figure 7.11c). Breakdown of the microtubule array with APM induced a discernible change in MAP7A-GFP localisation: the filament network displayed by MAP7A-GFP in untreated cells (figure 7.11b) was no longer present, yet residual punctae remained (figure 7.11f). Treatment of control leaf sections with 1% DMSO did not result in MAP7A-GFP filament dissolution (figure 7.11d).

Next, it was investigated whether the MAP7A-GFP fusion protein associated with the actin cytoskeleton. Leaf sections of *N. benthamiana* transient expressing MAP7A-GFP were incubated with the actin depolymerising drugs, Cytochalasin D, or Latrunculin B. Cytochalasin D and Latrunculin B have different mechanisms of action: Cytochalasin D disrupts actin by binding to the barbed end of actin filaments preventing actin polymerisation, whereas Latrunculin B prevents polymerisation by sequestering free G-actin (Wakatsuki et al. 2001).

It was observed that 30 minutes incubation with 40 µM Cytochalasin D or 50 µM Latrunculin B was sufficient to depolymerise the actin cytoskeleton in leaf sections

expressing the actin marker, RFP-Lifeact (figure 7.12e and 7.12g). Incubation in 0.5% DMSO, the highest concentration of DMSO present in the actin depolymerisation treatment, was unable to cause actin depolymerisation (figure 7.12c). Latrunculin B and Cytochalasin D treatments, however, did not induce dissolution of the MAP7A-GFP filament network (figure 7.12d and 7.12f).

The data described in this section indicates that the filamentous MAP7A-GFP network observed in transient expression assays was dependent on the integrity of the microtubule cytoskeleton, but not actin. This suggests that the MAP7s are able to associate with microtubules *in vivo*.

7.3.2.4. Subcellular Localisation of MAP7A Sub-Domains in *N. benthamiana* Transient Expression Assays.

Having established that the MAP7s associate with microtubules *in vivo*, functional analysis of MAP7A truncations was performed to establish which specific subdomains localise to microtubules *in vivo*. MAP7A subdomains were transiently expressed as GFP fusion proteins in *N. benthamiana* and their subcellular localisation visualised using CLSM.

As described in section 7.2, $MAP7A^{1-46}$ corresponds to the highly conserved SERF N-terminal domain, present in both MAP7A and MAP7B and conserved throughout plant and animal kingdoms. $MAP7^{47-69}$ corresponds to the unconserved C-terminal domain. The MAP7A subdomains were PCR amplified using the MAP7A-pB7FGW2 construct as template and cloned into pDONR207. The subdomains were then cloned into pB7FGW2 to facilitate their expression as C-terminal fusion proteins in *N. benthamiana* transient assays (figure 7.13a).

The MAP7A-SERF-GFP construct was shown to localise to a filamentous network (figure 7.13b) similar to full length MAP7A-GFP. MAP7A-SERF-GFP also localised to the cytosol and formed prominent protein aggregates. MAP7A-C-GFP, in contrast did not decorate a filament network, and seemed to localise entirely to the cytosol (figure 7.13c) as did the GFP_{cyt} negative control (figure 7.13e). As a positive control, the microtubule marker, mCherry-TUA5, was also included to visualise the intact microtubule cytoskeleton (figure 7.13d).

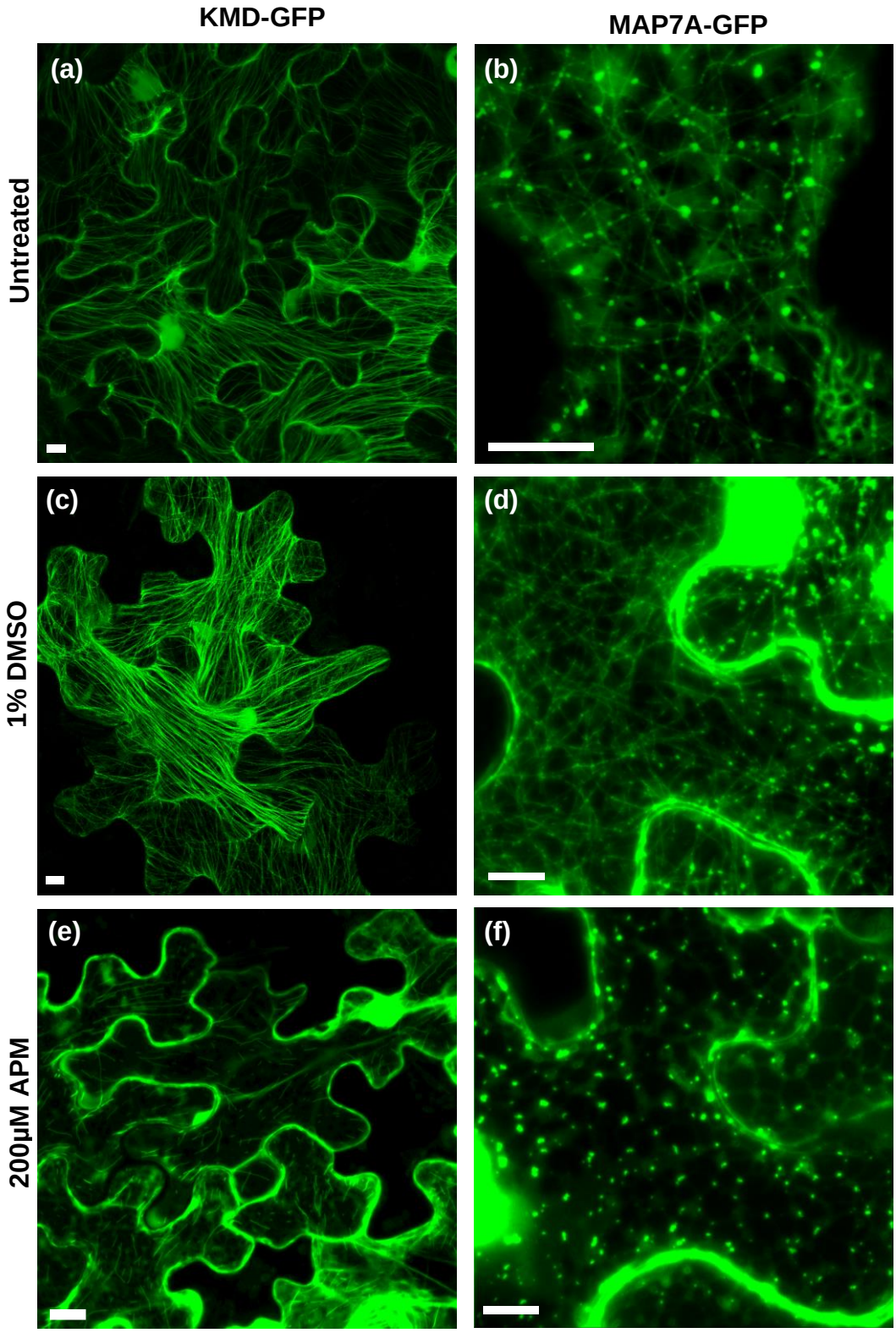

Figure 7.11: Effect of Pharmacological Disruption of the Microtubule Cytoskeleton on MAP7A-GFP Localisation in *N. benthamiana* Leaf Epidermal Cells. (a), (c) and (e): cells expressing the microtubule marker, KMD-GFP. (b), (d) and (f): cells expressing MAP7A-GFP. (a) and (b): untreated. (c) and (d): treated with 1% DMSO. (e) and (f): treated with 200 µM APM. Scale bar: 10 µm.

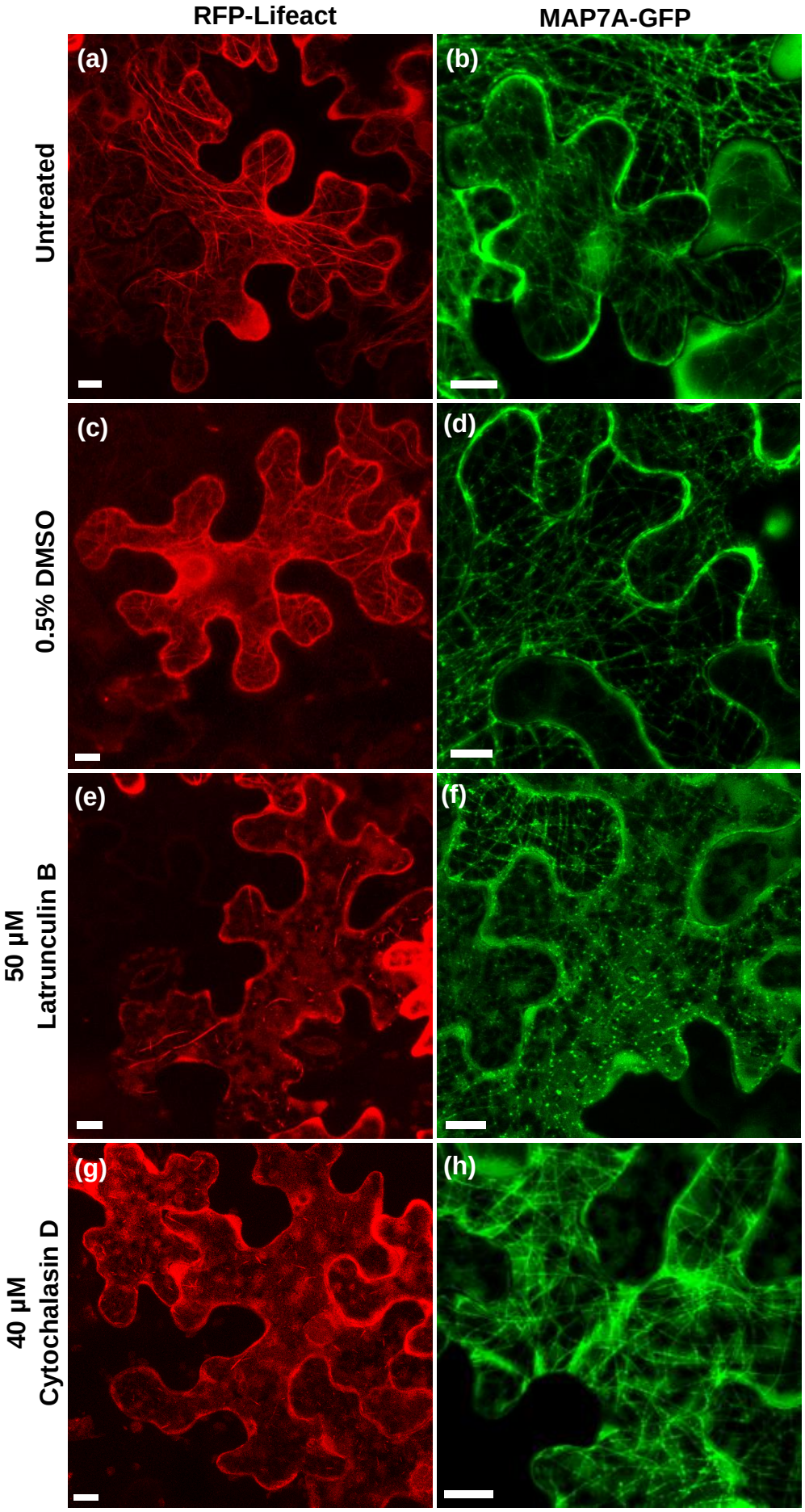

Figure 7.12: Effect of Pharmacological Disruption of the Actin Cytoskeleton on MAP7A-GFP Localisation. (a), (c), (e) and (g): cells expressing the actin marker, RFP-Lifeact. (b), (d), (f) and (h): cells expressing MAP7A-GFP. (a) and (b): untreated. (c) and (d): treated with 1% DMSO. (e) and (f): treated with 50 µM Latrunculin B. (g) and (h) treated with 40 µM Cytochalasin D. Scale bar: 10 µm.

The data indicates that the MAP7 N-terminal SERF domain is responsible for localising MAP7A-GFP to the microtubule cytoskeleton. This domain is highly conserved amongst plant and animal SERF proteins; the data presented here implies that SERF proteins may serve as microtubule-associated proteins in multiple eukaryotic kingdoms.

7.3.2.5. Subcellular Localisation of MAP7A-GFP in *CaMV 35s*:MAP7A-GFP Stable Lines.

Having established that MAP7 proteins can bind microtubules in transient expression assays, the ability of stably expressed MAP7A-GFP to bind microtubules was assessed.

Arabidopsis Col-0 plants were stably transformed with the MAP7A-pB7FGW2 expression construct using the floral dipping method (as described in chapter 2.2.15), to constitutively express MAP7A-GFP under the *CaMV 35s* promoter. Transformed plants were selected from the T1 generation of seed on ½MS plates containing 10 µg/ml BASTA. Subsequently, selected seedlings were manually screened for GFP fluorescence in leaf and root tissue using the Leica M165FC fluorescent stereo microscope.

The subcellular localisation of MAP7A-GFP in leaf sections of fluorescing stable lines was analysed using CLSM. 5 independently transformed stable lines were analysed. Strong GFP signal was clearly detectable in the pavement cells and guard cells of fluorescing leaf sections. MAP7A-GFP decorated filamentous networks similar to those observed in *N. benthamiana* transient assays, at the cortex of leaf epidermal cells (figure 5.6b), and exhibited a highly defined, radially-organised filamentous network in guard cells (figure 5.6a), characteristic of those formed by microtubules (Marc et al. 1989; Lahav et al. 2004). Pharmacological disruption of the microtubule cytoskeleton in *CaMV 35*s:MAP7A-GFP stable lines with APM (as performed in 5.2.2) resulted in dissolution of the MAP7A-GFP filament system (figure 5.6c - e), proving that MAP7A-GFP was associated with microtubules.

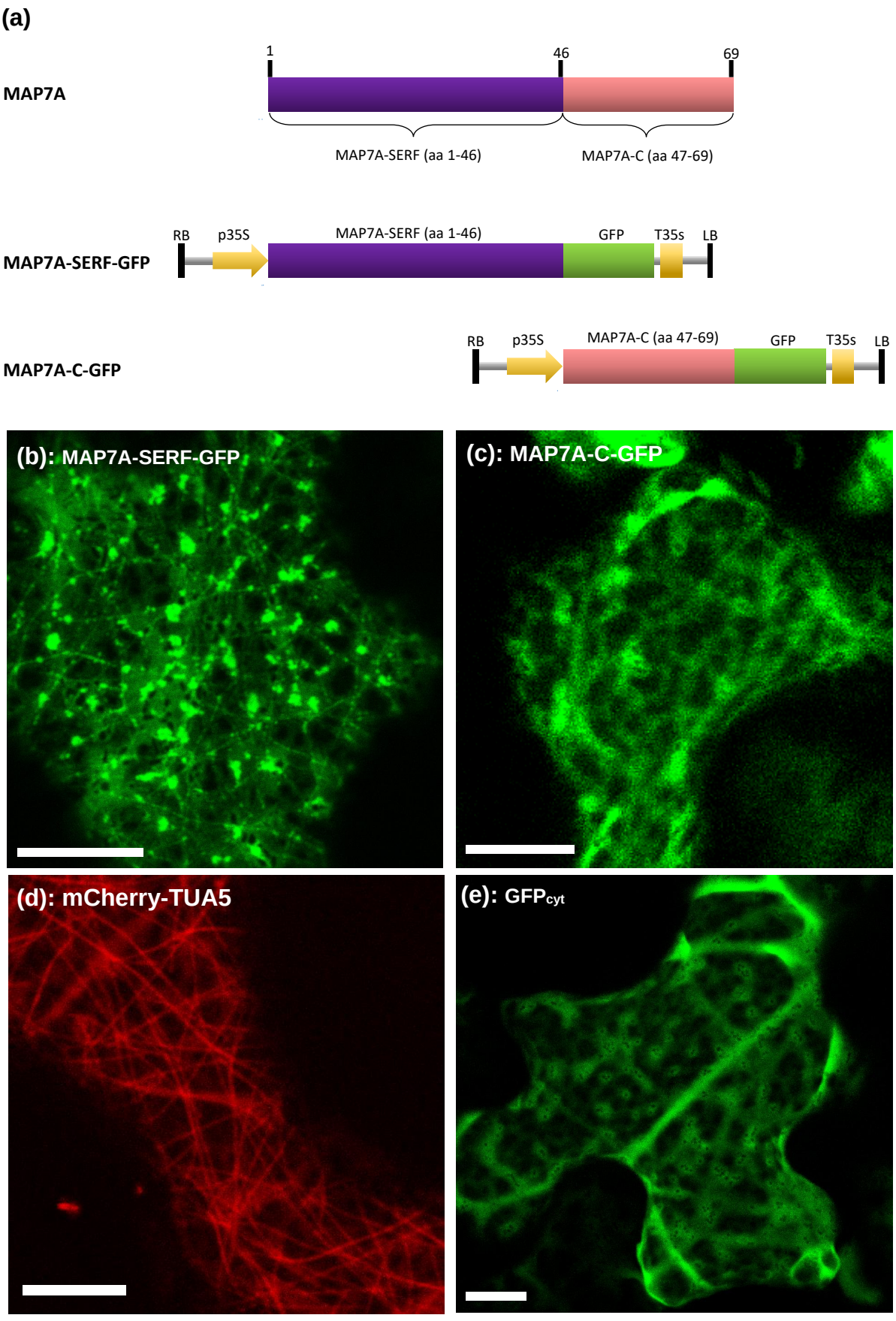

Figure 7.13: Subcellular Localisation of MAP7A Subdomains in *N. benthamiana* Leaf Epidermal Cells. (a): Schematic diagram of MAP7A subdomain fusion proteins. RB = T-DNA right border. p35s = CaMV 35s promoter sequence. T35s = CaMV 35s terminator sequence. LB = T-DNA left border. (b): MAP7A-SERF-GFP, (c): MAP7A-C-GFP, (d): mcherry-TUA5, (e): $GFP_{cyt.}$ Scale bar: 10 µm.

The data shows that MAP7A-GFP is able to associate with microtubules under stable expression conditions in *Arabidopsis*. This adds further evidence to suggest that the WT MAP7 proteins may serve as endogenous microtubule-associated proteins *in Arabidopsis.*

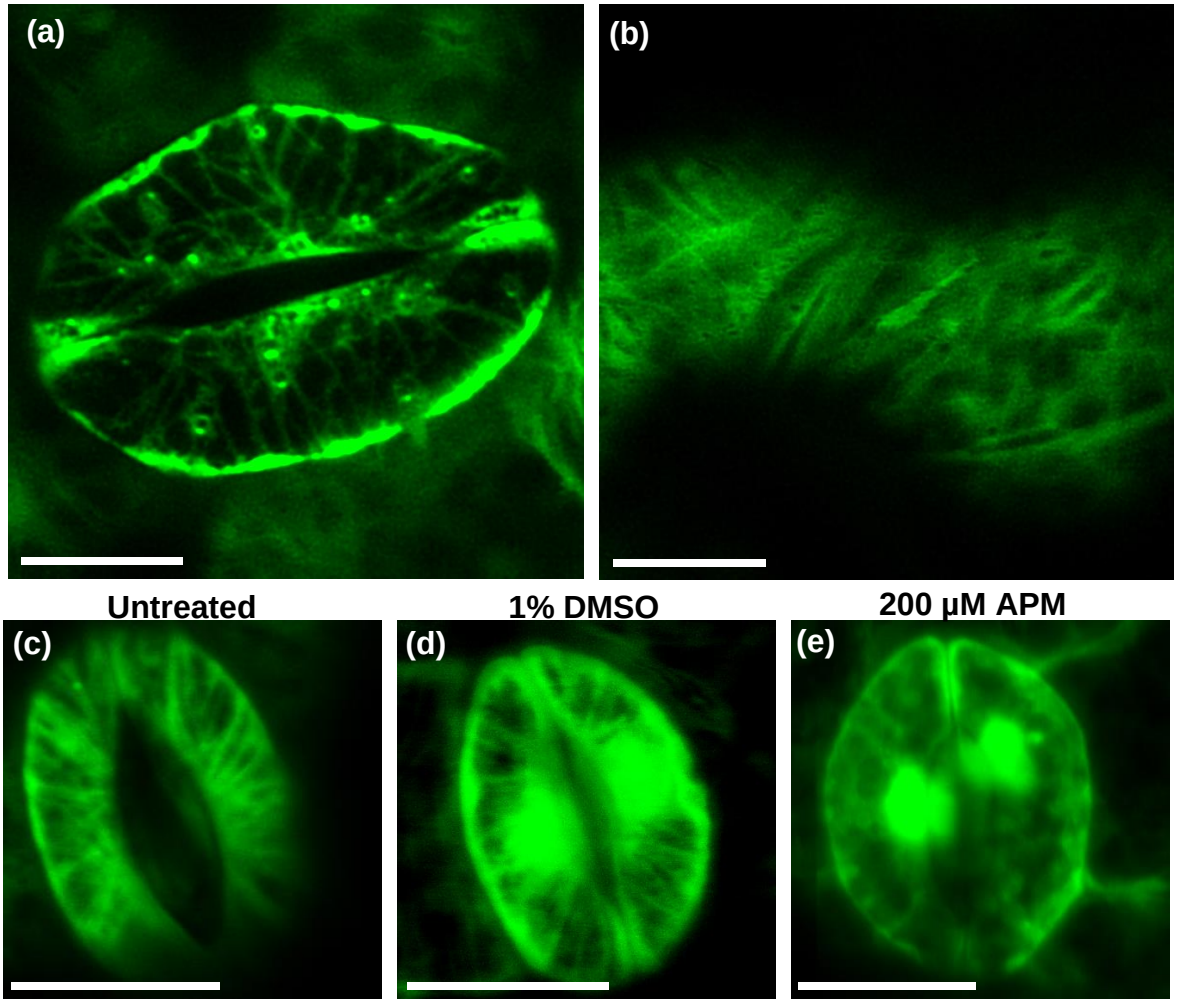

Figure 7.14: Subcellular Localisation of MAP7A-GFP in *CaMV 35s*:MAP7A-GFP Stable *Arabidopsis* lines. (a), (c), (d) and (e): Guard cells expressing MAP7A-GFP. (b): Subcellular localisation of MAP7A-GFP in *Arabidopsis* leaf epidermal cells. (c): Untreated. (d): Treated with 1% DMSO. (e): Treated with 200 µM APM. Scale bar: 10 µm.

7.3.3. *In vitro* Microtubule-Binding Assay.

Having established that MAP7A-GFP can associate with microtubules in transient assays in *N. benthamiana,* the association of MAP7s with microtubules was studied *in vitro*, to determine whether MAP7s bind to microtubules directly, or whether they may associate with microtubules through a secondary intermediate. To investigate, a microtubule co-sedimentation assay was performed. Microtubule co-sedimentation assays are based on separation of soluble unpolymerised tubulin and insoluble, polymerised microtubules through sedimentation by ultracentrifugation. Unpolymerised tubulin remains in the soluble supernatant fraction, whilst polymerised tubulin is separated into the pellet fraction. Direct microtubule-binding activity of a protein of interest can be determined if it is also partitioned into the pellet fraction after ultracentrifugation following incubation with polymerised tubulin.

7.3.3.1. Expression and Purification of Recombinant MAP7A.

The full-length MAP7A was cloned into the protein expression vector, pET28, facilitating the expression of an N-terminal 6xHistidine-fusion protein, which can be purified using nickel-nitrilotriacetic acid (Ni-NTA) agarose resin. To achieve this, the full-length MAP7A coding sequence was PCR amplified from MAP7A-pDONR207 with added 5' *NdeI* and 3' *NotI* restriction sites (for primers see appendix 1). The PCR product was subcloned into the *NdeI/NotI* sites of the pET28a multiple cloning site (MCS), in frame with N-terminal 6x-HIS tag, using the double digest restriction cloning method to generate the MAP7A-pET28a expression construct.

The resulting MAP7A-pET28a construct was transformed into and expressed in the Rossetta2 *E.coli* strain (figure 7.15) and the 6x-HIS fusion protein was purified using a Ni-NTA purification column (as described in chapter 2.4.1). On an SDS-PAGE gel, the purified 6xHIS-MAP7A protein ran at an approximate size of 15 kDa, compared to its predicted size of 10.8 kDa. The identity of the purified recombinant protein was confirmed as MAP7A by MALDI-TOF, performed by the SBBS Proteomics Centre.

Purified 6xHIS-MAP7A was then dialysed in 2x Buffer C. Prior to use in the microtubule co-sedimentation assay, aliquots of MAP7A in 2x Buffer C were ultracentrifuged to pellet insoluble, denatured MAP7A, and a Bradford assay was

performed to quantify the concentration of soluble MAP7A remaining in the supernatant.

7.3.3.2. Microtubule Co-Sedimentation Assay.

The microtubule co-sedimentation assay was performed by Dr Ian Cummins using purified tubulin. Per reaction, 10 µM tubulin was allowed to polymerise by incubation at 37 ˚C in the presence of 1 mM GTP. Three experimental series were performed in this assay: one with tubulin only, one with 6xHIS-MAP7A only, and one with tubulin and 6xHIS-MAP7A incubated together. Separation of insoluble pellet and soluble supernatant fractions by ultracentrifugation was performed to determine if 6xHIS-MAP7A co-sedimented with polymerised tubulin in the pellet fraction. The soluble and pellet fractions of each experimental series were analysed by SDS-PAGE electrophoresis.

Following ultracentrifugation, 6xHIS-MAP7A was observed to be completely soluble when incubated alone under tubulin-polymerising conditions, and was observed only in the soluble fraction. Tubulin, when incubated alone, could be seen in both the soluble fraction and the pellet fraction, indicating the incomplete polymerisation of soluble tubulin subunits into insoluble microtubule filaments. 6xHIS-MAP7A, when co-incubated with tubulin, was present in the pellet fraction following ultracentrifugation, indicating that the protein had co-sedimented with insoluble polymerised microtubules.

The co-sedimentation of 6xHIS-MAP7A with polymerised tubulin indicates that the full-length MAP7 proteins have the ability to bind microtubules directly, and constitute a novel family of plant microtubule-binding proteins.

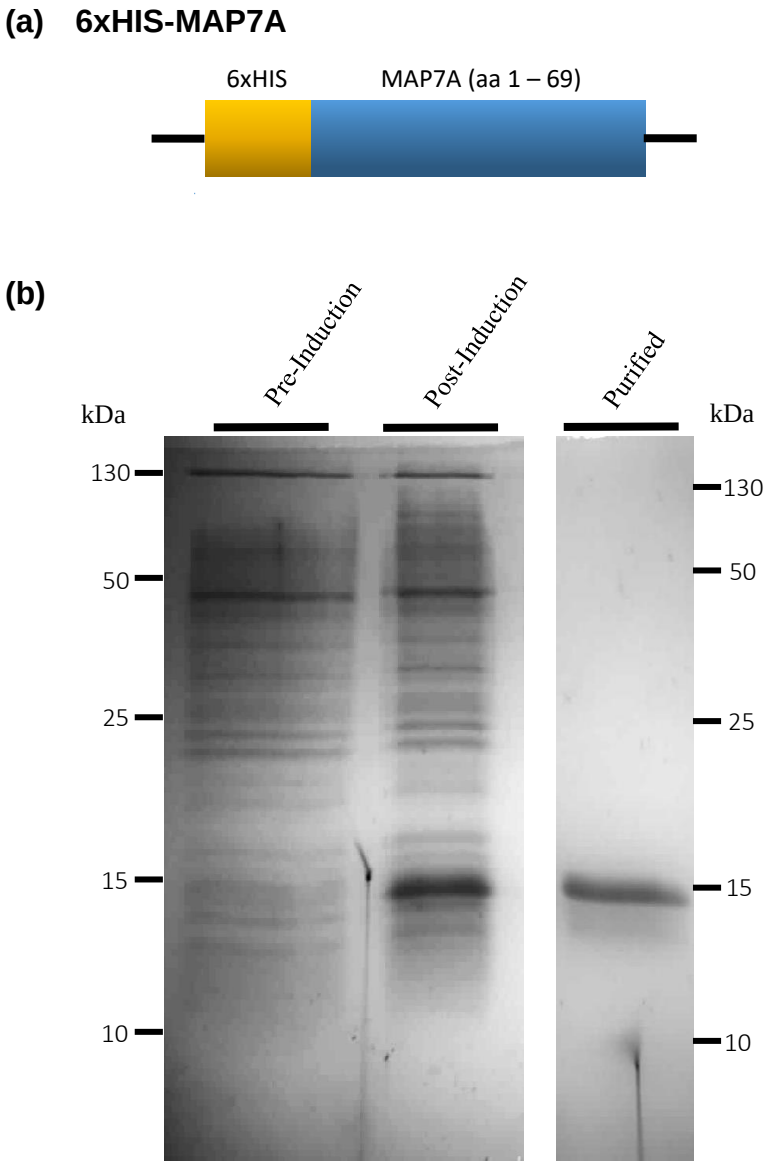

Figure 7.15: Expression and Purification of Recombinant 6xHIS-MAP7A. (a): Schematic diagram of 6xHIS-MAP7A expression construct. (b): Coomassie Brilliant Blue-stained SDS-PAGE gel showing purification of 6xHIS-MAP7A from *E.coli* total protein. Pre-Induction: *E. coli* total protein before autoinduction, Post-Induction: *E. coli* total protein after autoinduction. Purified: recombinant protein purified using Ni-NTA resin.

.

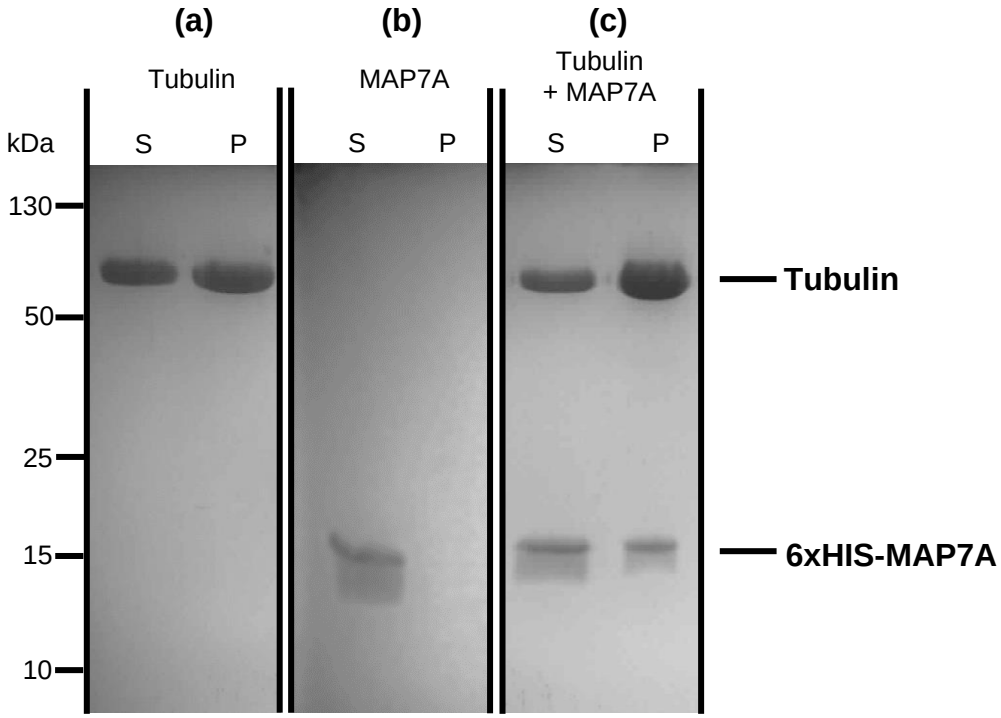

Figure 7.16: Microtubule Co-sedimentation Assay. Coomassie Brilliant Blue-stained SDS-PAGE gel showing soluble (S) and pellet fractions (P) of co-sedimentation series following ultracentrifugation. (a): Tubulin alone. (b): 6xHIS-MAP7A alone. (c): Tubulin + 6xHIS-MAP7A.

7.3.4. Summary.

As described above, initial analysis of MAP7A in *N. benthamiana* transient assays revealed a potential cytoskeletal association of MAP7A *in vivo*. Deduced from further investigation of this initial observation, the data presented in this section clearly characterises the Arabidopsis MAP7s as novel microtubule-associated proteins.

Firstly, it was observed that MAP7A-GFP decorates an extensive filament network when expressed in *N. benthamiana* leaf epidermal cells. The MAP7A-GFP filament system co-localised with microtubules, and was disrupted by depolymerisation of the microtubule cytoskeleton. This evidence was further corroborated through studies in *Arabidopsis,* in which stably-expressed MAP7A-GFP was also observed to form filamentous networks that were broken down by disruption of the microtubule

cytoskeleton. Through *in vitro* microtubule-binding assays, it was established that MAP7A was able to bind to microtubules directly.

The characterisation of MAP7A and MAP7B as a novel microtubule-binding proteins is highly significant in developing our understanding of how pollen tube growth may be regulated by the cytoskeleton. Firstly, an interaction between NET2A and the microtubule-binding MAP7A would be suggestive of a role for NET2A in mediating actin-microtubule interactions in growing pollen tubes. Interplay between the microtubule and actin cytoskeleton is thought to be important in the regulation of pollen tube growth (Gossot and Geitmann et al. 2007), and a potential interaction between NET2A and MAP7A may be involved in facilitating this. Furthermore, the discovery of a novel family of plant microtubule-binding proteins is likely to be highly important in understanding how the cytoskeleton is able to regulate plant growth, development and signalling. Also, identification of microtubule-binding activity in the conserved SERF domain of MAP7A suggests that SERF proteins may serve as microtubule-binding proteins in Kingdoms Animalia and Fungi: characterisation of MAP7 proteins in Arabidopsis may increase our understanding of the regulation of the cytoskeleton in multiple kingdoms.

7.4. Investigating MAP7A as an Interactor of NET2A.

7.4.1. Introduction.

MAP7A was identified as a potential interactor of NET2A in the SU-Y2H screen, as described in chapter 5.4.3. This section describes the attempts made to corroborate the MAP7A-NET2A interaction observed in the SU-Y2H, using the matchmaker Y2H system, and FRET-FLIM. As described below, an interaction between MAP7A and NET2A could not be demonstrated using these techniques.

7.4.2. Investigating MAP7A-NET2A Interactions Using the Clontech Matchmaker Y2H System.

7.4.2.2. Introduction.

MAP7A was pulled back as an interactor of NET2A in a SU-Y2H screen. To validate and further investigate this result, 1-on-1 Y2H interaction tests between NET2A and MAP7A were performed using the Clontech Matchmaker GAL4 Y2H system. Although the interaction between NET2A and MAP7A was originally identified using the SU-Y2H system, validation of the interaction using the Clonetech GAL4 Y2H system would substantiate the observed SU-Y2H result, and would permit further investigation of the NET2A-MAP7A interaction in-house, such as identification of protein domains and motifs responsible for mediating the interaction.

7.4.2.2. Generation, Transformation and Validation of Bait and Prey Fusion Protein Constructs in Yeast.

Generation of bait and prey constructs was performed as described in chapters 6.3.2.1 and 2.3. To analyse the interactions of NET2A and MAP7A in yeast, tests of interactions between BD-NET2A and AD-MAP7A were performed, as were AD-NET2A and BD-MAP7A. Using NET2A-pDONR207 (chapter 5.2.2), and MAP7A-pDONR207 (chapter 7.3.2), full length NET2A and MAP7A were cloned into pGBKT7 to generate the bait constructs BD-NET2A and BD-MAP7A, and full-length MAP7A was cloned into pGADT7 to generate AD-MAP7A. The cloning of NET2A-pGADT7 is described in chapter 6.3.2.1.

As described previously, autoactivation of selection markers by BD- and AD-constructs can give rise to false positive results. Therefore, it was assessed whether the generated constructs were able to autoactivate transcription of selection markers in the yeast reporter strain, AH109, which carries the reporter genes *HIS3* and *ADE2*. pGBKT7-NET2A, pGBKT7-MAP7A, and pGADT7-MAP7A were transformed into AH109, and grown on selective media. Yeast containing BD-NET2A and BD-MAP7A were grown on -W (to select for the bait construct), -WA (to select for autoactivation of *ADE2*), -WH (to select for autoactivation of *HIS3*) and -WH + 2.5 mM 3AT (to repress potential autoactivation of *HIS3*). Yeast containing

AD-MAP7A was grown on -L medium (to select for the prey construct), and -LA, -LH and -LH + 2.5 mM as described. Figure 7.17 shows the growth of the AH109 containing the bait or prey constructs on selective media. Bait constructs were able to grow on -W, and prey constructs were able to grow on -L. However, no growth was observed on -A, indicating no transcription of *ADE2* occurred in the absence of a bait-prey interaction. No growth of bait or prey-containing yeast occurred on -H, or -H + 2.5 mM 3AT, indicating that the *HIS3* reporter was not autoactivated by the bait and prey constructs. In addition to this, it was previously determined that AD-NET2A was unable to autoactivate the *HIS3* and *ADE2* reporter genes in AH109 (chapter 6.3.2.1).

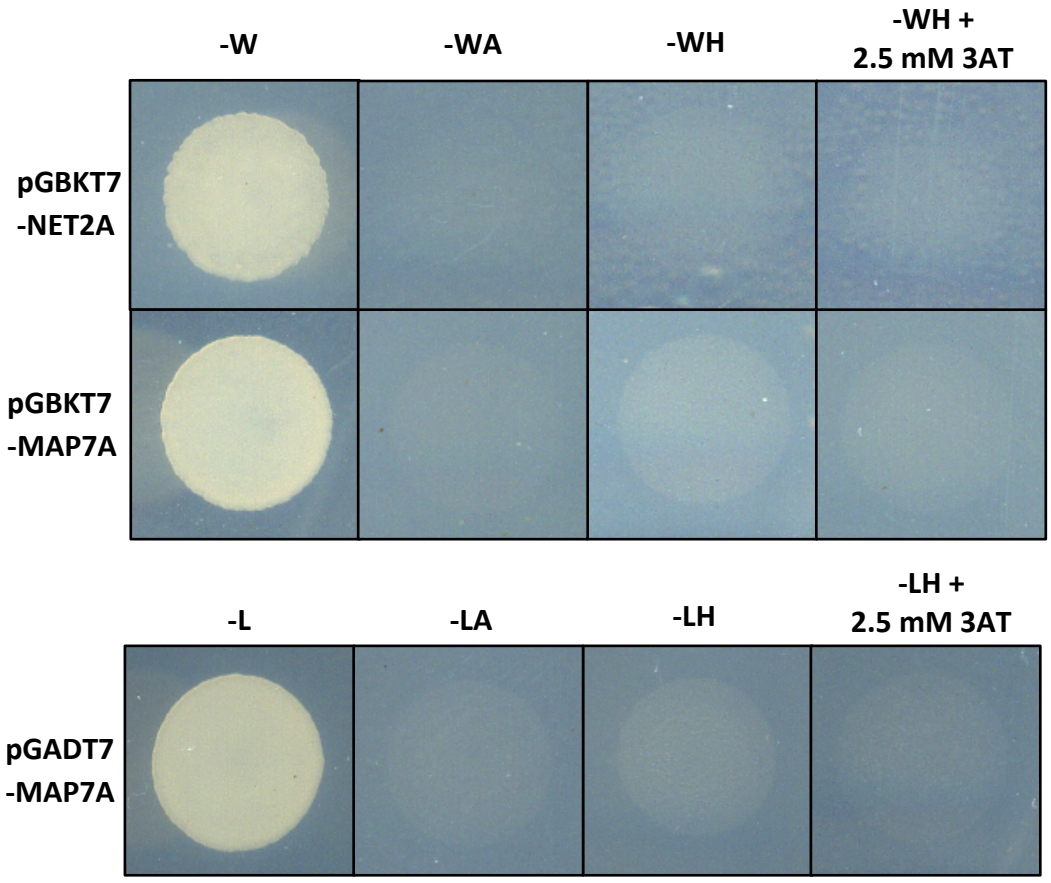

Figure 7.17: Autoactivation Assays of BD-NET2A, BD-MAP7A and AD-MAP7A in the AH109 Yeast Reporter Strain. NET2A-pGBKT7, MAP7A-pGBKT7 and MAP7A-pGADT7 were transformed into the AH109 yeast reporter strain. Yeast containing bait constructs in pGBKT7 were selected on -W selective media, and yeast containing prey constructs in pGADT7 were selected on -L media. The yeast were then selected on media also lacking -A, -H or -H + 2.5 mM 3AT to determine whether the constructs could autoactivate expression of *ADE2* and *HIS3*.

7.4.2.3. Testing NET2A-MAP7A Interactions using One-on-One Y2H Matings.

Having ascertained that the bait and prey constructs did not induce autoactivation of reporter genes in AH109, interactions between NET2A and MAP7A were investigated. Prey constructs in pGADT7 were transformed into the yeast strain, AH109, and bait constructs in pGBKT7 were transformed into Y187. As negative controls, the prey constructs were mated with empty pGBKT7 vector, and bait constructs with the empty pGADT7 vector, to ensure that activation of reporter genes did not occur in the absence of an interaction. Diploid yeast resulting from the one-on-one matings were grown on selective -WL media to select for yeast cells carrying both bait and prey constructs. Selected diploids were then grown on -WLH plates and -WLA plates to select for activation of *HIS3* and *ADE2* reporter genes, and also onto -WL media to show that growth could occur in the absence of -H and -A selection. As a positive control, pGBKT7-NET3C was mated with pGADT7-NET3C: an interaction between BD-NET3C and AD-NET3C has been demonstrated using the matchmaker Y2H system previously (Dr Pengwei Wang, unpublished data).

As shown in figure 7.18, it was clear that no interaction between NET2A and MAP7A could be observed. Firstly, an interaction between BD-MAP7A bait and AD-NET2A prey constructs was investigated. Diploid yeast containing pGBKT7-MAP7A and pGADT7-NET2A were able to grow on -WL selective media, but not on -WLH, or -WLA. Secondly, diploids containing pGADT7-MAP7A and pGBKT7-NET2A were able to grow on -WL, but not on -WLH or -WLA. In contrast, diploids containing pGBKT7-NET3C and pGADT7-NET3C were able to grow on -WLH and -WLA media. It was concluded that an interaction between NET2A and MAP7A could not be demonstrated using the Clontech Matchmaker Y2H System. Therefore, FRET-FLIM was performed to investigate the interaction between NET2A and MAP7A observed in the SU-Y2H screen. It is possible that a genuine interaction of NET2A and MAP7A may exist, which cannot be detected using the GAL4 Y2H system. One possible reason that no interaction was detected may be because full-length MAP7A was tested for an interaction with NET2A. In the SU-Y2H screen, only a fragment of MAP7A (aa 5 - 38) was pulled back as an interactor of NET2A, and it is possible that full length MAP7A may not interact with NET2A in the yeast system. Unfortunately, MAP7A (aa 5 - 38) could not be cloned for use in Y2H. It is also possible that MAP7A may be rendered non-functional by N-terminal GAL4 AD or BD fusions, which may distort the native confirmation of MAP7A and prevent an

interaction. Conversely, MAP7A may distort the conformation of GAL4 AD or BD tags, preventing their activation of *ADE2* and *HIS3* even in the presence of an interaction (Sobhanifar. 2003).

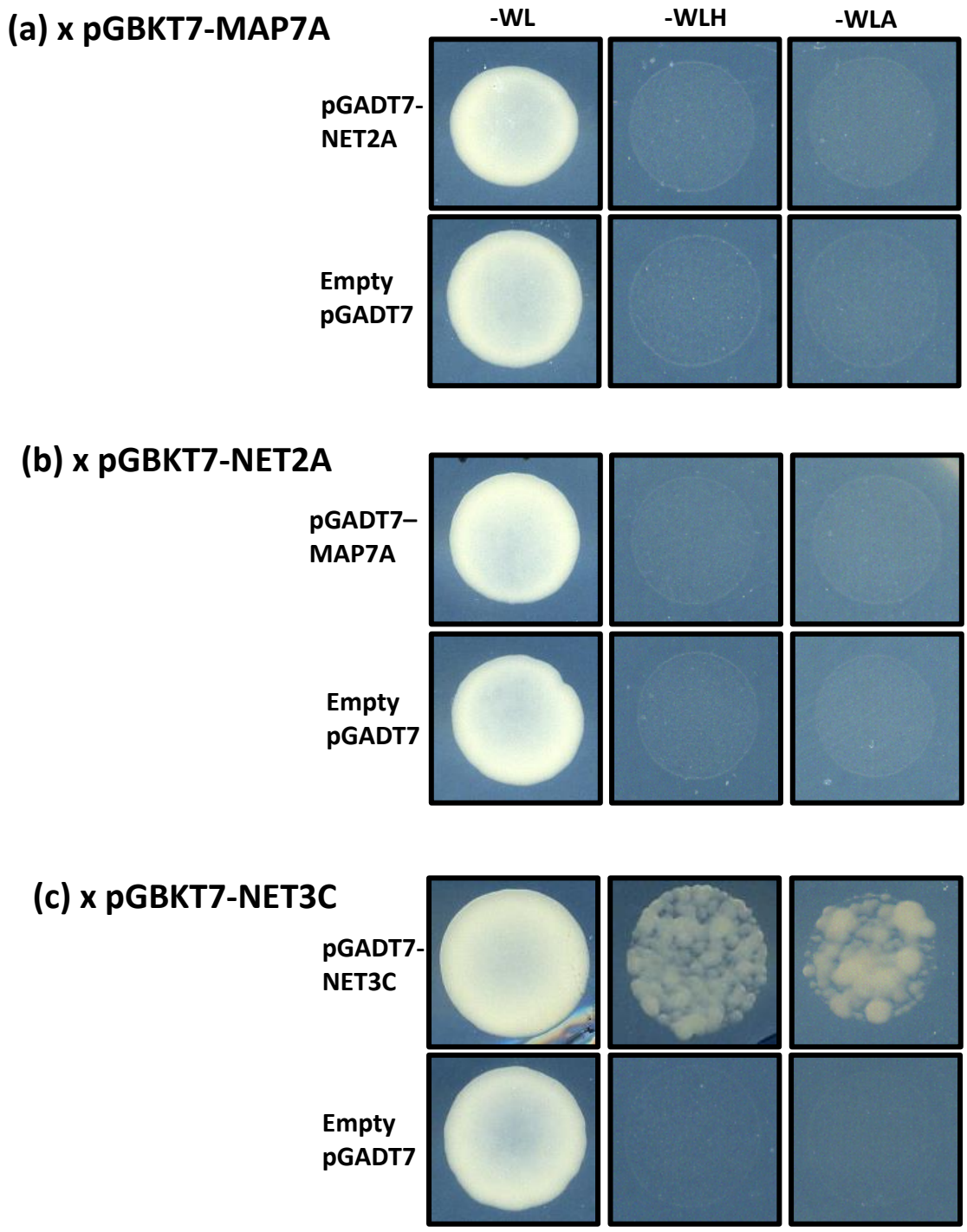

Figure 7.18: One-on-One Y2H Assay Between NET2A and MAP7A. (a): the bait construct pGBKT7-MAP7A was mated against the prey construct, pGADT7-NET2A, and the negative control, empty pGADT7. (b): the bait construct, pGBKT7-NET2A was mated against the prey construct, pGADT7-MAP7A, and the negative control, empty pGADT7. (c): as a positive control, the bait vector, pGBKT7-NET3C was mated against the prey construct, pGADT7-NET3C and empty pGADT7. Diploids were grown on selective media, -WL to select for diploids, and -WLH, and -WLA to select for positive interactions through activation of *HIS3* and *ADE2* respectively.

7.4.3. Analysis of NET2A-MAP7A Interactions *in vivo* using FRET-FLIM.

7.4.3.1. Analysis of MAP7A-GFP and NET2A-mCherry Co-localisation *in vivo*.

Before FRET-FLIM was performed to investigate a potential interaction between MAP7A-GFP and NET2A-mCherry, it was investigated as to whether the two constructs may occupy the same subcellular localisation; a pre-requisite for protein-protein interactions to occur. MAP7A-GFP is known to localise to the microtubule cytoskeleton, where it forms punctae and filaments (section 7.3.2). NET2A-mCherry is known to localise to the actin cytoskeleton with a 'beads-on-a-string' distribution (chapter 6.3.3.2) characteristic of NET superfamily proteins (Deeks et al. 2012). To analyse whether the two proteins may co-localise *in vivo*, MAP7A-GFP and NET2A-mCherry were co-expressed in *N. benthamiana* leaf tissue using agrobacterium-mediated infiltration so that they may be visualised together.

Figure 7.19 shows the subcellular localisation of MAP7A-GFP with NET2A-mCherry co-expressed in *N. benthamiana* leaf epidermal cells. MAP7A-GFP and NET2A-mCherry appeared to co-localise *in vivo*: co-alignment of MAP7A-GFP and NET2A-mCherry-labelled filaments was clearly observable, and co-localisation of MAP7A-GFP and NET2A-mCherry punctae was evidently apparent. It was observed that 84.5 ± 8.3% of MAP7A-GFP punctae co-localised with NET2A-mCherry (n = 1181 MAP7A-GFP punctae analysed in 10 cells). Having ascertained that the MAP7A-GFP and NET2A-mCherry constructs co-localised *in vivo*, FRET-FLIM was performed to investigate a potential physical interaction between the two proteins.

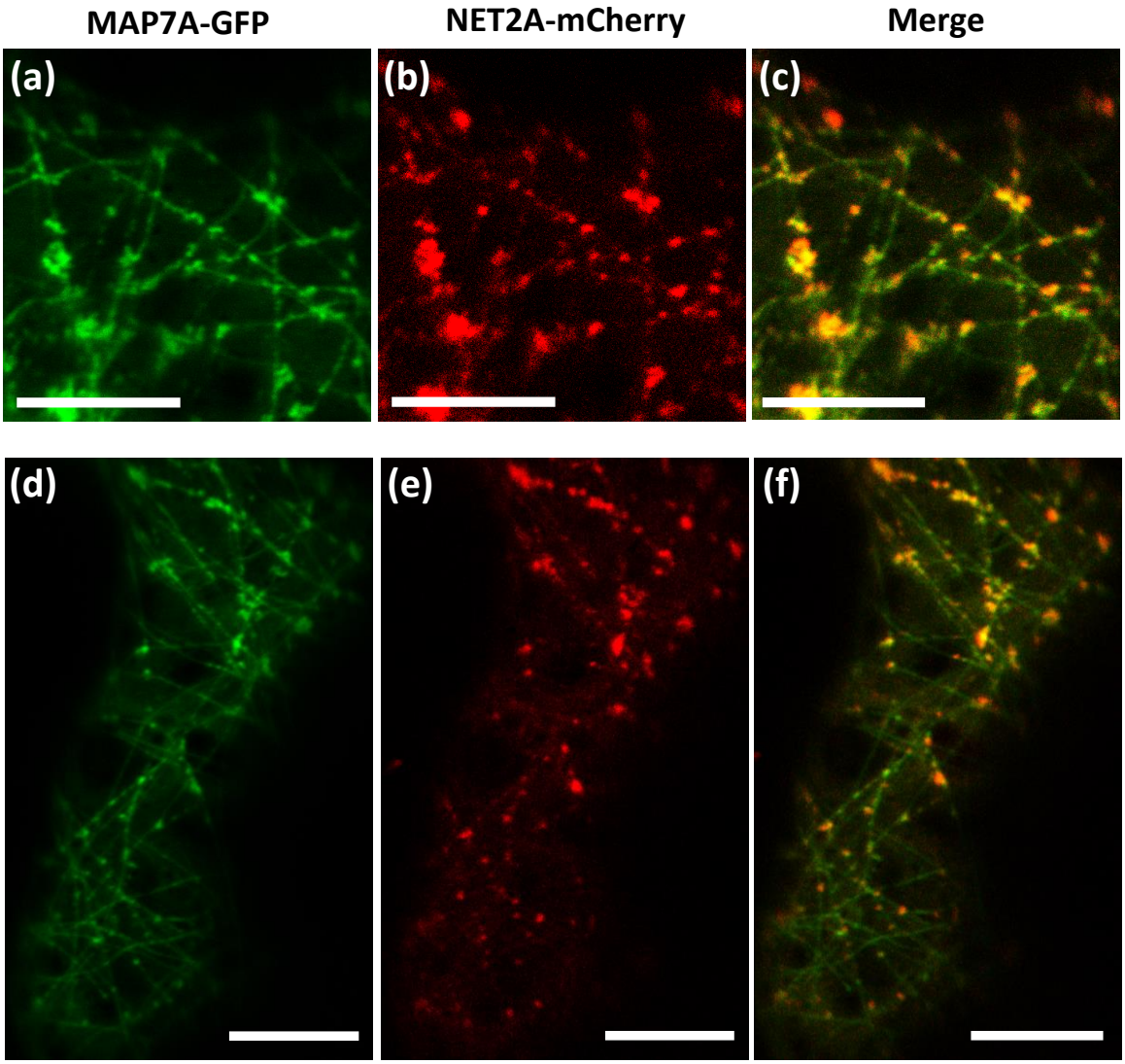

Figure 7.19: Co-localisation of MAP7A-GFP with NET2A-mCherry *in vivo*. *N benthamiana* leaf epidermal cells expressing MAP7A-GFP and NET2A-mCherry. (a) and (d): MAP7A-GFP visualised using a 488 nm excitation laser. (b) and (e): NET2A-mCherry visualised using a 594 nm excitation laser. (c) and (f): overlay of images of corresponding GFP and RFP channels, with yellow indicating regions of co-localisation between MAP7A-GFP and NET2A-mCherry. Scale bar: 10 µm.

7.4.3.2. FRET-FLIM Analysis of MAP7A-GFP and NET2A-mCherry Interactions.

FRET-FLIM was performed to investigate a potential direct interaction between MAP7A-GFP and NET2A-mCherry. MAP7A-GFP and NET2A-mCherry are suitable donor and acceptor fluorophore-fusion protein partners, due to their overlapping spectral profiles (see chapter 5.3), and are known to co-localise *in vivo*, as demonstrated above. Analysis of FRET between the two constructs, observable by

measuring differences in MAP7A-GFP fluorescence lifetime when expressed alone and with NET2A-mCherry, would indicate whether the two proteins physically interact *in vivo*. *N. benthamiana* leaf sections were transiently transformed with MAP7A-GFP and NET2A-mCherry using agrobacterium infiltration, and FRET-FLIM was performed as described in chapters 5.3 and 2.5.3.

As demonstrated in figures 7.20 and 7.21, MAP7A-GFP; when expressed alone, exhibited an average fluorescence lifetime of 2.54 ± 0.03 ns, which remained practically unaffected when co-expressed alongside NET2A-mCherry. The average fluorescence lifetime of MAP7A-GFP when co-expressed with NET2A-mCherry was 2.51 ± 0.01 ns, constituting a fluorescence lifetime decrease of 0.03 ns, from MAP7A-GFP expressed alone. This difference in fluorescence lifetime is negligible, and is far below the decrease in fluorescence lifetime of 0.2 ns, accepted to indicate an interaction between donor and acceptor fluorophore-fusion proteins. In comparison, the fluorescence lifetime of the positive control GFP-mCherry fusion protein was 2.07 ± 0.04 ns. Therefore, no interaction between MAP7A-GFP and NET2A-mCherry could be detected using FRET-FLIM.

It is surprising that no interaction between MAP7A-GFP and NET2A-mCherry could be detected using FRET-FLIM: clear co-localisation between the two proteins is evident, and they have been shown to interact in a SU-Y2H assay. It is possible that MAP7A-GFP and NET2A-mCherry may physically interact in *N. benthamiana*, but no observable interaction was detected using FRET-FLIM. This could be caused if the interaction of the MAP7A and NET2A proteins does not result in the positioning of the GFP and mCherry fluorophore tags within close enough proximity for FRET to occur (Sun et al. 2011; Day and Davidson. 2012), Alternatively, unfavourable alignment of fluorophore dipoles can prevent FRET occurring between closely positioned donor and acceptor fluorophores (Day and Davidson. 2012): perhaps FRET cannot occur between MAP7A-GFP and NET2A-mCherry as the steric orientation of the fluorophore tags is not favourable for energy transfer. However, a physical association between NET2A and MAP7A could not be demonstrated using FRET-FLIM, and further attempts to study the interaction were subsequently abandoned.

Constructs Expressed	Mean GFP Fluorescence Lifetime	Standard Deviation	n
MAP7A-GFP	2.54 ns	0.03	5
MAP7A-GFP + NET2A-mCherry	2.51 ns	0.01	5
GFP-mCherry positive control	2.07 ns	0.04	5

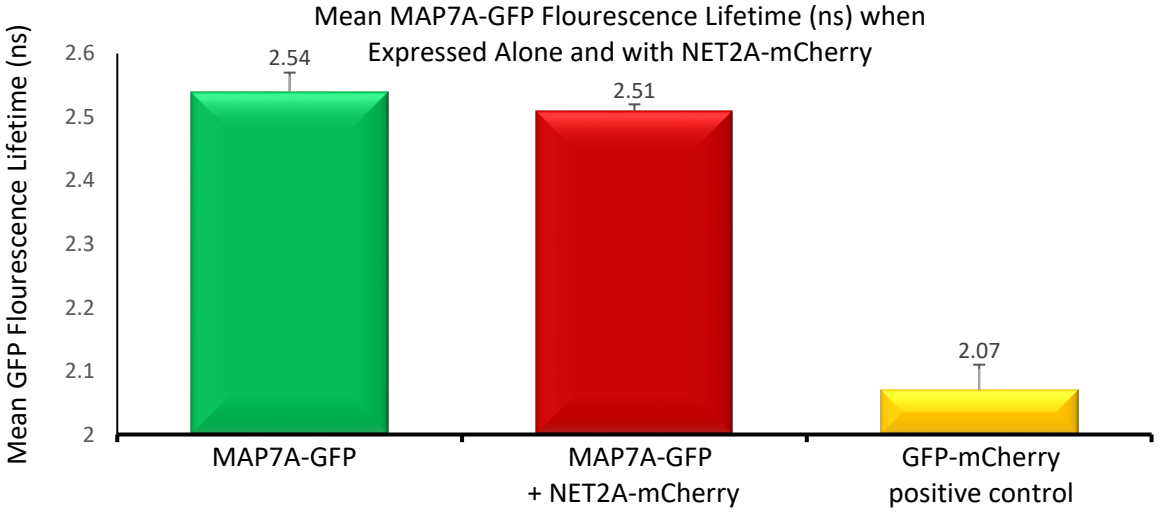

Figure 7.20: NET2A-mCherry Induces no Decrease in MAP7A-GFP Fluorescence Lifetime when Co-expressed in *N. benthamiana* Epidermal Cells. n = number of cells analysed.

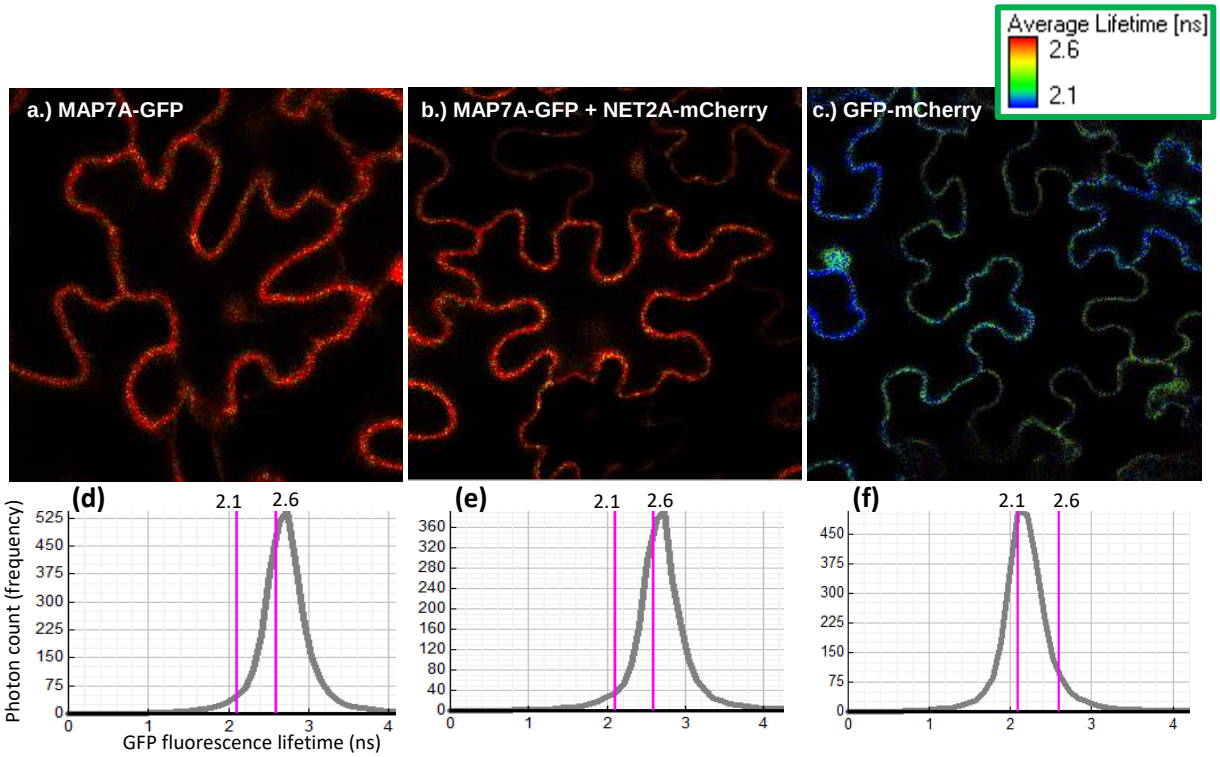

Figure 7.21: Visualisation of MAP7A-GFP Fluorescence Lifetime *in vivo* when Expressed Alone, and with NET2A-mCherry (a)–(c): Example images of GFP fluorescence detected in *N. benthamiana* leaf epidermal cells, pseudocoloured according to GFP fluorescence lifetime. (d)-(f): charts associated with images (a)-(c) respectively, show the frequency distributions of the fluorescence lifetimes (ns) of detected photons in each image. A leftward shift in peak GFP fluorescence lifetime is indicative of reduced average lifetime. (a) and (d): MAP7A-GFP expressed alone. (b) and (e): MAP7A-GFP co-expressed with NET2A-mCherry. (c) and (f): GFP-mCherry positive control.

7.4.4. Summary.

MAP7A was pulled back as a potential interactor of NET2A in the SU-Y2H screen. This section describes the experiments performed to corroborate the identified interaction. Firstly, 1-on-1 Y2Hs were performed using the matchmaker Y2H system to attempt to replicate the observed interaction between NET2A and MAP7A in the SU-Y2H screen. In contrast to the SU-Y2H, the matchmaker Y2H did not prove an interaction. FRET-FLIM was also unable to prove an interaction between MAP7A-GFP and NET2A-mCherry, despite co-localisation between the two proteins.

It seems likely that NET2A and MAP7A may share some involvement with each other *in vivo*, based on the interaction between the two proteins observed in the SU-Y2H, and co-localisation between MAP7A-GFP and NET2A-mCherry observed in *N. benthamiana*. It is possible that interactions occurring between NET2A and MAP7A could not be detected using the GAL4 Y2H system or FRET-FLIM. However, an alternative explanation is that NET2A and MAP7A do not interact directly, and the interaction detected in the SU-Y2H may have occurred indirectly through a third intermediary protein (Sobhanifar. 2003). Binding of NET2A-Cub bait and MAP7A-Nub prey constructs to a common intermediary protein may have bought the Cub and Nub moieties in close enough proximity to generate split ubiquitin, causing growth of yeast on selective media and indicating a positive interaction.

As the interaction between NET2A and MAP7A could not be validated using GAL4 Y2H or FRET-FLIM assays, no further attempts were made to prove and characterise an interaction between the two proteins. However, further characterisation has revealed MAP7A to be a cytoskeletal-associated protein (section 7.3) that appears to be expressed specifically in pollen (section 7.5). It is therefore likely that MAP7A may be involved in the regulation of the pollen tube cytoskeleton, warranting full characterisation of the MAP7 proteins as a novel family of microtubule-binding proteins.

7.5. Analysis of MAP7 Expression and Localisation *in situ.*

7.5.1. Introduction.

In section 7.3, the MAP7s were described as a novel family of microtubule-associated proteins, deduced from *in vitro* studies and expression of MAP7A-GFP *in vivo*. This section summarises the characterisation of the MAP7 protein family's expression patterns and subcellular localisation *in situ*.

Firstly, the GUS reporter system was employed to study the expression patterns of MAP7A and MAP7B *in situ*, in transgenic lines expressing the GUS reporter under control of the MAP7A and MAP7B promoters.

Secondly, the *in situ* subcellular localisation of the MAP7 proteins was analysed using immunofluorescent labelling of *Narcissus* pollen tubes using anti-MAP7A antibodies.

7.5.2. Analysis of MAP7A and MAP7B Transcriptional Expression Patterns using the GUS Reporter System.

7.5.2.1. An Introduction to the GUS Reporter System.

Due to a lack of availability of bioinformatic data pertaining to the expression patterns of MAP7A and MAP7B in Arabidopsis tissues, the GUS reporter system was used to analyse the transcriptional expression patterns of the MAP7 family. This method relies on the expression of the *E. coli* GUS (β-glucuronidase) enzyme under the control of the promoter of a gene of interest. GUS catalyses the cleavage of the substrate, X-Gluc (5-bromo-4-chloro-3-indolyl-β-D-glucuronic acid) into glucuronic acid and chloro-bromoindigo; a blue-coloured breakdown product (Jefferson et al. 1987). The cell-specific activity of a promoter can be visualised in GUS reporter lines by observing blue staining in tissues incubated in solutions of X-Gluc. This permits the mapping of promoter activity in various plant tissues at different stages of development.

Analysis was performed on *pMAP7A*:GUS and *pMAP7B*:GUS stable transgenic lines. To generate these lines, the GUS expression vector, pBI101G was used. Cloning of the promoter sequences of *MAP7A* (*pMAP7A*) and *MAP7B* (*pMAP7B*) into pBI101G, directly upstream of the GUS coding sequence, facilitated the expression of GUS under control of *pMAP7A* and *pMAP7B*. The *pMAP7A*-pBI101G and *pMAP7B*-pBI101G constructs (figure 7.22) were generated by PCR amplifying a ≈ 2 KB DNA fragment, immediately upstream of the *MAP7A* and *MAP7B* start codons, and cloning them into pDONR207 using gateway cloning. The promoter fragments were then cloned into pBI101G. Floral dipping was used to stably transform the *pMAP7A*-GUS and *pMAP7B:*GUS constructs into *Arabidopsis* (chapter 2.2.15*)*. The T1 seed of dipped plants was selected on 1/2 MS media supplemented with 50 µg/ml Kanaymcin. Kanamycin-resistant plants were then manually screened for GUS reporter activity in whole inflorescences, to confirm expression of the transgene. GUS-positive T1 plants were permitted to self-fertilise and analysis was performed on progeny of the T2 generation. The progeny of 10 independently transformed lines was analysed for both *pMAP7A*-GUS and *pMAP7B*-GUS.

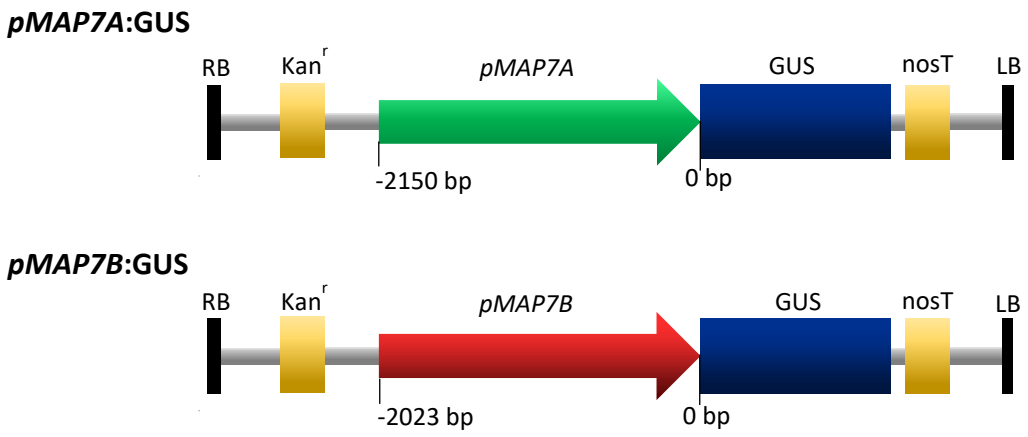

Figure 7.22: Schematic Diagram of *pMAP7A*:GUS and *pMAP7B*:GUS Constructs Generated using the pBI101G Expression Vector. RB = T-DNA right border. Kan^r = kanamycin resistance marker. p35s = *CaMV* 35s promoter sequence. GUS = β-glucuronidase coding sequence. nosT = nopaline synthase terminator sequence. LB = T-DNA left border. *pMAP7A* = fragment of MAP7A promoter (2150 bp pairs upstream of the MAP7A start codon as indicated in diagram). *pMAP7B* = fragment of MAP7B promoter (2023 bp pairs upstream of the MAP7B start codon as indicated in diagram).

7.5.2.2. Expression of MAP7A and MAP7B in 7-10 Day Old Seedlings.

The transcriptional expression patterns of MAP7A and MAP7B were analysed in developing seedlings at 7-10 days after germination. As described in chapter 2.5.9, *pMAP7A:*GUS and *pMAP7B:*GUS seedlings were vacuum infiltrated with GUS

buffer: both lines were incubated at 37 ºC for 1 hour, after which GUS staining of *pMAP7B:*GUS seedlings was clearly observable. As no staining of *pMAP7A:GUS* seedlings was detected after 1 hour, seedlings were also analysed after 48 hours incubation to determine whether MAP7A may be expressed at low levels. The seedlings were then cleared of pigment using a graded series of ethanol washes (30%, 50%, 70%, 100% respectively). Samples were mounted in 20% glycerol and imaged using the Leica M165FC Fluorescent Stereo Microscope.

MAP7A did not appear to express strongly in the roots, leaf or shoot tissue of Arabidopsis seedlings, and no GUS staining was observable after 1 hour of incubation of *pMAP7A*:GUS seedlings in GUS buffer (figure 7.23a, c and e). In contrast, strong staining was observed in the root vasculature of *pMAP7B:*GUS seedlings after just one hour incubation in GUS buffer, with diffuse staining observable in the surrounding tissue (figure 7.23b). It is possible that MAP7B is expressed at low levels in the root epidermis and cortex, however staining of tissue surrounding the intensely-stained root vasculature could have resulted through bleeding of chloro-bromoindigo pigment into surrounding cells. Strikingly, expression of MAP7B appeared to be entirely absent from the growing root tip (figure 7.23c) and was confined to mature tissues of the root. In addition to being expressed in the root, strong MAP7B expression was observed at discreet zones at the base of developing shoots (figure 7.23f). It should be noted that no staining was observable in Col-0 seedlings. A complete summary on the staining patterns of seedlings of all *pMAP7A:*GUS and *pMAP7B*:GUS lines analysed can be found in appendix 5.

7.5.2.3. Expression of MAP7A and MAP7B in Floral Tissue.

The expression of MAP7A and MAP7B was then analysed in floral tissue. Whole inflorescences were vacuum infiltrated in GUS buffer and incubated at 37 ºC for either 1-3 hours or 48 hours. Samples were then cleared of pigment by multiple washes in 70% ethanol and were mounted in 20% glycerol before imaging.

As shown in figure 7.24 (a) and (b), vivid staining of the anthers of *pMAP7A*:GUS and *pMAP7B*:GUS plants was clear after 48 hours of incubation. No staining was observable in Col-0 inflorescences. The level of MAP7A and MAP7B expression observed appeared to intensify in the anthers of older buds, indicating that MAP7A

and MAP7B expression may be upregulated during anther maturation. After 1 - 3 hours of incubation in GUS buffer, MAP7A and MAP7B expression was only observable in the anthers of mature flowers, but not in those of developing buds. Upon closer inspection of mature anthers, GUS staining appeared to be localised to pollen grains (figure 7.24c and d). The data indicates the MAP7 proteins are expressed in pollen grains and are transcriptionally upregulated during maturation. It can be concluded that expression of MAP7B was stronger in the root tissue than in pollen: intense GUS staining was observable in root tissue after just 1 hour of incubation in GUS buffer, whereas only weak staining was seen in pollen grains after 1 - 3 hours in the same independent transgenic lines. A complete summary of the staining patterns of inflorescences of all *pMAP7A:*GUS and *pMAP7B*:GUS lines analysed can be found in appendix 5.

7.5.3. Analysis of MAP7A Subcellular Localisation *in situ* using Immunofluorescence.

7.5.3.1. An Introduction to Immunofluorescence.

Immunofluorescence permits visualisation of the subcellular localisations of proteins *in situ*. This entails probing fixed tissues with primary antibodies which specifically recognise and bind a protein of interest. The primary antibodies are in turn, recognised by fluorochrome-conjugated secondary antibodies; fluorescently labelling the locations of the protein within a cell.

In order to detect MAP7A using immunofluorescence, polyclonal anti-MAP7A antibodies, specifically recognising MAP7A, were raised. Primary polyclonal antibodies are raised in a host organism (typically mice or rabbits), as an immune response to inoculation with an antigen from a protein of interest. As a result, the antibodies raised will recognise and bind the protein used for inoculation. The serum of inoculated animals, containing the generated antibodies, is collected for use in immunological detection protocols. The antibodies described in this section are classed as polyclonal antibodies: recognising multiple epitopes on the surface of the antigen they are raised to. This section describes the production and validation of anti-MAP7A mouse polyclonal antibodies and their use in immunofluorescence analysis on *Narcissus* pollen tubes.

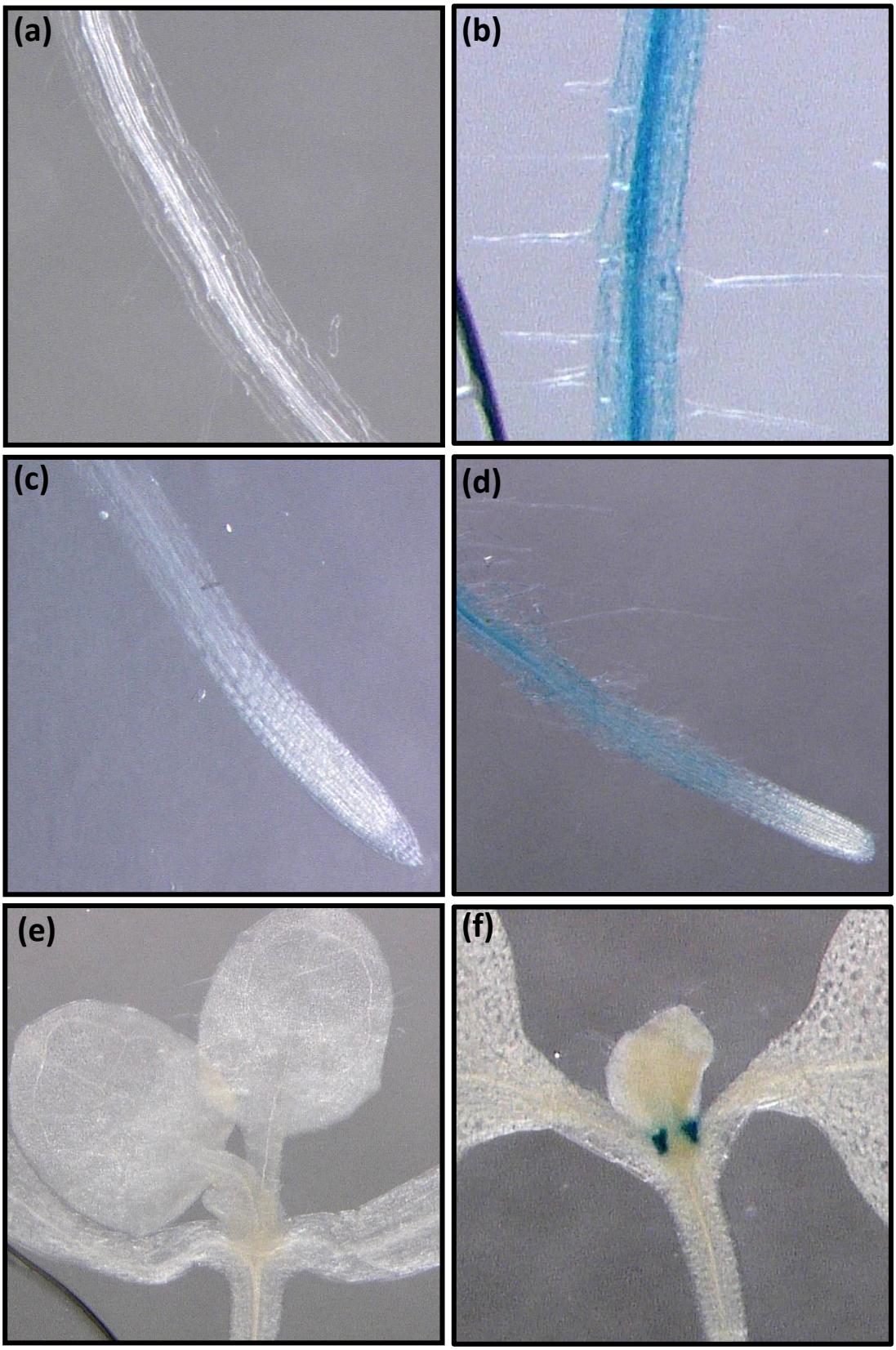

Figure 7.23: Expression Patterns of MAP7A and MAP7B in 7-10 day Old Seedlings. *pMAP7A*:GUS seedlings (a), (c) and (e), and *pMAP7B*:GUS seedlings (b), (d) and (f) incubated in GUS buffer for 1 hour at 37 °C. (a)-(d): GUS staining in root tissue. (e)-(f): GUS staining in developing shoots.

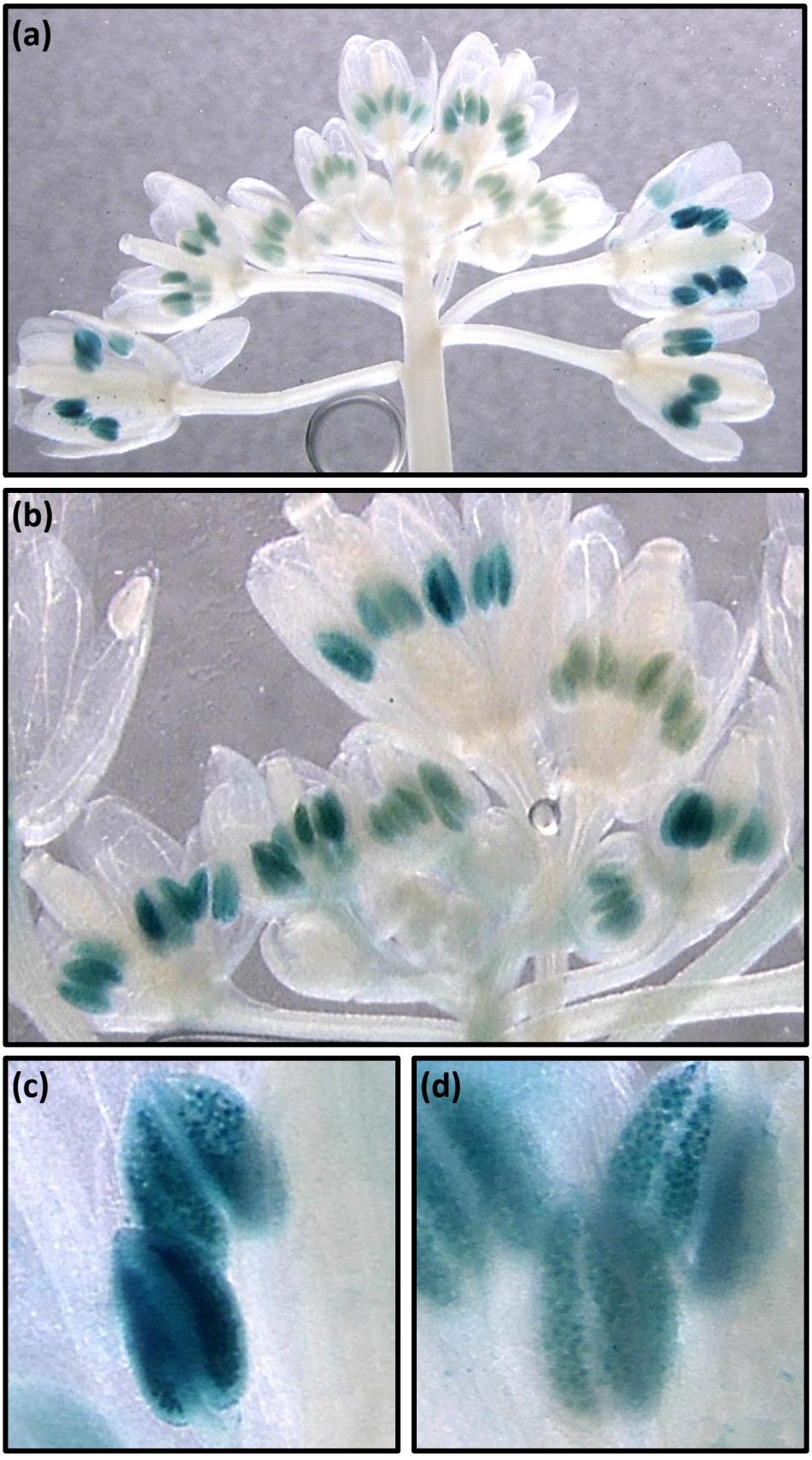

Figure 7.24: Expression Patterns of MAP7A and MAP7B in Whole Inflorescences. Inflorescences of plants expressing *pMAP7A*:GUS (a), and inflorescences of plants expressing *pMAP7B*:GUS (b) incubated in GUS buffer for 48 hours at 37 °C. GUS staining indicates pollen-localised expression of MAP7A (c), and MAP7B (d) in mature anthers.

7.5.3.2. Production of Mouse Polyclonal Antibodies to MAP7A.

In order to generate polyclonal antibodies to MAP7A, mice were inoculated with 6xHIS-MAP7A (7.3.3.1) as described in chapter 2.4.4, to raise antibodies against full-length MAP7A.

Achieving high specificity of antibody recognition of epitopes is of great importance when raising primary antibodies, as non-specific recognition of other epitopes would result in the unwanted detection of other proteins. To raise antibodies of high specificity, it is necessary to inoculate the host organism with a unique antigen, specific to the protein of interest. This may often require inoculation with a specific fragment of a protein of interest, with low homology to other proteins. This however, was not possible when raising antibodies to MAP7A, which is highly homologous to MAP7B; with which it exhibits no regions of low homology. Furthermore, due to the small size of MAP7A, raising antibodies to smaller fragments of MAP7A was not desirable. Therefore, antibodies were raised to full-length MAP7A, by inoculating mice with 6xHIS-MAP7A.

Purified recombinant 6xHIS-MAP7A (7.3.3.1) was dialysed in 1 x PBS and inoculation of mice was performed as described in chapter 2.4.4. The immune responses of different mice may be variable, so 3 different mice (named mice 3 - 5) were inoculated. The specificity of the antibodies to MAP7A was analysed using Western blot analysis. Total protein was extracted from whole Arabidopsis inflorescences and separated by molecular weight using SDS-PAGE gel electrophoresis, before being transferred to a nitrocellulose membrane as described in chapter 2.4.6. Sera from the terminal bleeds of mice 3 - 5 was used to probe the nitrocellulose membrane at 1:250, 1:500 and 1:1000 dilutions (figure 7.25). At a dilution of 1:1000, the sera of mice 3-5 detected a band of ≈ 15 kDa, similar to the molecular weight of 6xHIS-MAP7A observed using SDS-PAGE electrophoresis. However, the sera derived from mouse 5 also detected additional bands at ≈10 and ≈20 kDa and was deemed non-specific. At a dilution of 1:500, the mouse 4 sera exhibited a high level of background signal, indicating that it was non-specific at this dilution, and less specific than the sera derived from mouse 3. Therefore, anti-MAP7A antibodies from mouse 3 were used in further experiments.

The specificity of the antibodies from mouse 3 to MAP7A was then validated. Comparison of the pre-bleed sera from mouse 3 (taken before immunization), with

the sera of the terminal bleed was performed using Western blot analysis on recombinant 6xHIS-MAP7A. Nitrocellulose membranes were probed with pre-bleed sera and terminal bleed sera of mouse 3, at a dilution of 1/500 (figure 7.26). The predicted band of ≈15 kDa was clearly visible when probed with the terminal bleed sera, but no band was observable after probing with the pre-bleed sera. This indicates that the antibodies recognising the observed ≈15 kDa band were generated as an immune response to inoculation with 6xHIS-MAP7A, and that the antibodies contained in the mouse 3 serum are specific to MAP7A.

Having confirmed that the antibodies raised in mouse 3 were specific to MAP7A, immunostaining of Narcissus pollen tubes was performed to investigate the subcellular localisation of MAP7A *in situ*.

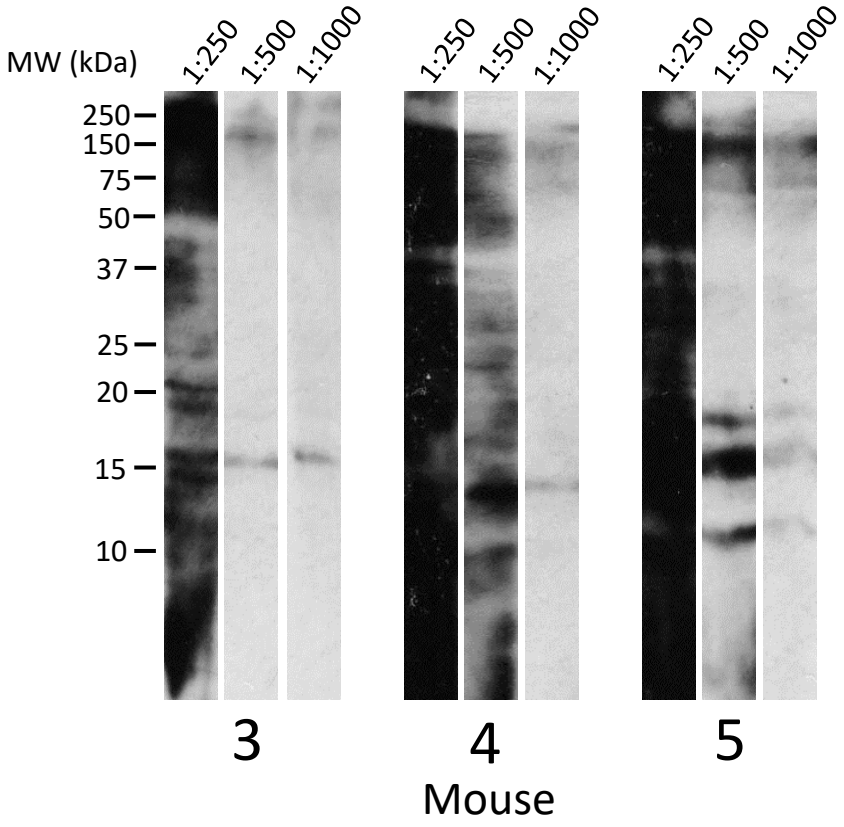

Figure 7.25: Western Blot Analysis of Mouse anti-MAP7A Antibodies. Performed on total protein extracted from whole Arabidopsis inflorescences. The nitrocellulose membrane was cut into strips, separately probed with anti-MAP7A primary antibodies from mice 3, 4 or 5 at a dilution of 1:250, 1:500 or 1:1000. Bio-Rad Precision Plus Protein Dual Colour was used as a molecular weight marker.

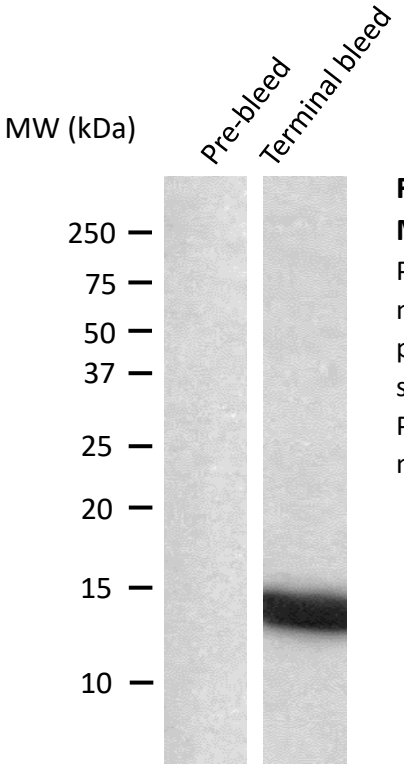

Figure 7.26: Western Blot Analysis of anti-MAP7A Pre-bleed and Terminal Bleed Sera. Performed on recombinant 6xHIS-MAP7A. The nitrocellulose membrane was cut into strips and probed with either the pre-bleed or terminal bleed sera of mouse 3, at a dilution of 1:500. Bio-Rad Precision Plus Protein Dual Colour was used as a molecular weight marker.

7.5.3.3. *In situ* Analysis of MAP7A Subcellular Localisation in Narcissus Pollen Tubes Using Immunofluorescence.

Having validated the specificity of the anti-MAP7A antibodies, immunostaining was used to detect and visualise the subcellular localisation of MAP7A *in situ*. Analysis of MAP7A subcellular localisation was performed on Narcissus pollen tubes; reportedly an excellent model on which to study the cytoskeleton and cell structure using immunofluorescence (Smertenko et al. 2001; Heslop-Harrison and Heslop-Harrison. 1992).

As described in chapter 2.5.6, germinated Narcissus pollen tubes were simultaneously fixed with 3.7% paraformaldehyde, 0.02% glutaraldehyde, and 100 µM MBS ester to preserve cellular structure, and permeablised with 0.02% saponin in PEM buffer to order to permit the antibodies access to intracellular epitopes. Saponin is a detergent-based permeabilisation agent which selectively interacts with cholesterol, forming small holes in plasma membranes whilst leaving the membrane

structure intact (Jamur and Oliver. 2009). This form of membrane permeabilisation was used as not to disrupt membrane systems to which MAP7A may localise. Fixed pollen tubes were incubated with primary antibodies at a dilution of 1:300. Visualisation of primary antibodies was facilitated by incubation with anti-mouse IgG secondary antibodies conjugated to FITC at a dilution of 1:50. To assess good fixation and preservation of cell structure during the immunostaining procedure, pollen tubes were co-stained with 0.825 nM rhodamine-phalloidin to visualise F-actin and the preserved integrity of the actin cytoskeleton. Visualisation of immunostained pollen tubes was performed using CLSM using the Leica Sp5 confocal laser scanning microscope. No FITC fluorescence was observable in pollen tubes that had not been incubated with anti-MAP7A primary antibodies.

Figures 7.27, 7.28 and 7.29 show the subcellular localisation of MAP7A in Narcissus pollen tubes. Initially, visualisation of MAP7A and actin in pollen tubes was performed to observe MAP7A subcellular localisation in pollen tubes known to have well-preserved subcellular structure. As shown in figure 7.27, the fixation procedure had maintained the subcellular architecture as indicated by the clearly apparent actin filaments, labelled by rhodamine-phalloidin. MAP7A appeared to localise to punctae at the plasma membrane of pollen tubes in both the shank and tip regions, but not at the plasma membrane of the pollen grain. The subcellular localisation of MAP7A did not appear to co-localise with that of rhodamine-phalloidin-stained actin filaments. Figure 7.28 shows magnified images of MAP7A subcellular localisation to the pollen tube plasma membrane at cortical and medial cross sections of the tube. The localisation of MAP7A to punctae at the pollen tube membrane draws similarities to the subcellular localisation of NET2A in pollen tubes. Although an interaction between NET2A and MAP7A could not be demonstrated in this study, it is possible that the two proteins may co-localise or even physically associate at these membrane punctae.

MAP7A was also seen to localise to the periphery of a subcellular compartment, clearly encircling a structure visible using brightfield microscopy, with a punctate distribution (figure 7.29). As discussed below, it was demonstrated that MAP7A localises to the generative cell nucleus, where is can be seen to co-localise to microtubules.

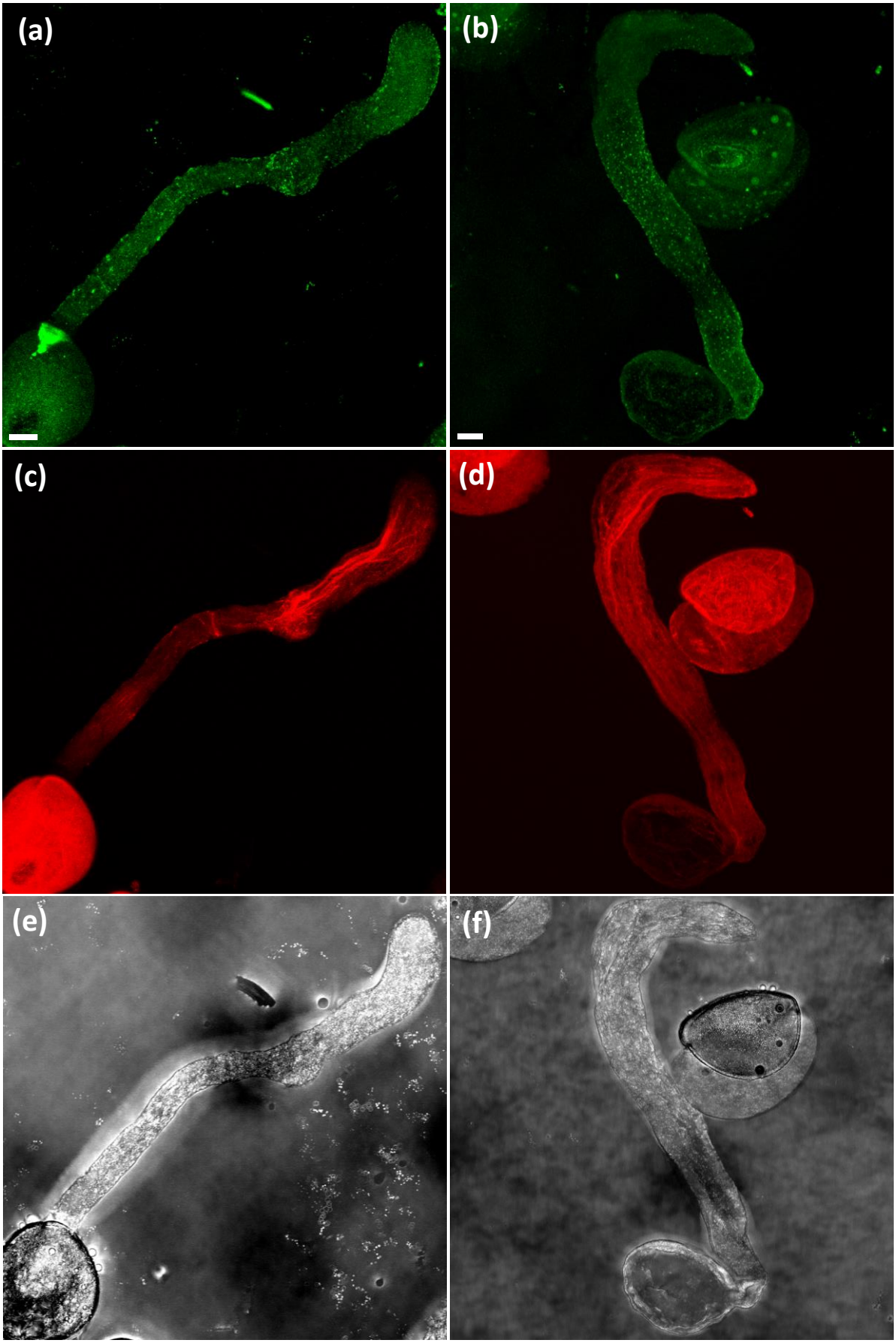

Figure 7.27: *In situ* Localisation of MAP7A in Narcissus Pollen Tubes. (a) and (b): subcellular localisation of MAP7A visualised using anti-MAP7A primary antibodies recognised by FITC-conjugated anti-mouse IgG secondary antibodies. (c) and (d): actin cytoskeleton labelled with the F-actin stain, rhodamine-phalloidin in the same cells. (e) and (f): brightfield images of the same cells. Scale bar: 10 µm.

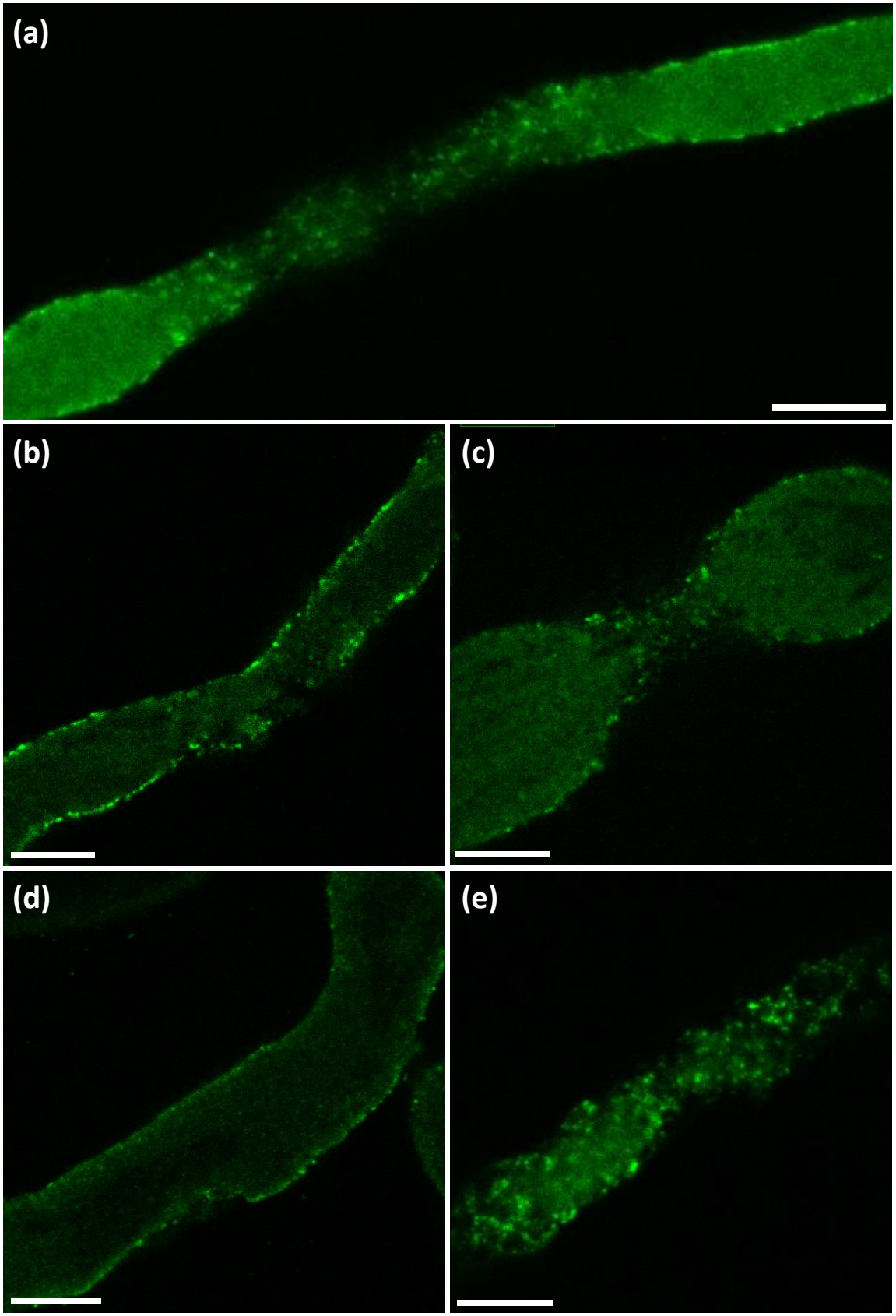

Figure 7.28: High-Magnification Images of MAP7A Localisation at the Plasma Membrane of Narcissus Pollen Tubes. MAP7A visualised using anti-MAP7A primary antibodies, detected by FITC-conjugated anti-mouse IgG secondary antibodies. (a) and (c): single Z-planes showing cortical and medial cross-sections of pollen tubes. (b) and (d): single Z-plane showing medial cross-section of pollen tubes. (e): pollen tube cortex. Scale bar: 10µm.

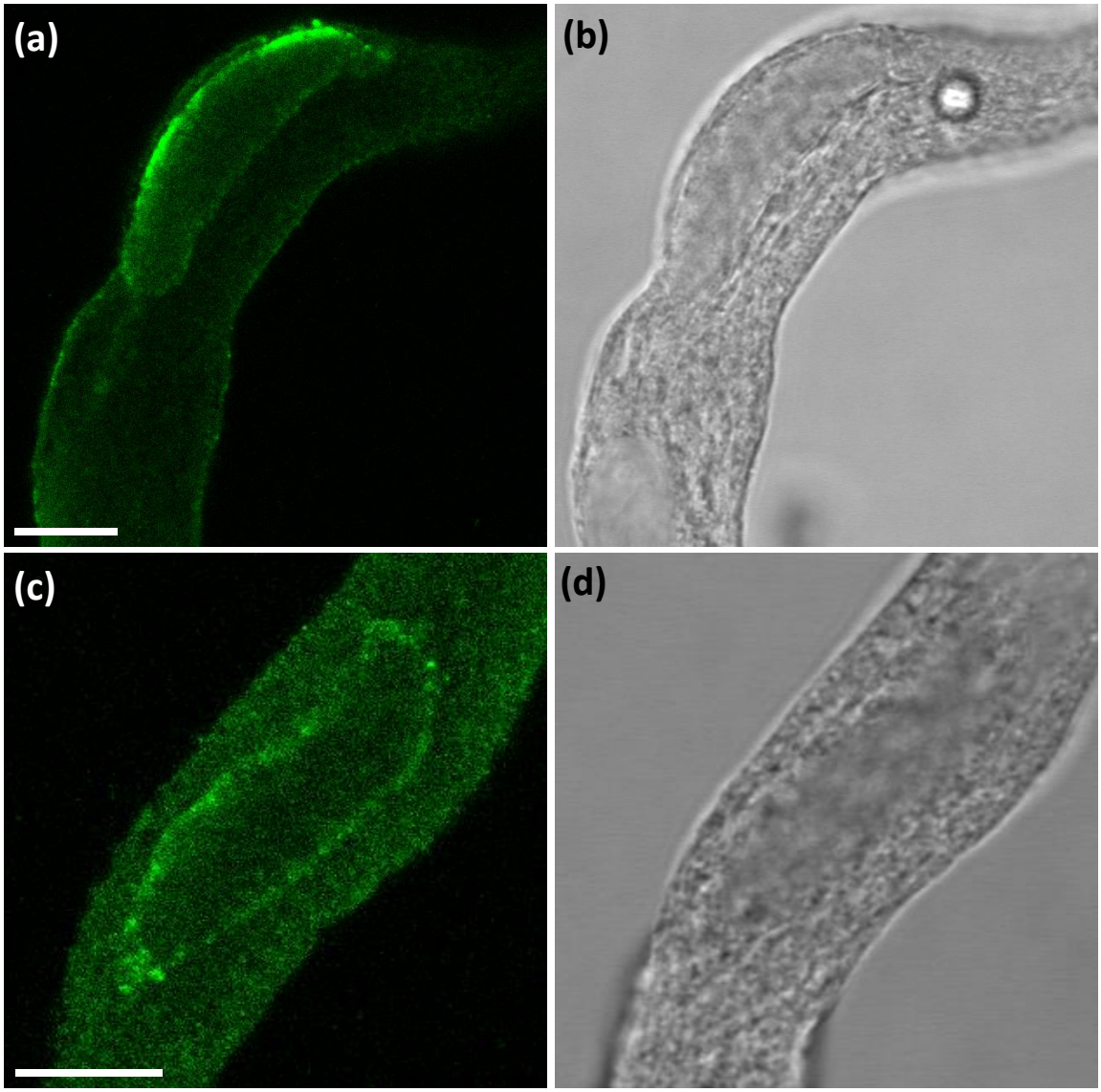

Figure 7.29: Localisation of MAP7A to the Generative Cell Nucleus of Narcissus Pollen Tubes. (a) and (c): MAP7A visualised using anti-MAP7A primary antibodies, detected by FITC-conjugated anti-mouse IgG secondary antibodies. (b) and (d): corresponding brightfield images of the same pollen tubes. Scale bar: 10 µm.

7.5.3.4. *In situ* Co-localisation of MAP7A with Microtubules at the Generative Cell of Narcissus Pollen Tubes.

In section 7.3, it was demonstrated that MAP7A is able to associate with microtubules *in vivo*. To investigate whether MAP7A may associate with microtubules in germinated pollen tubes, co-visualisation of MAP7A alongside microtubules was performed in Narcissus pollen tubes using immunofluorescence. Narcissus pollen tubes were fixed and permeablised as described above, and co-incubated with anti-MAP7A, and rat YL1/2 anti-tubulin antibodies at dilutions of 1:300 and 1:200 respectively. Visualisation of anti-MAP7A and anti-tubulin primary antibodies was performed by labelling with anti-mouse IgG FITC-conjugated

secondary antibodies, and anti-rat IgG TRITC-conjugated secondary antibodies at dilutions of 1:50. Therefore, MAP7A was indirectly labelled with FITC, and microtubules with TRITC, allowing separate visualisation of each antigen. Staining of the pollen tube nuclei was also performed using the nucleic acid stain, DAPI.

Figure 7.30 and 7.31 shows the localisations of MAP7A, microtubules and nuclei in the immunostained pollen tubes. Microtubule staining was clearly observable at one of the two nuclei in Narcissus pollen tubes, identifiable as the generative cell (GC) by the presence of the observed microtubule cage, which characteristically encircles the nucleus of the GC, but is absent from the vegetative cell (VC; Joos et al. 1994; Yu and Russel. 1993). Staining of microtubules was not apparent elsewhere in the pollen tube or grains. Cortical microtubule networks have reportedly been observed in the pollen tubes of angiosperms such as maize and *Nicotiana* (Joos et al. 1994; Kliwer and Dresselhaus 2010): it could be that the microtubules of the GC, which are reportedly more stable to depolymerisation than cortical microtubules (Joos et al. 1994; Kliwer and Dresselhaus 2010), were able to withstand the fixation process used, whereas cortical microtubules were not.

MAP7A was observed to localise to the GC in Narcissus pollen tubes, accounting for the observed subcellular localisation described in figure 7.29, but did not seem to associate with the VC. At the generative cell nucleus, MAP7A appeared to co-localise with microtubules. This co-localisation seemed most prominent at the external, or cytoplasmic, face of the GC microtubule cage; apparently encircling the microtubule cage itself. The observed co-localisation of MAP7A with microtubules *in situ* corroborates the observed microtubule-binding activity of MAP7A described in section 7.3, and suggests a direct association of MAP7A with the GC microtubules, providing evidence of MAP7A microtubule-binding activity *in situ*.

During this procedure, preservation of the actin, and GC microtubule arrays was clearly possible, however cortical microtubule arrays were not observed. It is possible that the MAP7A punctae observed at the PM in figure 7.28 also co-localise with and bind microtubules, but this could not be observed without visualisation of cortical microtubule arrays. Fixation and observation of cortical microtubules in Narcissus pollen tubes would help to provide useful information as to the nature of MAP7A punctae at the plasma membrane.

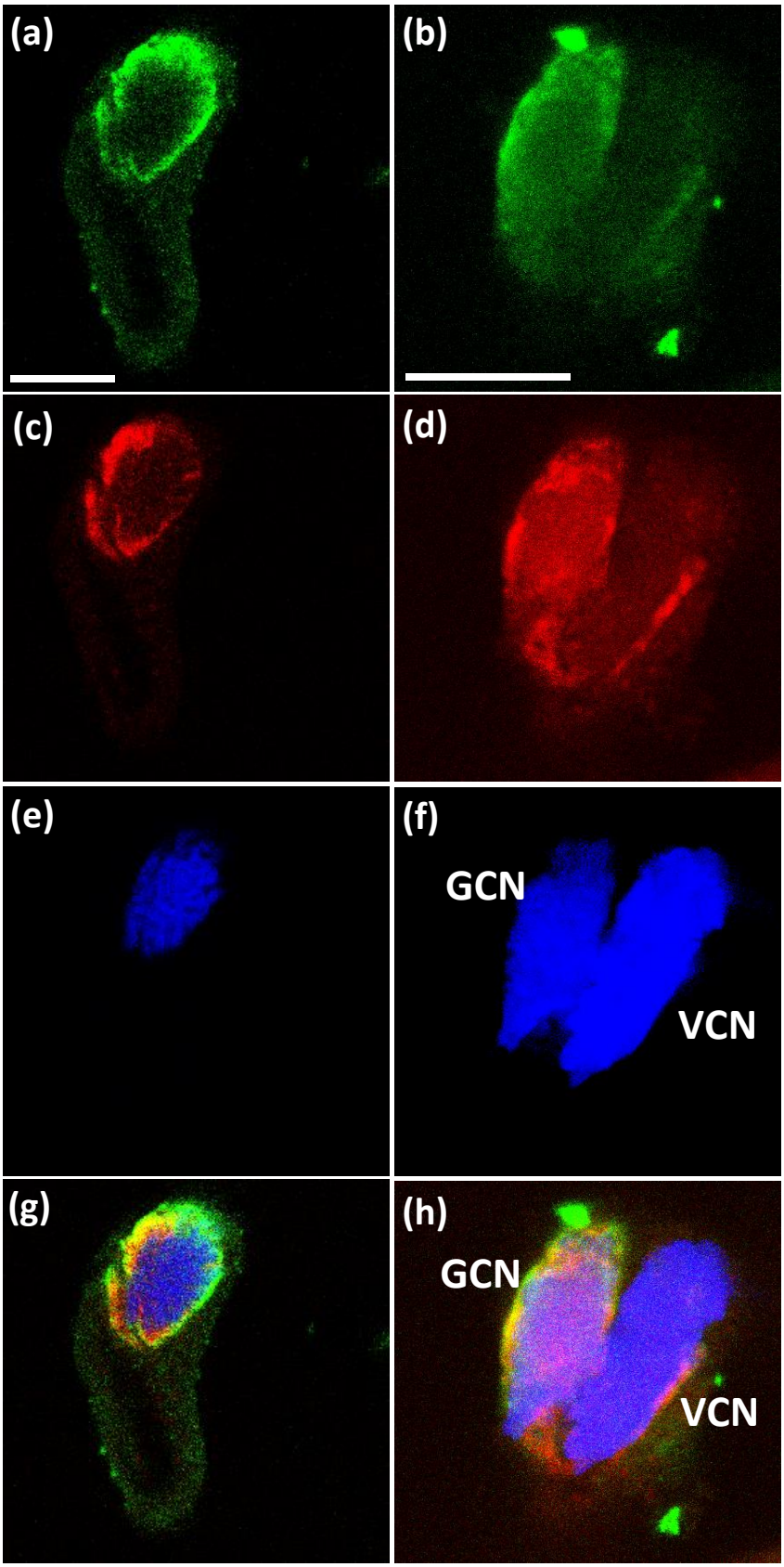

Figure 7.30: Co-localisation of MAP7A with Microtubules at the Generative Cell Nucleus of Narcissus Pollen Tubes. (a) and (b): MAP7A visualised with mouse anti-MAP7A primary antibodies, detected with FITC-conjugated anti-mouse IgG secondary antibodies. (c) and (d): microtubules visualised with rat anti-tubulin primary antibodies detected by TRITC-conjugated anti-rat IgG secondary antibodies. (e) and (f): DAPI-staining of cell nuclei. (g) and (h): merge of (a),(c) and (e), and (b),(d) and (f) respectively. GCN: generative cell nucleus. VGN: vegetative cell nucleus. Scale bar: 10 µm.

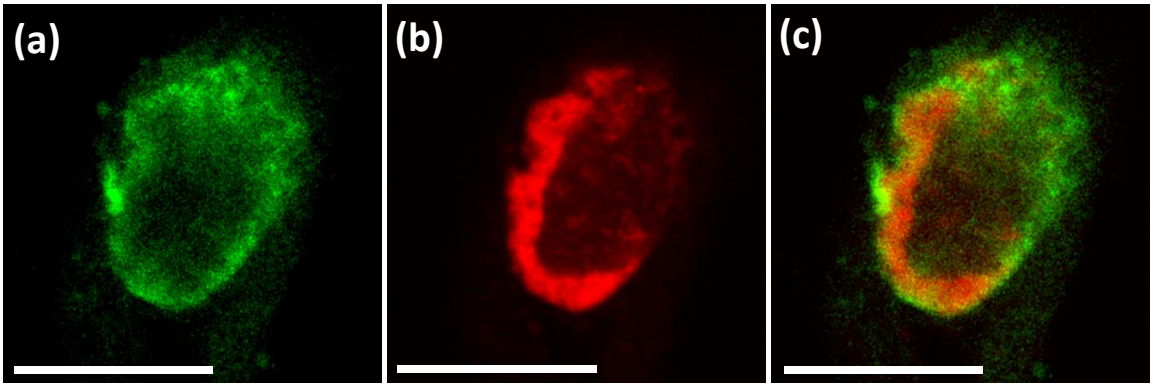

Figure 7.31: MAP7A Localises to the Periphery of the Generative Cell Microtubule Cage. (a): MAP7A visualised with mouse anti-MAP7A primary antibodies, detected with FITC-conjugated anti-mouse IgG secondary antibodies. (b): microtubules visualised with rat anti-tubulin primary antibodies, detected by TRITC-conjugated anti-rat IgG secondary antibodies. (c): merge of (a) and (b). Scale bar: 10 µm.

7.5.4. Summary.

This section details the experiments used to characterise the expression patterns of the MAP7 protein family, and the subcellular localisation of MAP7A *in situ*.

By visualising GUS-staining in *pMAP7A:GUS* and *pMAP7B:GUS*, the transcriptional expression profiles of MAP7A and MAP7B were characterised. MAP7A expression was observable only in floral tissue, specifically localised to the pollen of analysed plants. MAP7B expression in Arabidopsis floral tissue appeared highly similar to that of MAP7A, with GUS staining detected specifically in pollen grains. The transcriptional activity of MAP7A and MAP7B detected in pollen grains seemed to increase throughout grain maturation, with progressively more intense staining observable in older floral buds. In addition to this, MAP7B transcriptional activity was prominent in the root vasculature, whereas no MAP7A expression was observable, indicating the root tissue to be a zone of MAP7B-specific expression.

Having determined the expression patterns of the MAP7 protein family, the subcellular localisation of MAP7A was investigated *in situ*. Polyclonal antibodies were raised to full-length MAP7A, and their specificity validated. Following this, immunofluorescent staining was employed to visualise the localisation of MAP7A in Narcissus pollen tubes. It could be observed that MAP7A localised to discreet foci at the plasma membrane of pollen tubes, and could also be seen to form punctae at

the periphery of the generative cell of germinated tubes. Co-labelling of MAP7A and tubulin permitted visualisation of the co-localisation between MAP7A and the microtubule cage of the generative cell, with MAP7A appearing to encircle the microtubule cage at its outermost face.

It has been demonstrated that the MAP7 protein family associates with microtubules *in vivo*. This section describes the tissue-specific locations of MAP7 expression and details *in situ* examples of MAP7A association with microtubules in these tissues, specifically at the microtubule cage of the generative cell of germinated pollen tubes. Given that the expression of both MAP7A and MAP7B increases during pollen maturation, it could be likely that these proteins may function in germinating pollen grains or germinated pollen tubes. Roles for the microtubule cytoskeleton have been speculated in the regulation of pollen tube growth, and of particular interest, in nuclear division and transport (chapter 1.6.2 and 1.6.3). It is possible that MAP7A, being localised to the GCN of pollen tubes, may play an important role in co-ordinating pollen cell division, nuclear transport or tube growth. Therefore, the next chapter investigates the potential roles of the observed associations of MAP7 proteins with the microtubule cytoskeleton using reverse-genetic analysis.

7.6. Functional Analysis of Arabidopsis MAP7s Using Reverse Genetic Analysis.

7.6.1. Introduction.

Thus far, characterisation of the Arabidopsis MAP7 proteins has revealed the expression patterns, subcellular localisation and microtubule-binding activity of MAP7A. In this section, reverse-genetic analysis of the MAP7 protein family was performed to elucidate the function of MAP7A and MAP7B in Arabidopsis. This section describes the identification and validation of *map7a* and *map7b* T-DNA mutant lines and the generation of *map7a*/*map7b* double mutants, on which phenotypic analysis could be performed.

7.6.2. Analysis of *map7* Mutant Lines.

7.6.2.1. Analysis of Available *map7a* and *map7b* T-DNA Mutant Lines.

As described in chapter 3.2.2, The SIGnAL T-DNA Express Arabidopsis Gene Mapping Tool was used to identify mutant lines with T-DNA insertions lying in the MAP7A and MAP7B genes. Table 7.7 displays a summary of promising T-DNA mutant lines of *MAP7A* and *MAP7B*, along with the primers used to genotype them. Schematics of the T-DNA alleles and genotyping primer annealing sites are shown in figure 7.32.

For *MAP7A*, two T-DNA lines were selected for analysis. The first, SALK_069232, contains a T-DNA insertion located in the second exon of the *MAP7A* coding sequence, and was deemed very likely to disrupt MAP7A expression, as is characteristic of T-DNA insertions lying in gene exons (Wang. 2008). The second T-DNA insertion line, GABI_488G06, resides in the 3' untranslated region (3' UTR) of *MAP7B*, 36 bp after the stop codon. It is known that T-DNA insertions located downstream of gene stop codons are much less likely to result in altered transcript levels compared to those in exons, and promoter regions, but still have the potential to reduce or abolish transcription. Therefore, the GABI_488H06 T-DNA line was selected for further analysis. Henceforth, SALK_069232 was referred to as *map7a.1*, and GABI_488H06 was *map7a.2*.

One T-DNA allele of *MAP7B,* SALK_063967, was selected for analysis. SALK_063967 contains a T-DNA insertion lying in the second exon of *MAP7B* and was deemed highly likely to disrupt transcription. SALK_063967 was henceforth referred to as *map7b.1*.

Having identified promising T-DNA mutant lines that were likely to be transcriptional null knockouts of *MAP7A* and *MAP7B*, PCR genotyping was performed to identify homozygous plants for each T-DNA allele.

MAP7A

SALK_069232
(*map7a.1*)

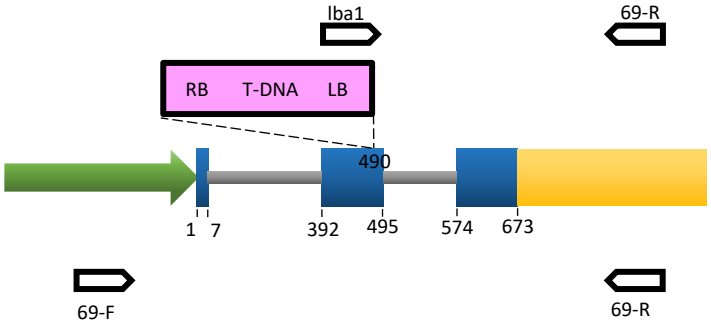

GABI_488H06
(*map7a.2*)

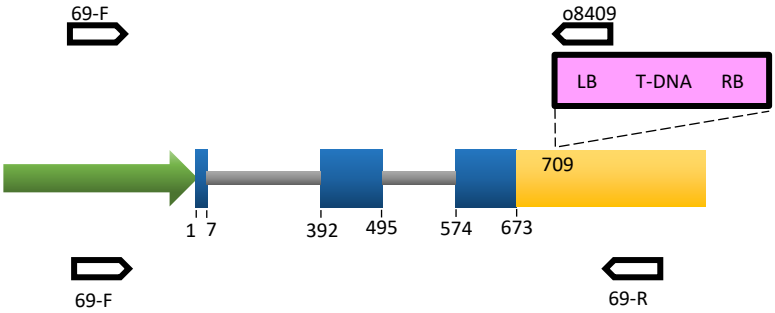

SALK_063967
(*map7b.1*)

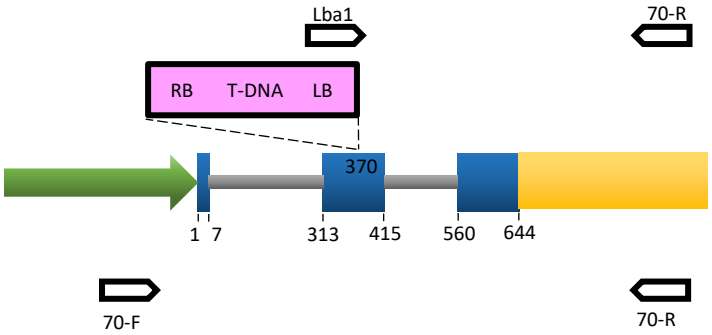

Figure 7.32: Schematic Diagram of T-DNA Mutant Alleles Selected for Analysis, Including Positions of the T-DNA Insertion Sites and Primers Used for Genotyping. Promoter regions are shown in green, exons in blue, introns in grey and the 3' UTR in yellow. The T-DNA insertions are represented by the pink box, labelled with the left border (LB) and right border (RB). Primers used for genotyping are represented by white arrows, with insert-specific primers above, and gene-specific primers below the gene. Numbers below the gene diagram correspond to base pairs after the start codon.

Mutant Line	T-DNA Allele	Insert Position	Insertion Type	Primers for Insert PCR	Insert PCR Size (bp)	Primers for WT PCR	WT PCR Size (bp)
MAP7A							
map7a.1	SALK_069212	490 bp	exon	Lba1 + 69-R	1112 bp	69-F + 69-R	1031 bp
map7a.2	GABI_488G06	709 bp	3' UTR	o8409 + 69-F	816 bp	69-F + 69-R	1031 bp
MAP7B							
map7b.1	SALK_063967	370 bp	exon	Lba1+ 70-R	1069 bp	70-F + 70-R	1056 bp

Table 7.7: Details of *map7a and map7b* T-DNA Insertion Mutants Selected for Analysis. Included are the locations of the T-DNA insertions for each mutant, the primers used for PCR genotyping and the expected sizes of insert and WT PCR bands.

7.6.2.2. Identification of Homozygous *map7a*, and *map7b* T-DNA Mutants, and Generation of *map7a/map7b* Double Mutants.

Having identified T-DNA insertion lines that were likely to result in disrupted transcription of *MAP7A* and *MAP7B*, PCR genotyping was performed to identify plants homozygous for identified T-DNA alleles (as described in chapter 3.2.3). Genomic DNA was extracted from Col-0 and T-DNA mutants, and PCR genotyping was performed using the primers listed in table 7.7 and displayed in figure 7.32.

Figure 7.33 shows examples of insert PCRs performed on gDNA extracted from homozygous T-DNA mutants using the primers listed in table 7.7. The SALK_069212 T-DNA insertion was demonstrated to be present in the *map7a.1* mutant by PCR amplification of a 1112 bp band using the T-DNA primer, Lba1, and the *MAP7A* gene-specific primer 69-R, which could not be amplified from Col-0 gDNA. *map7a.2* was shown to contain the GABI_488H06 T-DNA insert by amplification of an 816 bp band using the T-DNA primer o8409, and the *MAP7A* gene-specific primer, 69-F. *map7b.1* was shown to carry the SALK_063967 T-DNA insert by PCR amplification of a 1069 bp band using the T-DNA primer Lba1 and the *MAP7B* gene-specific primer 70-R.

Having identified plants carrying the T-DNA insertions of interest, WT-PCRs were performed to identify plants homozygous for the T-DNA alleles, using the primers listed in table 7.7. *map7a.1* and *map7a.2* were both genotyped using the primers 69-F and 69-R, which were able to amplify a band of 1031 bp from Col-0 gDNA. No such band could be amplified from the gDNA of *map7a.1* and *map7a.2* plants, indicating that they did not contain the WT *MAP7A* allele, and were homozygous for the SALK_069212 and GABI_488G06 T-DNA alleles respectively. WT-PCR was performed on *map7b.1* mutant gDNA using the primers 70-F and 70-R. PCR-amplification of a 1056 bp band was observable from Col-0 gDNA, but not from *map7b.1*, indicating that the *map7b.1* plants were homozygous for the SALK_063967 allele.

Having identified homozygous plants for *map7a.1*, *map7a.2*, and *map7b.1*, *map7a/map7b* double mutants were generated to knock out both *MAP7A* and *MAP7B* expression in Arabidopsis. It is known that the disruption of one gene may be compensated for by that of a closely related family member. Therefore, disruption of multiple members of a gene family may be necessary to elicit a phenotype through reverse genetics. Cross-pollination of *map7a.1* and *map7b.1* homozygous plants was performed as described in chapter 2.6.3 to generate *map7a.1/map7b.1* double mutant T-DNA lines. Following cross-pollination, the resulting F1 seeds were collected and germinated. Insert PCR was performed to identify individual plants conveying both SALK_069212 and SALK_063967 T-DNA alleles, which were permitted to self-pollinate. F2 seed collected from these plants was germinated and PCR genotyping was performed to identify individual plants homozygous for SALK_069212 and SALK063967; constituting *map7a.1*/*map7b.1* double mutants. Example insert and WT-PCRs of *map7a.1/map7b.1* homozygotes are shown in figure 7.34 and 7.35.

Having identified homozygous plants of the *map7a.1*, *map7a.2*, *map7b.1* and *map7a.1/map7b1* mutant lines, RT-PCR was performed to determine whether transcription of the mutant alleles had been disrupted.

7.6.2.3. Transcriptional Analysis of *MAP7A* and *MAP7B* in *map7a.1*, *map7a.2* and *map7b.1* and *map7a.1/map7b.1* T-DNA Mutant Lines.

Having identified homozygous *map7a* and *map7b* T-DNA insertion lines, RT-PCR was performed to analyse the transcriptional activity of the mutant T-DNA alleles in each mutant line.

As described in chapter 2.2.7, RNA was extracted from whole inflorescences of Col-0, *map7a.1*, *map7a.2*, *map7b.1*, and *map7a.1/map7b.1* plants, and cDNA was generated using 1µg RNA with the GoScript Reverse Transcriptase System using oligo(dT)15 primers.

The primers used for RT-PCR analysis of the *map7* T-DNA mutants, their relative annealing sites and predicted amplicon lengths are detailed in table 7.8, and figure 7.35.

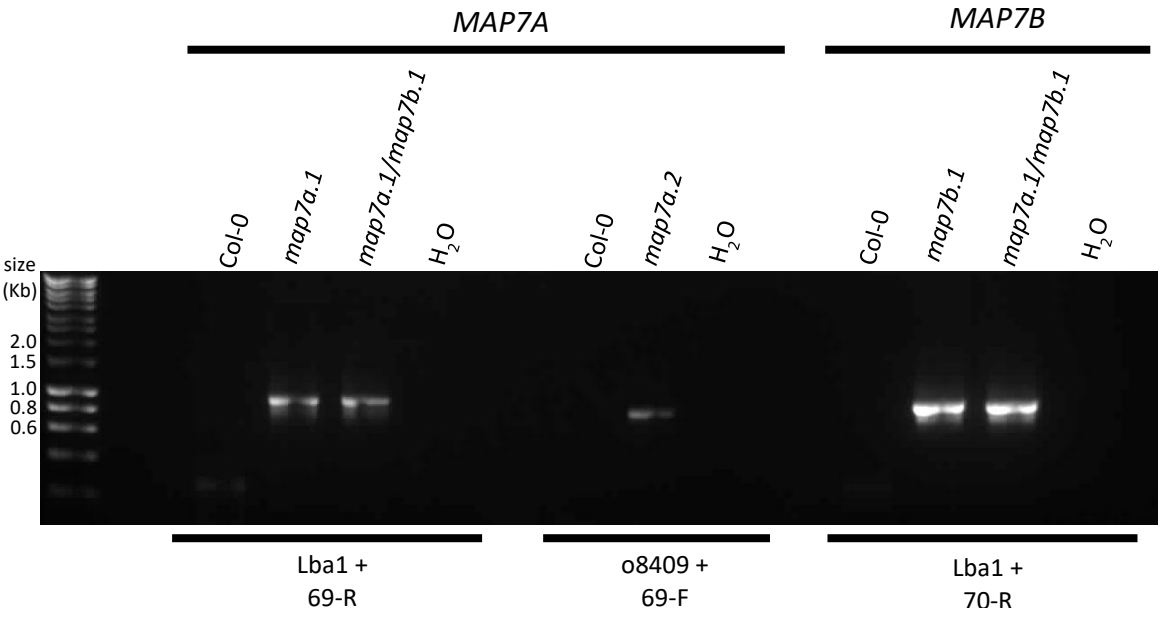

Figure 7.33: Example Insert PCR Reactions Performed to Genotype *map7a* and *map7b* T-DNA Mutants. PCR reactions performed on genomic DNA extracted from homozygous T-DNA mutant lines and Col-0 plants. The insert-specific primers used to amplify the insert band are stated below the gel. Bioline DNA Hyperladder I was used as a molecular weight marker.

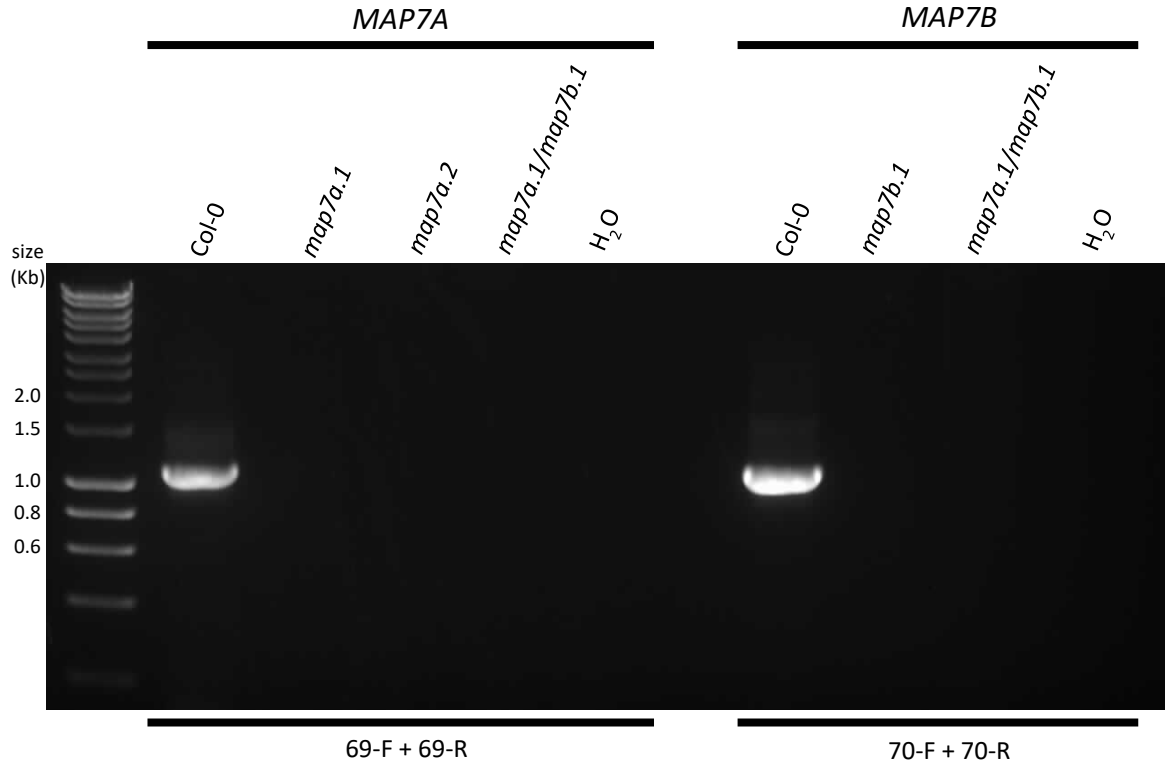

Figure 7.34: Example WT PCR Reactions Performed to Genotype *map7a* and *map7b* T-DNA Mutants. PCR reactions performed on genomic DNA extracted from homozygous T-DNA mutant lines and Col-0 plants. The gene-specific primers used to amplify the WT band are stated below the gel. Bioline DNA Hyperladder I was used as a molecular weight marker.

For RT-PCR analysis of *map7a.1*, amplification of target sequences in the *MAP7A* transcript, upstream and downstream of the T-DNA insertion site were performed, as well as across the T-DNA insertion site itself. *MAP7A* transcriptional analysis was performed on the *map7a.1* single mutant and *map7a.1/map7b.1* double mutant. During RT-PCR analysis of the *map7a.2* T-DNA allele, only amplification of the transcript sequence upstream of the T-DNA insertion site was performed, as the T-DNA insertion lies in the 3' UTR. Transcriptional analysis of *MAP7B* was performed on *map7b.1* single and *map7a.1/map7b.1* double mutants. RT-PCR amplification of target sequences within the *MAP7B* transcript was performed upstream of, downstream of, and across the T-DNA insertion site. As a positive control, amplification of a 187 bp sequence of the housekeeping gene EF-1α was performed to ensure equal quantities of cDNA template were used per PCR reaction.

The results of the RT-PCR analysis are shown in figure 7.36. Firstly, it was ascertained that the *map7a.1* T-DNA line was a transcriptional null. RT-PCR of *MAP7A* transcript-specific sequences upstream, downstream and across the T-DNA insertion site generated amplicons of predicted size using Col-0 cDNA, but no PCR product was generated from the cDNA of *map7a.1* or *map7a.1/map7b.1* mutants. This indicates total disruption of *MAP7A* transcription in these lines.

It was then determined that the transcriptional activity of *map7b* was also disrupted in the *map7b.1* single and double mutant lines. RT-PCR analysis could detect no amplicon of predicted size from primers designed to amplify across the T-DNA insertion site and upstream of the insertion site, indicating that transcription of these target sequences was disrupted. However, amplification of a PCR product of predicted size was observed using the downstream primer sets. Therefore, it seems that *MAP7B* transcript sequences downstream of the T-DNA insertion sites are still present in the *map7b.1* and *map7a.1*/*map7b.1* mutants. It is probable that the transcription of this sequence may be driven by an element within the T-DNA itself, and the transcript would not be functional. Regardless, *MAP7B* transcription was disrupted upstream of the T-DNA insertion site, and the *map7b.1* and *map7a.1/map7b.1* mutants are defective in *MAP7B* transcription.

MAP7A

map7a.1

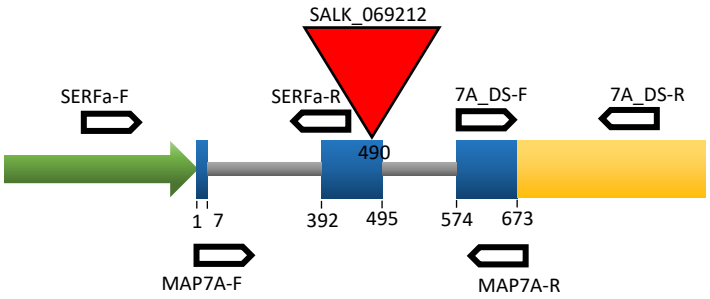

map7a.2

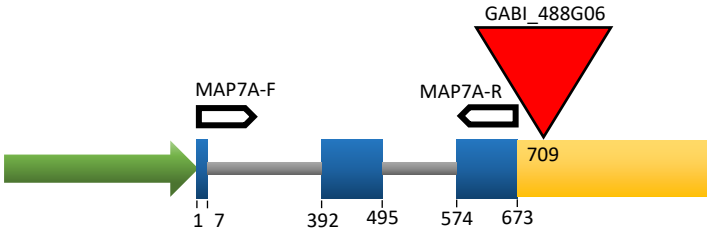

MAP7B

map7b.1

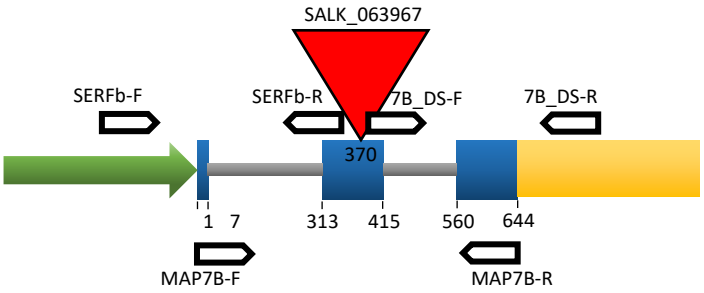

Figure 7.35: Schematic Diagram of *map7* T-DNA Mutant Alleles, Including Positions of Primers used for RT-PCR Analysis of Transcriptional Activity. Promoter regions are shown in green, exons in blue, introns in grey and the 3' UTR in yellow. The T-DNA insertions are represented by the red triangle. Primers used for genotyping are represented by white arrows, labelled with the identity of each specific primer. Numbers below the gene diagram correspond to base pairs after the start codon.

Gene	Mutant Line	Upstream Primers	Upstream Band Size	Flanking Primers	Flanking Band Size	Downstream Primers	Downstream Band Size
MAP7A	*map7a.1*	SERFa-F + SERFa-R (1)	102 bp	MAP7A-F + MAP7A-R (2)	207 bp	7A_DS-F + 7A_DS-R (5)	231 bp
	map7a.2	MAP7A-F + MAP7A-R (2)	207 bp	N/A	N/A	N/A	N/A
MAP7B	*map7b.1*	SERFb-F + SERFb-R (3)	145 bp	MAP7B-F + MAP7B-R (4)	210 bp	7B_DS-F + 7B_DS-R (6)	242 bp

Table 7.8: List of Primers used for RT-PCR Transcriptional Analysis of *map7a.1*, *map7a.2*, and *map7b.1* T-DNA Alleles. Upstream primers used to amplify PCR product from template sequences upstream of the T-DNA insert. Flanking primers amplify gene-specific sequences spanning the T-DNA insertion site of the corresponding mutant. Downstream primers amplify sequences downstream up the T-DNA insertion site. Included are the predicted sizes of amplicons generated using each primer set. Numbers associated with each primer pair correspond to the amplified PCR products shown in figure 7.36. Diagrammatic details of the locations of each primer are displayed in figure 7.35, and sequences of each primer are shown in Appendix 1.

RT-PCR analysis of *map7a.2* indicated that the T-DNA line was transcriptionally active. PCR amplification of the full-length *MAP7A* coding sequence was performed: PCR product of the predicted size was clearly amplified from Col-0 cDNA, and was also abundantly amplified from the cDNA of *map7a.2*. It can therefore be concluded that the GABI_488H06 T-DNA insertion, located in the *MAP7A* 3' UTR, was not effective in disrupting gene transcription. Further analysis of *map7a.2* was subsequently abandoned.

In summary, two T-DNA mutants, *map7a.1* and *map7b.1* were confirmed to be transcriptionally disrupted by RT-PCR analysis. The transcription of both *MAP7A* and *MAP7B* was determined to be abolished in the *map7a.1/map7b.1* double mutant also. Further analysis of *map7a.2* was not performed. Having validated that the *map7a.1*, *map7b.1* and *map7a.1/map7b.1* mutants were transcriptionally defective, phenotypic analysis was performed to elucidate the functional roles of MAP7A and MAP7B in *Arabidopsis*.

7.6.3. Phenotypic Analysis of *map7* Mutants.

As described above, T-DNA mutants for *MAP7A* (*map7a.1*), and *MAP7B* (*map7b.1*) were identified, from which a *map7a.1/map7b.1* double mutant line was generated. Subsequently, phenotypic analysis was performed in order to identify a potential role for the MAP7 proteins in pollen.

Thus far, MAP7A and MAP7B have been characterised as pollen-expressed microtubule-binding proteins that appear to localise to the pollen tube plasma membrane and GCN. The microtubule cytoskeleton is known to play an important role in pollen grain development; regulating nuclear migration and cell division (Twell et al. 2011) and nuclear morphology and development (Zonia et al. 1999; Oh et al. 2010). In pollen tubes, microtubules have been reported to play roles in regulating pollen tube growth and morphology and in achieving successful fertilisation (Zhu et al. 2013; Gossot and Geitmann. 2007; Onelli et al. 2015). Furthermore, microtubules are reported to be important in nuclear transport and positioning in growing pollen tubes (Joos et al. 1994; Laitianen et al. 2002). To investigate whether MAP7A, or MAP7B may be involved in the regulation of these cytoskeletal processes, a battery

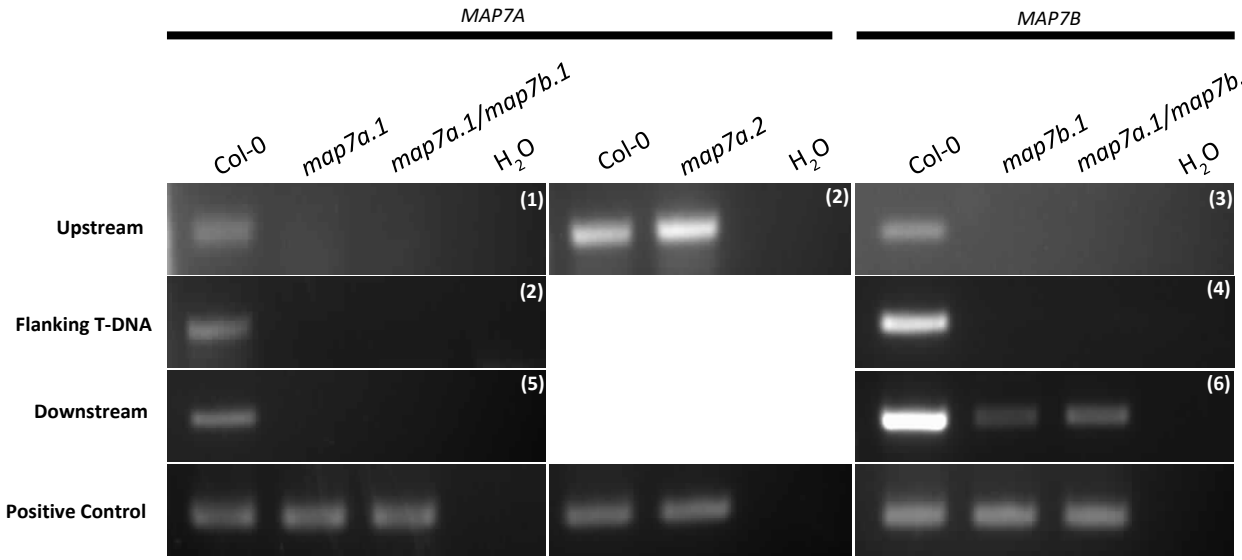

Figure 7.36: RT-PCR Analysis of the Transcriptional Activity of *MAP7A* in *map7a.1, map7a.2* and *map7a.1/map7b.1* T-DNA Lines, and *MAP7B* in *map7b.1* and *map7a.1/map7b.1* T-DNA Lines. Using gene-specific primers**,** bands were generated by PCR amplification of sequences upstream (top row), across (second row) and downstream (third row) of the T-DNA insertion site of each mutant. To ensure each cDNA sample contained similar quantities of cDNA template, amplification of a 187 bp sequence from the housekeeping gene, EF-1α, was performed (bottom row). Using each gene-specific primer set, RT-PCR was performed on Col-0 cDNA, the corresponding *map7* mutant cDNA, and deionised water as a negative control. The numbers in the top right-hand corner of each panel correspond to the specific primer pairs used to amplify the PCR product, as shown in table 7.8. The predicted sizes of the PCR products amplified are also shown in table 7.8.

of phenotypic analysis assays was performed on *map7a.1* and *map7b.1* single mutants, and *map7a.1/map7b.1* double mutants. Firstly, analysis of pollen grain development was performed using DAPI staining to determine whether the mutant lines may have failed to mature, and to identify potential defects in nuclear morphology and organisation. Analysis of the pollen grain germination efficiency, pollen tube morphology and growth rate was then performed to identify potential roles of MAP7A and MAP7B in pollen tube growth. Analysis of the potential roles of the MAP7 proteins in transport and organisation of the MGU in growing pollen tubes was assessed using of DAPI staining of *map7* mutant pollen tubes. Finally, analysis of potential fertilisation defects in the *map7* mutants was investigated by analysis of seed set in the *map7* mutant lines.

7.6.3.1. DAPI Staining of *map7* Mutant Pollen Grains.

DAPI staining of dehisced pollen grains from Col-0, *map7a.1, map7b.1* and *map7a.1/map7b.1* plants was performed as previously described in chapter 3.3.1. A minimum of 70 grains was analysed per line. As shown in figure 7.37, all pollen grains analysed from *map7a.1, map7b.1* and *map7a.1/map7b.1* plants had reached maturity, judging by the centrally organised vegetative and sperm nuclei, in identical fashion to pollen grains from Col-0 plants. This indicates that the *map7* mutant pollen grains were not defective in cell division. Likewise, the mutant pollen grains did not appear to have any noticeable defects in nuclear morphology or positioning. Based on this analysis, it must be concluded that MAP7A and MAP7B, themselves possess no essential function in regulating pollen grain development, cell division and nuclear morphology.

7.6.3.2. Analysis of Pollen Germination Efficiency in *map7* Mutants.

To investigate whether MAP7A or MAP7B may be involved in the regulation of pollen germination, *in-vitro* germination of Col-0, *map7a.1, map7b.1* and *map7a.1/map7b.1* plants was performed as described in chapter 2.5.2. The rate of pollen tube germination, (percentage grains to extend a pollen tube) was recorded after 24 hours of incubation in germination media.

As shown in figure 7.38, pollen grains from Col-0, *map7a.1, map7b.1* and *map7a.1/map7b.1* lines had all germinated at a high rate following 24 hours of incubation in germination media. Quantified analysis of pollen germination in each line using CLSM revealed little difference in the germination rates between Col-0 pollen and those of *map7a.1, map7b.1* and *map7a.1/map7b.1*, and no significant difference was identified using statistical analysis (appendix 2.4). Whilst the germination rate of Col-0 pollen was observed to be 44.9 ± 8.1 %, the germination rates of *map7a.1, map7b.1* and *map7a.1/map7b.1* mutant pollen was 51.9 ± 8.7 %, 54.5 ± 9.0 % and 54.5 ± 19.6 %, respectively. These differences in pollen germination rate were very slight, and it can be concluded that *map7* mutant pollen grains are not impaired in their ability to germinate. It is therefore unlikely that MAP7A and MAP7B, alone, are essential in the regulation of pollen germination.

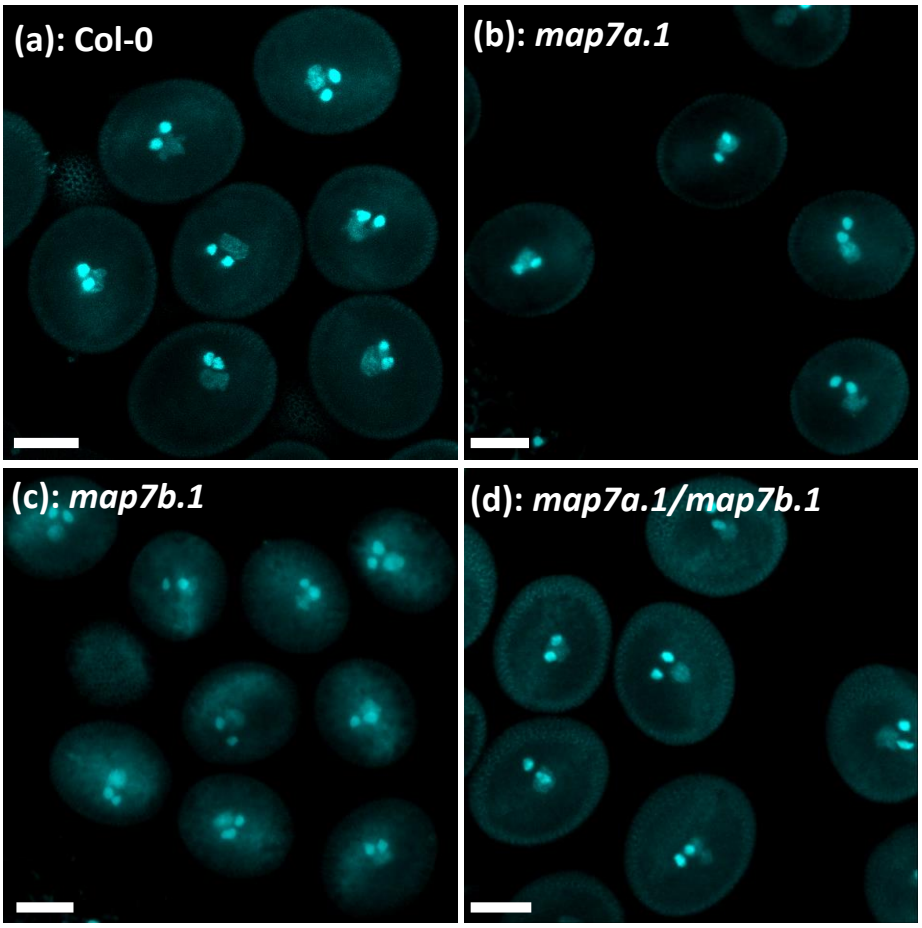

Figure 7.37: Analysis of *map7* Mutant Pollen Grain Development and Nuclear Morphology using DAPI staining of cell nuclei. DAPI-stained nuclei were visualised by CLSM using 405 nm excitation and 415 – 500 nm emission detection. (a): Col-0 pollen grains. (b): *map7a.1* pollen grains. (c): *map7b.1* pollen grains (d): *map7a.1/map7b.1* pollen grains. Scale bar: 10 µm.

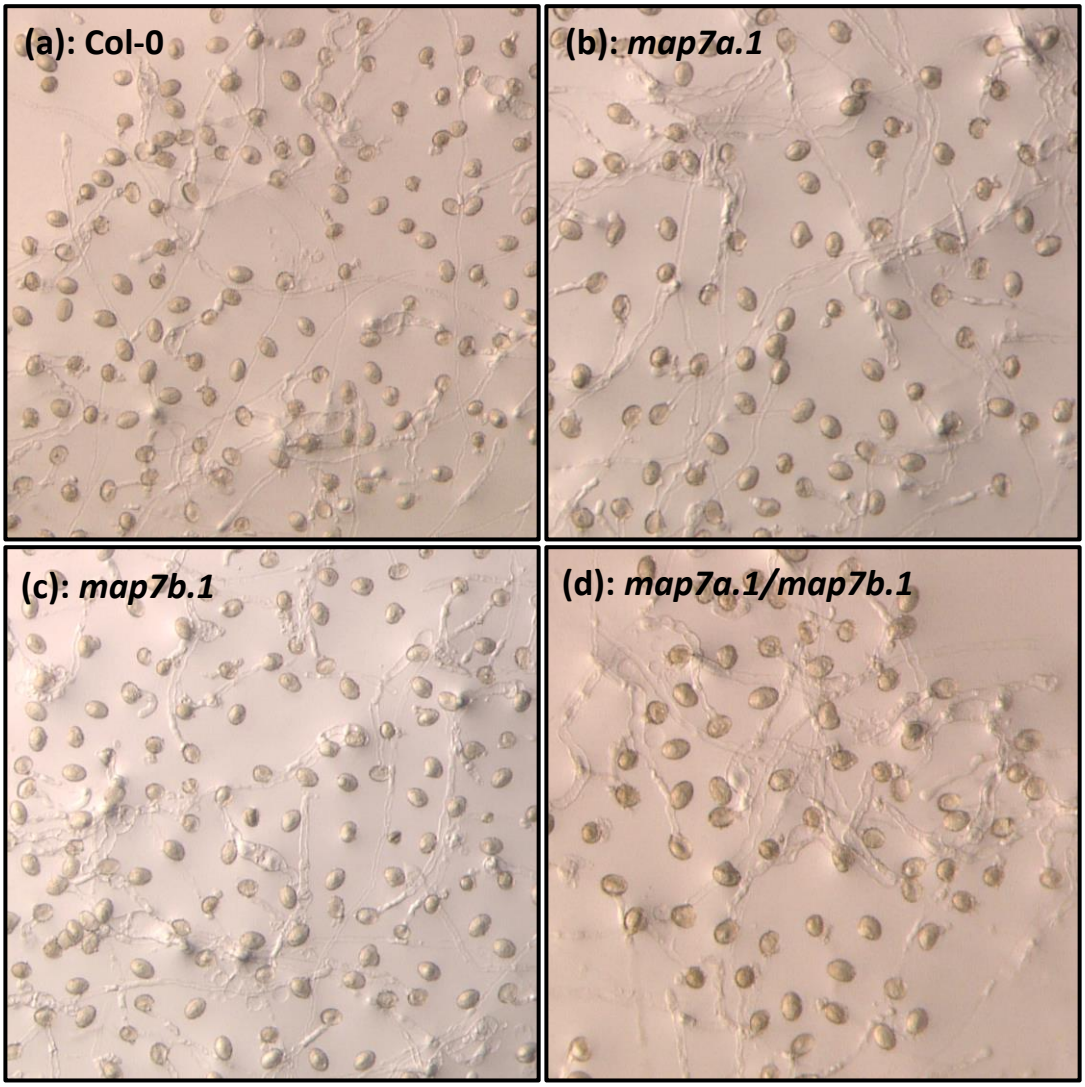

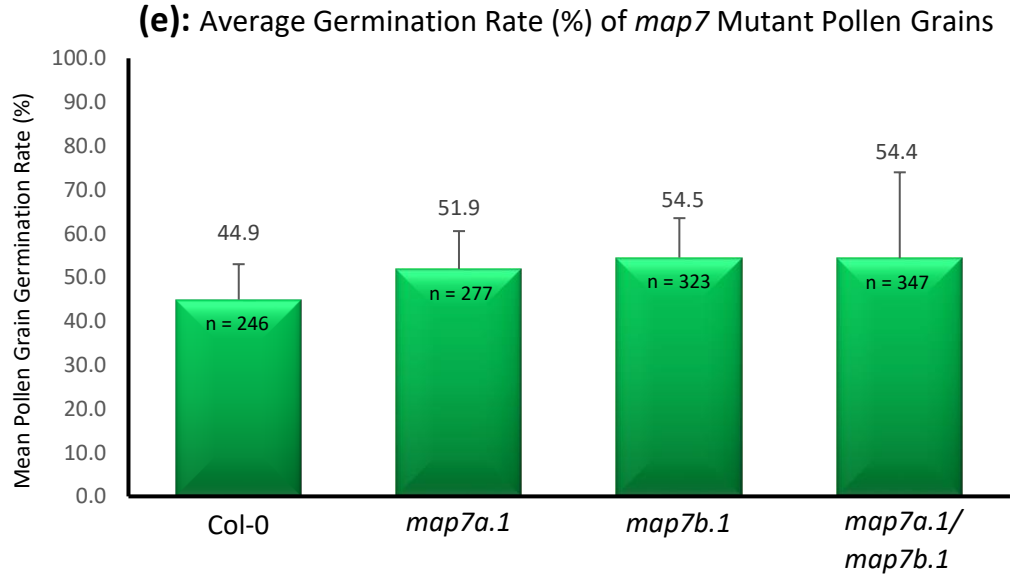

Figure 7.38: Germination of *map7* mutant Pollen Grains *in vitro*. Pollen grains of Col-0 plants and *map7a.1*, *map7b.2* and *map7a.1/map7b.1* mutants were germinated *in vitro* for 24 hours to assess their ability to germinate. Widefield images of germinated pollen from (a): Col-0, (b): *map7a.1*, (c): *map7b.1* and (d): *map7a.1/map7b.1* plants left to germinate for 24 hours. (e): chart represents the average germination rate (%) of pollen grains after 24 hours. n = number of pollen tubes analysed.

7.6.3.3. Phenotypic Analysis of *map7* Mutant Pollen Tubes.

The roles of MAP7A and MAP7B were then investigated in growing pollen tubes. Pollen from Col-0, *map7a.1, map7b.1* and *map7a.1/map7b.1* plants were germinated under SIV conditions as described in chapter 3.3.3. As shown in figures 7.39 and 7.40, pollen tubes of *map7a.1, map7b.1* and *map7a.1/map7b.1* mutants were able to grow under SIV conditions without major defects. Using time-lapse CLSM imaging, the growth of the mutant pollen tubes was analysed over time. It was determined that pollen tubes of *map7a.1* and *map7b.1* single mutants, and *map7a.1/map7b.1* double mutants extended at a slightly reduced rate to that of Col-0 pollen tubes. Pollen tubes from Col-0 plants were observed to grow at a rate of 2.29 ± 0.41 µm/min, whilst the growth rates of pollen tubes from *map7a.1, map7b.1* and *map7a.1/map7b.1* plants were 1.93 ± 0.28 µm/min, 1.99 ± 0.31 µm/min and 1.99 ± 0.34 µm/min respectively. There was determined to be a statistically significant difference between the growth rates of the *map7a.1*, *map7b.1* or *map7a.1/map7b.1* mutant pollen tubes compared to the Col-0 control (appendix 2.5), however this difference is materially small, and it is unlikely that MAP7A or MAP7B loss of function has a major impact on pollen tube growth rate.

The width of pollen tubes from *map7a.1*, *map7b.1* and *map7a.1/map7b.1* mutants was analysed, 5 µm behind the tip, in order to quantify potential morphological abnormalities such as swelling of the pollen tube tip, as a result of depolarised growth. The average pollen tube diameter appeared to be unaffected in the *map7* mutants compared to that of Col-0, which was determined to be 6 ± 0.66 µm. Similarly, the average widths of pollen tubes from *map7a.1, map7b.1* and *map7a.1/map7b.1* plants was found to be 5.96 ± 0.82 µm, 5.79 ± 0.86 µm and 6.07 ± 0.95 µm respectively, showing that the average pollen tube diameters were quite consistent between Col-0 plants and *map7* mutants. No statistically significant difference in pollen tube diameter was observed between *map7a.1, map7b.1* or *map7a.1/map7b.1* mutant plants and the Col-0 control (appendix 2.6). The *map7a.1, map7b.1* and *map7a.1/map7b.1* mutant pollen tubes were therefore not deemed to be morphologically defective.

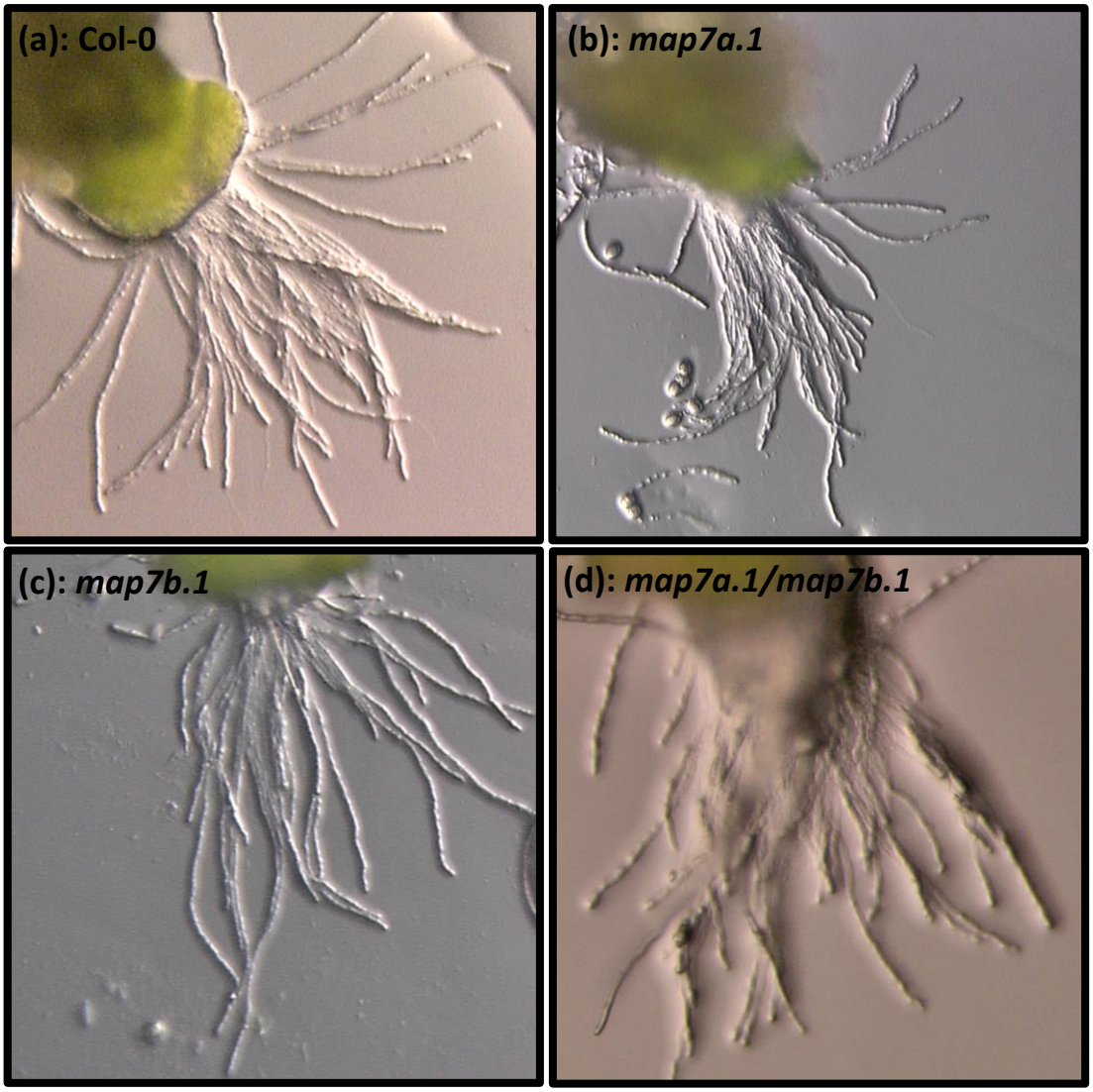

Figure 7.39*: Semi-in vivo* Germination of *map7* Mutant Pollen. Pollen grains of Col-0, *map7a.1*, *map7b.1* and *map7a.1/map7b.1* plants were germinated under semi-*in vivo* conditions. Widefield images of SIV-germinated pollen tubes from (a): Col-0, (b): *map7a.1* (c): *map7b.1,* (d): *map7a.1/map7b.1* plants growing from excised pistils.

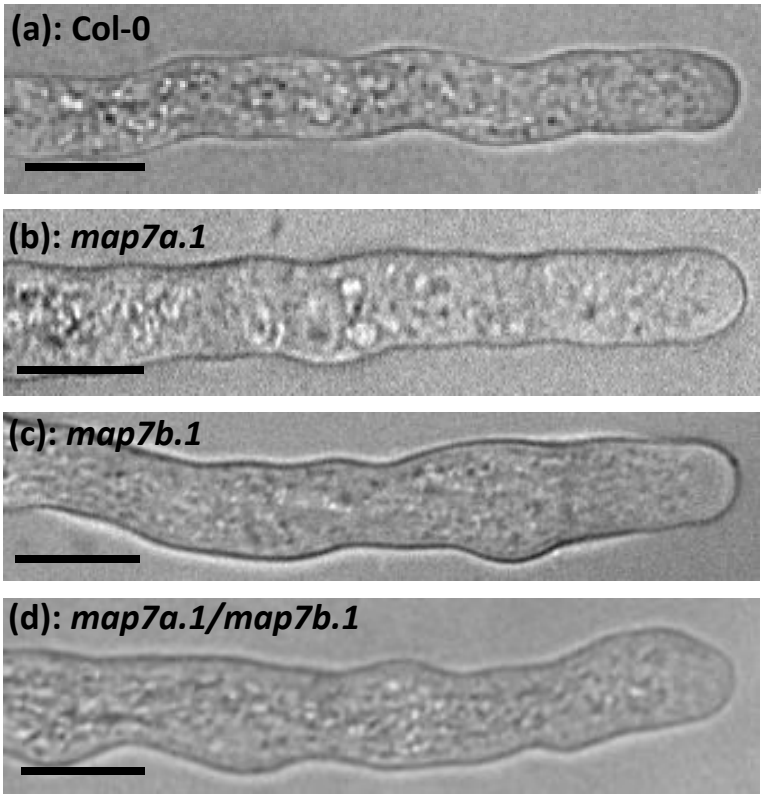

Figure 7.40*:* Example Pollen Tubes from *map7* Mutant Plants. Brightfield images of growing pollen tubes from Col-0 plants and *map7a.1, map7b.1, map7a.1/map7b.1* mutants acquired using CLSM. Scale bar: 10 µm.

7.6.3.4. DAPI Staining of *map7* Mutant Pollen Tubes.

The microtubule cytoskeleton has been implicated in facilitating the transport of the MGU in growing pollen tubes, and maintaining organisation and polarity of the vegetative and sperm nuclei. To investigate as to whether MAP7A and MAP7B may be involved in the regulation of nuclear transport and organisation in growing pollen tubes, DAPI staining of *map7* mutant pollen tubes was performed to visualise the pollen tube nuclei and identify potential defects in the MGU organisation.

Pollen of Col-0, *map7a.1, map7b.1* and *map7a.1/map7b.1* plants was germinated *in vitro* in liquid pollen germination medium (chapter 2.5.2.1.) Light fixation of pollen tubes was performed using 100 µM MBS ester in PEM buffer to preserve the pollen tubes during the staining procedure. Pollen tubes were stained with 0.4 µg/ml DAPI in PBS as described in chapter 2.5.8.

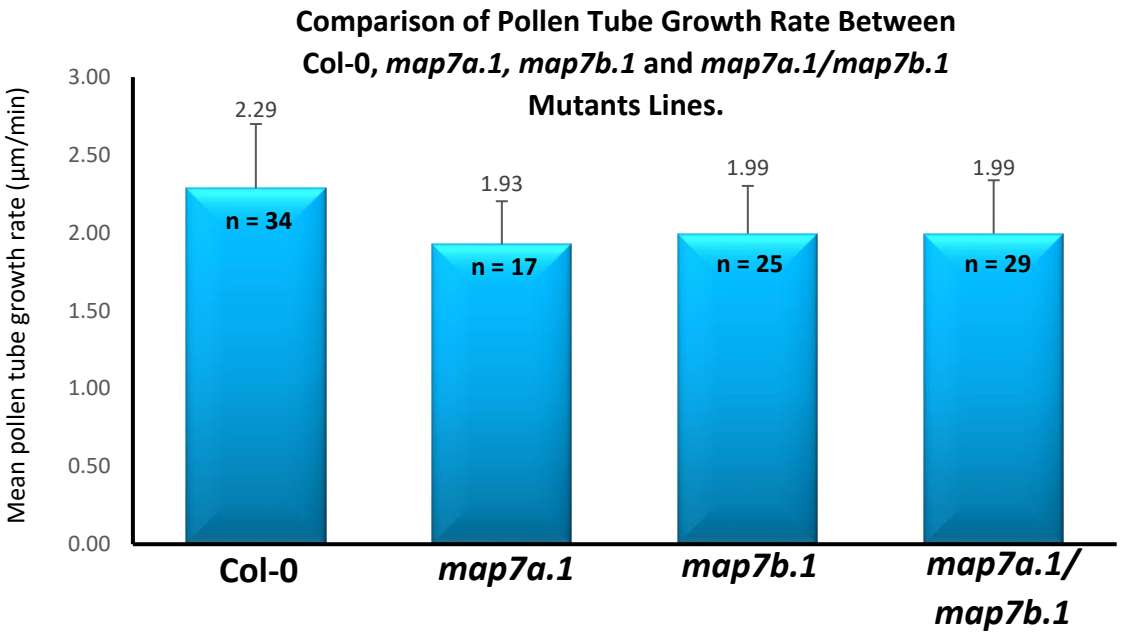

Figure 7.41*:* Quantitative Analysis of Pollen Tube Growth Rate of *map7* Mutants. Pollen grains of Col-0 plants and *map7a.1*, *map7b.1, map7a.1/map7b.1* mutants were germinated under semi-*in vivo* conditions. Time-lapse imaging using CLSM was used to acquire brightfield images of growing pollen tubes at regular intervals, in order to visualise the growth of pollen tubes over time (µm/min). n = number of pollen tubes analysed.

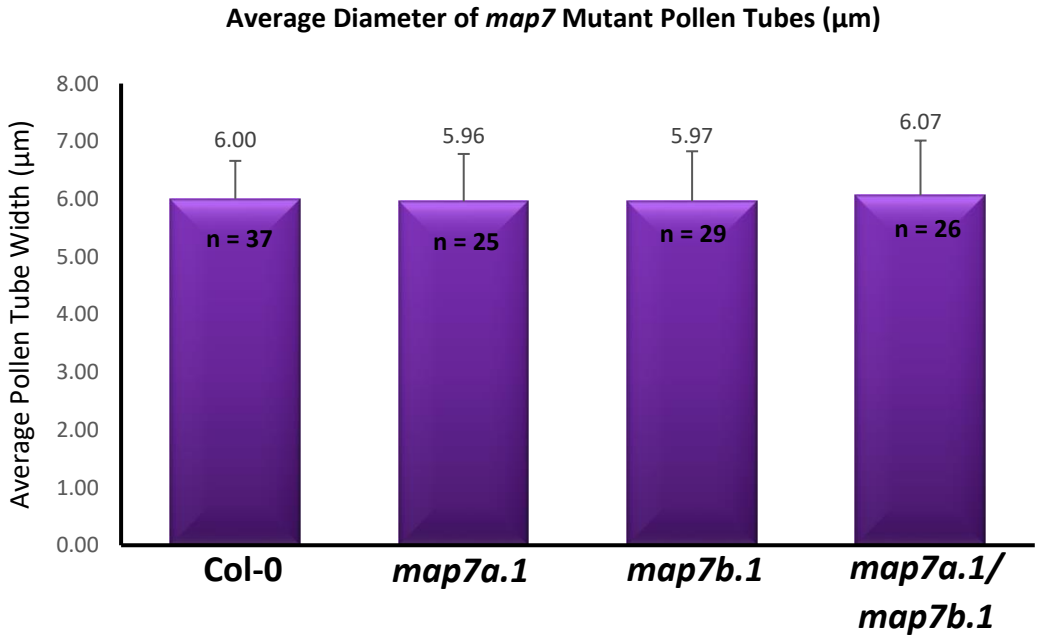

Figure 7.42: Quantitative Analysis of *map7* Mutant Pollen Tube Diameter. Pollen grains of Col-0 plants and *map7a.1*, *map7b.1, map7a.1/map7b.1* mutants were germinated under semi-*in vivo* conditions. CLSM was used to acquire brightfield images of growing pollen tubes. ImageJ image analysis software was used to measure the diameters of each pollen tube 5 µm behind the tip. n = number of pollen tubes analysed.

No significant differences were observed in the organisations of the pollen tube nuclei in Col-0 pollen tubes, and pollen tubes of *map7a.1*, *map7b.1* and *map7a.1/map7b.1* mutant plants. The sperm cell nuclei (SCN) and VCN of Col-0 pollen tubes were clearly stained and were observed to be tightly associated. Consistent with previous reports (Laitiainen et al. 2002), the VCN regularly preceded, and was located proximally to the SCN: the MGU had moved into the pollen tube, no longer residing in, or close to, the germinated grain. The organisation of the MGU in *map7a.1*, *map7b.1* and *map7a.1/map7b.1* mutant pollen tubes was observed to be similar to those of Col-0, with tightly organised nuclei and a forwardly positioned vegetative cell nucleus. It could not be concluded that *map7* mutants exhibited phenotypic defects in nuclear organisation or transport, or that MAP7A or MAP7B have essential functions in regulating these processes.

7.6.3.5. Analysis of *map7* Mutant Seed Set.

The potential roles of MAP7A and MAP7B in the regulation of fertilisation were then investigated. As described in chapter 3.3.4, siliques from Col-0 and *map7a.1*, *map7b.1* and *map7a.1/map7b.1* mutant plants were collected and cleared using serial washes in 70% ethanol in order to visualise developing seeds within the silique pod. For each mutant line, the seed content of 5 siliques from 3 individual plants was analysed.

As displayed in figure 7.44, the *map7a.1* and *map7b.1* single mutants, as well as the *map7a.1/map7b.1* double mutant plants had produced high percentages of fertilised seeds, indicating that the mutant pollen tubes were able to achieve fertilisation of the female gametes, at comparable levels to that of Col-0. Quantification of the seed set of the *map7* mutants, indicated no differences between the average fertilisation efficiency (% ovules fertilised to form seeds) of *map7a.1*, *map7b.1* and *map7a.1/map7b.1* mutants and Col-0. It was observed that the average fertilisation efficiency of the Col-0 plants analysed in this experiment was 98.9 ± 1.5 %, whereas the average fertilisation efficiency of *map7a.1*, *map7b.1* and *map7a.1/map7b.1* mutants was 99.0 ± 1.4 %, 98.3 ± 2.2 % and 98.6 ± 1.9 % respectively. The near-identical levels of seed production between Col-0 and *map7* mutant plants indicates that the mutants are not impaired in their ability to achieve

fertilisation and it cannot be concluded that MAP7A and MAP7B, alone, are essential in regulating this function.

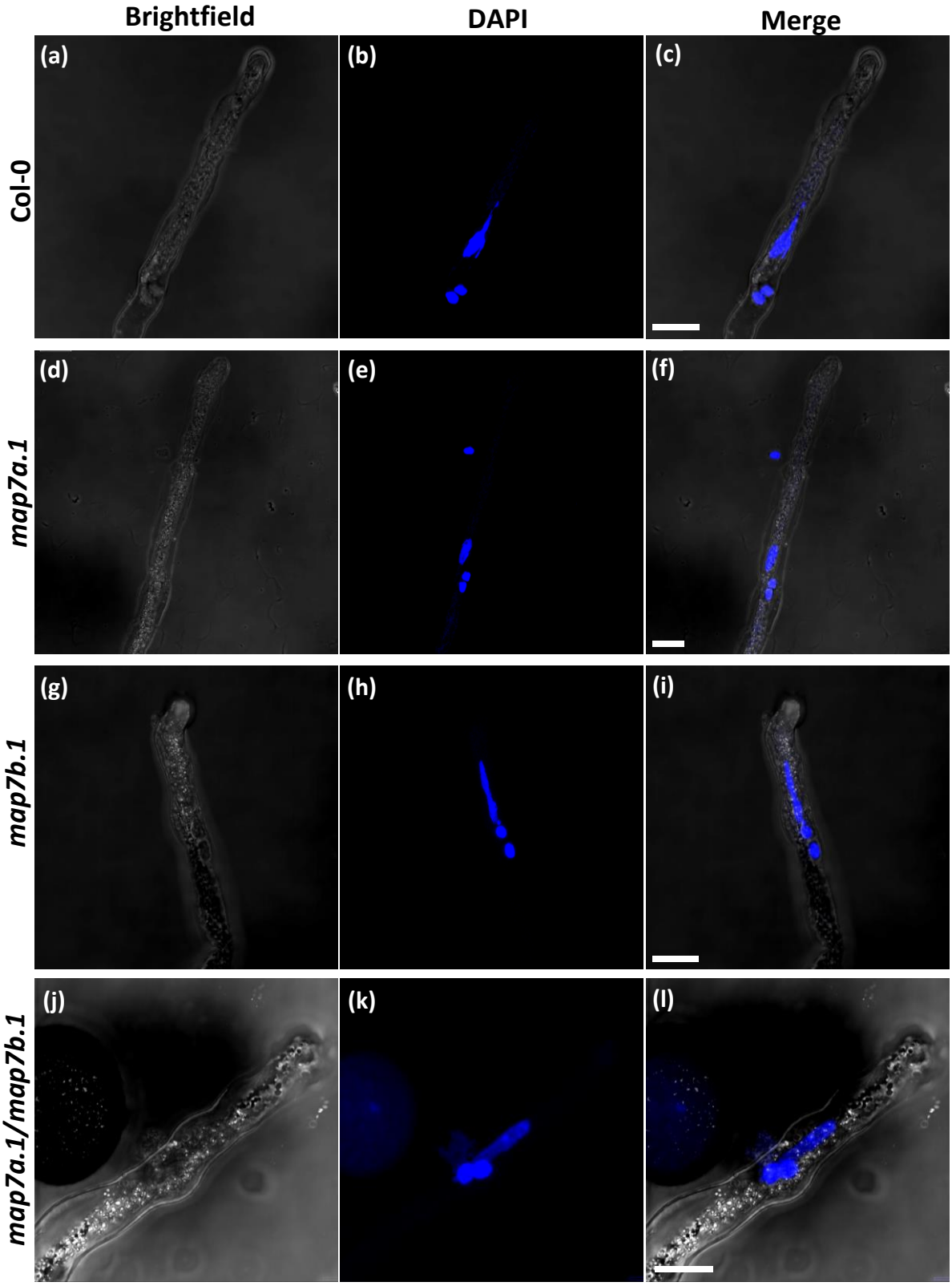

Figure 7.43: Analysis of Pollen Tube Nuclei in *map7* Mutant Plants. Pollen from Col-0, *map7a.1*, *map7b.1* and *map7a.1/map7b.1* plants were germinated *in vitro* and stained with the nucleic acid stain, DAPI. (a) - (c): Col-0 pollen tube. (d) - (f): *map7a.1* mutant pollen tube. (g) - (i): *map7b.1* mutant pollen tube. (j) and (l): *map7a.1/map7b1* double mutant pollen tube. (a), (d), (g) and (j): DAPI-stained nuclei visualised by CLSM using 405 nm excitation and 415 – 500 nm emission detection. (b), (e), (h) and (k): brightfield images of the same cells. (c), (f), (i) and (j): merge of brightfield and DAPI channels. Scale bar: 10 µm.

7.6.4. Summary.

Throughout the course of this section, reverse genetic analysis of MAP7A and MAP7B was employed to ascertain the functions of the MAP7 proteins in Arabidopsis. *map7a* and *map7b* single T-DNA mutants were identified and were demonstrated to be transcriptionally defective. From these single mutants, a *map7a/map7b* double mutant was generated, defective in transcription of both *MAP7A* and *MAP7B*, on which to perform reverse-genetic analysis of MAP7 function.

Phenotypic analysis of *map7a* and *map7b* single mutants, and *map7a/map7b* double mutants was performed to investigate potential defects in pollen grain development, germination, pollen tube growth and morphology, and fertilisation. No phenotypic defects could be observed in the mutant pollen during any of these developmental processes. It could not be concluded from the observations made during this study, that MAP7A and MAP7B, alone, perform any essential functions in pollen.

One explanation for the lack of an observable *map7* phenotype might be due to potential functional redundancy of MAP7A and MAP7B to other proteins. In section 7.2, MAP7C was identified as a SERF protein with a potentially conserved relationship to MAP7A and MAP7B. MAP7C was determined to have relatively low protein sequence homology compared to MAP7A and MAP7B, and was therefore not investigated in this study. However, MAP7C, like MAP7A and MAP7B, is identified as a SERF protein family member and may share functional redundancy to MAP7A and MAP7B in Arabidopsis, despite its relatively low conservation.

It is also possible that MAP7A and MAP7B may have essential roles in Arabidopsis that could not be identified using the tests described in this section. MAP7A and MAP7B may play important roles in regulating pollen development or fertilisation under stress conditions such as high temperature, as has been described for other pollen-expressed proteins (Endo et al. 2013). MAP7B was observed to be expressed in the root tissue of developing seedlings (section 7.5.2): phenotypic analysis of the MAP7 proteins was restricted to pollen in this investigation, however it is possible that the MAP7 proteins may play important roles in developing roots.

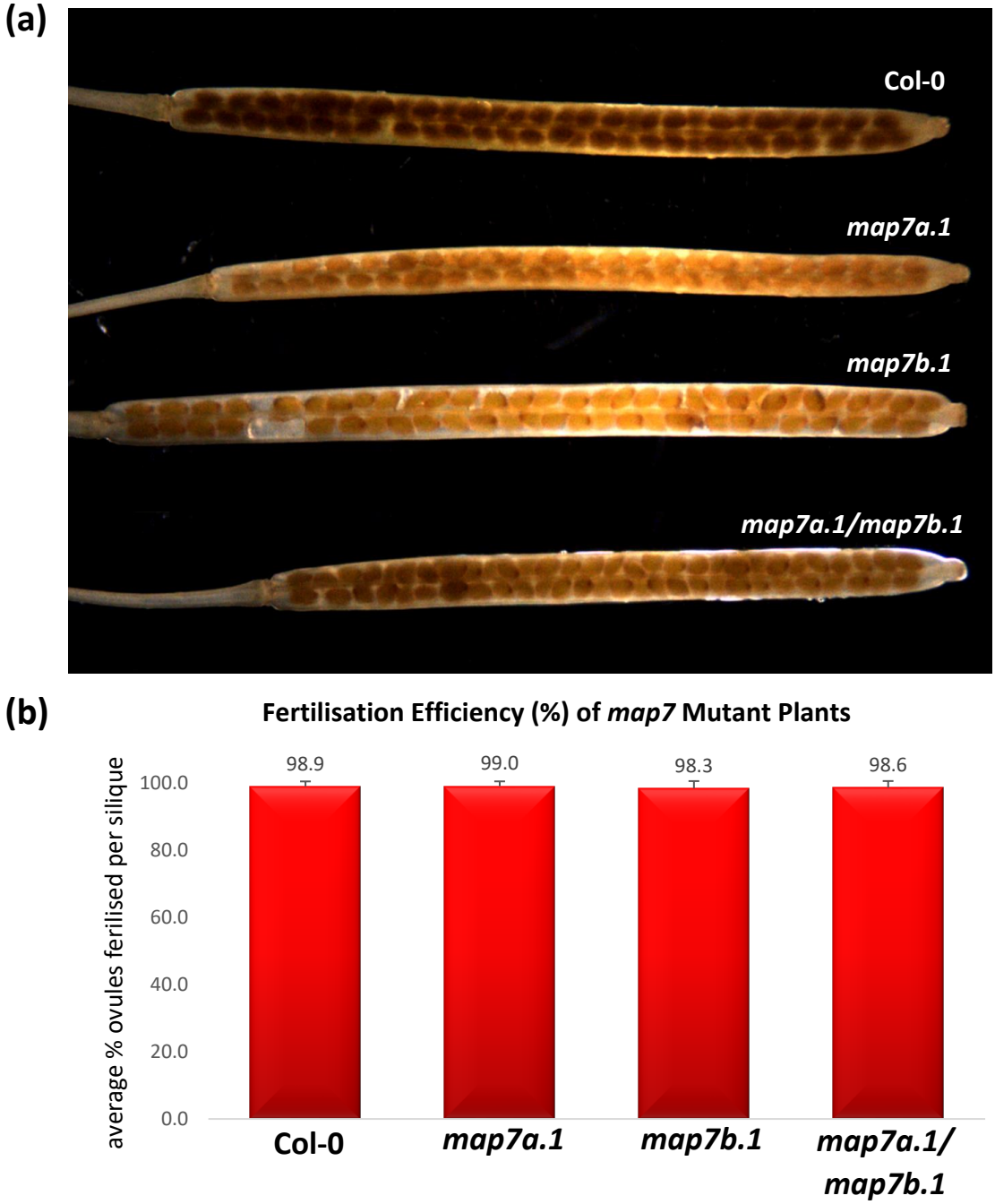

Figure 7.44*:* Quantitative Analysis of *map7* Mutant Seed Set. Developing siliques of Col-0, *map7a.1*, *map7b.1* and *map7a.1/map7b.1* plants were collected and their seed content quantified. (a): Example siliques collected from Col-0, *map7a.1*, *map7b.1* and *map7a.1/map7b.1* plants, with developing seeds clearly visible. (b): Quantification of average fertilisation efficiency (% ovules fertilised to produce seeds per silique) of Col-0, *map7a.1*, *map7b.1* and *map7a.1/map7b.1* plants. For each line, 5 siliques were analysed from 3 individual plants.

7.7. Conclusion.

Throughout the course of this chapter, the data presented has described MAP7A and the related protein, MAP7B, as a novel family of pollen-expressed microtubule-associated proteins in Arabidopsis. MAP7A, was originally identified as an interactor

of NET2A in a SU-Y2H screen. In this study, further attempts to substantiate an interaction between NET2A and MAP7A were unsuccessful, perhaps due to technical limitations in the experiments used to investigate the interaction. However, the discovery of novel cytoskeletal-associated proteins is highly valuable in advancing current understanding of plant cell biology, and may expand our understanding of the role of microtubules in pollen development, pollen tube growth and fertilisation. Therefore, detailed characterisation of MAP7A was performed to investigate its potential regulation of the microtubule cytoskeleton in Arabidopsis pollen.

Bioinformatic analysis revealed other Arabidopsis proteins conserved with MAP7A, of which MAP7B was selected for further analysis as a close relative of MAP7A. Another Arabidopsis protein, MAP7C, was suggested to be a relative of MAP7A, but due its relatively poor conservation with MAP7A, was not studied further. The Arabidopsis MAP7 proteins were determined to be members of a highly conserved family of SERF proteins, present in Planta, Animalia and Fungi, each possessing a highly conserved N-terminal SERF domain, which is responsible for mediating microtubule-binding in Arabidopsis. In animals, SERF proteins are implicated in the pathogenesis of age-related proteotoxic amyloid diseases (Van Ham et al. 2010). It is probable that SERF proteins in Animals and Fungi may also bind microtubules. Whether microtubules, through their interactions with SERF proteins, are involved in amyloid formation in Animals has yet to be determined. Furthermore, potential roles for MAP7A and MAP7B in the regulation of protein aggregate formation may exist in Arabidopsis, which have not thus far been studied.

The binding of MAP7A and MAP7B to microtubules was demonstrated *in vivo* and *in vitro*. When expressed in *N. benthamiana*, MAP7A-GFP associated with microtubule filament systems, determined by co-localisation with microtubule markers and pharmacological analysis. Recombinant MAP7A protein was demonstrated to bind microtubules directly *in vitro*. As stated above, it was discovered that the conserved MAP7A N-terminal SERF domain was responsible for microtubule-binding activity, suggesting that SERF proteins in Animalia and Fungi may also bind microtubules *in vivo*.

In situ analysis of MAP7A and MAP7B also demonstrated proof of endogenous MAP7 association with microtubules in growing pollen tubes. Firstly, GUS staining assays revealed MAP7A to be specifically expressed in pollen, whilst MAP7B was

expressed in pollen and root tissue. Increasing expression of MAP7A and MAP7B throughout pollen grain development suggests a role for these proteins in the mature gametophyte. Therefore, immunofluorescent staining of Narcissus pollen tubes was performed to investigate the subcellular localisation of MAP7A and its potential association with microtubules *in situ*. MAP7A was observed to localise to punctae at the plasma membrane, and at the periphery of the GCN of Narcissus pollen tubes. MAP7A was clearly determined to co-localise with microtubules at the periphery of the GCN, demonstrating association of MAP7A and microtubules *in situ*. No cortical microtubule filaments were observed in this experiment with which to study co-localisation with MAP7A punctae at the plasma membrane. It is likely that cortical microtubules were not preserved during fixation, and it is probable that the MAP7A punctae may co-localise with microtubule filaments at the membrane of growing pollen tubes: MAP7A punctae have been demonstrated to reside on microtubule filaments in *N. benthamiana* transient assays (section 7.3.2). However, association of MAP7A with microtubules at the GCN was clearly observed: microtubules are known to regulate the division of the generative cell nucleus, as well as the organisation of the male germ unit in pollen tubes (chapter 1.6.2), and it is possible that MAP7A may regulate these processes in Arabidopsis.

To identify a potential function of MAP7A and MAP7B in Arabidopsis, *map7a* and *map7b* T-DNA mutants were identified to investigate potential phenotypic defects arising from loss of MAP7 function. Additionally, *map7a/map7b* double mutants were generated to account for potential functional redundancy between MAP7A and MAP7B. No phenotypic defects were observed in the pollen of *map7a* and *map7b* single mutants, or *map7a/map7b* double mutants: pollen cell division and development, pollen germination, pollen tube growth and morphology, and fertilisation appeared normal in the T-DNA mutant lines. In addition to this, the organisation of the male germ units of *map7* mutant pollen tubes did not appear to disrupted. Therefore, no essential role has thus far been elucidated for MAP7A or MAP7B in pollen from this study. One possible explanation for this could perhaps be due to functional redundancy of MAP7A and MAP7B to another Arabidopsis SERF protein, MAP7C, which was not investigated in this study due to its relatively low conservation with MAP7A and MAP7B. However, MAP7C is also a designated SERF protein, and may also associate with microtubules in pollen, with functionally redundant roles to MAP7A and MAP7B. To test this hypothesis, reverse genetic analysis of *map7a/map7b/map7c* triple mutants must be performed. It is also possible that MAP7 proteins may regulate pollen tube growth only under stress

conditions, which were not analysed in this study. The possibility of MAP7A serving as a mediator of actin-microtubule interactions has also been discussed. Previous studies highlighting the importance of actin-microtubule associations in pollen tube growth have demonstrated the synergistic role of each cytoskeletal element: whilst disruption of microtubules induces only minor defects in pollen tube growth, disruption of actin and microtubules has severe effects (Gossot and Geitmann. 2007). Investigating the effects of disruption of the actin cytoskeleton in *map7* mutant pollen may therefore expose a potential role for MAP7 proteins in regulating actin-microtubule interactions, if the roles of MAP7-regulated microtubules may be synergistic to those of actin. However, during the course of this study, the roles of MAP7A and MAP7B have not yet been determined.

Therefore, the Arabidopsis MAP7s were characterised as novel microtubule-binding proteins in pollen. An interaction between MAP7A and NET2A *in vivo* could not be demonstrated in this study, however several clues may indicate the involvement of the two proteins in pollen. MAP7A was identified as an interactor of NET2A in a SU-Y2H screen: during further attempts to validate the interaction, clear co-localisation between NET2A and MAP7A *in vivo* was demonstrated in *N. benthamiana* transient expression assays. *In situ,* MAP7A could be seen to localise to punctae at the plasma membrane of growing pollen tubes in a pattern reminiscent of the subcellular localisation of NET2A as described by Deeks et al. (2012). Similar to NET2A, the expression pattern of MAP7A appeared to be specific to pollen. As an interaction between NET2A and MAP7A could not be demonstrated during this project, the roles of this hypothetical interaction can only be speculated. However, it is possible that an interaction between NET2A and MAP7A may co-ordinate interplay between actin and microtubules in growing pollen tubes. Associations of NET2A with *At*PRK proteins at punctae at the pollen tube membrane were demonstrated in chapter 6.4.4; it is possible that physical associations of NET2A and MAP7A at punctae may also occur to mediate actin-microtubule interactions at the pollen tube cortex. Co-dependence of the organisation of actin and microtubule cytoskeletal arrays has been suggested to exist in pollen, which may be important in regulating pollen tube germination and growth (Gossot and Geitmann. 2007). It is possible that an interaction between MAP7A and NET2A may be important in mediating such processes. However, the potential roles of interactions between NET2A and MAP7A can only be speculated.

Chapter 8: Discussion.

8.1. Introduction.

NET2A belongs to the NET superfamily of actin-binding proteins, which bind actin at various membrane compartments through their conserved N-terminal NAB domains (Deeks et al. 2012). Previous studies on NET2A have revealed it to be a pollen-specific actin-binding protein. NET2A localises to punctae at the plasma membrane, which align along, and associate with actin filaments, putatively linking them to the membrane (Dixon et al. 2013). However, the role of NET2A in pollen tube growth and fertilisation remains unknown. The aim of this project was to elucidate the functions of NET2A in the male gametophyte, and understand how it may regulate the actin cytoskeleton to orchestrate pollen grain development, pollen tube growth and fertilisation. As described below, several strategies were employed to articulate the function of NET2A in Arabidopsis.

Firstly, reverse-genetic analysis of multiple members of the NET2 subfamily was performed. Identification of a phenotype from loss-of-function *net2* mutants would provide valuable insights as to their roles *in vivo*. The results of this endeavour will be discussed in section 8.2.

Secondly, *in situ* analysis of NET2A subcellular localisation was performed in developing pollen grains. NET2A was previously demonstrated to localise to filamentous networks in developing pollen grains (Dixon et al. 2013). In chapter 4, thorough investigation into the association of NET2A with actin throughout pollen grain development was performed, and will be discussed in section 8.3.

To identify potential functions of NET2A *in vivo*, multiple protein-protein interaction screens were performed to identify potential binding partners of NET2A. By identifying the proteins with which NET2A interacts, it could be possible to articulate the processes with which NET2A may be involved *in vivo*. As a result of these screens, it was determined that NET2A was able to self-interact to form homodimers, and interact with NET2B to form heterodimers. This will be discussed in section 8.4.

The interactions between NET2 proteins, and Pollen Receptor-Like Kinases (PRKs) were also investigated, as described in chapter 6. NET2A was determined to interact with *At*PRK4, and *At*PRK5, implicating the NET2s in the regulation of fertilisation in Arabidopsis, and providing potential insights as to how NET2A may be regulated *in vivo*. The significance of the interactions between NET2s and PRKs will be discussed in section 8.5

Finally, the characterisation of MAP7A; a novel microtubule-associated protein identified as an interactor of NET2A in the SU-Y2H screen, will be discussed in section 8.6. The role of MAP7A in the regulation of the pollen microtubule cytoskeleton will be hypothesised. The interaction between NET2A and MAP7A may mediate associations between actin and microtubules in growing pollen tubes: the potential role and importance of NET2A in actin-microtubule crosstalk will be speculated.

8.2. NET2 Reverse-Genetics.

8.2.1. NET2A Reverse-Genetic Analysis Indicates Functional Redundancy Between NET2 Family Members.

Reverse-genetic analysis of *net2a, net2b* and *net2d* single T-DNA knockout mutants was performed during this investigation. Identification of potential phenotypes arising from the loss-of-function of a *NET2* gene would indicate a role for that NET2 in pollen grain development and pollen tube growth. No defects in pollen grain development, pollen tube growth or fertilisation were observed in the *net2a, net2b* and *net2d* single mutant lines, suggesting that each NET2 analysed, alone, plays no essential function in pollen.

This result was unsurprising: functional redundancy between NET subfamily members has been reported previously, and loss of function of one single NET protein within a subfamily has not yet been reported to elicit a phenotype. Phenotypic defects have only been observed in plants that do not express multiple members of the same NET subfamily (Calcutt. 2009; Ingle. 2011; Wang et al. 2014). It can therefore be assumed that in the examples given above, the loss of function of one NET family member can be compensated for by the function of another. It is

highly likely that individual members of the NET2 subfamily are also functionally redundant to one another, and may share overlapping roles in the functions they regulate.

Therefore, it will be necessary to develop *net2* double mutant plant lines, in which the expression of multiple *NET2* subfamily members is disrupted, in order ascertain their roles using reverse genetics. During the course of this project, the *net2a, net2b* and *net2d* single T-DNA mutant lines described in chapter 3 were used to generate such *net2* double mutants, which could not be analysed within the timeframe of this investigation. Analysis of these mutant lines may reveal potential roles for individual members of the NET2 family in future studies.

Phenotypic analysis of *net2a/net2d* double mutants should be performed on developing pollen grains. NET2A and NET2D are both expressed highly during pollen grain maturation, perhaps indicating a role for them in pollen grain development, or pollen germination (Dixon. 2013). As discussed below in section 8.3, NET2A was observed to associate with the actin cytoskeleton of developing pollen grains, indicating a potential role for its regulation of actin-dependent processes occurring during gametogenesis. Furthermore, NET2 proteins are interactors of PRKs (chapter 6, chapter 8.5): in Petunia, mutants of *Pi*PRK1 (with which the NET2 orthologue, *Pi*KIP1, interacts), fail to develop viable pollen (Lee et al. 1996), perhaps implicating the NET2 proteins in pollen grain development through their associations with PRKs. NET2B is unlikely to be involved in pollen grain development, and does not appear to be expressed in ungerminated pollen (Dixon. 2013; Leydon et al. 2013).

Phenotypic analysis of *net2a/net2b, net2a/net2d,* and *net2b/net2d* double mutants must also be performed in the growing pollen tube and during fertilisation, in which NET2 proteins are predicted to play important roles. NET2A and NET2B are very likely to share functional redundancy in regulating pollen tube growth and fertilisation, and analysis of *net2a*/*net2b* double mutants, lacking expression of both genes, may reveal their importance in growing pollen tubes. NET2A has for some time been predicted to play a major role in pollen tube growth, and is known to bind actin at the pollen tube plasma membrane (Dixon et al. 2013). NET2B, the closest relative of NET2A, is expressed specifically in pollen tubes having penetrated the stigma, under the regulation of transcription factors that coordinate fertilisation (Dixon et al. 2013; Leydon et al. 2013). Therefore, the role of NET2B appears to be

specific in promoting pollen tube growth though the stigma during fertilisation (Dixon. 2013). NET2A and NET2B have been shown to interact with each other (section 8.4), implicating their involvement in common processes. Both NET2A and NET2B have been shown to bind common interacting partners: each NET2 protein is able to interact with *At*PRK4 and *At*PRK5 (section 8.5), indicating functional redundancy between NET2A and NET2B in the regulation of pollen tube growth under control of *At*PRKs. Therefore, *net2a/net2b* double mutants may be defective in pollen tube growth *in vivo*: investigation of these potential defects may elucidate the importance of NET2A and NET2B in Arabidopsis. NET2D may also have a major role in pollen tube growth and its expression is upregulated slightly in pollen tubes having penetrated the stigma (Dixon. 2013). NET2D may also interact with PRKs: its putative orthologue in Petunia, *Pi*KIP1, interacts with *Pi*PRK1, potentially implicating the role of NET2D in pollen tube growth during fertilisation. Therefore, NET2D may also play a role in pollen tube growth and fertilisation with functional redundancy to NET2A and/or NET2B. Analysis of pollen tube growth in *net2a/net2d*, and *net2b/net2d* mutants must therefore be investigated.

8.3. NET2A in Developing Pollen Grains.

8.3.1. Summary of Results.

Chapter 4 describes the characterisation of NET2A subcellular localisation during pollen grain development in *pNET2A*:NET2A-GFP stable transgenic lines. The subcellular localisation of NET2A underwent striking changes throughout gametogenesis, timed to specific developmental events. The association of NET2A with actin in developing grains was investigated using plants co-expressing natively-driven NET2A-GFP, and the actin marker FABD2-RFP under the *pLAT52* promoter. At each developmental stage, NET2A-GFP associated with actin filaments, indicating a functional role for NET2A during gametophyte maturation.

8.3.2. The Actin Cytoskeleton of Developing Pollen in Arabidopsis.

The actin cytoskeleton is known to be important for pollen grain development, and regulates specific developmental events including nuclear positioning, mitosis, and

pollen grain growth (Gervais et al. 1994; Zonia et al. 1999). A small number of studies have mapped the behaviour of the actin cytoskeleton during pollen grain development (Gervais et al. 1994; Zonia et al. 1999). However, these observations were made on samples prepared with harsh chemical fixations, using epifluorescence microscopy and may be considered of relatively low quality compared to modern standards of bioimaging. In an important distinction to these previous works, this study employed CLSM to gather high-resolution images of the actin cytoskeleton *in vivo*, in live cells stably expressing the actin marker, FABD2-RFP. Furthermore, whereas previous studies have visualised the actin cytoskeleton in the developing gametophytes of *N. tabacum* and *B. napus*, the developmental rearrangements of the actin network are here characterised in the model organism, Arabidopsis, in which the genetic, molecular and cellular processes orchestrating gametogenesis are better studied. Therefore, this study presents a novel insight into the coordination of the actin cytoskeleton during pollen grain development in Arabidopsis, and provides high quality images of the dynamic reorganisation of actin during gametogenesis.

It was observed that the actin cytoskeleton displayed many different localisation patterns during gametophyte maturation in Arabidopsis, and reorganised to form distinctive arrays at specific developmental events (figure 8.1). *pLAT52*-driven expression of the actin reporter, FABD2-RFP was first detected in mid-bicellular pollen, in which actin filaments formed transversely orientated cables at the equatorial regions of the cell cortex. This ‘girdle-like’ actin structure was reminiscent of the pre-prophase band formed by the cytoskeleton during mitosis. Also observed was a fine cytosolic network of actin filaments. In late bicellular and early tricellular pollen, the actin cytoskeleton manifested as a prominent filamentous network at the cell cortex and throughout the cytoplasm. Actin appeared to surround the vegetative cell nucleus, and connect it to the cytosolic actin network. Prior to anthesis, tricellular pollen grains exhibited a different actin network array, forming a dense meshwork of fine actin filaments at the cell cortex, with a sparse distribution of fine filaments present throughout the cytosol.

The dynamic restructuring of the actin cytoskeleton during development appears to be similar to the previous studies performed on *N. tabacum* and *B. napus* (Gervais et al. 1994; Zonia et al. 1999). The transverse cortical cables observed during mid-bicellular pollen are also a feature of developing *B. napus* grains, but however have not been reported to form in *N. tabacum*. It is possible that this actin girdle structure

is a feature unique to tricellular pollen grains such as those of Arabidopsis and Brassica, but does not manifest in species with bicellular grains such as tobacco. However, it is also possible that this actin structure was not well-preserved following fixation of *N. tabacum* grains, or could not be visualised using wide-field microscopy and was therefore not documented. The putative function of this structure is unknown. *In B. napus* and *N. tabacum*, pharmacological disruption of the actin cytoskeleton in mid-bicellular microspores inhibited the growth and elongation of the grain (Gervais et al. 1994). It is therefore likely that the transverse cortical actin cables may regulate the growth and morphology of the developing grain. Potentially, the cortical actin cables may mark the position to which the vegetative cell nucleus (VCN) and generative cell (GC) may migrate following PMI, and may play a role in nuclear positioning leading into mid-bicellular pollen. In *N. tabacum*, pharmalogical disruption of the actin cytoskeleton of early bicellular grains induces defects in nuclear positioning (Zonia et al. 1999). Differences in the structures of the actin cytoskeleton exist in the mid-bicellular pollen grains of Arabidopsis and *B. napus*. In *B. napus*, actin surrounds the GC, which does not occur in Arabidopsis: the function of actin at the GC of mid-bicellular *B. napus* pollen is unknown, and no predictions as to the significance of this observed difference can be made.

In late-bicellular/early-tricellular grains of Arabidopsis, actin microfilaments surround the VCN, and extend a filamentous network through the cytoplasm, connecting to a filament system at the membrane. This seems to be mirrored by the actin cytoskeleton in *B. napus* and *N. tabacum* pollen grains. The role of this actin array is unknown, and no defects in pollen grain development have been reported to arise as a result of its pharmacological disruption. This actin array arises during a period of cell growth and elongation in pollen grains, and the actin cytoskeleton may play an important role in this aspect of development. Several cellular processes occur during this stage of pollen development, which may be dependent on actin. For example, fragmentation and dispersal of the vacuole takes place in bicellular pollen, through a series of invaginations of the vacuole tonoplast. The plasma membrane also becomes increasingly convoluted (Yamamoto et al. 2003). These process appear to be regulated somehow by clathrin-mediated endocytosis (Kang et al. 2003; Kim et al. 2013), likely under control of actin (Konopka et al. 2008). It is possible that actin regulates endocytosis at this stage of pollen development: the actin array of late-bicellular/early tricellular pollen has also been shown to co-localise with endocytic trafficking bodies, labelled with the styryl-dye, FM4-64; a commonly used marker of endocytic vesicles. It is possible that actin may mediate

endocytosis in pollen grains to facilitate uptake of nutrients and synthetic material from the anther locules to support growth and development (Ye and Xu. 2012).

The dense cortical actin network observed in *tricellular* Arabidopsis grains has also been documented in *B. napus*, and *N. tabacum* prior to anthesis. Therefore, the organisation of the pollen actin cytoskeleton at this stage of development is highly similar between species. The role of these actin structures has not yet been elucidated, but it is possible that the actin cytoskeleton may regulate endocytosis and maintenance of the plasma membrane prior to anthesis: mutants defective in clathrin-mediated endocytosis exhibit severe defects in plasma membrane morphology at this stage of pollen grain development (Kang et al. 2003).

Therefore, the observations of the dynamic reorganisations of the actin cytoskeleton made on Arabidopsis pollen appear to corroborate previous observations made on *B. napus* and *N. tabacum*. The actin cytoskeleton is known to be important in the regulation of PMI and its associated nuclear migrations, as well as in controlling microspore growth and elongation (Gervais et al .1994; Zonia et al. 1999). This project focusses on the regulation of the actin cytoskeleton following PMI, after which NET2A is expressed. It is after PMI that actin-driven cell growth and elongation occurs, but the mechanisms by which actin may regulate these processes is unknown. It is possible that the actin cytoskeleton plays important roles in the organisation of the cell's cytoplasmic contents, the plasma membrane, and endocytotic processes. However, the potential functions of actin following PMI can only be speculated.

8.3.3. NET2A in Developing Pollen Grains.

It was observed that NET2A-GFP co-localised with actin filaments in each array described above. This proves that NET2A associates with the actin cytoskeleton during pollen grain development, and indicates its involvement in the regulation of actin to orchestrate specific developmental events.

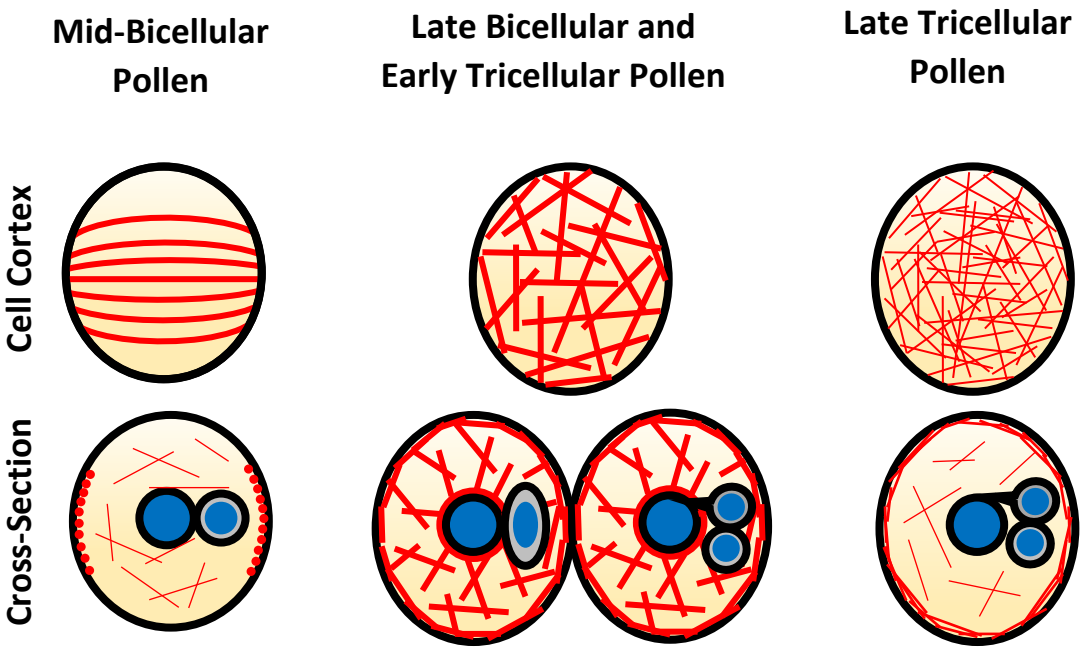

Figure 8.1: Dynamic Reorganisation of the Actin Cytoskeleton Throughout Pollen Grain Development. Diagrammatic representation of the structures of the actin cytoskeleton in mid-bicellular, late bicellular/early tricellular and late tricellular pollen grains. The depictions are based on observations of *pLAT52*:FABD2-RFP stable transgenic lines. F-actin filaments are depicted in red, and cell nuclei in blue. Original figure.

In the transverse array, NET2A co-localised with actin at the transverse cortical actin cables and fine cytoplasmic filaments, decorating them in the 'beads-on-a-string' pattern characteristic of NET proteins. It is possible that NET2A may bind the cortical actin cables to the plasma membrane of the developing pollen grain at this stage. A role for NET2A in the organisation of this actin structure must also be considered: NET2A may stabilise, cross-link or bundle actin filaments to form this cytoskeletal array.

In late-bicellular/early tricellular grains, NET2A associates with actin surrounding the VCN, and the actin filaments of cytoplasmic and cortical networks. At the cell cortex, it is conceivable that NET2A will serve to bind actin to the pollen grain membrane, as is thought to occur in growing pollen tubes (Dixon. 2013; Deeks et al. 2012). As discussed above, the actin cytoskeleton is implicated in the maintenance of plasma membrane morphology through clathrin-mediated endocytosis (Kang et al. 2003; Kim et al. 2013). By binding actin at the plasma membrane, it is possible NET2A may be involved in regulating membrane morphology and endocytosis at this stage of development.

The binding of actin by NET2A at periphery of the VCN during this stage of development is likely to be of great significance. It is believed that the VCN envelope is physically tethered to the actin cytoskeleton through an interaction between myosin XI-I and components of the LINC (Linker of Nucleoskeleton and Cytoskeleton) complex (figure 8.2). The LINC complex spans the nuclear envelope double membrane, consisting of SUN proteins spanning the inner nuclear membrane, that interact with WPP Domain-Interacting Proteins (WIPs), that traverse the outer nuclear membrane. An interaction between WIPs and WPP Domain-Interacting Tail-Anchored Proteins (WITs) associates the LINC complex with actin through the interaction of WITs and myosin XI-I (figure 8.2; Tamura et al. 2013; Zhou and Meirer. 2014). Components of the LINC complex regulate nuclear morphology, movement, and the transport of the VCN during pollen tube growth (Oda and Fukuda. 2011; Zhou et al. 2014b; Tamura et al. 2013). It is possible that NET2A may also be involved in binding actin to the VCN envelope, perhaps as part of the LINC complex: NET2A may bind actin to the outer nuclear membrane through an interaction with WITs or WIPs or perhaps acts as an adaptor protein to mediate the recruitment of myosin XI-I. It is also possible that NET2A may tether actin to the nucleus independently of the LINC complex. By linking actin to the nuclear envelope, NET2A may serve to regulate the morphology and movements of the VCN.

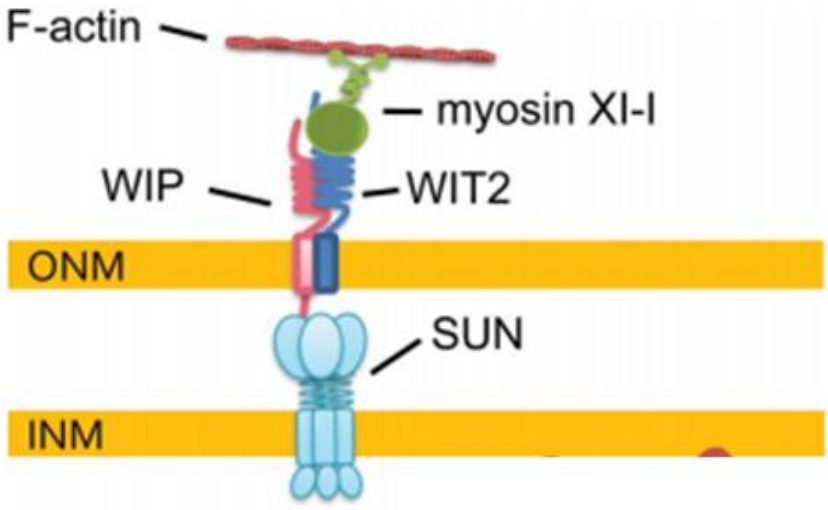

Figure 8.2: The Structure of the LINC Complex. Diagrammatic representation of the LINC protein complex that links the nuclear envelope to the actin cytoskeleton. SUN proteins integral to the inner nuclear membrane (INM), interact with the outer nuclear membrane (ONM)-integral protein, WIP1, in the perinuclear space. WIP1 interacts with WIT1 on the cytosolic face of the ONM, which associates with myosin XI-I to bind actin at the nuclear envelope. Taken from Zhou et al. (2015).

Cytoplasmic actin filaments are also bound by NET2A during the late-bicellular/early tricellular stage. As described above, the actin cytoskeleton may be involved in clathrin-mediated endocytosis and rearrangements of the vegetative cell organelles, including separation and dispersal of the vacuole. NET2A, bound to actin filaments may offer points of contact between organelle membranes and the cytoskeleton during actin-mediated reorganisation of intracellular compartments. NET2A may also serve to regulate the actin cytoskeleton by stabilising, cross-linking or bundling actin filaments to organise this distinctive cytoskeletal network.

In late-tricellular pollen grains prior to anthesis, NET2A is associated with the dense meshwork of cortical actin filaments. It is very likely that NET2A will bind these filaments at the plasma membrane, and may organise the cortical filament system by cross-linking or stabilising individual filaments. NET2A may be involved in the regulation of actin-controlled membrane morphology or endocytosis at the pollen grain plasma membrane.

8.3.4. NET2A in Mature Pollen Grains and Germination.

In mature, dehiscent pollen, NET2A was observed to be cytosolic and did not decorate actin filaments (Dixon. 2013). During the onset of pollen germination, NET2A localised to punctae at the plasma membrane facing the site of germination. In recently germinated pollen, NET2A formed punctae at the plasma membrane of the shank region of nascent pollen tubes and at the pollen grain membrane in the immediate vicinity of the germination site.

The dynamic behaviour of the actin cytoskeleton has been documented during pollen grain germination (Volger et al. 2015). Prior to germination, the actin cytoskeleton localises to the cell periphery opposite the site of germination. However, during the initiation of pollen tube outgrowth, longitudinal actin cables form facing the bulge site, extending into the incipient pollen tube as tip-focussed exocytotic vesicle trafficking ensues. The NET2A punctae that form at the site of pollen tube outgrowth may bind the longitudinal actin cables to the plasma membrane of the bulge site. This may tether cytosolic actin filaments to the membrane of the bugle site, directing trafficking of exocytotic vesicles and synthetic materials to the nascent tube tip to drive elongation. As the pollen tube begins to

extend, the membrane of the bulge region becomes increasingly distal to the pollen tube tip, and begins to mature into shank. NET2A punctae at the membrane of the germination bulge may bind and organise actin into cortical longitudinal filaments as the pollen tube extends, generating the longitudinal actin cables of the pollen tube shank region, as it begins to form (figure 8.3).

8.3.5. Future Perspectives of the Role of NET2A in Gametogenesis.

The association of NET2A with actin throughout pollen grain development indicates it may play an important role in the regulation of the cytoskeleton, and in the regulation of pollen grain development. Further research must be performed to establish the importance of NET2A in gametogenesis, and the specific developmental events which it may co-ordinate. Then, it may be possible to understand how NET2A may regulate the cytoskeleton to orchestrate pollen grain development.

Reverse-genetic analysis of NET2A will be critical to understand the importance of NET2A in gametogenesis. Developmental defects arising from the loss of function of NET2A will provide valuable insights into NET2A's roles in pollen grain development. As described previously, *net2a* single null mutants did not display significant developmental phenotypes, indicating that the role of NET2A in pollen grain development may be functionally redundant to other NET2 subfamily members. Analysis of *net2a/net2d* double mutants may be likely to reveal potential clues as to the roles of NET2A and NET2 proteins in grain development.

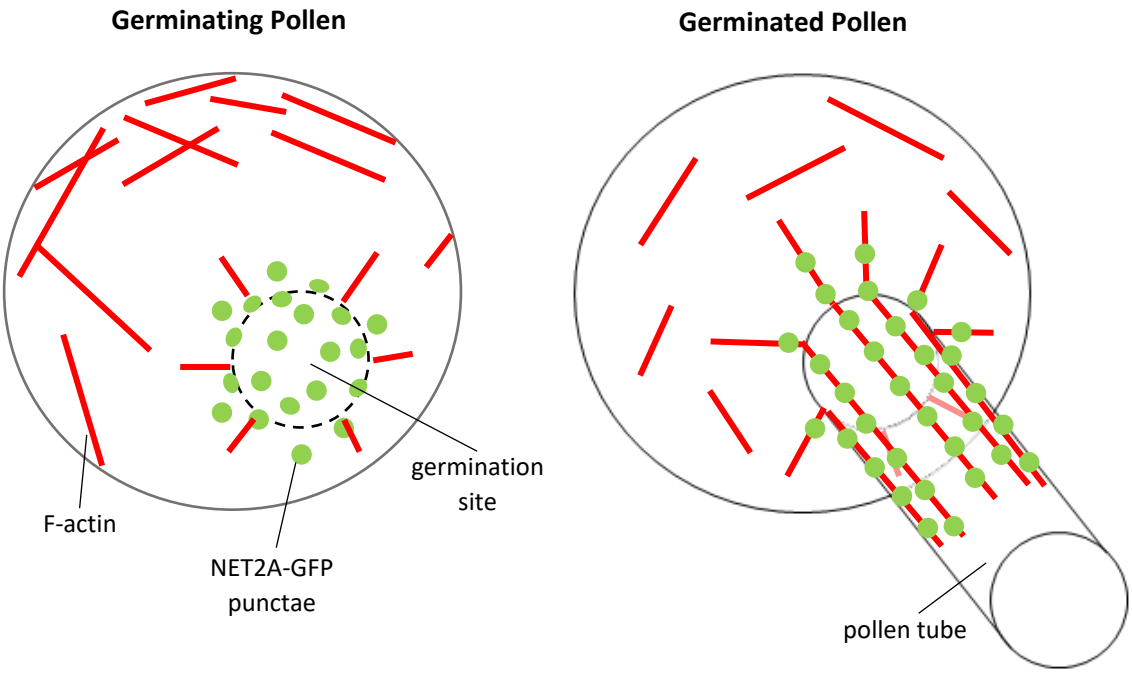

Figure 8.3: A Potential Model for NET2A Association with Actin at the Site of Germination. NET2A punctae form at the membrane of the germination bulge, from which the pollen tube will extend. The NET2A punctae bind actin filaments at the plasma membrane to form the cortical longitudinal actin cables of the shank as the pollen tube extends. F-actin shown in red. NET2A-GFP punctae shown in green. Original figure.

8.4. The Oligomerisation of NET2 Proteins.

8.4.1. Summary of Results.

As described in chapter 5, a series of protein-protein interaction screens were performed to identify potential interacting partners of NET2A. It was observed that NET2A was able to self-interact to form homo-oligomers, and could also interact with NET2B to form hetero-oligomers. NET2A was identified to interact with itself in the SU-Y2H and TAP-MS screens. In the TAP-MS screen, an interaction between NET2A and NET2B was also identified, and was subsequently corroborated using FRET-FLIM. Therefore, the observed interactions of NET2A with itself and with NET2B were both corroborated using multiple experimental techniques. It is unsurprising that members of the NET2 subfamily may self-interact: dimerisation of NET3C has been reported previously, as have NET4A-NET4A, NET4A-NET4B and NET4B-NET4B oligomerisations (Wang et al. 2014; Mentlak. 2015).

8.4.2. Putative Protein Domains Responsible for Mediating NET2A Homo-Oligomerisation.

In the SU-Y2H, full-length NET2A was found to interact with another cDNA fragment of NET2A, corresponding to aa 36 – 136 of the protein. This indicates that aa 36 - 136 of the protein may be responsible for mediating the homomeric interaction, and may contain a NET2A-binding motif. NET2A$^{36-136}$ incorporates a large proportion of the NET2A NAB domain (aa 1 – 93). Therefore, it is possible that the NET2A NAB domain may mediate a the homomeric interaction. Interestingly, it has been reported previously that NET2A$^{1-93}$ may exhibit actin-bundling activity *in vivo*: dimerisation or oligomerisation of the NAB domain may form cross-bridges between actin filaments to promote filament bundling. This can only be speculated however; it is unknown as to which region of the full length NET2A protein that the NET2A$^{36-136}$ fragment may interact with.

*Pi*KIP1, a NET2 orthologue in Petunia, has been shown to self-interact through a central region of the protein: the observed interaction between *Pi*KIP1$^{333 - 724,}$ and an identical protein fragment (*Pi*KIP1$^{333 - 724}$), indicates that the domains responsible for the self-interaction lie centrally within the protein sequence, well outside the NAB domain. It is possible that NET2A may self-interact at multiple regions, or even along the full length of the protein. Conversely however, differences may exist between the mechanisms by which NET2A and *Pi*KIP1 self-interact.

8.4.3. The NET2A-NET2B Hetero-oligomerisation.

The observed interaction between NET2A and NET2B indicates that both proteins may cooperate in regulating common subcellular processes in Arabidopsis. However, little work has been performed to characterise NET2B, and the role of the heteromeric NET2A-NET2B interaction can only be speculated.

As described previously, NET2B appears to be implicated in the regulation of fertilisation, and is expressed in pollen tubes only upon penetration of the stigma (Dixon. 2013), under control of a group of transcription factors that control fertilisation in Arabidopsis (Leydon et al. 2013). Therefore, through its interactions with NET2B, NET2A may also be implicated in the regulation of fertilisation in

growing pollen tubes. NET2A and NET2B both interact with *At*PRK4, and *At*PRK5 (section 8.5), further implicating both NET2A and NET2B, together, in the regulation of fertilisation in Arabidopsis.

NET2B has been shown to have a functional NAB domain, indicating it is an actin-binding protein (Dixon. 2013). In this study, full-length NET2B also appeared to bind actin; forming the 'beads-on-a-string' pattern characteristic of NET proteins, including NET2A (Deeks et al. 2012). Significantly, NET2A-GFP and NET2B-RFP co-localised on actin filaments and also at punctae in *N. benthamiana* leaf-epidermal cells. It is therefore very probable that NET2A and NET2B will also co-localise in growing pollen tubes; at the discreet membrane foci formed by NET2A (Deeks et al. 2012).

To fully understand the role of the interaction between NET2A and NET2B, it will be necessary to further investigate the subcellular localisation and role of NET2B in Arabidopsis.

8.4.4. The Potential Regulation of Actin by NET2 Oligomers.

The ability of NET2A and NET2B to oligomerise may be conferred by their coiled-coil domains. NET2A and NET2B are both long coiled-coil proteins, containing three and four coiled-coil domains respectively at their c-termini (Dixon. 2013; Deeks et al. 2012). Coiled-coil domains consist of multiple α-helices wrapped around each other in a left-handed helix to form a supercoil (Mason and Arndt. 2004). A key feature of long coiled-coil proteins is their ability to form dimers and oligomers (Rose and Meier. 2004). Dimerisation of coiled-coil proteins can create a rod-structured protein complex, with functional domains at each end (Rose and Meier. 2004). It is possible that NET2A and NET2B may oligomerise in this fashion, which may be an important mechanism in their regulation of the actin cytoskeleton.

There are known examples of coiled-coil proteins that regulate the actin cytoskeleton through oligomerisation. STOMATAL CLOSURE-RELATED ACTIN BINDING1 (SCAB1) is an actin-binding, coiled-coil protein that promotes bundling of F-actin: dimerisation of SCAB1 forms 'cross-bridges' between filaments, causing them to bundle (Zhao et al. 2011; Zhang et al. 2012). In mammalian cells, the

organisation of actin into higher-order structures can be mediated by dimerising coiled-coil proteins: α-actinin dimers cross-link actin filaments into bundles, whereas another protein, filamin, dimerises to cross-link F-actin filaments into a loose web-like network of orthogonal (non-bundled) filaments (Matsudaira. 1991; Wachsstock et al. 1993). Similarly, NET2s may dimerise to form a protein complex with multiple actin-binding sites, which may cross-link or bundle actin filaments (figure 8.4).

NET2A and NET2B may bind and regulate actin differentially. The ability of NET2A to form NET2A-NET2A homodimers, and NET2A-NET2B heterodimers may modulate the actin-binding activity of the NET2 dimer, and its potential regulation, or organisation of actin. Interestingly, NET2A is expressed in pollen prior to germination and penetration of the stigma, whereas NET2B is not (Dixon. 2013; Leydon et al. 2013). Therefore, NET2A would exist only in NET2A homodimers prior to penetration of the stigma by the pollen tube, following which the upregulated expression of NET2B may increase the prevalence of NET2A-NET2B heterodimers in the pollen tube. The increase in NET2B expression following penetration of the stigma by the growing pollen tube may therefore differentially modulate the way NET2A regulates the actin cytoskeleton, in order to perform actin-dependent processes that occur specifically during fertilisation. NET2A, as NET2A-NET2A homodimers may regulate actin to drive pollen tube germination and early growth (Volger et al. 2015; Gibbon et al. 1999), but may regulate actin differently as part of a NET2A-NET2B heterodimer to drive rapid pollen tube growth rates observed in the pistil during fertilisation (Cheung et al. 2010; Qin et al. 2009; Taylor and Helper. 1997).

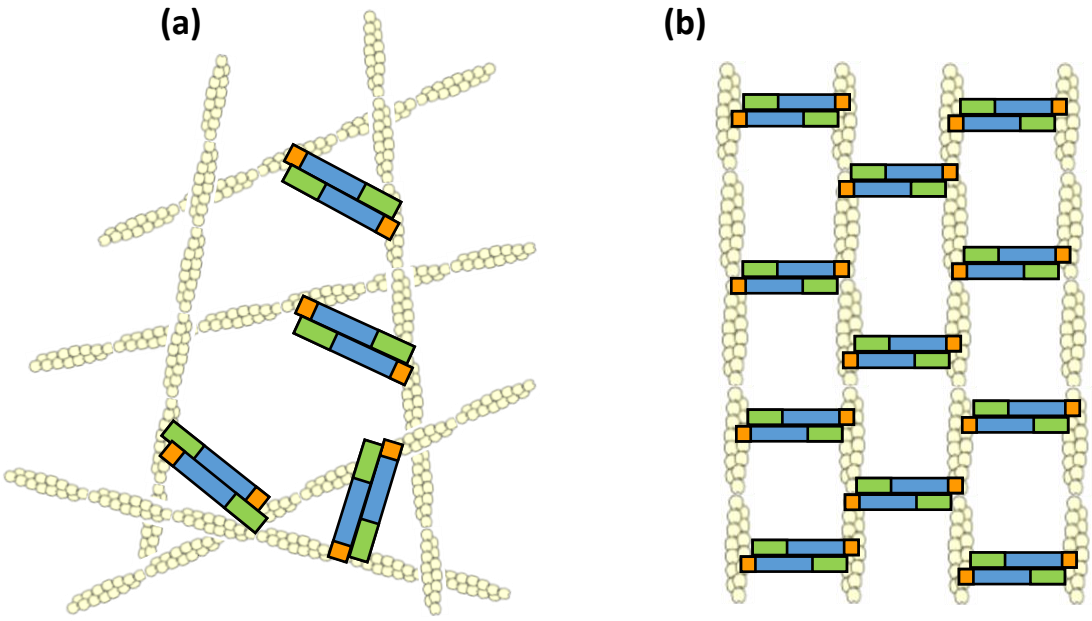

Figure 8.4: Potential Mechanisms of Actin Organisation by NET2 Dimers. (a): Cross-linking of actin filaments by NET2 dimers to create a loose filament network. (b): Bundling of actin filaments by NET2 dimers. Actin (white helices), NET2 dimers (blue) with NAB domain (orange), and coiled-coil domains (green). Original figure.

8.5. Interactions of NET2s and PRKs at the Actin-Membrane Interface.

8.5.1. Summary of Results

In chapter 6, the interactions between members of the NET2 family and PRKs were investigated. Firstly, the previously reported interaction between *Pi*KIP1 and *Pi*PRK1 (Skirpan et al. 2001) was confirmed *in vivo* using FRET-FLIM. Subsequently, it was determined that NET2A and NET2B are able to bind the Arabidopsis PRKs, *At*PRK4 and *At*PRK5, using Y2H assays and FRET-FLIM.

Having identified *At*PRK proteins that interact with NET2s, their subcellular localisations were analysed *in vivo*, by expressing them in pollen as fluorophore fusion proteins, under the pollen-specific *pLAT52* promoter. It was observed that *At*PRK4 and *At*PRK5 localised to discreet punctae at the pollen tube shank. NET2A and *At*PRK4 co-localised at these punctae, indicating that they interact at the pollen tube shank membrane, at specific foci. Discussed below are the implications of

these observed interactions, and what can be ascertained as to the potential function of NET2A's involvement with *At*PRKs in Arabidopsis.

8.5.2. NET2 Proteins Bind Actin at the Pollen Tube Plasma Membrane.

As a result of this investigation, it can be concluded that NET2A binds actin at the pollen tube plasma membrane through interactions with *At*PRK4 and *At*PRK5. In previous studies by Dixon. (2013), NET2A was demonstrated to be a functional actin-binding protein that could bind actin *in vivo* through its NAB domain. NET2A localises to punctae at the plasma membrane of the pollen tube shank, aligning along and binding actin at the membrane. The identification of the interaction between NET2A and *At*PRK4 & *At*PRK5 characterises a physical link at the actin-membrane interface of plants, and elucidates the mechanism by which the cortical actin cables of the pollen tube shank are bound at the membrane.

It was observed that *At*PRK4 & *At*PRK5 also formed discreet punctae at the plasma membrane of the growing pollen tube. It was at the punctae of NET2A and *At*PRK4 that co-localisation was observed between the two proteins, indicating that the actin-associated NET2A punctae observed by Dixon. (2013), are sites of physical interaction between the actin cytoskeleton and plasma membrane.

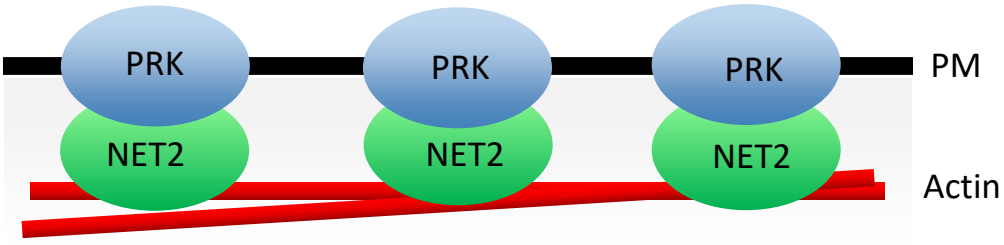

Figure 8.5: NET2s Bind Actin to the Plasma Membrane Through Interactions with Membrane-Integral PRKs. Original figure.

8.5.3. Multiple NET2 Family Members Interact with *At*PRKs.

Several lines of evidence suggest that NET2A may cooperate functionally with other members of the NET2 subfamily. As described above, NET2A has been shown to interact with NET2B, indicating both NET2s are involved in performing a common function. Reverse-genetic analysis of NET2A, NET2B and NET2D suggests functional redundancy between members of the NET2 protein family, as has been observed in other the NET families.

In this study, it was demonstrated that NET2A and NET2B share common interacting partners in *At*PRK4 and *At*PRK5, providing further evidence that the functionalities of both NET2s are linked to the same subcellular processes. Inferences can be made as to the functions of one NET2 based on the observations of another. NET2B is implicated in the delivery of sperm to the egg cell during fertilisation: it is expressed specifically upon the penetration of the pistil by the growing pollen tube, by a specific group of MYB transcription factors required for the delivery of sperm to the egg cell (Leydon et al. 2013). It is very likely that NET2A cooperates with NET2B to achieve this function, under control of PRKs.

The involvement of NET2C & NET2D alongside NET2A & NET2B through their interactions with *At*PRKs is also open to speculation. *Pi*KIP1, which is an interactor of *Pi*PRK1, is most conserved with NET2C and NET2D in Arabidopsis (Skirpan et al. 2001; Deeks et al. 2012). It can therefore be expected that NET2C and NET2D will also interact with PRK proteins in Arabidopsis.

8.5.4. The Function of PRKs in Pollen.

The interaction observed between NET2A & NET2B and *At*PRK4 & *At*PRK5 indicates a functional involvement of NET2s with PRKs in pollen.

It is possible that the interaction between NET2A and *At*PRK4 & *At*PRK5 may be important in the regulation of pollen grain development. In Petunia, *Pi*PRK1 mediates the development of microspores, and pollen of *Pi*PRK1 mutants fail to develop (Lee et al. 1996), indicating an essential role for *Pi*PRK1 in pollen development in which *Pi*KIP1 may be involved. It may be that *At*PRK4 and *At*PRK5

too are important for pollen grain development in Arabidopsis, and may play a role in the regulation of actin, mediated through involvement with NET2A. However, the interaction of NET2B, which is specifically expressed after penetration of the stigma by the pollen tube, with *At*PRK4 and *At*PRK5, may suggest that the importance of the NET2/PRK interaction lies in fertilisation, as the pollen tube grows through the pistil (Leydon et al. 2013).

PRKs are known to be involved in the regulation of polarised growth in pollen tubes. It has been reported that pollen tubes overexpressing *At*PRK1, *At*PRK2 *At*PRK3, *At*PRK4 or *At*PRK5 exhibited increased width and reduced growth rate (Chang et al. 2013). The regulation of pollen tube growth *in vivo* by PRKs appears to be especially important: *At*PRK1, *At*PRK3, *At*PRK6 and *At*PRK8 cooperate to regulate the growth of pollen tubes through the stigma and targeting to the ovule during fertilisation in a functionally redundant manner (Takeuchi and Higashiyama. 2016). Similarly, in *L. esculentum*, mutants of *Le*PRK2 display reduced fertility due to reduced pollen tube elongation rates during fertilisation (Huang et al. 2014).

The specific roles of PRKs *in vivo* seem to be in their regulation of pollen tube growth in response to external signals. The chemoattractant, *At*LURE1, is secreted by synergid cells of the ovule, and is important for guidance of the pollen tube to the egg cell during fertilisation (Takeuchi and Higashiyama. 2012). In Arabidopsis, *At*LURE1 is perceived by *At*PRK1, *At*PRK3 and *At*PRK6 which respond to the perception of the chemoattractant to guide pollen tube growth into the ovules (Takeuchi and Higashiyama. 2016).

Of particular interest to this study is the promotion of pollen tube growth in *L. esculentum* by the pistil-secreted peptide, *Le*STIG1. *Le*STIG1 is important in pollen tube growth and fertilisation, and is an extracellular binding partner of *Le*PRK1 and *Le*PRK2. *Le*PRK2 promotes pollen tube growth downstream of binding *Le*STIG1, indicating its importance as a transducer of external signals to regulate pollen tube growth. *Le*STIG1 is an orthologue of Arabidopsis GRI, which is a known ligand of *At*PRK4 and *At*PRK5. Binding of GRI by *At*PRK4 and *At*PRK5 induces ROS-induced cell death in leaf tissue (Wrzaczek et al. 2015). GRI is strongly expressed in the pistil and is important for fertilisation (Wrzaczek et al. 2009). It is therefore likely that *At*PRK4 and *At*PRK5 serve parallel roles to *Le*PRK2 in *L. esculentum,* and promote pollen tube growth in response to binding GRI. *Le*PRK2 also binds the extracellular signalling ligands, *Le*SHY, which is important in fertilisation, and *Le*STIL, which also

promotes pollen tube growth (Wengier et al. 2010; Guyon et al. 2004). It is probable that *At*PRK4 and *At*PRK5 bind Arabidopsis orthologues of *Le*STIL and *Le*SHY to regulate pollen tube growth and fertilisation. It can be predicted, based on their involvements with *At*PRK4 & *At*PRK5, that NET2s may have functional importance in regulating pollen tube growth in response to pistil-secreted signals such as GRI. It is currently unknown as to how *At*PRK4 and *At*PRK5 may regulate pollen tube growth in response to such signalling peptides. Therefore, the regulation of actin by NET2A downstream of *At*PRK4 & *At*PRK5 may represent a novel mechanism by which pollen tube growth is mediated in response to extracellular signals. PRKs are implicated in the control of the actin cytoskeleton during pollen tube growth, as will be described below.

8.5.5. Regulation of the Actin Cytoskeleton by PRKs.

Examples of the regulation of the actin cytoskeleton by PRKs have been demonstrated previously. In *L. esculentum*, *Le*PRK1 and *Le*PRK2 regulate the organisation of actin filaments at the pollen tube tip, and their overexpression induces depolarised growth through disorganisation of the apical actin cytoskeleton (Salem et al. 2011; Gui et al. 2014). Functional kinase activity of *Le*PRK2 is required for its regulation of the actin cytoskeleton, indicating the it regulates actin through phosphorylation of downstream signalling intermediates (Salem et al. 2011). Likewise, *At*PRK2 also regulates the organisation of actin filaments in the pollen tube tip in Arabidopsis (Zhao et al. 2013).

The best characterised mechanism of actin regulation by PRKs, is through their association with the Rop signalling pathway. In Arabidopsis, Rop1 regulates actin organisation and dynamics at the pollen tube apex, and localises to the membrane of the growing tip to coordinate polar cell growth (Lin et al. 2006; Fu et al. 2001; Gu et al. 2005). Rop1 activates two counteracting signalling pathways at the pollen tube apex: firstly, activation of RIC4-dependent assembly of the actin fringe permits the transport of secretory vesicles to the pollen tube tip. Subsequently, activation of the RIC3 pathway increases $[Ca^{2+}_{cyt}]$ in the apex, inducing disassembly of apical F-actin and exocytosis of vesicles at the pollen tube tip, driving polar cell growth (Lee et al. 2008; Gu et al. 2005). PRKs are believed to regulate Rop-driven cell growth through their associations with RopGEFs (Chang et al. 2013; Zhao et al. 2013; Gui et al.

2014; Zhang and McCormick. 2007). RopGEFs are activators of Rop signalling and promote Rop-driven tip growth in pollen tubes (Mucha et al. 2011; Gu et al. 2006). In *L. esculentum, Le*PRK1 and *Le*PRK2 regulate pollen tube growth through association with the RopGEF, KPP, which promotes Rop-driven actin organisation and subsequent tip extension (Kaothien et al. 2005; Gui et al. 2014). In Arabidopsis, *At*PRK2 binds and phosphorylates RopGEFs to activate Rop1 at the pollen tube tip, and subsequently drives tip growth through regulation of the actin cytoskeleton (Chang et al. 2013; Zhao et al. 2013; Zhang and McCormick. 2007). There is also evidence to suggest that PRKs may associate with Rops directly (Locke et al. 2010; Chang et al. 2013). Therefore, PRKs are able to regulate the actin cytoskeleton of pollen tubes, through controlling the Rop signalling pathway which in turn regulates actin dynamics at the pollen tube apex. Through PRKs, the actin cytoskeleton may be controlled in response to external signals such as GRI.

In Arabidopsis, multiple *At*PRKs have been demonstrated to interact with a wide variety of RopGEFs. *At*PRK1, *At*PRK2, *At*PRK3, *At*PRK4 and *At*PRK6 are each known to associate with RopGEFs in Arabidopsis. *At*PRK2 binds at least two RopGEFs (RopGEF1 and RopGEF12), whereas *At*PRK6 interacts with RopGEF8, RopGEF9, RopGEF12 and RopGEF13 (Takeuchi and Higashiyama. 2016; Chang et al. 2013; Zhang and McCormick. 2007). These numerous signalling components appear to be functionally redundant to one another, and cooperate in the same signalling pathways (Takeuchi and Higashiyama. 2016; Chang et al. 2013), however it cannot be ruled out that distinct roles exist for individual *At*PRKs and RopGEFs. As discussed in the next section, the data observed in this report may indicate a functional niche for *At*PRK4 and *At*PRK5. Interestingly however, the association of *At*PRK4 and RopGEF1 may implicate the *At*PRK4-NET2 complex in the regulation of Rop1, and its control of pollen tube growth. As described below, it seems unlikely that *At*PRK4 may be involved in the regulation of actin at the apex: it is therefore remotely possible that *At*PRK4 and NET2A might have a role in regulating Rop1 at the pollen tube shank.

There is also evidence to suggest that PRKs may regulate the actin cytoskeleton through direct association with actin-binding proteins in pollen. *Le*PRK1 for example, has been demonstrated to interact with tomato ADF (Gui et al. 2014): in Arabidopsis, ADF7 regulates organisation of actin filaments in the pollen tube shank by severing F-actin and promoting filament turnover (Zheng et al. 2013). Turnover of actin filaments in *L. esculentum* could be promoted by tomato ADF downstream of

*Le*PRK1 perception of extracellular signalling ligands such as *Le*STIG1. *Le*PRK2 has also been shown to interact with the LIM domain protein, δlim2 of tomato (Gui et al. 2014). LIM proteins are known to bundle and stabilise actin filaments (Papuga et al. 2010), and the Arabidopsis LIM protein, CROLIN1 is suggested to bundle and stabilise actin filaments in the pollen tube shank. It is possible that δlim2 may perform a similar role in tomato pollen tubes. Therefore, there exist possible mechanisms by which *Le*PRKs are able to regulate the actin cytoskeleton through direct association with actin-regulatory proteins, which may have roles in the organisation of the actin cytoskeleton during pollen tube growth. Whether these interactions constitute potential signalling links is unknown, but it is possible that PRKs may be able to control these proteins downstream of binding extracellular signalling ligands such as *Le*STIG1, in order to regulate the actin cytoskeleton downstream of external signal perception. In parallel, *At*PRK4 and *At*PRK5 may regulate the organisation of actin filaments in response to binding GRI through controlling the activities of actin-binding proteins like ADFs and LIMs; a process in which NET2s may be involved.

8.5.6. The *At*PRK4 and *At*PRK5 Subclade of *At*PRK Proteins Appears Functionally Unique.

It was observed that the interaction of NET2A & NET2B with Arabidopsis PRK proteins was restricted specifically to *At*PRK4 & *At*PRK5, whereas no interactions of NET2s were observed with *At*PRK1, *At*PRK2, *At*PRK3 or *At*PRK6. Therefore, *At*PRK4 & *At*PRK5 possess unique involvement with the actin cytoskeleton that is not found in other *At*PRK proteins. *At*PRK4 and *At*PRK5 represent a discreet evolutionary subclade of Arabidopsis PRKs, separate from *At*PRK1, *At*PRK2 & *At*PRK7, and *At*PRK3, *At*PRK6 & *At*PRK8, both sets of which comprise separate subgroups.

There is evidence to suggest that *At*PRK4 and *At*PRK5 occupy a separate functional niche from other *At*PRKs in Arabidopsis. This is firstly evident in their subcellular localisations, characterised in this investigation. Both *At*PRK4 and *At*PRK5 localised preferentially to the shank plasma membrane as discreet foci. This is distinct from the reported distributions of *At*PRK1, *At*PRK2, *At*PRK3 and *At*PRK6, which localise preferentially or exclusively to the pollen tube tip, and do not form punctae in the

shank regions. This is strongly suggestive of a unique function for *At*PRK4 and *At*PRK5. *At*PRK proteins have been implicated in the control of pollen tube growth through regulation of cellular processes occurring at the apex. *At*PRK2 for example is believed to regulate Rop1 signalling, which controls apical actin dynamics in growing pollen tubes. Working at the pollen tube tip, *At*PRK3 & *At*PRK6 also mediate the growth of pollen tubes towards the chemoattractant, *At*LURE1, most likely through regulation of Rop1. Being shank-localised, *At*PRK4 and *At*PRK5 are therefore unlikely to be involved in tip-localised processes such as the regulation of Rop1-controlled actin dynamics, and are likely to regulate pollen tube growth through an alternative, shank-specific pathway. The localisation of *At*PRK4 and *At*PRK5 may be indicative of potential roles in the organisation of the longitudinal cortical actin cables of the pollen tube shank.

8.5.7. Potential Mechanisms of NET2 Regulation by *At*PRKs in Arabidopsis.

Insights as to how Arabidopsis NET2s may be regulated by *At*PRK4 & *At*PRK5 can be drawn from studies made on the interaction between *Pi*KIP1 and *Pi*PRK1. Using FRET-FLIM, it was determined that the Petunia NET2 orthologue, *Pi*KIP1, interacts with *Pi*PRK1, confirming previous observations made from *in vitro* studies (Skirpan et al. 2001). The interaction constitutes a potential link between the plasma membrane and actin cytoskeleton: *Pi*KIP1 has a functional NAB domain which can bind actin *in vivo* (Calcutt. 2009), and could feasibly link it to the plasma membrane through an interaction with *Pi*PRK1.

It can be predicted that NET2 proteins are downstream effectors of PRKs, controlled by phosphorylation. Skirpan et al. (2001), demonstrated that *Pi*KIP1 is phosphorylated by *Pi*PRK1, indicating that *Pi*KIP1 may be a downstream signalling component of *Pi*PRK1. The phosphorylation of *Pi*KIP1 by *Pi*PRK1 is likely to be a highly significant regulatory mechanism, and appears to be important for the interaction between the two proteins. During this investigation, it was observed that *Pi*PRK1 appeared to be able to recruit *Pi*KIP1 to the plasma membrane during transient expression assays in *N. benthamiana* leaf epidermal cells. Likewise, *At*PRK4 & *At*PRK5 were also able to recruit NET2A & NET2B to the membrane in a similar manner. Therefore, PRKs may probably serve to recruit and bind NET2s at the pollen tube plasma membrane, most likely dependent on phosphorylation of

the NET2s by PRKs. This could explain a possible mechanism by which NET2 proteins may localise to the pollen tube membrane. *Pi*PRK1 interacts with and phosphorylates a fragment of *Pi*KIP1 (aa 333 – 724) consisting of the central region of the full-length protein, indicating that the phosphorylation site lies within the centre of *Pi*KIP1 (Skirpan et al. 2001). Therefore, NET2s are likely to be controlled by phosphorylation of specific sites within their central region. Phosphorylation of such sites may regulate the actin-binding activity of NET2s, as has been reported for members of other NET subfamilies: for example, phosphorylation of the c-terminal region of NET4B is believed to promote its binding to actin (Bush. 2015). Identification of the specific serine, threonine or tyrosine residues of NET2A that are phosphorylated by *At*PRKs would greatly advance our understanding of how NET2s are regulated by PRKs *in vivo*, and would permit further investigation into the effects that their phosphorylation would have on NET2 function and activity.

8.5.8. Putative Functions of NET2-PRK Interactions.

So far, it has been discussed that Arabidopsis NET2s bind actin at the plasma membrane at the shank region of growing pollen tubes at discreet foci through interactions with *At*PRK4 and *At*PRK5. This elucidates a novel mechanism by which actin is bound to the plasma membrane of plant cells, and also implicates NET2s in a signal transduction mechanism in which the actin cytoskeleton may be regulated in response to extracellular signals during fertilisation. It seems probable that NET2 proteins are downstream signalling intermediates of PRKs, which may phosphorylate and subsequently recruit NET2 proteins to the plasma membrane, perhaps in response to binding extracellular ligands. The way in which NETs may regulate pollen tube growth in response to external signals is likely to be novel, and localised to the pollen tube shank, as *At*PRK4 and *At*PRK5 appear to be spatially distinct from other *At*PRKs that regulate actin at the pollen tube tip. Discussed below are potential mechanisms by which NET2A may regulate pollen tube growth through its interactions with *At*PRKs.

8.5.8.1. NET2s as Actin-Membrane Anchors May Organise the Pollen Tube Cytoskeleton.

As discussed in chapter 1.4, the actin cytoskeleton of the growing pollen tube is highly organised to facilitate polar cell growth. Rapid, long-distance, actomyosin-based targeting of organelles and vesicles to the pollen tube tip is permitted using reverse fountain streaming in the pollen tube shank, in which anterograde transport is conducted by actin cables at the shank cortex, whilst recycling of organelles is permitted by retrograde transport along cytoplasmic actin cables (Qu et al. 2015b). The actin cytoskeleton of the pollen tube shank is considered to be highly stable, undergoing few severing events, and a high frequency of bundling events, explaining why actin exists as stable longitudinal cables in the pollen tube shank (Zheng et al. 2013; Qu et al. 2015b). Consistent with this, shank-specific actin-mediated processes such as cytoplasmic streaming are more resistant to actin disruption than tip growth, mediated by fine, unstable actin filaments at the tip (Gibbon et al. 1999; Vidali et al. 2001; Qu et al. 2015b). It is likely that the binding of actin filaments at the plasma membrane by NET2-PRK complexes may serve a role in the spatial organisation of shank actin cables, and their stabilisation during pollen tube growth.

The interaction of *At*PRKs and NET2s seems to occur at specific punctae at the pollen tube plasma membrane, constituting actin-membrane contact sites (AMCSs; figure 8.6). These AMCSs are likely to be stable anchors between the actin and membrane: analysis of dynamic movements of NET2A and PRK punctae (not discussed in this report), indicate them to be highly static, with the exception of infrequent and short linear movements along presumptive actin filaments. NET2s, through their interactions with PRKs, may serve to anchor cortical longitudinal actin filaments to the plasma membrane at AMCSs, and attach the actin cables to the membrane in a longitudinal orientation, therefore aiding to organise the ‘reverse-fountain’ structure of the actin cytoskeleton in the shank region of the pollen tube. Polymerisation of actin filaments in the pollen tube shank is initiated by membrane-bound FH3 in Arabidopsis (Ye et al. 2009). NET2A punctae at the plasma membrane may be responsible for the anchorage of extending filaments to the plasma membrane as they are polymerised, and may guide the longitudinal extension of the filament along the membrane (figure 8.7).

AMCSs formed by PRK-NET2 interactions may themselves be sites of actin regulation. NET2A may organise the actin cytoskeleton specifically at AMCSs by cross-linking actin filaments, bundling actin filaments into actin cables, or perhaps acting as adaptor proteins for the regulation of actin by other protein complexes. Noted by Dixon. (2013), was the actin-bundling ability of the NET2A NAB domain *in vivo*, perhaps indicating that NET2A may bundle actin filaments at AMCSs at the pollen tube plasma membrane. In chapter 4, it was demonstrated that NET2A was able to homodimerise, and heterodimerise with NET2B. It could be possible that the recruitment of NET2s to AMCSs by *At*PRK4 and *At*PRK5 could lead to the bundling of filaments through dimerisation of NET2s at these sites. Likewise, the dimerisation of NET2s recruited to the plasma membrane could cross-link actin filaments intersecting at AMSCs (figure 8.8). It is probable that the organisation of actin filaments into higher order structures in this manner may help to stabilise actin filaments in the pollen tube shank.

As discussed above, PRKs have been shown to interact with other actin-regulatory proteins including actin-severing ADFs and actin-bundling LIM domain proteins (Gui et al. 2014). LIMs may bundle and stabilise actin cables at AMCSs, whereas ADFs may work to sever actin cables at AMCSs to promote their turnover. It is therefore possible that NET2s serve as mediators or adaptors of actin regulation by these proteins, perhaps binding actin to the sites of ADF or LIM recruitment (figure 8.9).

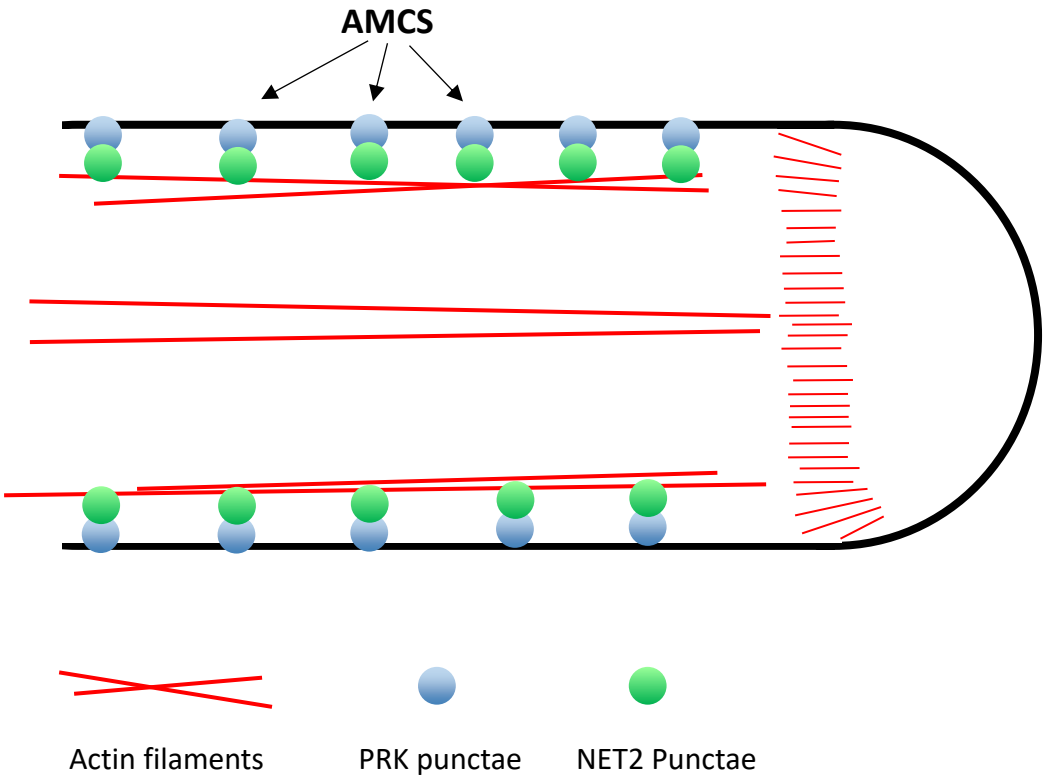

Figure 8.6: NET2A Forms Discreet Actin-Membrane Contact Sites (AMCSs) at the Shank Region of the Pollen Tube Plasma Membrane. The interaction of NET2 proteins with PRKs at individual punctae forms localised sites of physical contact between actin filaments and the plasma membrane. Original figure.

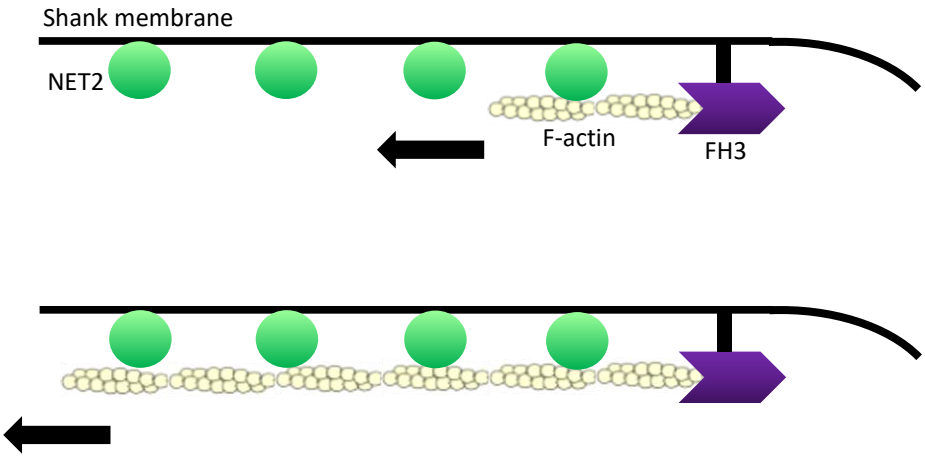

Figure 8.7: A Potential Role for NET2A in Binding Newly Polymerised Actin Filaments to the Shank Membrane. Membrane-localised Formin3 (FH3; purple chevron) initiates polymerisation of new actin filaments at the plasma membrane. Membrane-localised NET2A punctae may bind the filament to the membrane as it extends, perhaps serving to stabilise the nascent filament, or guide its polymerisation in a longitudinal orientation. Original figure.

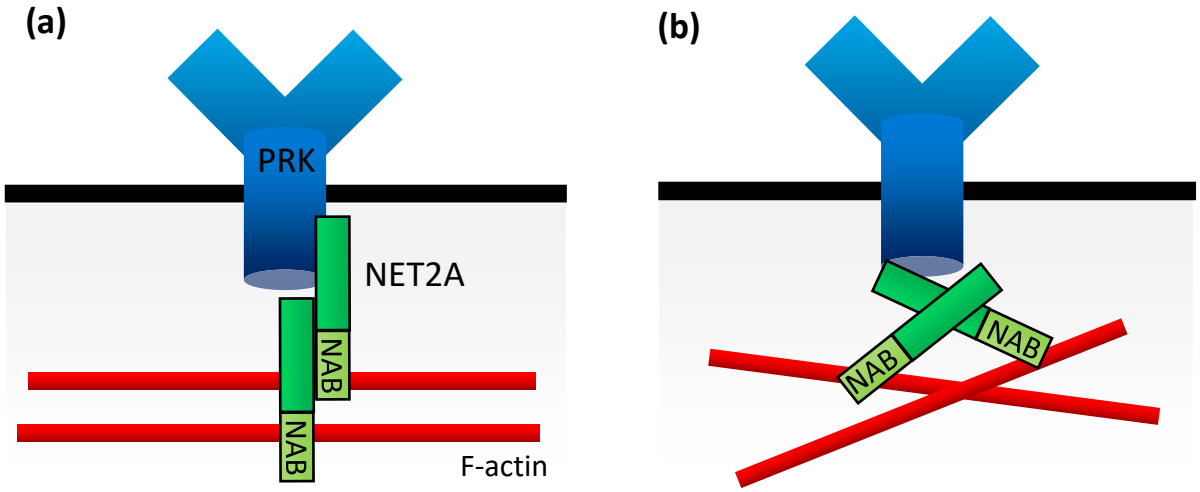

Figure 8.8: Hypothetical Organisation of Actin at AMCSs by NET2A. NET2A in AMCSs may mediate organisation of actin filaments into higher-order structures. (a): Bundling of actin filaments by NET2A at AMCSs. (b): Cross-linking of actin filaments by NET2A at AMCSs. Original figure.

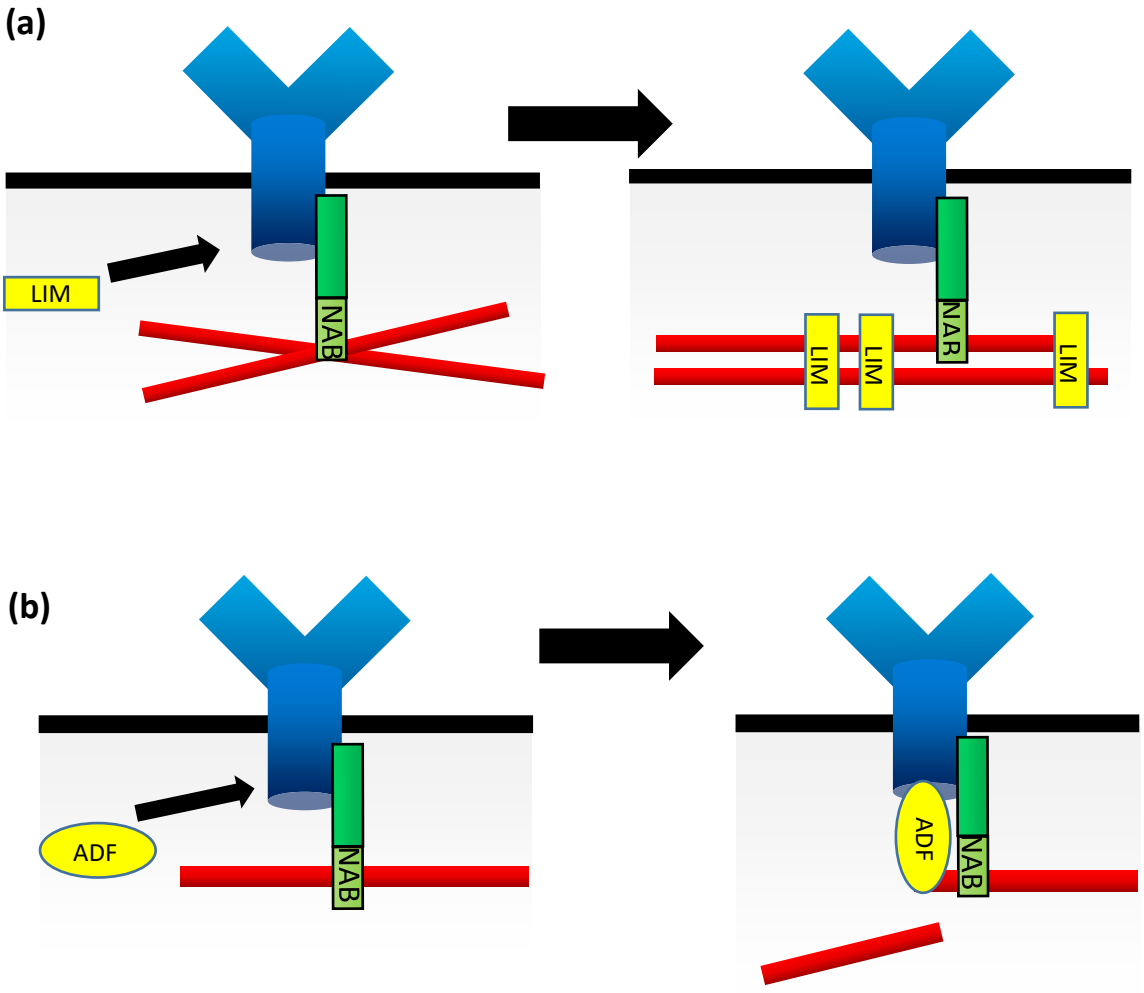

Figure 8.9: NET2A may Mediate the Organisation of Actin by Other Actin Regulatory Proteins at AMCS. (a): NET2A may mediate the bundling of actin filaments by LIM domain proteins recruited to AMCSs by PRKs. (b): NET2A may mediate the severing of actin filaments by ADFs recruited to AMCSs by PRKs. Original figure.

8.5.8.2. Potential Involvement of NET2A in Signal Transduction to the Actin Cytoskeleton During Fertilisation.

As discussed above, it is likely that *At*PRK4 and *At*PRK5 have roles in signal transduction during fertilisation, and promote pollen tube growth through the stigmatic tissues in response to binding the pistil-secreted ligand, GRI. It is possible that NET2A may be involved in this process: the actin cytoskeleton is a known target for regulation by other PRKs, and NET2s are likely downstream signalling intermediates of PRKs. It can be predicted therefore that NET2A may be involved in signal transduction; regulating the actin cytoskeleton downstream of the perception of GRI by *At*PRK4 and *At*PRK5 to promote pollen tube growth.

Whilst the role of GRI in the regulation of pollen tube growth is unknown, it appears to be important for fertilisation (Wrzaczek et al. 2009). It can be predicted that the importance of GRI in fertilisation will lie in its ability to promote pollen tube growth through the stigma, as has been reported for the tomato orthologue of GRI, *Le*STIG1, a ligand of *Le*PRK2 through which the growth signal is transduced (Huang et al 2014; Tang et al. 2004). Whereas the pistil-secreted peptide, *At*LURE1; perceived by *At*PRK6, is a chemoattractant that influences the directionality of pollen tube growth, GRI/*Le*STIG1 is predicted to influence the growth rate of pollen tubes, but not pollen tube navigation (Tang et al. 2004; Takeuchi and Higashiyama. 2016; Takeuchi and Higashiama. 2012). The role of NET2A and NET2B may well likely be tied to the regulation of actin downstream of GRI perception by *At*PRK4 and *At*PRK5 to facilitate increased rates of pollen tube elongation. Consistent with this hypothesis, the expression of NET2B appears to coincide with pollen tube growth through the stigma (see above; Dixon. 2013; Leydon et al. 2013), further implicating the NET2s' involvement during fertilisation.

The mechanisms by which NET2A may transduce pistil-secreted growth factors to regulate pollen tube growth is unknown, mainly because the role of actin in GRI/STIG1-stimulated pollen tube growth has not been studied. Indeed, no investigation of the actin cytoskeleton has been performed in pollen tubes growing through the pistil *in vivo*, or germinated under semi-*in vivo* conditions. *In vivo*, pollen tubes are known to extend at much faster rates than *in vitro*-germinated pollen tubes, most likely occurring in response to signalling cues (such as GRI/STIG1) secreted from the pistil (Qin et al. 2009; Taylor and Helper. 1997; Cheung et al. 2010). This increase in growth rate must certainly be facilitated by increased rates

of cytoplasmic streaming and apically-targeted exocytosis in order to deliver greater quantities of growth materials to the extending tip. These enhanced rates of growth must therefore be accommodated by the actin cytoskeleton, which regulates cytoplasmic streaming and targeted apical exocytosis that is crucial for pollen tube growth (Vidali et al. 2001; Gibbon et al. 1999; Qu et al. 2015b). How the actin cytoskeleton is regulated to achieve these higher rates of elongation in response to pistil-secreted factors such as GRI/STIG1 is unknown, and it cannot yet be predicted as to how NET2 proteins may be involved. Discussed below are further experiments which may elucidate the role of NET2A in fertilisation through its associations with *At*PRK4 and *At*PRK5.

8.5.9. Future Perspectives: Investigating NET2-PRK Interactions.

During this study, it was determined that NET2A binds actin at the pollen tube plasma membrane at discreet sites through interactions with *At*PRK4 and *At*PRK5, which are likely to have niche functional roles in regulating the actin cytoskeleton in response to extracellular signals during pollen tube growth and fertilisation. To elucidate the specific role of the PRK-NET2 complex in the organisation of the actin cytoskeleton, and its involvement in signal transduction, some further experiments must be performed, as outline below.

Firstly, it is necessary to understand the importance of the AMCSs established through the interactions between NET2A & NET2B and *At*PRK4 & *At*PRK5, in order to understand how they may organise the actin cytoskeleton of pollen. Disruption of AMCSs, achieved by preventing interactions between NET2s and PRKs, may elicit defects in the organisation of the pollen tube cytoskeleton and therefore its growth and morphology, making it possible to evaluate the importance of NET2-PRK interactions. Several approaches may be employed to achieve this. Firstly, reverse-genetic analysis of NET2 mutants would be a powerful tool: in *net2* transcriptional null mutants, actin could no longer be bound at AMCSs, perhaps inducing disorganisation of the actin cytoskeleton. As described previously, analysis of *net2* double mutants should be performed, which may help to elucidate the role of NET2 proteins at AMCSs. Secondly, reverse-genetic analysis of *atprk4* and *atprk5* mutants may establish a role for AMCSs: in mutants lacking *At*PRK4 and *At*PRK5, NET2s may not be recruited to the membrane to bind actin there, and

disorganisation of the actin cytoskeleton may be caused as a result. Performed during this study, but not described, was the analysis of NET2A-GFP subcellular localisation in pollen tubes of *prk4* and *prk5* mutants characterised previously (Chang et al. 2013; Wrzaczek et al. 2015). The localisation of NET2A-GFP appeared unaffected in these mutants, indicating NET2A could still be recruited to the membrane normally. The previously described *prk5* mutants are unlikely to be suitable for reverse-genetic analysis. The first available *prk5* mutant; *prk5-1* is insubstantially designated as a 'suppression' mutant (Chang et al. 2013) and appears to be transcriptionally active (Takeuchi and Higashiyama. 2016). The second, *prk5-2*, appears to be a truncation, lacking only a small c-terminal fragment (Wrzaczek et al. 2015; Takeuchi and Higashiyama. 2016), and may still be fully functional. This may explain the lack of a defect in NET2A localisation and pollen tube growth in these lines. Functional redundancy between *At*PRK4 and *At*PRK5 may explain why NET2A localisation was unaffected in *prk4* mutants: NET2A can interact with both PRKs, the loss of *At*PRK4 alone may not be enough to elicit a phenotype. The generation of *prk4/prk5* knockout mutants using alternative methods such as RNAi could be employed to further this avenue of research, however, insufficient time remained to perform these experiments. Thirdly, dominant negative mutants could be used to prevent the interaction between NET2A and *At*PRK4 & *At*PRK5. It was noted during this study, (but not described in this thesis) that truncations of *At*PRK4 and *At*PRK5 lacking c-terminal kinase domains could not interact with NET2A and recruit it to the membrane in *N. benthamiana* leaf epidermal cells. Overexpression of these constructs in pollen may displace endogenous *At*PRK4 & *At*PRK5 at AMCSs, preventing the recruitment of NET2A and binding of actin to the membrane: it would be highly insightful to visualise NET2A subcellular localisation in such lines, as well as the organisation of the actin cytoskeleton.

The effects of GRI on the regulation of actin by NET2A should also be investigated. Purification of recombinant GRI would allow its application to growing pollen tubes as has been performed using *Le*STIG1 previously (Tang et al. 2004; Huang et al. 2014). This would permit investigation into its effects on pollen tube growth, actin organisation and potential changes in NET2A subcellular localisation at the pollen tube membrane. It is possible that binding of GRI by *At*PRK4 and *At*PRK5 may cause them to phosphorylate NET2s, and alter their subcellular localisation or their regulation of, or association with actin. The effects of GRI on pollen tube growth and actin organisation could also be investigated in the *net2*, *prk,* and dominant negative

mutants discussed above, to see if the NET2-PRK complex may be important in transducing extracellular signals such as GRI during pollen tube growth.

8.6. The MAP7s as Novel Plant Microtubule-Associated Proteins.

8.6.1. Summary of Results.

In chapter 7, MAP7A was identified as a potential interactor of NET2A in a SU-Y2H screen. This protein was determined to be a microtubule-associated protein in a series of *in vivo* and *in vitro* assays, and full and thorough investigation of MAP7A as a novel plant microtubule-associated protein ensued. Bioinformatic analysis indicated MAP7A to be a member of a highly conserved family of SERF proteins, present in Planta, Animalia and Fungi. In Arabidopsis, two other SERF proteins were identified: MAP7B was also investigated, whereas MAP7C was not studied further as it showed little homology to MAP7A. *In situ* analysis of MAP7A and MAP7B indicated both proteins to be expressed in pollen, at increasing levels throughout pollen grain development. Additionally, MAP7B was expressed in the root vasculature in the zone of elongation. Using immunofluorescent staining of Narcissus pollen tubes, MAP7A was observed to localise to punctae at the pollen tube plasma membrane, and also at punctae associated with microtubules of the generative cell. *map7a* and *map7b* single mutants, and *map7a/map7b* double mutants were generated and analysed to identify a potential role for MAP7 proteins in Arabidopsis, but no phenotype could be observed in these lines.

Although MAP7A was identified as an interactor of NET2A in the SU-Y2H screen, proof of an interaction between NET2A and MAP7A could not be substantiated further. However, the identification of a novel family of microtubule-binding proteins is highly significant, and understanding the importance of MAP7A's functions in Arabidopsis could greatly increase current understanding of how microtubules are regulated in plants, and the importance of microtubules in pollen tube growth and fertilisation. Discussed below are the potential implications of the discovery of MAP7A, and how it might function in plants.

8.6.2. The MAP7 Proteins as Microtubule-Associated Proteins.

MAP7A and MAP7B were both determined to be microtubule-associated proteins in chapter 7.2. Both proteins decorated a similar network of filaments when expressed as fluorophore fusion proteins in *N. benthamiana* leaf epidermal cells. The filament system formed by MAP7A-GFP co-localised with microtubule marker constructs and was disrupted by pharmacological breakdown of the microtubule cytoskeleton. MAP7A associated with microtubules directly *in vitro*, as determined by microtubule co-sedimentation. Therefore, it was clearly determined through multiple methods that MAP7 proteins could associate with microtubules directly, indicating that the MAP7 protein family are a novel group of microtubule-associate proteins in Arabidopsis.

When expressed in *N. benthamiana* leaf epidermal cells, both MAP7A-GFP and MAP7B-GFP appeared to associate with microtubules in similar arrangements to each other. Each protein formed a fine filament system and did not appear to induce bundling of microtubules. MAP7A-GFP filaments were highly static, and growth and shrinkage of microtubules labelled with MAP7A-GFP was observed very rarely. It is unsurprising that the microtubule-binding activity of MAP7A and MAP7B are similar, due their very high degree of conservation. It could be predicted, based on observations of MAP7A-GFP and MAP7B-GFP *in vivo*, that MAP7s are unlikely to exhibit microtubule-bundling activity in Arabidopsis, but may serve as microtubule-stabilising proteins.

The high degree of conservation between Arabidopsis MAP7A and MAP7B, and SERF proteins from Yeast (such as YDL085-C), and Animals (MOAG-4 and SERF2C), may indicate a similar function for these proteins across Eukaryota. It is therefore possible that SERF proteins may bind and regulate microtubules in Fungi and Animals. The particularly high degree of conservation between the N-terminal SERF domains of these proteins, which has been demonstrated to mediate the association of MAP7A with microtubules, is likely to confer microtubule-binding function to SERF proteins in Animals and Fungi. Not examined during this study, was MAP7C, a previously uncharacterised protein encoded by the gene locus, At2g23090, designated as a putative relative of MAP7A due its N-terminal Pfam 4F5 SERF domain. Although this protein exhibited a low level of homology to MAP7A and MAP7B, it is possible that MAP7C could also associate with microtubules through its N-terminal SERF domain.

8.6.3. The Potential Role of MAP7A at the Pollen Tube Plasma Membrane.

It was revealed using the GUS-reporter system, that MAP7A and MAP7B were expressed in pollen at increasing levels throughout pollen grain development, indicating a role of MAP7 proteins in mature pollen. Therefore, the subcellular localisation of MAP7A was analysed in pollen tubes using immunofluorescence. It was observed that MAP7A localised to discreet foci at the pollen tube plasma membrane. Discussed below are the potential functions that MAP7A could perform at the plasma membrane of growing pollen tubes.

In growing pollen tubes, microtubules are organised into stable longitudinal bundles at the cell cortex of the pollen tube shank, and are present as short, dynamic, randomly orientated filaments in the apical region (Idilli et al. 2013; Cheung. 2008). Microtubules are predicted to have minor roles in pollen tube growth, but are believed to have roles in maintaining pollen tube morphology and growth direction (Gossot and Geitmann. 2007; Idilli et al. 2013). Slow, short range transport of vesicles and organelles by the microtubule cytoskeleton has been predicted to mediate 'fine-positioning' of organelles in pollen tubes, and microtubules are believed to regulate actin-independent modes of exocytosis and endocytosis at the pollen tube tip (Romagnoli et al. 2007; Idilli et al. 2013). Transport of the MGU during pollen tube growth is also suspected to be dependent on microtubules (Heslop-Harrison et al. 1988; Joos et al. 1994; Astrom et al. 1995). Finally, the microtubule cytoskeleton is thought to facilitate the deposition of callose to the cell wall in the shank regions of the pollen tube, and a physical association of callose synthase with microtubules has been documented (Cai et al. 2011). It is possible that MAP7A and MAP7B may be involved in the regulation of microtubule-dependent process occurring in the growing pollen tube.

MAP7A and MAP7B are likely to bind microtubules at the pollen tube membrane. During this study it was not possible to visualise the association of MAP7A with the cortical microtubules of the pollen tube shank, which were not preserved during the immunofluorescence fixation process. However, similar to the punctate localisation of MAP7A at the pollen tube membrane, MAP7A-GFP also formed punctae when expressed in *N. benthamiana*, which aligned along microtubules. It is probable therefore, that the MAP7A punctae observed at the pollen tube membrane could also be associated with microtubules *in vivo*. It is possible that MAP7s may be involved in linking the cortical longitudinal microtubules to the pollen tube plasma

membrane. No transmembrane domain is present in the MAP7A and MAP7B protein sequence: it is therefore likely that their localisation to the membrane, or cortical regions of the cell, is dependent on interactions with other proteins, or lipids of the plasma membrane. Through interactions with other proteins, or direct association with the membrane, MAP7 proteins may link microtubules to the cell cortex of growing pollen tubes. Discussed later is the potential for such a mechanism to occur through an interaction between MAP7A, and NET2A. MAP7A and MAP7B may have a role in organising the microtubule cytoskeleton in the pollen tube shank. Microtubules at the pollen tube shank are known to be immobile and stable. As described above, it can be predicted that MAP7A may act to stabilise microtubule filaments, and these proteins may be responsible for conferring this observed stability to the microtubules of the pollen tube shank.

Similar to MAP7A, a plasma membrane localisation has been observed for other microtubule-binding proteins in growing pollen tubes. MAP18 and MDP25 are both known to associate with, and regulate microtubules in somatic tissues, and localise to the plasma membrane in pollen, similar to MAP7A. However, in pollen tubes, MAP18 and MDP25 are reported to mediate severing of F-actin (Zhu et al. 2013; Qin et al. 2014). A role for MAP7A and MAP7B in the regulation of the actin cytoskeleton was not investigated during this study, and it is possible that they may regulate the actin cytoskeleton during pollen tube growth.

From the data gathered, it can only be speculated as to whether MAP7A and MAP7B may have a role in organelle transport, vesicle trafficking, nuclear positioning or cell wall deposition. During reverse-genetic analysis, no essential function for MAP7A or MAP7B was observed in pollen grain development, pollen tube growth, or fertilisation. It is possible that the roles of MAP7A and MAP7B may be functionally redundant to those of MAP7C, which was not studied during this investigation. It may be necessary to generate *map7a/map7b/map7c* triple mutants in order to ascertain a functional role of the MAP7 proteins at the pollen tube plasma membrane.

8.6.4. The Potential Role of MAP7A in the Generative Cell.

Immunofluorescence analysis of MAP7A subcellular localisation in Narcissus pollen tubes also revealed it to localise to the GC, where it could be observed to associate with microtubules.

Microtubules are known to form a cage-like structure at the cortex of the generative cell, which is thought to be responsible for the formation and maintenance of the GC's elongated morphology (Theunis et al. 1992; Oh et al. 2010; McCue et al. 2011). During PMII, the GC microtubules assemble into the spindle and phragmoplast arrays to co-ordinate the division and separation of the GC into two daughter sperm cells (SCs; Palevitz. 1993; Oh et al. 2010; Joos et al. 1994; Kliwer and Dressehaus. 2010). Following PMII, microtubules form a cage around the sperm cell nuclei (SCN), which extends a tail connecting the SCs to the VCN. The role of these microtubules following PMII appears structural: the SCs of the MGU remained linked to the VCN by a cytoplasmic projection, for which the microtubule cytoskeleton of the interconnected SCs is believed to provide a mechanical framework. The microtubules of the GC orchestrate cell division during PMII, and are thought to regulate the organisation of MGU morphology following PMII (Oh et al. 2010; McCue et al. 2011). It is possible that MAP7A may have a role in the regulation of microtubules in the GC, during PMII, and perhaps in the MGU.

It was observed that MAP7A associated with the microtubules of the generative cell in Narcissus pollen tubes. Specifically, MAP7A appeared to localise to the periphery of the microtubule cage. The GC microtubules have been described to form a basket at the cortex of the GC, surrounding the nucleus (Theunis et al. 1992). The association of MAP7A with the periphery of the microtubule basket may suggest a role for MAP7A in binding these cortical microtubules at the cortex, or membrane of the generative cell. As described above, MAP7A localises to punctae at the pollen tube plasma membrane, and it is therefore likely that the MAP7A punctae of the GC are, likewise, membrane-associated. MAP7A may link the microtubule basket to the membrane of the GC, or may regulate the organisation or dynamics of the microtubules.

MAP7A may be involved in the microtubule-controlled elongation of the GC that occurs in late bicellular pollen. As discussed above, MAP7A may be predicted to stabilise microtubules, and stabilisation of the GC microtubule basket by MAP7A

may confer structural rigidity to the cytoskeletal framework that maintains the elongated morphology of the GC.

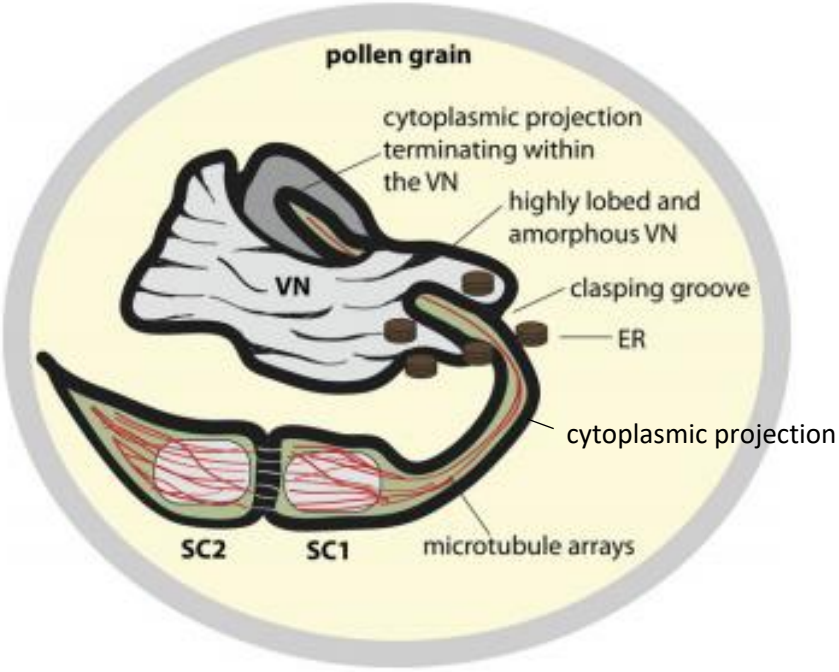

Figure 8.10: The Microtubules of the Male Germ Unit. A microtubule basket surrounds the two sperm cell nuclei and extends a tail connecting the sperm cells to the vegetative cell nucleus via the cytoplasmic projection. SC1 = sperm cell 1. SC2 = sperm cell 2. VN = vegetative nucleus. Taken from McCue et al. (2011).

During PMII, a physical connection between the GC microtubules and membrane may help to facilitate the separation of chromosomes by the mitotic spindle. The microtubule spindle is known to exert both inward forces, towards the plane of cell division, and outward forces towards the cell poles (Masoud et al. 2013; Dixit and Cyr. 2002; Ambrose and Cyr. 2007; Chen et al. 2002), necessary to facilitate the separation of chromosomes towards each cell pole. In mammalian cells, anchorage of microtubules at the spindle poles is necessary to bear the load of forces generated by the kinetochore-associated motor proteins during the movement of chromosomes (Gordon et al. 2001). MAP7A, by binding microtubules to the GC membrane, may serve to bear the load of mechanical forces exerted by the spindle during PMII. Therefore, the GC membrane may act as a substrate against which microtubules may be able to exert forces needed to separate chromosomes during PMII.

Although the subcellular localisation of MAP7A was observed in the GC, its subcellular localisation in the SCs following PMII was not documented. The two SCs of the MGU are physically connected, perhaps sharing plasma membrane and cytoplasm (McCue et al. 2011). The SCs also contain cortical cytoskeletal arrays, inherited from the GC, which link the two SCs to the VCN through the cytoplasmic projection (McCue et al. 2011; Oh et al. 2010). Whether the association of MAP7A with the microtubules of the GC persists as an association with the SC microtubules after PMII remains to be seen. MAP7A may have an important role in regulating or organising the microtubules of the MGU. The role of the microtubule cytoskeleton within the MGU is thought to be structural, and contributes to the morphology of the sperm nuclei and integrity of the MGU (Ge et al. 2011; Theunis et al. 1992; McCue et al. 2011). MAP7A may be important in regulating the SC microtubules to mediate the organisation and structuring of the MGU. It is possible that stabilisation of microtubules by MAP7A, as hypothesised above, may confer structural integrity to the MGU. Perhaps, interactions between microtubules and the SC membranes mediated through MAP7A may be vital in shaping and organising the MGU membranes and the cytoplasmic projection. It is possible that MAP7A may associate with the microtubules of the SCs and the cytoplasmic projection, however further investigation will be needed to confirm this.

8.6.5. MAP7A as an Interacting Partner of NET2A.

MAP7A was originally identified as an interacting partner of NET2A, in a SU-Y2H screen. However, this result could not be substantiated using 1-on-1 GAL4 Y2H assays, or by FRET-FLIM. It is possible that MAP7A may be a genuine interactor of NET2A, and that an interaction between these two proteins could not be detected with the techniques employed.

Interestingly, when co-expressed in *N. benthamiana*, co-localisation was observed between MAP7A-GFP and NET2A-mCherry. The proteins appeared to co-localise along filaments, and also at punctae. In Arabidopsis, both proteins are pollen-specific, and form punctae at the pollen tube plasma membrane. Based on observations made in *N. benthamiana*, it could be predicted that MAP7A may co-localise with NET2A punctae at the pollen tube membrane.

Whether or not MAP7A and NET2A may interact directly can, for now, only be speculated. Further analysis of the interaction must be performed using alternative methodologies to corroborate the interaction observed in the SU-Y2H screen. However, hypotheses regarding the roles of a speculative interaction between NET2A and MAP7A will be discussed below.

8.6.6. MAP7A as an Actin-Microtubule Linker Protein.

An association between NET2A and MAP7A would implicate the two proteins as mediators of actin-microtubule interactions, at the cortex of growing pollen tubes. As discussed previously, NET2A is predicted to bind actin at specific foci at the plasma membrane of growing pollen tubes, at discreet AMCSs. It was also observed that MAP7A localises to punctae at the pollen tube membrane. It could be speculated that MAP7A localises to AMCSs through an interaction with NET2A, binding microtubules to these sites of actin-membrane interactions. Therefore, AMCSs would in fact constitute discreet sites of actin-microtubule-membrane interactions at the pollen tube cortex. Such functions have been reported of the NET superfamily previously, and NET3C is involved in mediating the interactions of actin and microtubules at discreet sites of the endoplasmic reticulum membrane (Wang et al. 2014).

Interactions between actin and microtubules are believed to occur in pollen tubes. Co-alignment between longitudinal actin and microtubule cables in the pollen tube shank has been documented (Pierson et al. 1989), and functional synergy between both cytoskeletal networks has also been observed, leading to suggestions that the microtubule cytoskeleton may stabilise actin filaments or guide their polymerisation. Inversely, actin filaments may guide the polymerisation of, or stabilise microtubules (Gossot and Geitmann. 2007). In cells of somatic tissues, it is known that the polymerisation of actin occurs along microtubule filaments, and polymerisation of microtubules is also guided by actin filaments. Reorganisations of actin filaments in response to external stimuli is also dependent on microtubules, which undergo co-ordinated rearrangements in tandem with the actin cytoskeleton (Sampathkumar et al. 2011). Therefore, the dynamic spatial organisation of the actin cytoskeleton is dependent on microtubules, and vice versa. In pollen tubes, a role for microtubules in the regulation of the actin cytoskeleton is possible.

The actin cytoskeleton is essential for pollen tube growth through regulation of cytoplasmic streaming and delivery of secretory vesicles to the pollen tube tip (Vidali et al. 2001; Gibbon et al. 1999; Lee et al. 2008). In contrast, disruption of the microtubule cytoskeleton induces only minor defects in pollen tube growth and morphology. Therefore, the roles of microtubules are likely to be subsidiary to those of actin, and microtubules may serve to direct, or 'fine-tune' the organisation of actin filaments in the pollen tube shank. Therefore, the longitudinal microtubule cables of the pollen tube may serve to organise actin filaments of the pollen tube shank. As described above, the dynamic and spatial organisation of actin is dependent on its interactions with microtubules (Sampathkumar et al. 2011). An interaction between NET2A and MAP7A may mediate rearrangements of the actin cytoskeleton under control of microtubules by bridging a physical link between the two filament systems. The microtubule cytoskeleton may also provide guidance for the polymerisation of actin filaments at the shank membrane: an interaction between MAP7A and NET2A may bind polymerising actin filaments to microtubules, to guide microfilament extension longitudinally, along the length of microtubule tracks.

MAP7A may also stabilise actin filaments at the pollen tube shank. Stabilisation of microtubules by MAP7A, as hypothesised above, may also indirectly stabilise actin filaments bound to microtubules through the interaction of MAP7A and NET2A. It has been observed that disruption of the microtubule cytoskeleton renders the actin cytoskeleton hypersensitive to pharmacological disruption (Collings et al. 2006), indicating that the microtubular cytoskeleton is important in maintaining the stability of the actin network in plant cells. MAP7A may stabilise the microtubule cytoskeleton and therefore the actin cytoskeleton, physically linked to microtubules through the NET2A-MAP7A complex.

Finally, it is also possible that MAP7 proteins may regulate actin directly. Two microtubule-binding proteins, MAP18 and MDP25, which both localise to the pollen tube plasma membrane, have been demonstrated to regulate actin dynamics by severing F-actin filaments in growing pollen tubes (Zhu et al. 2013; Qin et al. 2014). MAP7A might also regulate actin directly in growing pollen tubes, in a similar manner to MAP18 and MDP25. It is possible in this scenario that NET2A may act as an adaptor protein, to mediate the association of MAP7A and actin at the plasma membrane.

8.6.7. Future Perspectives: Further Characterisation of MAP7A.

To fully understand the role of MAP7A and MAP7 proteins in Arabidopsis, further experiments could be performed, as described below.

Firstly, the potential association of cortical MAP7A punctae with microtubules at the pollen tube plasma membrane should be further investigated. During this study, preservation of the cortical microtubule array was not observed during immunofluorescence analysis of MAP7A subcellular localisation in Narcissus pollen tubes. Therefore, analysis of MAP7A co-localisation with microtubules at the cell cortex could not be performed. Analysis of the potential association of MAP7A with microtubules is crucial in understanding how it may function, and whether it may regulate the microtubule cytoskeleton at the pollen tube plasma membrane. Preservation of the cortical microtubule array using chemical fixation has been performed in tobacco pollen tubes (Astrom et al. 1995; Joos et al. 1994). The co-localisation of MAP7A and microtubules could be studied using these methods of immunofluorescence microscopy in tobacco, in the future.

Secondly, the subcellular localisation of MAP7A within the generative cell should be analysed in more detail, to investigate whether MAP7A may bind microtubules at the generative cell membrane. Transmission electron microscopy (TEM) would reveal the subcellular localisation of MAP7A in ultra-high resolution that could not be acquired using CLSM, and distinguish the specific subcellular structures with which MAP7A associates in the generative cell. This may provide insight into the nature and potential role of MAP7A's association with the GC microtubule cage, and would determine whether MAP7A associates with the GC membrane.

It has been speculated during this investigation that MAP7A may stabilise microtubules *in vivo*. The direct effects of MAP7A on microtubules could be investigated *in vitro*, by observing the dynamics and organisation of purified microtubules in the presence of purified recombinant MAP7A. Microtubule turbidity assays can be used to measure the effects of MAP7A on microtubule polymerisation and depolymerisation. Visualisation of fluorescently-labelled microtubules *in vitro* can be performed to observe the effects of MAP7A on microtubule dynamics and organisation. For example, MAP65-1 has been demonstrated to bundle suspensions of fluorescently-labelled microtubules *in vitro*, and promote polymerisation of microtubule filaments from purified tubulin in turbidity assays

(Smertenko et al. 2004; Mao et al. 2005). To test the ability of MAP7A to stabilise microtubules, cold-induced depolymerisation of fluorescently-labelled microtubules *in vitro* can be performed in the presence of MAP7A, to determine whether it may stabilise the microtubules against depolymerisation. This method has been used to demonstrate microtubule-stabilising functions of proteins such as MAP60 (Rutten et al. 1997).

To understand the role of MAP7 proteins in Arabidopsis, reverse genetics should be continued to elicit a phenotype from loss-of-function *map7* mutants. No major defects in pollen development, tube growth or fertilisation could be observed in *map7a, map7b* or *map7a/map7b* knockout mutants, indicating they had no essential role in the regulation of these processes. MAP7C, which although is relatively poorly conserved with MAP7A & MAP7B, is predicted to be a SERF family protein, and contains an N-terminal Pfam 4F5 domain, characteristic of SERF proteins. It is therefore possible that MAP7C may also function alongside MAP7A & MAP7B as a microtubule-binding protein in pollen tubes. *map7a/map7b/map7c* triple knockout mutants should be developed and analysed, to assess whether the function of MAP7A and MAP7B are functionally redundant to MAP7C. Phenotypic defects arising in triple knockout mutants may elucidate roles for MAP7s in the regulation of the microtubule cytoskeleton in pollen. Cloning and expression of MAP7C as a fluorophore fusion protein in *N. benthamiana* leaf epidermal cells may also be a rapid and effective means of determining whether MAP7C may associate with microtubules in a similar manner to MAP7A and MAP7B.

Further investigation into the interaction of NET2A and MAP7A should also be considered. The co-localisation of NET2A and MAP7A in *N. benthamiana* leaf epidermal cells, and the strikingly similar subcellular localisation patterns formed by these proteins at the pollen tube plasma membrane suggests that the two proteins may interact directly or indirectly. Further interaction studies, such as co-immuno precipitations or pulldown assays could be employed to test their interaction. Analysis of co-localisation between NET2A and MAP7A in pollen tubes would greatly help to determine whether the two proteins may associate, and function together at the pollen tube membrane.

The role of MAP7s in the regulation of the actin cytoskeleton was not analysed during this study. MAP7A may regulate the actin cytoskeleton through an association with NET2A, or could regulate actin directly as has been reported for

other microtubule-binding proteins in pollen, such as MAP18 and MDP25 (Zhu et al. 2013; Qin et al. 2014). Various reports have indicated a role for the microtubule cytoskeleton in the stabilisation and organisation of actin (Sampathkumar et al. 2011; Collings et al. 2006; Gossot and Geitmann. 2007), which may be mediated by MAP7A. Simple pharmacological analysis of potential regulation of actin by MAP7 proteins could be performed by treating *map7* mutant pollen tubes with low doses of actin-depolymerising drugs, to determine if mutant pollen tubes are hypersensitive to actin disruption. Visualisation of actin in *map7* mutant pollen tubes, using fluorescent actin reporter constructs (as described in chapter 4) could allow analysis of potential disorganisation of the actin cytoskeleton, and determine a role for MAP7s in the regulation of actin. To determine whether MAP7A may bind actin directly, *in vitro* F-actin binding assays could be performed, similar to the microtubule co-sedimentation assay performed in chapter 7.

8.7. Conclusion.

The aim of this thesis was to analyse the potential functions of NET2A in Arabidopsis, through the use of reverse-genetic analysis, *in situ* analysis of NET2A's associations with actin, and identification of interacting partners of NET2A, to identify the cellular processes with which NET2A is involved *in vivo*. The finds of this investigation suggest that NET2A is likely to play an important role in pollen grain development and fertilisation.

In situ analysis of NET2A subcellular localisation in developing pollen grains was performed to research its potential roles in gametogenesis. NET2A was observed to associate with the actin cytoskeleton, as it underwent dynamic reorganisations at specific stages of pollen grain development. This indicates an important role for NET2A in the regulation of actin in gametogenesis. Based on reverse-genetic analysis of NET2 subfamily members, the role of NET2A in gametogenesis is likely to be shared with other NET2s, most likely NET2D. Analysis of pollen grain development in *net2* double mutants will be imperative in understanding NET2A's importance during pollen maturation.

NET2A and NET2B were demonstrated to interact with a specific subclade of PRKs; comprised of *At*PRK4 and *At*PRK5, but not *At*PRK1, *At*PRK2, *At*PRK3, and *At*PRK6.

NET2 proteins interact with PRKs at discreet punctae at the plasma membrane, forming specific actin-membrane contact sites (AMCSs) at which actin is physically linked to the plasma membrane. It is likely that NET2A is a downstream signalling component of *At*PRK4 & *At*PRK5: NET2A & NET2B are recruited to the membrane by, and are probably phosphorylated by *At*PRK4 & *At*PRK5 *in vivo*. The involvement of the NET2s with PRKs implicates them in the regulation of pollen tube growth in response to extracellular signals in the pistil tissue during fertilisation. As is evident from reverse genetic analysis, these roles of NET2A will be shared between multiple NET2 subfamily members, probably through their interactions with *At*PRK4 & *At*PRK5. At AMCSs, NET2A may form NET2A-NET2A homodimers and NET2A-NET2B heterodimers, perhaps serving to organise the actin cytoskeleton at these foci. The importance of NET2A in AMCSs remains an exciting prospect for future study and is likely to play a crucial role in the organisation of the cytoskeleton, with potential signalling functions.

From the protein-protein interaction screens performed during this investigation, a previously uncharacterised protein, named MAP7A in this study, was characterised as a novel microtubule-binding protein. MAP7A, belongs to a family of SERF proteins, highly conserved in plants, animals and fungi, all of which contain a conserved N-terminal SERF domain, through which MAP7A was shown to associate with microtubules directly. The expression of MAP7A was revealed to be specific to pollen, in which it localises to punctae at the pollen tube plasma membrane, and associates with microtubules in the pollen generative cell. This implicates MAP7A in the regulation of cortical longitudinal microtubules in the pollen tube shank, and perhaps in the regulation of PMII or the organisation of the MGU. Further investigation of the interaction between NET2A and MAP7A may highlight a novel mechanism that mediates the interaction of actin and microtubule cytoskeletal arrays in plants.

Appendix 1: Primers.

1.1. Primers used to Amplify Full-Length Coding Sequences from cDNA.

Primer name	Sequence	Tm (ºC)	Target gene
NET2A_F	ATGTTGCAGAGAGCAGCGAGCAATG	62.3	At1g58210 (*NET2A*)
NET2A_R	TTATTCAGGGAGCTTCCCA	52.0	
***Pi*PRK1_F**	GCAATGCTTATGCCTCAAATTGTG	59.3	AAA33715.1 (*PiPRK1*)
***Pi*PRK1_R**	TCGGCAGGTTTATTTCCGCATCAG	62.7	
***Pi*KIP1_F**	TTGACAAGATGTTGCAGAGAG	55.9	AY029758 (*PiKIP1*)
***Pi*KIP1_R**	TTGGCAGCCTATCCAGATAC	57.3	
***At*PRK1_F**	ATGCCTCCCATGCAGGCGCGTACCC	68	At5g35390 (*AtPRK1*)
***At*PRK1_R**	TCATGCAAAGCTGATACTCTCGCATGACTCT	63	
***At*PRK2_F**	ATGGAATCCAAATGTCTCATGTTCG	56	At2g07040 (*AtPRK2*)
***At*PRK2_R**	TCATGACAAGTTAATTCCCTCACTTGATAGTCCC	61	
***At*PRK3_F**	ATGACTGCTGTTCTATTTCTCTGCTTCC	59	At3g42880 (*AtPRK3*)
***At*PRK3_R**	CAAAGTGTTACTCGTTCTATCCTTCTAACAA	57	
***At*PRK4_F**	ATGCTAACTTGGGAGACCCCAG	58	At3g20190 (*AtPRK4*)
***At*PRK4_R**	TCGATTCATGGCGAAACCAAAGT	57	
***At*PRK5_F**	ATGCGCAATTGGGAGGACCCGTTT	63	At1g50610 (*AtPRK5*)

***At*PRK5_R**	TCGATTCATCGAGAAACCAAAGTCATCATCGTC	62	At1g50610 (*AtPRK5*)
***At*PRK6_F**	ATGGCTGCTGCTGTTCTGAATC	57	At5g20690 (*AtPRK6*)
***At*PRK6_R**	AGTTTTTACTTGTTCTATCCTTCTAACAGC	55	
MAP7A_F	ATGACTCGAGGAAGTCAAAGAGA	55	At3g24100 (*MAP7A*)
MAP7A_R	TCACTTATTGTTTCCTTTGCCTCCTC	57	
MAP7B_F	ATGACTCGTGGAAGTCAGAGAGA	56.8	At4g13615 (*MAP7B*)
MAP7B_R	CTTCTTAGCAGCAGCTCCTTTTCCTC	60	

1.2. Primers Used for Amplifying Full-Length Coding Sequences for Insertion into pDONR207.

Primer name	Sequence	Tm (ºC)	Target gene
NET2A_GatF	GGGGACAAGTTTGTACAAAAAAGCAGGCTT CACCATGTTGCAGAGAGCAGCGAGC	73	At1g58210 (*NET2A*)
NET2A_GatR	GGGGACCACTTTGTACAAGAAAGCTGGGTC TTCAGGGAGCTTCCCAGGTG	73	
NET2B_GatF	GGGGACAAGTTTGTACAAAAAAGCAGGCTT CACCATGTTGCAGAGAGCAGCGAGC	73	At1g09720 (*NET2B*)
NET2B_GatR	GGGGACCACTTTGTACAAGAAAGCTGGGTC GCTTCTTTTGACATATTCAGG	70	
***Pi*PRK1_GatF**	GGGGACAAGTTTGTACAAAAAAGCAGGCTT CACCATGATGACGGAGGTGCATGA	> 75	AAA33715.1 (*PiPRK1*)
***Pi*PRK1_GatR**	GGGGACCACTTTGTACAAGAAAGCTGGGTC AACTCCAGCATCATGCATTTG	> 75	
***Pi*KIP1_GatF**	GGGGACAAGTTTGTACAAAAAAGCAGGCTT CACCATGTTGCAGAGAGCTGCCA	> 75	AY029758 (*PiKIP1*)

***Pi*KIP1_GatR**	GGGGACCACTTTGTACAAGAAAGCTGGGTC GAATTTCCTATTGGGATTCATGCGT	> 75	AY029758 (*PiKIP1*)
***At*PRK1_GatF**	GGGGACAAGTTTGTACAAAAAAGCAGGCTT CACCATGCCTCCCATGCAGGCG	74	At5g35390 (*AtPRK1*)
***At*PRK1_GatR**	GGGGACCACTTTGTACAAGAAAGCTGGGTC TGCAAAGCTGATACTCTC	70	
***At*PRK2_GatF**	GGGGACAAGTTTGTACAAAAAAGCAGGCTT CACCATGGAATCCAAATGTCTCATGTTCG	70	At2g07040 (*AtPRK2*)
***At*PRK2_GatR**	GGGGACCACTTTGTACAAGAAAGCTGGGTC TGACAAGTTAATTCCCTCAC	69	
***At*PRK3_GatF**	GGGGACAAGTTTGTACAAAAAAGCAGGCTT CACCATGACTGCTGTTCTATTT	69	At3g42880 (*AtPRK3*)
***At*PRK3_GatR**	GGGGACCACTTTGTACAAGAAAGCTGGGTC AAGTGTTACTCGTTCTAT	68	
***At*PRK4_GatF**	GGGGACAAGTTTGTACAAAAAAGCAGGCTT CACCATGCTAACTTGGGAGACC	71	At3g20190 (*AtPRK4*)
***At*PRK4_GatR**	GGGGACCACTTTGTACAAGAAAGCTGGGTC TCGATTCATGGCGAAACC	71	
***At*PRK5_GatF**	GGGGACAAGTTTGTACAAAAAAGCAGGCTT CACCATGCGCAATTGGGAGGAC	72	At1g50610 (*AtPRK5*)
***At*PRK5_GatR**	GGGGACCACTTTGTACAAGAAAGCTGGGTC TCGATTCATCGAGAAACCA	70	
***At*PRK6_GatF**	GGGGACAAGTTTGTACAAAAAAGCAGGCTT CACCATGGCTGCTGCTGTTCTG	72	At5g20690 (*AtPRK6*)
***At*PRK6_GatR**	GGGGACCACTTTGTACAAGAAAGCTGGGTC AGTTTTTACTTGTTCTATCCTTCTA	68	
MAP7A_GatF	GGGGACAAGTTTGTACAAAAAAGCAGGCTT CACCATGACTCGAGGAAGTCAAAGAGA	71	At3g24100 (*MAP7A*)
MAP7A_GatR	GGGGACCACTTTGTACAAGAAAGCTGGGTC CTTATTGTTTCCTTTGCCT	70	
MAP7B_GatF	GGGGACAAGTTTGTACAAAAAAGCAGGCTT CACCATGACTCGTGGAAGTCAGAG	71	At4g13615 (*MAP7B*)
MAP7B_GatR	GGGGACCACTTTGTACAAGAAAGCTGGGTC CTTCTTAGCAGCAGCTCCTTTTCCTCC	73	

1.3. Primers Used to Amplify *MAP7A* and *MAP7B* Promoter Regions.

Primer name	Sequence	Tm (ºC)	Target gene
pMAP7A_F	GATTCATTCACTTTTCGCACTTTCTCAAGC	56	*MAP7A* Promoter (-2150 – 0 bp)
pMAP7A_R	GGCAGGTGAGATCTGCGTAGCGAACAA	65	
pMAP7B_F	GTGTTTTGTTTGGTTGGTGTGTATAGGTG	60	*MAP7B* Promoter (-2026 – 0 bp)
pMAP7B_R	GGTTGAAACGAAGATAAATCGG	52	

1.4. Primers used to Amplify *MAP7A* and *MAP7B* Promoter Regions for Insertion into pDONR207 and use in the GUS Reporter System.

Primer name	Sequence	Tm (ºC)	Target gene
pMAP7A_ **GatF**	GGGGACAAGTTTGTACAAAAAAGCAGGCTTCACCGATTCATTCACTTTTCGCACTTTCTCAAGC	72	*MAP7A* Promoter (-2150 – 0 bp)
pMAP7A_ **GatR**	GGGGACCACTTTGTACAAGAAAGCTGGGTCGGCAGGTGAGATCTGCGTAGCGAACAA	75	
pMAP7B_ **GatF**	GGGGACAAGTTTGTACAAAAAAGCAGGCTTCACCGTGTTTTGTTTGGTTGGTGTGTATAGGTG	71	*MAP7B* Promoter (-2026 – 0 bp)
pMAP7B_ **GatR**	GGGGACCACTTTGTACAAGAAAGCTGGGTCGGTTGAAACGAAGATAAATCGG	71	

1.5. Amplification of MAP7A Subdomains for Insertion into pDONR207 and Expression as GFP Fusion Proteins.

Primer name	Sequence	Tm (ºC)	Target
MAP7A-SERF_R	GGGGACCACTTTGTACAAGAAAGCTG GGTCCTTCTCTTGCAATGCTTT	70	MAP7A (aa 1 - 46)
MAP7A-C_F	GGGGACAAGTTTGTACAAAAAAGCAG GCTTCACCATGACTGCAAAGAAAGCT GCT	71	MAP7A (aa 47 - 69)

1.6. Primers Used to Amplify *At*PRK Y2H Constructs for Insertion into pDONR207 and Use in the GAL4 Y2H System.

Primer name	Sequence	Tm (ºC)	Target gene
***At*PRK1_Y2H_F**	GGGGACAAGTTTGTACAAAAAAGCAGGCTT CCGCAGCTATAAGAATAAAAAACCG	69	At5g35390 (*AtPRK1*)
***At*PRK1_Y2H_R**	GGGGACCACTTTGTACAAGAAAGCTGGGTC TCATGCAAAGCTGATACTC	70	
***At*PRK2_Y2H_F**	GGGGACAAGTTTGTACAAAAAAGCAGGCTT CACCTTCCTTATCCGAAGACGAAAG	70	At2g07040 (*AtPRK2*)
***At*PRK2_Y2H_R**	GGGGACCACTTTGTACAAGAAAGCTGGGTC TCATGACAAGTTAATTCCCTCACTTG	70	
***At*PRK3_Y2H_F**	GGGGACAAGTTTGTACAAAAAAGCAGGCTT CAGATGGAAGAAGAAGAGGCAACC	70	At3g42880 (*AtPRK3*)
***At*PRK3_Y2H_R**	GGGGACCACTTTGTACAAGAAAGCTGGGTC TCAAAGTGTTACTCGTTCTATC	69	
***At*PRK4_Y2H_F**	GGGGACAAGTTTGTACAAAAAAGCAGGCTT CCATACCAGAAGACGCAAGAG	70	At3g20190 (*AtPRK4*)
***At*PRK4_Y2H_R**	GGGGACCACTTTGTACAAGAAAGCTGGGTC TCATCGATTCATGGCGAAAC	71	At3g20190 (*AtPRK4*)

***At*PRK5_Y2H_F**	GGGGACAAGTTTGTACAAAAAAGCAGGCTT CCAATCAAGAAGACGTAATTTCTTG	68	At1g50610 (*AtPRK5*)
***At*PRK5_Y2H_R**	GGGGACCACTTTGTACAAGAAAGCTGGGTC TCATCGATTCATCGAGAAAC	69	
***At*PRK6_Y2H_F**	GGGGACAAGTTTGTACAAAAAAGCAGGCTT CATAAAGAGGCGAAATAAG	67	At5g20690 (*AtPRK6*)
***At*PRK6_Y2H_R**	GGGGACCACTTTGTACAAGAAAGCTGGGTC TCAAGTTTTTACTTGTTC	67	

1.7. Primers used to Amplify Insert PCR Fragments for Use in Vector Modification by Restriction Cloning.

Primer name	Sequence	Tm (ºC)	Target gene
***pLAT52*-SacI_F**	TCAGGAGCTCTTGAGGAATGATCG ATTCTGG	62	*pLAT52*
***pLAT52*-SpeI_R**	CCATACTAGTGAATTTTTTTTTTGGT GTGTG	56	
mCherry-AscI_F	CTTGGCGCGCCATGGTGAGCAAGG GCGAGGAGGATAA	73	mCherry CDS
mCherry-BstBI_R	TCTTTCGAATTACTTGTACAGCTCG TCCATGCC	63	

1.8. Primers used to Amplify MAP7A Insert PCR Fragment to Generate 6xHIS-MAP7A Protein Expression Construct.

MAP7A-NdeI_F	GATATACATATGATGACTCGAGGAA GTCAAAGAGAGCG	62	MAP7A CDS
MAP7A-NotI_R	AGTGCGGCCGCCTTATTGTTTCCTT TGCCT	67	MAP7A CDS

1.9. Primers used to Amplify Constructs for the Generation of GFP-mCherry and GFP-RFP FRET-FLIM Controls

Primer name	Sequence	Tm (ºC)	Target gene
mCherry_GatF	GGGGACAAGTTTGTACAAAAAAGCAGGC TTCACCATGGTGAGCAAGGGCGAG	73	mCherry CDS
mCherry_GatR	GGGGACCACTTTGTACAAGAAAGCTGGG TCCTACTTGTACAGCTC GTCCATGCCG	73	
DsRED_GatF	GGGGACAAGTTTGTACAAAAAAGCAGGC TTCACCATGGCCTCCTCCGAGGACGTCA	74	DsRED CDS
DsRED_GatR	GGGGACCACTTTGTACAAGAAAGCTGGG TCTTAGGCGCCGGTGGAGTG	74	

1.10. Genotyping Primers (Gene-Specific).

Primer name	Sequence	Tm (ºC)	Target gene
H12 LP	GAAGCTGAAGATCTGGTGAC G	55	At1g58210 (*NET2A*)
H12 RP	CTTGCTTGGAGTTGTTCTTG C	54	At1g58210 (*NET2A*)
E08-F	GAGCGGAGATGTATTACCGT AAAAGGCCAGAGA	64	At1g09720 (*NET2B*)
E08-R	GACATGCCTTGTCTTTCTCT ACATCACGGATATGGT	63	At1g09720 (*NET2B*)
H06-F	GTGTTGGGTCTTGGATGGTT AGACG	59	At1g09720 (*NET2B*)
2D-F	GAGAGGATCTGTGGTTTGCA GGATG	59	At2g22560 (*NET2D*)
2D-R	CTGTCTGATCAGATGCAGCT TGGTTC	60	At2g22560 (*NET2D*)
69-F	GCTTGTTCGCTACGCAGATC TCACCT	66	At3g24100 (*MAP7A*)
69-R	GGGTTGGTCTTGATGATGCA GATGATGATTTTATGAGC	70	At3g24100 (*MAP7A*)
70-F	GGTAAAGTCAATGCCGAAGA AAAACGCGAAGCAG	70	At4g13615 (*MAP7B*)
70-R	GCCCCAAAAGAGAGACTAAA CAAGCCTTCACC	70	At4g13615 (*MAP7B*)

1.11. Genotyping Primers (T-DNA – Specific)

o8409	ATATTGACCATCATACTCATTGC	50	GABI KAT T-DNA left border
Lba1	TGGTTCACGTAGTGGGCCATCG	61	SALK TDNA left border

1.12. Primers used for RT-PCR.

Primer name	Sequence	Tm (ºC)	Target gene
2A_US-F	GAGAGCAGCGAGCAATGCTT ATTCATGG	62	At1g58210 (*NET2A*)
2A_US-R	GATGCTTAGGCGGTTTTCGT GGCCTTCC	65	At1g58210 (*NET2A*)
2A_Insert-F	CAGACGCAGATCAGTACTCT TGAAACAG	59	At1g58210 (*NET2A*)
2A_Insert-R	GCAACTGCAGTATTACTACT ACTTCTTGGAG	59	At1g58210 (*NET2A*)
2A_DS-F	GACAGCAAAAGCAATCAGCA TCATCCC	61	At1g58210 (*NET2A*)
2A_DS-R	CGGTGAAAGCAAGAACATTC ACTTTGG	59	At1g58210 (*NET2A*)
2B_US-F	GAACACAATCTCCAAGTCCT AGATATGGAGGAGAAG	62	At1g09720 (*NET2B*)
2B_US-R	GCGTTCTGCTAAAGCACGGT ATG	58	At1g09720 (*NET2B*)
E08-F	GAGCGGAGATGTATTACCGT AAAAGGCCAGAGA	64	At1g09720 (*NET2B*)
E08-R	GACATGCCTTGTCTTTCTCT ACATCACGGATATGGT	63	At1g09720 (*NET2B*)
2B_DS-F	GGGTTGGTGGAGAGATCGAA GATGG	60	At1g09720 (*NET2B*)
2B_DS-R	CACACCTTTCTGTTGCAGTA TCAATCCTTTC	60	At1g09720 (*NET2B*)
2D_US-F	CGAAAACTTTACGACGATGC TGC	57	At2g22560 (*NET2D*)
2D_US-R	CGCAAACGAATCTCCATCTT CTTG	56	At2g22560 (*NET2D*)
2D_Insert-F	CAGACGCAGATCAGTACTCT TGAAACAG	59	At2g22560 (*NET2D*)
2D-R	CTGTCTGATCAGATGCAGCT TGGTTC	59	At2g22560 (*NET2D*)

2D_DS-F	GTACCATCCCAAGTACAAAT CCAGACAC	59	At2g22560 (*NET2D*)
2D_DS-R	CCTTCTTTCTCCTTTTGATC CTCTTGTTGTTCACC	62	At2g22560 (*NET2D*)
SERFa-F	GACTCGAGGAAGTCAAAGAG AGC	56	At3g24100 (*MAP7A*)
SERFa-R	CGACGTTGCTCAGGAGTTA ATC	55	At3g24100 (*MAP7A*)
MAP7A-F	ATGACTCGAGGAAGTCAAAG AGA	55	At3g24100 (*MAP7A*)
MAP7A-R	TCACTTATTGTTTCCTTTGC CTCCTC	57	At3g24100 (*MAP7A*)
7A_DS-F	GACTGCAAAGAAAGCTGCTC AAG	57	At3g24100 (*MAP7A*)
7A_DS-R	CTTGTAATCATAGATATTGT AAGAGTAATCATTGG	54	At3g24100 (*MAP7A*)
SERFb-F	CCTCTGCTTCGCGTTTTTCT TCG	59	At4g13615 (*MAP7B*)
SERFb-R	CTTTCCACCAGCACGAGC	55	At4g13615 (*MAP7B*)
MAP7B-F	ATGACTCGTGGAAGTCAGAG AGA	56	At4g13615 (*MAP7B*)
MAP7B-R	CTTCTTAGCAGCAGCTCCTT TTCCTC	59	At4g13615 (*MAP7B*)
7B_DS-F	GAATGGTGACGATGGTTTGA CG	56	At4g13615 (*MAP7B*)
7B_DS-R	GATTTCAGACAAGAGTCAAA GCTTCAGG	58	At4g13615 (*MAP7B*)
ACT2_F	GGATCGGTGGTTCCATTCTT GC	58	A13g18780 (*ACT2*)
ACT2_R	AGAGTTTGTCACACACAAGT GCA	57	A13g18780 (*ACT2*)
EF-1a_F	CCCATTTGTGCCAATCTCT	52	At1g07940 (*EF-1a*)
EF-1a_R	CACCGTTCCAATACCACCAA	54	At1g07940 (*EF-1a*)

Appendix 2: Statistical Analysis of Mutant Phenotypes.

2.1: Statistical Analysis of Pollen Germination Rates in *net2a* and *net2d* T-DNA Mutant lines.

Genetic background	Significant difference vs control?	P-value
net2a.2	No	0.97
net2d.1	No	0.48
net2d.2	No	0.48

Statistical comparison of pollen germination rates of *net2a.1*, *net2d.1* and *net2d.2* mutant lines (figure 3.11) against their respective Col-0 controls analysed in the same experiment. Statistical analysis was performed using a Student's T-Test (2-tailed, assuming unequal variance, critical value = 0.05).

2.2: Statistical Analysis of Pollen Tube Growth Rates in *net2a, net2b* and *net2d* T-DNA Mutant lines.

Genetic background	Significant difference vs control?	P-value
net2a.2	Yes	5.91×10^{-06}
net2b.1	No	0.47
net2b.2	No	0.79
net2d.1	Yes	0.04
net2d.2	No	0.05

Statistical comparison of pollen tube growth rates of *net2a.1*, *net2b.1*, *net2b.2* *net2d.1* and *net2d.2* mutant lines (figure 3.14) against their respective Col-0 controls analysed in the same experiment. Statistical analysis was performed using a Student's T-Test (2-tailed, assuming unequal variance, critical value = 0.05).

2.3: Statistical Analysis of Pollen Tube Diameter in *net2a, net2b* and *net2d* T-DNA Mutant lines.

Genetic background	Significant difference vs control?	P-value
net2a.2	No	0.90
net2b.1	No	0.22
net2b.2	No	0.24
net2d.1	No	0.32
net2d.2	No	0.52

Statistical comparison of pollen tube diameter between *net2a.1*, *net2b.1*, *net2b.2* *net2d.1* and *net2d.2* mutant lines (figure 3.15) against their respective Col-0 controls analysed in the same experiment. Statistical analysis was performed using a Student's T-Test (2-tailed, assuming unequal variance, critical value = 0.05).

2.4: Statistical Analysis of Pollen Germination Rates in *map7a, map7b* and *map7a/map7b* T-DNA Mutant lines.

Genetic background	Significant difference vs control?	P-value
map7a.1	No	0.74
map7b.1	No	0.85
map7a.1/map7b.1	No	0.17

Statistical comparison of pollen germination rates of *map7a.1*, *map7b.1* and *map7a.1/map7b.1* mutant lines (figure 7.38) against their respective Col-0 controls analysed in the same experiment. Statistical analysis was performed using a Student's T-Test (2-tailed, assuming unequal variance, critical value = 0.05).

2.5: Statistical Analysis of Pollen Tube Growth Rates in *map7a, map7b* and *map7a/map7b* T-DNA Mutant lines.

Genetic background	Significant difference vs control?	P-value
map7a.1	Yes	6.2×10^{-6}
map7b.1	Yes	0.01
map7a.1/map7b.1	Yes	3.9×10^{-3}

Statistical comparison of pollen tube growth rates in *map7a.1*, *map7b.1* and *map7a.1/map7b.1* mutant lines (figure 7.41) against their respective Col-0 controls analysed in the same experiment. Statistical analysis was performed using a Student's T-Test (2-tailed, assuming unequal variance, critical value = 0.05).

2.6: Statistical Analysis of Pollen Tube Diameter in *map7a, map7b* and *map7a/map7b* T-DNA Mutant lines.

Genetic background	Significant difference vs control?	P-value
map7a.1	No	0.80
map7b.1	No	0.85
map7a.1/map7b.1	No	0.77

Statistical comparison of pollen tube diameter between *map7a.1*, *map7b.1*, *map7a.1/map7b.1* mutant lines (figure 7.42) against their respective Col-0 controls analysed in the same experiment. Statistical analysis was performed using a Student's T-Test (2-tailed, assuming unequal variance, critical value = 0.05).

Appendix 3: Modified Vectors.

3.1: pMDC83-mCherry Vector Sequence.

cgtaatcatggtcatagctgtttcctgtgtgaaattgttatccgctcacaattccacacaacatacgagccggaagcataaagtgtaaagcct
ggggtgcctaatgagtgagctaactcacattaattgcgttgcgctcactgcccgctttccagtcgggaaacctgtcgtgccagctgcattaatg
aatcggccaacgcgcggggagaggcggtttgcgtattggctagagcagcttgccaacatggtggagcacgacactctcgtctactccaa
gaatatcaaagatacagtctcagaagaccaaagggctattgagacttttcaacaaagggtaatatcgggaaacctcctcggattccattgc
ccagctatctgtcacttcatcaaaaggacagtagaaaaggaaggtggcacctacaaatgccatcattgcgataaaggaaaggctatcgtt
caagatgcctctgccgacagtggtcccaaagatggacccccacccacgaggagcatcgtggaaaaagaagacgttccaaccacgtctt
caaagcaagtggattgatgtgataacatggtggagcacgacactctcgtctactccaagaatatcaaagatacagtctcagaagaccaa
agggctattgagacttttcaacaaagggtaatatcgggaaacctcctcggattccattgcccagctatctgtcacttcatcaaaaggacagta
gaaaaggaaggtggcacctacaaatgccatcattgcgataaaggaaaggctatcgttcaagatgcctctgccgacagtggtcccaaaga
tggacccccacccacgaggagcatcgtggaaaaagaagacgttccaaccacgtcttcaaagcaagtggattgatgtgatatctccactg
acgtaagggatgacgcacaatcccactatccttcgcaagaccttcctctatataaggaagttcatttcatttggagaggacacgctgaaatc
accagtctctctctacaaatctatctctctcgagctttcgcagatcccgggggcaatgagatatgaaaaagcctgaactcaccgcgacgtc
tgtcgagaagtttctgatcgaaaagttcgacagcgtctccgacctgatgcagctctcggagggcgaagaatctcgtgctttcagcttcgatgt
aggagggcgtggatatgtcctgcgggtaaatagctgcgccgatggtttctacaaagatcgttatgtttatcggcactttgcatcggccgcgctc
ccgattccggaagtgcttgacattggggagtttagcgagagcctgacctattgcatctcccgccgtgcacagggtgtcacgttgcaagacct
gcctgaaaccgaactgcccgctgttctacaaccggtcgcggaggctatggatgcgatcgctgcggccgatcttagccagacgagcgggtt
cggcccattcggaccgcaaggaatcggtcaatacactacatggcgtgatttcatatgcgcgattgctgatccccatgtgtatcactggcaaa
ctgtgatggacgacaccgtcagtgcgtccgtcgcgcaggctctcgatgagctgatgctttgggccgaggactgccccgaagtccggcacc
tcgtgcacgcggatttcggctccaacaatgtcctgacggacaatggccgcataacagcggtcattgactggagcgaggcgatgttcgggg
attcccaatacgaggtcgccaacatcttcttctggaggccgtggttggcttgtatggagcagcagacgcgctacttcgagcggaggcatccg
gagcttgcaggatcgccacgactccgggcgtatatgctccgcattggtcttgaccaactctatcagagcttggttgacggcaatttcgatgat
gcagcttgggcgcagggtcgatgcgacgcaatcgtccgatccggagccgggactgtcgggcgtacacaaatcgcccgcagaagcgcg
gccgtctggaccgatggctgtgtagaagtactcgccgatagtggaaaccgacgccccagcactcgtccgagggcaaagaaatagagta
gatgccgaccggatctgtcgatcgacaagctcgagtttctccataataatgtgtgagtagttcccagataagggaattagggttcctataggg
tttcgctcatgtgttgagcatataagaaaccttagtatgtatttgtatttgtaaaatacttctatcaataaaatttctaattcctaaaaccaaaatcc
agtactaaaatccagatcccccgaattaattcggcgttaattcagtacattaaaaacgtccgcaatgtgttattaagttgtctaagcgtcaattt
gtttacaccacaatatatcctgccaccagccagccaacagctccccgaccggcagctcggcacaaaatcaccactcgatacaggcagc
ccatcagtccgggacggcgtcagcgggagagccgttgtaaggcggcagactttgctcatgttaccgatgctattcggaagaacggcaact
aagctgccgggtttgaaacacggatgatctcgcggagggtagcatgttgattgtaacgatgacagagcgttgctgcctgtgatcaccgcgg
tttcaaaatcggctccgtcgatactatgttatacgccaactttgaaaacaactttgaaaaagctgttttctggtatttaaggttttagaatgcaagg
aacagtgaattggagttcgtcttgttataattagcttcttggggtatctttaaatactgtagaaaagaggaaggaaataataaatggctaaaat
gagaatatcaccggaattgaaaaaactgatcgaaaaataccgctgcgtaaaagatacggaaggaatgtctcctgctaaggtatataagct
ggtgggagaaaatgaaaacctatatttaaaaatgacggacagccggtataaagggaccacctatgatgtggaacgggaaaaggacat
gatgctatggctggaaggaaagctgcctgttccaaaggtcctgcactttgaacggcatgatggctggagcaatctgctcatgagtgaggcc
gatggcgtcctttgctcggaagagtatgaagatgaacaaagccctgaaaagattatcgagctgtatgcggagtgcatcaggctctttcactc
catcgacatatcggattgtccctatacgaatagcttagacagccgcttagccgaattggattacttactgaataacgatctggccgatgtggat
tgcgaaaactgggaagaagacactccatttaaagatccgcgcgagctgtatgatttttaaagacggaaaagcccgaagaggaacttgtc
ttttcccacggcgacctgggagacagcaacatctttgtgaaagatggcaaagtaagtggctttattgatcttgggagaagcggcagggcgg
acaagtggtatgacattgccttctgcgtccggtcgatcagggaggatatcggggaagaacagtatgtcgagctatttttgacttactggggat
caagcctgattgggagaaaataaaatattatatttttactggatgaattgttttagtacctagaatgcatgaccaaaatcccttaacgtgagttttc
gttccactgagcgtcagaccccgtagaaaagatcaaaggatcttcttgagatccttttttctgcgcgtaatctgctgcttgcaaacaaaaaaa
ccaccgctaccagcggtggtttgtttgccggatcaagagctaccaactcttttccgaaggtaactggcttcagcagagcgcagataccaaa
tactgtccttctagtgtagccgtagttaggccaccacttcaagaactctgtagcaccgcctacatacctcgctctgctaatcctgttaccagtgg
ctgctgccagtggcgataagtcgtgtcttaccgggttggactcaagacgatagttaccggataaggcgcagcggtcgggctgaacggggg
gttcgtgcacacagcccagcttggagcgaacgacctacaccgaactgagatacctacagcgtgagctatgagaaagcgccacgcttcc
cgaagggagaaaggcggacaggtatccggtaagcggcagggtcggaacaggagagcgcacgagggagcttccagggggaaacg
cctggtatctttatagtcctgtcgggtttcgccacctctgacttgagcgtcgatttttgtgatgctcgtcaggggggcggagcctatggaaaaac
gccagcaacgcggcctttttacggttcctggccttttgctggccttttgctcacatgttctttcctgcgttatcccctgattctgtggataaccgtatta
ccgcctttgagtgagctgataccgctcgccgcagccgaacgaccgagcgcagcgagtcagtgagcgaggaagcggaagagcgcctg
atgcggtattttctccttacgcatctgtgcggtatttcacaccgcatatggtgcactctcagtacaatctgctctgatgccgcatagttaagccagt
atacactccgctatcgctacgtgactgggtcatggctgcgccccgacacccgccaacacccgctgacgcgccctgacgggcttgtctgctc
ccggcatccgcttacagacaagctgtgaccgtctccgggagctgcatgtgtcagaggttttcaccgtcatcaccgaaacgcgcgaggcag
ggtgccttgatgtgggcgccggcggtcgagtggcgacggcgcggcttgtccgcgccctggtagattgcctggccgtaggccagccatttttg
agcggccagcggccgcgataggccgacgcgaagcggcggggcgtagggagcgcagcgaccgaagggtaggcgctttttgcagctct

tcggctgtgcgctggccagacagttatgcacaggccaggcgggttttaagagttttaataagttttaaagagttttaggcggaaaaatcgcctt
ttttctcttttatatcagtcacttacatgtgtgaccggttcccaatgtacggctttgggttcccaatgtacgggttccggttcccaatgtacggctttg
ggttcccaatgtacgtgctatccacaggaaagagacctttttcgacctttttcccctgctagggcaatttgccctagcatctgctccgtacattag
gaaccggcggatgcttcgccctcgatcaggttgcggtagcgcatgactaggatcgggccagcctgccccgcctcctccttcaaatcgtact
ccggcaggtcatttgacccgatcagcttgcgcacggtgaaacagaacttcttgaactctccggcgctgccactgcgttcgtagatcgtcttga
acaaccatctggcttctgccttgcctgcggcgcggcgtgccaggcggtagagaaaacggccgatgccgggatcgatcaaaaagtaatcg
gggtgaaccgtcagcacgtccgggttcttgccttctgtgatctcgcggtacatccaatcagctagctcgatctcgatgtactccggccgcccg
gtttcgctctttacgatcttgtagcggctaatcaaggcttcaccctcggataccgtcaccaggcggccgttcttggccttcttcgtacgctgcatg
gcaacgtgcgtggtgtttaaccgaatgcaggtttctaccaggtcgtctttctgctttccgccatcggctcgccggcagaacttgagtacgtccg
caacgtgtggacggaacacgcggccgggcttgtctcccttcccttcccggtatcggttcatggattcggttagatgggaaaccgccatcagt
accaggtcgtaatcccacacactggccatgccggccggccctgcggaaacctctacgtgcccgtctggaagctcgtagcggatcacctc
gccagctcgtcggtcacgcttcgacagacggaaaacggccacgtccatgatgctgcgactatcgcgggtgcccacgtcatagagcatcg
gaacgaaaaaatctggttgctcgtcgcccttgggcggcttcctaatcgacggcgcaccggctgccggcggttgccgggattctttgcggatt
cgatcagcggccgcttgccacgattcaccggggcgtgcttctgcctcgatgcgttgccgctgggcggcctgcgcggccttcaacttctccac
caggtcatcacccagcgccgcgccgatttgtaccgggccggatggtttgcgaccgtcacgccgattcctcgggcttgggggttccagtgcc
attgcagggccggcagacaacccagccgcttacgcctggccaaccgcccgttcctccacacatggggcattccacggcgtcggtgcctg
gttgttcttgattttccatgccgcctcctttagccgctaaaattcatctactcatttattcatttgctcatttactctggtagctgcgcgatgtattcagat
agcagctcggtaatggtcttgccttggcgtaccgcgtacatcttcagcttggtgtgatcctccgccggcaactgaaagttgacccgcttcatgg
ctggcgtgtctgccaggctggccaacgttgcagccttgctgctgcgtgcgctcggacggccggcacttagcgtgtttgtgcttttgctcattttct
ctttacctcattaactcaaatgagttttgatttaatttcagcggccagcgcctggacctcgcgggcagcgtcgccctcgggttctgattcaagaa
cggttgtgccggcggcggcagtgcctgggtagctcacgcgctgcgtgatacgggactcaagaatgggcagctcgtacccggccagcgc
ctcggcaacctcaccgccgatgcgcgtgcctttgatcgcccgcgacacgacaaaggccgcttgtagccttccatccgtgacctcaatgcgc
tgcttaaccagctccaccaggtcggcggtggcccatatgtcgtaagggcttggctgcaccggaatcagcacgaagtcggctgccttgatcg
cggacacagccaagtccgccgcctggggcgctccgtcgatcactacgaagtcgcgccggccgatggccttcacgtcgcggtcaatcgtc
gggcggtcgatgccgacaacggttagcggttgatcttcccgcacggccgcccaatcgcgggcactgccctggggatcggaatcgactaa
cagaacatcggccccggcgagttgcagggcgcgggctagatgggttgcgatggtcgtcttgcctgacccgcctttctggttaagtacagcg
ataaccttcatgcgttccccttgcgtatttgtttatttactcatcgcatcatatacgcagcgaccgcatgacgcaagctgttttactcaaatacaca
tcacctttttagacggcggcgctcggtttcttcagcggccaagctggccggccaggccgccagcttggcatcagacaaaccggccaggatt
tcatgcagccgcacggttgagacgtgcgcgggcggctcgaacacgtacccggccgcgatcatctccgcctcgatctcttcggtaatgaaa
aacggttcgtcctggccgtcctggtgcggtttcatgcttgttcctcttggcgttcattctcggcggccgccagggcgtcggcctcggtcaatgcgt
cctcacggaaggcaccgcgccgcctggcctcggtgggcgtcacttcctcgctgcgctcaagtgcgcggtacagggtcgagcgatgcacg
ccaagcagtgcagccgcctctttcacggtgcggccttcctggtcgatcagctcgcgggcgtgcgcgatctgtgccggggtgagggtaggg
cgggggccaaacttcacgcctcgggccttggcggcctcgcgcccgctccgggtgcggtcgatgattagggaacgctcgaactcggcaat
gccggcgaacacggtcaacaccatgcggccggccggcgtggtggtgtcggcccacggctctgccaggctacgcaggcccgcgccgg
cctcctggatgcgctcggcaatgtccagtaggtcgcgggtgctgcgggccaggcggtctagcctggtcactgtcacaacgtcgccagggc
gtaggtggtcaagcatcctggccagctccgggcggtcgcgcctggtgccggtgatcttctcggaaaacagcttggtgcagccggccgcgt
gcagttcggcccgttggttggtcaagtcctggtcgtcggtgctgacgcgggcatagcccagcaggccagcggcggcgctcttgttcatggc
gtaatgtctccggttctagtcgcaagtattctactttatgcgactaaaacacgcgacaagaaaacgccaggaaaagggcagggcggcag
cctgtcgcgtaacttaggacttgtgcgacatgtcgttttcagaagacggctgcactgaacgtcagaagccgactgcactatagcagcggag
gggttggatcaaagtactttgatcccgaggggaaccctgtggttggcatgcacatacaaatggacgaacggataaacctttcacgccctttt
aaatatccgttattctaataaacgctcttttctcttaggtttacccgccaatatatcctgtcaaacactgatagtttaaactgaaggcgggaaacg
acaatctgatccaagctcaagctgctctagcattcgccattcaggctgcgcaactgttgggaagggcgatcggtgcgggcctcttcgctatta
cgccagctggcgaaaggggatgtgctgcaaggcgattaagttgggtaacgccagggttttcccagtcacgacgttgtaaaacgacggc
cagtgccaagcttggcgtgcctgcaggtcaacatggtggagcacgacacacttgtctactccaaaaatatcaaagatacagtctcagaag
accaaagggcaattgagacttttcaacaaagggtaatatccggaaacctcctcggattccattgcccagctatctgtcactttattgtgaagat
agtggaaaaggaaggtggctcctacaaatgccatcattgcgataaaggaaaggccatcgttgaagatgcctctgccgacagtggtccca
aagatggacccccacccacgaggagcatcgtggaaaaagaagacgttccaaccacgtcttcaaagcaagtggattgatgtgataacat
ggtggagcacgacacacttgtctactccaaaaatatcaaagatacagtctcagaagaccaaagggcaattgagactttcaacaaaggg
taatatccggaaacctcctcggattccattgcccagctatctgtcactttattgtgaagatagtggaaaaggaaggtggctcctacaaatgcc
atcattgcgataaaggaaaggccatcgttgaagatgcctctgccgacagtggtcccaaagatggacccccacccacgaggagcatcgtg
gaaaaagaagacgttccaaccacgtcttcaaagcaagtggattgatgtgatatctccactgacgtaagggatgacgcacaatcccactat
ccttcgcaagacccttcctctatataaggaagttcatttcatttggagaggacctcgactctagaactagttaattaagaattagcttgcatgcct
gcaggtcgactctagaggatccccgggtaccgagctcgaattatcacaagtttgtacaaaaaagctgaacgagaaacgtaaaatgatat
aaatatcaatatattaaattagattttgcataaaaaacagactacataatactgtaaaacacaacatatccagtcactatggcggccgcatta
ggcaccccaggctttacactttatgcttccggctcgtataatgtgtggattttgagttaggatccggcgagattttcaggagctaaggaagcta
aaatggagaaaaaaatcactggatataccaccgttgatatatcccaatggcatcgtaaagaacattttgaggcatttcagtcagttgctcaat
gtacctataaccagaccgttcagctggatattacggccttttaaagaccgtaaagaaaaataagcacaagttttatccggcctttattcacatt
cttgcccgcctgatgaatgctcatccggaattccgtatggcaatgaaagacggtgagctggtgatatgggatagtgttcacccttgttacacc
gttttccatgagcaaactgaaacgttttcatcgctctggagtgaataccacgacgatttccggcagtttctacacatatattcgcaagatgtggc
gtgttacggtgaaaacctggcctatttccctaaagggtttattgagaatatgtttttcgtctcagccaatccctgggtgagtttcaccagttttgattt
aaacgtggccaatatggacaacttcttcgcccccgttttcaccatgggcaaatattatacgcaaggcgacaaggtgctgatgccgctggcg

attcaggttcatcatgccgtctgtgatggcttccatgtcggcagaatgcttaatgaattacaacagtactgcgatgagtggcagggcggggc
gtaaacgcgtggatccggcttactaaaagccagataacagtatgcgtatttgcgcgctgatttttgcggtataagaatatatactgatatgtata
cccgaagtatgtcaaaaagaggtgtgctatgaagcagcgtattacagtgacagttgacagcgacagctatcagttgctcaaggcatatatg
atgtcaatatctccggtctggtaagcacaaccatgcagaatgaagcccgtcgtctgcgtgccgaacgctggaaagcggaaaatcaggaa
gggatggctgaggtcgcccggtttattgaaatgaacggctcttttgctgacgagaacagggactggtgaaatgcagtttaaggtttacaccta
taaaagagagagccgttatcgtctgtttgtggatgtacagagtgatattattgacacgcccgggcgacggatggtgatccccctggccagtg
cacgtctgctgtcagataaagtctcccgtgaactttacccggtggtgcatatcggggatgaaagctggcgcatgatgaccaccgatatggc
cagtgtgccggtctccgttatcggggaagaagtggctgatctcagccaccgcgaaaatgacatcaaaaacgccattaacctgatgttctgg
ggaatataaatgtcaggctcccttatacacagccagtctgcaggtcgaccatagtgactggatatgttgtgttttacagtattatgtagtctgttttt
tatgcaaaatctaatttaatatattgatatttatatcattttacgtttctcgttcagctttcttgtacaaagtggtgatagcttggcgcgccATGGT
GAGCAAGGGCGAGGAGGATAACATGGCCATCATCAAGGAGTTCATGCGCTTCAAGGTGCACA
TGGAGGGCTCCGTGAACGGCCACGAGTTCGAGATCGAGGGCGAGGGCGAGGGCCGCCCCT
ACGAGGGCACCCAGACCGCCAAGCTGAAGGTGACCAAGGGTGGCCCCCTGCCCTTCGCCTG
GGACATCCTGTCCCCTCAGTTCATGTACGGCTCCAAGGCCTACGTGAAGCACCCCGCCGACA
TCCCCGACTACTTGAAGCTGTCCTTCCCCGAGGGCTTCAAGTGGGAGCGCGTGATGAACTTC
GAGGACGGCGGCGTGGTGACCGTGACCCAGGACTCCTCCCTGCAGGACGGCGAGTTCATCT
ACAAGGTGAAGCTGCGCGGCACCAACTTCCCCTCCGACGGCCCCGTAATGCAGAAGAAGAC
CATGGGCTGGGAGGCCTCCTCCGAGCGGATGTACCCCGAGGACGGCGCCCTGAAGGGCGA
GATCAAGCAGAGGCTGAAGCTGAAGGACGGCGGCCACTACGACGCTGAGGTCAAGACCACC
TACAAGGCCAAGAAGCCCGTGCAGCTGCCCGGCGCCTACAACGTCAACATCAAGTTGGACAT
CACCTCCCACAACGAGGACTACACCATCGTGGAACAGTACGAACGCGCCGAGGGCCGCCAC
TCCACCGGCGGCATGGACGAGCTGTACAAGTAGttcgaaagatcccaacgaaaagagagaccacatggtccttc
ttgagtttgtaacagctgctgggattacacatggcatggtagaactatacaaacaccaccaccaccaccactaagagctcgaatttccccg
atcgttcaaacatttggcaataaagtttcttaagattgaatcctgttgccggtcttgcgatgattatcatataatttctgttgaattacgttaagcatgt
aataattaacatgtaatgcatgacgttatttatgagatgggtttttatgattagagtcccgcaattatacatttaatacgcgatagaaaacaaaat
atagcgcgcaaactaggataaattatcgcgcgcggtgtcatctatgttactagatcgggaatt

Feature	Colour
2x CaMV 35s: promoter	**Green**
attR1 recombination site	**Cyan**
ccdB gateway cassette	**Grey**
attR2 recombination site	Blue
AscI ligation site (ggcgcggc)	**Red**
mCherry coding sequence	Purple
BstBI ligation site (ttcgaa)	**Red**

3.2. pB7FGW52 Vector Sequence.

ggccctctagaggatccccgggtaccctcgaattatcatacatgagaattaagggagtcacgttatgacccccgccgatgacgcgggaca
agccgttttacgtttggaactgacagaaccgcaacgttgaaggagccactgagccgcgggtttctggagtttaatgagctaagcacatacgt
cagaaaccattattgcgcgttcaaaagtcgcctaaggtcactatcagctagcaaatatttcttgtcaaaaatgctccactgacgttccataaat
tcccctcggtatccaattagagtctcatattcactctcaactcgatcgaggggatctaccatgagcccagaacgacgcccggccgacatcc
gccgtgccaccgaggcggacatgccggcggtctgcaccatcgtcaaccactacatcgagacaagcacggtcaacttccgtaccgagcc
gcaggaaccgcaggagtggacggacgacctcgtccgtctgcgggagcgctatccctggctcgtcgccgaggtggacggcgaggtcgc
cggcatcgcctacgcgggtccctggaaggcacgcaacgcctacgactggacggccgagtcgaccgtgtacgtctccccccgccaccag
cggacgggactgggctccacgctctacacccacctgctgaagtccctggaggcacagggcttcaagagcgtggtcgctgtcatcgggct
gcccaacgacccgagcgtgcgcatgcacgaggcgctcggatatgccccccgcggcatgctgcgggcggccggcttcaagcacggga
actggcatgacgtgggtttctggcagctggacttcagcctgccggtgccgccccgtccggtcctgcccgtcaccgaaatctgatgaccccta
gagtcaagcagatcgttcaaacatttggcaataaagtttcttaagattgaatcctgttgccggtcttgcgatgattatcatataatttctgttgaatt
acgttaagcatgtaataattaacatgtaatgcatgacgttatttatgagatgggtttttatgattagagtcccgcaattatacatttaatacgcgat
agaaaacaaaatatagcgcgcaaactaggataaattatcgcgcgcggtgtcatctactatgttactagatcgaccggcatgcaagctgat
aattcaattcggcgttaattcagtacattaaaaacgtccgcaatgtgttattaagttgtctaagcgtcaatttgtttacaccacaatatatcctgcc
accagccagccaacagctccccgaccggcagctcggcacaaaatcaccactcgatacaggcagcccatcagtccgggacggcgtca
gcgggagagccgttgtaaggcggcagactttgctcatgttaccgatgctattcggaagaacggcaactaagctgccgggtttgaaacacg
gatgatctcgcggagggtagcatgttgattgtaacgatgacagagcgttgctgcctgtgatcaattcgggcacgaacccagtggacataag
cctcgttcggttcgtaagctgtaatgcaagtagcgtaactgccgtcacgcaactggtccagaaccttgaccgaacgcagcggtggtaacgg
cgcagtggcggttttcatggcttcttgttatgacatgttttttggggtacagtctatgcctcgggcatccaagcagcaagcgcgttacgccgtgg
gtcgatgtttgatgttatggagcagcaacgatgttacgcagcagggcagtcgccctaaaacaaagttaaacatcatgggggaagcggtga
tcgccgaagtatcgactcaactatcagaggtagttggcgtcatcgagcgccatctcgaaccgacgttgctggccgtacatttgtacggctcc
gcagtggatggcggcctgaagccacacagtgatattgatttgctggttacggtgaccgtaaggcttgatgaaacaacgcggcgagctttga
tcaacgacctttttggaaacttcggcttcccctggagagagcgagattctccgcgctgtagaagtcaccattgttgtgcacgacgacatcattc
cgtggcgttatccagctaagcgcgaactgcaatttggagaatggcagcgcaatgacattcttgcaggtatcttcgagccagccacgatcga
cattgatctggctatcttgctgacaaaagcaagagaacatagcgttgccttggtaggtccagcggcggaggaactctttgatccggttcctga
acaggatctatttgaggcgctaaatgaaaccttaacgctatggaactcgccgcccgactgggctggcgatgagcgaaatgtagtgcttacg
ttgtcccgcatttggtacagcgcagtaaccggcaaaatcgcgccgaaggatgtcgctgccgactgggcaatggagcgcctgccggccca
gtatcagcccgtcatacttgaagctagacaggcttatcttggacaagaagaagatcgcttggcctcgcgcgcagatcagttggaagaatttg
tccactacgtgaaaggcgagatcaccaaggtagtcggcaaataatgtctagctagaaattcgttcaagccgacgccgcttcgccggcgtt
aactcaagcgattagatgcactaagcacataattgctcacagccaaactatcaggtcaagtctgcttttattatttttaagcgtgcataataagc
cctacacaaattgggagatatatcatgcatgaccaaaatcccttaacgtgagttttcgttccactgagcgtcagaccccgtagaaaagatca
aaggatcttcttgagatcctttttttctgcgcgtaatctgctgcttgcaaacaaaaaaaccaccgctaccagcggtggtttgtttgccggatcaa
gagctaccaactctttttccgaaggtaactggcttcagcagagcgcagataccaaatactgtccttctagtgtagccgtagttaggccaccac
ttcaagaactctgtagcaccgcctacatacctcgctctgctaatcctgttaccagtggctgctgccagtggcgataagtcgtgtcttaccgggtt
ggactcaagacgatagttaccggataaggcgcagcggtcgggctgaacgggggttcgtgcacacagcccagcttggagcgaacgac
ctacaccgaactgagatacctacagcgtgagctatgagaaagcgccacgcttcccgaagggagaaaggcggacaggtatccggtaag
cggcagggtcggaacaggagagcgcacgagggagcttccagggggaaacgcctggtatctttatagtcctgtcgggtttcgccacctctg
acttgagcgtcgatttttgtgatgctcgtcaggggggcggagcctatggaaaaacgccagcaacgcggccttttacggttcctggccttttgc
tggccttttgctcacatgttctttcctgcgttatcccctgattctgtggataaccgtattaccgcctttgagtgagctgataccgctcgccgcagccg
aacgaccgagcgcagcgagtcagtgagcgaggaagcggaagagcgcctgatgcggtattttctccttacgcatctgtgcggtatttcaca
ccgcatatggtgcactctcagtacaatctgctctgatgccgcatagttaagccagtatacactccgctatcgctacgtgactgggtcatggctg
cgccccgacacccgccaacacccgctgacgcgccctgacgggcttgtctgctcccggcatccgcttacagacaagctgtgaccgtctccg
ggagctgcatgtgtcagaggttttcaccgtcatcaccgaaacgcgcgaggcagggtgccttgatgtgggcgccggcggtcgagtggcga
cggcgcggcttgtccgcgccctggtagattgcctggccgtaggccagccatttttgagcggccagcggccgcgataggccgacgcgaag
cggcggggcgtagggagcgcagcgaccgaagggtaggcgctttttgcagctcttcggctgtgcgctggccagacagttatgcacaggcc
aggcgggttttaagagttttaataagttttaaagagttttaggcggaaaaatcgccttttttctctttatatcagtcacttacatgtgtgaccggttcc
caatgtacggctttgggttcccaatgtacgggttccggttcccaatgtacggctttgggttcccaatgtacgtgctatccacaggaaagagac
cttttcgaccttttccccctgctagggcaatttgccctagcatctgctccgtacattaggaaccggcggatgcttcgccctcgatcaggttgcggt
agcgcatgactaggatcgggccagcctgccccgcctcctccttcaaatcgtactccggcaggtcatttgacccgatcagcttgcgcacggt
gaaacagaacttcttgaactctccggcgctgccactgcgttcgtagatcgtcttgaacaaccatctggcttctgccttgcctgcggcgcggcgt
gccaggcggtagagaaaacggccgatgccgggatcgatcaaaaagtaatcggggtgaaccgtcagcacgtccgggttcttgccttctgt
gatctcgcggtacatccaatcagctagctcgatctcgatgtactccggccgcccggtttcgctctttacgatcttgtagcggctaatcaaggctt
caccctcggataccgtcaccaggcggccgttcttggccttcttcgtacgctgcatggcaacgtgcgtggtgtttaaccgaatgcaggtttctac
caggtcgtctttctgctttccgccatcggctcgccggcagaacttgagtacgtccgcaacgtgtggacggaacacgcggccgggcttgtctc
ccttcccttcccggtatcggttcatggattcggttagatgggaaaccgccatcagtaccaggtcgtaatcccacacactggccatgccggcc
ggccctgcggaaacctctacgtgcccgtctggaagctcgtagcggatcacctcgccagctcgtcggtcacgcttcgacagacggaaaac

ggccacgtccatgatgctgcgactatcgcgggtgcccacgtcatagagcatcggaacgaaaaaatctggttgctcgtcgcccttgggcgg
cttcctaatcgacggcgcaccggctgccggcggttgccgggattctttgcggattcgatcagcggccgcttgccacgattcaccggggcgtg
cttctgcctcgatgcgttgccgctgggcggcctgcgcggccttcaacttctccaccaggtcatcacccagcgccgcgccgatttgtaccggg
ccggatggtttgcgaccgtcacgccgattcctcgggcttgggggttccagtgccattgcagggccggcagacaacccagccgcttacgcct
ggccaaccgcccgttcctccacacatggggcattccacggcgtcggtgcctggttgttcttgattttccatgccgcctcctttagccgctaaaat
tcatctactcatttattcatttgctcatttactctggtagctgcgcgatgtattcagatagcagctcggtaatggtcttgccttggcgtaccgcgtac
atcttcagcttggtgtgatcctccgccggcaactgaaagttgacccgcttcatggctggcgtgtctgccaggctggccaacgttgcagccttg
ctgctgcgtgcgctcggacggccggcacttagcgtgtttgtgcttttgctcattttctctttacctcattaactcaaatgagttttgatttaatttcagc
ggccagcgcctggacctcgcgggcagcgtcgccctcgggttctgattcaagaacggttgtgccggcggcggcagtgcctgggtagctca
cgcgctgcgtgatacgggactcaagaatgggcagctcgtacccggccagcgcctcggcaacctcaccgccgatgcgcgtgcctttgatc
gcccgcgacacgacaaaggccgcttgtagccttccatccgtgacctcaatgcgctgcttaaccagctccaccaggtcggcggtggcccat
atgtcgtaagggcttggctgcaccggaatcagcacgaagtcggctgccttgatcgcggacacagccaagtccgccgcctggggcgctcc
gtcgatcactacgaagtcgcgccggccgatggccttcacgtcgcggtcaatcgtcgggcggtcgatgccgacaacggttagcggttgatct
tcccgcacggccgcccaatcgcgggcactgccctggggatcggaatcgactaacagaacatcggccccggcgagttgcagggcgcgg
gctagatgggttgcgatggtcgtcttgcctgacccgcctttctggttaagtacagcgataaccttcatgcgttcccttgcgtatttgtttatttactc
atcgcatcatatacgcagcgaccgcatgacgcaagctgttttactcaaatacacatcacctttttagacggcggcgctcggtttcttcagcgg
ccaagctggccggccaggccgccagcttggcatcagacaaaccggccaggatttcatgcagccgcacggttgagacgtgcgcgggcg
gctcgaacacgtacccggccgcgatcatctccgcctcgatctcttcggtaatgaaaaacggttcgtcctggccgtcctggtgcggtttcatgct
tgttcctcttggcgttcattctcggcggccgccagggcgtcggcctcggtcaatgcgtcctcacggaaggcaccgcgccgcctggcctcggt
gggcgtcacttcctcgctgcgctcaagtgcgcggtacagggtcgagcgatgcacgccaagcagtgcagccgcctctttcacggtgcggcc
ttcctggtcgatcagctcgcgggcgtgcgcgatctgtgccggggtgagggtagggcgggggccaaacttcacgcctcgggccttggcggc
ctcgcgcccgctccgggtgcggtcgatgattagggaacgctcgaactcggcaatgccggcgaacacggtcaacaccatgcggccggcc
ggcgtggtggtgtcggcccacggctctgccaggctacgcaggcccgcgccggcctcctggatgcgctcggcaatgtccagtaggtcgcg
ggtgctgcgggccaggcggtctagcctggtcactgtcacaacgtcgccagggcgtaggtggtcaagcatcctggccagctccgggcggt
cgcgcctggtgccggtgatcttctcggaaaacagcttggtgcagccggccgcgtgcagttcggcccgttggttggtcaagtcctggtcgtcg
gtgctgacgcgggcatagcccagcaggccagcggcggcgctcttgttcatggcgtaatgtctccggttctagtcgcaagtattctactttatgc
gactaaaacacgcgacaagaaaacgccaggaaaagggcagggcggcagcctgtcgcgtaacttaggacttgtgcgacatgtcgttttc
agaagacggctgcactgaacgtcagaagccgactgcactatagcagcggaggggttggatcaaagtactttgatcccgaggggaaccc
tgtggttggcatgcacatacaaatggacgaacggataaacctttcacgccctttaaatatccgttattctaataaacgctcttttctcttaggttt
acccgccaatatatcctgtcaaacactgatagtttaaactgaaggcgggaaacgacaatctgatccaagctcaagctaagcttgagctcT
TGAGGAATGATCGATTCTGGGTCATTTGTGTGGTTAATCACCCTCCAAATCAACTAAGTCATCC
TGAAGGACAATATCCTATTTTTTCTCTCGTAGGTTTATCATTTAAATTACTATCGCGTGATAATT
TTGTAACGTAGAAAAATAATACCATTAATCCAAACGTTATATTCATTAAAATAATTATGATACATT
TAAAAATATTTCGTGACCTCTCAATTATTGCAAATTCTAAGCCATCCCAAGTTTTGAGGCTAATT
TTTTTTACTATACTATTTTTACAACCACAAAAACATAAAAAATAAAAAATAAAAAAATAAACCGA
GTCAATTGCTACAATCACTTCATTATTAATTTTAATTAATATTATGTGGTTATATATGAAACTGTT
AGAGAAATAATAGCTCCACCATATTTTTTTCTCAATTTATTTTCACTATAAAAAGGCTATTTCATT
ATAATCAAAACAAGACACACACAAAGAGAAGGAGCAATAAAATAAAAGTAAACAACAATTTGTG
TGTTTAAAAAAAAAAAAAAAGTACACACACCAAAAAAAAAATTCactagtgatatcacaagtttgtacaaaaaa
gctgaacgagaaacgtaaaatgatataaatatcaatatattaaattagattttgcataaaaaacagactacataatactgtaaaacacaac
atatccagtcactatggcggccgcattaggcaccccaggctttacactttatgcttccggctcgtataatgtgtggattttgagttaggatccgg
cgagattttcaggagctaaggaagctaaaatggagaaaaaaatcactggatataccaccgttgatatatcccaatggcatcgtaaagaac
attttgaggcatttcagtcagttgctcaatgtacctataaccagaccgttcagctggatattacggccttttaaagaccgtaaagaaaaataa
gcacaagttttatccggcctttattcacattcttgcccgcctgatgaatgctcatccggaattccgtatggcaatgaaagacggtgagctggtg
atatgggatagtgttcaccttgttacaccgttttccatgagcaaactgaaacgttttcatcgctctggagtgaataccacgacgatttccggca
gtttctacacatatattcgcaagatgtggcgtgttacggtgaaaacctggcctatttccctaaagggtttattgagaatatgtttttcgtctcagcc
aatccctgggtgagtttcaccagttttgatttaaacgtggccaatatggacaacttcttcgcccccgttttcaccatgggcaaatattatacgca
aggcgacaaggtgctgatgccgctggcgattcaggttcatcatgccgtctgtgatggcttccatgtcggcagaatgcttaatgaattacaaca
gtactgcgatgagtggcagggcggggcgtaaacgcgtggatccggcttactaaaagccagataacagtatgcgtatttgcgcgctgatttttt
gcggtataagaatatatactgatatgtatacccgaagtatgtcaaaaagaggtgtgctatgaagcagcgtattacagtgacagttgacagc
gacagctatcagttgctcaaggcatatatgatgtcaatatctccggtctggtaagcacaaccatgcagaatgaagcccgtcgtctgcgtgcc
gaacgctggaaagcggaaaatcaggaagggatggctgaggtcgcccggtttattgaaatgaacggctcttttgctgacgagaacaggga
ctggtgaaatgcagtttaaggtttacacctataaaagagagagccgttatcgtctgtttgtggatgtacagagtgatattattgacacgcccgg
gcgacggatggtgatccccctggccagtgcacgtctgctgtcagataaagtctcccgtgaactttacccggtggtgcatatcggggatgaa
agctggcgcatgatgaccaccgatatggccagtgtgccggtctccgttatcggggaagaagtggctgatctcagccaccgcgaaaatga
catcaaaaacgccattaacctgatgttctggggaatataaatgtcaggctcccttatacacagccagtctgcaggtcgaccatagtgactgg
atatgttgtgttttacagtattatgtagtctgttttttatgcaaaatctaatttaatatattgatatttatatcattttacgtttctcgttcagctttcttgtacaa
agtggtgatatcaatggtgagcaagggcgaggagctgttcaccggggtggtgcccatcctggtcgagctggacggcgacgtaaacggcc
acaagttcagcgtgtccggcgagggcgagggcgatgccacctacggcaagctgaccctgaagttcatctgcaccaccggcaagctgcc
cgtgccctggcccaccctcgtgaccaccctgacctacggcgtgcagtgcttcagccgctaccccgaccacatgaagcagcacgacttctt
caagtccgccatgcccgaaggctacgtccaggagcgcaccatcttcttcaaggacgacggcaactacaagacccgcgccgaggtgaa

gttcgagggcgacaccctggtgaaccgcatcgagctgaagggcatcgacttcaaggaggacggcaacatcctggggcacaagctgga
gtacaactacaacagccacaacgtctatatcatggccgacaagcagaagaacggcatcaaggtgaacttcaagatccgccacaacatc
gaggacggcagcgtgcagctcgccgaccactaccagcagaacaccccatcggcgacggccccgtgctgctgcccgacaaccacta
cctgagcacccagtccgccctgagcaaagaccccaacgagaagcgcgatcacatggtcctgctggagttcgtgaccgccgccgggatc
actctcggcatggacgagctgtacaagtaaccgcggccatgctagagtccgcaaaaatcaccagtctctctctacaaatctatctctctctat
ttttctccagaataatgtgtgagtagttcccagataagggaattagggttcttatagggtttcgctcatgtgttgagcatataagaaacccttagt
atgtatttgtatttgtaaaatacttctatcaataaaatttctaattcctaaaaccaaaatccagtgacctgcaggcatgcgacgtcg

Feature	Colour
SacI ligation site (gagctc)	**Red**
pLAT52 promoter Insert	**Yellow**
SpeI ligation site (actagt)	**Red**
attR1 recombination site	**Cyan**
ccdB gateway Cassette	**Grey**
attR2 recombination site	**Blue**
N-terminal GFP tag	**Green**

Appendix 4: MAP7A and MAP7B Nucleotide and Protein Sequences.

4.1. MAP7A Nucleotide Coding Sequence.

ATGACTCGAGGAAGTCAAAGAGAGCGTGACCGTGAAAGGGCTCTAGCTCGA
ACCGGAGGCAAAGGAAAGAACAAAGATGATGGATTAACTCCTGAGCAACGTC
GTGAAAGAGATGCAAAAGCATTGCAAGAGAAGACTGCAAAGAAAGCTGCTCA
AGCCGCTGCTGCAGCTAGTTCCGGAGGAGGAGGAGGCAAAGGAAACAATAA
GTGA

4.2. MAP7B Nucleotide Coding Sequence.

ATGACTCGTGGAAGTCAGAGAGAGCGTGACCGTGAAAGAGCTGCCGCTCGT
GCTGGTGGAAAGGGTAAGAATGGTGACGATGGTTTGACGCCGGAGCAACGC
CGTGAAAGAGATGGGAAAGCATTGCAAGAGAAAGCGGCTAAGAAAGCTGCT
CAAGCTGCAGGTGCGAGTTCTGGTGGTGCAGCTGGAGGAAAAGGAGCTGCT
GCTAAGAAGTGA

4.3. MAP7A Promoter Sequence.

ACGTGCTGATATAGGCCACTAGCCACTGTCCCTAAGTTCAGATCAATTCATAA
TTAAATACAGTAAAAATCAATTCATAATTAGGAATCTCTCTGTTTTGAACATGT
GGTTTATAAGTTATCATTATGTTAATCAAGTTTCAAAAGCCAAATATCAATCTA
AATAGAATAGTAGACACAATATCCTAATTAACCCTAACAAACCAAATACTTCCC
TTAACAAAAAAAAAAACACAACATTCTACCGTACCCAATCAAAAACAACCAATGA
TTCATTCACTTTTCGCACTTTCTCAAGCGACTTTGTTCTGTTCTTGAGCAACTC
GTTGTACTTCCTCTGCAAATTTGGTAAAATTCTTCTAACTCCAAGTTTCGGATC
TTTCATGATTCCTCGTGGCAACTTTCTGCGTCGTTGTTTGTAAAACCGTCTAAT
GGCTCCATAAACACCCACCTCCGGCTTCTCATTATCCTCCGCCACCGCAAAC
TTAATGGCCGATTCTATGGCATGAAAGTACATATCATCTTTGAACAGCTCGTC
CTCTTCCCCACGCGTCATCTCATCTCGTTTCTCATCTTGTATTAAACCGTGGT
CGAGTAGGATCATCCTAAACTCCTCTTTTAGACGAGGATAATCTCGTAACATT
AGGTCAACATCATCTTTTAAAATCTGCACATCGTTATGTTCCTTGAACCTCACG
AAAGCCTCTATAAGCACTCCACATAATTCCTCGCAGTCTCTTCTCAACGACTT
TAAGAACTCCTTTATTCGTTTAACATTCTTTGGATCAACAAAAACTTCCTTTTGA
CGAGAACTGGAATTCGAATCTTCCAGAAATCGATCAAAGGCATCGAGCAAAA
CGTCGCAGTTCTTGAAAATAGTCGTGATTCTGTTTTTGAGATCGACTTCGCTC
AAAGATCCAGAATAGTAAAGCTTCATTGCAGTAGTATATCGAAGGAAGATTCC
TCTGTGGTTTCCTTTTTCATCAATCTCTTTTACTTTCTTCACGAACTCCAACGC
TCGCTTAAACTCTTTCTGCGAGCAATCGTTGGGGAGTTTTATCGGATACTTGT
TCGTCGTATGCATTATCATAAACTTGTTAATCTCTCTTCTGTGTTTGTATTTTTT
GTTGAGTAAAAATGTAAACTTATCTCTATATATATAGGAGATAGTCAGATAGAG

CTGTTTCTATTTCCTAATCCATATCCGAGTAGGCGTTTTTAGAAAATGGAAAAT
CTGCTGTCAAACAAAAAAAAAAATGGAAATCCTAATACATATTATATTTTAAA
CTTAATAAAATATATCATGTCATACACATGGCAATCCCATTTTTATTATATTGTT
TCATGGTATATACAATGCTCTGTTTTAGTCATGTGCAAATTCTAATGATTTTTAT
TAATAATTCACTTATAAATATATATATCATAAAAATCAACAACATGTCATACATC
AACAGAAGTAGTGTCTTTATAAAACTTGAAAATAATCATAGTAAAATTAGTAGT
GACAGATTTTAAAAAATGACAAGCTTATGCTAGTACTTTACAAAATAAATAGCA
TTATATAAATATTTTACTGTAGTATGAGTCAATACTTTTTAAATTATTAATTTAGT
CAATATATGTTAGATGCAAATGTATTTTAATTATTTTTTTTATTGACCAATACTTT
GGTAGTATAATATTAGTAGTATTAGATATTATTGGCTATAAATAGATTCAACATT
GAAACACAAATACAATTAAAACCAAAACAAAAAGTAAAAAATGGCTAAGTTCAT
TGTACTCAAAATCACATCAAGAAAAAGCACTGAAATCATACATAGGTCTCAATT
TGGTGCCCCCAAACCGGATTTTTAACAAACCGAAAATGTACATTAATTTCCCT
CAAAATAGGAAAACCGGAAAACCAAAAAAATCAGTAAACCGAACCCAACGGA
TAATAAAGAAAAGAAAACCAAAGTCTAGGCCTAGAAATTTCGATGGTATGGAA
ATTACGATTTTGGACCCAAAACAATATGTACAAAAAATCATATAAATAATCGAA
TTTATTCCATCAAATCTTCTTCCTTGTCTGGATTTGGTTCACCATCGTCGGAAA
TCTCTGATCTCTCTCAGGATCGCTTGTTCGCTACGCAGATCTCACCTGCC

4.4. MAP7B Promoter Sequence.

GTGTTTTGTTTGGTTGGTGTGTATAGGTGGATCATGTTTTGTGCAAGATTTATC
TGACTCCATCGGCAGCAAAGAAGAAGAAAATGAGGAGCTGAAGAAGATGATC
AAGTGGTCGTAAAAAGAGGAGCAGCTGGATTTGCATTAATCGCAGCCTCATG
ATATTGTGTATCAGCCGCATCTTTTTCCTTATAACTTGGATAACATTTCTAAGT
TGATCAGTTTTGAACAACAACCAGTGATCCCAGAGGATTTTGAAGATTTTTTG
GCTGACTTCATGAAGCAGGATGGAGATGAAGAATCCATCGACACTGAAGGAA
TGATGGAACACTACACTAACTGATCTCAGCCAGCTTATAGTTTTTTTTTTCATT
TTGGTTTGCGTTTTTGTTATACGGGTTTTGTTATCAGAAAGAAAAAACAGAGA
GAAGATTTCATTATGTCTTAGTTGCTAATTGCTATGTTTCCTATAGGTAGTGTT
CTCCAAAACAAGAGATAATTCTCCCTGTTGTTATTGCTTTTGATGCCTAGATAC
ACAATTTATTCAACATTTTCTAATCATCTTAGAATTTCAAATATACACTAACATG
TTACCGTTGTAAAACACCAGAGTCTTGTTCTTCTTCATGTTCTTCTCCTAAGCA
TTTGTCTTCCTCTGAAAAAAGAAAAAATATAGAATATACCGGGTCTTTATAAGT
CTGATGTTCGGAAGATTCATTTAGCTCATTTGCATCCTCAATCTTTGTTTTTCT
CATCTAGTACGTCAGATGTCAAGAGCCATTGAATAAACTCAGATCTTTTCGTC
TGCTCTCCCTGATCTTGTGTTGAGACAGATGAGGAAGATTAACCAAACTATCC
CATTCATTGTTAATCTGGTACCTTCTGAAGAAGATAACAACATCTTTACCCAGA
GTTCAATCAAGTATATTTTGCAAAAACTAGCCTAGTATAAGTCACGTGTAAGAT
GCATGTAGAACACAGAATTTTTTTTGTTTTGATATCAATGTTAAGTATTTATACC
ATTTTCGAAGTTTTGACAGAAGTTATAAAGAATACAAGTAATGGAAAAATAAAT
CTACAGAAAGCACAAACAAAAACAAACAGTAATGGAGGAAATCTTTAACCAAG
AGCGGAAACAAGAAAAGAAACACCGATTCCGAGAAGCTAAACTCGAAAATTT
CAGTGATTTCCACAACTCGAAAATACCAAGGAGCTGGAATCTCATCTTACTTG
CCACGAGCAAACCTTAGCAGAGGTCCGTCCTCAAAACCTCTCGAGTAAGGCA
CATTAACTTCTCTTCAAACTAACGCAAAACGTAAAGATAATAGAGAACTTAAAC
ACAAATCCGACGAAGTCCTCTTGACAAGAAGATGGAGGGTTGTTCTCGTACT
CGCTTGGCGGGATGGGCATTCTTAGTTGTTTAAAACTTCACCAATTGAAGTCT

TATGGTTCATCATCATCCGTTGTAAGTTCCGCTTAACATCGCTATCACCGACA
AGCTGATTTTCTTGTAGATGCAAGATTTACCACAACAATAAATCATCTGTTGAC
TCCGAGAAACCGCTTGAAAAATCTGTCTACAAACACTGCAAAATTGGAATTCT
ATAAAAAAAAAAAAAATTCTGTTTCGATACAAACTAAACCGAGGCATAAGCTTCA
CCTATAGACCTAACCTGAAGTCTACTCCATTATTCATTAACGAATAATCTTTTG
GCAAAAATATTAATCAAATGGCAATTTTGACCAAATTCTCATTTCATATCCGCT
CAAGTTGGTAATAAAATTACCAAATATTTTATTAACAAAACAATATGAAAAAGA
AAGAATTATATAATCGAGAAAAATAGAGAATATGGAAAAGTAGAGGCGTACGA
CAAAGAAGACCTTAACACACACAATTCAAGCAATATATAAAAAAAAAATCCAAT
CTTTGTTCCTCAAAAATCCTCTGCTTCGCGTTTTTCTTCGGCATTGACTTTACC
AATCACAACTTTCTCCGGGATCGCCGATTTATCTTCGTTTCAACC

4.5. MAP7A Protein Sequence.

MTRGSQRERDRERALARTGGKGKNKDDGLTPEQRRERDAKALQEKTAKKAAQ
AAAAASSGGGGGKGNNK*

4.6. MAP7B Protein Sequence.

MTRGSQRERDRERAAARAGGKGKNGDDGLTPEQRRERDGKALQEKAAKKAAQ
AAGASSGGAAGGKGAAAKK*

Appendix 5: Summary of GUS Histochemical Staining in Transgenic *pMAP7A:GUS* and *pMAP7B:GUS* Lines.

5.1 GUS-Staining in Seedlings.

5.1.1. MAP7A.

Line	Root Tip	Root Vasculature	Root Hair	Leaf Vasculature	stipule	Trichomes
1				x		
2				x		
3		x		x		
4						
5						
6						
7						
8				x		
9				X		
10						

5.1.2. MAP7B.

Line	Root Tip	Root Vasculature	Root Hair	Leaf Vasculature	Stipules	Trichomes
1		x				
2		x	x	x	x	
3		x	x	x	x	
4		x	x	x	x	
5		x			x	
6		x		x	x	
7		x	x	x	x	x
8		x	x	x	x	
9		x	x	x	x	
10		x	x	x	x	

5.2. GUS-Staining in Leaf Tissue.

5.2.1. MAP7A.

Line	Leaf Vasculature	Stomata	Trichomes	Serrate Margin	Leaf Tissue
1		x(1)			
2		x(1)			
3					
4					
5					
6					
7					
8					
9					
10					

5.2.2. MAP7B.

Line	Leaf Vasculature	Stomata	Trichromes	Serrate Margin	Leaf Tissue
1					
2	x	x(1)	x	x	
3	x	x(1)	x	x	x(2)
4				x	
5					x(2)
6					
7	x	x(1)	x	x	x(2)
8	x	x(1)	x	x	x(2)
9	x	x(1)	x	x	
10	x	x(1)	x	x	

1 – Observation inconsistent between samples, and the strength of the signal did not correspond to length of incubation in GUS buffer. Staining was localised to clusters of stomata in isolated regions of the leaf tissue sample. Expression may have been activated at localised sites in individual plants a stress-response.

2 – Localised blotches of stained tissue sample, apparently non-specific to a certain cell type. Localised expression may be a response to stress, such as pathogen attack.

5.3. GUS-Staining in Floral Tissue

5.3.1. MAP7A.

Line	Pollen	Sepal Vasculature	Pistil	Trichomes
1	x			
2	x			
3	x			
4	X			
5	X			
6	X			
7	X			
8	X			
9	X			
10	X			

5.3.2. MAP7B.

Line	Pollen	Sepal Vasculature	Pistil	Trichomes
1				
2	x	x		
3	x	x		
4	x	x		
5	x			
6	x			
7	x			
8	x	x		
9	x	x		
10	x			

References.

Allwood EG, Anthony RG, Smertenko AP, Reichelt S, Drobak BK, Doonan JH, Weeds AG, Hussey PJ. (2002). Regulation of the Pollen-Specific Actin-Depolymerizing Factor LlADF1. *The Plant Cell*. **14**: 2915 - 2927

Alonso JM, Stepanova AN, Leisse TJ, Kim CJ, Chen H, Shinn P, Stevenson DK, Zimmerman J, Barajas P, Cheuk R. (2003). Genome-wide insertional mutagenesis of *Arabidopsis thaliana*. *Science*. **301**: 653 – 657.

Ambrose CJ, & Cyr R. (2007). The kinesin ATK5 functions in early spindle assembly in Arabidopsis. *The Plant Cell*. **19**: 226 – 236.

Astrom H, Sorri O, Raudaskoski. (1995). Role of microtubules in the movement of the vegetative nucleus and generative cell in tobacco pollen tubes. *Sex Plant Reprod.* **8**: 61 – 69.

Aouar L, Chebli Y, Geitmann A. (2010). Morphogenesis of complex plant cell shapes: the mechanical role of crystalline cellulose in growing pollen tubes. *Sex Plant Reprod,* **23**: 15 – 27.

Bao CC, Wang J, Zhang RH, Zhang BC, Zhang H, Zhou YH. Huang S. (2012). Arabidopsis VILLIN2 and VILLIN3 act redundantly in sclerenchyma development via bundling of actin filaments. *Plant J.* **71**: 962 – 975.

Baskin TI. (2001). On the alignment of cellulose microfibrils by cortical microtubules: a review and a model. *Protoplasma*. **215**: 150– 171.

Beh T, McCaster CR, Kozminski KG, Menon AK. (2012). A detour for Yeast oxysterol binding proteins. *J Biol Chem*. **287**: 11481 – 11488.

Blackmore S, Wortley AH, Skvarla JJ, Rowley JR. (2007). Pollen wall development in flowering plants. *New Phytol*. **174**: 483 – 498.

Borg M, Brownfield L & Twell D. (2009). Male gametophyte development: a molecular perspective. *J. Exp. Bot*. **60**: 1485 – 1478.

Borg M, & Twell D. (2011). Pollen: structure and development. *eLS.* DOI: 10.1002/9780470015902.a0002039.pub2

Bosch M, Poulter NS, Vatovec S, Franklin-Tong VE. (2008). Initiation of programmed cell death in self-incompatibility: role for cytoskeleton modifications and several caspase-like activities. *Mol Plant*. **1**: 879 – 887.

Bou Daher F & Geitmann A. (2012). Actin depolymerizing factors ADF7 and ADF10 play distinct roles during pollen development and pollen tube growth. *Plant Signal Behav*. **7**: 879 - 881.

Bosch M, Cheung AY, Hepler PK. (2005). Pectin methylesterase, a regulator of pollen tube growth. *Plant Physiol.* **138**: 1334 – 1346.

Bush S. (2014). Investigating post-translational modification of the NET protein superfamily .*M.Sc thesis, University of Durham, Durham, UK.*

Cai G, Cresti M. (2006). The microtubular cytoskeleton in pollen tubes: structure and role in organelle trafficking. *Plant Cell Monographs.* **3**: 157 – 175.

Cai G, Del Casino C, Cresti M. (2000). Cytoskeletal basis of organelle trafficking in the angiosperm pollen tube. *Ann. Bot.* **85:** 69 – 78.

Cai G, Faleri C, Del Casino C, Emons AMC, Cresti M. (2011). Distribution of callose synthase, cellulose synthase, and sucrose synthase in tobacco pollen tube is controlled in dissimilar ways by actin filaments and microtubules. *Plant Physiol* **155**: 1169 – 1190.

Calcutt, JR. (2009). ABP195, a novel plant actin-binding protein. *PhD Thesis, University of Durham, Durham, UK.*

Chang F, Gu Y, Ma H, Yang Z. (2013). AtPRK2 promotes ROP1 activation via RopGEFs in the control of polarized pollen tube growth. *Mol Plant*. **6**: 1187 – 1201.

Chebli Y, Kaneda M, Zerzour R, Geitmann A. (2012). The cell wall of the Arabidopsis pollen tube—spatial distribution, recycling, and network formation of polysaccharides. *Plant Physiol*. **160**. 1940 – 1955.

Chen C, Marcus A, Li W, Hu Y, Calzada JP, Grossniklaus U, Cyr RJ, Ma H. (2002). The Arabidopsis ATK1 gene is required for spindle morphogenesis in male meiosis. *Development.* **129**: 2401 -2409.

Chen M, & Thelen JJ. (2010). The plastid isoform of triose phosphate isomerase Is required for the postgerminative transition from heterotrophic to autotrophic growth in Arabidopsis. *Plant Cell*. **1**: 77 – 90.

Chen N, Qu X, Wu Y, and Huang S. (2009). Regulation of actin dynamics in pollen tubes: control of actin polymer level. *J. Integr. Plant Biol.* 51: 740 – 750.

Cheung AY, & Wu H. (2004). Overexpression of an Arabidopsis formin stimulates supernumerary actin cable formation from pollen tube cell membrane. *The Plant Cell*. **16**: 257 – 269.

Cheung A, Niroomand S, Zou Y, Wu H. (2010). A transmembrane formin nucleates subapical actin assembly and controls tip-focused growth in pollen tubes. *PNAS*. **107**: 16390 – 16395.

Cheung AY, Boavida LC, Aggarwal M, Wu HM, Fejo JA. (2010). The pollen tube journey in the pistil and imaging the *in vivo* process by two-photon microscopy. *J Exp Bot*. **61**: 1907 – 1915.

Clough SJ, & Bent AF. (1998). Floral dip: A simplified method for Agrobacterium-mediated transformation of *Arabidopsis thaliana*. *The Plant Journal*. **16**: 735 – 743.

Coles CH, & Bradke F. (2015). Coordinating neuronal actin-microtubule dynamics. *Curr Biol*. **25**: 677 – 691.

Collings D.A. (2008). Crossed wires: Interactions and cross-talk between the microtubule and microfilament networks in plants. *Plant Cell Mono.* **11**: 47 – 82.

Collings, DA, Lill AW, Himmelspach R, Wasteneys GO. (2006). Hypersensitivity to cytoskeletal antagonists demonstrates microtubule-microfilament cross-talk in the control of root elongation in *Arabidopsis thaliana*. *New Phyto*l. **170**: 275 – 290.

Curtis MD, & Grossniklaus U. (2003). A Gateway cloning vector set for high-throughput functional analysis of genes in planta. *Breakthrough Technologies,* **133**: 462 – 469.

Cvrčková F. (2013). Formins and membranes: anchoring cortical actin to the cell wall and beyond. *Frontiers in Plant Science*. **4**: 436, DOI: 10.3389/fpls.2013.00436

Czechowski T, Stitt M, Altmann T, Udvardi MK. (2005). Genome-wide identification and testing of superior reference genes for transcript normalization. *Plant Physiology*. **139**: 5 – 17. DOI:10.3389/fpls.2013.00436

Daher FB, Van Oostende C, Geitmann A. (2011). Spatial and temporal expression of actin depolymerizing factors ADF7 and ADF10 during male gametophyte development in *Arabidopsis thaliana*. *Plant Cell Physiol.* **52**: 1177 – 1192.

Danquah JO, Botchway S, Jeshtadi A, King L, (2012). Direct interaction of Baculovirus Capsid proteins VP39 and EXON0 with Kinesin-1 in insect cells determined by fluorescence resonance energy transfer-fluorescence lifetime imaging microscopy. *J Virol*. **86**: 844 – 853.

Day RN, & Davidson MW. (2012). Fluorescent proteins for FRET microscopy: Monitoring protein interactions in living cells. *Bioassays*. **34**: 341 - 350.

Deeks, M, Calcutt JR, Ingle ES, Hawkins TJ, Chapman S, Richardson AC, Mentlak DA, Dixon MR, Cartwright F, Smertenko AP, Oparka K, Hussey PJ. (2012). A superfamily of actin-binding proteins at the actin-membrane nexus of higher plants. *Current Biology.* **22**: 1595 – 600.

Deeks MJ, Rodrigues C, Dimmock S, Ketelaar T, Maciver SK, Malho R, Hussey, PJ (2007). *Arabidopsis* CAP1 – a key regulator of actin organisation and development. *J. Cell Sci.***120:** 2609–2618

de la Cruz EM, Mandinova A, Steinmetz MO, Stoffler D, Aebi U & Pollard TD. (2000). Polymerization and structure of nucleotide-free actin filaments. *J Mol Biol.* **295**: 517 - 526.

Dhonukshe P, Vischer N, Theodorus WJ, Gadella JR. (2006). Contribution of microtubule growth polarity and flux to spindle assembly and functioning in plant cells. *J Cell Sci*. **119**: 3193 – 3205.

Dievart A, & Clark SE. (2004). LRR-containing receptors regulating plant development and defense. *Development*. **131**: 251 – 261

Dixit R, & Cyr R. (2002). Spatio-temporal relationship between nuclear-envelope breakdown and preprophase band disappearance in cultured tobacco cells. *Protoplasma.* **219**: 116 – 121.

Dixon MR. (2013). NET2A: bridging the gap in plant-specific actin-membrane interactions. *PhD thesis, University of Durham, Durham, UK*.

Djinovic-Carugo K, Gautel M, Ylänne J, Young P. (2002). The spectrin repeat: A structural platform for cytoskeletal protein assemblies. *FEBS Letters*. **513**: 119 – 123.

Eady C, Lindsey K, Twell D. (1994). Differential activation and conserved vegetative cell-specific activity of a late pollen promoter in species with bicellular and tricellular pollen. *Plant Journal*. **5**: 543 – 550.

Eaves D, Flores-Ortiz C, Haque T, Lin Z, Teng N, Franklin-Tong V. (2014). Self-incompatibility in Papaver: advances in integrating the signalling network. *Biochemical Society Transactions*. **42**: 370 – 376.

Edwards K, Johnstone C, Thompson C. (1991). A simple and rapid method for the preparation of plant genomic DNA for PCR analysis. *Nucleic Acids Research*, **19**: 1349.

Eleftheriou EP, and Palevitz BA. (1992). The effect of cytochalasin-D on preprophase band organization in root-tip cells of *Allium*. *J. Cell Sci*. **103:** 989 – 998.

Endo M, Tsuchiya T, Hamada K, Kawamura S, Yano K, Ohshima M, Higashitani A, Watanabe M, Kawagishi-Kobayashi M. (2009). High temperatures cause male sterility in rice plants with transcriptional alterations during pollen development. *Plant Cell Physiol*. **50**: 1911 – 1922.

Escobar NM, Haupt S, Thow G, Boevnik P, Chapman S, Oparka K. (2003). High-throughput viral expression of cDNA-green fluorescent protein fusions reveals novel subcellular addresses and identifies unique proteins that interact with plasmodesmata. *The Plant Cell*, **15**: 1507 – 1523.

Esseling-Ozdoba A, Houtman D, van Lammeren AAM, Eiser E, Emons AMC. (2008). Hydrodynamic flow in the cytoplasm of plant cells. *Journal of Microscopy*, **231**: 274 – 283.

Eun SO, & Lee Y. (1997). Actin filaments of guard cells are reorganized in response to light and abscisic acid. *Plant Physiol*. **115:** 1491 – 1498.

Feng QN, Kang H, Song SJ, Ge FR, Zhang YL, Li E, Li S, Zhang Y. (2016). Arabidopsis RhoGDIs are critical for cellular homeostasis of pollen tubes. *Plant Physiol*. **170**: 841 – 856.

Ferguson C, Teeri TT, Siika-aho M, Read SM, Bacic A. (1998). Location of cellulose and callose in pollen tubes and grains of *Nicotiana tabacum*. *Planta*. **206**: 452 - 460.

Finn RD, Bateman A, Clements J, Coggill P, Eberhardt RY, Eddy SR, Heger A, Hetherington K, Holm L, Mistry J, Sonnhammer ELL, Tate J, Punta M. (2014). Pfam: The protein families database. *Nucleic Acids Research*. **42**: D222 – D230.

Fu Y, Li H, Yang Z. (2002). The ROP2 GTPase controls the formation of cortical fine F-actin and the early phase of directional cell expansion during Arabidopsis organogenesis. *Plant Cell*. **14**: 777 – 794.

Fu Y, Wu G, and Yang Z. (2001). ROP GTPase–dependent dynamics of tip-localized F-actin controls tip growth in pollen tubes. *J Cell Biol*. **152:** 1019 – 1032.

Fu Y, Xu T, Zhu L, Wen M, Yang Z. (2009). A ROP GTPase signaling pathway controls cortical microtubule ordering and cell expansion in Arabidopsis. *Curr Biol*. **19**: 1827 - 1832.

García-Cerdán JG, Sveshnikov D, Dewez D, Jansson S, Funk C, Schröder WP. (2009). Antisense inhibition of the PsbX protein affects PSII integrity in the higher plant *Arabidopsis thaliana*. *Plant Cell Physiol*. **50**: 191 - 202

Granger CL & Cyr RJ (2000). Use of abnormal preprophase bands to decipher division plane determination. *J Cell Sci.* **114**: 599 - 607.

Ge L, Gou X, Yuan T, Strout GW, Nakashima J, Blancaflor EB, Tian HQ, Russell SD. (2011). Migration of sperm cells during pollen tube elongation in *Arabidopsis thaliana*: behaviour during transport, maturation and upon dissociation of the male germ unit associations. *Planta*. **233:** 325 – 332.

Geitmann A. (2010). How to shape a cylinder: pollen tube as a model system for the generation of complex cellular geometry. *Sex Plant Reprod*. **23**: 63 – 71.

Gervais C, Simmonds DH, Newcomb W. (1994). Actin microfilament organization during pollen development of Brassica napus cv. Topas. *Protoplasma* **183**: 67 – 76.

Gibbon BC, Kovar DR, Staiger CJ. (1999). Latrunculin B has different effects on pollen germination and tube growth. *Plant Cell.* **11:** 2349 – 2363.

Gordon MB, Howard L, Compton DA. (2001). Chromosome movement in mitosis requires microtubule anchorage at spindle poles. *J Cell Biol*. **152**: 425 – 434.

Gossot O, & Geitmann A. (2007). Pollen tube growth: coping with mechanical obstacles involves the cytoskeleton. *Planta.* **226**: 405 – 416.

Gu Y, Vernoud V, Fu Y, Yang Z. (2003). ROP GTPase regulation of pollen tube growth through the dynamics of tip-localized F-actin. *J Exp Bot*. **54**: 93 – 101.

Gu Y, Fu Y, Dowd P, Li S, Vernoud V, Gilroy S, Yang Z. (2005). A Rho family GTPase controls actin dynamics and tip growth via two counteracting downstream pathways in pollen tubes. *J Cell Biol*. **169**: 127 – 138.

Gu Y, Li S, Lord E, Yang Z. (2006). Members of a novel class of *Arabidopsis* Rho Guanine Nucleotide Exchange Factors control Rho GTPase-dependent polar growth. *Plant Cell.* **18**: 366 – 381.

Gui CP, Dong X, Liu HK, Huang WJ, Zhang D, Wang SJ, Barberini ML, Gao XY, Muschietti J, McCormick S, Tang WH. (2014). Overexpression of the Tomato Pollen Receptor Kinase LePRK1 rewires pollen tube growth to a blebbing mode. *Plant Cell*. **26**: 3538 – 3555.

Gunning BES, & Wick SM. (1985). Preprophase bands, phragmoplasts and spatial control of cytokinesis. *J. Cell Sci*. *Suppl.* **2**: 157 - 179.

Gutierrez R, Lindeboom JJ, Paredez AR, Emons AM, Ehrhardt DW. (2009). Arabidopsis cortical microtubules position cellulose synthase delivery to the plasma membrane and interact with cellulose synthase trafficking compartments. *Nat Cell Biol.* **11:** 797 – 806.

Guyon V, Tang WH, Monti MM, Raiola A, Lorenzo GD, McCormick S, Taylor LP. (2004). Antisense phenotypes reveal a role for SHY, a pollen-specific leucine-rich repeat protein, in pollen tube growth. *Plant Journal* **39**: 643 – 654.

Hardham AR, Jones DA, Takemoto D. (2007). Cytoskeleton and cell wall function in penetration resistance. *Curr Op Plant Biol*, **10**: 342 – 348.

Hammer JA, & Sellers JR. (2012). Walking to work: roles for class V myosins as cargo transporters. *Nat Rev. Mol Cell Biol*, **13**: 13 – 26.

Hashimoto T. (2015). Microtubules in Plants. *The Arabidopsis Book*. DOI: 10.1199/tab.0179.

Hawkins TJ, Deeks MJ, Wang P, Hussey PJ. (2014). The evolution of the actin binding NET superfamily. *Front Plant Sci*. doi: 10.3389/fpls.2014.00254.

Helper PK, Vidali L., Cheung AY. (2001). Polarised cell growth in higher plants. *Annu Rev Cell Dev Biol*. **17**: 159 - 187.

Helper PK, Lovy-Wheeler A, McKenna S, Kunkel J. (2006). Ions and pollen tube growth. *Plant Cell Mono*. **3**: 47 – 69.

Henty-Ridilla JL, Shimono M, Li J, Chang JH, Day B, Staiger C.J. (2013). The Plant Actin Cytoskeleton Responds to Signals from Microbe-Associated Molecular Patterns. *PLoS Pathogens*, **9**: e1003290.

Henty-Ridilla JL, Li JJ, Day B, Staiger CJ. (2014). ACTIN DEPOLYMERIZING FACTOR4 regulates actin dynamics during innate immune signaling in Arabidopsis. *The Plant Cell*. **26**: 340 – 352.

Heslop-Harrison Y, & Heslop-Harrison J. (1992). Germination of monocolpate angiosperm pollen: evolution of the actin cytoskeleton and wall during hydration, activation and tube emergence. *Annals Bot.* **69:** 385 – 394.

Heslop-Harrison J, Heslop-Harrison Y, Cresti M, Tiezzi A, Moscatelli A. (1988). Cytoskeletal elements, cell shaping and movement in the angiosperm pollen tube. *J. Cell Sci*. **91**: 49 – 60.

Huang S, Blanchoin L, Kovar DR, Staiger CJ. (2003). Arabidopsis capping protein (AtCP) Is a heterodimer that regulates assembly at the barbed ends of actin filaments. *J Biol Chem*, **278**: 44832 – 44842.

Huang S. Jin L, Du K, Li H, Zhao Q, Ou G, Ao G, Yuan M. (2007). SB401, a pollen-specific protein from Solanum berthaultii, binds to and bundles microtubules and F-actin. *Plant Journal*. **51**: 401 – 418.

Huang WJ, Liu HJ, McCormick S, Tang WH. (2014). Tomato pistil factor STIG1 promotes *in vivo* pollen tube growth by binding to phosphatidylinositol 3-phosphate and the extracellular domain of the pollen receptor kinase LePRK2. *Plant Cell*. **26**: 2505 – 2523.

Huang S, Robinson RC, Gao LY, Matsumoto T, Brunet A, Blanchoin L, Staiger CJ. (2005). VILLIN1 generates actin filament cables that are resistant to depolymerization. *Plant Cell*. **17**: 486 - 501.

Hussey PJ. (2004). The plant cytoskeleton in cell differentiation and development. *Blackwell Scientific Publishers, Oxford.*

Hussey PJ, Ketelaar T, Deeks M.J. (2006). Control of the actin cytoskeleton in plant cell growth. *Annual Review of Plant Biology*, **57**: 109 – 125.

Hwang JU, Wu G, Yan A, Lee YJ, Grierson CS, Yang Z. (2010). Pollen-tube tip growth requires a balance of lateral propagation and global inhibition of Rho-family GTPase activity. *J Cell Sci*. **123**: 340 – 350.

Hwang JU, Vernoud V, Szumlanski A, Nielsen E, Yang Z. (2008). A tip-localized RhoGAP controls cell polarity by globally inhibiting Rho GTPase at the cell apex. *Curr Biol* **18**: 1907 - 1916.

Idilli A, Morandini P, Onelli E, Rodighiero S, Caccianiga M, Moscatelli A. (2013). Microtubule depolymerization affects endocytosis and exocytosis in the tip and influences endosome movement in tobacco pollen tubes. *Mol Plant*. **6**: 1109 – 1130.

Igarashi H, Orii H, Mori H, Shimmen T, Sonobe S. (2000). Isolation of a novel 190-kDa protein from tobacco BY2 cells: possible involvement in the interactions between actin filaments and microtubules. *Plant Cell Physiol*. **41:** 920 – 931.

Ingle EKS. (2011). An analysis of the NET1 proteins, a group of novel plant actin-binding proteins. *PhD thesis, University of Durham, Durham, UK.*

Ischebeck T, Stenzel I, Heilmann I (2008). Type B phosphatidylinositol-4-phosphate 5-kinases mediate Arabidopsis and *Nicotiana tabacum* pollen tube growth by regulating apical pectin secretion. *Plant Cell*. **20**; 3312 – 3330.

Ischebeck T, Stenzel I, Hempel F, Jin X, Molsbleh A, Heilmann I. (2011). Phosphatidylinositol-4,5-bisphosphate influences Nt-Rac5-mediated cell expansion in pollen tubes of *Nicotiana tabacum*. *The Plant Journal.* **65**: 453 – 468.

Ishikawa-Ankerhold HC, Ankerhold R, Drummen GPC. (2012). Advanced fluorescence microscopy techniques—FRAP, FLIP, FLAP, FRET and FLIM. *Molecules.* **17**: 4047 – 4132.

James P, Halladay J, Craig EA. (1996). Genomic libraries and a host strain designed for highly efficient two-hybrid selection in yeast. *Genetics*. **144**: 1425 - 1436.

Jamur MC, & Oliver C. (2009). Permeabilization of cell membranes. *Methods Mol Biol*. **588**: 63 – 66.

Jefferson RA, Kavanagh TA, Bevan MW. (1987). GUS fusions: beta-glucuronidase as a sensitive and versatile gene fusion marker in higher plants. *The EMBO Journal*. **6**: 3901 – 3907.

Jeshtadi A, Burgos P, Stubbs CD, Parker AW, King LA, Skinner MA, Botchway SW (2010). Interaction of poxvirus intracellular mature virion proteins with the TPR domain of kinesin light chain in live infected cells revealed by two-photon-induced fluorescence resonance energy transfer fluorescence lifetime imaging microscopy. *J. Virol* **84**:12886 –12894.

Jia H, Li J, Zhu J, Fan T, Qian D, Zhou Y, Wang J, Ren H, Xiang Y, An L. (2013). Arabidopsis CROLIN1, a novel plant actin binding protein, functions in cross-linking and stabilizing actin filaments. *Journal of Biological Chemistry*. **288**: 32277 - 32288.

Jiang K, Sorefan K, Deeks MJ, Bevan MW, Hussey PJ, Hetherington AM. (2012). The ARP2/3 complex mediates guard cell actin reorganization and stomatal movement in Arabidopsis. *The Plant Cell*. **24**: 2031 – 2040.

Joos U, Vanaken J, Kristen U. (1994). Microtubules are involved in maintaining the cellular polarity in pollen tubes of Nicotiana sylvestris. *Protoplasma*.**179**: 5 –15.

Kabsch W, Mannherz HG, Suck D, Pai EF, Holmes KC. (1990). Atomic structure of the actin:DNase I complex. *Nature* **347**: 37 – 44.

Kadota A, Yamada N, Suetsugu N, Hirose M, Saito C, Shoda K, Ichikawa S, Kagawa T, Nakano A, Wada M. (2009). Short actin-based mechanism for light-directed chloroplast movement in Arabidopsis. *PNAS.* **106**: 13106 – 13111.

Kang BH, Rancour DM, Benarek SY. (2003). The dynamin-like protein ADL1C is essential for plasma membrane maintenance during pollen maturation. *The Plant Journal.* **35**: 1 – 15.

Kaothien P, Ok SH, Shuai B, Wengier D, Cotter R, Kelley D, Kiriakopolos S, Muschietti J, McCormick S. (2005). Kinase partner protein interacts with the LePRK1 and LePRK2 receptor kinases and plays a role in polarized pollen tube growth. *Plant Journal.* **42**: 492 – 503.

Kapila J, de Rycke R, van Montagu, M, Angenon G. (1997). An Agrobacterium mediated transient gene expression system for intact leaves. *Plant Science* **122**: 101 - 108.

Karimi M, Inzé D, Depicker A. (2002). Gateway vectors for Agrobacterium-mediated plant transformation. *Trends Plant Sci.* **7:** 193 - 195.

Khlare U & Kost B. (2006). Tobacco RhoGTPase ACTIVATING PROTEIN1 spatially restricts signaling of RAC/Rop to the apex of pollen tubes. *Plant Cell*. **18**: 3033 – 3046.

Klahre U, Becker C, Schmitt AC, Kost B. (2006). Nt-RhoGDI2 regulates Rac/Rop signaling and polar cell growth in tobacco pollen tubes. *Plant J*. **46**: 1018 – 1031.

Kliwer I, & Dresselhaus T. (2010). Establishment of the male germline and sperm cell movement during pollen germination and tube growth in maize. *Plant Signal Behav.* **5**: 885 – 889.

Kim HU, Cotter R, Johnson S, Senda M, Dodds P, Kulikauskas R, Tang W, Ezcurra I, Herzmark P, McCormick S. (2002). New pollen- specific receptor kinases identified in tomato, maize and Arabidopsis: the tomato kinases show overlapping but distinct localization patterns on pollen tubes. *Plant Mol Biol.* **50**: 1 – 16.

Kim S, Mollet JC, Dong J, Zhang K, Park SY, Lord EM. (2003). Chemocyanin, a small basic protein from the lily stigma, induces pollen tube chemotropism. *PNAS*. **100**: 16125 – 16130.

Kim SY, Xu ZY, Song K, Kim DH, Kang H, Reichardt I, Sohn EJ, Friml J, Jeurgens G, Hwang I. (2013). Adaptor protein complex 2–mediated endocytosis is crucial for male reproductive organ development in Arabidopsis. *Plant Cell*. **25**: 2970 – 2985.

Konopka CA, Backues SK, Bednarek SY. (2008). Dynamics of Arabidopsis dynamin-related protein 1C and a clathrin light chain at the plasma membrane. *Plant Cell*. **20**: 1363 – 1380.

Kost B, Mathur J, Chua NH. (1999). Cytoskeleton in plant development. *Curr Op Plant Biol*. **2**: 462 - **470**.

Kozminski KG, Alfaro G, Dighe S, Beh CT. (2006). Homologs of oxysterol binding proteins affect Cdc42p- and Rho1p-mediated cell polarization in Saccharomyces cerevisiae. *Traffic.* **7**: 1224 – 1242.

Krysan PJ, Young JC, Sussman MR. (1999). T-DNA as an insertional mutagen in Arabidopsis. *Plant Cell*. **11**: 2283 - 2290.

Lahav M, Abu-Abied M, Belausov E, Schwartz A, Sadot E. (2004). Microtubules of guard cells are light sensitive. *Plant Cell Physiol*. **45**: 573 – 582.

Lalanne E, & Twell D. (2002). Genetic control of the male germ unit organisation in Arabidopsis. *Plant Physiol*. **129**: 865 – 875.

Larkin MA, Blackshields G, Brown NP, Chenna R, Mcgettigan PA, McWilliam H, Valentin F, Wallace IM, Wilm A, Lopez R, Thompson JD, Gibson TJ, Higgins DG. (2007). Clustal W and Clustal X version 2.0. *Bioinformatics*. **23:** 2947 – 2948.

Laitiainen E, Nieminen KM, Vihinen H, and Raudaskoski M. (2002). Movement of generative cell and vegetative nucleus in tobacco pollen tubes is dependent on microtubule cytoskeleton but independent of the synthesis of callose plugs. *Sex Plant Reprod*. **15**: 195 – 204.

Lee, YJ, Szumlanski A, Nielsen E, and Yang ZB. (2008). Rho-GTPase dependent filamentous actin dynamics coordinate vesicle targeting and exocytosis during tip growth. *J. Cell Biol*. **181:** 1155 – 1168.

Lee HS, Karunanandaa B, McCubbin A, Gilroy A, Kao TH. (1996). PRK1, a receptor-like kinase of *Petunia inflata*, is essential for postmeiotic development of pollen. *Plant Journal*. **9**: 613 – 624.

Leydon AR, Beale KM, Woroniecka K, Castner E, Chen J, Horgan C, Palanivelu R, Johnson MA. (2013). Three MYB transcription factors control pollen tube differentiation required for sperm release. *Curr Biol*. **23**: 1209 – 1214.

Li H, Lin Y, Heath RM, Zhu MX, Yang Z. (1999). Control of pollen tube tip growth by a Rop GTPase-dependent pathway that leads to tip-localized calcium influx. *Plant Cell.* **11**: 1731 - 1742

Li JJ, Wang XL, Qin T, Zhang Y, Liu XM, Sun JB, Zhou Y, Zhu L, Zhang Z, Yuan M, Mao T. (2011). MDP25, a novel calcium regulatory protein, mediates hypocotyl cell elongation by destabilizing cortical microtubules in Arabidopsis. *Plant Cell*. **23**: 4411 – 4427.

Lin Y, Wang Y, Zhu JK., and Yang Z. (1996). Localization of a Rho GTPase implies a role in tip growth and movement of the generative cell in pollen tubes. *Plant Cell*. **8**: 293 – 303.

Liu J, Zhong S, Guo X, Hao L, Wei X, Huang Q, Hou Y, Shi J, Wang C, Gu H, Qu LJ. (2013). Membrane-bound RLCKs LIP1 and LIP2 are essential male factors controlling male-female attraction in Arabidopsis. *Curr Biol*. **23**: 993 – 998.

Lloyd C. (2009). Plant microtubules: their role in growth and development. eLS. DOI: 10.1002/9780470015902.a0001685.pub2.

Löcke S, Fricke I, Mucha E, Humpert ML, Berken A. (2010). Interactions in the pollen-specific receptor-like kinases-containing signaling network. *Eur J Cell Biol*. **89**: 917 – 923

Lovy-Wheeler A, Kunkel JG, Allwood EG, Hussey PJ, Helper PK. (2006). Oscillatory increases in alkalinity anticipate growth and may regulate actin dynamics in pollen tubes of lily. *Plant Cell*. **18**: 2182 – 2193.

Lovy-Wheeler A, Wilsen KL, Baskin TI, and Hepler PK. (2005). Enhanced fixation reveals the apical cortical fringe of actin filaments as a consistent feature of the pollen tube. *Planta*. **221**: 95 – 104.

Lou Y, Schwender J, Shanklin J. (2014). FAD2 and FAD3 desaturases form heterodimers that facilitate metabolic channeling *in vivo*. *J Biol Chem.* **289**: 17996 – 18007.

Ma H. (2005). Molecular genetic analyses of microsporogenesis and microgametogenesis in flowering plants. *Annu Rev Plant Biol.* **56**: 393 - 434.

Marc J, Mineyuki Y, Palevitz BA. (1989). The generation and consolidation of a radial array of cortical microtubules in developing guard cells of Allium cepa L. *Planta*. **179:** 516 – 529.

Madison SL, Buchanan ML, Glass JD, McClain TF, Park E, Nebenführ A. (2015). Class XI Myosins move specific organelles in pollen tubes and are required for normal fertility and pollen tube growth in Arabidopsis. *Plant Physiol*. **169**: 1946 - 1960.

Mao T, Jin L, Li H, Liu B, Yuan M. (2005). Two microtubule-associated proteins of the Arabidopsis MAP65 family function differently on microtubules. *Plant Physiol*. **138**: 654 – 622.

Martinière A, Gayral P, Hawes C, Runions J. (2011). Building bridges: Formin1 of Arabidopsis forms a connection between the cell wall and the actin cytoskeleton. *The Plant Journal*. **66**: 354 – 365.

Mason JM, & Arndt KM. (2004). Coiled coil domains: stability, specificity, and biological implications. *Chembiochem*. **5**: 170 – 176.

Masoud K, Herzog E, Chaboute EM, Schmitt AC. (2013). Microtubule nucleation and establishment of the mitotic spindle in vascular plant cells. *Plant Journal.* **75**: 245 – 257.

Mathur J, Spielhofer P, Kost B, Chua NH. (1999). The actin cytoskeleton is required to elaborate and maintain spatial patterning during trichome cell morphogenesis in *Arabidopsis thaliana*. *Development.* **126**: 5559 - 5568.

McCue AD, Cresti M, Feijo JA, Slotkin RK. (2011). Cytoplasmic connection of sperm cells to the pollen vegetative cell nucleus: potential roles of the male germ unit revisited. *J Exp Bot*. **62**: 1621 – 1631.

McCurdy DW, & Kim M. (1998). Molecular cloning of a novel fimbrin-like cDNA from *Arabidopsis thaliana*. *Plant Mol Biol.* **36**: 23 - 31.

Mentlak D. (2015). Studies on NET4B and associated proteins. *PhD thesis, University of Durham, Durham, UK*.

Michelot A, Derivery E, Paterski-Boujemaa R, Guerin C, Huang S, Parcy F, Staiger CJ, Blanchoin L. (2006). A novel mechanism for the formation of actin-filament bundles by a nonprocessive formin. *Curr Biol*. **16**: 1924 - 1930.

Michelot A, Guerin C, Huang S, Ingouff M, Richard S, Rodiuc N, Staiger CJ, Blanchoin L. **(2005).** The Formin homology 1 domain modulates the actin nucleation and bundling activity of Arabidopsis FORMIN1. *The Plant Cell*, **17**: 2296 – 2313.

Mineyuki Y, & Palevitz BA. (1990). Relationship between preprophase band organization, F-actin and the division site in Allium. *J. Cell Sci*. **97**: 283 - 295.

Miyawaki KN, & Yang Z. (2014). Extracellular signals and receptor-like kinases regulating ROP GTPases in plants. *Front Plant Sci*. **22**: 449, doi: 10.3389/fpls.2014.00449.

Möckli N, Deplazes A, Hassa PO, Zhang Z, Peter M, Hottiger MO, Stagljar I, Auerbach D. (2007). Yeast split-ubiquitin-based cytosolic screening system to detect interactions between transcriptionally active proteins. *Biotechniques.* **42**: 725 – 730.

Morejohn LC, & Fosket DE. (1984). Inhibition of plant microtubule polymerization *in vitro* by the phosphoric amide herbicide amiprophos-methyl. *Science*. **224**: 874 – 876.

Moscatelli A, Idiili A, Rodighiero S, Caccianiga M. (2012). Inhibition of actin polymerisation by low concentration Latrunculin B affects endocytosis and alters exocytosis in shank and tip of tobacco pollen tube. *Plant Biology*. **14**: 770 – 782.

Moscatelli A, & Idilli A (2009). Pollen Tube Growth: a Delicate Equilibrium Between Secretory and Endocytic Pathways. *J Integr Plant Biol.* **51**: 727 – 739.

Mu JH, Lee HS, Kao TH. (1994). Characterization of a pollen-expressed receptor-like kinase gene of *Petunia inflata* and the activity of its encoded kinase. *Plant Cell.* **6**: 709 – 721.

Mucha E, Fricke I, Schaefer A, Wittinghofer A, Berken A. (2011). Rho proteins of plants--functional cycle and regulation of cytoskeletal dynamics. *Eur J Biol*. **90**: 934 – 943.

Murthy JV, Kim HH, Hanesworth VR, Hugdahl JD, Morejohn LC. (1994). Competitive Inhibition of High-Affinity Oryzalin Binding to Plant Tubulin by the Phosphoric Amide Herbicide Amiprophos-Methyl. *Plant Physiology*. **105**: 309 – 320.

Muschietti J, Dircks L, Vancanneyt G, McCormick S. (1994). LAT52 protein is essential for tomato pollen development: pollen expressing antisense LAT52 RNA hydrates and germinates abnormally and cannot achieve fertilization. *Plant Journal* **6**: 321 – 338.

Muschietti J, Eyal Y, McCormick S. (1998). Pollen tube localization implies a role in pollen-pistil interactions for the tomato receptor-like protein kinases LePRK1 and LePRK2. *Plant Cell.* **10**: 319 – 330.

Nebenführ A, Gallagher LA, Dunahay TG, Frohlick JA, Mazurkiewicz AM, Meehl JB, Staehelin LA. (1999). Stop-and-go movements of plant Golgi stacks are mediated by the acto-myosin system. *Plant Physiology*, **121**: 1127–1141.

Oda Y, & Fukuda H. (2011). Dynamics of Arabidopsis SUN proteins during mitosis and their involvement in nuclear shaping. *The Plant Journal*. **66**: 629 – 641.

Oh SA, Pal MD, Park SK, Johnson JA, Twell D. (2010). The tobacco MAP215/Dis1-family protein TMBP200 is required for the functional organization of microtubule arrays during male germline establishment. *J Exp Bot.* **61:** 969 – 981.

Ohlrogge J. B., Browse J., Somerville C. R. (1991). The genetics of plant lipids. *Biochim. Biophys. Acta*. **1082**: 1 – 26.

Osaskabe Y, Yamaguchi-Shinozaki K, Shinozaki K, Phan Tran LS. (2013). Sensing the environment: key roles of membrane-localized kinases in plant perception and response to abiotic stress. *J Exp Bot.* **64:** 445 – 458.

Osterrieder A, Carvalho CM, Latijnhouwers M, Johansen JN, Stubbs C, Botchway S, Hawes C. (2009). Fluorescence lifetime imaging of interactions between Golgi tethering factors and small GTPases in plants. *Traffic.* **10:** 1034 – 1046.

Pacini E. (1996). Types and meaning of pollen carbohydrate reserves. *Sex Plant Reprod* **9**: 362 – 366.

Palevitz BA. (1993). Organization of the mitotic apparatus during generative cell division in *Nicotiana tabacum*. *Protoplasma* **174:** 25 – 35.

Palevitz BA, & Cresti M. (1989). Cytoskeletal changes during generative cell division and sperm formation in Tradescantia virginiana. *Protoplasma.* **150**. 54 – 71.

Palanivelu R, & Preuss D. (2006). Distinct short-range ovule signals attract or repel *Arabidopsis thaliana* pollen tubes *in vitro*. *BMC Plant Biol*. **6**: doi:10.1186/1471-2229-6-7.

Palin R, & Geitmann A. (2012). The role of pectin in plant morphogenesis. *Biosystems*. **109**: 397 – 402.

Pantaloni D, & Carlier MF. (1993). How profilin promotes actin filament assembly in the presence of thymosin β4. *Cell*. **75**: 1007 – 1014.

Papuga J, Hoffmann C, Dieterle M, Moes D, Moreau F, Tholl S, Steinmetz A, Thomas C. (2010). Arabidopsis LIM proteins: A family of actin bundlers with distinct expression patterns and modes of regulation. *The Plant Cell*. **22**: 3034 – 3052.

Park SK, Howden R, Twell D. (1998). The *Arabidopsis thaliana* gametophytic mutation gemini pollen1 disrupts microspore polarity, division asymmetry and pollen cell fate. *Development*. **125**: 3789 – 3799.

Parre E, & Geitmann, A. (2005a). Pectin and the role of the physical properties of the cell wall in pollen tube growth of Solanum chacoense. *Planta*. **220**: 582 – 592.

Parre E, & Geitmann A (2005b). More than a leak sealant. The mechanical properties of callose in pollen tubes. *Plant Physiol.* **137**: 274 – 286.

Pastuglia M, Azimzadeh J, Goussot M, Camilleri C, Belcram K, Evrard JL, Schmit AC, Guerche P, Bouchez D. (2006). Gamma-tubulin is essential for microtubule organization and development in *Arabidopsis*. *Plant Cell.* **18**: 1412 – 1425.

Peaucelle A, Baybrook S, Hofte H. (2012). Cell wall mechanics and growth control in plants: the role of pectin revisited. *Front Plant Sci*. **3**: 121 doi: 10.3389/fpls.2012.00121.

Pierson ES, Kengen HMP, Derksen J. (1989). Microtubules and actin filaments co-localize in pollen tubes of *Nicotiana tabacum* L. and *Lilium longiflorum* Thunb. *Protoplasma.* **150:** 75 – 77.

Peremyslov VV, Mockler TC, Filichkin SA, Fox SE, Jaiswal P, Makarova KS, Koonin EV, Dolja VV. (2011). Expression, splicing, and evolution of the myosin gene family in plants. *Plant Physiology*. **155**: 1191 – 1204.

Peremyslov VV, Morgun EA, Kurth EG, Makarova KS, Koonin EV, Dolja VV. (2013). Identification of myosin XI receptors in Arabidopsis defines a distinct class of transport vesicles. *The Plant Cell*, **25**: 3022 - 3038.

Peremyslov, VV, Prokhnevsky AI, and Dolja VV. (2010). Class XI myosins are required for development, cell expansion, and F-Actin organization in Arabidopsis. *Plant Cell.* **22**: 1883 – 1897.

Peremyslov VV, Prokhnevsky AI, Avisar D, Dolja VV. (2008). Two class XI myosins function in organelle trafficking and root hair development in Arabidopsis. *Plant Physiology*. **146**: 1109 – 1116.

Pollard TD, & Borisy, GG. (2003). Cellular motility driven by assembly and disassembly of actin filaments. *Cell*, **112**: 453 – 465.

Potocky M, Jones MA, Bezvoda R, Zarsky V. (2007). Reactive oxygen species produced by NADPH oxidases are involved in pollen tube growth. *New Phytol*. **174**: 742 – 751.

Qin T, Liu XM, Li JJ, Sun JB, Song LN, Mao, TL. (2014). Arabidopsis microtubule-destabilizing protein 25 functions in pollen tube growth by severing actin filaments. *Plant Cell.* **26**: 325 – 339.

Qin Y, Leydon AR, Manziello A, Pandey R, Mount D, Denic S, Vasic B, Johnson MA, Palanivelu R. (2009). Penetration of the stigma and style elicits a novel transcriptome in pollen tubes, pointing to genes critical for growth in a pistil. *PLoS Genetics.* **5**: doi/10.1371/journal.pgen.1006210.

Qu LJ, Li L, Lan Z, Dresselhaus T. (2015a). Peptide signalling during the pollen tube journey and double fertilization. *J Exp Bot*. **66:** 5139 – 5150

Qu X, Jiang Y, Chang M, Liu X, Zhang R, Huang S. (2015b). Organisation and regulation of the actin cytoskeleton in the pollen tube. *Front Plant Sci.* doi: 10.3389/fpls.2014.00786

Qu XL, Zhang H, Xie YR, Wang J, Chen NZ, and Huang SJ. (2013). Arabidopsis villins promote actin turnover at pollen tube tips and facilitate the construction of actin collars. *Plant Cell*. **25**: 1803 – 1817.

Reagan S, & Moffat BA. (1990). Cytochemical analysis of pollen development in wild-type Arabidopsis and a male-sterile mutant. *Plant Cell*. **2**: 877 – 889.

Reddy AS, & Day IS. (2001). Analysis of the myosins encoded in the recently completed *Arabidopsis thaliana* genome sequence. *Genome Biology*, **2**: RESEARCH0024.1–0024.17

Rhee SY, Dickerson J, Xu D (2006). Bioinformatics and its applications in plant biology. *Ann Rev Plant Biol.* **57**: 335 - 360.

Romagnoli S, Cai G, Faleri C, Yokota E, Shimmen T, Cresti M. (2007). Microtubule- and actin filament-dependent motors are distributed on pollen tube mitochondria and contribute differently to their movement. *Plant Cell Physiol*. **48**: 345 – 361.

Rose A, & Meier I. (2004). Scaffolds, levers, rods and springs: diverse cellular functions of long coiled-coil proteins. Cell Mol Life Sci. **61**: 1996 – 2009.

Rounds CM, Hepler, PK, Winship LJ. (2014). The apical actin fringe contributes to localized cell wall deposition and polarized growth in the lily pollen tube. *Plant Physiol*, **166**: 139 – 151.

Rutten T, Chan J, Lloyd CW. (1997). A 60-kDa plant microtubule-associated protein promotes the growth and stabilization of neurotubules *in vitro*. *PNAS*. **94**: 4469 - 4474

Salem T, Mazzella A, Barberini ML, Wengier D, Motillo V, Parisi G, Muschietti J. (2011). Mutations in two putative phosphorylation motifs in the tomato pollen receptor kinase LePRK2 show antagonistic effects on pollen tube length. *J Biol Chem*. **286**: 4882 – 4891.

Sampathkumar A, Lindeboom JJ, Debolt S, Gutierrez R, Erdheart DW, Ketelaar T, Persson S. (2011). Live cell imaging reveals structural associations between the actin and microtubule cytoskeleton in Arabidopsis. *Plant Cell*. **23**: 2302 – 2313.

Sattarzadeh A, Krahmer J, Germain AD & Hanson MR. (2009). A myosin XI tail domain homologous to the yeast myosin vacuole-binding domain interacts with plastids and stromules in Nicotiana benthamiana. *Mol. Plant*. **2**: 1351 – 1358.

Scharf JM, Endrizzi MG, Wetter A, Huang S, Thompson TG, Zerres K, Dietrich WF, Wirth B, Kunkel LM. (1998). Identification of a candidate modifying gene for spinal muscular atrophy by comparative genomics. *Nat Genetics*. **20**: 83 – 86.

Schliwa M, & Woehlke G. (2003). Molecular motors. *Nature*. **422**: 759 – 765.

Schmit AC, & Lambert AM. (1990). Microinjected fluorescent phalloidin *in vivo* reveals the F-actin dynamics and assembly in higher plant mitotic cells*. Plant Cell* **2**: 129 - 138.

Schneider R, & Persson S. (2015). Connecting two arrays: the emerging role of actin-microtubule cross-linking motor proteins. *Front Plant Sci*. **6**: doi: 10.3389/fpls.2015.00415.

Schwacke R, Grallath S, Breitkreuz KE, Stransky E, Stransky H, Frommer WB, Rentsch D. (1999). LeProT1, a transporter for proline, glycine betaine, and {Gamma}-amino butyric acid in tomato pollen. *The Plant Cell*. **11**: 377 - 392.

Scott RJ, Spielman M, Dickinson HG. (2004). Stamen structure and function. *The Plant Cell*: **16**: S46 – S60.

Sellers JR. (2000). Myosins: A diverse superfamily. *Biochimica et Biophysica Acta.* **1496**: 3 – 22.

Shiu SH, Bleecker AB. (2001). Plant receptor-like kinase gene family: diversity, function, and signaling. *Sci Signal Transduction Knowledge Environ.* **113**: RE22.

Skirpan AL, McCubbin AG, Ishimizu T, Wang X, Hu Y, Dowd PE, Ma H, Kao T-H. (2001). Isolation and characterization of kinase interacting protein 1, a pollen protein that interacts with the kinase domain of PRK1, a receptor-like kinase of Petunia. *Plant Physiology* **126**: 1480 - 1492.

Skirpan AL, Dowd PE, Sijacic P, Jaworski CJ, Gilroy S, Kao TH. (2006). Identification and characterization of PiORP1, a Petunia oxysterol-binding-protein related protein involved in receptor-kinase mediated signalling in pollen, and analysis of the ORP gene family in Arabidopsis. *Plant Mol Biol*. **61**: 553 - 565.

Smertenko AP, Chang HY, Wagner V, Kaloriti D, Fenyk S, Sonobe S, Lloyd C, Hauser MT, Hussey PJ. (2004). The Arabidopsis microtubule-associated protein AtMAP65-1: molecular analysis of Its microtubule bundling activity. *Plant Cell.* **16**: 2035 – 2047.

Sobhanifar S. (2003). Yeast Two Hybrid Assay: A Fishing Tale. *BioTeach Journal*. **1**: 81 – 88.

Sparkes, I.A, Runions, J., Kearns, A., Hawes, C. (2006). Rapid, transient expression of fluorescent fusion proteins in tobacco plants and generation of stably transformed plants. *Nat Prot*, **1**: 2019 – 2025.

Sparkes I, Tolley N, Aller I, Svozil J, Osterrieder A, Botchway S, Mueller C, Frigerio L, Hawes C. (2010). Five Arabidopsis reticulon isoforms share endoplasmic reticulum location, topology, and membrane-shaping properties. *Plant Cell*. **22**: 1333 – 1343.

Staiger CJ, & Franklin-Tong VE. (2003). The actin cytoskeleton is a target of the self-incompatibility response in Papaver rhoeas. *J Exp Bot*. **54**: 103 - 113

Staiger CJ, Gibbon BC, Kovar DR, Zonia LE. (1997). Profilin and actin-depolymerizing factor: Modulators of actin organization in plants. *Trends in Plant Science*, **2**: 275 – 281.

Staiger CJ & Hussey PJ. (2004). Actin and actin-modulating proteins. In Hussey PJ (ed) The Plant Cytoskeleton in Cell Differentiation and Development. *Blackwell Scientific Publishers, Oxford:* 32 - 80.

Staiger CJ, Sheahan MB, Khurana P, Wang X, McCurdy DW, Blanchoin L. (2009). Actin filament dynamics are dominated by rapid growth and severing activity in the Arabidopsis cortical array. *Journal of Cell Biology*. **184**: 269 – 280.

Staiger, CJ, Poulter NS, Henty JL, Franklin-Tong VE. Blanchoin L. (2010). Regulation of actin dynamics by actin-binding proteins in pollen. *J Exp Bot.* **61**: 1969 – 1986.

Steinhorst L, & Kudla J. (2013). Calcium and reactive oxygen species rule the waves of signalling. *Plant Physiol*, **163**: 471 – 485.

Steinmetz MO, Goldie KN, Aebi U. (1997). A correlative analysis of actin filament assembly, structure, and dynamics. *J Cell Biol*, **138**: 559 – 574.

Stewman S, Jones-Rhoades M, Bhimalapuram P, Tchernookov M, Preuss D, Dinner AR. (2010). Mechanistic insights from a quantitative analysis of pollen tube guidance. *BMC Plant Biol*. **10**:32 DOI: 10.1186/1471-2229-10-32.

Stubbs CD, Botchway SW, Slater SJ, Parker AW. (2005). The use of time-resolved fluorescence imaging in the study of protein kinase C localisation in cells. *BMC Cell Biol*. **6**: 22 – 34.

Su H, Wang T, Dong H, Ren H. (2007). The villin/gelsolin/fragmin superfamily proteins in plants. *J Int Plant Biol*. **49**: 1183 – 1191.

Su H, Zhu JS, Cai C, Pei WK, Wang JJ, Dong HJ. Ren H. (2012). FIMBRIN1 is involved in lily pollen tube growth by stabilizing the actin fringe. *Plant Cell.* **24**. 4539 –4554.

Su T. (2012). Proteins that interact with Arabidopsis TANGLED. *M.Sc Thesis. University of California San Diego, San Diego, USA.*

Sun Y, Day RN, Periasamy A. (2011). Investigating protein-protein interactions in living cells using fluorescence lifetime imaging microscopy. *Nat Prot*. **6**: 1324 – 1340.

Sylvester AW. (2000). Division decisions and the spatial regulation of cytokinesis. *Curr Op Plant Biol.* **3**: 58 - 66.

Szymanski DB, Marks MD & Wick SM. (1999). Organized F-actin is essential for normal trichome morphogenesis in Arabidopsis. *Plant Cell.* **11**: 2331 - 2347.

Takeuchi H, & Higashiyama T. (2012). A species-specific cluster of Defensin-like genes encodes diffusible pollen tube attractants in Arabidopsis. *PLOS Biol*. **10**: e1001449.

Takeuchi H, & Higashiyama T. (2016). Tip-localized receptors control pollen tube growth and LURE sensing in Arabidopsis. *Nature*. **531:** 245 – 248.

Takemoto D, Jones DA, Hardham AR. (2003). GFP-tagging of cell components reveals the dynamics of subcellular re-organization in response to infection of Arabidopsis by oomycete pathogens. *The Plant Journal*. **33**: 775 – 792.

Tamura K, Iwabuchi K, Fukao Y, Kondo M, Okamoto K, Ueda H, Nishimura M, Hara-Nishimura I. (2013). Myosin XI-i links the nuclear membrane to the cytoskeleton to control nuclear movement and shape in Arabidopsis. *Curr. Biol*. **23**: 1776 – 1781.

Tang W, Kelley D, Ezcurra I, Cotter R, McCormick S. (2004). LeSTIG1, an extracellular binding partner for the pollen receptor kinases LePRK1 and LePRK2, promotes pollen tube growth *in vitro*. *Plant J.* **39**: 343 – 353

Tang W, Ezcurra I, Muschietti J, McCormick S. (2002). A cysteine-rich extracellular protein, LAT52, interacts with the extracellular domain of the pollen receptor kinase LePRK2. *Plant Cell.* **14**: 2277 – 2287.

Taylor LP, Hepler PK. (1997). Pollen Germination and Tube Growth. *Annu Rev Plant Physiol Plant Mol Biol.* **48**: 461 – 491.

Theunis CH, Pierson ES, Cresti M. (1992). The microtubule cytoskeleton and the rounding of isolated generative cells of *Nicotiana tabacum*. *Sex Plant Reprod.* **5**: 64 – 71.

Thompson JD, Gibson TJ, Plewniak F, Jeanmougin F, Higgins DG. (1997). The CLUSTAL X windows interface: Flexible strategies for multiple sequence alignment aided by quality analysis tools. *Nucleic Acids Research.* **25**: 4876 – 4882.

Traas JA, Burgain S, Dumas de Vaulx R. (1989). The organization of the cytoskeleton during meiosis in eggplant (Solanum melongena L.): microtubules and F-actin are both necessary for coordinated meiotic division. *J Cell Sci.* **92**: 541 – 550

Tripathi LP, & R Sowdhamini (2006). Cross genome comparisons of serine proteases in Arabidopsis and rice. *BMC Genomics.* **7**: 200 - 231

Twell D. (2010). Pollen: structure, development and function. *eLS*. 0002039

Twell D. (2011). Male gametogenesis and germline specification in flowering plants. *Sex Plant Reprod.* **24**: 149 – 160.

Twell D, Park SK, Hawkins TJ, Schubert D, Schmidt R, Smertenko A, Hussey PJ. (2002). MOR1/GEM1 has an essential role in the plant-specific cytokinetic phragmoplast. *Nat Cell Biol.* **4**: 711 - 714

Ueda H, Yokota E, Kutsuna N, Shimada T, Tamura K, Shimmen T, Hasezawa S, Dolja VV, Hara-Nishimura I. (2010). Myosin-dependent endoplasmic reticulum motility and F-actin organization in plant cells. *PNAS.* **107**: 6894 – 6899.

Valster A, Pierson E, Valenta R, Hepler P, Emons A. (1997). Probing the plant actin cytoskeleton during cytokinesis and interphase by profilin microinjection. *The Plant Cell*. **9**: 1815 – 1824.

van Criekinge W, & Beyaert R. (1999). Yeast Two-Hybrid: State of the Art. *Biol Proceed Online*. **4**: 1 – 38.

van Ham TJ, Thijssen KL, Breitling R, Hofstra RM, Plasterk RH, Nollen EA. (2008). *C. elegans* model identifies genetic modifiers of alpha-synuclein inclusion formation during aging. *PLoS Genet*. **4**: e1000027.

van Ham TJ, Holmberg MA, van der Goot AT, Teuling E, Garcia-Arencibia M, Kim HE, Du D, Thijssen KL, Wiersma M, Burggraaff R, van Bergeijk P, van Rheenen J, Jerre van Veluw G, Hofstra RM, Rubinsztein DC, Nollen EA. (2010). Identification of MOAG-4/SERF as a regulator of age-related proteotoxicity. *Cell*. **142**: 601 - 612

van Gestel K, Kohler RH, Verbelen J-P. (2002). Plant mitochondria move on F-actin, but their positioning in the cortical cytoplasm depends on both F-actin and microtubules. *J Exp Bot*. **53**: 659 - 667.

van Gisbergen PAC, Li M, Wu SZ, Benzanilla M. (2012). Class II formin targeting to the cell cortex by binding PI(3,5)P_2 is essential for polarized growth. *JCB*. **198**: 235 - 250

Van Leene J, Eeckhout D, Cannoot B, De Winne N, Persiau G, Van De Slijke E, Vercruysse L, Dedecker M, Verkest A, Vandepoele K, Martens L, Witters E, Gevaert K, De Jaeger G. (2014). An improved toolbox to unravel the plant cellular machinery by tandem affinity purification of Arabidopsis protein complexes. *Nat Protocols*. **10:** 169 - 187.

Vanstraelen M, Van Damme D, De Rycke R, Mylle E, Inzé D, Geelen D. (2006). Cell cycle-dependent targeting of a kinesin at the plasma membrane demarcates the division site in plant cells. *Curr Biol.* **7**: 308 - 314.

Verchot-Lubicz J, Goldstein RE. (2010). Cytoplasmic streaming enables the distribution of molecules and vesicles in large plant cells. *Protoplasma*, **240**: 99 – 107.

Vidali L, & Hepler PK. (2001). Actin and pollen tube growth. *Protoplasma*. **215**: 64 - 76.

Vidali L, Yokota E, Cheung AY, Shimmen T, Hepler PK (1999). The 135 kDa actin bundling protein from *Lilium longiflorum* pollen is the plant homologue of villin. *Protoplasma.* **209**: 283 - 291.

Vidali L, Mckenna ST, Hepler PK. (2001). Actin polymerization is essential for pollen tube growth. *Mol Biol Cell.* **12**: 2534 – 2545.

Volger F, Konrad SSA, Sprunck S. (2015). Knockin' on pollen's door: live cell imaging of early polarization events in germinating Arabidopsis pollen. *Front Plant Sci*. 10.3389/fpls.2015.00246

Wachsstock DH, Schwarz WH, Pollard TD. (1993). Affinity of a-Actinin for actin determines the structure and mechanical properties of actin filament gels. *Biophysical Journal*. **65**: 205 – 214.

Wakatsuki T, Schwab B, Thompson NC, Elson EL. (2001). Effects of cytochalasin D and latrunculin B on mechanical properties of cells. J Cell Sci. **114**: 1025 – 1036.

Wang C, Tian Q, Hou Z, Mucha M, Aukerman M, Olsen OA. (2007). The *Arabidopsis thaliana* AT PRP39-1 gene, encoding a tetratricopeptide repeat protein with similarity to the yeast pre-mRNA processing protein PRP39, affects flowering time. *Plant Cell Rep*. **26**: 1375 – 1366.

Wang HY. (2008). How effective is T-DNA insertional mutagenesis in Arabidopsis? *J Biochem Tech.* **1**: 11 – 20.

Wang P, Hawkins TJ, Richardson C, Cummins I, Deeks MJ, Sparkes I, Hawes C, Hussey PJ. (2014). The plant cytoskeleton, NET3C, and VAP27 mediate the link between the plasma membrane and endoplasmic reticulum. *Curr Biol.* **24**: 1397 - 1405

Wang P, & Hussey PJ. (2015). Interactions between plant endomembrane systems and the actin cytoskeleton. *Front Plant Sci*. **6**: 422, DOI: 10.3389/fpls.2015.00422

Wang X, Zhu L, Liu B, Wang C, Jin L, Zhao Q, Yuan M. (2007). Arabidopsis MICROTUBULE-ASSOCIATED PROTEIN18 functions in directional cell growth by destabilizing cortical microtubules. *Plant Cell.* **19**: 877 – 889.

Waterhouse AM, Procter JB, Martin DMA, Clamp M, Barton GJ. (2009). Jalview Version 2- A multiple sequence alignment editor and analysis workbench. *Bioinformatics.* **25**: 1189 – 1191.

Welch MD, Mallavarapu A, Rosenblatt J, Mitchison TJ. (1997). Actin dynamics *in vivo*. *Current Opinion in Cell Biology*, **9**: 54–61.

Wengier DL, Mazzella, MA, Salem TM, McCormick S, Muschietti JP. (2010). STIL, a peculiar molecule from styles, specifically dephosphorylates the pollen receptor kinase LePRK2 and stimulates pollen tube growth *in vitro.* ***BMC Plant Biol*****.** **10**: 33, DOI: 10.1186/1471-2229-10-33

Wengier D, Valsecchi I, Cabanas ML, Tang WH, McCormick S, Muschietti J. (2003). The receptor kinases LePRK1 and LePRK2 associate in pollen and when expressed in yeast, but dissociate in the presence of style extract. *PNAS.* **100**: 6860 – 6865.

Wilson ZA, & Yang C. (2004). Plant gametogenesis: conservation and contrasts in development. *Reproduction*. **128**: 483 – 492

Wolf S, Mouille G, Pelloux K. (2009). Homogalacturonan methyl-esterification and plant development. *Mol Plant*. **2**: 851 – 860

Wootton J, & Federhen S. (1996). Analysis of compositionally biased regions in sequence databases. *Methods Enzymol.* **266**: 554 - 571.

Wrzaczek M, Broschéa M, Kollista H, Kangasjärvi J. (2009). Arabidopsis GRI is involved in the regulation of cell death induced by extracellular ROS. *PNAS.* **106**: 5412 - 5417

Wrzaczek M, Vainonen JP, Stael S, Tsiatsiani L, Help-Rinta-Rahko H, Gauthier A, Kaufholdt D, Bollhöner B, Lamminmäki A, Staes A, Gevaert K, Tuominen H, Van Breusegem F, Helariutta Y, Kangasjärvi J. (2015). GRIM REAPER peptide binds to receptor kinase PRK5 to trigger cell death in Arabidopsis. *EMBO J*. **34**: 55 – 66.

Wu SZ, & Benzanilla M. (2014). Myosin VIII associates with microtubule ends and together with actin plays a role in guiding plant cell division. **eLIFE** 3:e03498

Wu Y, Yan J, Zhang R, Qu X, Ren S, Chen N, Huang S. (2010). *Arabidopsis* FIMBRIN5, an actin bundling factor, Is required for pollen germination and pollen tube growth. *Plant Cell.* **22**: 3745 - 3763

Xia G, Ramachandran S, Hong Y, Chan YS, Simanis V, Chua NH. (1996). Identification of plant cytoskeletal, cell cycle-related and polarity-related proteins using Schizosaccharomyces pombe. *Plant Journal*. **10**: 761 – 769.

Xue XH, Guo CQ, Du F, Lu QL, Zhang CM, Ren HY. (2011). AtFH8 is involved in root development under effect of low-dose latrunculin B in dividing cells. *Molecular Plant*. **4**: 264 – 278.

Yamamoto Y, Nishimura M, Nishimura-Hara I, Noguchi T. (2003). Behaviour of vacuoles during microspore and pollen development in *Arabidopsis thaliana*. *Plant Cell Physiol*. **44:** 1192 – 1201.

Yang Y, Sage TL, Liu Y, Ahmad TR, Marshall WF, Shiu SH, Froelich Jem Ime KM, Osteryoung KW. (2011). CLUMPED CHLOROPLASTS 1 is required for plastid separation in Arabidopsis. *PNAS.* **108**: 18530 - 18535.

Ye J, Zheng Y, Yan A, Chen N, Wang Z, Huang S, Yang Z. (2009). Arabidopsis formin3 directs the formation of actin cables and polarized growth in pollen tubes. *Plant Cell:* **21**, 3868 – 3884

Ye J, & Xu M. (2012). Actin bundler PLIM2s are involved in the regulation of pollen development and tube growth in Arabidopsis. *J Plant Physiol.* **169**: 516 – 522.

Ye JR, Zhou LM, Xu ML. (2013). *Arabidopsis* LIM proteins PLIM2a and PLIM2b regulate actin configuration during pollen tube growth. *Biologia Plantarium*. **57:** 433 - 441

Yokota E, & Shimmen T. (1999). The 135-kDa actin-bundling protein from lily pollen tubes arranges F-actin bundles with uniform polarity. *Planta.* **209**: 264 - 266.

Yu HS, & Russell SD. (1993). Three-dimensional ultrastructure of generative cell mitosis in the pollen tube of *Nicotiana tabacum*. *Eur J Cell Biol*. **61**: 338 – 348.

Zhang D, Diego W, Shuai B, Gui C, Muschietti J, McCormick S, Tang WH. (2008). The pollen receptor kinase LePRK2 mediates growth promoting signals and positively regulates pollen germination and tube growth. *Plant Physiol* **148**: 1368 – 1379.

Zhang H, Qu XL, Bao CC, Khurana P, Wang, QN, Xie YR, Zheng Y, Chen N, Blanchoin L, Staiger CJ, Huang S. (2010). Arabidopsis VILLIN5, an actin filament bundling and severing protein, is necessary for normal pollen tube growth. *Plant Cell.* **22**: 2749 – 2767.

Zhang W, Zhao Y, Guo Y, Ye K. (2012). Plant actin-binding protein SCAB1 is dimeric actin cross-linker with atypical pleckstrin homology domain. *J Biol Chem*. **287**: 11981 – 11990.

Zhang Y, & McCormick S. (2007). A distinct mechanism regulating a pollen-specific guanine nucleotide exchange factor for the small GTPase Rop in *Arabidopsis thaliana*. *PNAS*. **104:** 18830 - 18835

Zhao XY, Wang Q, Li S, Ge FR, Zhou LZ, McCormick S, Zhang Y. (2013). The juxtamembrane and carboxy-terminal domains of Arabidopsis PRK2 are critical for ROP-induced growth in pollen tubes. *J Exp Bot*. **64**: 5599 – 5610

Zhao Y, Zhao S, Mao T, Qu X, Cao W, Zhang L, Zhang W, He L, Li S, Ren S, Zhao J, Zhu G, Huang S, Ye K, Yuan M, Guo Y. (2011). The plant-specific actin binding protein SCAB1 stabilizes actin filaments and regulates stomatal movement in Arabidopsis. *The Plant Cell*. **23**: 2314 – 2330.

Zheng, Y, Xie Y, Jiang, Y, Qu X, Huang S. (2013). Arabidopsis ACTIN-DEPOLYMERIZING FACTOR7 severs actin filaments and regulates actin cable turnover to promote normal pollen tube growth. *The Plant Cell*. **25**: 3405 – 3423.

Zhou X, Graumann K, Wirthmueller L, Jones JDG, Meier I. (2014). Identification of unique SUN-interacting nuclear envelope proteins with diverse functions in plants. *Journal of Cell Biology*. **205**: 677 – 692.

Zhou X, & Meier I. (2013). How plants LINC the SUN to KASH. *Nucleus*, **4**: 206 – 215.

Zhou X, & Meier I. (2014b). Efficient plant male fertility depends on vegetative nuclear movement mediated by two families of plant outer nuclear membrane proteins. *PNAS*. **111**: 11900 – 11905.

Zhou X, Groves NR, Meier I. (2015). Plant nuclear shape is independently determined by the SUN-WIP-WIT2-myosin XI-I complex and CRWN1. *Nucleus*. **6**: 144 – 153.

Zhu L, Zhang Y, Kang E, Xu Q, Wang M, Rui Y, Liu B, Yuan M, Fu Y (2013). MAP18 regulates the direction of pollen tube growth in Arabidopsis by modulating F-actin organization. *Plant Cell*. **25**: 851 – 867.

Zonia L, Tupý J, Staiger CJ. (1999). Unique actin and microtubule arrays co-ordinate the differentiation of microspores to mature pollen in *Nicotiana tabacum*. *J Exp Bot.* **50**: 581–594

Zupan JR, & Zambryski P. (1995). Transfer of T-DNA from Agrobacterium to the plant cell. *Plant Physiol.* **107**: 1041 - 1047.